Phosphorus-Containing Tetrahedranes:

Synthesis and Reactivity Studies

Dissertation

Zur Erlangung des Doktorgrades der Naturwissenschaften

Dr. rer. nat.

an der Fakultät Chemie und Pharmazie der Universität Regensburg

vorgelegt von:

Gabriele Hierlmeier

aus Kelheim

Regensburg, April 2021

Der experimentelle Teil der vorliegenden Arbeit wurde in der Zeit zwischen November 2017 und Februar 2021 unter Anleitung von Prof. Dr. Robert Wolf am Institut für Anorganische Chemie der Universität Regensburg angefertigt.

Die Arbeit wurde angeleitet von: Prof. Dr. Robert Wolf

Promotionsgesuch eingereicht am: 22.04.2021

Tag der mündlichen Prüfung: 10.06.2021

Promotionsausschuss:	Vorsitz	Prof. Dr. Patrick Nürnberger
	Erstgutachter	Prof. Dr. Robert Wolf
	Zweitgutachter	Prof. Dr. Manfred Scheer
	Dritter Prüfer	Prof. Dr. Frank-Michael Matysik

Prologue

This thesis primarily reports on the synthesis and reactivity of phosphorus-containing tetrahedranes. Chapter 1 reviews the chemistry of p-block tetrahedranes, covering the synthesis of both organic tetrahedranes - exemplified by tetra-*tert*-butyltetrahedrane - and inorganic tetrahedranes such as white phosphorus (P_4). Chapter 2 describes the release of P_2 units from a nickel butterfly complex, which ultimately gives access to white phosphorus. In chapter 3 the aggregation and degradation of P_4 using N-heterocyclic carbene (NHC) nickel(0) complexes is described. The use of NHC-Ni(0) complexes has also allowed access to the mixed "hybrid" of (*t*BuC)$_4$ and P_4, di-*tert*-butyldiphosphatetrahedrane. The synthesis of this mixed group 14 / group 15 tetrahedrane by a simple nickel-catalysed dimerisation reaction of *tert*-butylphosphaalkyne is described in chapter 4 as is its characterisation. The stability and photochemistry of di-*tert*-butyldiphosphatetrahedrane is reported in chapter 5. Chapters 6-8 describe the reactivity of di-*tert*-butyldiphosphatetrahedrane toward carbenes (chapter 6), nickel NHC complexes (chapter 7) and metalate anions (chapter 8). Chapter 9 covers a distinct project and describes the synthesis of a penta-terphenyl cyclopentadienyl ligand and attempts to use it to generate dimetallocenes. Finally, chapter 10 gives a summary of the results described in this thesis and provides a short outlook.

Prolog

Diese Dissertation behandelt hauptsächlich die Synthese und Reaktivität von Phosphor-haltigen Tetrahedranen. Kapitel 1 gibt einen Überblick über die Chemie von p-Block Tetrahedranen und beschreibt unter anderem die Synthese des organischen Tetrahedrans Tetra-*tert*-butyltetrahedran und anorganischen Tetrahedranen wie z.B. weißem Phosphor. In Kapitel 2 wird die Freisetzung von P_2-Fragmenten durch einen Nickel-Schmetterlings Komplex beschrieben, wodurch letztendlich P_4 freigesetzt wird. Kapitel 3 befasst sich mit Aufbau- und Abbaureaktionen von weißem Phosphor mithilfe von N-heterocyclischen Carbenkomplexen von Nickel(0). NHC-Nickel(0)-Komplexe ermöglichten ebenfalls den Zugang zu dem gemischten „Hybrid" aus (*t*BuC)$_4$ und P_4, Di-*tert*-butyldiphosphatetrahedran. Die Synthese und Charakterisierung dieses gemischten Gruppe 14 / Gruppe 15- Tetrahedrans durch eine einfache nickelkatalysierte - Dimerisierungsreaktion von *tert*-Butylphosphaalkin wird in Kapitel 4 behandelt. Die Stabilität und Photochemie von Di-*tert*-butyldiphosphatetrahedran wird anschließend in Kapitel 5 beschrieben. Kapitel 6-8 handeln von der Reaktivität dieser Verbindung mit Carbenen (Kapitel 6), Nickel-NHC-Komplexen (Kapitel 7) und Metallaten (Kapitel 8). Kapitel 9 beschreibt ein unabhängiges Projekt und handelt von der Synthese eines penta-Terphenylcyclopentadienylliganden und Versuchen zur Darstellung eines Dimetallocenes mit diesem Liganden. Das letzte Kapitel fasst die Ergebnisse dieser Arbeit zusammen und gibt einen kurzen Ausblick.

Table of Contents

1 Tetrahedranes Composed of p-Block Elements: Topical Molecules with a Long History[a]

Abstract:

Tetrahedranes have fascinated the chemical community due to their structural elegancy and aesthetic simplicity, yet they are synthetically difficult to access. While the tetrahedral phosphorus molecule has been discovered in the 17th century, it was only in the late 20th century when a purely carbon based tetrahedrane could be isolated. Besides P and C-based tetrahedranes, this structural motif can be found in group 13 of the periodic table with compounds in the +I oxidation state which form electron-deficient tetrahedral cages.

This review provides an overview of tetrahedral molecules in the p-block of the periodic table. The synthesis, bonding situation, and properties of group 13, 14 and 15 tetrahedranes are described, with a particular emphasis on recent developments in the field of 'mixed' tetrahedranes.
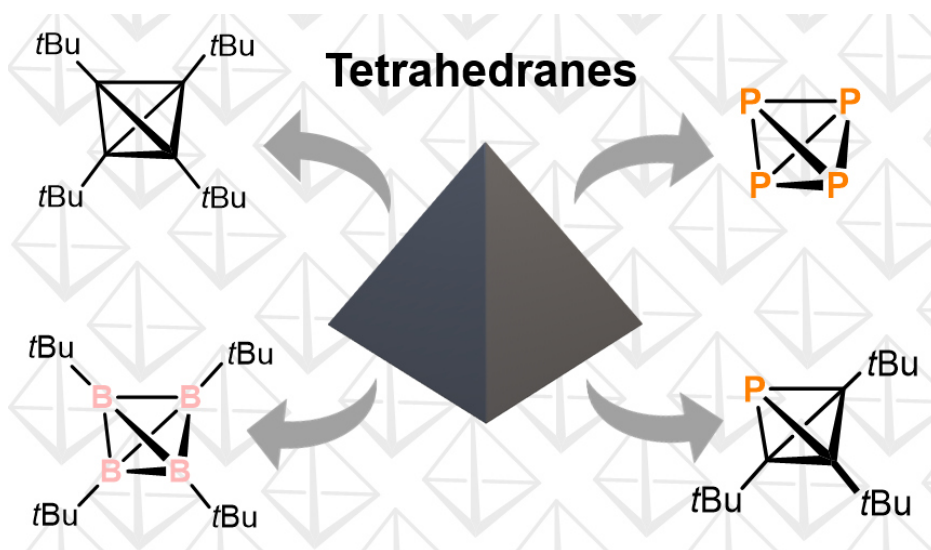
1.1 Platonic Solids and Hydrocarbons

The fascination for Platonic solids – tetrahedron, cube, octahedron, icosahedron and dodecahedron – dates back to antiquity.[1] Due to their high symmetry and apparent beauty, people have long associated them with significant and familiar concepts such as the ancient elements fire, air, earth, water and aether (Figure 1). The interest for these regular polyhedra was shared by Johannes Kepler, who even stated in his cosmological theory, that the orbits of the known planets around the sun and eventually the structure of the universe can be predicted by ordering the five polyhedra correctly.[2]

Tetrahedrane	Cubane	Dodecahedrane
	Eaton, **1964**	*Paquette*, **1982**
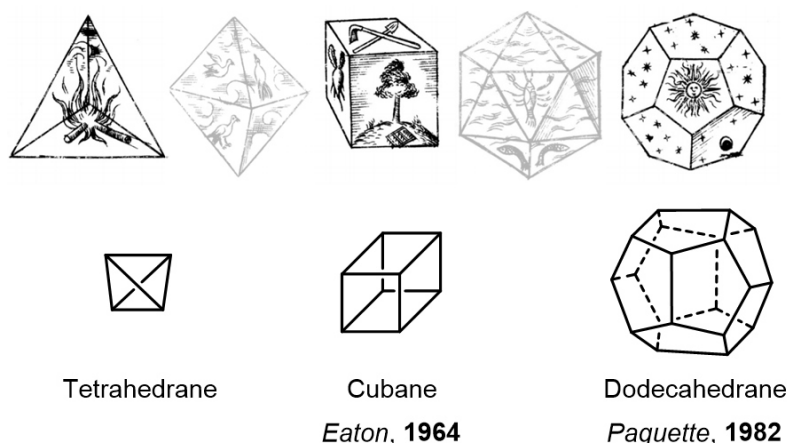
Figure 1. Drawing of the five Platonic solids representing the elements and the related Platonic hydrocarbons.[3]

In the early 20th century, it was recognised that the Platonic polyhedra represent fundamental und ubiquitous structures of chemical compounds. Examples are structures of Werner type metal complexes (octahedron and tetrahedron), boranes such as $(B_{12}H_{12})^{2-}$ (icosahedron),[4] and the structure of water clusters such as $(H_2O)_{20}$ (dodecahedron).[5] While these examples stem from the realm of inorganic chemistry, the idea of formally replacing each corner of the polyhedron with a methine group (CH) brought up the challenge of synthesising these Platonic hydrocarbons, which are only feasible for the tetrahedron, cube and dodecahedron due to the valency of carbon. In 1964, Eaton reported the synthesis of cubane C_8H_8.[6] This was followed by the synthesis of dodecahedrane $C_{20}H_{20}$ reported by Paquette in 1982.[7] The parent tetrahedrane C_4H_4 (tricyclo[1.1.0.0^{2,4}]butane, **1**), however, has not yet been isolated and researchers are still investigating the stability of this molecule.[8–13] This is not surprising, considering that tetrahedranes are the platonic hydrocarbons with the highest ring strain. Hence, their synthesis has been a challenge for the chemical community ever since they were proposed. It is the purpose of this review to summarise the chemistry of tetrahedranes with a focus on neutral p-block tetrahedranes of groups 13, 14 and 15.

1.2 The Parent Tetrahedrane C4H4

Numerous research groups have attempted to synthesise the missing parent tetrahedrane C_4H_4 (**1**) in the last decades.[8–12] However, only three studies suggest the formation of tetrahedrane as an intermediate.[14–16] In 1969 and 1970, Shevlin and Wolf as well as Peterson Jr., Baker and Wolfgang independently reported the intermediacy of tetrahedrane in the gas phase photolysis of carbon suboxide (C_3O_2) in the presence of cyclopropene.[14,15] The mechanism of this reaction is shown in Scheme 1a. Decarbonylation of carbon suboxide leads to ketocarbene C_2O, a suitable source to provide a single carbon atom. Subsequent reaction with cyclopropene affords a bicyclic carbene intermediate (**2**), which can undergo ring opening to vinylacetylene or ring closure to tetrahedrane. Analysis of the obtained gas mixture showed the presence of vinylacetylene and acetylene, the latter stemming from fragmentation of tetrahedrane. According to Shevlin and Wolf, their deuteration studies rule out the presence of any other intermediate than the (deuterated) tetrahedrane.[14,15] A similar approach was used by Rodewald and co-workers and involved the pyrolysis of the dilithium salt of *trans*-butenedial bistosylhydrazone (**3**, Scheme 1b). In this case, the tetrahedrane is possibly formed via a cyclopropenylcarbene intermediate (**4**). The authors suggest that the final product acetylene can form from this carbene intermediate or from a tetrahedrane. However, the observed product distribution in the deuterium scrambling experiments could only be explained through the formation of tetrahedrane.[16]
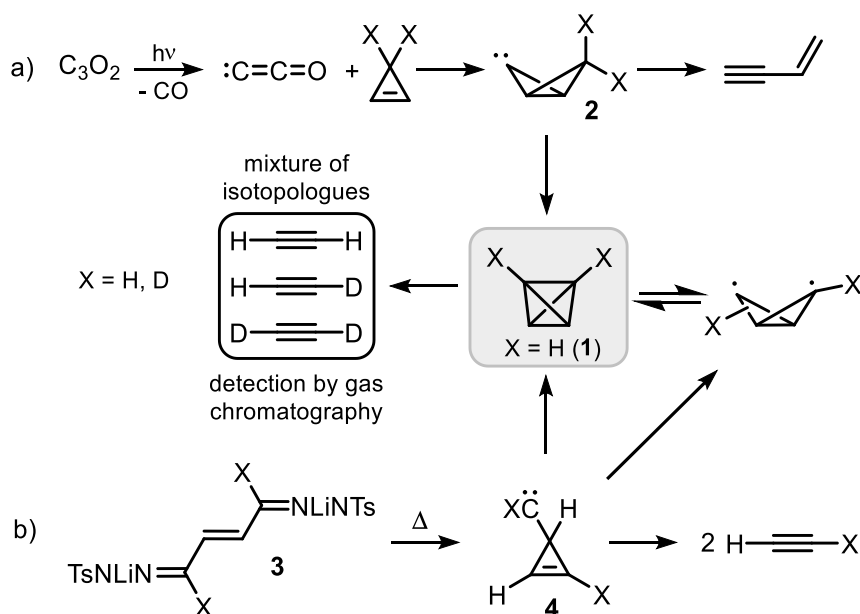
Scheme 1. Early attempts to generate tetrahedrane via photolysis (a) or thermolysis (b), and resulting acetylenes.[14–16]

In a more recent study, Schreiner and co-workers re-investigated the reaction of cyclopropene with atomic carbon in a low-temperature matrix-isolation experiment. In contrast to Shevlin's suggestion, Schreiner's study shows that the intermediacy of tetrahedrane is not necessary to

explain the observed product distribution. Nevertheless, calculations show that C_4H_4 should be an isolable molecule and is therefore still an interesting synthetic target.[13]

1.3   Main Group Tetrahedranes

1.3.1   Overview

In a broader sense, tetrahedranes are any molecules with a tetrahedral core structure. Beyond purely carbon-based tetrahedranes, a range of tetrahedranes containing other elements of the periodic table have been isolated or at least characterised spectroscopically. Indeed, the very first tetrahedrane to be isolated was white phosphorus, P_4 (*vide infra*). In addition to p-block elements, transition metals are also easily incorporated into tetrahedral structures due to their specific coordination requirements and, hence, a vast number of transition metal-based tetrahedranes is known. The chemistry of specific transition metal-based metallotetrahedranes has been explored thoroughly and only a few selected examples are given in Figure 2.[17–25] It is notable that such complexes vary in charge and symmetry, and a number of different p-block elements can also be incorporated alongside the transition metal(s).
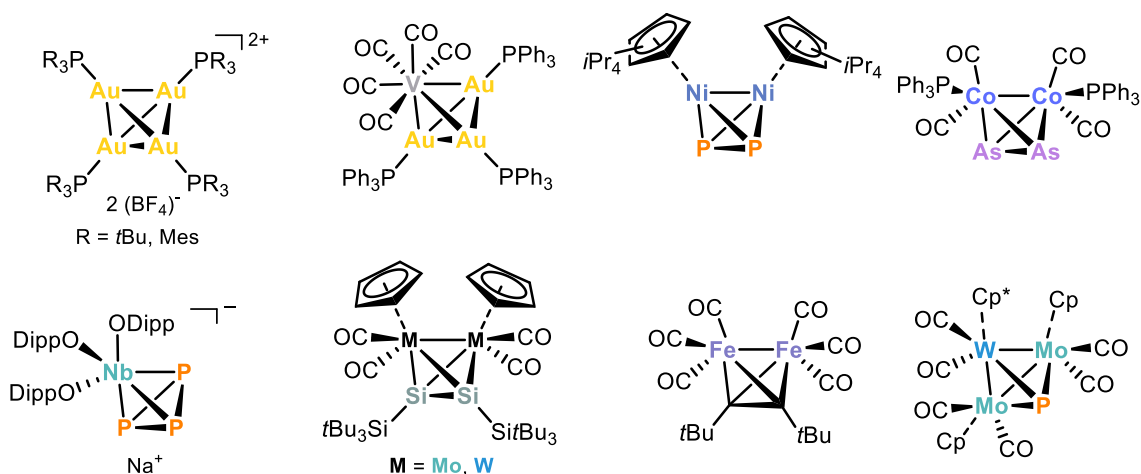
Figure 2. Examples of tetrahedranes containing transition metals.[17–25]

While transition metal-based tetrahedranes are rather common, tetrahedranes purely based on main group elements are much scarcer. Figure 3 gives an overview of the main group tetrahedranes that have been described in the literature. These known examples can be divided according to their molecular charge. Anionic, p-block element-based tetrahedranes are a well-developed family that have been reviewed in detail and so only the most pertinent, recent developments will be discussed below.[26–29] By contrast, examples of neutral tetrahedranes are very limited (isolable ones in particular), while cationic examples are even scarcer still. The following sections will give an overview of the bonding in tetrahedranes followed by an account of the chemistry of anionic, neutral and cationic tetrahedranes.
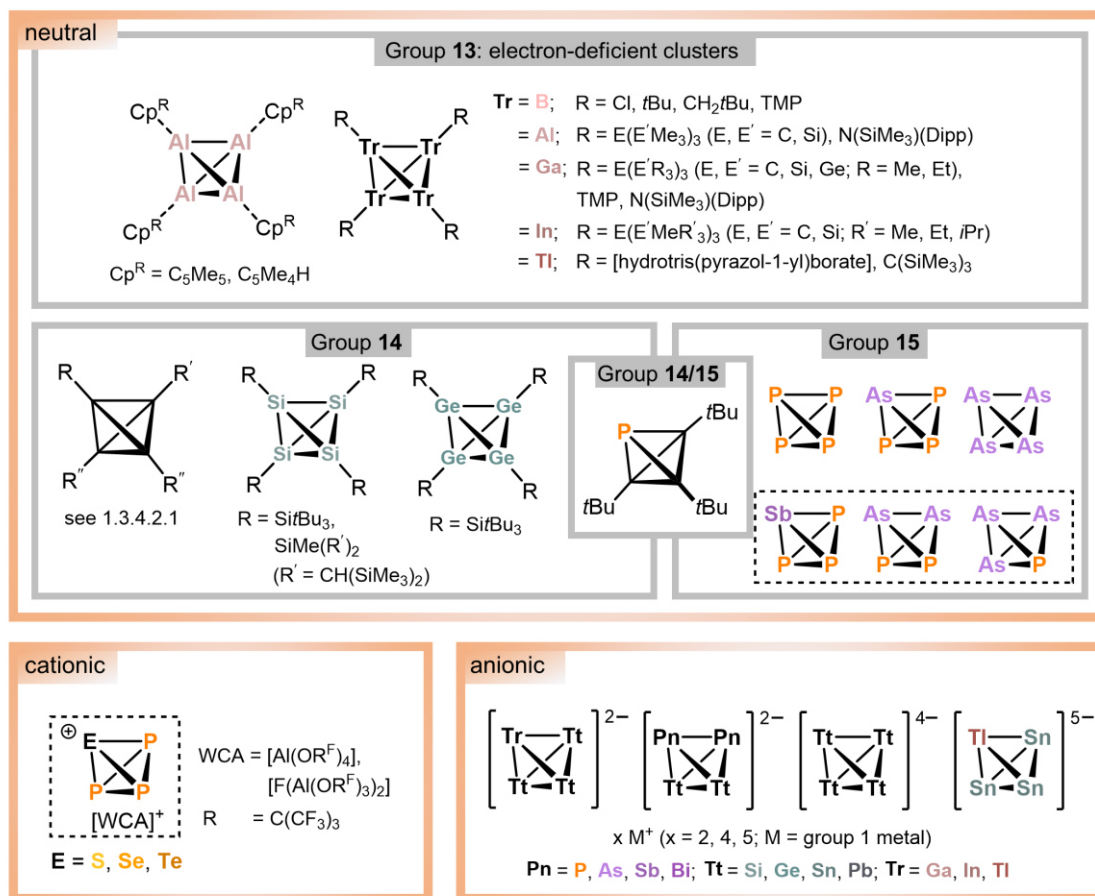
Figure 3. An overview of reported main group tetrahedranes. Species observed but not isolated are indicated by dashed boxes.

1.3.2   Bonding in Main Group Tetrahedranes

There has been widespread interest in understanding the bonding situation in main group tetrahedranes. The types of bonding observed for tetrahedranes composed of p-block elements can be divided into two groups: electron-deficient tetrahedranes (Group 13) form three-centre-two-electron (3c2e) bonds and electron precise tetrahedranes (Groups 14 and 15) form classic two-centre-two-electron (2c2e) bonds. Tetrahedranes from groups involving group 13, 14 and 15 elements additionally display spherical aromaticity (Figure 4).[30–32]

Group 13 tetrahedranes Tr_4R_4 (Tr = B, Al, Ga, In, Tl) possess eight cluster electrons. This electron count is not in line with the Wade-Mingos rules (ten electrons for *closo*-system), nor with classic 2c2e bonds (twelve electrons).[33] Calculation of the localised molecular orbitals on B_4H_4 showed that this electron-deficient system forms four 3c2e bonds, which are located within the B_3-triangles.[34] Moreover, for substituted derivatives B_4R_4 back donation of electrons from the substituents to the B_4 core was considered as a stabilising factor for R = F and Cl.[35]
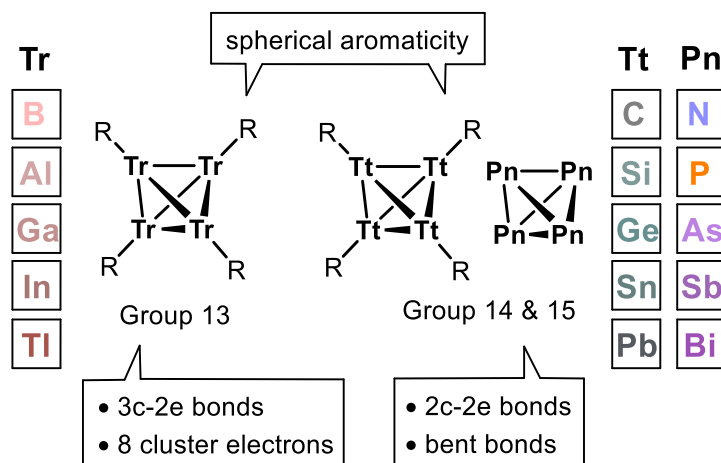
Figure 4. Bonding in Group 13, 14 and 15 tetrahedranes.

In contrast, Group 14 and 15 tetrahedranes form 2c2e bonds. However, chemists recognised as early as the late 19th century that covalent bonds in smaller cycloalkanes (e.g. in cyclopropane) are strained.[36] Following Baeyer's strain theory, the formation of bent bonds in cyclopropane was proposed in the 20th century.[37] These theoretical considerations were later confirmed by electron density measurements, which showed a deformation of the electron density away from the line of centres between atoms.[38] Considering the formation of six bent bonds, the ring strain in tetrahedrane was calculated to be as high as 141 kcal·mol^{-1}.[39,40] (The stability of isolable carbon-based tetrahedranes and other substituted carbon-based tetrahedranes will be discussed in 1.3.4.2.1.) Similarly, the electronic structure of P_4 is also dominated by bent bonds, which mainly have p-character and lone pairs of high s-character.[40]

While bent bonds significantly destabilise group 14 and 15 tetrahedranes, spherical aromaticity plays a major role in the bonding of group 13, 14 and 15 tetrahedranes (Table 1) and has a great stabilising effect.[41] This type of aromaticity was introduced as an extension of classical Hückel-

aromaticity and occurs in three-dimensional systems that have "abnormal stability, reactivity, and structural and magnetic properties".[32] The strength of these aromatic ring currents can be determined by nucleus-independent chemical shift (NICS) calculations. This method was initially introduced by Schleyer and co-workers and works as an aromaticity probe.[42] Negative NICS values are typically obtained at ring centres, indicating large induced diatropic ring currents and, hence, aromaticity.[32] With a value of ca. -48, the NICS value at the cage centre of C_4H_4 is extremely low, suggesting a high spherical aromaticity with strong diatropic ring current effects.[31,43] The spherical aromaticity of the heavier homologues Si_4H_4 and Ge_4H_4, however, is much less pronounced, as indicated by the low NICS values of -1.0 and 1.9, respectively.[43] In contrast, the NICS values of all group 15 tetrahedranes are strongly negative, suggesting pronounced diamagnetic ring currents even for the heavier analogues.[30] In these Pn_4 (Pn = N…Bi) tetrahedranes, all σ- and π-orbitals are completely filled which results in the special case of double spherical aromaticity.[30,44] In contrast, the NICS value calculated for B_4H_4 of 34.7 is highly paratropic, indicating a strong antiaromaticity in the tetrahedral cage.[45]

Table 1. Calculated NICS values for group 14 and 15 tetrahedranes. Values were calculated at the B3LYP level of theory using the 6-311*G** basis set for E = N, P, As and the LANL2DZp basis set for E = Sb, Bi and ωB97XD/6-311++G(d,p) for group 14 compounds.[30,43] Values are given for the cage centre.[46]

	NICS value (ppm)
C_4H_4	-48.5
Si_4H_4	-1.0
Ge_4H_4	1.9
N_4	-69.6
P_4	-52.9
As_4	-53.3
Sb_4	-38.8
Bi_4	-36.3

1.3.3   Ionic Main Group Tetrahedranes

Isoelectronic replacement of elements in neutral tetrahedranes such as P_4 can lead to valence-isoelectronic cationic or anionic species. Until lately, cationic species were only observed in the gas phase by Stoppioni, Vaglio and Sheldrick,[47] while isolable cationic tetrahedranes were elusive. Very recently, the Krossing group accessed the first cationic tetrahedranes in the condensed phase upon reacting group 16 salts $ECl_3[WCA]$ (E = S, Se, Te) with white phosphorus P_4 (Scheme 2). The resulting $[EP_3]^+$ cations with weakly coordinating aluminate counterions (= WCA = $[Al(OR^F)_4]^-$, $[F(Al(OR^F)_3)_2]^-$, $R^F = C(CF_3)_3$) were characterised by NMR spectroscopy and quantum chemical calculations. The $^{31}P\{^1H\}$ NMR spectra reveal characteristic high-field

singlet signals at $\delta = -399.3$ (E = S), -360.6 (E = Se), -342.9 (E = Te) ppm, which are very upfield-shifted, similarly to P_4. The formation of side-products such as $[P_5Cl_2]^+$ and $[P_3Se_4]^+$ and slow decomposition of the counteranions could not be circumvented in these reactions and prevented isolation of the pure materials.
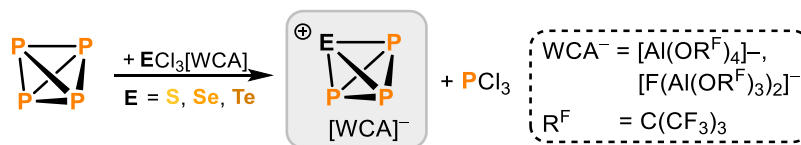
Scheme 2. Formation of cationic tetrahedranes [EP₃][WCA].[48]

In contrast to the very limited number of examples for cationic tetrahedranes, a vast number of anionic tetrahedranes has been characterised by single crystal X-ray diffraction. The structures and properties of anionic Zintl-type tetrahedranes are covered in several recent review articles and will not be discussed in detail in this chapter.[26–29] These Zintl-type anions are the smallest deltahedral clusters and commonly available by solid-state reactions of the corresponding elements. For instance, the Zintl-phase sodium silicide was synthesised from the elements at 700 °C in a corundum crucible, affording metallic needles of Na_4Si_4 which contain Si_4^{4-} tetrahedra.[49] Structure determination of solvate-free Zintl-phases or the corresponding ammonia solvates in the presence of sequestering agents such as crown-ethers or cryptands reveals the availability of both homo- and heteroatomic tetrahedranes.[50],[51] Moreover, the groups of Korber and Fässler recently detected some of these ions (e.g. $[Si_4]^{4-}$ and $[Sn_4]^{4-}$) as well as the mono-protonation products (e. g. $[\mu-HSi_4]^{3-}$) in solution.[52,53] The transition from the $[Tt_4]^{4-}$ Zintl-anions to neutral main group tetrahedranes by addition of electrophiles (alkyl, silyl) seems conceivable, yet only the above-mentioned protonation ($[Si_4]^{4-} + H^+ \rightarrow [\mu-HSi_4]^{3-}$) has been accomplished.[53]

1.3.4 Neutral Main Group tetrahedranes

Neutral main group tetrahedranes are far less explored than their "naked" Zintl-analogues. Nevertheless, those examples that have been characterised can be divided into three different categories. First: electron-deficient group 13 elements in the +I oxidation state formed from tetrameric aggregates. Second: tetrahedral group 14 compounds of the type Tt_4R_4. Third: group 15 compounds such as white phosphorus and yellow arsenic. The synthesis and properties of all known p-block tetrahedranes will be discussed in this chapter. In particular, recent developments in the synthesis of heteroatomic tetrahedranes will be highlighted.

1.3.4.1 Group 13

B_4Cl_4 was the first isolated group 13 tetrahedrane and obtained in a low yield from decomposition of B_2Cl_4.[54] Characterisation by X-ray crystallography in 1953 revealed its tetrahedral core.[55] Subsequently, chemists attempted to use this compound in salt metathesis reactions for the preparation of alkyl-substituted tetraboratetrahedranes.[56,57]

Thereafter, a variety of group 13 tetrahedranes have been prepared. Mainly three strategies have been used (Scheme 3): a) salt metathesis of Tr(I)X compounds, b) reduction of group 13 (=Tr) halide precursors RTr(II)X or RTr(III)X$_2$, and c) reductive elimination of silyl-radicals from [R$_2$TrTrR]$_2$ compounds.
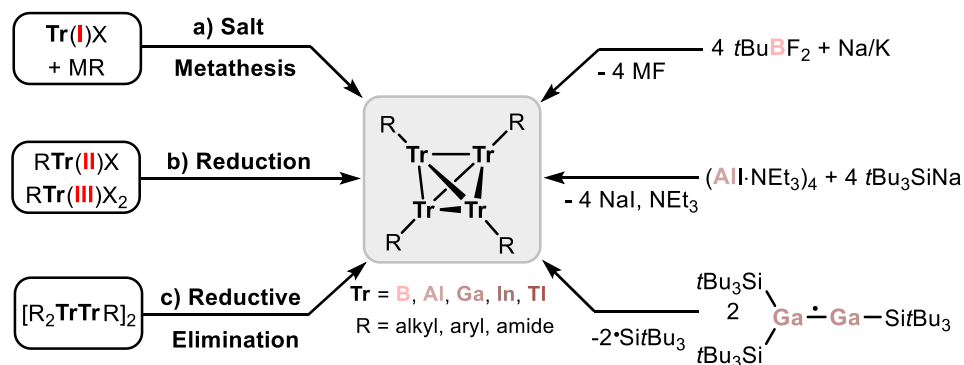
Scheme 3. General synthetic routes toward group 13 tetrahedranes (left) and selected examples (right).[58–60]

An example for the salt metathesis approach is the synthesis of the alkyl-substituted tetrahedrane B$_4$tBu$_4$ by reaction of B$_4$Cl$_4$ with tBuLi by Morrison and co-workers.[57] Although this species was not characterised by X-ray crystallography initially, the structure was later assigned by Paetzold and Boese.[58] This synthetic approach of salt metathesis has been very successfully used in subsequent years for the synthesis of a variety of other group 13 tetrahedranes, e.g. Al$_4$(SitBu$_3$)$_4$, Ga$_4$[N(SiMe$_3$)(Dipp)]$_4$, In$_4$[Si(SiMe$_3$)]$_4$, Tl$_4$[C(SiMe$_3$)$_3$]$_4$.[59,61,62]

In 1991 Paetzold and Boese accessed tetra-*tert*-butylboratetrahedrane by reduction of tBuBF$_2$ with a Na/K alloy, thus employing the second approach for the synthesis of tetratrielatetrahedranes.[58,63] Reduction of [RTr(II)X]$_2$, RTr(III)X$_2$ or M[RTr(III)Cl$_3$] (Tr = B, Al) with group 1 or 2 metals was also used by the groups of Uhl, Roesky and Siebert for the synthesis of similar B$_4$R$_4$ and Al$_4$R$_4$ tetrahedranes.[64]

Apart from reduction by external reductants and salt metathesis, the reductive elimination of silyl radicals has been successfully employed to obtain tetrahedranes,[65] for instance by elimination of SitBu$_3$ radicals from a radical Ga species.[60] This reductive approach was used in combination with salt metathesis for the synthesis of Ga$_4$R$_4$ tetrahedranes by reaction of GaCl$_2$·dioxane with LiR (R = Si(SiMe$_3$)$_3$[66], C(SiMe$_3$)$_3$[67]).

One particularly notable class of group 13 tetrahedranes are cyclopentadienyl aluminium(I) derivatives. These compounds are usually prepared by salt metathesis with aluminium subhalides or reduction of the Al(III) precursors. While the tetrahedral structures of [Cp^{R}Al]$_4$ (Cp^R = Cp*, C$_5$Me$_4$H)[62,68] were confirmed by Schnöckel and co-workers, the corresponding gallium and indium compounds crystallise in hexameric forms as Tr$_6$ (Tr = Ga, In) octahedrons.[69] The group of Schnöckel also found that salt metathesis of GaBr with LiC(SiMe$_3$)$_3$ and AlCl with LiN(SiMe$_3$)$_2$ results in formation of small amounts of anionic Al$_7$[N(SiMe$_3$)$_2$]$_6^-$ (**5**) and Ga$_8$[C(SiMe$_3$)$_3$]$_6$ (**6**) clusters, both featuring connected tetrahedra (Figure 5).[70,71] The vertex-

connected Al_7 cluster has a highly unusual arrangement of the Al atoms resembling the cubic close packed (ccp) solid-state structure of metallic Al, whereas the Ga_8 compound features two separate Ga_4 tetrahedra connected via a Ga−Ga bond.
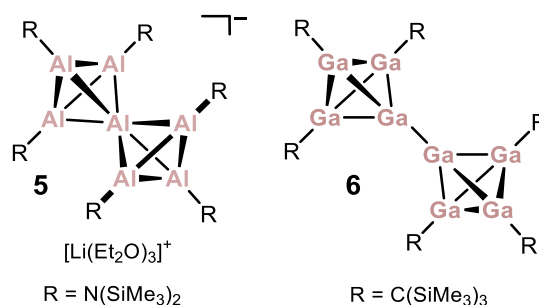
Figure 5. "Dimeric" tetrahedranes synthesised by the group of Schnöckel.[70,71]

Notably, for some of the group 13 tetrahedranes, dissociation in solution has been reported. For instance, Uhl and co-workers reported that $[Ga_4(CSiMe_3)_4]$ can dissociate into the monomer as determined by cryoscopic molar mass determination and gas-phase electron diffraction.[67,72]

1.3.4.2   Group 14

The synthesis of group 14 tetrahedranes has undoubtedly proved more challenging compared to the neighbouring groups in the periodic table. Therefore, theoretical chemists have striven to develop a detailed understanding for ring strain in such systems.[73] The calculated strain energy of tetrahedrane itself is extremely high at 141 kcal·mol^{-1} (Figure 6).[74,75] Tetrasilatetrahedrane (140.9 kcal·mol^{-1}) is as strained as its carbon analogue, whereas the related heavier tetrahedranes (E = Ge, Sn, Pb) are slightly more stable. As shown in Figure 6, the number of four-membered rings increases - in prismane or cubane - the strain energy of the carbon compounds increases even more, while it is significantly reduced for the heavier homologues. Nagase attributed this behaviour to the lower tendency of heavier group 14 elements to form s-p hybrid orbitals compared to carbon. This property makes it more favourable for the heavier atoms to form 90° bond angles, which accounts for the higher stability of the prismane and cubane systems. In contrast, the formation of three-membered rings with angles of 60° is similarly unfavourable for carbon and its heavier congeners, resulting in only small energy differences in the strain of the tetrahedranes.
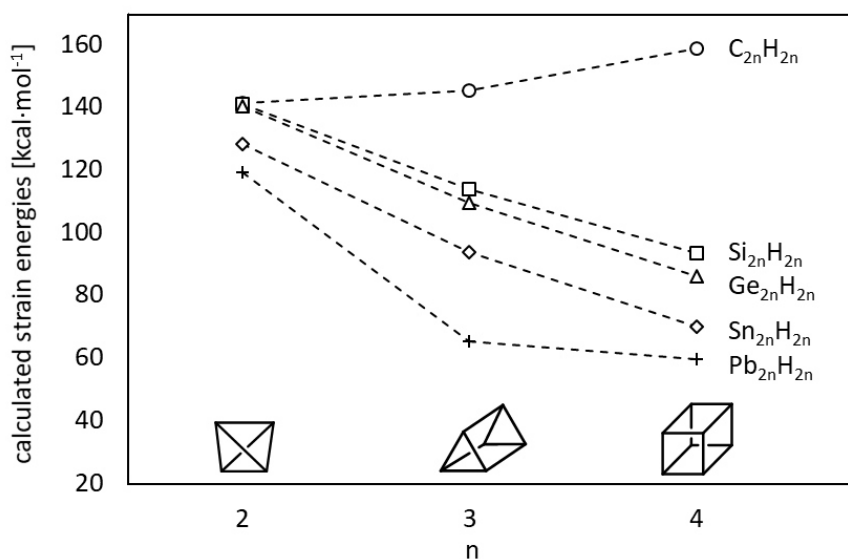
Figure 6. Calculated strain energies for group 14 tetrahedranes, prismanes and cubanes. Calculated at the HF/6-31G*
(Tt = C, Si) and HF/DZ(d) (Tt = Ge, Sn) level of theory; adapted from references [73,74].

1.3.4.2.1 Carbon - Organic Tetrahedranes

In a review article from 1974, Maier states that the chances to isolate an all-carbon tetrahedrane "appear very remote".[76] However, theoretical calculations that showed the high ring strain and instability were seen "as a challenge to defy the theorists". And, indeed, only four years later Maier and co-workers were successful in the synthesis of the first stable, organic tetrahedrane, tetra-*tert*-butyltetrahedrane ($tBuC)_4$ (**7**, Scheme 4a).[77] This achievement was a milestone in organic synthesis and laid the foundation for the subsequent synthesis of many other organic and heteronuclear tetrahedranes.[78] The synthesis of $(tBuCP)_4$ was initially accomplished by irradiation of tetra-*tert*-butylcyclopentadienone (**8**) to give the isomeric tricyclopentanone (**9**). Upon prolonged irradiation of this compound, a cyclopropenylketene (**10**) is formed. However, when these experiments were conducted at −100 °C in diethyl ether, decarbonylation occurred and the tetrahedrane **11** could be detected and subsequently isolated in 35% yield by column chromatography. **11** is a colourless, air-stable solid with a melting point of 135 °C and a core C signal in the ^{13}C NMR spectrum at 10.2 ppm. Heating the tetrahedrane in solution to 130 °C results in quantitative isomerisation to tetra-*tert*-butylcyclobutadiene. Irradiation of the latter in argon at 10 K regenerates the tetrahedrane.

Given the elaborate, multi-step synthesis of **11**, the group of Maier subsequently developed a more efficient route via N_2 liberation starting from a synthetically more easily available cyclopropenyldiazomethane precursor (**12**, Scheme 4b). In this synthesis, tetra-*tert*-butylcyclobutadiene (**13**) was detected as an intermediate and the tetrahedrane **11** was isolated in 65% yield.[79]
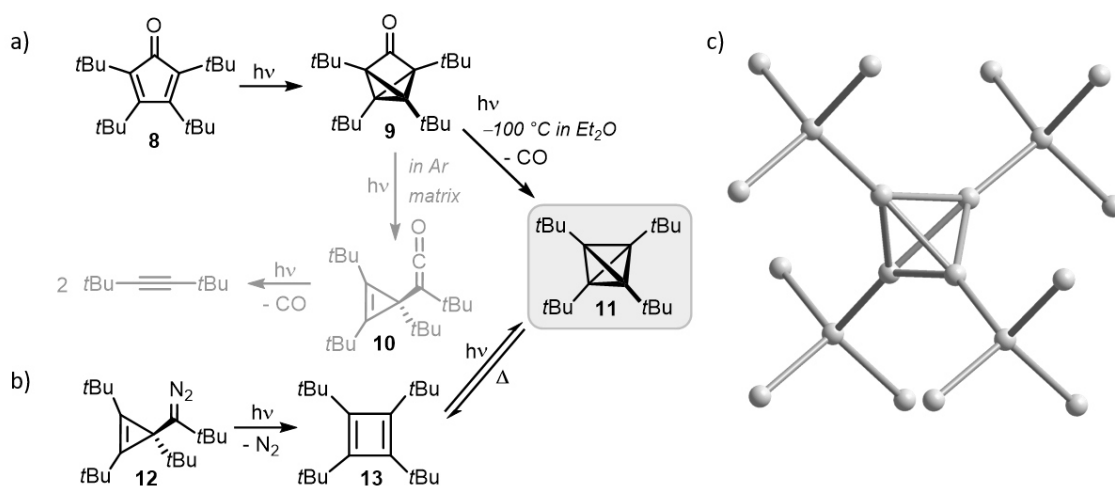
Scheme 4. a, b) Syntheses of tetra-*tert*-butyltetrahedrane (**11**); c) molecular structure of **11** in the solid state.[77,79]

The molecular structure of **11** in the solid state was investigated by Irngartinger.[80] **11** crystallises in the hexagonal crystal system at −60 °C. The molecular structure shows only slight deviations from the ideal T_d symmetry with average C−C bond lengths of 1.485(5) Å in the tetrahedron (Scheme 4b), which is significantly shorter than a typical C−C single bond. This shortness can be attributed to the bending of the bonds outwards from the edge of the ideal tetrahedron. **11** has a significantly higher bent bond character (28.4°) compared to cyclopropane (21.3°) as determined by NMR spectroscopic methods.[81]

The stability of **11** was attributed to the so-called "corset effect". According to Maier, the intramolecular repulsion of the *tert*-butyl groups is smallest when they are arranged in a tetrahedral geometry. Bond cleavage in **11** is less favourable compared to C_4H_4 as it would result in a smaller distance between the *tert*-butyl groups and higher steric repulsion. A more recent computational study on the stability of tetrahedranes has revealed that hydrogen bonding between H-atoms of the *t*Bu substituents also plays an important role in the stabilisation of **11**.[82]

In the following years, the Maier group succeeded in the synthesis of various asymmetric and symmetric tetrahedranes from the related cyclopropenyldiazomethane precursors,[83] including silyl-substituted tetrahedranes such as tetrakis(trimethylsilyl)tetrahedrane, $(Me_3SiC)_4$ (**14**) starting from **15** (Scheme 5).[84] Sekiguchi and co-workers were able to isolate the same compound from the cyclobutadiene **16** generated from the dianionic precursor $Li_2[(CSiMe_3)_4]$ (**17**) by oxidation with 1,2-dibromoethane.
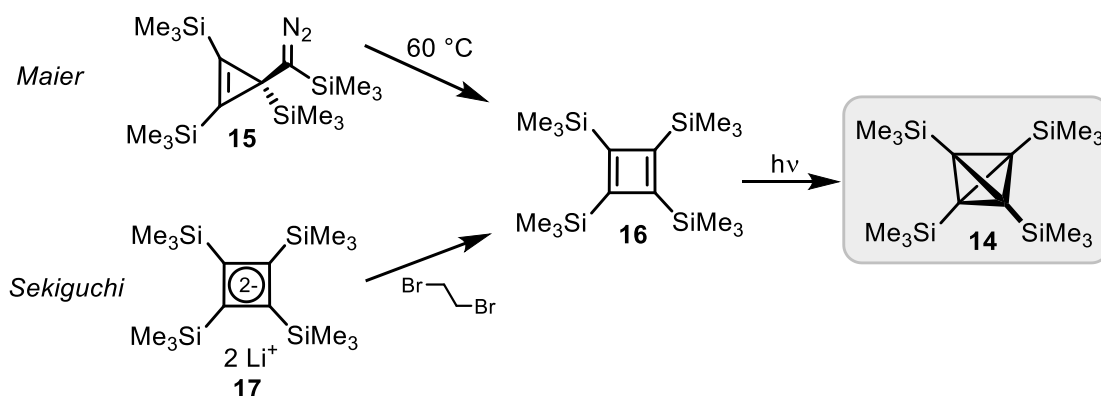
Scheme 5. Syntheses of tetrakis(trimethylsilyl)tetrahedrane (**14**) by the Maier and Sekiguchi routes.[84]

Despite the less pronounced corset effect in **14** (due to the longer C−Si bonds compared to C−C bonds), the tetrasilylated tetrahedrane features an unusually high thermal stability up to 300 °C. This is attributed to the electronic stabilisation from the $SiMe_3$ groups, offering both a strong σ-donor effect and a π-acceptor effect with electron donation from the bent C−C bonds of the tetrahedron to σ*-orbitals of the Si−Me bonds. This effect is so dominant that **14** is the first example of a tetrahedrane that is more stable than its cyclobutadiene isomer **16** (according to calculations).

The group of Sekiguchi later explored the chemistry of **14** and showed that tris(trimethylsilyl)tetrahedranyllithium (**18**) can be isolated from the reaction of **14** with methyl lithium (Scheme 6).[85] This lithiated tetrahedrane is a particularly useful compound for subsequent functionalisation reactions.
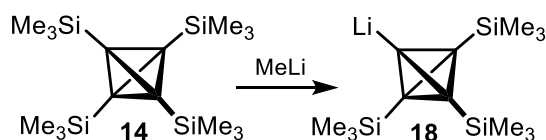
Scheme 6. Synthesis of a tetrahedranyllitihium.[85]

Using **18**, Sekiguchi and co-workers were able to isolate a plethora of asymmetrically substituted tetrahedranes by substitution of the lithium atom.[85–90] Treatment of **18** with dimethylsulfate affords the methyl-substituted derivative **19**, whereas addition of cyclopentadiene yields $(HC)(CSiMe_3)_3$ (**20**, Scheme 7).[85] The latter compound is surprisingly stable despite the reduced number of bulky substituents and features a ^1H NMR signal of the skeleton H at the relatively downfield shift of 2.85 ppm due to the high s-character of the hybrid orbital. The vertex-connected hexakis(trimethylsilyl)tetrahedranyltetrahedrane (**21**) was synthesised by oxidative coupling of two molecules of **18**.[86] Structural analysis by X-ray crystallography revealed a staggered conformation with an extremely short linking C−C bond (1.436(3) Å). A range of aryl-functionalised tetrahedranes (**22**) was accessed by palladium-catalysed cross-coupling reactions of **18** with aryl iodides. These compounds feature HOMO orbitals that result from mixing of the

tetrahedral σ-core with the aryl π-systems. The presence of three more silyl groups in **22** allows for a second functionalisation after treatment with MeLi and subsequent methylation, protonation and cross-coupling reactions.[90] Furthermore, sulfur-substituted tetrahedranes **23** were obtained from reaction of **18** with diaryldisulfides.[88] Analysis of their electronic structures by DFT revealed the interaction of lone pairs on the sulfur atoms with the tetrahedral core, leading to a batochromic shift in the UV/Vis absorption spectra of these compounds. Oxidation of the tetrahedranylphenylsulfide with *m*CPBA afforded the sulfone **24**. Collectively, the rich follow-up chemistry of the tetrahedranyllithium **18** suggests a certain robustness of the tetrahedrane motif, especially when combined with SiMe$_3$-groups.
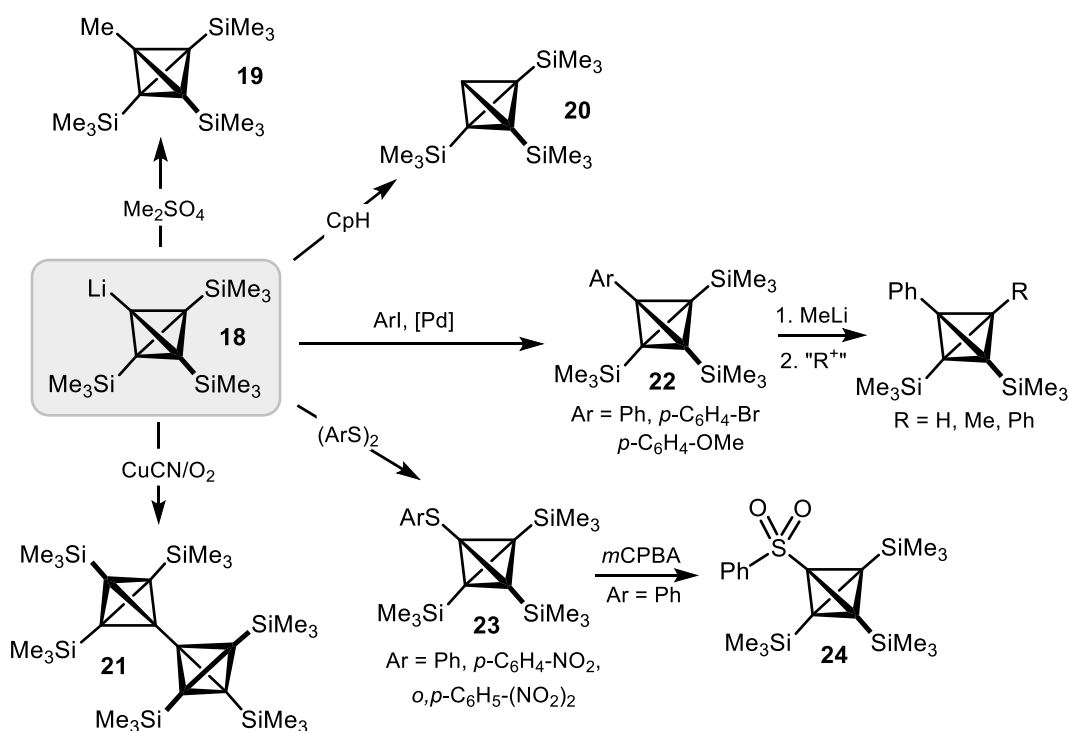
Scheme 7. A tetrahedranyllithium as a building block for the synthesis of asymmetric tetrahedranes.[85–90]

In 1978, Schleyer and co-workers reported the synthesis of tetralithiotetrahedrane (**25**) by photolysis of dilithium diacetylide (Scheme 8).[91] The hypothesis of its formation was based on ^{13}C NMR spectroscopy and hydrolysis experiments that showed the formation of acetylene. Computational studies revealed that tetralithiotetrahedrane might indeed be stable kinetically as an isomer in which each lithium atom is located over a C$_3$ triangle (**25**-T$_d$), though the thermodynamically more favourable **25**-D$_{2h}$ isomer of C$_4$Li$_4$ also exists.[92] One year later, the methylation of tetralithiotetrahedrane was erroneously reported to yield tetramethyltetrahedrane.[93] The group of Maier subsequently checked several routes towards tetramethyltetrahedrane and showed that this species is not stable.[94]
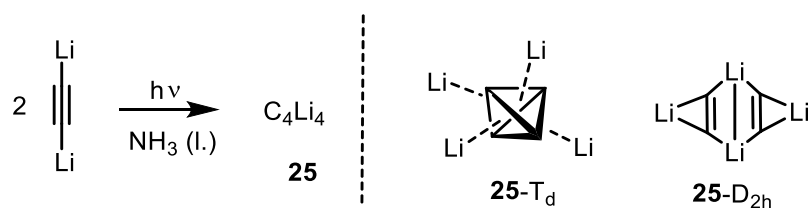
Scheme 8. Synthesis of tetralithiotetrahedrane and minima structures of **25**.[91]

1.3.4.2.2 Heavier Group 14 Tetrahedranes

Even though the strain energy for tetrasilatetrahedrane $(HSi)_4$ is similarly high as for the carbon analogue (see Figure 6), the replacement of carbon with silicon could be accomplished. The group of Wiberg has shown that tetrakis(tri-*tert*-butylsilyl)-tetrasilatetrahedrane, $[(tBu_3Si)Si]_4$ (**26**, Scheme 9) can be synthesised by reaction of the tetrabromotetrasilane precursor **27** with supersilylsodium tBu_3SiNa (Scheme 9, left).[95] Concomitant elimination of tBu_3SiBr and NaBr affords **26** as air- and moisture-stable yellow-orange needles. X-ray crystallography revealed an average Si−Si bond length in the Si_4 tetrahedron of 2.318(2) Å and exocyclic Si−Si bond lengths of 2.360(2) Å. A one pot procedure for the synthesis of the same compound starting from $HSiCl_3$ and one equivalent of supersilylsodium was found more recently.[96]
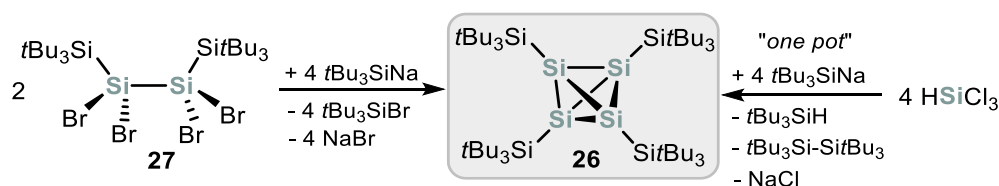
Scheme 9. Synthesis of the tetrasilatetrahedrane **26** according to Wiberg's original procedure (left) and a "one-pot" procedure (right).[95,96]

A related Si_4R_4 tetrahedrane (**28**) featuring a different silyl substituent $(R = SiMeR'_2, R' = CH(SiMe_3)_2)$ has also been synthesised by Sekiguchi and co-workers by a salt metathesis reaction similar to that reported by Wiberg.[97,98] Sekiguchi and co-workers investigated the reaction of this tetrasilatetrahedrane with reducing agents. The reaction of **28** with KC_8 resulted in bond cleavage of an exocyclic Si−Si bond to afford the anionic tetrasilatetrahedranide **29** as part of a separated ion pair (Scheme 10).[98] A similar reaction was reported by Klapötke and co-workers for $Si_4(SitBu_3)_4$.[99] Addition of iodine to **28** afforded a trans-substituted cyclotetrasilene (**30**), which could be converted back to the tetrasilatetrahedrane by addition of the $NaSitBu_3$.[100] Moreover, the group of Wiberg investigated the reactivity of tetrasilatetrahedranes toward a series of other reagents (e.g. dioxygen and elemental sodium), but reported no unambiguous structural proof of the outcome of these reactions.[101]
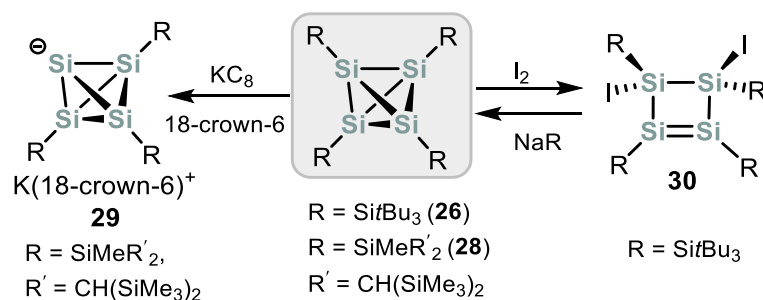
Scheme 10. Reactivity of tetrasilatetrahedranes.[98–100]

Using the heavier germanium precursor **31**, Wiberg and co-workers were also successful in preparing the germanium tetrahedrane $[(t\text{Bu}_3\text{Si})\text{Ge}]_4$ (**32**, Scheme 11) in an analogous fashion.[102] However, the yield was significantly improved when simply using GeCl_2 as a precursor. In contrast to its lighter homologues, **32** is very air-sensitive and hydrolyses slowly in the presence of water. Structural analysis of deep red crystals of **32** by X-ray crystallography revealed a Ge_4 tetrahedron with an average Ge–Ge distance of 2.442(3) Å, which is significantly shorter than the bond length in digermanes such as $t\text{Bu}_3\text{Ge}$–$\text{Ge}t\text{Bu}_3$ (2.710(1) Å).[103]
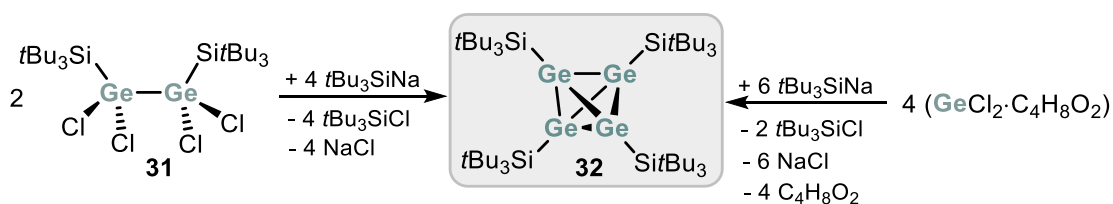
Scheme 11. Synthesis of tetragermatetrahedrane **32** by Wiberg.[102]

The heavier homologues, tetrastannatetrahedrane and the lead derivative have not been reported up to now. However, the cubane derivative octastannacubane $(2,6\text{-Et}_2\text{-C}_6\text{H}_3)_8\text{Sn}_8$ is accessible.[104] The availability of this octastanncacubane raises the question whether a related tetrastannatetrahedrane might be stable and should stimulate further research in this area.[105]

1.3.4.3 Group 15

Heavier Group 15 elements commonly form three- and five-membered ring structures.[106] Therefore, the formation of a tetrahedron, consisting of four three-membered rings, is easily achieved for phosphorus and its heavier elements, while tetrahedral N_4 is unknown. The reason for the higher stability of the diatomic species N_2 over N_4 compared to the higher stability of P_4 over P_2 is that the nitrogen atoms encounter a stronger Pauli repulsion in N_4 due to the similar radii of 2s and 2p orbitals compared to the 3s and 3p orbitals.[107] Despite the strong N≡N triple bond (BDE = 228 kcal·mol^{-1}), the existence of a neutral tetraazene molecule, N_4, has been subject of several studies.[108] While the tetrahedral isomer of N_4 was discussed heavily, the group of Cacace could detect the open-chain N_4 molecule in neutralisation-reionisation mass spectrometry experiments with a life time of more than one microsecond.[109]

In contrast, P_4 was the first tetrahedrane that was isolated as early as 1669 by Hennig Brand on his search for the "Philosopher's stone".[110]

White phosphorus is the least stable and most reactive form of phosphorus. It is of tremendous importance both in academia and industry as the key starting material for the synthesis of most organophosphorus compounds.[110,111] In the chemical industry, P_4 is generated from calcium apatite, quartz sand and coke at 1500 °C in an electric arc furnace (Scheme 13a).[112] This process requires an enormous amount of energy (ca. 737 kcal·mol^{-1}) and researchers worldwide continue to strive to functionalise P_4 selectively and even catalytically.[113]

a) $2 \, Ca_3(PO_4)_2 + 6 \, SiO_2 + 10 \, C \xrightarrow[\text{electric arc furnace}]{+ \, 3084 \, kJ} 6 \, CaSiO_3 + 10 \, CO +$

b) $As_{grey} \xrightarrow{\text{ca. 600 °C}}$
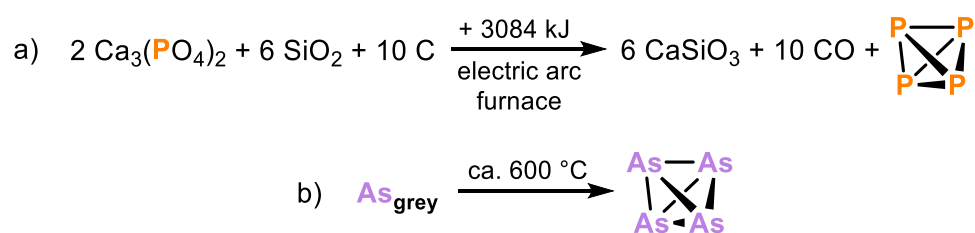
Scheme 12. Syntheses of white phosphorus P_4 (a) and yellow arsenic (b).[112,114]

The structure of P_4 has been intensely investigated over decades. Gas-phase electron diffraction studies revealed a P−P bond length of 2.1994(3) Å.[115] The determination of the solid-state structure of P_4 has been a formidable challenge.[116] P_4 forms poorly diffracting, waxy crystals and shows pronounced tendency for disorder in the solid state. The α-modification has 58 positions in the unit cell with partially occupied and disordered P_4 molecules similar to the α-manganese structure.[117] Upon cooling to −76.4 °C, the α-modification transforms into the ordered β-modification, which is related to the structure of γ-Pu and contains six P_4 molecules per unit cell. From this modification, the bond length in P_4 was determined as 2.209(5) Å.[118]

Similarly to white phosphorus, yellow arsenic is generated at high temperatures (ca. 600 °C) and forms tetrahedral As_4 molecules in the gas phase (Scheme 12b). Condensation of these arsenic vapours on cold surfaces leads to solid arsenic As_4, which is highly air- and light-sensitive.[114] Condensation of arsenic vapours in organic solvents in an air-free set-up containing a furnace tube yields solutions of yellow arsenic which can be handled under rigorous exclusion of light. While the condensation of As_4 vapours was originally described in 1867 by Bettendorf,[119] it is only much more recently the groups of Scherer, Scheer and Cummins used and developed this method for studying the reactivity of As_4 (which has similarities to that of P_4).[114,120] Notably, the group of Scheer also improved the inconvenient handling of photosensitive As_4 solutions by incorporation of As_4 in porous carbon materials, making them air- and light-stable.[121]

A comparable solid modification of antimony containing Sb_4 tetrahedrons has not yet been isolated. However, Sb_4 has been detected by Raman spectroscopy of noble gas matrices and in thin antiomony films.[122] Bi_4 was only detected in the gas phase.[123]

Mixed tetrahedral interpnictogen compounds, containing P, As or Sb in the core, were detected by Ozin in 1970 by gas-phase Raman spectroscopy.[124] Mixing of phosphorus and antimony vapours results in the formation of the entire series of compounds P_nAs_{4-n} ($n = 0-4$). SbP_3 was detected in a similar way. In 2009, Cummins and co-workers developed a tailored synthetic route toward one of these compounds, AsP_3.[125] The selective synthesis of this compound was achieved by using the anionic niobium complex $Na[P_3Nb(ODipp)_3]$ (**33**) as a cyclo-P_3^- transfer reagent (Scheme 13). Salt metathesis of this complex with $AsCl_3$ affords the dichloridoniobium complex **34** and AsP_3, which could be isolated in 75% yield. Similarly, SbP_3 was detected (but not isolated) by reaction of **33** with $SbCl_3$ by ^{31}P NMR spectroscopy. AsP_3 is a bright white solid with a melting point of 73 °C that is thermally stable up to 130 °C and not light sensitive. The distorted tetrahedral structure was proven by coordination to a molybdenum complex as $[(AsP_3)Mo(CO)_3(PiPr_3)_2]$ with the P atom coordinating to the Mo centre. In this complex the P−P bond lengths average to 2.177 Å and the P−As bonds are longer with an average of 2.305 Å . Gas phase electron diffraction studies on uncoordinated AsP_3 reveal similar bond lengths of 2.1949(28) (P−P) and 2.3041(12) Å (P−As). AsP_3 shows a resonance at a chemical shift of −484 ppm in the $^{31}P\{^1H\}$ NMR spectrum, which is similar to the chemical shift observed for P_4 (−520 ppm).[115]
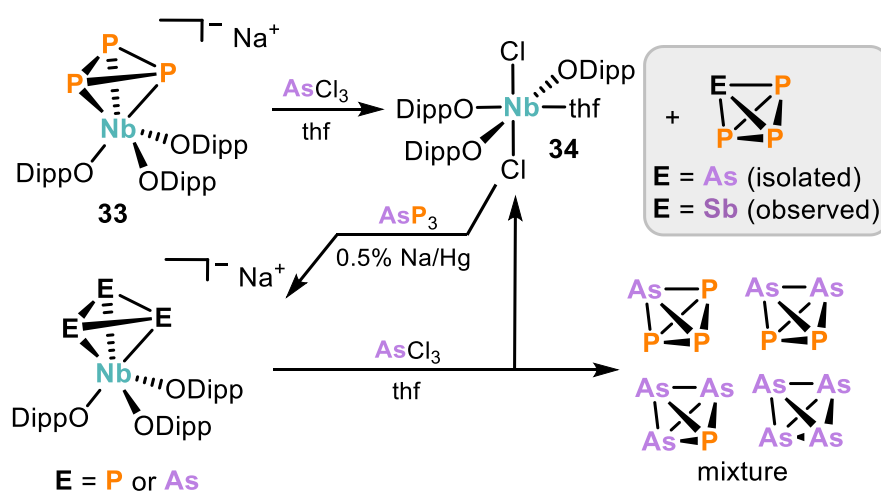
Scheme 13. Synthesis of tetrahedral interpnictogen compounds by Cummins.[126]

When the dichlorido niobium complex by-product $[Nb(ODipp)_3Cl_2(thf)]$ (**34**) was reacted with AsP_3 in the presence of a reducing agent, the whole series of P/As-containing complexes $[(E_nE'_{3-n})Nb(ODipp)_3]^-$ (E, E' = P, As) containing P_3^-, P_2As^-, PAs_2^- and As_3^- was formed. Treatment of this mixture with $AsCl_3$ again recovers $[Nb(ODipp)_3Cl_2(thf)]$ along with the mixed tetraatomic interpnictides AsP_3, As_2P_2, As_3P, and As_4 as evidenced by gas chromatography and ^{31}P NMR spectroscopy. The chemical shifts of the phosphorus containing species are given in Table 2. Comparison of these shifts reveals that introduction of As atoms to the P_4 tetrahedron leads to a stepwise low-field shift of the ^{31}P NMR signal from −521 (P_4) over −484 (AsP_3) and

−452 (As_2P_2) to −432 ppm (As_3P). Similarly, the ^{31}P NMR signals of SbP_3 at −462 ppm is low-field shifted compared to P_4 and additionally in comparison to AsP_3, which shows that substitution of a P atom in P_4 with antimony has an even larger effect compared to arsenic substitution.

Table 2. ^{31}P NMR shifts of mixed group 15 / group 14 tetrahedranes

	^{31}P shift (ppm)
P_4	−521
AsP_3	−484
As_2P_2	−452
As_3P	−432
SbP_3	−462
$P(CtBu)_3$	−488

1.3.4.4   Mixed Group 14 / Group 15 Tetrahedranes

Considering the isolobal analogy between P and CR fragments, the replacement of one or several vertices of P_4 by CR fragments seems conceivable. The group of Cummins was successful in this approach by developing a synthetic route toward tri-*tert*-butylphosphatetrahedrane (**35**).[127] This molecule was synthesised according to the multi-step procedure shown in Scheme 14. Irradiation of the anthracene precursor [$C_{14}H_8P(CtBu)_3$] (**36**) led to formation of **35** in small amounts, as detected by ^{31}P NMR spectroscopy. A subsequent adjustment of the synthetic route to classic salt elimination chemistry from **37** allowed the isolation of $P(CtBu)_3$ in 19% yield as a low-melting, colourless and light-sensitive solid. The tetrahedral structure was confirmed by a single-crystal X-ray diffraction study. Unfortunately, the quality of the data set does not allow any interpretation of the bond metric data. Nevertheless, the spectroscopic analysis of **35** reveals a singlet resonance in the ^{31}P NMR spectrum at −488 ppm, which compares well to the resonances of P_4 and the P_nAs_{4-n} ($n = 0−3$) series (Table 2).
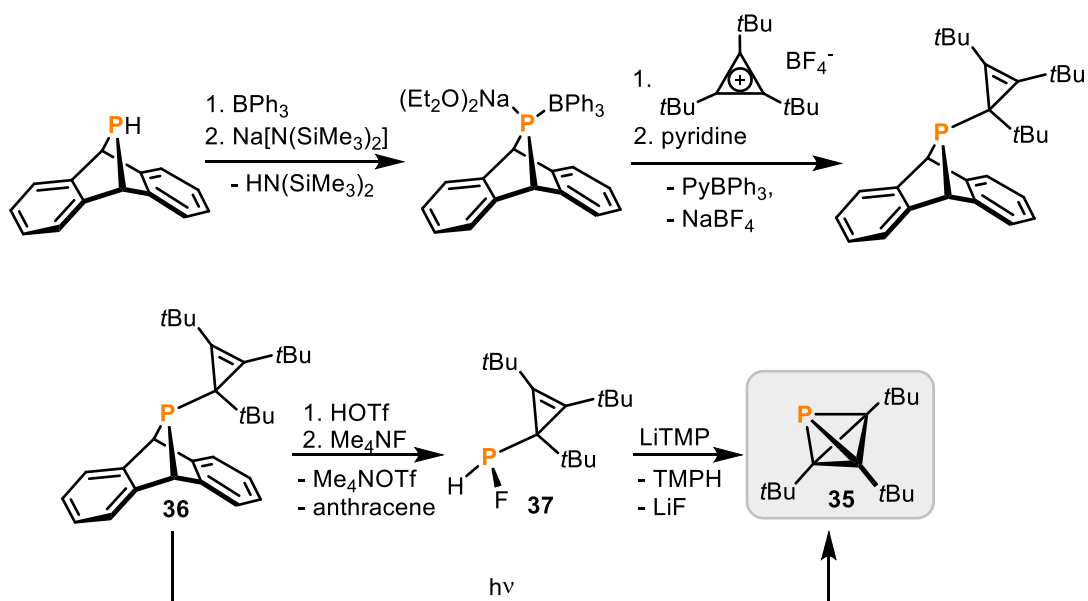
Scheme 14. Synthesis of tri-*tert*-butylphosphatetrahedrane.[127]

Initial reactivity studies on tri-*tert*-butylphosphatetrahedrane show a high tendency towards dimerisation and opening of the tetrahedron. Addition of Lewis acids such as [W(CO)$_5$(thf)] affords an uncomplexed housene (**38**, Scheme 15). Moreover, irradiation of **35** leads to a mixture of several products including the symmetrically cyclopropenyl-substituted diphosphene (**39**).
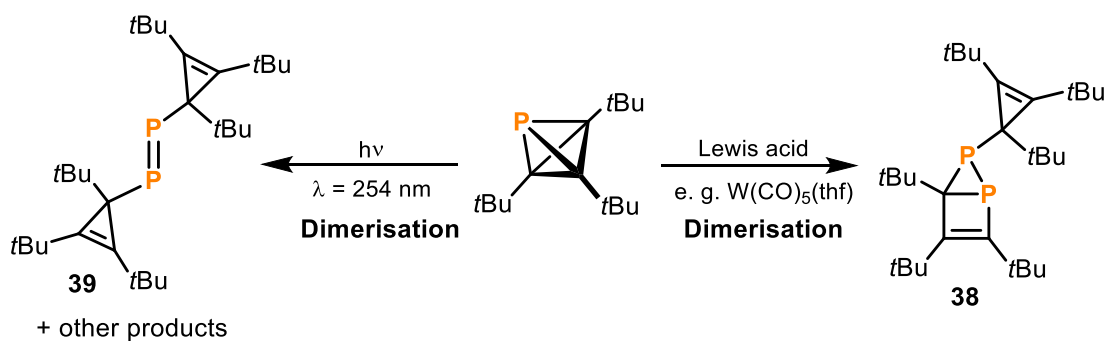
Scheme 15. Reactivity of tri-*tert*-butylphosphatetrahedrane.[127]

1.4 Conclusion and Outlook

The first heteroatomic tetrahedrane, P_4, was discovered by Brand in 1669.[110] While its tetrahedral structure was only recognised in the early 20th century,[128] the rise of inorganic molecular chemistry in the late 20th century was accompanied with the discovery of many other tetrahedral main group clusters. A great variety of group 13 compounds in the +I oxidation state aggregate to form electron deficient tetrahedral clusters with 3c2e bonds.

In contrast to the trieles, the tetrahedral arrangement of carbon atoms to form organic tetrahedranes has been a challenge for synthetic chemists and was attempted by several groups. Following Maier's pioneering work, carbon tetrahedranes C_4R_4 were established as stable, yet highly strained compounds with a rich follow-up chemistry.[129] Moreover, the heavier homologues E_4R_4 (E = Si, Ge) were accessed as tetrahedral compounds.[97] In contrast to the lighter carbon homologue, the tetrasila- and tetragermatetrahedranes can be prepared by facile one-pot procedures, e.g. starting from $HSiCl_3$. However, the heavier tetrastanna- and tetraplumbatetrahedranes have not yet been isolated.

Recent advances in the field of main group tetrahedranes have focused on the synthesis of mixed p-block tetrahedranes, containing more than one element in the tetrahedral core. The synthesis of mixed group 15 tetrahedranes by the group of Cummins was a major breakthrough in this area.[125] Very recently, Cummins also showed that tetrahedranes with both group 14 and group 15 elements in the tetrahedral core can be synthesised.[127] While $P(CtBu)_3$ contains one P-atom and three C-atoms, the synthesis of related diphosphatetrahedranes $P_2(CR)_2$ or $P_3(CR)$ represents an attractive target for future studies. Moreover, while the chemistry of P_4 has been studied extensively, the reactivity of related phosphatetrahedranes remains almost unexplored, despite the potential use of these molecules as building blocks in the synthesis of organophosphorus compounds.

References

[1] M. Atiyah, P. Sutcliffe, *Milan J. Math.* **2003**, *71*, 33–58.

[2] a) J. Kepler, Harmonices mundi libri V., **1619**; b) J. V. Field, *Q. Jl. R. Astr. Soc.* **1982**, *23*, 556–568.

[3] Partially reproduced from: J. Kepler, Harmonices mundi libri V., **1619**.

[4] I. Tiritiris, T. Schleid, K. Müller, W. Preetz, *Z. Anorg. Allg. Chem.* **2000**, *626*, 323–325.

[5] a) J. K. Kazimirski, V. Buch, *J. Phys. Chem. A* **2003**, *107*, 9762–9775; b) H. Kabrede, R. Hentschke, *J. Phys. Chem. B* **2003**, *107*, 3914–3920.

[6] a) P. E. Eaton, T. W. Cole, *J. Am. Chem. Soc.* **1964**, *86*, 3157–3158; b) James C. Barborak, L. Watts, R. Pettit, *J. Am. Chem. Soc.* **1966**, *88*, 1328–1329.

[7] Leo A. Paquette, Walter Bauer, Mark R. Sivik, Michael Buehl, Martin Feigel, Paul von Ragué Schleyer, *J. Am. Chem. Soc.* **1990**, *112*, 8776–8789.

[8] H. W. Lage, H. P. Reisenauer, G. Maier, *Tetrahedron Lett.* **1982**, *23*, 3893–3896.

[9] G. Maier, M. Hoppe, H. P. Reisenauer, *Angew. Chem. Int. Ed. Engl.* **1983**, *22*, 990–991.

[10] G. Maier, M. Hoppe, K. Lanz, H. P. Reisenauer, *Tetrahedron Lett.* **1984**, *25*, 5645–5648.

[11] M. Christl, S. Freund, *Chem. Ber.* **1985**, *118*, 979–999.

[12] D. A. Kaisaki, D. A. Dougherty, *Tetrahedron Lett.* **1987**, *28*, 5263–5266.

[13] A. Nemirowski, H. P. Reisenauer, P. R. Schreiner, *Chem. Eur. J.* **2006**, *12*, 7411–7420.

[14] R. F. Peterson Jr., R. T. K. Baker, R. L. Wolfgang, *Tetrahedron Lett.* **1969**, *54*, 4749–4751.

[15] P. B. Shevlin, A. P. Wolf, *J. Am. Chem. Soc.* **1970**, *92*, 406–408.

[16] L. B. Rodewald, H.-K. Lee, *J. Am. Chem. Soc.* **1973**, *95*, 623–625.

[17] F. A. Cotton, J. D. Jamerson, B. R. Stults, *J. Am. Chem. Soc.* **1976**, *98*, 1774–1779.

[18] A. S. Foust, C. F. Campana, J. D. Sinclair, L. F. Dahl, *Inorg. Chem.* **1979**, *18*, 3047–3054.

[19] J. E. Ellis, *J. Am. Chem. Soc.* **1981**, *103*, 6106–6110.

[20] E. Zeller, H. Beruda, H. Schmidbaur, *Inorg. Chem.* **1993**, *32*, 3203–3204.

[21] Y. Yang, P. R. Sharp, *J. Am. Chem. Soc.* **1994**, *116*, 6983–6984.

[22] H. Shan, Y. Yang, A. L. James, P. R. Sharp, *Science* **1997**, *275*, 1460–1462.

[23] M. Scheer, D. Himmel, C. Kuntz, S. Zhan, E. Leiner, *Chem. Eur. J.* **2008**, *14*, 9020–9029.

[24] M. Wilfling, K. W. Klinkhammer, *Angew. Chem. Int. Ed.* **2010**, *49*, 3219–3223.

[25] G. Dübek, F. Hanusch, D. Munz, S. Inoue, *Angew. Chem. Int. Ed.* **2020**, *59*, 5823–5829.

[26] T. F. Fässler, Zintl Ions: Principles and Recent Developments, Springer, **2011**.

[27] S. Scharfe, F. Kraus, S. Stegmaier, A. Schier, T. F. Fässler, *Angew. Chem. Int. Ed.* **2011**, *50*, 3630–3670.

[28] K. Mayer, J. Weßing, T. F. Fässler, R. A. Fischer, *Angew. Chem. Int. Ed.* **2018**, *57*, 14372–14393.

[29] R. J. Wilson, N. Lichtenberger, B. Weinert, S. Dehnen, *Chem. Rev.* **2019**, *119*, 8506–8554.

[30] A. Hirsch, Z. Chen, H. Jiao, *Angew. Chem. Int. Ed.* **2001**, *40*, 2834–2838.

[31]   D. Moran, M. Manoharan, T. Heine, P. von Ragué Schleyer, *Org. Lett.* **2003**, *5*, 23–26.

[32]   Z. Chen, R. B. King, *Chem. Rev.* **2005**, *105*, 3613–3642.

[33]   a) K. Wade, *J. Chem. Soc., Chem. Commun.* **1971**, 792–793; b) A. J. Welch, *Chem. Commun.* **2013**, *49*, 3615–3616.

[34]   a) D. J. Swanton, R. Ahlrichs, *Theor. Chim. Acta* **1989**, *75*, 163–172; b) J. H. Hall Jr., I. R. Epstein, W. N. Lipscomb, *Inorg. Chem.* **1973**, *12*, 915–920; c) A. Burkhardt, U. Wedigg, H. G. von Schnering, A. Savin, *Z. Anorg. Allg. Chem.* **1993**, *619*, 437–441.

[35]   D. A. Kleier, J. Bicerano, W. N. Lipscomb, *Inorg. Chem.* **1980**, *19*, 216–218.

[36]   A. Baeyer, *Ber. Dtsch. Chem. Ges.* **1885**, *18*, 2269–2281.

[37]   a) T. Förster, *Z. Phys. Chem.* **1939**, *B43*, 58–78; b) C. A. Coulson, W. E. Moffitt, *J. Chem. Phys.* **1947**, *15*, 151; c) K. B. Wiberg, *Acc. Chem. Res* **1996**, *29*, 229–234.

[38]   a) P. Chakrabarti, P. Seiler, J. D. Dunitz, A. D. Schluter, G. Szeimies, *J. Am. Chem. Soc.* **1981**, *103*, 7378–7380; b) R. Boese, T. Miebach, A. De Meijere, *J. Am. Chem. Soc.* **1991**, *113*, 1743–1748.

[39]   K. B. Wiberg, R. F. W. Bader, C. D. H. Lau, *J. Am. Chem. Soc.* **1987**, *109*, 985–1001.

[40]   M. F. Guest, I. H. Hillier, V. R. Saunders, *J. Chem. Soc., Faraday Trans. 2* **1972**, *68*, 2070–2074.

[41]   Z.-H. Li, D. Moran, K.-N. Fan, P. von Ragué Schleyer, *J. Phys. Chem. A* **2005**, *109*, 3711–3716.

[42]   P. von Ragué Schleyer, C. Maerker, A. Dransfeld, H. Jiao, N. J. R. van Eikema Hommes, *J. Am. Chem. Soc.* **1996**, *118*, 6317–6318.

[43]   N. K. V. Monteiro, J. F. de Oliveira, C. L. Firme, *New J. Chem.* **2014**, *38*, 5892–5904.

[44]   P. von Ragué Schleyer, H. Jiao, M. N. Glukhovtsev, J. Chandrasekhar, E. Kraka, *J. Am. Chem. Soc.* **1994**, *116*, 10129–10134.

[45]   a) C. Corminboeuf, R. B. King, P. von Ragué Schleyer, *ChemPhysChem* **2007**, *8*, 391–398; b) J. Aihara, *J. Am. Chem. Soc.* **1978**, *100*, 3339–3342.

[46]   The NICS value of P_4 was also calculated by Cummins (−59.4) and Krossing (−61.9), also see: B. M. Cossairt, C. C. Cummins, *J. Am. Chem. Soc.* **2009**, *131*, 15501–15511, P. Weis, D. C. Röhner, R. Prediger, B. Butschke, H. Scherer, S. Weber, I. Krossing, *Chem. Sci.* **2019**, *48*, 295.

[47]   a) G. J. Penney, G. M. Sheldrick, *J. Chem. Soc. A* **1971**, 243–245; b) L. Operti, G. A. Vaglio, M. Peruzzini, P. Stoppioni, *Inorg. Chim. Acta* **1985**, *96*, 43–47.

[48]   P. Weis, D. C. Röhner, R. Prediger, B. Butschke, H. Scherer, S. Weber, I. Krossing, *Chem. Sci.* **2019**, *48*, 295.

[49]   a) E. Hohmann, *Z. Anorg. Chem.* **1948**, *257*, 113–126; b) J. Witte, H. G. Schnering, W. Klemm, *Z. Anorg. Allg. Chem.* **1964**, *327*, 260–273.

[50]   a) I. F. Hewaidy, E. Busmann, W. Klemm, *Z. Anorg. Allg. Chem.* **1964**, *328*, 283–293; b) J. Witte, H. G. von Schnering, *Z. Anorg. Allg. Chem.* **1964**, *327*, 260–273; c) H. G. von Schnering, M. Schwarz, R. Nesper, *Angew. Chem. Int. Ed. Engl.* **1986**, *6*, 566–567; d) J. Llanos, R. Nesper, H. G. von Schnering, *Angew. Chem.* **1983**, *95*, 1026–1027; e) K. H. Janzon, H. Schäfer, A. Weiss, *Z. Anorg. Allg. Chem.* **1970**, *372*, 87–99; f) V. Quéneau, E. Todorov, S. C. Sevov, *J. Am. Chem. Soc.* **1998**, *120*, 3263–3264; g) H. G. von Schnering, M. Baitinger, U. Bolle, W. Carrillo-Cabrera, J. Curda, Y. Grin, F. Heinemann, J. Llanos, K. Peters, A. Schmeding, M. Somer, *Z. Anorg. Allg. Chem.* **1997**, *623*, 1037–1039; h) J. Curda, W. Carrillo-Cabrera, A. Schmeding, K. Peters, M. Somer, H. G. von Schnering, *Z. Anorg. Allg. Chem.* **1997**, *623*, 929–936; i) C. R. C. Hoch, *Z. Anorg. Allg. Chem.* **2002**, *628*, 1541–1548; j) C. Hoch, M. Wendorff, C. Röhr, *Z. Anorg. Allg. Chem.* **2003**, *629*, 2391–2397; k) S. Bobev and S. C. Sevov, *Polyhedron* **2002**, *21*, 641; l) C. Lorenz, S. Gärtner, N. Korber, *Z. Anorg. Allg. Chem.* **2017**, *643*, 141–145; m) C. B. Benda, T. Henneberger, W. Klein, T. F. Fässler, *Z. Anorg. Allg. Chem.* **2017**, *643*, 146–148; n) E. Busmann, *Z. Anorg. Allg. Chem.* **1961**, *313*, 90–106.

[51]   a) S. C. Critchlow, J. D. Corbett, *Inorg. Chem.* **1982**, *21*, 3286–3290; b) S. C. Critchlow, J. D. Corbett, *Inorg. Chem.* **1985**, *24*, 979–981; c) G. C. W. Blase, *Z. Kristallogr. – Cryst. Mater.* **1991**, *196*, 207–211; d) L. Xu, S. C. Sevov, *Inorg. Chem.* **2000**, *39*, 5383–5389; e) F. Lips, I. Schellenberg, R. Pöttgen, S. Dehnen, *Chem. Eur. J.* **2009**, *15*, 12968–12973; f) F. Lips, M. Raupach, W. Massa, S. Dehnen, *Z. Anorg. Allg. Chem.* **2011**, *637*, 859–863; g) U. Friedrich, M. Neumeier, C. Koch, N. Korber, *Chem. Commun.* **2012**, *48*, 10544–10546; h) R. Ababei, J. Heine, M. Hołyńska, G. Thiele, B. Weinert, X. Xie, F. Weigend, S. Dehnen, *Chem. Commun.* **2012**, *48*, 11295–11297; i) S. Mitzinger, L. Broeckaert, W. Massa, F. Weigend, S. Dehnen, *Nat. Commun.* **2016**, *7*, 10480; j) S. Mitzinger, J. Bandemehr, K. Reiter, J. Scott McIndoe, X. Xie, F. Weigend, J. F. Corrigan, S. Dehnen, *Chem. Commun.* **2018**, *54*, 1421–1424; k) K. Wiesler, K. Brandl, A. Fleischmann, N. Korber, *Z. Anorg. Allg. Chem.* **2009**, *635*, 508–512.

[52]   M. Neumeier, F. Fendt, S. Gärtner, C. Koch, T. Gärtner, N. Korber, R. M. Gschwind, *Angew. Chem. Int. Ed.* **2013**, *52*, 4483–4486.

[53]   F. Hastreiter, C. Lorenz, J. Hioe, S. Gärtner, N. Lokesh, N. Korber, R. M. Gschwind, *Angew. Chem. Int. Ed.* **2019**, *58*, 3133–3137.

[54]   a) G. Urry, T. Wartik, H. I. Schlesinger, *J. Am. Chem. Soc.* **1952**, *74*, 5809; b) G. Urry, A. G. Garrett, H. I. Schlesinger, *Inorg. Chem.* **1963**, *2*, 396–400.

[55]   M. Atoji, W. N. Lipscomb, *J. Chem. Phys.* **1953**, *21*, 172.

[56]   B. Wrackmeyer, *Annu. Rep. NMR Spectrosc.* **1988**, *20*, 61–203.

[57]   T. Davan, J. A. Morrison, *J. Chem. Soc., Chem. Commun.* **1981**, *5*, 250–251.

[58]   T. Mennekes, P. Paetzold, R. Boese, D. Bläser, *Angew. Chem. Int. Ed. Engl.* **1991**, *30*, 173–175.

[59]   A. Purath, C. Dohmeier, A. Ecker, H. Schnöckel, K. Amelunxen, T. Passler, N. Wiberg, *Organometallics* **1998**, *17*, 1894–1896.

[60]   N. Wiberg, K. Amelunxen, H.-W. Lerner, H. Nötz, W. Ponikwar, H. Schwenk, *J. Organomet. Chem.* **1999**, *574*, 246–251.

[61]   a) H. S. A. Purath, *J. Organomet. Chem.* **1999**, *579*, 373–375; b) M. Huber, H. Schnöckel, *Inorg. Chim. Acta* **2008**, *361*, 457–461; c) A. R. G. Linti, *Chem. Commun.* **2000**, 127–128; d) A. Seifert, G. Linti, *Eur. J. Inorg. Chem.* **2007**, *2007*, 5080–5086; e) W. Uhl, S. U. Keimling, K. W. Klinkhammer, W. Schwarz, *Angew. Chem. Int. Ed. Engl.* **1997**, *36*, 64–65; f) M. Bühler, G. Linti, *Z. Anorg. Allg. Chem.* **2006**, *632*, 2453–2460; g) R. D. Schluter, A. H. Cowley, D. A. Atwood, R. A. Jones, J. L. Atwood, *J. Coord. Chem.* **2006**, *30*, 25–28; h) W. Uhl, A. Jantschak, W. Saak, M. Kaupp, R. Wartchow, *Organometallics* **1998**, *17*, 5009–5017; i) W. Uhl, R. Graupner, M. Layh, U. Schütz, *J. Organomet. Chem.* **1995**, *493*, C1-C5.

[62]   C. Dohmeier, C. Robl, M. Tacke, H. Schnöckel, *Angew. Chem. Int. Ed. Engl.* **1991**, *30*, 564–565.

[63]   A. Neu, T. Mennekes, P. Paetzold, U. Englert, M. Hofmann, P. von Ragué Schleyer, *Inorg. Chim. Acta* **1999**, *289*, 58–69.

[64]   a) C.-J. Maier, H. Pritzkow, W. Siebert, *Angew. Chem. Int. Ed.* **1999**, *38*, 1666–1668; b) C. Schnitter, H. W. Roesky, C. Röpken, R. Herbst-Irmer, H.-G. Schmidt, M. Noltemeyer, *Angew. Chem. Int. Ed.* **1998**, *37*, 1952-1955; c) M. Schiefer, N. D. Reddy, H. W. Roesky, D. Vidovic, *Organometallics* **2003**, *22*, 3637–3638; d) A. J. W. Uhl, *J. Organomet. Chem.* **1998**, *555*, 263–269.

[65]   N. Wiberg, T. Blank, K. Amelunxen, H. Nöth, H. Schnöckel, E. Baum, A. Purath, D. Fenkse, *Eur. J. Inorg. Chem.* **2002**, 341–350.

[66]   G. Linti, *J. Organomet. Chem.* **1996**, *520*, 107–113.

[67]   W. Uhl, W. Hiller, M. Layh, W. Schwarz, *Angew. Chem. Int. Ed. Engl.* **1992**, *31*, 1364–1366.

[68]   H. Sitzmann, M. F. Lappert, C. Dohmeier, C. Üffing, H. Schnöckel, *J. Organomet. Chem.* **1998**, *561*, 203–208.

[69]   a) D. Loos, E. Baum, A. Ecker, H. Schnöckel, A.J. Downs, *Angew. Chem. Int. Ed. Engl.* **1997**, *36*, 860–862; b) O. T. Beachley, R. Blom, M. R. Churchill, K. Faegri Jr., J. C. Fettinger, J. C. Pazik, L. Victoriano, *Organometallics* **1989**, *8*, 346–356.

[70]   A. Purath, R. Köppe, H. Schnöckel, *Angew. Chem. Int. Ed.* **1999**, *38*, 2926–2928.

[71]   A. Schnepf, R. Köppe, H. Schnöckel, *Angew. Chem. Int. Ed.* **2001**, *7*, 1241–1243.

[72] A. Haaland, K.-G. Martinsen, H. V. Volden, W. Kaim, E. Waldhör, W. Uhl, U. Schütz, *Organometallics* **1996**, *15*, 1146–1150.

[73] S. Nagase, *Acc. Chem. Res* **1995**, *28*.

[74] S. Nagase, *Angew. Chem. Int. Ed. Engl.* **1989**, *28*, 329–330.

[75] a) S. Nagase, K. Kobayashi, M. Nagashima, *J. Chem. Soc., Chem. Commun.* **1992**, 1302–1304; b) S. Nagase, M. Nakano, R. Kudo, *J. Chem. Soc., Chem. Commun.* **1987**, 60–62.

[76] G. Maier, *Angew. Chem. Int. Ed. Engl.* **1974**, *13*, 425–490.

[77] G. Maier, S. Pfriem, U. Schäfer, R. Matusch, *Angew. Chem. Int. Ed. Engl.* **1978**, *17*, 520–521.

[78] A. de Meijere, S. I. Kozhushkov, H. Schill, *Chemical reviews* **2006**, *106*, 4926–4996.

[79] F. Fleischer, G. Maier, *Tetrahedron Lett.* **1991**, *32*, 57–60.

[80] H. Irngartinger, A. Goldmann, R. Jahn, M. Nixdorf, H. Rodewald, G. Maier, K.-D. Malsch, R. Emrich, *Angew. Chem. Int. Ed. Engl.* **1984**, *23*, 993–994.

[81] T. Loerzer, R. Machinek, W. Lüttke, L. H. Franz, K.-D. Malsch, G. Maier, *Angew. Chem. Int. Ed. Engl.* **1983**, *11*, 878–879.

[82] N. K. V. Monteiro, J. F. de Oliveira, C. L. Firme, *New J. Chem.* **2014**, *38*, 5892–5904.

[83] G. Maier, R. Wolf, H.-O. Kalinowski, R. Boese, *Chem. Ber.* **1994**, *127*, 191–200.

[84] G. Maier, J. Neudert, O. Wolf, D. Pappusch, A. Sekiguchi, M. Tanaka, T. Matsuo, *J. Am. Chem. Soc.* **2002**, *124*, 13819–13826.

[85] A. Sekiguchi, M. Tanaka, *J. Am. Chem. Soc.* **2003**, *125*, 12684–12685.

[86] M. Tanaka, A. Sekiguchi, *Angew. Chem. Int. Ed.* **2005**, *44*, 5821–5823.

[87] M. Nakamoto, Y. Inagaki, M. Nishina, A. Sekiguchi, *J. Am. Chem. Soc.* **2009**, *131*, 3172–3173.

[88] T. Ochiai, M. Nakamoto, Y. Inagaki, A. Sekiguchi, *J. Am. Chem. Soc.* **2011**, *133*, 11504–11507.

[89] Y. Kobayashi, M. Nakamoto, Y. Inagaki, A. Sekiguchi, *Angew. Chem. Int. Ed.* **2013**, *52*, 10740–10744.

[90] Y. Kobayashi, M. Nakamoto, A. Sekiguchi, *Chem. Lett.* **2015**, *44*, 206–207.

[91] G. Rauscher, R. Clark, D. Poppinger, P. von Ragué Schleyer, *Angew. Chem. Int.* **1978**, *17*, 276–278.

[92] a) S. Y. Lee, B. H. Boo, H. K. Kang, D. Kang, K. Judai, J. Nishijo, N. Nishi, *Chem. Phys. Lett.* **2005**, *411*, 484–491; b) R. L. Disch, J. M. Schulman, J. P. Ritchie, *J. Am. Chem. Soc.* **1984**, *106*, 6246–6249.

[93] N. S. Zefirov, V. N. Kirin, N. M. Yur'eva, A. S. Koz'min, N. S. Kulikov, Y. N. Luzikov, *Tetrahedron Lett.* **1979**, *20*, 1925–1926.

[94]   a) G. Maier, M. Schneider, G. Kreiling, W. Mayer, *Chem. Ber.* **1981**, *114*, 3922–3934; b) G. Maier, W. Mayer, H.-A. Freitag, H. P. Reisenauer, R. Askani, *Chem. Ber.* **1981**, *114*, 3935–3958; c) G. Maier, H. P. Reisenauer, *Chem. Ber.* **1981**, *114*, 3859–3964.

[95]   N. Wiberg, C. M. M. Finger, K. Polborn, *Angew. Chem. Int. Ed. Engl.* **1993**, *32*, 1054–1056.

[96]   F. Meyer-Wegner, S. Scholz, I. Sänger, F. Schödel, M. Bolte, M. Wagner, H.-W. Lerner, *Organometallics* **2009**, *28*, 6835–6837.

[97]   A. Sekiguchi, H. Sakurai in *Advances in Organometallic Chemistry*, Elsevier, **1995**.

[98]   M. Ichinohe, M. Toyoshima, R. Kinjo, A. Sekiguchi, *J. Am. Chem. Soc.* **2003**, *125*, 13328–13329.

[99]   T. M. Klapötke, S. K. Vasisht, G. Fischer, P. Mayer, *J. Organomet. Chem.* **2010**, *695*, 667–672.

[100]   N. Wiberg, H. Auer, H. Nöth, J. Knizek, K. Polborn, *Angew. Chem. Int. Ed.* **1998**, *37*, 2869–2872.

[101]   N. Wiberg, H. Auer, S. Wagner, K. Polborn, G. Kramer, *J. Organomet. Chem.* **2001**, *619*, 110–131.

[102]   N. Wiberg, W. Hochmuth, H. Nöth, A. Appel, M. Schmidt-Amelunxen, *Angew. Chem. Int. Ed. Engl.* **1996**, *12*, 1333–1334.

[103]   M. Weidenbruch, F.-T. Grimm, M. Herrndorf, A. Schäfer, *J. Organomet. Chem.* **1988**, *341*, 335–343.

[104]   L. R. Sita, I. Kinoshita, *Organometallics* **1990**, *9*, 2865–2867.

[105]   Z. Rappoport (Editor), The Chemistry of Organic Germanium, Tin and Lead Compounds, Volume 2, John Wiley & Sons, pp. 935, **2002**.

[106]   H.-G. Von Schnering, W. Hönle, *Chem. Rev.* **1988**, *88*, 243–273.

[107]   P. Jerabek, G. Frenking, *Theor. Chem. Acc.* **2014**, *133*, 2317.

[108]   J. P. Zheng, J. Waluk, J. Spanget-Larsen, D. M. Blake, J. G. Radziszewski, *Chem. Phys. Lett.* **2000**, *329*, 227–233.

[109]   a) F. Cacace, G. de Petris, A. Troiani, *Science* **2002**, *295*, 480–481; b) E. E. Rennie, P. M. Mayer, *J. Chem. Phys.* **2004**, *120*, 10561–10578.

[110]   D. E. C. Corbridge, *Phosphorus 2000. Chemistry, Biochemistry and Technology*, (Elvesier, 2000).

[111]   O. Ganter, W. Schipper, J. J. Weigand, *Springer* **2014**, 237–242.

[112]   A. F. Holleman, E. Wiberg, N. Wiberg, Anorganische Chemie, Band 1 Grundlagen und Hauptgruppenelemente, de Gruyter, Berlin, **2017**.

[113]   a) B. M. Cossairt, N. A. Piro, C. C. Cummins, *Chem. Rev.* **2010**, *110*, 4164–4177; b) M. Caporali, L. Gonsalvi, A. Rossin, M. Peruzzini, *Chem. Rev.* **2010**, *110*, 4178–4235; c) B. M. Cossairt, C. C. Cummins, *New J. Chem.* **2010**, *34*, 1533; d) U. Lennert, P. B. Arockiam,

V. Streitferdt, D. J. Scott, C. Rödl, R. M. Gschwind, R. Wolf, *Nat. Catal.* **2019**, *2*, 1101–1106.

[114] M. Seidl, G. Balázs, M. Scheer, *Chem. Rev.* **2019**, *119*, 8406–8434.

[115] B. M. Cossairt, C. C. Cummins, A. R. Head, D. L. Lichtenberger, R. J. F. Berger, S. A. Hayes, N. W. Mitzel, G. Wu, *J. Am. Chem. Soc.* **2010**, *132*, 8459–8465.

[116] A. Simon, *J. Alloys Compd.* **1995**, *229*, 158–174.

[117] a) D. E. C. Corbridge, E. J. Lowe, *Nature* **1952**, *170*, 629; b) G. Natta, L. Passerini, *Nature* **1930**, *125*, 707–708.

[118] A. Simon, H. Borrmann, H. Craubner, *Phosphorus, Sulfur Relat. Elem.* **1987**, *30*, 507–510.

[119] A. Bettendorff, *Justus Liebigs Ann. Chem.* **1867**, *144*, 110–114.

[120] a) O. J. Scherer, H. Sitzmann, G. Wolmershäuser, *J. Organomet. Chem.* **1986**, *309*, 77–86; b) H. A. Spinney, N. A. Piro, C. C. Cummins, *J. Am. Chem. Soc.* **2009**, *131*, 16233–16243.

[121] A. E. Seitz, F. Hippauf, W. Kremer, S. Kaskel, M. Scheer, *Nat. Commun.* **2018**, *9*, 361.

[122] a) Andreas J. Kornath, Alexander Kaufmann, Sebastian Cappellacci, *J. Mol. Spectrosc.* **2009**, *255*, 189–193; b) T. M. Bernhardt, B. Stegemann, B. Kaiser, K. Rademann, *Angew. Chem. Int. Ed.* **2003**, *42*, 199–202.

[123] a) V. E. Bondybey, J. H. English, *J. Chem. Phys.* **1980**, *73*, 42–48; b) M. E. Geusic, R. R. Freeman, M. A. Duncan, *J. Chem. Phys.* **1988**, *88*, 163–166.

[124] G. A. Ozin, *J. Chem. Soc. A* **1970**, 2307–2310.

[125] B. M. Cossairt, M.-C. Diawara, C. C. Cummins, *Science* **2009**, *323*, 602.

[126] a) B. M. Cossairt, M.-C. Diawara, C. C. Cummins, *Science* **2009**, *323*, 602; b) B. M. Cossairt, C. C. Cummins, *J. Am. Chem. Soc.* **2009**, *131*, 15501–15511.

[127] M.-L. Y. Riu, R. L. Jones, W. J. Transue, P. Müller, C. C. Cummins, *Sci. Adv.* **2020**, *6*, eaaz3168.

[128] O. Reinmuth, *J. Chem. Educ.* **1928**, *5*, 1473.

[129] G. Maier, *Angew. Chem. Int. Ed. Engl.* **1988**, *27*, 309–332.

2 Release of P₂ Units from a Ni₂P₂ Butterfly Complex[a]

Abstract:

The mild generation of diphosphorus molecules P$_2$ in solution is a convenient strategy to generate diphosphine *via* [4+2] cycloadditions. We recently described the formation of P$_4$ from the nickel butterfly complex [{(IMes)Ni(CO)}$_2$(μ^2,η^2:η^2-P$_2$)] upon addition of CO (g). Herein, we developed an alternative protocol for the release of P$_2$ units from the same nickel complex using heterocumulenes. The nickel-containing by-products possess novel pincer-type ligands. Aryl isothiocyanates undergo a trimerisation within the coordination sphere of nickel and afford square planar nickel complexes with S-C-S pincer-ligand frameworks. Carbon disulfide coordinates to the [(IMes)Ni]-fragment in an η^2-fashion, affording a dinuclear complex.
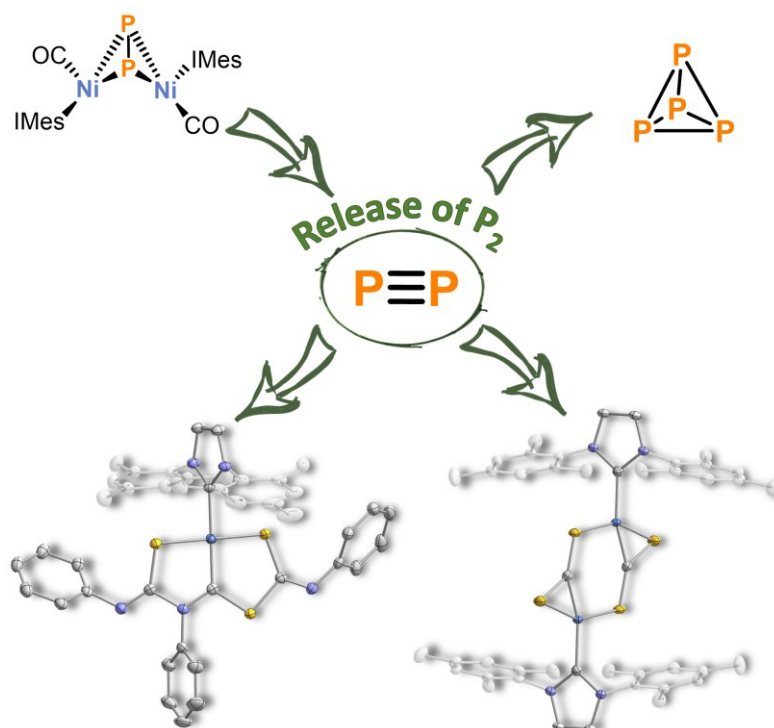
2.1 Introduction

The low tendency of the heavier members of the p-block elements to form multiple bonds is known as the double bond rule.[1] In the last decades, however, main group chemists have shown that this rule can be overcome, e.g. by introduction of bulky substituents. A noteworthy example for this kinetic stabilisation is the isolation of a disilyne by Sekiguchi and co-workers.[2] For group 15 elements, the formation and detection of the P_2 molecule showing a P≡P triple bond has been investigated intensively. Upon heating white phosphorus to over 1000 K, dissociation into diphosphorus occurs.[3,4] However, the conditions of this gas-phase reaction render further reactions with P_2 difficult. Therefore, several compounds which generate P_2 under milder conditions in solution have been developed (Figure 1).

The group of Cummins showed that the niobium complex **A** transfers a P_2 unit to cyclohexadiene in a Diels-Alder reaction to afford the diphosphine **B**.[5] The molecular structure was confirmed by single crystal X-ray crystallography of a tungsten pentacarbonyl adduct of **B**.
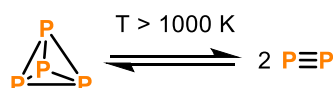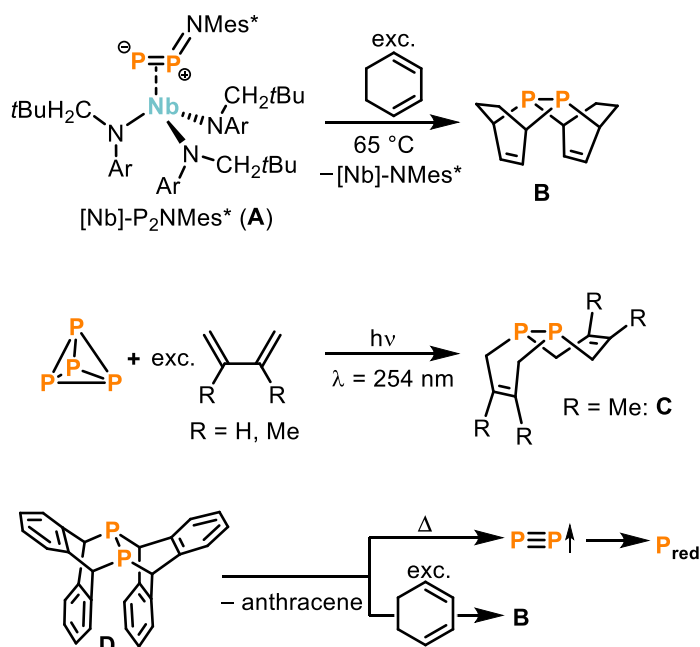
Figure 1. Examples of compounds capable of P_2 transfer; Mes* = 2,4,6-tri-*tert*-butylphenyl.[3–7]

A similar [4+2]-cycloaddition was achieved by photolysis directly from P_4 in the presence of butadiene or dimethylbutadiene affording the diphosphines **B** and **C**.[6,8] Moreover, Cummins and co-workers showed that the diphosphanorbornadiene compound **D** efficiently transfers P_2 to butadienes. Under mild thermal activation, **D** releases P_2 which could be detected by molecular

beam mass spectrometry and ultimately transforms to red phosphorus.[7] Recently, the group of Ghadwal showed that P$_2$ units are also released upon reaction of a phosphorus analogue of *p*-quinodimethane [(IPr=C)$_2$P$_4$] (IPr = 1,3-bis(2,6-di-*iso*-propylphenyl)imidazolin-2-ylidene) containing a planar P$_4$ ring with cyclohexadiene.[9] However, this reaction was not selective, affording both P$_4$ and the cycloaddition product **B**.

In 2018, our group showed that the release of P$_2$ units is also viable using the dinuclear nickel butterfly complex [{(IMes)Ni(CO)}$_2$(μ^2,η^2:η^2-P$_2$)] (Figure 2, IMes = 1,3-bis(2,4,6-trimethylphenyl)imidazolin-2-ylidene) upon addition of carbon monoxide. In the presence of 2,3-dimethylbutadiene (dmb), the formation of the diphosphine **C** was observed. In the absence of other reagents, however, the formation of P$_4$ was observed. The dimerisation of P$_2$-type units presumably takes place through a nickel-coordinated equivalent, since the dimerisation of free P$_2$ to P$_4$ is symmetry forbidden and therefore cannot take place under mild conditions.[3,10]
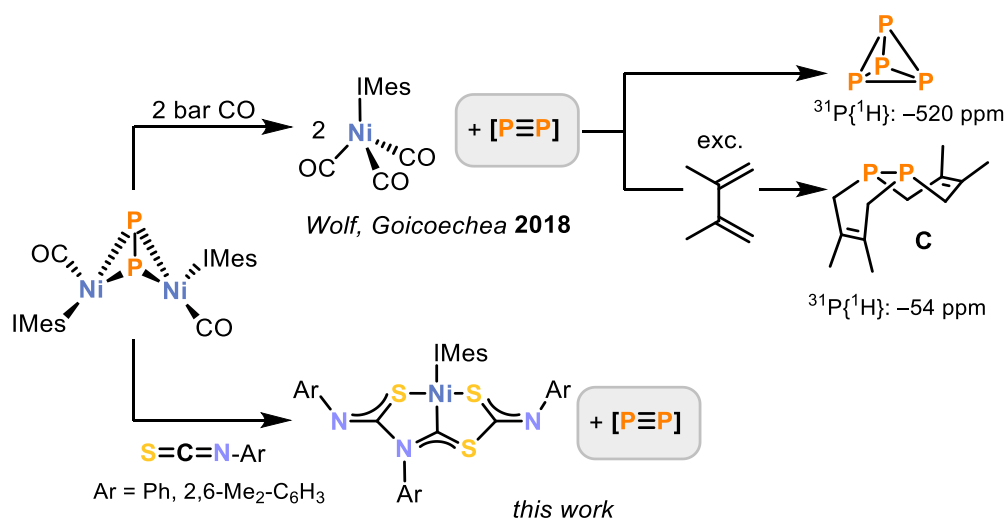
Figure 2. P$_4$ release via P$_2$-type intermediates from a nickel butterfly complex.[11]

Nevertheless, the use of CO gas comprises a significant drawback of this method due to its toxicity and the need for complicated handling. Therefore, finding alternatives for carbon monoxide for the release of P$_2$ from [{(IMes)Ni(CO)}$_2$(μ^2,η^2:η^2-P$_2$)] would be advantageous. Herein, we describe our efforts to use more convenient 2-electron donor ligands and heterocumulenes for the generation of diphosphorus and white phosphorus from [{(IMes)Ni(CO)}$_2$(μ^2,η^2:η^2-P$_2$)].

2.2   Results and Discussion

This study commenced with reactions of isonitriles with [{(IMes)Ni(CO)}$_2$(μ^2,η^2:η^2-P$_2$)]. Isonitriles were chosen because they are isoelectronic to carbon monoxide and often show similar reactivity. As such, the reaction of Cy-N≡C with [{(IMes)Ni(CO)}$_2$(μ^2,η^2:η^2-P$_2$)] afforded an intractable reaction mixture displaying multiple signals in the ^{31}P{^{1}H} NMR spectrum. We therefore turned our attention towards other two-electron donor ligands such as carbenes. Addition of excess amounts (8 eq.) of the carbene TMC (TMC = 2,3,4,5-tetramethylimidazolin-2-ylidene, Figure 3) to an orange solution of [{(IMes)Ni(CO)}$_2$(μ^2,η^2:η^2-P$_2$)] in C$_6$D$_6$ resulted in a colour change to dark red. Analysis of the reaction mixture by ^{31}P{^{1}H} NMR spectroscopy revealed complete consumption of the starting material [{(IMes)Ni(CO)}$_2$(μ^2,η^2:η^2-P$_2$)] and formation of a single species characterised by a singlet resonance at 34.7 ppm. Notably, no P$_4$ was detected in the spectrum. Slow diffusion of *n*-hexane into the C$_6$H$_6$ solution afforded orange needles suitable for single crystal X-Ray diffraction (SCXRD), which revealed the formation of the dinuclear complex [{(TMC)$_2$Ni}$_2$(μ^2,η^2:η^2-P$_2$)] (**1**, Figure 3a).
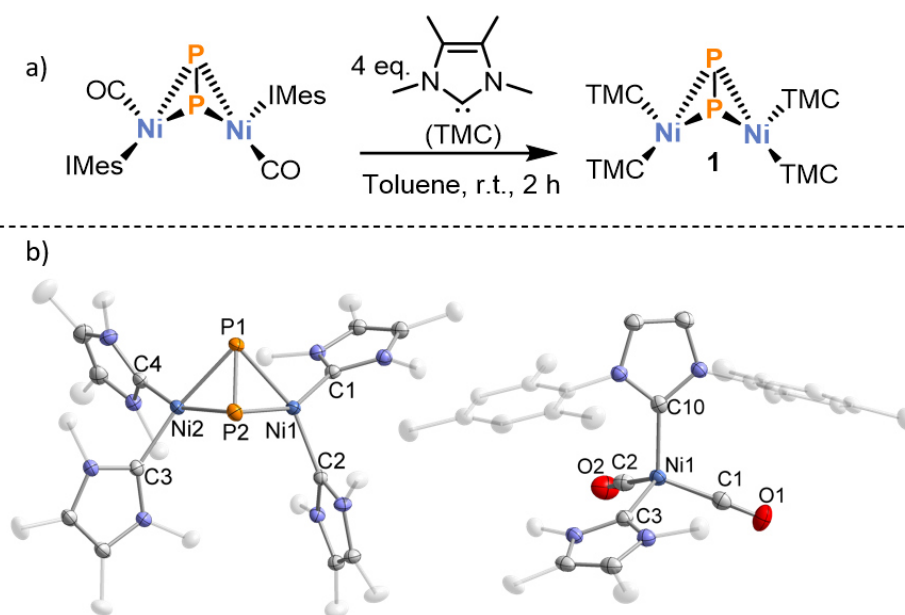
Figure 3. Synthesis of **1** (a) and molecular structures of **1** and **2** in the solid state (b). Thermal ellipsoids are set at the 50% probability level. Hydrogen atoms and solvent molecules (in case of **1**) are omitted for clarity. For **2**, 4 molecules with similar bond metric data are present in the asymmetric unit; the data for only one molecule are given below. Selected bond lengths [Å] and angles [°] for **1**: Ni1···Ni2 2.9712(4), P1−P2 2.0949(6), Ni1−P1 2.2419(5), Ni1−P2 2.2660(5), Ni1−C1 1.9135(16), Ni1−C2 1.9173(16), Ni2−P1 2.2640(5), Ni2−P2 2.2317(5), Ni2−C3 1.9113(17), Ni2−C4 1.8999(18), P1−Ni1−P2 55.382(17), P2−Ni2−P1 55.542(17), C1−Ni1−C2 106.52(7), C4−Ni2−C3 100.95(7), P2−P1−Ni2 61.447(17), P2−P1−Ni1 62.893(18), P1−P2−Ni2 63.011(18), Ni1−P1−Ni2 82.506(16), Ni2−P2−Ni1 82.687(17), Ni1/P1/P2 to Ni2/P1/P2 plane to plane fold angle 83.5(2); selected bond lengths [Å] and angles [°] for **4**: Ni1−C1 1.7644(15), Ni1−C2 1.7679(15), Ni1−C3 1.9825(14), Ni1−C10 1.9656(14), O1−C1 1.1530(18), O2−C2 1.1528(18), C10−Ni1−C3 108.08(6), C1−Ni1−C10 109.88(6), C1−Ni1−C3 107.49(6), C1−Ni1−C2 110.36(7), C2−Ni1−C10 109.08(6), C2−Ni1−C3 111.91(6).

Unexpectedly, **1** forms through ligand exchange of the carbonyl and IMes-ligands, retaining the Ni$_2$P$_2$ butterfly core. The P−P bond length of 2.0949(6) Å compares well to the bond length in the starting material (2.076(2) Å).[11] Moreover, the Ni−C and Ni−P bond lengths (1.8999(18) to 1.9173(16) Å and 2.2317(5) to 2.2660(5) Å, respectively) are in a comparable range to those observed for [{(IMes)(CO)Ni}$_2$(μ^2,η^2:η^2-P$_2$)]. **1** was isolated in a yield of 31% as a bright orange powder. The low yield is attributed to the presence of several other species in the ^{1}H NMR spectrum. One of these compounds was identified as the new NHC carbonyl complex [(IMes)(TMC)Ni(CO)$_2$] (**2**, Figure 3b) by SCXRD.

The ^{1}H NMR spectrum of **1** shows two signals at 1.97 and 3.58 ppm corresponding to the methyl groups of the carbene ligand. In the ^{31}P{^{1}H} NMR spectrum a singlet resonance at 34.7 ppm (*vide supra*) is observed. This resonance is in a comparable region as the related complex [{(*i*PrIm^{Me})$_2$Ni}$_2$(μ^2,η^2:η^2-P$_2$)] [*i*PrIm^{Me} = 1,3-di-*iso*-propyl-4,5-dimethylimidazolin-2-ylidene, δ (^{31}P{^{1}H}) = 70.7 ppm].[12] The UV/Vis spectrum of **1** shows a broad band at 320 nm tailing into the green region of the spectrum (ca. 500 nm), which accounts for its orange colour.

We next assessed the reactivity of [{(IMes)Ni(CO)}$_2$(μ^2,η^2:η^2-P$_2$)] toward heterocumulenes. While di-*iso*-propylcarbodiimide does not react with [{(IMes)Ni(CO)}$_2$(μ^2,η^2:η^2-P$_2$)] even at elevated temperatures, phenyl isothiocyanate and 2,6-dimethylphenyl isothiocyanate readily react to form a purple solution and P$_4$ as assayed by ^{31}P{^{1}H} NMR spectroscopy. Structural characterisation of deep purple crystals obtained from toluene revealed the formation of the mononuclear complexes [(IMes)Ni(η^3-(PhNCS)$_3$)] (**3a**) and [(IMes)Ni(η^3-(2,6-Me$_2$-C$_6$H$_3$-NCS)$_3$)] (**3b**) as by-products. Complexes **3a** and **3b** contain a pincer-type ligand formed through trimerisation of three PhNCS molecules in the coordination sphere of nickel. These complexes can also be synthesised by reacting the vinyltrimethylsilane (vtms) nickel(0) complex [(IMes)Ni(vtms)$_2$] with PhNCS or 2,6-Me$_2$-C$_6$H$_3$NCS in 44% or 77% yield, respectively.

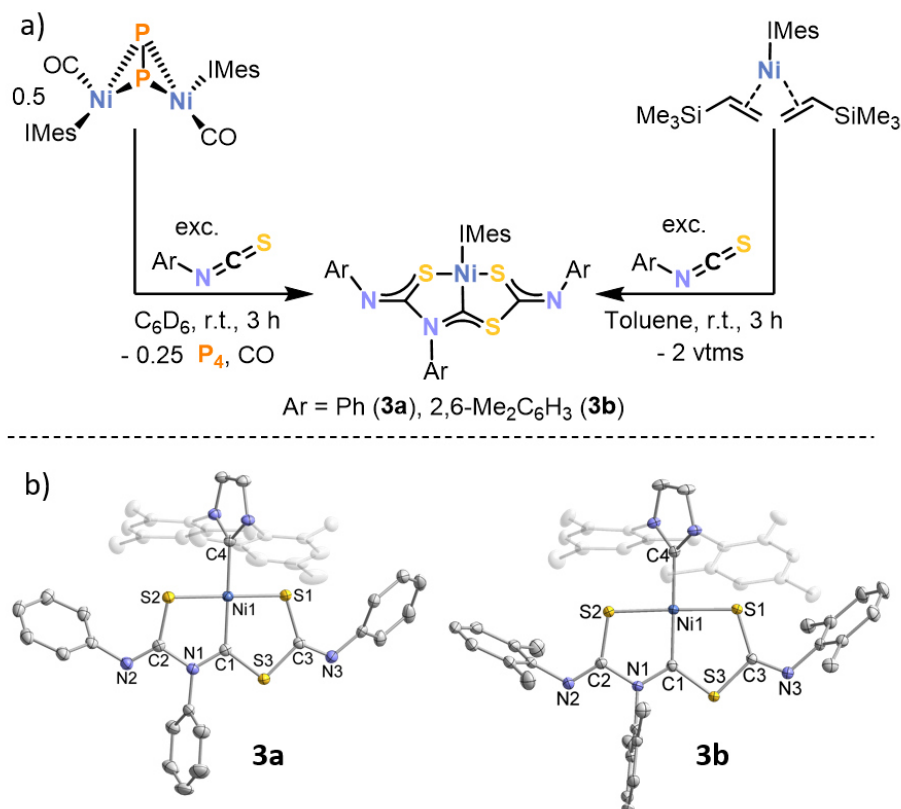**Figure 4.** Synthesis (a) and molecular structures (b) of **3a** and **3b**. Thermal ellipsoids are set at the 50% probability level. Hydrogen atoms are omitted for clarity. Selected bond lengths [Å] and angles [°] for **3a**: Ni1−C1 1.8723(15), Ni1−C4 1.9353(15), Ni1−S1 2.1309(5), Ni1−S2 2.1414(4), S3−C1 1.7337(15), N1−C1 1.337(2), N1−C2 1.447(2), S2−C2 1.7347(15), N2−C2 1.269(2), S3−C3 1.7892(15), S1−C3 1.7361(15), N3−C3 1.276(2), S1−Ni1−S2 175.76(2), C4−Ni1−S2 91.76(5), C4−Ni1−S1 88.71(5), C1−Ni1−S2 87.40(5), C1−Ni1−S1 92.24(5), C1−Ni1−C4 178.26(6), S3−C1−Ni1 124.21(9), N1−C1−Ni1 121.35(11), N1−C1−S3 114.44(11), NHC to Ni/S/C/N plane to plane twist angle 73.0(2). C2/N1/C1/Ni1/S2 to C1/S3/C3/S1/Ni1 plane to plane twist angle 3.13(2); for **3b**: Ni1−C1 1.8716(13), Ni1−C4 1.9363(13), Ni1−S1 2.1392(4), Ni1−S2 2.1679(4), S3−C1 1.7268(13), N1−C1 1.3356(16), N1−C2 1.4384(16), S2−C2 1.7335(13), N2−C2 1.2726(17), S3−C3 1.7840(13), S1−C3 1.7296(13), N3−C3 1.2772(17), S1−Ni1−S2 177.162(16), C4−Ni1−S2 92.09(4), C4−Ni1−S1 89.79(4), C1−Ni1−S2 86.83(4), C1−Ni1−S1 91.51(4), C1−Ni1−C4 174.17(5), S3−C1−Ni1 124.94(7), N1−C1−Ni1 121.65(9), N1−C1−S3 113.29(9), NHC to Ni/S/C/N plane to plane twist angle 57.2(1). C2/N1/C1/Ni1/S2 to C1/S3/C3/S1/Ni1 plane to plane twist angle 2.85(2)

The molecular structures of **3a** and **3b** in the solid state confirm the η³-coordination of the LX₂-type (PhNCS)₃ ligand via two sulfur atoms and one carbon atom. The coordination environment around the central nickel atom is almost planar (sum of angles 360.1(2)° for **3a** and 360.2(4)° for **3b**). The two planar pentagons C2/N1/C1/Ni1/S2 and C1/S3/C3/S1/Ni1 are almost coplanar with a plane to plane twist angle of 3.13(2)° for **3a** and 2.85(2)° for **3b**, whereas the imidazole rings of the NHC are significantly displaced with respect to the planar (PhNCS)₃ scaffold with a plane to plane twist angle of 73.0(2)° for **3a** and 57.2(1)° for **3b**. The Ni1−C1 bond lengths of 1.8723(15) Å (**3a**) and 1.8716(13) Å (**3b**) are shorter than the Ni1−C4 bond lengths (1.9353(15) Å (**3a**) and 1.9363(13) Å (**3b**)), which can be attributed to a stronger double bond character of the C1-nickel bond. NMR spectra of complexes **3a** and **3b** were recorded at 0 °C due to slow

decomposition in solution at room temperature. The ^{1}H NMR spectra are in good agreement with the molecular structures determined by SCXRD. Three signals were observed for the methyl-groups of the IMes ligand, which indicates a hindered rotation around the N−C(Mes) bonds. Additional signals in the aromatic region (**3a** and **3b**) and the aliphatic region (**3b**) arise from the aryl residues of the former isothiocyanates. In the ^{13}C{^{1}H} NMR spectrum the two carbene resonances of C4 and C1 were detected at 173.5 and 238.8 ppm (**3a**) and 179.2 and 239.1 ppm (**3b**), respectively, and identified by ^{1}H-^{13}C-HMBC. The UV/Vis spectra feature absorption bands at 580 nm (**3a**) and 560 nm (**3b**), which account for the purple colours in solution.

It is worth noting that the reaction of cyclohexyl isothiocyanate CyNCS with [(IMes)Ni(vtms)₂] afforded a different product (**4**, Scheme 1). In this case, dimerisation of the isothiocyanate on the nickel occurs to form [(IMes)Ni(η³-(Cy-NCS)₂)] (**4**). A similar product was obtained in a recent study when [(IPr)Ni(styrene)₂] (IPr = 1,3-bis(2,6-di-*iso*-propylphenyl)imidazolin-2-ylidene) was used instead of [(IMes)Ni(vtms)₂] (see the Experimental Section for preparation and characterisation data of **4**).[13]
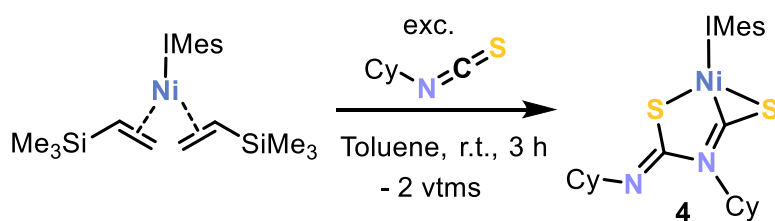
Scheme 1. Synthesis of [(IMes)Ni(η³-(Cy-NCS)₂)] (**4**).

In order to gain further information about the electronic structure density functional theory (DFT) calculations were performed on the smaller example **3a**. The optimised structure (BP86/def2-TZVP level of theory) compares well with the experimental data. The HOMO of **3a** is mainly located at the two sulfur atoms coordinating to the Ni atom and the Ni atom itself (Figure 5 top). The LUMO is mostly located at the C1 atom with contributions from the adjacent nitrogen and carbon atoms. Inspection of the Mayer bond orders reveals a significant delocalisation of electrons along the N1−C1−S3 motif, as anticipated for a Fischer-type carbene (Figure 5 bottom). Moreover, the N2−C2−S2 and N3−C3−S1 moieties can be considered as delocalised heteroallylic systems. This is also in agreement with the positive Löwdin atomic charges on the N2 and N3 atoms with values of 0.17 and 0.13, respectively.
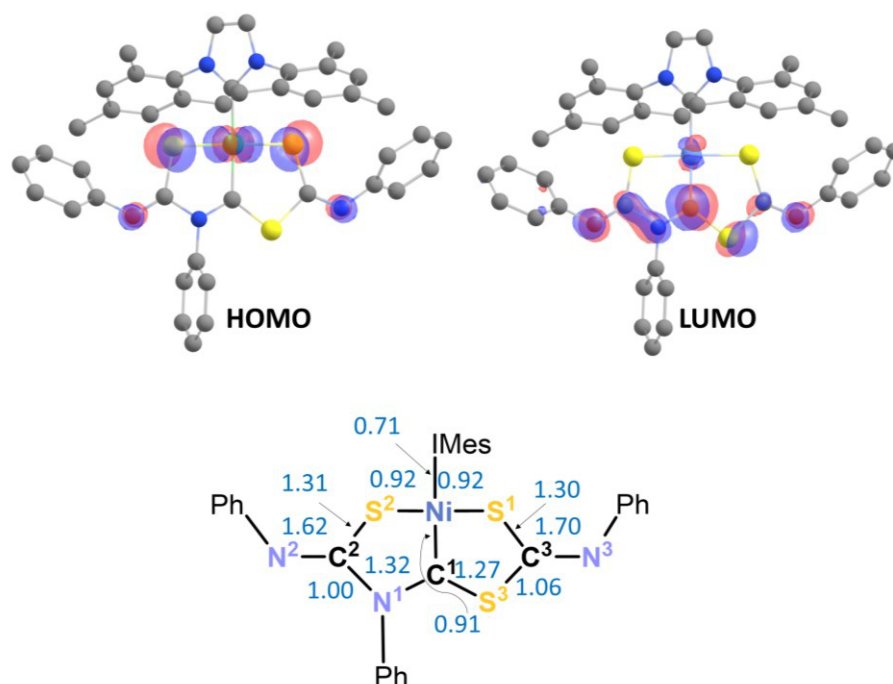
Figure 5. HOMO and LUMO orbitals of **3a** (isosurface value 0.05) (top) and Mayer bond orders in **3a** (bottom).

Notably, several reactions of organic isothiocyanates with transition metals have been reported to date, with some of them resulting in insertions or oligomerisation reactions on the metal centre.[13,14] Only one system with a comparable ligand to the (PhNCS)₃ scaffold in **3a/b** was described in the literature (Figure 6 left).[15] This complex contains rhodium in a similar coordination environment with two PPh₃ and an additional chloride ligand and an S-C-S pincer-type ligand obtained from ethoxycarbonyl isothiocyanate. However, in this case, a 1,3-shift of one of the substituents was observed, leading to an unsubstituted N1-atom. A different P-C-S-type pincer system was reported recently by Gessner and co-workers.[16] This complex contains a PMe₃ ligand instead of the N-heterocyclic carbene in **3a/b** and a P-C-S-pincer ligand.
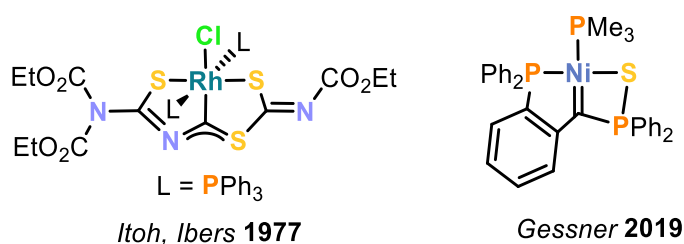
Figure 6. P-C-S- and S-C-S-type pincer ligands similar to those in **5** described in literature.

The reaction of [{(IMes)Ni(CO)}₂(μ²,η²:η²-P₂)] with isothiocyanates in the presence of 2,3-dimethylbutadiene did not afford the diphosphine **C**, which was the major product when CO gas was used. Instead, the formation of several doublet resonances was observed (see Figure S 12). Even though these signals hint towards the formation of nickel complexes of **C**, the isolation of cycloaddition products from [{(IMes)Ni(CO)}₂(μ²,η²:η²-P₂)] remains elusive.

Inspection of the coordination of the S-C-S pincer ligand in **3a/b** suggests that the nitrogen atoms in ArNCS play a minor role in the coordination behaviour. Therefore, it was hypothesised that isoelectronic carbon disulfide, CS_2, might undergo a similar reaction with $[\{(\text{IMes})\text{Ni(CO)}\}_2(\mu^2,\eta^2:\eta^2\text{-}P_2)]$ or $[(\text{IMes})\text{Ni(vtms)}_2]$. Indeed, addition of a CS_2 solution in THF to solutions of either of the complexes in benzene afforded a colour change from orange to red and precipitation of a red powder. ^{1}H NMR spectra of the red solid in THF-d_8 confirm the presence of one distinct IMes signal set, whereas the ^{31}P$\{^1$H$\}$ NMR spectrum reveals formation of P_4 when $[\{(\text{IMes})\text{Ni(CO)}\}_2(\mu^2,\eta^2:\eta^2\text{-}P_2)]$ is used as Ni-precursor. Single crystals suitable for SCXRD analysis grown from fluorobenzene reveal the formation of the dinuclear complex $[\{(\text{IMes})\text{Ni}(\mu^2,\eta^1:\eta^2\text{-}CS_2)\}_2]$ (**5**, Figure 7), which was isolated in good yields of 88% starting from $[\{(\text{IMes})\text{Ni(CO)}\}_2(\mu^2,\eta^2:\eta^2\text{-}P_2)]$.
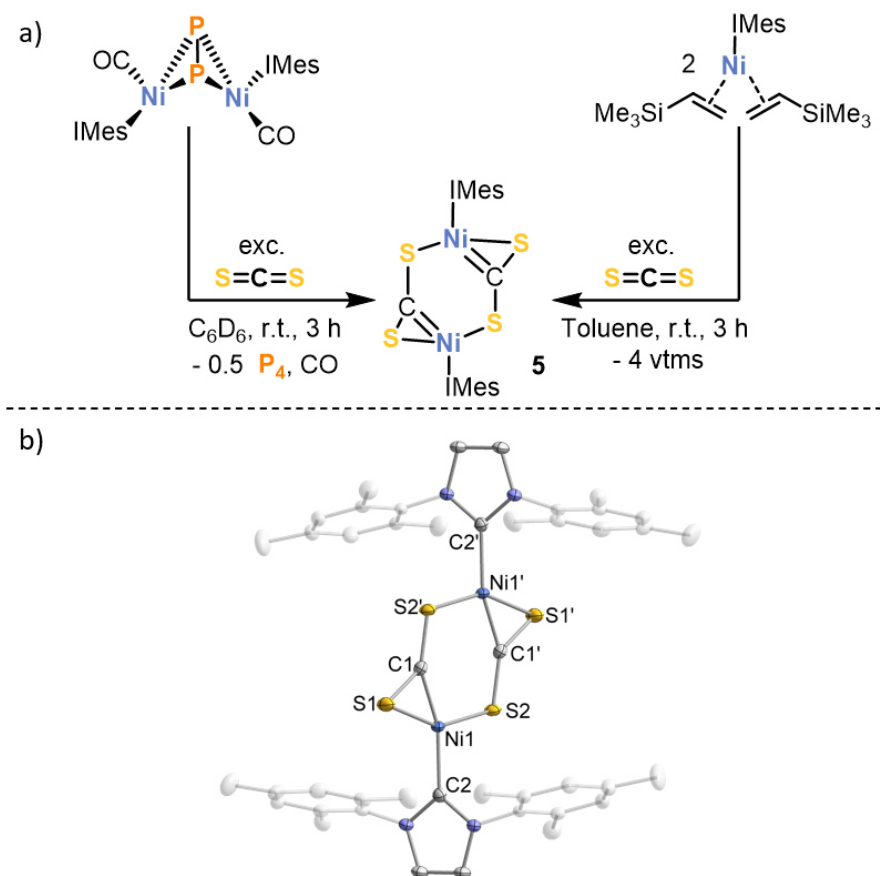
Figure 7. Synthesis (a) and molecular structure (b) of **5**. Thermal ellipsoids are set at the 50% probability level. Hydrogen atoms and solvent molecules are omitted for clarity. Selected bond lengths [Å] and angles [°]: Ni1−S1 2.1812(6), Ni1−S2 2.1589(5), Ni1−C1 1.8134(18), Ni1−C2 1.9379(18), S1−C1 1.6646(19), S2−C1' 1.6624(18), S2−Ni1−S1 150.82(2), C1−Ni1−S1 48.18(6), C1−S1−Ni1 54.27(6), S1−C1−Ni1, C1−S2−Ni1 110.07(7), C1−Ni1−S2 102.66(6), S2−C1−Ni1 147.25(12), C2−Ni1−S2 97.96(5), C2−Ni1−S1 111.20(5), NHC to Ni/S/C plane to plane twist angle 70.5(2).

It is important to note that a handful of compounds with structures closely related to **5** have been reported in the literature as deep red to purple solids. These compounds were also obtained from

the reactions of nickel(0) complexes with CS_2 and feature additional N-heterocyclic carbene or phosphine ligands.[17,18]

The structure of **5** shows two sulfur atoms and a carbene-like carbon coordinating to the nickel atoms. In contrast to **3a/b**, however, the complex is dinuclear and the CS_2-moieties are not directly connected, as was the case for the trimerised $(PhNCS)_3$ unit in **3a/b**. The coordination around the nickel atom is planar (sum of angles 360.0(22)°). Each CS_2 moiety in **5** is η^2-bonded via a C=S bond to one nickel atom and σ-bonded to the other nickel atom via the other sulfur atom. The C1−Ni1 bond of 1.8134(18) Å is shorter than the C2−Ni1 bond (1.9379(18) Å) and both of them compare well to the bond metric data of $[\{(tBu_2Im)Ni(\mu^2,\eta^1{:}\eta^2{-}CS_2)\}_2]$ (tBu_2Im = 1,3-di-*tert*-butylimidazolin-2-ylidene; C1−Ni1: 1.810(2) Å, C2−Ni1 1.968(2) Å).[18] A similar difference in bond lengths was observed for **3a/b** (*vide supra*), however, in case of **5** the difference in the C−Ni bond lengths is larger due to the small NiSC-ring.

The ^1H NMR spectrum of **5** is in line with the molecular structure determined by SCXRD with a total of four singlet signals as expected for a C_{2v}-symmetric IMes ligand. The $^{13}C\{^1H\}$ NMR spectrum shows a strongly low-field-shifted carbene resonance for C1 at 285.6 ppm, which was assigned by ^1H-^{13}C-HMBC NMR spectroscopy. This shift is in good agreement with the related resonance of $[\{(tBu_2Im)Ni(\mu^2,\eta^1{:}\eta^2{-}CS_2)\}_2]$ at 283.5 ppm.[18] The signal of the NHC-carbene atom (C2) is observed at 189.2 ppm, which is in a similar range as the shifts observed for **3a/b** [173.5 (**3a**) and 173.4 (**3b**)]. The UV/Vis absorption spectrum of **7** reveals an absorption band at 550 nm, which accounts for its red colour in solution.

It is noteworthy that the reaction of $[\{(IMes)Ni(CO)\}_2(\mu^2,\eta^2{:}\eta^2{-}P_2)]$ with CS_2 in the presence of excess amounts of 2,3-dimethylbutadiene also does not afford the diphosphine **C** (see Figure S13).

2.3 Conclusion

Reactions of suitable two-electron donors with the Ni_2P_2 complex $[\{(IMes)Ni(CO)\}_2(\mu^2,\eta^2{:}\eta^2{-}P_2)]$ were investigated in order to study the release of P_2 units. While addition of tetramethylcarbene (TMC) to $[\{(IMes)Ni(CO)\}_2(\mu^2,\eta^2{:}\eta^2{-}P_2)]$ only resulted in a ligand exchange reaction to form the symmetric complex **1**, heterocumulenes replaced the P_2 ligand effectively to afford P_4. Unfortunately, the formation of the diphosphine **C** was not observed when heterocumulenes such as PhNCS were employed. While the reasons for this reactivity are currently unclear, it is tempting to speculate that the cycloaddition products coordinate to nickel fragments to form several unidentified complexes. Furthermore, it is possible that the P_2 type fragments undergo unselective reactions with heterocumulenes themselves. Nevertheless, this work demonstrates that the P_2 ligand in $[\{(IMes)Ni(CO)\}_2(\mu^2,\eta^2{:}\eta^2{-}P_2)]$ is highly labile and thus provides access to new nickel(0) complexes. The molecular structures of the new complexes **3a/b** and **5** obtained in this manner contain S-C-S pincer-type carbene ligands with planar coordination geometries around the nickel atom and an NHC ancillary ligand. Aryl-substituted isocyanates

ArNCS undergo a trimerisation within the coordination sphere of nickel to form unusual (ArNCS)$_3$ scaffolds observed in the structures of **3a/b**, while CS_2 coordinates in an η^2-fashion and forms a dinuclear complex. The simple preparation of the nickel complexes **3a/b** and **5** together with their pincer-type ligands could make them interesting complexes for catalytic applications.

2.4 Experimental Details

General Synthetic Methods

All reactions and product manipulations were carried out in flame-dried glassware under an inert atmosphere of argon using standard Schlenk-line or glovebox techniques (maintained at <0.1 ppm H_2O and <0.1 ppm O_2). Tetramethylcarbene (TMC)[19], [{(IMes)Ni(CO)}$_2(\mu^2,\eta^2:\eta^2$-P$_2$)] (**1**)[11] and [(IMes)Ni(vtms)$_2$]][20] were prepared according to procedures previously reported in the chemical literature. All other chemicals were purchased from commercial suppliers and used without further purification.

Solvents were dried and degassed with a MBraun SPS800 solvent purification system. Fluorobenzene was dried over sodium and distilled. All dry solvents except *n*-hexane and *n*-pentane were stored under argon over activated 3 Å molecular sieves in gas-tight ampules. *n*-Hexane and *n*-pentane were stored over potassium mirrors.

General Analytical Techniques

NMR spectra were recorded on Bruker Avance 300 or 400 spectrometers at 300 K unless otherwise noted and internally referenced to residual solvent resonances (^{1}H NMR: THF-d$_8$: 1.72 ppm, C$_6$D$_6$: 7.16 ppm, toluene-d$_8$: 2.08 ppm; ^{13}C{^{1}H} NMR: THF-d$_8$: 25.31 ppm, C$_6$D$_6$: 128.06 ppm). Chemical shifts δ are given in ppm referring to external standards of tetramethylsilane (^{1}H, ^{13}C{^{1}H}), 85% phosphoric acid (^{31}P and ^{31}P{^{1}H} spectra). ^{1}H and ^{13}C NMR signals were assigned based on 2D NMR spectra (^{1}H,^{1}H-COSY, ^{1}H,^{13}C-HSQC, ^{1}H,^{13}C-HMQC). UV/Vis spectra were recorded on an Ocean Optics Flame Spectrometer. Elemental analysis was performed by the Central Analytical Services department of the University of Regensburg.

Single-crystal X-ray diffraction data were recorded on a Rigaku Oxford Diffraction SuperNova Atlas or a XtaLAB Synergy R (DW system, Hypix-Arc 150) device with Cu-K_α radiation ($\lambda = 1.54184$ Å). Crystals were selected under mineral oil, mounted on micromount loops and quench-cooled using an Oxford Cryosystems open flow N$_2$ cooling device. Either semi-empirical multi-scan absorption corrections[21] or analytical ones[22] were applied to the data. The structures were solved with SHELXT[23] solution program using dual methods and by using Olex2 as the graphical interface.[24] The models were refined with ShelXL[25] using full matrix least squares minimisation on F^2.[26] The hydrogen atoms were located in idealised positions and refined isotropically with a riding model.

2.4.1   Synthesis of Compounds

[{(TMC)₂Ni}₂(μ²,η²:η²-P₂)] (1):

To a solution of [{(IMes)Ni(CO)}₂(μ²,η²:η²-P₂)]·(0.5 *n*-hexane) (110.0 mg, 0.124 mmol, 1.0 eq.) in toluene (6 mL) was added TMC (61.6 mg, 0.50 mmol, 4.0 eq.). Upon stirring at ambient temperature for 2 hours, a colour change from deep orange to deep red was observed. Subsequently, the solvent was removed and the dark red residue was dried *in vacuo*. The residue was washed with *n*-hexane (5 mL) and benzene (5 mL) and the resulting bright orange solid was dried *in vacuo* to afford pure [{(TMC)₂Ni}₂(μ²,η²:η²-P₂)].

Crystals of [{(TMC)₂Ni}₂(μ²,η²:η²-P₂)] (**1**) suitable for X-ray crystallography were grown by slow diffusion of *n*-hexane into a saturated solution of **1** in benzene. In addition, X-ray quality crystals of [(IMes)(TMC)Ni(CO)₂] (**2**) were obtained from the benzene washing solution after storage for 2 months at ambient temperature.

C₂₈H₄₈N₈Ni₂P₂, MW = 676.08 g/mol
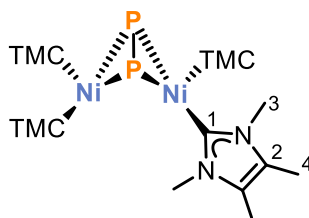
Yield: 26 mg (31%)

¹H NMR (400 MHz, 300 K, C₆D₆) δ = 1.97 (s, 24H, C⁴H), 3.58 (s, 24H, C³H) ppm.

¹³C{¹H} NMR (100 MHz, 300 K, C₆D₆) δ = 9.2 (s, C⁴), 34.8 (s, C³), 122.7 (s, C²), 203.5 (br s, C¹) ppm.

**³¹P{¹H}** (162 MHz, 300 K, C₆D₆) δ = 34.7 (s) ppm.

Elemental Analysis calcd. C 49.74, H 7.16, N 16.57; found C 49.46, H 7.21, N 15.28.

UV/Vis (THF): λ_{max} (nm, ε_{max} /L·mol⁻¹·cm⁻¹) 320 (21 000).

[(IMes)Ni(η³-(PhNCS)₃)] (3a):

To a solution of [(IMes)Ni(vtms)₂] (100.0 mg, 0.177 mmol, 1.0 eq.) in toluene (5 mL) was added phenyl isothiocyanate (0.1 mL, 113 mg, 0.84 mmol, 4.7 eq.). The colour of the reaction mixture changed from yellow over burgundy to deep purple while stirring at ambient temperature for 1.5 h. Subsequently, the solvent was removed and the dark residue was dried *in vacuo*. The residue was washed with *n*-hexane (20 mL), extracted in toluene (3 mL) and layered with *n*-hexane (20 mL). Storage at −30 °C for 3 days afforded microcrystalline [(IMes)Ni(η³-PhNCS)₃] which was isolated by decanting the supernatant and dried *in vacuo*.

Crystals of [(IMes)Ni(η³-PhNCS)₃] (**3a**) suitable for X-ray crystallography were grown by slow diffusion of *n*-hexane into a saturated solution of **3a** in toluene.
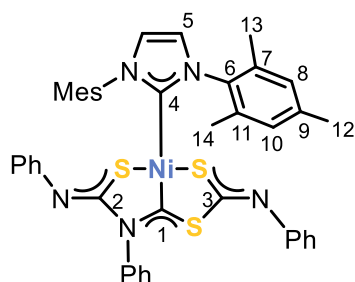
$C_{42}H_{39}N_5NiS_3$, MW = 768.68 g/mol

Yield: 60 mg (44%)

¹H NMR (400 MHz, 273 K, toluene-d⁸) δ = 2.03 (s, 6H, $C^{12}H$), 2.16 (s, 6H, $C^{13}H$), 2.19 (s, 6H, $C^{14}H$), 5.96 - 5.98 (m, 2H, H^{Ph}), 5.99 (s, 2H, C^5H), 6.69 - 6.73 (m, 4H, H^{Ph}), 6.75 (s, 2H, $C^{10}H$), 6.76 (s, 2H, C^8H), 7.22 - 7.34 (m, 9H, H^{Ph}) ppm.

¹³C{¹H} NMR (100 MHz, 273 K, toluene-d⁸) δ = 19.17 (s, C^{13}), 19.22 (s, C^{14}), 21.0 (s, C^{12}, overlapping with toluene signal), 122.2 (s, C^{Ar}), 122.6 (s, C^{Ar}), 123.6 (s, C^{Ar}), 123.7 (s, C^{Ar}), 124.5 (s, C^5), 126.8 (s, C^{Ar}), 128.47 (s, C^{Ar}), 128.5 (s, C^{Ar}), 129.3 (s, C^{Ar}), 129.5 (s, C^{10}), 129.6 (s, C^8), 135.7 (s, C^6), 135.9 (s, C^{11}), 136.0 (s, C^7), 139.2 (s, C^{Ar}), 143.1 (s, C^{Ar}), 149.6 (s, C^{Ar}), 151.5 (s, C^{Ar}), 169.8 (s, $C^{2/3}$), 173.5 (s, C^4), 180.4 (s, $C^{2/3}$), 238.8 (s, C^1) ppm.

Elemental Analysis calcd. C 65.63, H 5.11, N 9.11, S 12.51; found C 65.66, H 5.15, N 8.70, S 11.31.

UV/Vis (THF): λ_{max} (nm, ε_{max} /L·mol⁻¹·cm⁻¹) 280 (31 000), 340 (12 500sh), 580 (3200).

[(IMes)Ni(η³-(PhNCS)₃)] (**3a**) can also be prepared by an analogous procedure to the one described using 0.5 eq. [{(IMes)Ni(CO)}₂(μ²,η²:η²-P₂)] (40.0 mg, 0.045 mmol, 1.0 eq.).

Yield: 21 mg (30%)

Spectroscopic and analytical data of the isolated compound were identical to those given above.

[(IMes)Ni(η³-(2,6-Me₂-C₆H₃-NCS)₃)] (3b):

To a solution of [(IMes)Ni(vtms)₂] (30.0 mg, 0.053 mmol, 1.0 eq.) in toluene (2 mL) was added an excess amount of 2,6-dimethylphenyl isothiocyanate (0.1 mL, 109 mg, 0.67 mmol, 13.5 eq.). The colour of the reaction mixture changed from yellow over burgundy to deep purple while stirring at ambient temperature for 1.5 h. Subsequently, the solvent was removed and the dark residue was dried *in vacuo*. The residue was washed with *n*-hexane (5 mL), extracted in benzene (1 mL) and layered with *n*-hexane (5 mL). Storage at ambient temperature overnight afforded crystals of [(IMes)Ni(η³-(2,6-Me₂-C₆H₃-NCS)₃)] which were isolated by decanting the supernatant. The crystals were dried *in vacuo*.

Crystals of [(IMes)Ni(η³-(2,6-Me₂-C₆H₃-NCS)₃)] (**3b**) suitable for X-ray crystallography were grown by slow diffusion of *n*-hexane into a saturated solution of **3b** in benzene.
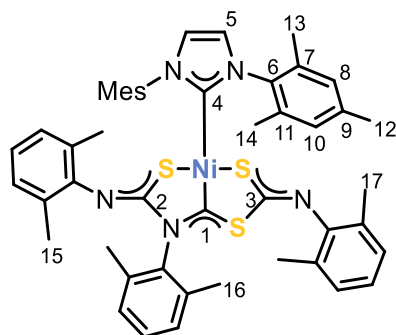
C$_{48}$H$_{51}$N$_5$NiS$_3$, MW = 852.84 g/mol

Yield: 35 mg (77%)

^{1}H NMR (400 MHz, 273 K, toluene-d^8) δ = 1.86 (s, 6H, CH$_3$), 1.97 (s, 6H, CH$_3$), 1.99 (s, 6H, CH$_3$), 2.11 (s, 6H, CH$_3$), 2.16 (s, 6H, CH$_3$), 2.26 (s, 6H, CH$_3$), 5.86 (s, 2H, C^{5}H), 6.64-6.72 (m, 4H, C^{Ar}H), 6.75 (s, 2H, C^{Ar}H), 6.83 (t, $^3J_{HH}$ = 7.6 Hz, C^{Ar}H), 6.93 (dd, 1H, J = 6.8, 8.0 Hz, C^{Ar}H), 6.99 (br s, 1H, overlapping with solvent signal, C^{Ar}H), 7.02-7.04 (m, 2H, overlapping with solvent signal, C^{Ar}H), 7.08-7.14 (m, 2H, overlapping with solvent signal, C^{Ar}H) ppm.

^{13}C{^{1}H} NMR (100 MHz, 273 K, toluene-d^8) δ = 17.4 (s, C$^{15/16/17}$), 18.4 (s, C$^{15/16/17}$), 19.0 (s, C$^{15/16/17}$), 19.1 (s, C$^{13/14}$), 19.2 (s, C$^{13/14}$), 21.1 (s, C^{12}), 123.0 (s, C^{Ar}), 124.3 (s, C^5), 127.2 (s, C^{Ar}), 127.37 (s, C^{Ar}), 127.43 (s, C^{Ar}), 129.37 (s, C^{Ar}), 129.41 (s, C^{Ar}), 134.2 (s, C^{Ar}), 135.5 (s, C^{Ar}), 135.6 (s, C^{Ar}), 135.88 (s, C^{Ar}), 135.90 (s, C^{Ar}), 138.6 (s, C^{Ar}), 142.3 (s, C^{Ar}), 147.7 (s, C^{Ar}), 150.6 (s, C^{Ar}), 167.9 (s, C$^{2/3}$), 173.4 (s, C^4), 179.2 (s, C$^{2/3}$), 239.1 (s, C^1) ppm.

**Elemental Analysis** calcd. C 65.63, H 5.11, N 9.11, S 12.51; found C 65.66, H 5.15, N 8.70, S 11.31.

UV/Vis (THF): λ_{max} (nm, ε_{max} /L·mol^{-1}·cm^{-1}) 280 (19 000), 380 (3000sh), 560 (1500).

[(IMes)Ni(η^3-2,6-Me$_2$-C$_6$H$_3$-NCS)$_3$)] (**3b**) can also be prepared by an analogous procedure to the one described using 0.5 eq. [{(IMes)Ni(CO)}$_2$(μ^2,η^2:η^2-P$_2$)]. NMR spectroscopic data of the isolated compound were identical to those given above.

[{(IMes)Ni(μ^2,η^1:η^2-CS$_2$)}$_2$] (5):

To a suspension of [{(IMes)Ni(CO)}$_2$(μ^2,η^2:η^2-P$_2$)]·(0.5 *n*-hexane) (40.0 mg, 0.045 mmol, 1.0 eq.) in *n*-hexane (5 mL) was added an excess amount of CS$_2$ (0.1 mL, 5 mol·L^{-1} in THF, 0.5 mmol, 11.0 eq.). While stirring at ambient temperature for 30 minutes a colour change from yellow to deep red and the formation of a red precipitate was observed. The reaction mixture was filtered and the remaining red powder was dried *in vacuo*, resulting in analytically pure [{(IMes)Ni(μ^2,η^1:η^2-CS$_2$)}$_2$] (**5**).

Crystals of [{(IMes)Ni(μ^2,η^1:η^2-CS$_2$)}$_2$] (**5**) suitable for X-ray crystallography were grown by slow diffusion of *n*-hexane into a saturated solution of **5** in fluorobenzene.

$C_{44}H_{48}N_4Ni_2S_4$, MW = 878.52 g/mol
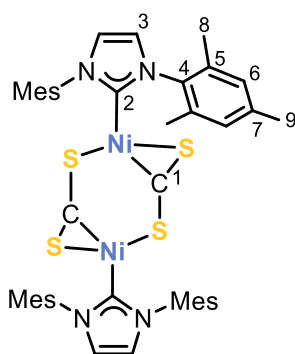
Yield: 35 mg (88%)

¹H NMR (400 MHz, 300 K, C_6D_6) δ = 1.99 (s, 24H, C^8H), 2.01 (s, 12H, C^9H), 6.04 (s, 4H, C^3H), 6.42 (s, 8H, C^6H) ppm.

¹³C{¹H} NMR (100 MHz, 300 K, C_6D_6) δ = 18.2 (s, C^8), 21.2 (s, C^9), 122.7 (s, C^3), 129.4 (s, C^6), 135.1 (s, C^4), 136.4 (s, C^5), 138.0 (s, C^7), 189.2 (s, C^2), 285.6 (s, C^1) ppm.

Elemental Analysis calcd. C 60.16, H 5.51, N 6.38; found C 60.11, H 5.57, N 6.83.

UV/Vis (THF): λ_{max} (nm, ε_{max} /L·mol⁻¹·cm⁻¹) 380 (11 500), 550 (7000).

[{(IMes)Ni(μ²,η¹:η²-CS₂)}₂] (**5**) can also be prepared from 2 eq. [(IMes)Ni(vtms)₂] using the same synthetic procedure. NMR spectroscopic data of the isolated compound were identical to those given above.

[(IMes)Ni(η²-(CyNCS))₂] (4):

To a solution of [(IMes)Ni(vtms)₂] (20.0 mg, 0.036 mmol, 1.0 eq.) in toluene (5 mL) was added an excess amount of cyclohexyl isothiocyanate (0.1 mL, 99.6 mg, 0.71 mmol, 19.6 eq.) at −30 °C. After stirring at ambient temperature for 5 minutes a colour change from yellow to orange was observed. The reaction mixture was stirred for 2 hours in total. Subsequently, the solvent was removed and the residue was dried *in vacuo*. The residue was extracted with *n*-hexane (5 mL) and stored at ambient temperature overnight to afford orange crystals of [(IMes)Ni(η²-(CyNCS))₂] (**4**) suitable for single crystal X-ray diffraction. The crystals were isolated by decanting the supernatant and dried *in vacuo*.

$C_{35}H_{46}N_4NiS_2$, MW = 645.59 g/mol
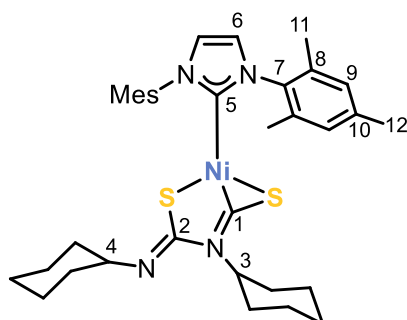
Yield: 17 mg (73%)

^{1}H NMR (400 MHz, 300 K, C$_6$D$_6$) δ = 0.60 - 1.84 (m, 20H, Cy-H), 2.03 (s, 6H, C^{12}H), 2.11 (m, 2H, Cy-H), 2.22 (s, 12H, C^{11}H), 4.23 (tt, $^3J_{HH}$ = 9.8 Hz, 4.3 Hz, C$^{3/4}$H), 4.50 (tt, 12.2 Hz, 3.6 Hz, C$^{3/4}$H), 6.21 (s, 2H, C^{6}H), 6.75 (s, 4H, C^{9}H) ppm.

^{13}C{^{1}H} NMR (100 MHz, 300 K, C$_6$D$_6$) δ = 18.2 (s, C^{11}), 21.09 (s, C^{12}), 23.1 (s, C^{Cy}), 23.2 (s, C^{Cy}), 25.0 (s, C^{Cy}), 25.3 (s, C^{Cy}), 25.5 (s, C^{Cy}), 25.6 (s, C^{Cy}), 26.7 (s, C^{Cy}), 30.3 (s, C^{Cy}), 33.0 (s, C^{Cy}), 34.1 (s, C^{Cy}), 58.0 (s, C$^{3/4}$), 58.7 (s, C$^{3/4}$), 122.4 (s, C^6), 129.5 (s, C^9), 135.6 (s, C^7), 136.8 (s, C^7), 138.8 (s, C^{10}), 168.4 (s, C$^{1/2}$), 190.7 (s, C^5), 229.9 (s, C$^{1/2}$) ppm.

Elemental Analysis calcd. [+ 0.2 molecules of *n*-hexane (see ^{1}H NMR)] C 65.60, H 7.42, N 8.45, S 9.67; found C 65.75, H 7.28, N 8.48, S 10.00.

UV/Vis (THF): $λ_{max}$ (nm, $ε_{max}$ /L·mol^{-1}·cm^{-1}) 270 (28 000), 380 (4 300, tailing to 520 nm).
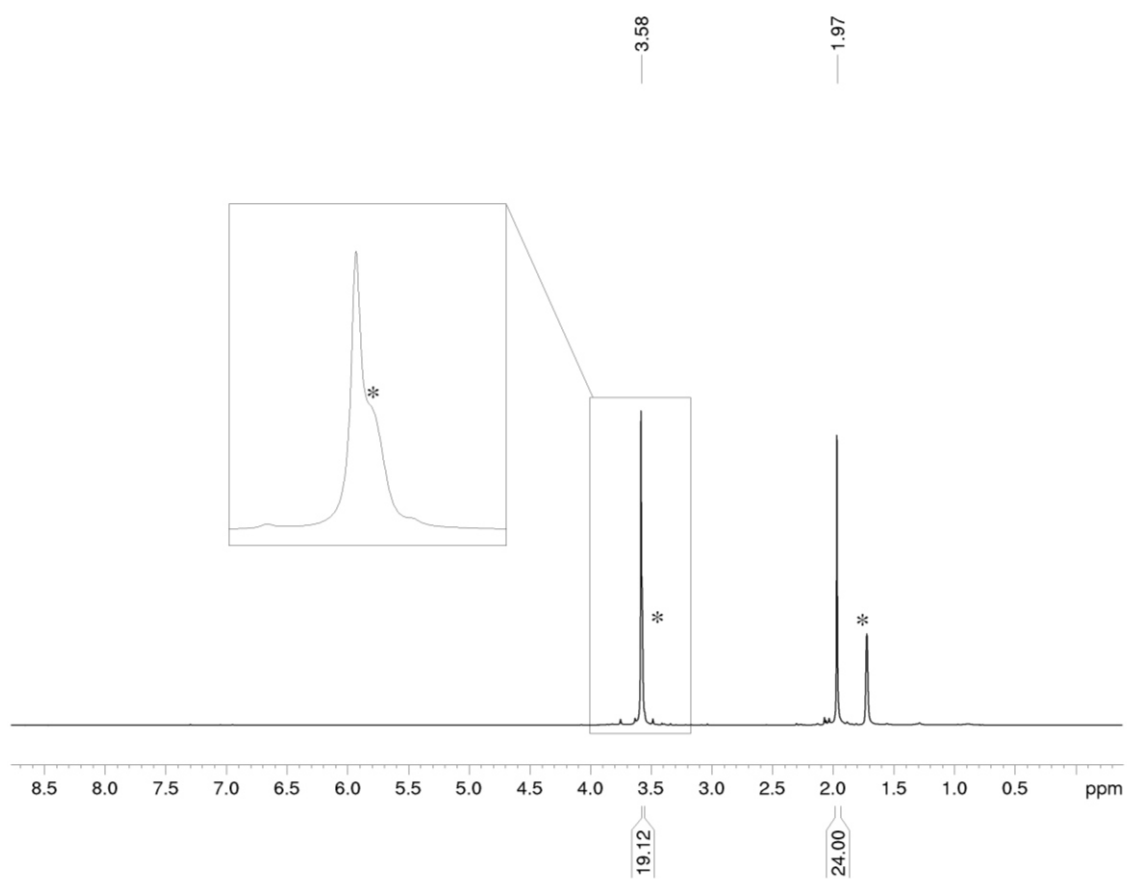
2.4.2   NMR Spectra

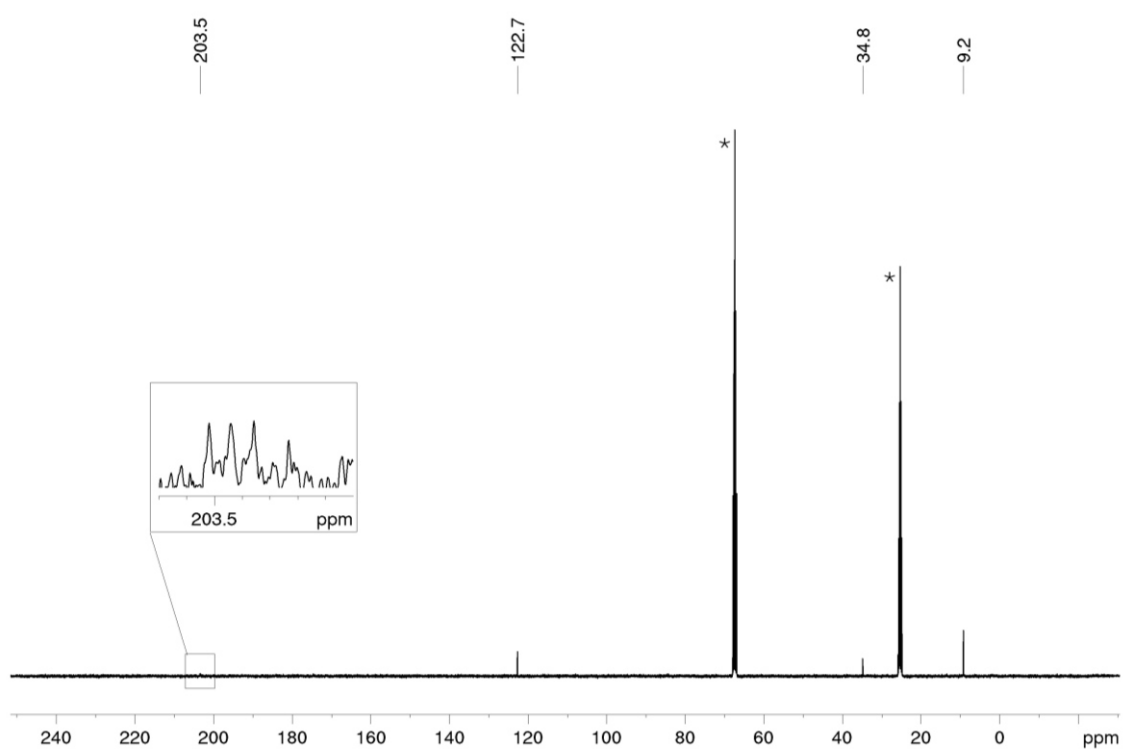**Figure S1.** ^{1}H NMR spectrum (400 MHz, 300 K, THF-d$_8$) of **1**; *THF-d$_8$.

Figure S2. ^{13}C{^{1}H} NMR spectrum (100 MHz, 300 K, THF-d$_8$) of **1**; *THF-d$_8$.
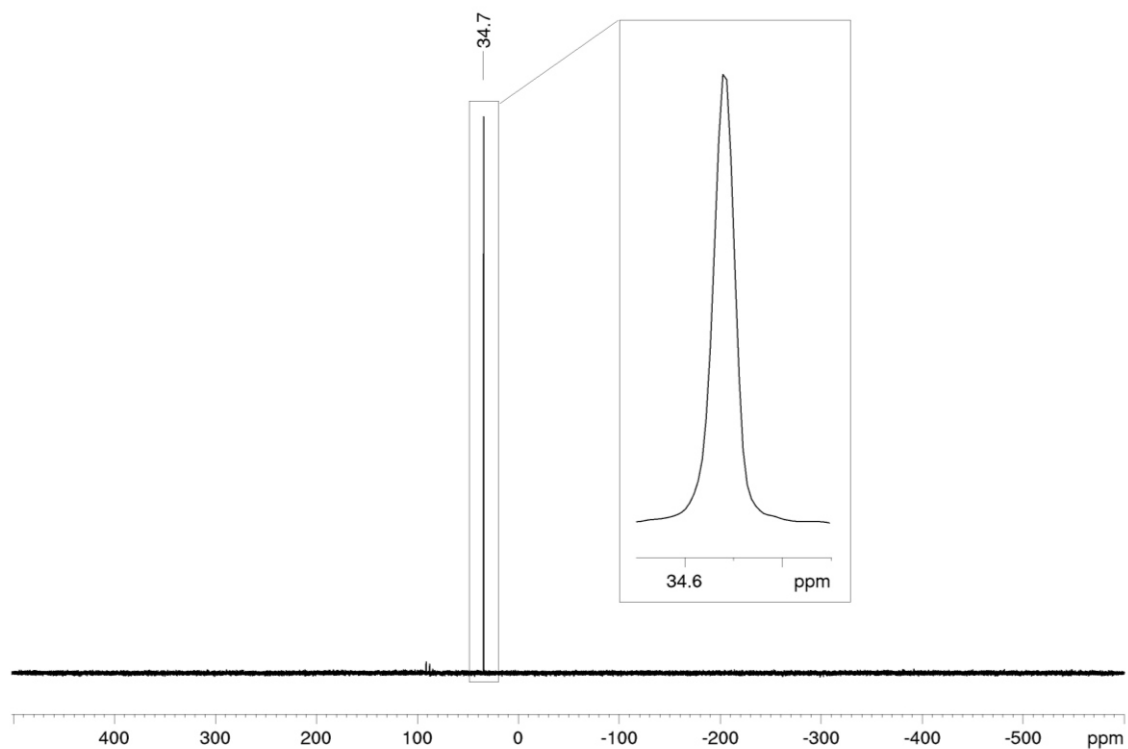
Figure S3. $^{31}P\{^{1}H\}$ NMR spectrum (162 MHz, 300 K, THF-d$_8$) of **1**.
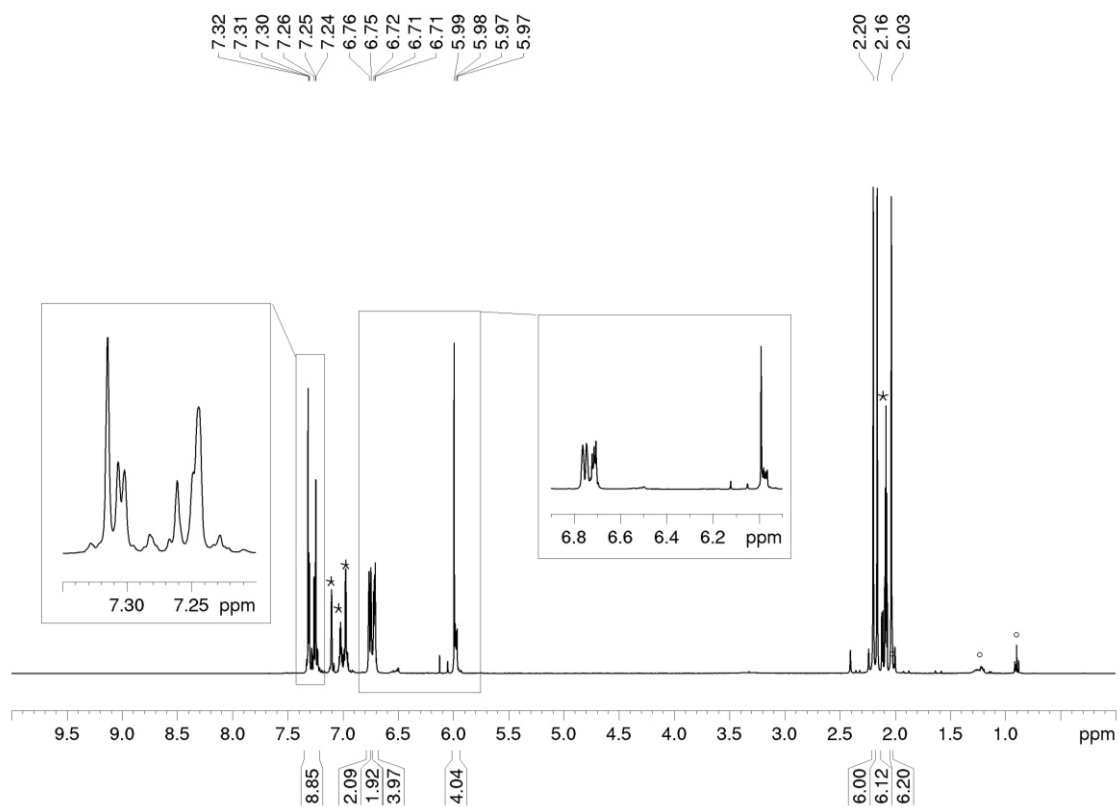
Figure S4. ^{1}H NMR spectrum (400 MHz, 273 K, toluene-d$_8$) of **3a**; * toluene-d$_8$.
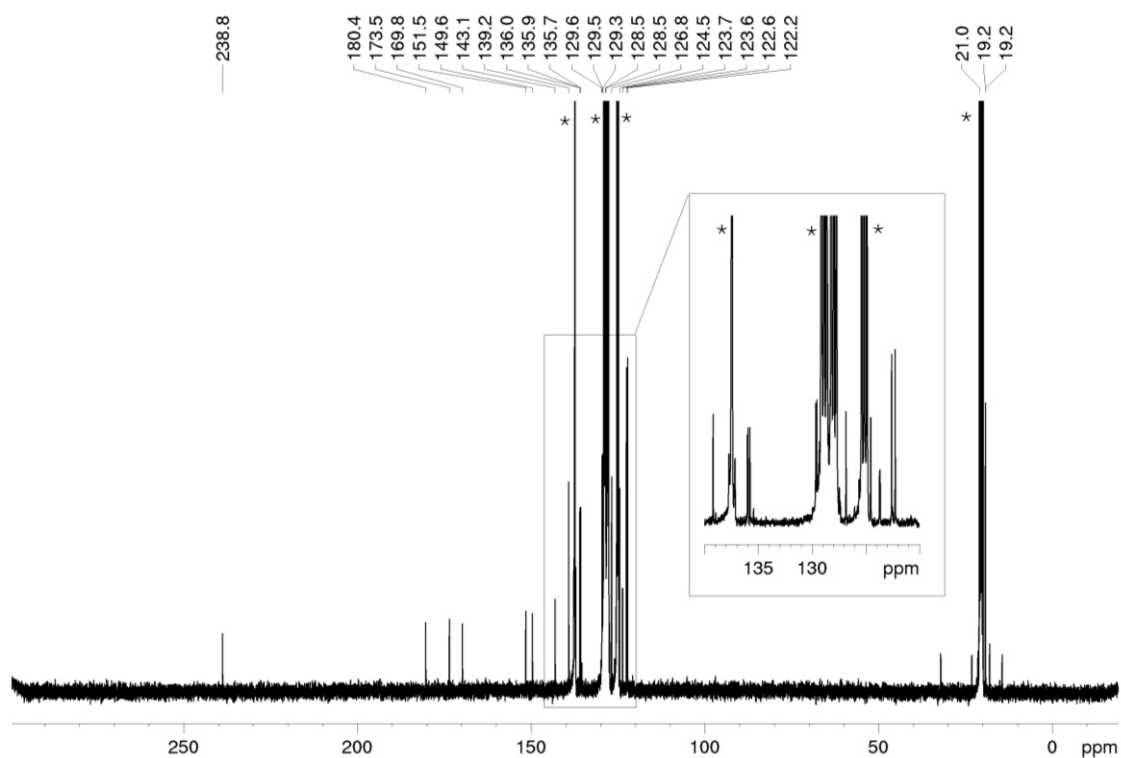
Figure S5. $^{13}C\{^1H\}$ NMR spectrum (100 MHz, 273 K, toluene-d$_8$) of **3a**; *toluene-d$_8$.
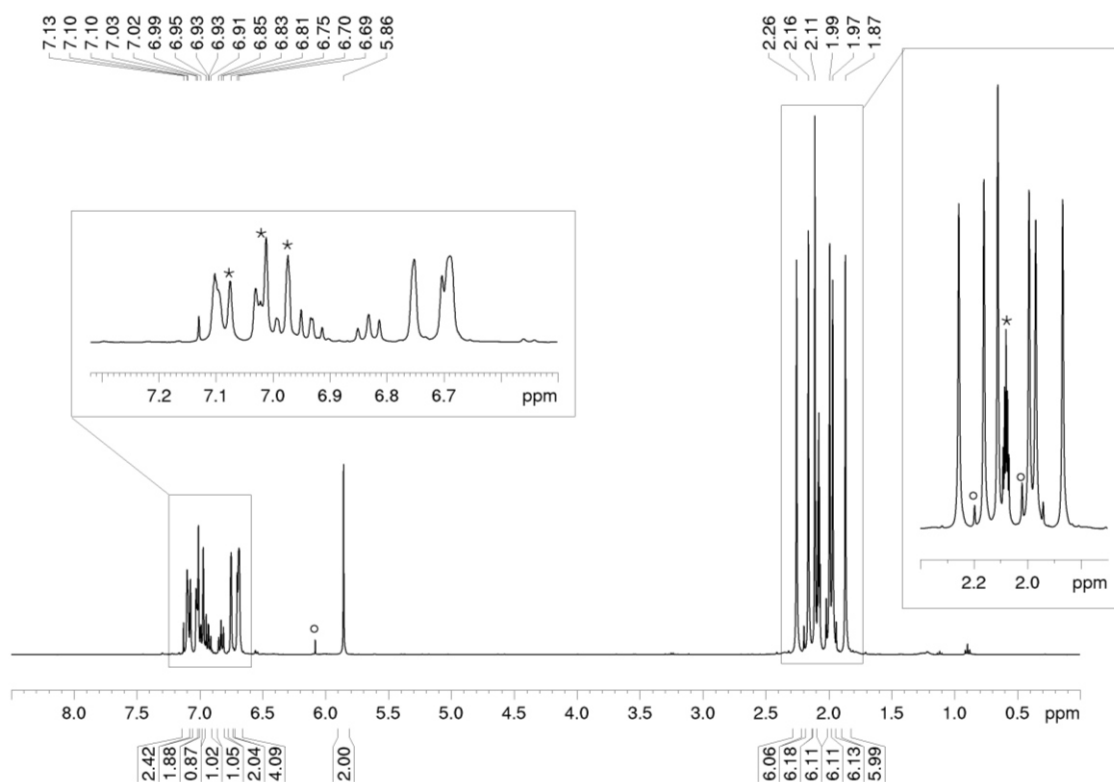
Figure S6. ^{1}H NMR spectrum (400 MHz, 273 K, toluene-d$_8$) of **3b**; * toluene-d$_8$; °minor impurity (<3%, forms upon storage of the sample at ambient temperature)

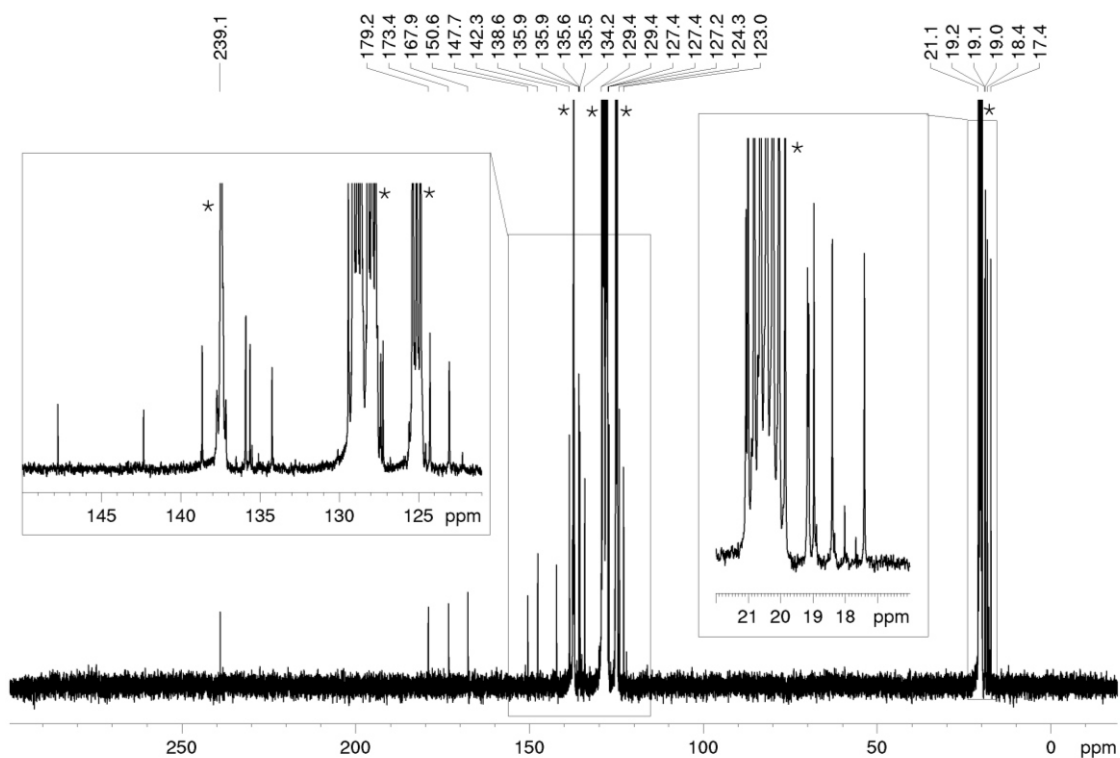**Figure S7.** $^{13}C\{^1H\}$ NMR spectrum (100 MHz, 273 K, toluene-d_8) of **3b**; *toluene-d_8.
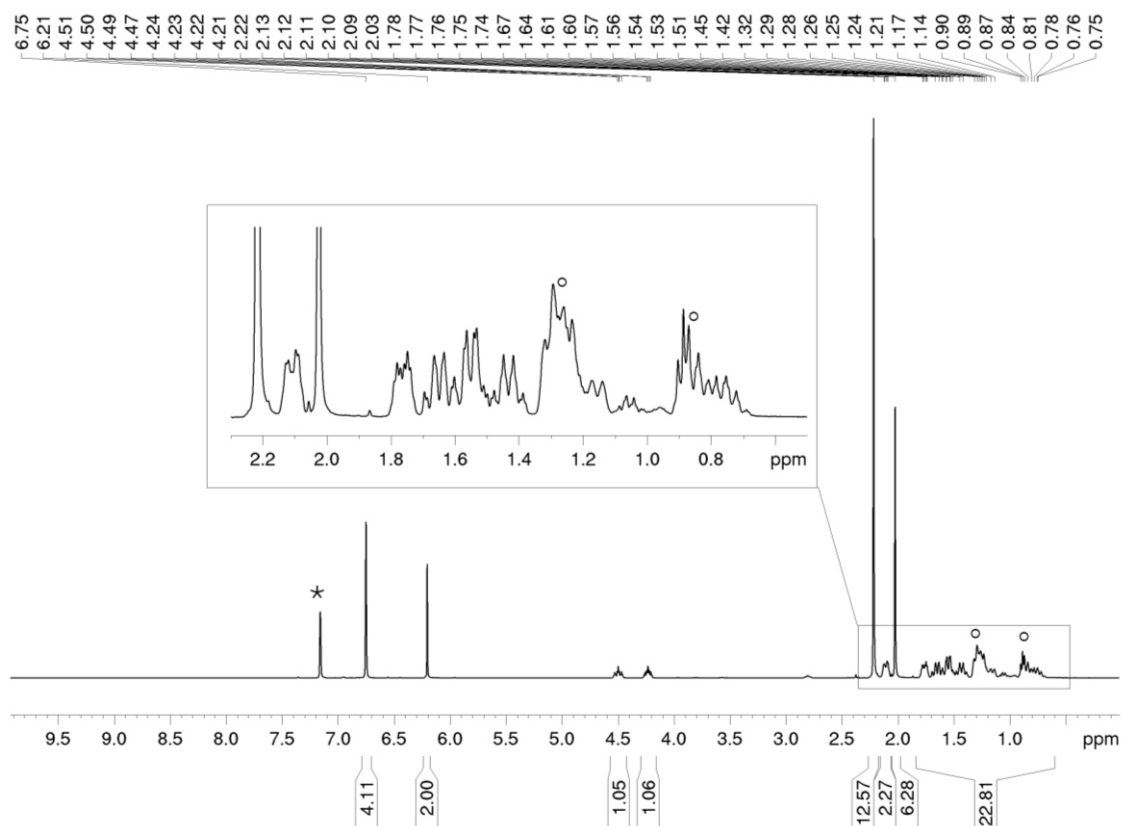

Figure S8. ^1H NMR spectrum (400 MHz, 300 K, C_6D_6) of **4**; *C_6D_6, °n-hexane (0.2 eq.).
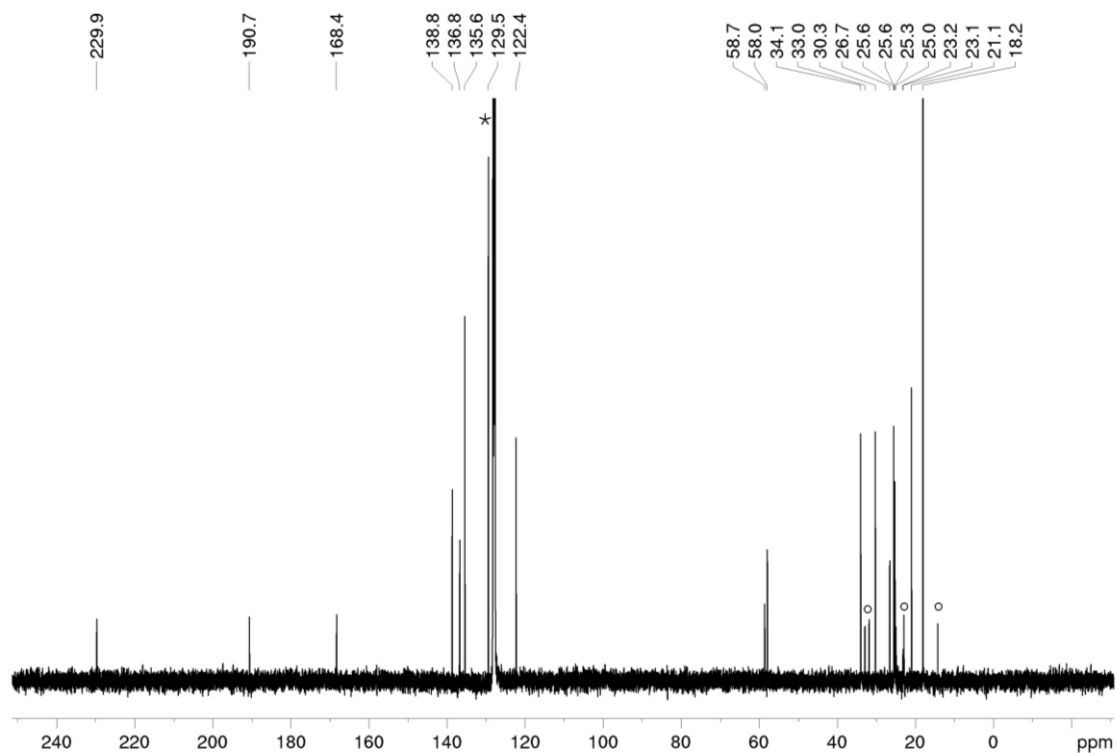
Figure S9. $^{13}C\{^1H\}$ NMR spectrum (100 MHz, 300 K, C_6D_6) of **4**; *C_6D_6, °*n*-hexane.
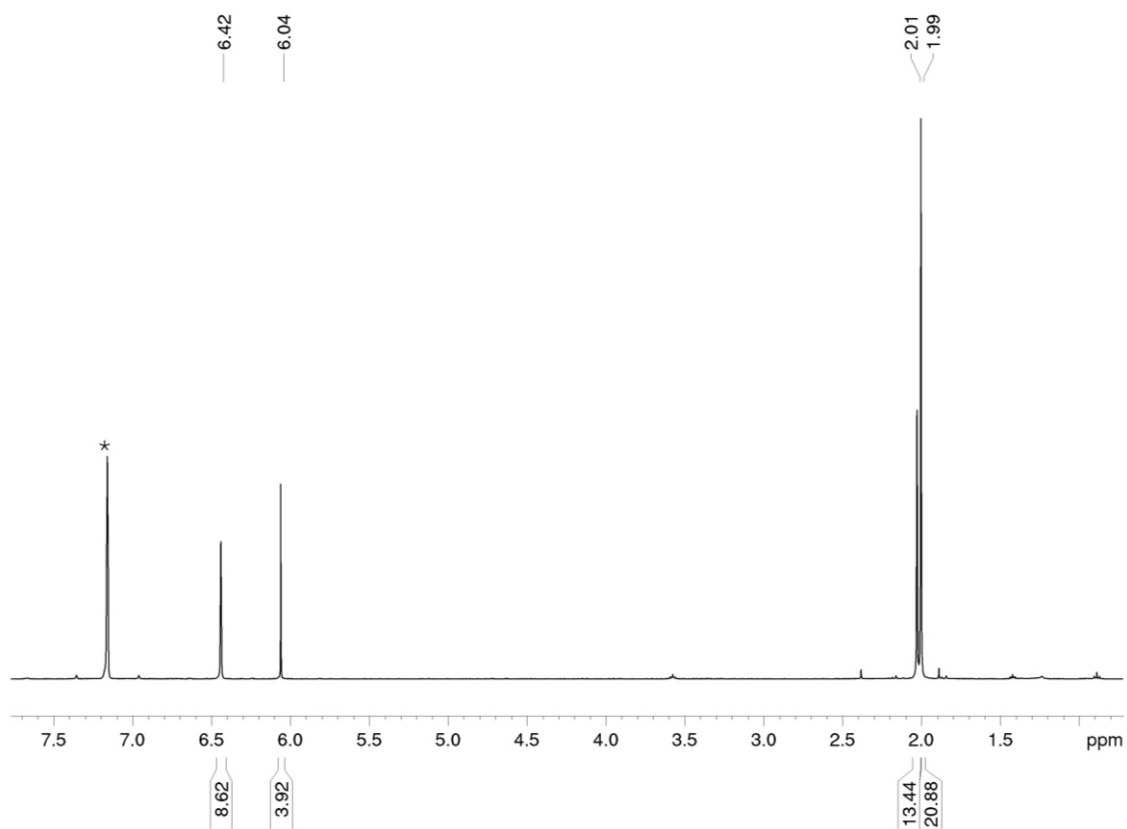
Figure S10. ^1H NMR spectrum (400 MHz, 300 K, C_6D_6) of **5**; *C_6D_6.
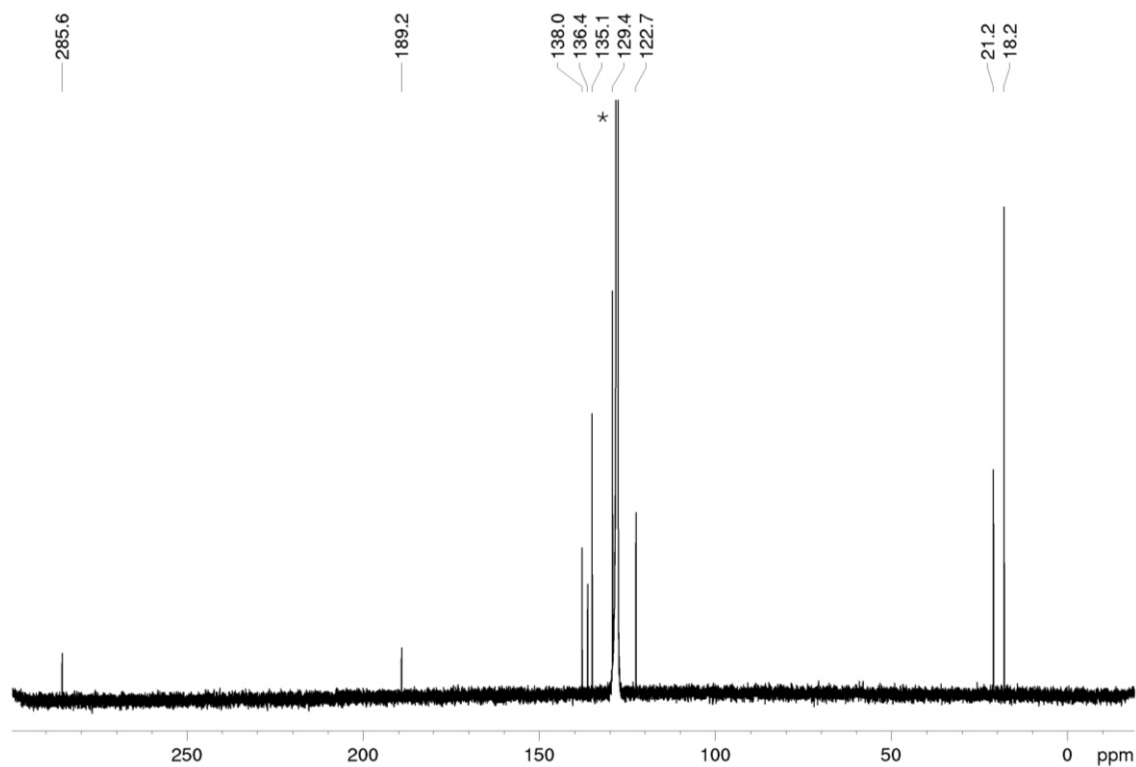
Figure S11. $^{13}C\{^1H\}$ NMR spectrum (100 MHz, 300 K, C_6D_6) of **5**; *C_6D_6.
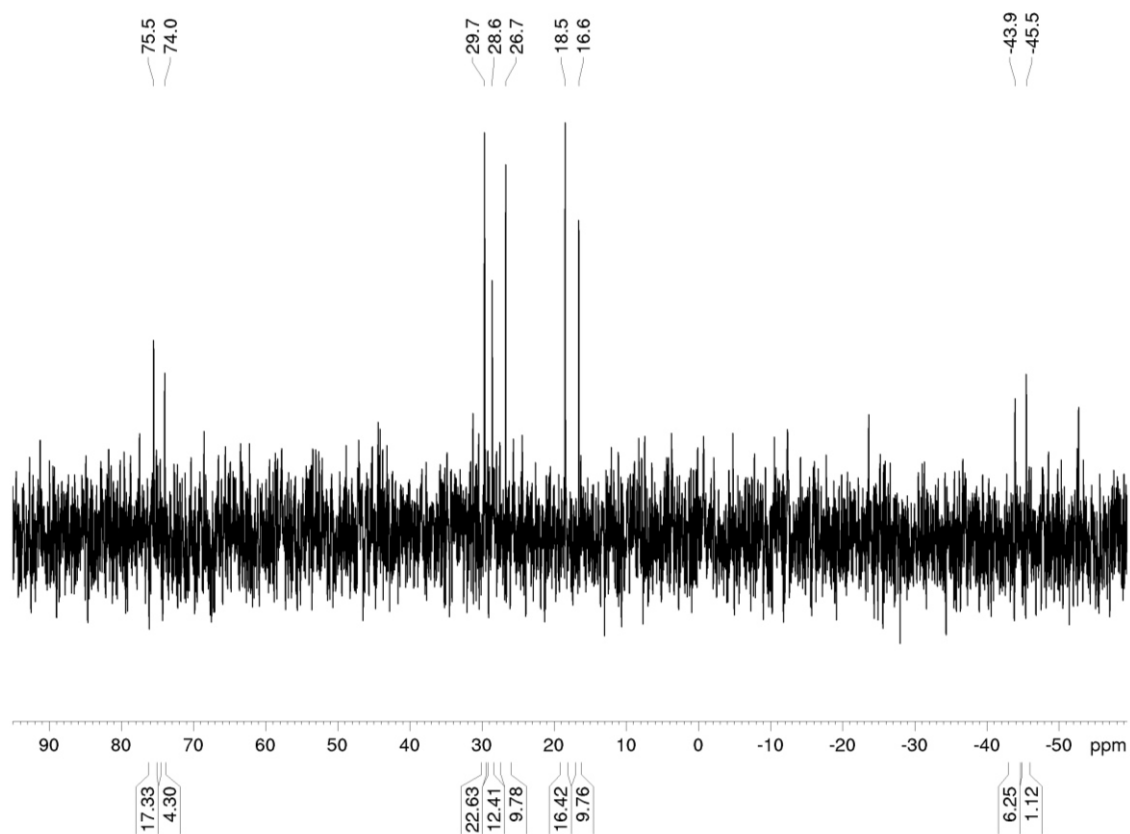
Figure S 12. $^{31}P\{^1H\}$ NMR spectrum (162 MHz, 300 K, C_6D_6) of the reaction of $[\{(IMes)Ni(CO)\}_2(\mu^2,\eta^2:\eta^2-P_2)]$ with CS_2 in the presence of excess amounts of 2,3-dimethylbutadiene.
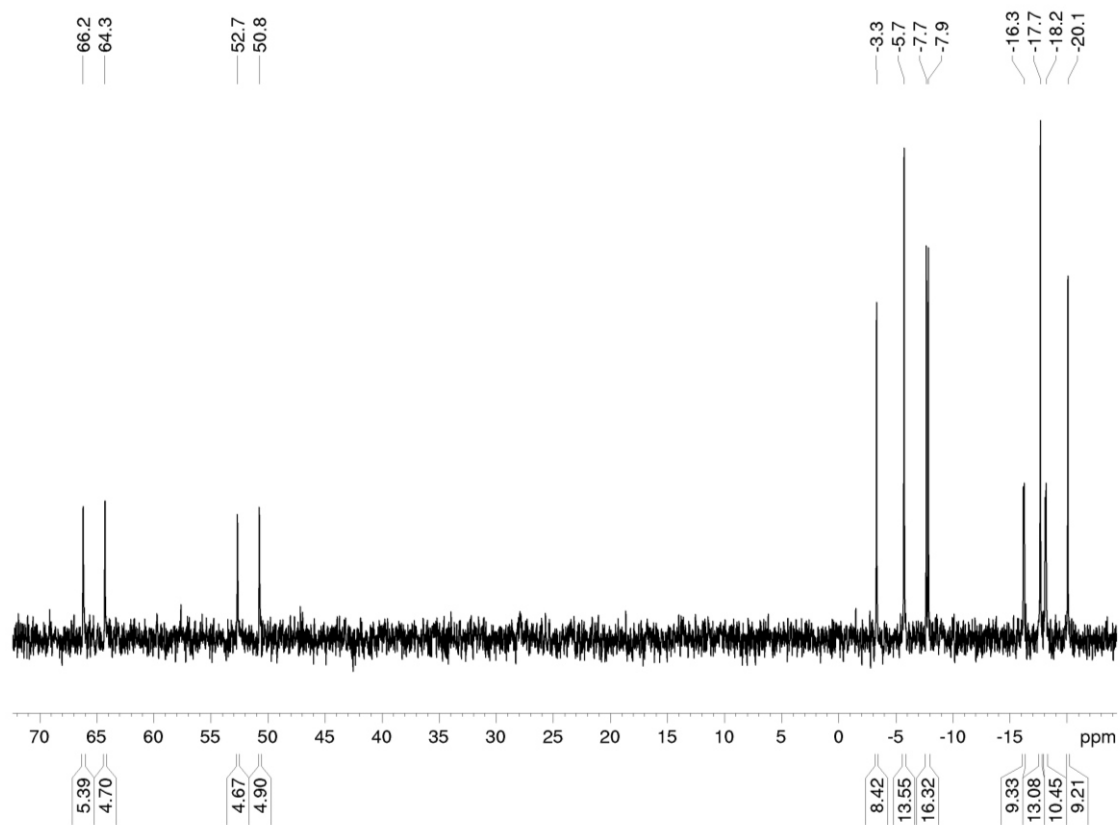
Figure S13. ^{31}P{^{1}H} NMR spectrum (162 MHz, 300 K, C$_6$D$_6$) of the reaction of [{(IMes)Ni(CO)}$_2$(μ^2,η^2:η^2-P$_2$)] with PhNCS in the presence of excess amounts of 2,3-dimethylbutadiene.

2.4.3 UV/Vis Spectra
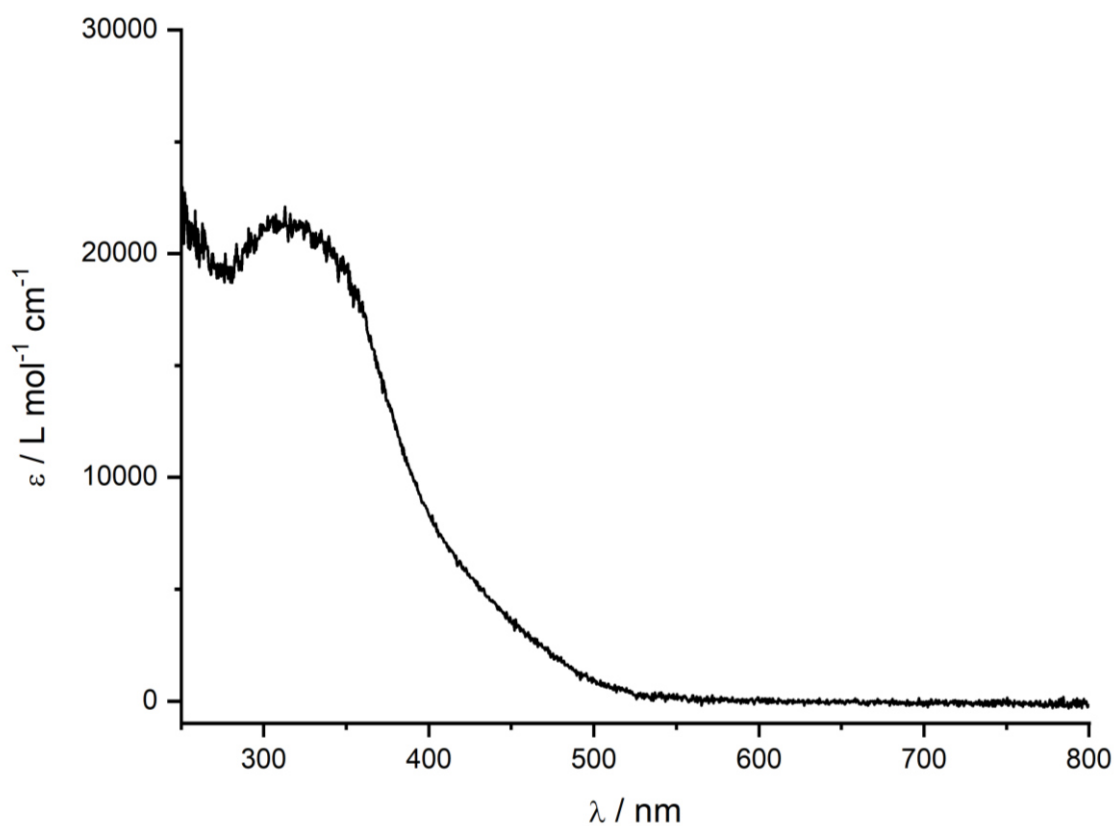
Figure S14. UV/Vis spectrum of [{(TMC)₂Ni}₂(μ²,η²:η²-P₂)] (**1**) recorded in THF.
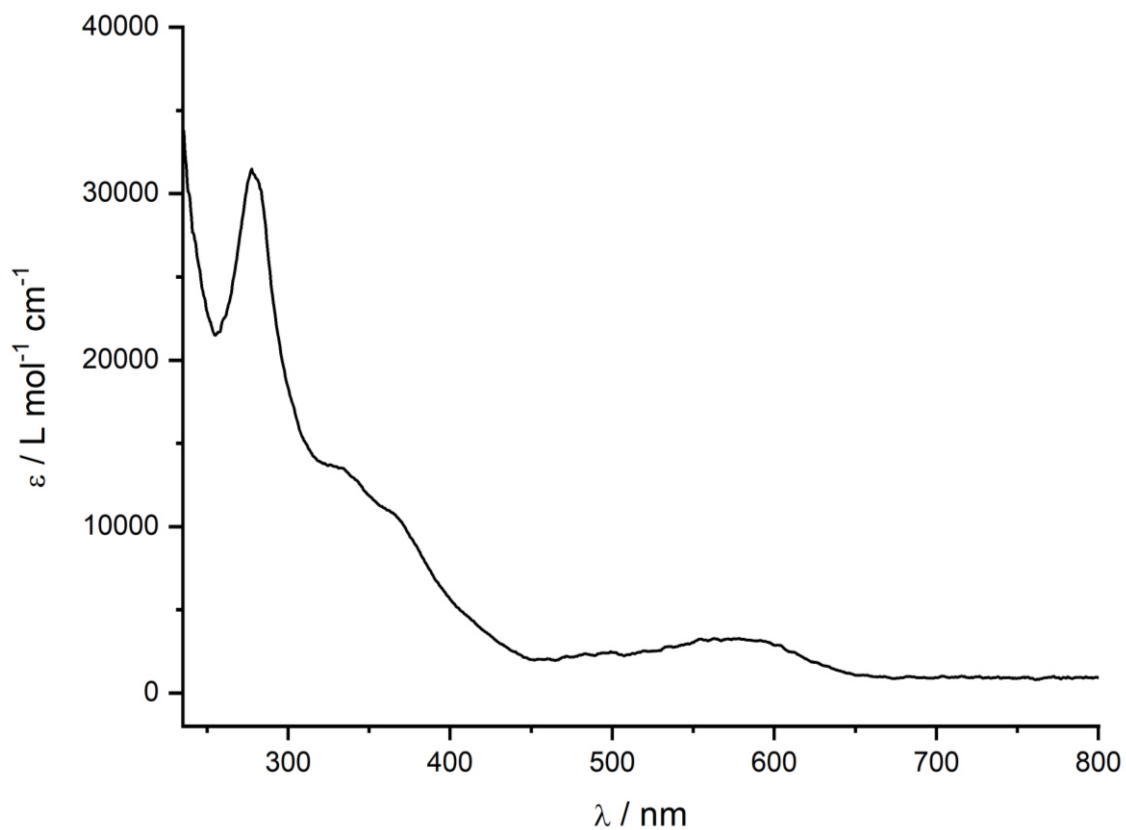
Figure S15. UV/Vis spectrum of [(IMes)Ni(η³-(PhNCS)₃)] (**3a**) recorded in THF.
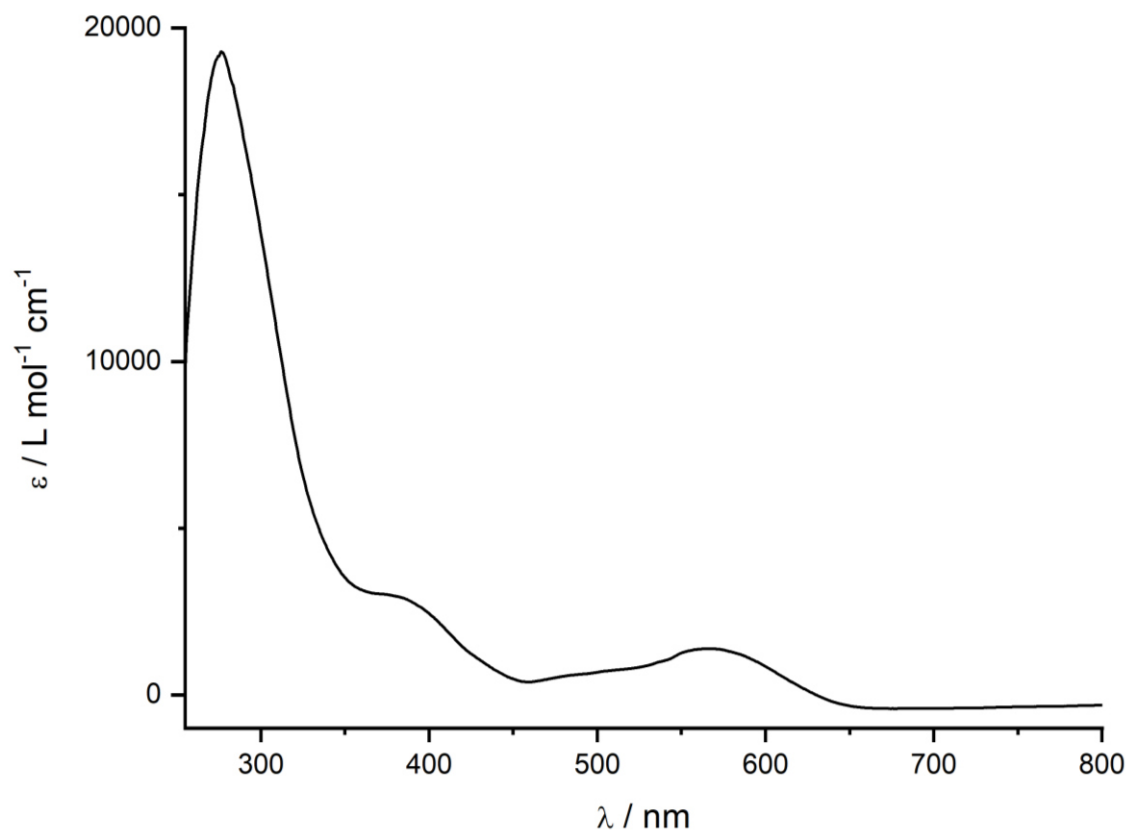
Figure S 16. UV/Vis spectrum of [(IMes)Ni(η^3-(2,6-Me$_2$-C$_6$H$_3$-NCS)$_3$)] (**3b**) recorded in THF.
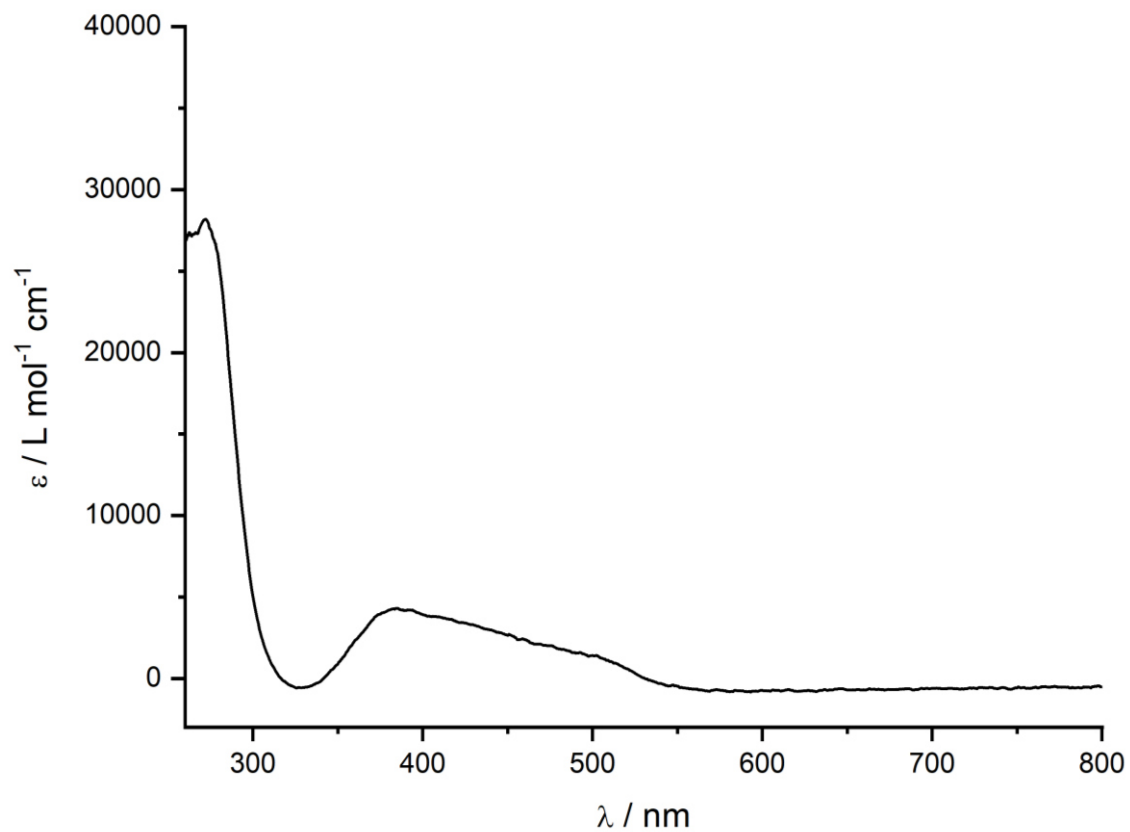
Figure S 17. UV/Vis spectrum of [(IMes)Ni(η^2-(CyNCS)$_2$)] (**4**) recorded in THF.

Figure S18. UV/Vis spectrum of [{(IMes)Ni(μ^2,η^1:η^2-CS$_2$)}$_2$] (**5**) recorded in THF.

2.4.4 Single Crystal X-Ray Diffraction Data

Table S1. Crystal data and structure refinement for compounds **3-6** and [(IMes)Ni(η^2-(CyNCS))$_2$].

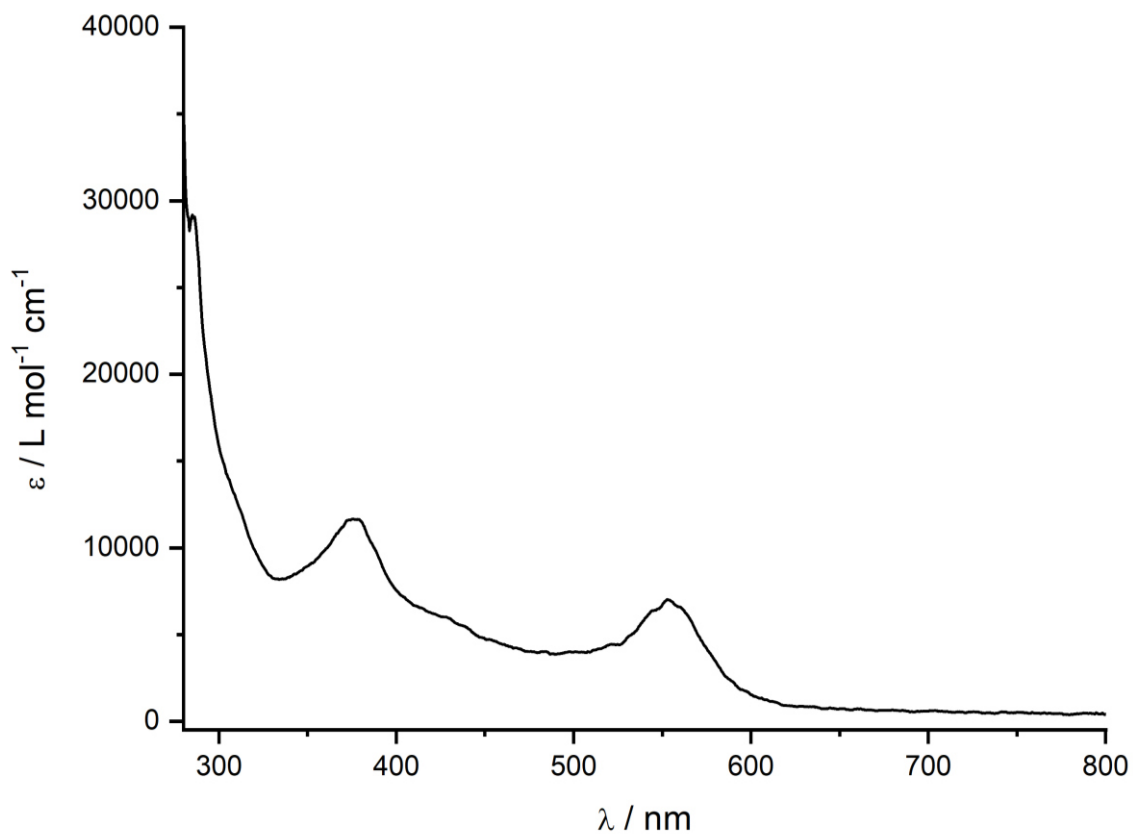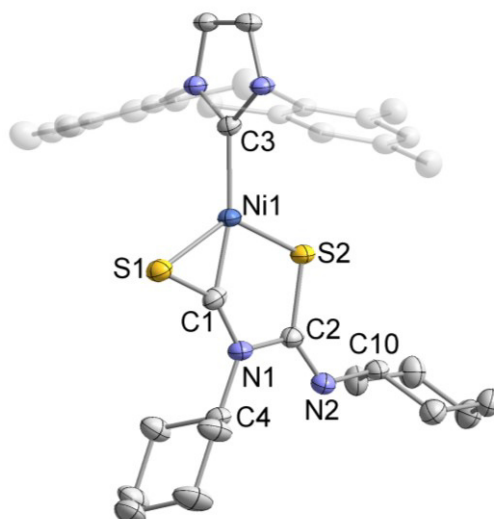|	1	2	3a	3b	4	5
Empirical formula	$C_{43}H_{63}N_8Ni_2P_2$	$C_{30}H_{36}N_4NiO_2$	$C_{42}H_{39}N_5NiS_3$	$C_{48}H_{51}N_5NiS_3$	$C_{35}H_{46}N_4NiS_2$	$C_{29}H_{30}FN_2NiS_2$
Formula weight	871.37	543.34	768.67	852.82	645.59	548.38
Temperature/K	123.0(1)	100.0(1)	123.1(1)	100.1(1)	100.0(1)	123.1(1)
Crystal system	triclinic	monoclinic	triclinic	monoclinic	hexagonal	trigonal
Space group	$P\bar{1}$	$P2_1/n$	$P\bar{1}$	$P2_1/c$	$P6_5$	$R\bar{3}$
a/Å	8.1593(2)	23.40218(11)	10.4206(5)	13.66226(6)	17.49340(10)	35.0705(3)
b/Å	16.6010(5)	14.48392(5)	12.0186(4)	11.10098(6)	17.49340(10)	35.0705(3)
c/Å	18.0971(5)	35.26725(15)	15.8459(7)	29.21385(12)	22.64210(10)	11.60940(10)
α/°	66.983(3)	90	93.313(3)	90	90	90
β/°	82.326(2)	105.6067(5)	103.684(4)	90.7383(4)	90	90
γ/°	79.881(2)	90	103.475(4)	90	120	120
Volume/Å³	2215.36(12)	11513.29(9)	1861.71(14)	4430.33(4)	6000.61(7)	12365.9(2)
Z	2	16	2	4	6	18
ρ_{calc}g/cm³	1.306	1.254	1.371	1.279	1.072	1.325
μ/mm⁻¹	2.038	1.220	2.614	2.247	1.857	2.645
F(000)	926.0	4608.0	804.0	1800.0	2064.0	5166.0
Crystal size/mm³	0.432 × 0.065 × 0.04	0.307 × 0.209 × 0.101	0.308 × 0.135 × 0.061	0.364 × 0.18 × 0.099	0.417 × 0.146 × 0.103	0.189 × 0.11 × 0.054
Radiation	CuKα (λ = 1.54184)	CuKα (λ = 1.54184)	CuKα (λ = 1.54184)	CuKα (λ = 1.54184)	CuKα (λ = 1.54184)	CuKα (λ = 1.54184)
2Θ range for data collection/°	9.268 to 145.726	4.08 to 148.038	7.618 to 147.258	6.052 to 151.986	5.834 to 151.506	8.154 to 147.196
Index ranges	-9 ≤ h ≤ 10, -20 ≤ k ≤ 20, -22 ≤ l ≤ 22	-26 ≤ h ≤ 28, -17 ≤ k ≤ 17, -43 ≤ l ≤ 43	-12 ≤ h ≤ 12, -13 ≤ k ≤ 14, -19 ≤ l ≤ 17	-17 ≤ h ≤ 17, -13 ≤ k ≤ 12, -28 ≤ l ≤ 36	-21 ≤ h ≤ 20, -21 ≤ k ≤ 21, -26 ≤ l ≤ 28	-37 ≤ h ≤ 43, -43 ≤ k ≤ 43, -14 ≤ l ≤ 10
Reflections collected	17350	116481	13723	50295	92802	24530
Independent reflections	8593 [R_{int} = 0.0313, R_{sigma} = 0.0414]	22606 [R_{int} = 0.0198, R_{sigma} = 0.0146]	7303 [R_{int} = 0.0239, R_{sigma} = 0.0340]	9098 [R_{int} = 0.0230, R_{sigma} = 0.0137]	8172 [R_{int} = 0.0281, R_{sigma} = 0.0101]	5499 [R_{int} = 0.0566, R_{sigma} = 0.0319]
Data/restraints/parameters	8593/0/512	22606/0/1373	7303/0/466	9098/0/526	8172/1/385	5499/6/250
Goodness-of-fit on F^2	1.021	1.039	1.038	1.051	1.034	1.058
Final R indexes [I>=2σ (I)]	R_1 = 0.0318, wR_2 = 0.0746	R_1 = 0.0333, wR_2 = 0.0924	R_1 = 0.0327, wR_2 = 0.0818	R_1 = 0.0287, wR_2 = 0.0769	R_1 = 0.0325, wR_2 = 0.0878	R_1 = 0.0454, wR_2 = 0.1241
Final R indexes [all data]	R_1 = 0.0404, wR_2 = 0.0801	R_1 = 0.0374, wR_2 = 0.0948	R_1 = 0.0380, wR_2 = 0.0858	R_1 = 0.0298, wR_2 = 0.0776	R_1 = 0.0327, wR_2 = 0.0881	R_1 = 0.0477, wR_2 = 0.1270
Largest diff. peak/hole / e Å⁻³	0.38/-0.32	0.36/-0.24	0.40/-0.27	0.34/-0.32	0.78/-0.28	0.37/-0.57
Flack parameter	/	/	/	/	0.011(8)	/

Figure S19. Molecular structure of [(IMes)Ni(η²-(CyNCS))₂] (**4**) in the solid state. Thermal ellipsoids are set at the 50% probability level. Hydrogen atoms are omitted for clarity. Selected bond lengths [Å] and angles [°]: Ni1–S1 2.2824(8), Ni1–S2 2.1508(7), Ni1–C1 1.755(3), Ni1–C3 1.933(3), S2–C2 1.772(3), S1–C1 1.646(3), N1–C1 1.319(3), N1–C2 1.437(3), N1–C4 1.488(3), N2–C2 1.266(4), S2–Ni1–S1 129.82(3), C1–Ni1–S2 83.96(9), C1–Ni1–S1 45.86(9), C1–Ni1–C3 166.51(11), C3–Ni1–S2 109.51(8), C3–Ni1–S1 120.66(8), C2–S2–Ni1 100.33(9), C1–S1–Ni1 49.89(10), N1–C2–S2 112.06(18) C1–N1–C2 111.9(2), N1–C1–Ni1 131.7(2).

2.4.5   Quantum Chemical Calculations

General Methods

All calculations were performed with the ORCA program package.[27] All calculations were conducted in the gas phase. The RI[28] approximation was used for GGA calculations. Geometry optimisations have been carried out at the BP86-D3BJ/def2-TZVP[29] level of theory. Chemcraft[30] was used to visualise the results.

Cartesian Coordinates for Optimised Structures

[(IMes)Ni(η³-PhNCS)₃] (3a)

```
Ni   1.98625332372706    1.58703957561642   11.25532597709465
S   -1.17044803488948    1.51210007558792   11.74367951381526
S    2.89280034351997    3.47173486319349   11.83008523241887
S    1.04343478083715   -0.26755863010329   10.68900126006957
N    4.33055134924548   -0.23560627704335   11.15800866080644
N    4.53868265599221    1.39717970261069    9.76250131810997
N    1.34126213838327    5.63471788375524   12.52015854445825
N    0.26486363486928    3.62083082105432   12.16189593181931
N   -1.57874974230275   -0.95241411327786   11.06903690672367
C    3.68925362082190    0.88878939596595   10.70975681202558
C    1.46506046972504    4.39680390265422   12.20211392845331
C    4.32124280376796    2.62113944136216    9.03805338473279
C    2.41507883985116    6.52799407615927   12.45703427543819
C    0.34557568943188    2.33530395107247   11.75911811198576
C    5.67637034063613    0.60715831034461    9.62495606252846
H    6.45636879427018    0.85153378549516    8.91567727135766
```

```
C   -1.33851550972632    -2.28866079252358    10.71906207781270
C    3.22635526454920     6.64743213060286    11.31083263594678
H    3.05409860092322     5.98367831173744    10.46380462583333
C    5.10117853529903     3.74090062405416     9.37416137071580
C   -0.63239911694243    -0.08780840531305    11.13835612350947
C    5.54679182567589    -0.41964255700873    10.50658789334000
H    6.19551390469977    -1.25433875158714    10.73793137582472
C    3.10713297148366     3.89029171088623     7.40941640103663
H    2.33011957606055     3.94697453745338     6.64357479299550
C   -0.98244652410922     4.25378457973628    12.51497828887343
C    4.85362119557055     4.93242325163633     8.68940839968631
H    5.44205521620296     5.81508933275915     8.94891249001959
C    3.81666020524089    -1.13340250903874    12.15803316287267
C    3.32926374199798     2.66372914670946     8.04824384381708
C    3.37889009245616    -2.40663718068522    11.75434983744868
C    3.84960647093519     5.03383864384817     7.71895641610075
C    2.63298495221906     7.39958594873818    13.53838338232206
H    1.98651728409807     7.31593272165767    14.41262615896058
C    4.23374852057305     7.60838830540416    11.26294731779717
H    4.84414011149600     7.69966787322365    10.36234858144048
C   -1.71345500601565     4.92258544344980    11.53293393443232
H   -1.32028616314728     4.98009651515997    10.51825940650422
C   -0.41163624109758    -3.08579558624393    11.41816764041506
H    0.18023967984170    -2.64030765965566    12.21753780362276
C   -2.10813282515846    -2.87142321854742     9.69798129179285
H   -2.83667607093854    -2.25101305354733     9.17510655198413
C    2.86329908463864    -3.25439237608772    12.73689733261807
H    2.50903424613948    -4.24292080452291    12.43794846860195
C    3.41647343520821    -2.84211452863345    10.31460224309586
H    3.09750945759896    -2.03111226933820     9.64644473427779
H    2.73843861177682    -3.68969849417280    10.15737622024407
H    4.42660126337629    -3.15273174300166    10.00495952300240
C    4.46487952325836     8.45519168328944    12.35213825963734
H    5.25799407788113     9.20262112930164    12.31073530861326
C    3.65920746520225     8.34249613883830    13.48941270184831
H    3.82395344002282     9.00269309121804    14.34254572173002
C   -1.93172343221543    -4.21322308056033     9.36120822586200
H   -2.52709950256504    -4.64830917504558     8.55681059881313
C    3.76071492074293    -0.70515624864816    13.49212242001754
C   -1.44560641821810     4.16332226525569    13.82773346516785
H   -0.84767973394134     3.63811207222291    14.57234267524302
C    2.51474061324577     1.45287742185841     7.69067101482778
H    3.14019883911023     0.55269346085885     7.60673762975687
H    1.99531708919558     1.60543809700003     6.73639287733303
H    1.75994571839484     1.23706350251062     8.46429892236922
C   -0.26233963672242    -4.43200315237580    11.09051510844413
H    0.44402644435179    -5.04565280650479    11.65273604997698
C    2.75632683632662    -2.85986301994673    14.07601036490174
C   -2.93441386443697     5.50505564776417    11.87279394497430
H   -3.51322644094886     6.03060933704464    11.11274178378276
C   -1.01074000501346    -5.00293235768218    10.05603601952193
H   -0.88593571662605    -6.05619324019244     9.80213117758422
C    3.56043117317598     6.35489568783638     7.05590467615873
H    4.48730074595970     6.87064983404607     6.76704042542957
H    3.01782268183072     7.02395171294357     7.74270242098409
H    2.94240315691397     6.22728695506375     6.15760678497155
```

```
C   6.13688028438778      3.68963508336616     10.46449683171919
H   5.77142922354935      3.12902135398563     11.33546577928425
H   6.38486181867521      4.70438338223653     10.79853258170115
H   7.06686554268109      3.20655189606693     10.12645980002716
C   3.21500684914461     -1.58839952632599     14.43211849165005
H   3.15269196270157     -1.26850951308033     15.47478076574484
C   4.24858747944947      0.65343371460087     13.90945669408034
H   5.20276923934137      0.90843655121860     13.42654939962379
H   4.38676700770070      0.69658232595622     14.99702345761578
H   3.53255101886825      1.43987131467220     13.62076843482913
C  -2.66840728927427      4.74758915004569     14.15920392811119
H  -3.04003444168345      4.68121819319717     15.18214589197804
C  -3.41221918267345      5.41670110497599     13.18340533035406
H  -4.36781655421196      5.87221547920801     13.44552485476949
C   2.13573604478064     -3.77888186084437     15.09543028393374
H   1.04622279278276     -3.84535004288882     14.94851913902118
H   2.31312625099778     -3.42205209116953     16.11824456055278
H   2.53625617904518     -4.79951738291411     15.01207167827166
```
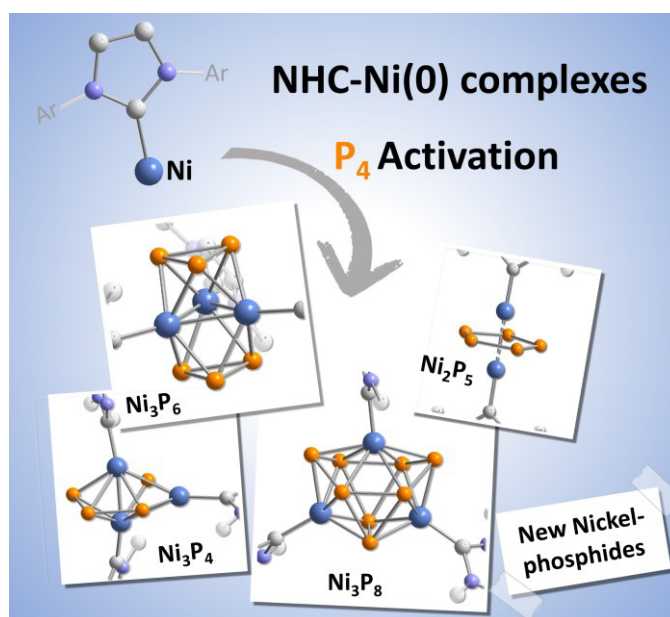
References

[1]   P. Jutzi, *Angew. Chem. Int. Ed. Engl.* **1975**, *14*, 232.

[2]   A. Sekiguchi, R. Kinjo, M. Ichinohe, *Science* **2004**, *305*, 1755.

[3]   H. Bock, H. Mueller, *Inorg. Chem.* **1984**, *23*, 4365.

[4]   O. J. Scherer, *Angew. Chem. Int. Ed.* **2000**, *39, 1029*, 1029.

[5]   N. A. Piro, J. Si Figueroa, J. T. McKellar, C. C. Cummins, *Science* **2006**, *313*, 1276.

[6]   D. Tofan, C. C. Cummins, *Angew. Chem. Int. Ed.* **2010**, *49*, 7516.

[7]   A. Velian, M. Nava, M. Temprado, Y. Zhou, R. W. Field, C. C. Cummins, *J. Am. Chem. Soc.* **2014**, *136*, 13586.

[8]   L.-P. Wang, D. Tofan, J. Chen, T. van Voorhis, C. C. Cummins, *RSC Adv.* **2013**, *3*, 23166.

[9]   D. Rottschäfer, B. Neumann, H.-G. Stammler, R. Kishi, M. Nakano, R. S. Ghadwal, *Chem. Eur. J.* **2019**, *25*, 3244.

[10]   H. W. Melville, S. C. Gray, *Trans. Faraday Soc.* **1936**, *32*, 271.

[11]   G. Hierlmeier, A. Hinz, R. Wolf, J. M. Goicoechea, *Angew. Chem. Int. Ed.* **2018**, *57*, 431.

[12]   B. Zarzycki, T. Zell, D. Schmidt, U. Radius, *Eur. J. Inorg. Chem.* **2013**, *2013*, 2051.

[13]   S. Pelties, R. Wolf, *Organometallics* **2016**, *35*, 2722.

[14]   a) C. Bianchini, D. Masi, C. Mealli, A. Meli, *J. Organomet. Chem.* **1983**, *247*, C29-C31; b) P. Jernakoffm, N. J. Cooper, *J. Am. Chem. Soc.* **1989**, *111*, 7424; c) Q. Shen, H. Li, C. Yao, Y. Yao, L. Zhang, K. Yu, *Organometallics* **2001**, *20*, 3070; d) Y.-J. Kim, J.-T. Han, S. Kang, W. S. Han, S. W. Lee, *Dalton Trans.* **2003**, 3357; e) C. Wycliff, A. G. Samuelson, M. Nethaji, *Inorg. Chem.* **1996**, *35*, 5427; f) W. Mei, L. Shiwei, B. Meizhi, G. Hefu, *J. Organomet. Chem.* **1993**, *447*, 227; g) L. D. Field, W. J. Shaw, P. Turner, *Organometallics* **2001**, *20*, 3491; h) J. Cámpora, I. Matas, P. Palma, E. Álvarez, C. Graiff, A. Tiripicchio, *Organometallics* **2007**, *26*, 3840; i) K.-E. Lee, X. Chang, Y.-J. Kim, H. S. Huh, S. W. Lee, *Organometallics* **2008**, *27*, 5566; j) S. H. Bertz, Y. Moazami, M. D. Murphy, C. A. Ogle, J. D. Richter, A. A. Thomas, *J. Am. Chem. Soc.* **2010**, *132*, 9549.

[15]   Kenji Itoh, I. Matsuda, F. Ueda, Y. Ishii, James A. Ibers, *J. Am. Chem. Soc.* **1977**, *99*, 2118.

[16]   L. T. Scharf, A. Kowsari, T. Scherpf, K.-S. Feichtner, V. H. Gessner, *Organometallics* **2019**, *38*, 4093.

[17]   a) C. Bianchini, C. A. Ghilardi, A. Meli, S. Midollini, A. Orlandini, *J. Chem. Soc., Chem. Commun.* **1983**, 753; b) R. Beck, M. Shoshani, J. Krasinkiewicz, J. A. Hatnean, S. A. Johnson, *Dalton Trans.* **2013**, *42*, 1461.

[18]   A. Bheemaraju, J. W. Beattie, E. G. Tabasan, P. D. Martin, R. L. Lord, S. Groysman, *Organometallics* **2013**, *32*, 2952.

[19]   T. K. N. Kuhn, *Synthesis* **1993**, 561.

[20]   M. R. Elsby, J. Liu, S. Zhu, L. Hu, G. Huang, S. A. Johnson, *Organometallics* **2019**, *38*, 436.

[21] a) Sheldrick, G. M. SADABS, Bruker AXS, Madison, USA **2007**; b) CrysAlisPro, Scale3 Abspack, Rigaku Oxford Diffraction **2019**.

[22] R. C. Clark, J. S. Reid, *Acta Cryst. A* **1995**, *51*, 887.

[23] G. M. Sheldrick, *Acta Cryst. A* **2015**, *71*, 3.

[24] O. V. Dolomanov, L. J. Bourhis, R. J. Gildea, J. A. K. Howard, H. Puschmann, *J .Appl. Crystallogr.* **2009**, *42*, 339.

[25] G. M. Sheldrick, *Acta Cryst. C* **2015**, *71*, 3.

[26] G. M. Sheldrick, *Acta Cryst. A* **2008**, *64*, 112.

[27] R. A. Kendall, H. A. Früchtl, *Theor. Chem. Acc.* **1997**, *97*, 158.

[28] F. Weigend, *Phys. Chem. Chem. Phys.* **2002**, *4*, 4285.

[29] a) Becke, *Physical Rev. A* **1988**, *38*, 3098; b) Perdew, *Phys. Rev. B* **1986**, *33*, 8822; c) S. Grimme, S. Ehrlich, L. Goerigk, *J. Comput. Chem.* **2011**, *32*, 1456; d) S. Grimme, J. Antony, S. Ehrlich, H. Krieg, *J. Chem. Phys.* **2010**, *132*, 154104; e) F. Weigend, R. Ahlrichs, *Phys. Chem. Chem. Phys.* **2005**, *7*, 3297.

[30] Chemcraft - graphical software for visualisation of quantum chemistry computations. https://www.chemcraftprog.com.

64

3   Aggregation and Degradation of White Phosphorus Mediated by N-Heterocyclic Carbene Nickel(0) Complexes[a,b]

Abstract: The reaction of zerovalent nickel compounds with white phosphorus (P_4) is a barely explored route to binary nickel phosphide clusters. Here, we show that coordinatively and electronically unsaturated N-heterocyclic carbene (NHC) nickel(0) complexes afford unusual cluster compounds with P_1, P_3, P_5 and P_8 units. Using [Ni(IMes)$_2$] [IMes = 1,3-bis(2,4,6-trimethylphenyl)imidazolin-2-ylidene], electron-deficient Ni$_3$P$_4$ and Ni$_3$P$_6$ clusters have been isolated, which can be described as *superhypercloso* and *hypercloso* clusters according to the Wade-Mingos rules. Use of the bulkier NHC complexes [Ni(IPr)$_2$] or [(IPr)Ni(η^6-toluene)] [IPr = 1,3-bis(2,6-di-*iso*-propylphenyl)imidazolin-2-ylidene] affords a *closo*-Ni$_3$P$_8$ cluster. Inverse-sandwich complexes [(NHC)$_2$Ni$_2$P$_5$] (NHC=IMes, IPr) with an aromatic cyclo-P$_5^-$ ligand were identified as additional products.

3.1   Introduction

Reactions of transition metal complexes with white phosphorus present a powerful strategy to access binary metal phosphide frameworks, and the structural motifs of the resulting compounds are highly diverse.[1,2] On the one hand, degradation of P_4 to products containing one to four phosphorus atoms is of tremendous industrial relevance, in order to improve the processes used in the production of organophosphorus compounds.[3] On the other hand, the aggregation of P_4 to polyphosphorus compounds with five or more phosphorus atoms is essential for understanding the structure and bonding in metal phosphides.[4]

The use of nickel as a metal for P_4 activation may result in unique nickel phosphide clusters. Besides a few reactions of P_4 with Ni(II) species, e.g. the formation of the sandwich compound $[\{(triphos)Ni\}_2(\mu_2,\eta^{3:3}\text{-}cyclo\text{-}P_3)](BF_4)_2$ (triphos $=$ $Me(CH_2CH_2PPh_2)_3$),[5] known examples typically involve Ni in the +I oxidation state. Cyclopentadienyl-substituted Ni(I) radicals are particularly useful, as the outcome of photolysis or thermolysis reactions of nickel complexes of the type $[Cp^xNi(CO)_2]_2$ with P_4 is highly dependent on the size of the Cp ligand used.[6] Relatively small cyclopentadienyl ligands such as Cp* or Cp'' (1,3-tBu$_2$C$_5$H$_3$) lead to the tetranuclear heterocubane clusters $[\{Cp^*Ni\}_3(\mu_3,\eta^{2:2:2}\text{-}P_4)(\mu_3\text{-}P)]$ and $[\{Cp^RNi(\mu_3\text{-}P)\}_4]$ (Cp^R = Cp*, Cp''], and the sandwich complex $[Cp^RNi(\eta^3\text{-}P_3)]$ (Cp^R = Cp*, 1,2,4-tBu$_3$C$_5$H$_2$), whereas a trigonal prismatic structure $[\{Cp^{iPr}Ni\}_2(\mu_2,\eta^{3:3}\text{-}P_4)]$ (Cp^{iPr} = 1,2,3,4-iPr$_4$C$_5$H) is accessed by using a superbulky tetra-*iso*-propylcyclopentadienyl ligand. Our group recently showed that [CpNi(NHC)] (NHC = IMes, IPr) radicals can selectively activate P_4 to afford $\mu_2,\eta^1{:}\eta^1\text{-}P_4$ butterfly complexes.[7]

In contrast to Ni(I) compounds, only a few examples of P_4 activation using Ni(0) sources have been reported (Figure 1).[8–10]
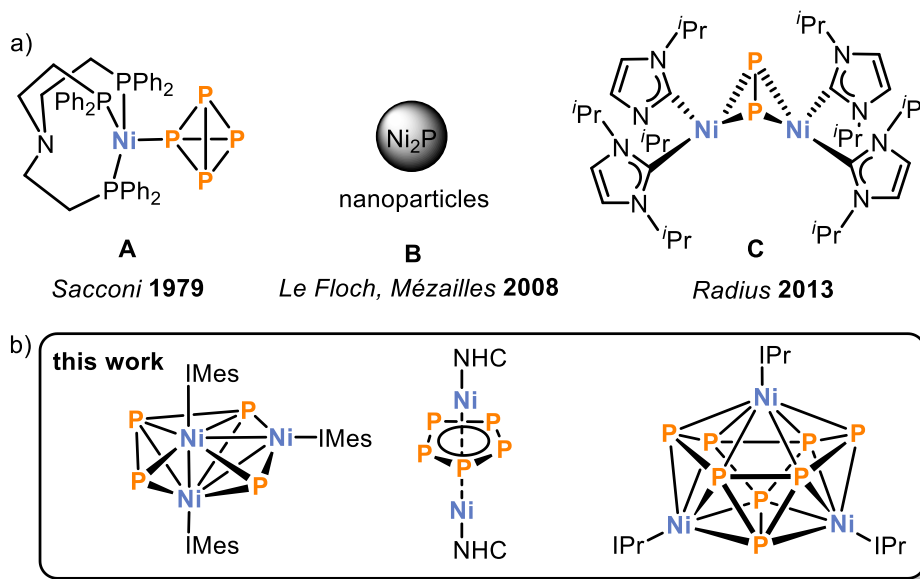

Figure 1. a) Overview of products resulting from P_4 activation using Ni(0) sources; [8-10] b) P_4 activation and aggregation products described herein.

In seminal work dating back to 1979, Sacconi and co-workers reported the formation of the complex [(κ^3-P,P,P-NP$_3$)Ni(η^1-P$_4$)] (**A**, NP$_3$ = tris(2-diphenylphosphinoethyl)amine) containing an intact, end-on coordinated P$_4$ tetrahedron.[8] Moreover, Le Floch and Mézailles reported on the use of [Ni(cod)$_2$] (cod = 1,4-cycloocta-1,5-diene) for the synthesis of nickel phosphide nanoparticles.[9] More recently, the group of Radius reported the synthesis of the butterfly compound [{Ni(ImiPr$_2$)$_2$}$_2$(μ,$\eta^{2:2}$-P$_2$)] (**C**, ImiPr$_2$ = 1,3-bis(*iso*-propyl)imidazolin-2-ylidene) by reaction of cod-stabilised Ni(ImiPr$_2$)$_2$ fragments with P$_4$.[10] While these examples demonstrate both the coordination and degradation of P$_4$ by 14 valence electron (VE) and 18 VE Ni(0) compounds, examples of P$_4$ aggregation using Ni(0) appear to be unknown, despite an unsuccessful attempt to synthesise a sandwich complex containing a pentaphosphacyclopentadienide ligand *cyclo*-P$_5^-$ by Hey-Hawkins and co-workers.[11]

3.2   Results and Discussion

Building on our previous work on P_4 activation with N-heterocyclic carbene (NHC) nickel(I) complexes,[7,12] we recently became interested in studying the reactivity of related Ni(0) complexes. NHC complexes seemed promising because they can be stabilised by various labile ligands, e.g. the carbenes themselves, alkenes, and arenes. After synthesising a range of known NHC compounds, including the bis(carbene) complexes [Ni(NHC)$_2$] (NHC = IMes, IPr),[13,14] vinyltrimethylsilane complexes [(NHC)Ni(η^2-H$_2$C=CHSiMe$_3$)$_2$][15,16] (NHC = IMes, IPr) and the toluene complex [(IPr)Ni(η^6-toluene)],[17] we proceeded to systematically study the reactivity of these compounds toward P_4. Reactions of [(NHC)Ni(η^2-H$_2$C=CHSiMe$_3$)$_2$] (NHC = IMes, IPr) with different amounts of P_4 afforded black, insoluble material that was not characterised any further. We next turned our attention from nickel complexes comprising labile alkene ligands to the less reactive [Ni(IMes)$_2$]. Gratifyingly, the ^{31}P{^{1}H} NMR spectrum of the reaction of [Ni(IMes)$_2$] with P_4 (0.5 equivalents) in toluene suggested formation of a major product, characterised by two main signals in a 1:1 ratio (Scheme 1). A single crystal X-ray diffraction (XRD) study of large block-shaped crystals grown from toluene revealed the formation of the trinuclear nickel phosphorus cluster [(IMes)$_3$Ni$_3$P$_4$] (**1**) (Figure 2).
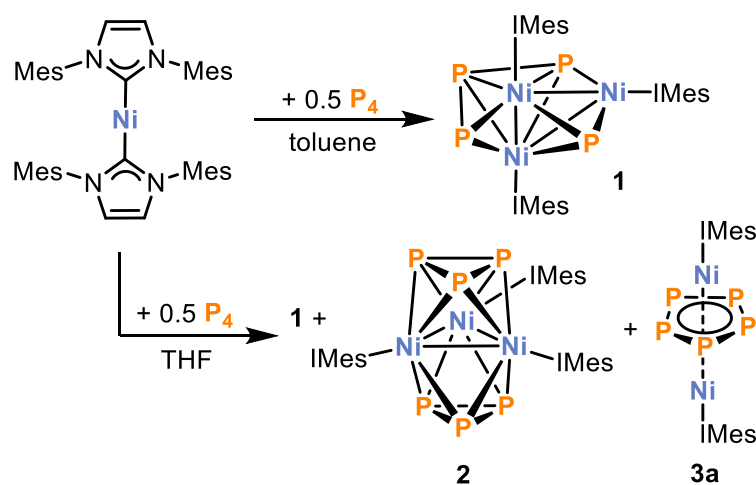
Scheme 1. Reactivity of [Ni(IMes)$_2$] toward P_4.

The molecular structure of **1** is reminiscent of the distorted kite-like *cyclo*-P_4 complex [(Cp′Fe)$_2$(μ-P_4)] reported by Walter and co-workers.[18] However, **1** can be described as a bicapped trigonal bipyramid featuring a Ni$_3$ triangle with one short Ni2−Ni3 bond (2.3720(3) Å) and two long nickel-nickel bonds (Ni1−Ni2: 2.7533(3) Å and Ni1−Ni3: 2.6528(3) Å). Ni$_3$ triangles are a common structure motif, e.g. in carbonyl or phosphine stabilised clusters.[19] The Ni$_3$ triangle is capped by two phosphorus atoms P1 and P4. The P4 atom is part of a P$_3$-chain with P−P bond lengths of 2.1671(5) (P2−P3) and 2.1754(5) Å (P3−P4), which are in the range commonly observed for P−P single bonds. Notably, the P_4 plane and the Ni$_3$ plane are almost perpendicular with a plane twist angle of 89.6 °.
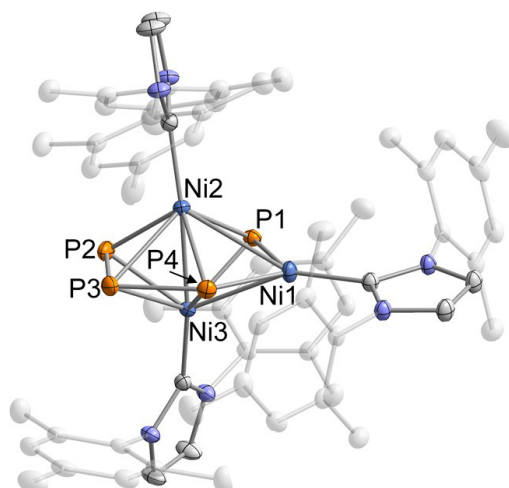
Figure 2. Molecular structure of **1** in the solid state. Thermal ellipsoids are set at the 50% probability level. Hydrogen atoms and solvent molecules are omitted for clarity. Selected bond lengths [Å] and angles [°]: Ni1−Ni2 2.7533(3), Ni2−Ni3 2.3720(3), Ni3−Ni1 2.6528(3), Ni1−P1 2.1045(4), Ni2−P1 2.1739(4), Ni3−P1 2.1720(4), P2−P3 2.1671(5), P3−P4 2.1754(5), Ni3−Ni2−Ni1 61.815(9), Ni2−Ni3−Ni1 66.177(9), Ni3−Ni1−Ni2 52.009(8), P2−P3−P4 106.89(2), Ni1−P4−P3 133.21(2), P1−Ni1−P4 99.288(16).

Compound **1** can be isolated in pure form as a black crystalline solid in 20% yield. As expected from analysis of the initial reaction mixture, $^{31}P\{^1H\}$ NMR measurements of pure **1** dissolved in C_6D_6 revealed two signals at chemical shifts of 463.1 ppm (P1/P4) and 105.6 ppm (P2/P3, averaged J_{PP} = 67.0 Hz), which are assigned to **1**. Notably, the observation of just two $^{31}P\{^1H\}$ NMR resonances is in apparent contrast with the presence of four distinct P atom positions in the solid-state XRD structure of **1**. An additional minor signal is observed at 134.0 ppm. This signal is assigned to an unidentified species, which may be an isomer of **1**. A variable temperature (VT) NMR study showed that the integral ratio of signal P1/P4 to P2/P3 remains constant at 1:1, whereas the intensity of the signal at 134.0 ppm increases with higher temperatures and disappears upon cooling the solution to 283 K (see the Supporting Information for spectra). In order to understand this dynamic behaviour, DFT calculations were performed on a truncated model compound, where the mesityl substituents at the NHC moieties were replaced by phenyl groups. The calculations reproduce the asymmetric molecular structure of **1**, but also reveal an isoenergetic isomer (ΔE = −0.3 kcal mol^{-1}) with a more symmetrical Ni_3P_4 core (see the Supporting Information for details). The fluxional behaviour observed by NMR spectroscopy can presumably be attributed to an exchange process between P1/P4 and P2/P3, which proceeds via this symmetrical isomer or a symmetrical transition state with a low energy (ΔE = 2.6 kcal mol^{-1}). The ^1H NMR spectra are in good agreement with these findings, exhibiting three different signal sets for the IMes ligand and similar thermal dependence of the integral ratios.

Analysis of **1** by liquid field ionisation desorption mass spectrometry (LIFDI-MS) revealed a molecular ion peak at m/z = 1212.295 in good agreement with the calculated molecular ion peak (1212.278). The cyclic voltammogram of **1** (THF/[nBu$_4$N]PF$_6$, depicted in the Supporting

Information of the thesis) features two reversible redox events at $E_{1/2} = -1.07$ and -2.76 V (vs. Fc/Fc$^+$), which may be assigned to the reversible oxidation and reduction of the complex, respectively.

The bonding situation in **1** was analysed by means of localised orbitals. In particular, intrinsic bond orbitals (IBO) were constructed starting from a BP86/def2-TZVP wavefunction. Looking at the composition of those orbitals, six filled orbitals involving multicentre bonds between the Ni and P atoms could be identified along with a $3d^{10}$ configuration for each Ni atom (see the Supporting Information for a depiction). This is consistent with classical electron-counting rules.[20] Thus, the cluster may be defined as a *superhypercloso*-cluster ($12 = 2(n-1)$, $n = 7$, number of cluster atoms).

The reaction of [Ni(IMes)$_2$] with P$_4$ is significantly less selective when THF is used as a solvent instead of toluene. Besides **1**, two other products formed could be identified by ^{31}P{^{1}H} NMR spectroscopy and X-ray crystallography. After work-up, brown crystals of the trinuclear cluster [(IMes)$_3$Ni$_3$P$_6$] (**2**) were obtained from *n*-hexane (Figure 3). Structural analysis of **2** reveals a distorted tricapped trigonal prism (or, equivalently, two facial Ni$_3$P$_3$ octahedra sharing a common Ni$_3$ face). Notably, compounds featuring pnictogen (P, As) prisms with iron or cobalt are usually stabilised by anionic cyclopentadienyl ligands.[21] Similar to **1**, an unsymmetrical Ni$_3$-triangle is observed (Ni1−Ni2 2.4835(3) Å, Ni1−Ni3 2.4882(3) Å, Ni2−Ni3 2.6429(3) Å). The P−P bond lengths range from 2.2055(4) to 2.2700(4) Å consistent with P−P single bonds. The ^{31}P{^{1}H} NMR spectrum in C$_6$D$_6$ shows a broad resonance at −8.6 ppm. The bonding situation in **2** was analysed similarly to that in cluster **1**. In accordance with electron-counting rules, nine doubly occupied orbitals of multicentre bonds between the cluster atoms were identified (see the Supporting Information for a depiction). Thus, due to its closed deltahedral structure (distorted tricapped trigonal prism) and fulfilment of the $2n$ cluster electron rule (n = 9), **2** can be described as a 9-vertex *hypercloso*-cluster. Additionally, a $3d^{10}$ configuration for each Ni atom in **2** could be derived from the analysis of the IBO (see the Supporting Information for details).
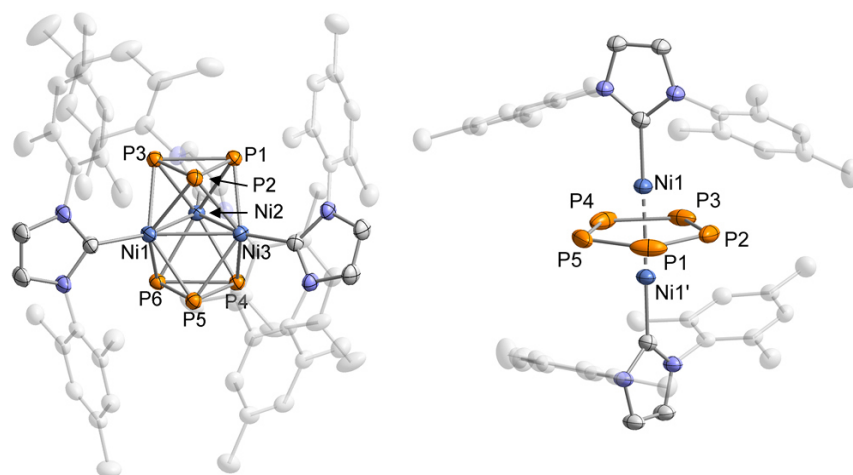
Figure 3. Molecular structure of **2** (left) and **3a** (right) in the solid state. Thermal ellipsoids are set at the 50% probability level. Hydrogen atoms, solvent molecules and disorder in the P_5 ring (3a) are omitted for clarity. Selected bond lengths [Å] and angles [°] for 2: Ni1−Ni2 2.4834(3), Ni1−Ni3 2.4883(3), Ni2−Ni3 2.6432(3), P1−P2 2.2087(5), P2−P3 2.2698(5), P1−P3 2.2156(5), P4−P5 2.2116(5), P5−P6 2.2822(5), P4−P6 2.2049(5), Ni2−Ni1−Ni3 64.233(10), Ni1−Ni2−Ni3 57.974(9), Ni1−Ni3−Ni2 57.793(9), P2−P1−P3 61.729(16), P1−P2−P3 59.285(16), P1−P3−P2 58.985(16), P6−P4−P5 62.226(16), P4−P5−P6 58.744(16), P4−P6−P5 59.030(16); 3a: Ni1−Ni1′ 2.6339(13), P1−P2 2.182(8), P2−P3 2.194(7), P3−P4 2.205(8) P4−P5 2.211(9), P5−P1 2.207(7), P2−P1−P5 108.2(2), P1−P2−P3 108.7(2), P2−P3−P4 107.6(3), P3−P4−P5 108.1(3), P1−P5−P4 107.4(3).

Moreover, we were able to identify [(IMes)$_2$Ni$_2$P$_5$] (**3a**) as a side product. This compound co-crystallises with **2** from the mother liquor of the reaction mixture of [Ni(IMes)$_2$] with P$_4$. Structural analysis of crystals of the composition [(IMes)$_3$Ni$_3$P$_6$]·[(IMes)$_2$Ni$_2$P$_5$] (**2·3a**) revealed that compound **3a** features a dinuclear inverse sandwich structure in the solid state with a bridging *cyclo*-P$_5^−$ ligand (Figure 3). The Ni1−Ni1′ distance is 2.6339(13) Å and the P−P bond lengths range from 2.182(8) to 2.211(9) Å, which is in the common range observed for dinuclear 3d transition metal complexes with bridging *cyclo*-P$_5^−$ ligands.[22] The pentaphosphacyclopentadienyl ligand is frequently observed in transition metal mediated P$_4$ activation.[1] However, most complexes comprising such a *cyclo*-P$_5^−$ ligand feature group 8 metals and there are only a few examples of other transition metal complexes.[23] Furthermore, all known *cyclo*-P$_5^−$ complexes additionally contain cyclopentadienyl ligands, while complex **3a** is stabilised by an L-type ligand.

Having established the ability of [Ni(IMes)$_2$] to act as a precursor to interesting Ni/P clusters, we proceeded with performing the analogous reactions using the bulkier carbene complex [Ni(IPr)$_2$] in order to examine if there is any difference in product distribution (Scheme 2). And, indeed, in contrast to observations made using [Ni(IMes)$_2$], ^{31}P{^{1}H} NMR spectroscopy revealed no resonances. Nevertheless, the ^{1}H NMR spectrum clearly showed the formation of free IPr and one new distinct diamagnetic IPr environment.
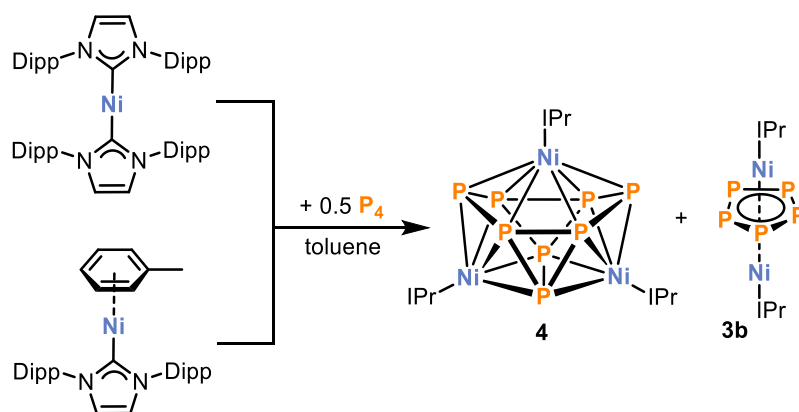
Scheme 2. Reactivity of [Ni(IPr)$_2$] and [(IPr)Ni(η^6-toluene)] toward P$_4$.

Furthermore, a single crystal X-ray diffraction study on crystals grown from toluene revealed the formation of [(IPr)$_3$Ni$_3$P$_8$] (**4**), an 11-vertex *closo*-cluster with 24 cluster electrons, adopting an octadecahedral geometry similar to the undecaborate anion [B$_{11}$H$_{11}$]$^{2-}$ (Figure 4).[24] The homoquadricyclane-like P$_8$ framework is reminiscent of the P$_8$ subunits in Hittorf's phosphorus and can be seen as a formal insertion product of Ni in one of the P−P bonds of such a subunit.[25] Nevertheless, to the best of our knowledge, this is the first example of such a P$_8$ framework in an isolated molecular compound.[4] The structure of compound **4** again comprises three Ni atoms, but the Ni⋯Ni distances are significantly longer than in complexes **1** and **2** [Ni1⋯Ni2 3.3246(18) Å and Ni2⋯Ni2′ 3.636(2) Å]. Ni1 is coordinated by six P atoms (P1, P1′, P2, P2′, P3, P3′) and Ni2/Ni2′ are coordinated by five P atoms (P1, P2, P3, P4, P4′ for Ni2 and P1′, P2′, P3′, P4, P4′ for Ni2′). The P$_8$-framework contains short P−P bonds ranging from 2.201(3) to 2.288(3) Å (P1−P3, P1−P2, P2−P3′), and long P−P bonds with bond lengths from 2.349(4) to 2.459(3) Å (P4−P4′, P3−P4′, P2−P4).
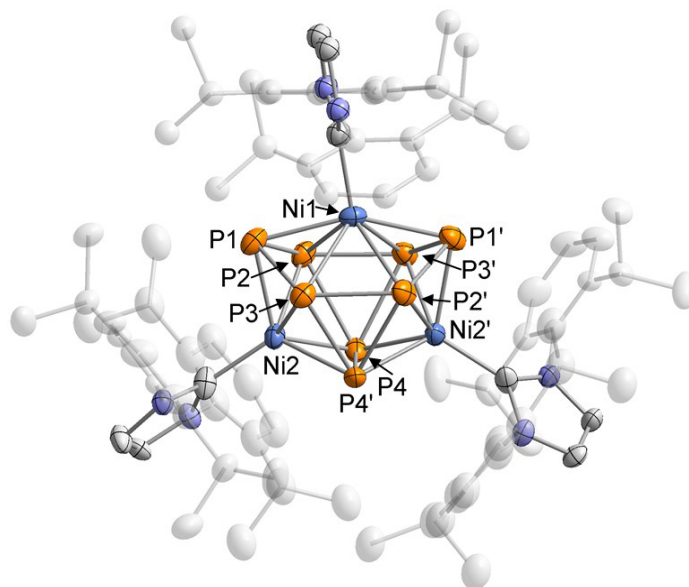
Figure 4. Molecular structure of **4** in the solid state. Thermal ellipsoids are set at the 50% probability level. Hydrogen atoms, solvent molecules and disorder in the IPr ligand are omitted for clarity. Selected bond lengths [Å] and angles [°]: Ni1…Ni2 3.3246(18), Ni2…Ni2′ 3.636(2), P1−P2 2.205(3), P1−P3 2.201(3), P2−P3′ 2.288(3), P2−P4 2.459(3), P3−P4′ 2.434(3), P4−P4′ 2.349(4), Ni2−Ni1−Ni1′ 66.31(5), Ni1−Ni2−Ni2′ 56.85(3), P3−P1−P2 103.21(11), P3′−P2−P4 61.57(8), P2′−P3−P4′ 62.67(9), P3′−P4−P2 55.77(8).

^{1}H and ^{13}C{^{1}H} NMR spectra of crystals of **4** dissolved in C$_6$D$_6$ showed only one set of IPr signals despite the presence of two distinct IPr environments in the solid-state structure. This evidence for fluxionality in solution was further confirmed by variable temperature ^{31}P{^{1}H} NMR spectroscopy (Figure 5). Coincidentally, the spectrum recorded at room temperature exhibits an extremely broad signal that could not be resolved. However, heating up the solution results in one broad resonance, whereas cooling the solution to 193 K afforded three signals with an integral ratio of 4 : 2 : 2, at chemical shifts of −136.2 (P2, P2′, P3, P3′), 97.0 (P1, P1′ or P4, P4′) and 124.6 ppm (P1, P1′ or P4, P4′), which is in agreement with the presence of three different P environments as suggested by the crystallographic study. Even at 193 K, the couplings could not be resolved completely.
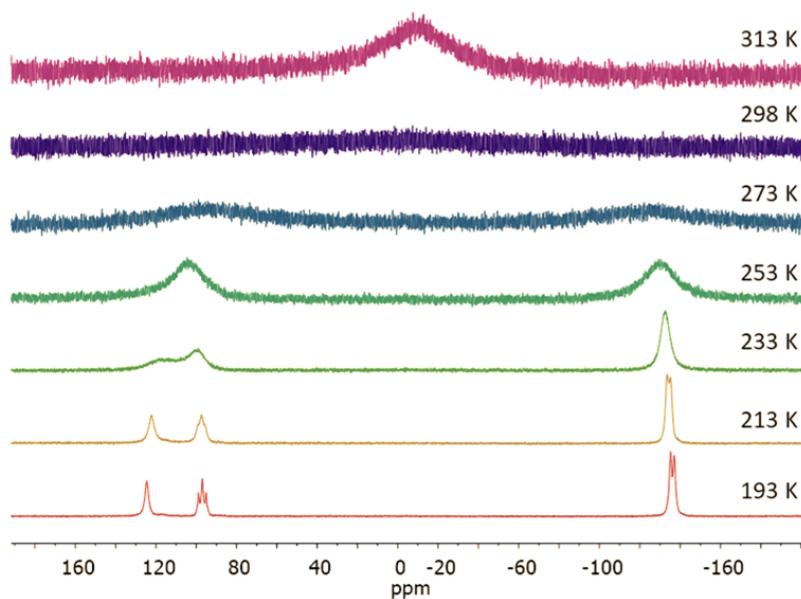
Figure 5. VT $^{31}P\{^{1}H\}$ NMR spectra of $[(IPr)_3Ni_3P_8]$ (**3**) in toluene-d_8.[26]

Unfortunately, separation of free IPr from compound **4** proved to be challenging. The use of $[(IPr)Ni(\eta^6\text{-toluene})]$ as an attractive precursor was therefore pursued and led to the isolation of pure **4** as a dark green powder in 41% yield. The cyclic voltammogram of **4** (THF/$[nBu_4N]PF_6$, see Supporting Information) shows one reversible oxidation wave at $E_{1/2}= -0.76$ V (vs. Fc/Fc$^+$). Analysis of the IBO reveals 12 orbitals that involve bonding between the cluster atoms again being in accordance with established electron-counting rules. Thus **4** obeys the $2(n+1)$ ($n = 11$) electron count rule of a 11-vertex *closo*-cluster (see the Supporting Information for a depiction of the IBO). The same analysis additionally allows for the assignment of a d^8-configuration for the Ni1 atom and d^{10}-configurations for Ni2/Ni2′.

Apart from **4**, the reaction of $[(IPr)Ni(\eta^6\text{-toluene})]$ with P_4 also affords green crystals of $[(IPr)_2Ni_2(\mu\text{-}P_5)]$ (**3b**), which were obtained from the *n*-hexane washing solution and identified by X-ray crystallography. Complex **3b** is isostructural with **3a** and features similar Ni−Ni and P−P bond lengths (see the Supporting Information for further details).

The electronic structure of a slightly truncated model complex **3′** ($[(IPh)_2Ni_2P_5]$, IPh = 1,3-diphenylimidazolin-2-ylidene) was calculated at the TPSSh/IGLO-III (CP(PPP) on Ni) level of theory.[27] This method was chosen since it has proven to yield reliable results for the calculation of magnetic properties. Significant interactions between the Ni atoms (Mayer bond order: 0.8) as well as the Ni atoms and the aromatic P_5 ring were found (Mayer bond order: 0.5). The X-band EPR spectrum of **3b** (Figure 6) recorded in a toluene glass at 20 K reveals an axial signal pattern for an $S = \frac{1}{2}$ system showing hyperfine interactions with all five phosphorus atoms. A satisfactory simulation of the experimental spectrum was obtained assuming hyperfine interactions with five equivalent phosphorus atoms ($g_{11} = g_{22} = 2.186$ (2.11), $g_{33} = 1.987$ (2.01), $A^{31P}_{33} = 30.0$ MHz (27.5 MHz, averaged value, DFT-calculated values of **3′** in parentheses; see the Supporting Information). Given the good agreement between the measured and DFT calculated EPR

parameters, the calculated and the true electronic structure should resemble each other closely. Thus, according to our DFT calculations, the spin density in **3′** is dominantly localised and evenly distributed between the Ni atoms (Figure 6).
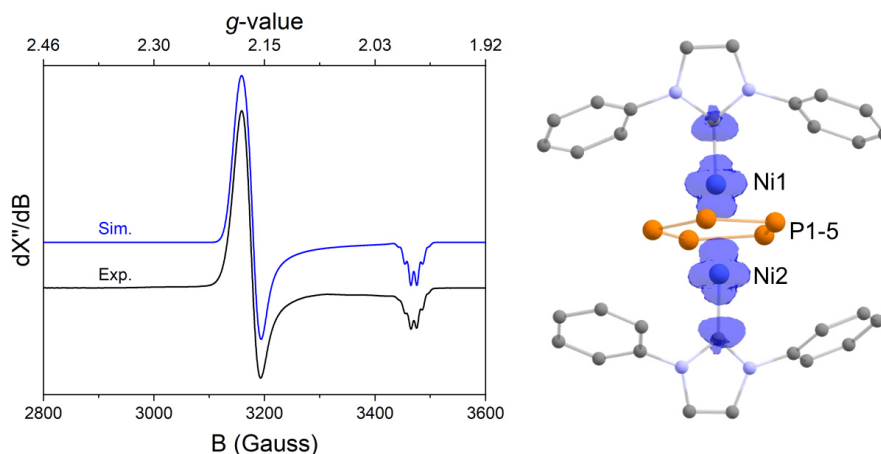

Figure 6. Left: spin density (blue) of [(IPh)$_2$Ni$_2$P$_5$] (**3′**), right: experimental and simulated X-band EPR spectrum of **3b** in a toluene glass at 20 K. Freq. 9.6508 GHz, 0.6325 mW, 20 K, mod. 4.000 Gauss; g-tensor parameters obtained from simulations and DFT calculations are: $g_{11} = g_{22} = 2.186$ (2.11), $g_{33} = 1.987$ (2.01) (DFT-calculated values for **3′** in parentheses).

3.3 Conclusion

To conclude, reactions of N-heterocyclic carbene nickel(0) complexes with P$_4$ afford unprecedented nickel phosphorus clusters. These reactions clearly show an impact of the size of the NHC ligand on the products obtained. Upon increasing the steric demand from I*i*Pr$_2$ to IMes, di- and trinuclear complexes with Ni$_3$P$_4$ (**1**), Ni$_3$P$_6$ (**2**) cores as well as Ni$_2$P$_5$ (**3a**) were obtained. Notably, **3a** represents the first nickel pentaphosphacyclopentadienyl complex. The bulky NHC IPr again changes the outcome of the reaction to afford a Ni$_3$P$_8$ (**4**) *closo*-cluster with a novel homoquadricyclane-like P$_8$-framework. Bulky substituents on the NHC ligands presumably facilitate the formation of monocarbene nickel fragments observed in the molecular structures of **1−4**. However, the mechanism of formation of these products is obviously complex, and the details of the initial P$_4$ activation process and the subsequent transformations of the resulting intermediates must be revealed by further studies. Moreover, we are currently investigating the use of **1−4** as single-source precursors for the preparation of nickel phosphides as electrocatalysts for hydrogen evolution.[28]

3.4   Experimental Details

General Synthetic Methods

All reactions and product manipulations were carried out in flame-dried glassware under an inert atmosphere of argon using standard Schlenk-line or glovebox techniques (maintained at <0.1 ppm H_2O and <0.1 ppm O_2). [Ni(IMes)$_2$],[13] [Ni(IPr)$_2$],[14] [Ni(IPr)(toluene)],[17] [(IMes)Ni(η^2-H$_2$C=CHSiMe$_3$)$_2$][16] and [(IPr)Ni(η^2-H$_2$C=CHSiMe$_3$)$_2$][15] were prepared according to procedures previously reported in the chemical literature. All other chemicals were purchased from commercial suppliers and used without further purification.

Solvents were dried and degassed with a MBraun SPS800solvent purification system. All dry solvents except *n*-hexane and *n*-pentane were stored under argon over activated 3 Å molecular sieves in gas-tight ampules. *n*-Hexane and *n*-pentane were instead stored over a potassium mirror.

General Analytical Techniques

NMR spectra were recorded on Bruker Avance 300 or 400 spectrometers at 300 K unless otherwise noted and internally referenced to residual solvent resonances (^{1}H NMR: THF-d$_8$: 1.72 ppm, C$_6$D$_6$: 7.16 ppm, toluene-d$_8$: 2.08 ppm; ^{13}C{^{1}H} NMR: THF-d$_8$: 25.31 ppm, C$_6$D$_6$: 128.06 ppm). Chemical shifts δ are given in ppm referring to external standards of tetramethylsilane (^{1}H, ^{13}C{^{1}H}), 85% phosphorus acid (^{31}P and ^{31}P{^{1}H} spectra). ^{1}H and ^{13}C NMR signals were assigned based on 2D NMR spectra (^{1}H,^{1}H-COSY, ^{1}H,^{13}C-HSQC, ^{1}H,^{13}C-HMQC).

UV/Vis spectra were recorded on an Ocean Optics Flame Spectrometer. Mass spectra were recorded by the analytical department at the University of Regensburg using a Jeol AccuTOF GCX. Elemental analysis was performed by the central analytics department of the University of Regensburg.

Cyclic voltammetry experiments were performed in a single-compartment cell inside a nitrogen-filled glovebox using a CH Instruments CHI600E potentiostat. The cell was equipped with a platinum disc working electrode (2 mm diameter) polished with 0.05 μm alumina paste, a platinum wire counter electrode and a silver/silver nitrate reference electrode. The supporting electrolyte, tetra-*n*-butylammonium hexafluorophosphate, was dried in vacuo at 110 °C for three days. All redox potentials are reported versus the ferrocene/ferrocenium (Fc/Fc$^+$) couple. The scan rate is v = 100 mV s^{-1} unless stated otherwise.

The single-crystal X-ray diffraction data were recorded on Rigaku Oxford Diffraction SuperNova Atlas or GV1000 Titan^{S2} diffractometers with Cu-K$_\alpha$ radiation (λ= 1.54184 Å). Crystals were selected under mineral oil, mounted on micromount loops and quench-cooled using an Oxford Cryosystems open flow N$_2$ cooling device. Either semi-empirical multi-scan absorption corrections[29] or analytical ones[30] were applied to the data. The structures were solved with SHELXT[31] solution program using dual methods and by using Olex2 as the graphical interface.[32] The models were refined with ShelXL[33] using full matrix least squares minimisation

on F^2.[34] The hydrogen atoms were located in idealised positions and refined isotropically with a riding model.

Cyclic voltammetry experiments were performed in a single-compartment cell inside a nitrogen-filled glovebox using a CH Instruments CHI600E potentiostat. The cell was equipped with a platinum disc working electrode (2 mm diameter) polished with 0.05 μm alumina paste, a platinum wire counter electrode and a silver/silver nitrate reference electrode. The supporting electrolyte, tetra-*n*-butylammonium hexafluorophosphate, was dried in vacuo at 110 °C for three days. All redox potentials are reported versus the ferrocene/ferrocenium (Fc/Fc$^+$) couple. The scan rate is v = 100 mV·s^{-1} unless stated otherwise.

Synthesis of Compounds

[(IMes)$_3$Ni$_3$P$_4$] (1):

To a mixture of [Ni(IMes)$_2$] (200 mg, 0.30 mmol, 1.0 eq.) and white phosphorus (18 mg, 0.15 mmol, 0.5 eq.) was added cold (−30 °C) toluene (10 mL). The dark blue reaction mixture underwent a colour change to yellow-brown within 1 hour. The solution was stirred at ambient temperature for 18 hours. Subsequently, the solvent was removed under reduced pressure and the dark residue was dried *in vacuo*. The residue was washed with *n*-hexane (3x2 mL) and extracted with toluene (1 mL). Slow diffusion of *n*-hexane into the toluene solution yielded dark black blocks of the solvate **1·toluene**, containing 1 molecule of toluene per molecule of **1**. The crystals were used for a single crystal X-ray structure determination, elemental analysis, LIFDI-MS and UV/Vis spectroscopy.

For NMR spectroscopy, the crystals of **1·toluene** were dissolved in C$_6$D$_6$. Subsequently, the solvent was removed in order to remove toluene. The resulting brown powder was re-dissolved in C$_6$D$_6$.
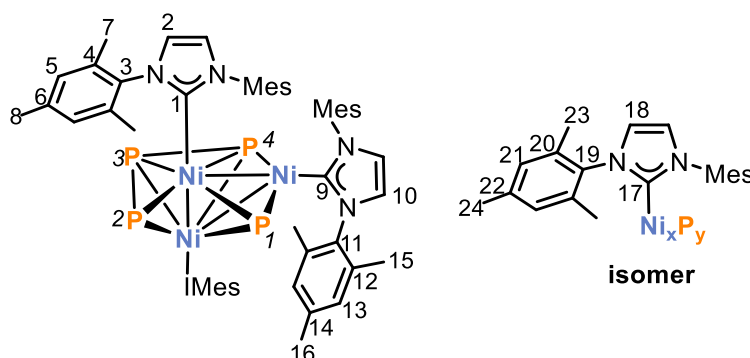
C$_{63}$H$_{72}$N$_6$Ni$_3$P$_4$, MW = 1213.29 g/mol (for dry powder sample)

C$_{70}$H$_{80}$N$_6$Ni$_3$P$_4$, MW = 1305.43 g/mol (for crystals containing 1 eq. of toluene)

Yield: 24 mg (20%)

^{1}H NMR (400 MHz, 300 K, C$_6$D$_6$) δ = 1.93 (s, 12H, C^{7}H), 2.09 (s, 2H, C^{23}H), 2.22 (s, 8H, C^{15}H+C^{24}H), 2.29 (s, 6H, C^{8}H), 2.47 (s, 3H, C^{16}H), 6.07 (s, 2H, C^{2}H), 6.22 (s, 0.4H, C^{18}H), 6.30 (s, 1H, C^{10}H), 6.79 (s, 0.8H, C^{21}H), 6.82 (s, 4H, C^{5}H), 7.00 (s, 2H, C^{13}H) ppm.

^{13}C{^{1}H} NMR (100 MHz, 300 K, C$_6$D$_6$) δ = 18.9 (s, C^{23}), 19.1 (s, C^7), 19.3 (s, C^{15}), 21.4 (s, C^{24}), 21.5 (s, C^8), 21.6 (s, C^{16}), 120.7 (s, C^{18}), 121.1 (s, C^{10}), 121.5 (s, C^2), 129.0 (s, C^5), 129.1 (s, C^{21}), 129.4 (s, C^{13}), 135.5 (s, C^{12}), 135.6 (s, C^{20}), 135.7 (s, C^4), 137.0 (s, C^6), 137.1 (s, C^{22}), 137.3 (s, C^{14}), 137.7 (s, C^{19}), 137.8 (s, C^3), 138.5, (s, C^{11}), 187.7 (brs, C$^{carbene(s)}$) ppm.

^{31}P{^{1}H} NMR (162 MHz, 300 K, C$_6$D$_6$) δ = 105.6 (t, J_{PP} = 67.0 Hz, P2/P3), 134.0 (br s, isomer), 463.1(br s, P1/P4) ppm.

Elemental Analysis calcd. for C$_{63}$H$_{72}$N$_6$Ni$_3$P$_4$·C$_7$H$_8$ (**1**·toluene) C 64.41, H 6.18, N 6.44; found C 64.72, H 6.39, N 6.40.

UV/Vis (THF): λ_{max} (nm, ε_{max} /L·mol^{-1}·cm^{-1}) 300 (17700), 370 (16600), 430 (10500sh).

LIFDI-MS m/z = 1212.295 (calc. 1212.278).

[(IMes)$_3$Ni$_3$P$_6$] (2) and [(IMes)$_3$Ni$_3$P$_6$]·[(IMes)$_2$Ni$_2$P$_5$] (2·3a):

To a mixture of [Ni(IMes)$_2$] (100 mg, 0.15 mmol, 1.0 eq.) and white phosphorus (9 mg, 0.75 mmol, 0.5 eq.) was added cold (−30 °C) THF (5 mL). The dark blue reaction mixture underwent a colour change to yellow-brown within 5 minutes. The solution was stirred at ambient temperature for 2 hours. Subsequently, the solvent was removed under reduced pressure and the dark residue was dried *in vacuo*. The residue was extracted with *n*-hexane (3 x 3 mL) and concentrated to ca. 5 mL. A ^{31}P{^{1}H} NMR spectrum of the crude mixture is shown in the Supporting Information. Dark brown needles of **2** suitable for single crystal X-ray crystallography were obtained by leaving the saturated solution in *n*-hexane at ambient temperature overnight. These crystals were characterised by ^{1}H and ^{31}P{^{1}H} NMR spectroscopy and elemental analysis. Dark blocks of **2·3a** were obtained by storing the supernatant solution at −30 °C for two weeks. These crystals were used for EPR spectroscopy (see Supporting Information).

Note that compound **2** is difficult to purify due to the formation of free IMes, which shows a similar solubility. IMes can be removed by fractional crystallisation. Unfortunately, attempts to purify crude **2** by column chromatography over silica gel or aluminium oxide were unsuccessful.

C$_{63}$H$_{72}$N$_6$Ni$_3$P$_6$, MW = 1275.23 g/mol
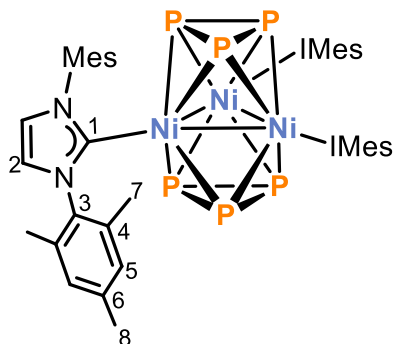
Yield: 6 mg (9%)

^{1}H NMR (400 MHz, 300 K, C_6D_6) δ = 2.23 (s, 18H, C^8H), 2.28 (s, 36H, C^7H), 6.87 (s, 12H, C^5H), 7.9 (s, 6h, C^2H) ppm.

A meaningful **$^{13}C\{^1H\}$ NMR** spectrum could not be obtained due to slow decomposition of **2** in solution over several hours.

**$^{31}P\{^1H\}$ NMR** (162 MHz, 300 K, C_6D_6) δ = −8.6 (brs) ppm.

Elemental Analysis calcd. C 59.34, H 5.69, N 6.59; found C 56.99, H 5.52, N 6.06. Low carbon values were found repeatedly in three independent samples.

[(IPr)$_3$Ni$_3$P$_8$] (4):

To a mixture of [(IPr)Ni($η^6$-toluene)] (130 mg, 0.24 mmol, 1.0 eq.) and white phosphorus (21 mg, 0.17 mmol, 0.67 eq.) was added cold (−30 °C) toluene (50 mL). The dark red reaction mixture underwent a colour change to dark green-brown within 5 minutes. The solvent was removed and the dark residue was dried *in vacuo*. Subsequently, the solid was washed with *n*-hexane (3 x 5 mL) until the filtrate was colourless. The remaining dark green powder was analytically pure **4**. Crystals suitable for X-ray crystallography were grown by cooling down a saturated solution of **4** in an appropriate solvent (*n*-hexane, *n*-heptane, toluene, Et$_2$O) from ambient temperature to −30 °C (see Supporting Information).

The solvent of the *n*-hexane washing solution was removed *in vacuo*. The ^{1}H NMR spectrum revealed a mixture of free IPr, **4** and **3b** (see Supporting Information). This sample was used for the EPR measurement.

$C_{81}H_{108}N_6Ni_3P_8$, MW = 1589.67 g/mol
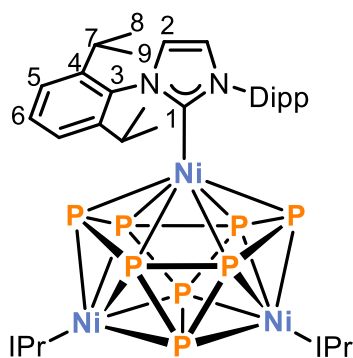
Yield: 53 mg (41%)

^{1}H NMR (400 MHz, 300 K, C_6D_6) δ = 1.14 (d, $^3J_{HH}$ = 6.8 Hz, 36H, C^8H), 1.41 (d, $^3J_{HH}$ = 6.7 Hz, 36H, C^9H), 3.16 (sept, $^3J_{HH}$ = 6.8 Hz, 12H, C^7H), 6.77 (s, 6H, C^2H), 7.13 (s, 18H, $C^{5/6}H$) ppm.

$^{13}C\{^1H\}$ NMR (400 MHz, 300 K, C_6D_6) δ = 23.7 (s, C^9), 26.4 (s, C^8), 28.9 (s, C^7), 124.1 (s, $C^{5/6}$), 124.4 (s, C2), 128.6 (s, $C^{5/6}$), 138.0 (s, C^3), 145.8 (s, C^4) ppm.

Elemental Analysis calcd. C 61.20, H 6.85, N 5.29; found C 60.84, H 6.77, N 4.94.

UV/Vis (THF): $λ_{max}$ (nm, $ε_{max}$ /L·mol^{-1}·cm^{-1}) 300 (14600).

3.5   **Supporting Information**

The Supporting Information of Chapter 3 can be found on the supplied CD-ROM and on https://onlinelibrary.wiley.com/doi/full/10.1002/anie.202004020. The Supporting Information contains: NMR and UV/Vis spectra, cyclic voltammograms, EPR details, X-ray crystallography details and results of quantum chemical calculations including Cartesian coordinates of all optimised structures.

References

[1] M. Caporali, L. Gonsalvi, A. Rossin, M. Peruzzini, *Chem. Rev.* **2010**, *110*, 4178.

[2] B. M. Cossairt, N. A. Piro, C. C. Cummins, *Chem. Rev.* **2010**, *110*, 4164.

[3] a) D. E. C. Corbridge, *Phosphorus 2000. Chemistry, Biochemistry and Technology*, (Elvesier, 2000); b) W. Schipper, *Eur. J. Inorg. Chem.* **2014**, *2014*, 1567.

[4] H.-G. Von Schnering, W. Hönle, *Chem. Rev.* **1988**, *88*, 243.

[5] a) M. Di Vaira, C. A. Ghilardi, S. Midollini, L. Sacconi, *J. Am. Chem. Soc.* **1978**, *100*, 2550; b) M. Di Vaira, S. Midollini, L. Sacconi, *J. Am. Chem. Soc.* **1979**, *101*, 1757.

[6] a) O. J. Scherer, T. Dave, J. Braun, G. Wolmershäuser, *J. Organomet. Chem.* **1988**, *350*, C20-C24; b) O. J. Scherer, J. Braun, G. Wolmershäuser, *Chem. Ber.* **1990**, 471; c) O. J. Scherer, J. Braun, P. Walther, G. Wolmershäuser, *Chem. Ber.* **1992**, *125*, 2661; d) E. Mädl, G. Balázs, E. V. Peresypkina, M. Scheer, *Angew. Chem. Int. Ed.* **2016**, *55*, 7702.

[7] S. Pelties, D. Herrmann, B. de Bruin, F. Hartl, R. Wolf, *Chem. Commun.* **2014**, *50*, 7014.

[8] P. Dapporto, S. Midollini, L. Sacconi, *Angew. Chem. Int. Ed. Engl.* **1979**, *18*, 469.

[9] S. Carenco, I. Resa, X. Le Goff, P. Le Floch, N. Mézailles, *Chem. Commun.* **2008**, 2568.

[10] B. Zarzycki, T. Zell, D. Schmidt, U. Radius, *Eur. J. Inorg. Chem.* **2013**, *2013*, 2051.

[11] V. Miluykov, A. Kataev, O. Sinyashin, P. Lönnecke, E. Hey-Hawkins, *Organometallics* **2005**, *24*, 2233.

[12] S. Pelties, A. W. Ehlers, R. Wolf, *Chem. Commun.* **2016**, *52*, 6601.

[13] A. J. Arduengo III, S. F. Gamper, J. C. Calabrese, F. Davidson, *J. Am. Chem. Soc.* **1994**, *116*, 4391.

[14] J. B. Diccianni, T. Heitmann, T. Diao, *J. Org. Chem.* **2017**, *82*, 6895.

[15] M. R. Elsby, S. A. Johnson, *J. Am. Chem. Soc.* **2017**, *139*, 9401.

[16] M. R. Elsby, J. Liu, S. Zhu, L. Hu, G. Huang, S. A. Johnson, *Organometallics* **2018**.

[17] Y. Hoshimoto, Y. Hayashi, H. Suzuki, M. Ohashi, S. Ogoshi, *Organometallics* **2014**, *33*, 1276.

[18] M. D. Walter, J. Grunenberg, P. S. White, *Chem. Sci.* **2011**, *2*, 2120.

[19] a) T. E. North, J. B. Thoden, B. Spencer, A. Bjarnason, L. F. Dahl, *Organometallics* **1992**, *11*, 4326; b) J. J. Maj, A. D. Rae, L. F. Dahl, *J. Am. Chem. Soc.* **1982**, *104*, 3054; c) P. Buchalski, P. Jadach, A. Pietrzykowski, K. Suwińska, L. Jerzykiewicz, J. Sadło, *Organometallics* **2008**, *27*, 3618; d) R. Beck, M. Shoshani, S. A. Johnson, *Angew. Chem. Int. Ed.* **2012**, *51*, 11753; e) G. Henkel, M. Kriege, K. Matsumoto, *J. Chem. Soc., Chem. Commun.* **1988**; f) J. H. J. Berthel, M. W. Kuntze-Fechner, U. Radius, *Eur. J. Inorg. Chem.* **2019**, *2019*, 2618.

[20] a) K. Wade, *J. Chem. Soc., Chem. Commun.* **1971**, 792; b) D. M. P. Mingos, *Nat. Phys. Sci.* **1972**, *236*, 99.

[21]   a) R. Ahlrichs, D. Fenske, K. Fromm, H. Krautscheid, U. Krautscheid, O. Treutler, *Chem. Eur. J.* **1996**, *2*, 238; b) G. Friedrich, O. J. Scherer, G. Wolmershäuser, *Z. Anorg. Allg. Chem.* **1996**, *622*, 1478; c) C. von Hänisch, D. Fenske, F. Weigend, R. Ahlrichs, *Chem. Eur. J.* **1997**, *3*, 1494; d) C. von Hänisch, D. Fenske, *Z. Anorg. Allg. Chem.* **1998**, *624*, 367; e) E.-M. Schnöckelborg, J. J. Weigand, R. Wolf, *Angew. Chem. Int. Ed.* **2011**, *50*, 6657; f) S. Heinl, A. Y. Timoshkin, J. Müller, M. Scheer, *Chem. Commun.* **2018**, *54*, 2244.

[22]   a) A. R. Kudinov, D. A. Loginov. Z. A. Starikova, P. V. Petrovskii, M. Corsini, P. Zanello, *Eur. J. Inorg. Chem.* **2002**, 3018; b) O. J. Scherer, T. Brück, G. Wolmershäuser, *Chem. Ber.* **1989**, *122*, 2049.

[23]   a) B. Rink, O. J. Scherer, G. Heckmann, G. Wolmershäuser, *Chem. Ber.* **1992**, *125*, 1011; b) S. Heinl, G. Balázs, M. Bodensteiner, M. Scheer, *Dalton Trans.* **2016**, *45*, 1962; c) C. M. Knapp, B. H. Westcott, M. A. C. Raybould, J. E. McGrady, J. M. Goicoechea, *Angew. Chem. Int. Ed.* **2012**, *51*, 9097; d) L. Y. Goh, R. C. S. Wong, C. K. Chu, T. W. Hambley, *J. Chem. Soc. Dalton Trans.* **1990**, 977; e) D. A. Loginov, Y. V. Nelyubina, A. R. Kudinov, *J. Organomet. Chem.* **2018**, *870*, 130; f) O. J. Scherer, J. Schwalb, G. Wolmershäuser, W. Kaim, R. Gross, *Angew. Chem. Int. Ed. Engl.* **1986**, *25*, 363.

[24]   O. Volkov, W. Dirk, U. Englert, P. Paetzold, *Z. Anorg. Allg. Chem.* **1999**, *625*, 1193.

[25]   H. Thurn, H. Krebs, *Acta Cryst.* **1969**, *B25*, 125.

[26]   Heating up the solution of **4** in toluene-d_8 to temperatures above 313 K led to decomposition to unidentified products.

[27]   a) V. N. Staroverov, G. E. Scuseria, J. Tao, J. P. Perdew, *J. Chem. Phys.* **2003**, *119*, 12129; b) S. Huzinaga, *J. Chem. Phys.* **1965**, *42*, 1293; c) F. Neese, *Inorg. Chim. Acta* **2002**, *337*, 181.

[28]   a) E. J. Popczun, J. R. McKone, C. G. Read, A. J. Biacchi, A. M. Wiltrout, N. S. Lewis, R. E. Schaak, *J. Am. Chem. Soc.* **2013**, *135*, 9267; b) H. Li, S. Lu, J. Sun, J. Pei, Di Liu, Y. Xue, J. Mao, W. Zhu, Z. Zhuang, *Chem. Eur. J.* **2018**, *24*, 11748.

[29]   a) Sheldrick, G. M. SADABS, Bruker AXS, Madison, USA **2007**; b) CrysAlisPro, Scale3 Abspack, Rigaku Oxford Diffraction **2019**.

[30]   R. C. Clark, J. S. Reid, *Acta Cryst. A* **1995**, *51*, 887.

[31]   G. M. Sheldrick, *Acta Cryst. A* **2015**, *71*, 3.

[32]   O. V. Dolomanov, L. J. Bourhis, R. J. Gildea, J. A. K. Howard, H. Puschmann, *J .Appl. Crystallogr.* **2009**, *42*, 339.

[33]   G. M. Sheldrick, *Acta Cryst. C* **2015**, *71*, 3.

[34]   G. M. Sheldrick, *Acta Cryst. A* **2008**, *64*, 112.

4 Di-*tert*-butyldiphosphatetrahedrane: Catalytic Synthesis of the Elusive Phosphaalkyne Dimer[a,b]

Abstract: While tetrahedranes as a family are scarce, neutral heteroatomic species are all but unknown, with the only reported example being AsP$_3$. Herein, we describe the isolation of a neutral heteroatomic X$_2$Y$_2$ molecular tetrahedron (X, Y = p-block elements), which also is the long-sought-after free phosphaalkyne dimer. Di-*tert*-butyldiphosphatetrahedrane, (*t*BuCP)$_2$, is formed from the monomer *t*BuCP in a nickel-catalysed dimerisation reaction using [(NHC)Ni(CO)$_3$]] (NHC=1,3-bis(2,4,6-trimethylphenyl)imidazolin-2-ylidene (IMes) and 1,3-bis(2,6-diisopropylphenyl)imidazolin-2-ylidene (IPr)). Single-crystal X-ray structure determination of (*t*BuCP)$_2$ confirms its tetrahedral structure. Moreover, a silver(I) complex containing η^2-coordinating (*t*BuCP)$_2$ is presented. The influence of the N-heterocyclic carbene ligand on the catalytic reaction was investigated, and a mechanism was elucidated using a combination of synthetic and kinetic studies and quantum chemical calculations.
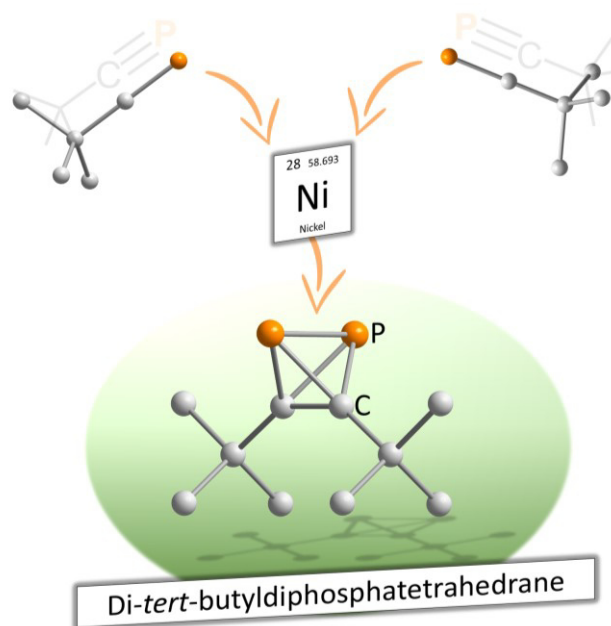
Di-*tert*-butyldiphosphatetrahedrane

4.1 Introduction

Tetrahedranes (tricyclo[1.1.0.0^{2,4}]butanes) have considerable practical and theoretical significance because of their high energy content, large bond strain and ensuing high reactivity.[1] While theoretical chemists have endeavored to determine the electronic structure and the thermodynamic stability of tetrahedranes with ever increasing accuracy,[2,3,4] synthetic chemists have striven to develop effective protocols for their preparation. The isolation by Maier and co-workers of the first organic tetrahedrane, (*t*BuC)$_4$, was a milestone in organic synthesis (Figure 1a).[5] Nevertheless, the number of well-characterised tetrahedranes remains small, even more than four decades later.[6] Some heavier congeners, e.g. (RE)$_4$ (E = Si and Ge, R = Si*t*Bu$_3$) and related group 13 element compounds, are also known,[7]] as are the structures adopted by white phosphorus (P$_4$) and yellow arsenic (As$_4$). Undoubtedly, P$_4$ is the most industrially significant tetrahedrane. Moreover, neutral tetrahedranes containing two different heteroatoms in their skeleton are almost unknown, the only example to have been isolated so far being AsP$_3$, which was synthesised by reaction of a niobium cyclotriphosphido complex with AsCl$_3$.[8]

Diphosphatetrahedranes, (RCP)$_2$, represent a particularly attractive target in this area, potentially providing a hybrid between the two most famous tetrahedral molecules, P$_4$ and (*t*BuC)$_4$. However, high level quantum chemical studies indicate that, similar to pure carbon-based tetrahedranes, such a species must be stabilised by bulky alkyl substituents (Figure 1b). Thus, while 1,2-diphosphatriafulvene (**IV**) is predicted to be the preferred isomer of (HCP)$_2$, the diphosphatetrahedrane (**I**) is the most stable isomer of (*t*BuCP)$_2$ (Figure 1b).[3,4] Related diphosphacyclobutadienes **II** and **III** are considerably higher in energy in both cases.
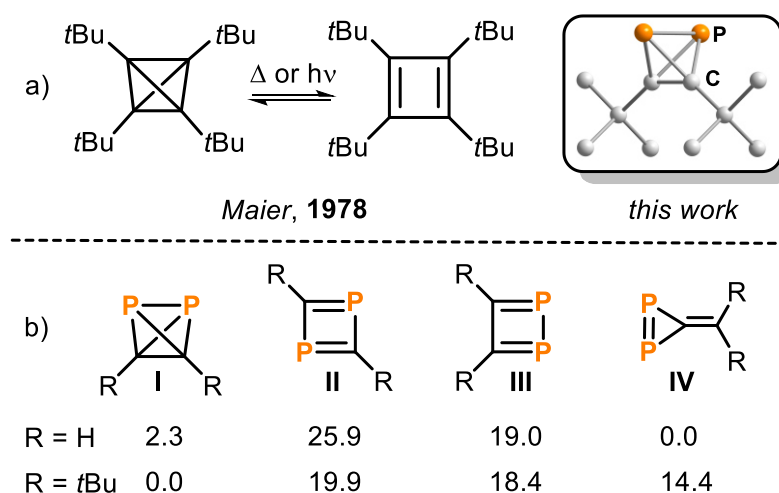

Figure 1. a) The tetrahedrane (*t*BuC)$_4$ in equilibrium with the cyclobutadiene isomer and DFT structure of (*t*BuCP)$_2$;[5] b) calculated relative electronic energies (ΔE in kcal·mol^{-1}) for (RCP)$_2$ with R = H (data from ref. [3]) and R = *t*Bu (see the SI).

We reasoned that the dimerisation of phosphaalkynes, R−C≡P, could present an elegant avenue toward elusive diphosphatetrahedranes. Indeed, transition metal-bound phosphaalkyne dimers

(most frequently 1,3-diphosphacyclobutadienes,[9] but also other isomers) commonly result from transition metal-mediated phosphaalkyne oligomerisation reactions. Free diphosphatetrahedranes have also been proposed as key intermediates in thermal and photochemical oligomerisation reactions of phosphaalkynes, which typically lead to higher phosphaalkyne oligomers (RCP)$_n$ (n = 3–6).[10,11] However, an uncomplexed phosphaalkyne dimer has never been observed.

4.2   Results and Discussion

Building on previous work on iron(–I)- and cobalt(–I)-mediated phosphaalkyne dimerisations,[12] we recently began studying the analogous reactivity of phosphaalkynes with nickel(0) species. Unexpectedly, the $^{31}P\{^{1}H\}$ NMR spectrum of the reaction of [Ni(CO)$_4$] with an excess of tBuCP (50 equivalents) exhibited a high field-shifted singlet at −468.2 ppm in addition to the signal of free tBuCP at −68.1 ppm. It was anticipated that such an upfield shift could be consistent with formation of a P$_2$C$_2$ tetrahedron (*cf.* P$_4$, δ = −521 ppm), through dimerisation of tBuCP. This assumption was later confirmed through isolation of the pure product **1a** (*vide infra*). A subsequent screening of various nickel tricarbonyl complexes [(NHC)Ni(CO)$_3$] (NHC = IMes, IPr, iPr$_2$Im^{Me} (= 1,3-di(*iso*-propyl)-4,5-di(methyl)-imidazolin-2-ylidene) for this dimerisation reaction of tBuCP revealed that the bulky NHC ligands IPr and IMes gave optimal results (see the Supporting Information catalyst screening), while the use of the smaller *iso*-propyl-substituted ligand iPr$_2$Im^{Me} resulted in only a low yield of **1a**. Using [(IMes)Ni(CO)$_3$], **1a** can be isolated in up to 55% yield on a 500 mg scale using just 2 mol% of the nickel catalyst in *n*-hexane for 18 h (Figure 2). Fractional condensation of the raw product affords pure **1a** as a pyrophoric, yellow oil with a melting point of −32 °C. Above the melting point, neat **1a** dimerises to the known ladderane-type tetramer tetraphosphatricyclo[4.2.0.0^{2,5}]octadiene (**2a**, Figure 2) within several hours.[10] Further details on the stability and the dimerisation process are discussed in the subsequent chapter 5 of this thesis. However, **1a** is stable at −80 °C for weeks without noticeable decomposition as evidenced by $^{31}P\{^{1}H\}$ NMR. Dimerisation of **1a** to **2a** is significantly slower in dilute solutions (e.g. 0.2 M in toluene). The use of 1-adamantylphosphalkyne under similar conditions results in the analogous formation of diadamantyldiphosphatetrahedrane (**1b**), as indicated by a resonance at −479.8 ppm in $^{31}P\{^{1}H\}$ NMR spectra. However, attempts to isolate **1b** in pure form have thus far been hampered by decomposition to higher phosphaalkyne oligomers (e.g. the ladderane (AdCP)$_4$ (**2b**) analogous to **2a**).
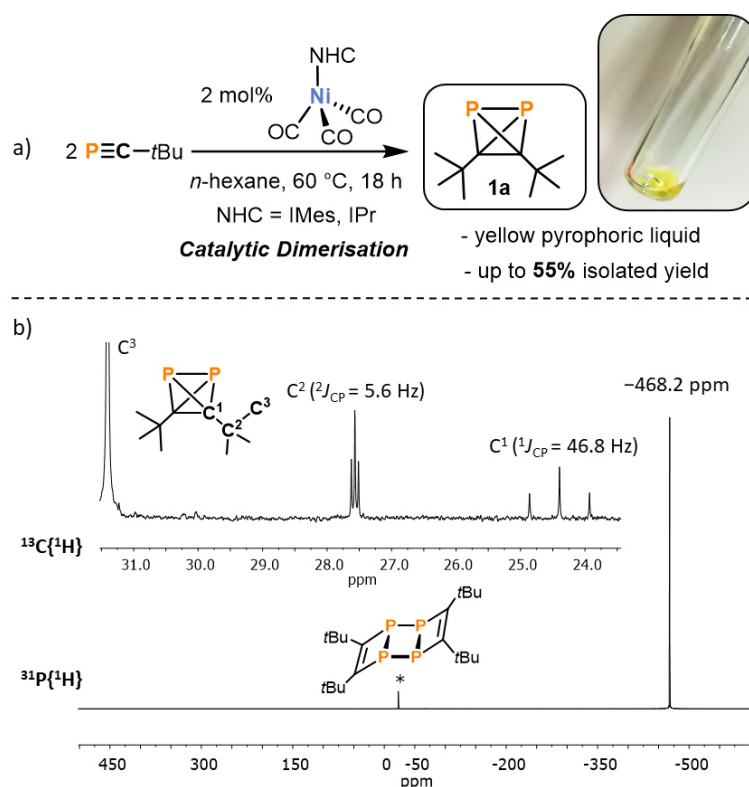
Figure 2. a) Synthesis of **1a** by [(NHC)Ni(CO)₃] (NHC = IMes, IPr) catalysed dimerisation of *t*BuCP, b) ³¹P{¹H} and ¹³C{¹H} NMR spectra for **1a** at 300 K in C₆D₆. The asterisk marks a trace of the tetramer (*t*BuCP)₄ (**2a**, i.e. the dimerisation product of **1a**).

Multinuclear NMR spectra of **1a** are in agreement with the tetrahedral structure with localised C_{2v} symmetry. The ³¹P{¹H} NMR spectrum of **1a** in C₆D₆ displays a singlet resonance at −468.2 ppm similar to other tetrahedral phosphorus compounds, e.g. P₄ (δ(³¹P) = −520 ppm) and AsP₃ (δ(³¹P) = −484 ppm).[13,14] The ¹H NMR spectrum shows a singlet resonance at 1.07 ppm for the *t*Bu group. In the ¹³C{¹H} spectrum, a singlet resonance is observed for the methyl groups, whereas the two other carbon signals split into triplets with $^{1}J_{\text{P–C}}$ = 46.7 Hz and $^{2}J_{\text{P–C}}$ = 5.7 Hz (Figure 2). **1a** was further characterised by elemental analysis, IR, UV/Vis spectroscopy and mass spectrometry. The UV/Vis spectrum reveals a weak absorption band at 275 nm (ε_{max} =1200 L·mol⁻¹·cm⁻¹) tailing into the visible region with a shoulder at 350 nm accounting for the yellow colour. Analysis of **1a** by EI-MS mass spectrometry revealed a molecular ion peak at m/z = 200.0879 in good agreement with the calculated molecular ion peak (m/z = 200.0878) and additionally showed fragmentation pathways via loss of P₂ units (e.g. M⁺−CH₃−P₂: 123.1172, calcd. 123.1173).

Attempts to grow single crystals of **1a** suitable for X-ray crystallography have been unsuccessful using standard techniques. For this reason, we pursued two alternative strategies. First, a mixture of **1a** and *n*-pentane was transferred to a capillary and crystallised *in-situ* on the diffractometer using the cryo-stream (Figure 3a).
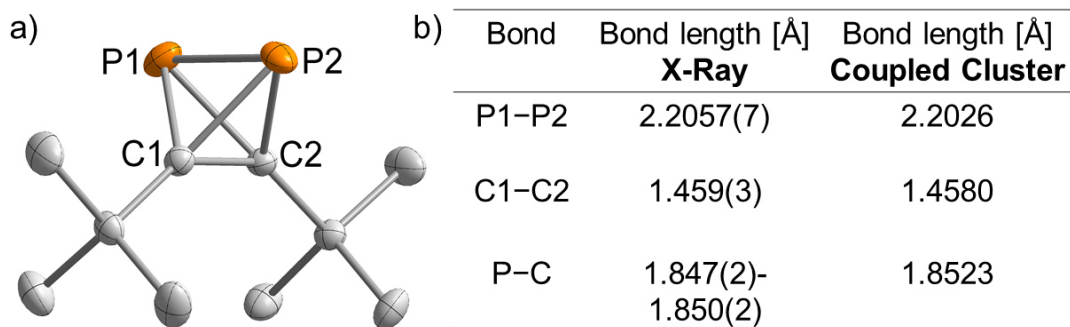
Bond	Bond length [Å] X-Ray	Bond length [Å] Coupled Cluster
P1−P2	2.2057(7)	2.2026
C1−C2	1.459(3)	1.4580
P−C	1.847(2)-1.850(2)	1.8523

Figure 3. a) Molecular structure of **1a** in the solid state. Thermal ellipsoids are set at the 50% probability level. Hydrogen atoms and the minor disordered component are omitted for clarity. Selected bond lengths [Å] and angles [°]: P1−P2 2.2057(7), P1−C1 1.850(2), P1−C2 1.8462(19), P2−C1 1.847(2), P2−C2 1.8476(19), C1−C2 1.459(3), C1−P1−P2 53.32(6), C2−P1−P2 53.36(6), C2−P1−C1 46.48(9), C1−P2−P1 53.43(6), C1−P2−C2 46.50(9), C2−P2−P1 53.30(6), P2−C1−P1 73.24(8), C2−C1−P1 66.62(10), C2−C1−P2 66.76(10), P1−C2−P2 73.33(7), C1−C2−P1 66.90(11), C1−C2−P2 66.74(11); b) Comparison of bond lengths in solid state structure with values obtained using DLPNO CCSD(T)/def2-QZVPP.

The P1−P2 bond length of 2.2057(7) Å in **1a** compares well to the bond length in P_4 determined by gas phase electron diffraction (2.1994(3) Å).[14] Moreover, the P−C bond lengths range from 1.8462(19) to 1.850(2) Å and the C1−C2 bond length of 1.459(3) Å is very similar to that of (*t*BuC)$_4$ (average: 1.485 Å).[15] Overall, the bond lengths compare very well to our calculations on the DLPNO-CCSD(T)/def2-QZVPP level of theory (Figure 3b).

Moreover, the preparation of a metal complex was attempted with [Ag(CH$_2$Cl$_2$)$_2$(pftb)] (pftb = Al{OC(CF$_3$)$_3$}$_4$).[16,17] A clean reaction was observed in toluene using two equivalents of **1a** per silver atom, and a species with a significantly downfield shifted $^{31}P\{^1H\}$ NMR signal (−446.8 ppm, cf. −468.2 ppm for **1a**) was detected. Further NMR monitoring also showed the slow formation of the tetramer **2a**. A single-crystal X-ray diffraction study on crystals grown from CH$_2$Cl$_2$ revealed the formation of [{Ag(**1a**)(**2a**)}$_2$][pftb]$_2$ (**3**), where both **1a** and **2a** are incorporated in the same complex (Figure 4).[18] Crucially, the X-ray diffraction experiment again confirms the tetrahedral structure of **1a**. The P$_2$C$_2$ tetrahedron is bound to the Ag$^+$ ion in an η^2 fashion *via* the P−P bond. While the four P–C bond lengths in the tetrahedron (1.821(9)-1.836(9)Å) and the C−C bond length (C1-C2 1.462(12) Å) are comparable to the values in uncoordinated **1a**, the P1−P2 bond is significantly elongated (P1−P2 2.308(3) Å) as a consequence of coordination to Ag$^+$. Broadened singlet resonances are observed in the $^{31}P\{^1H\}$ NMR spectrum at −19.8 and −446.8 ppm when crystals of **3** are dissolved in CD$_2$Cl$_2$, and the ^1H NMR data are also consistent with the molecular structure obtained by X-ray crystallography.[19]
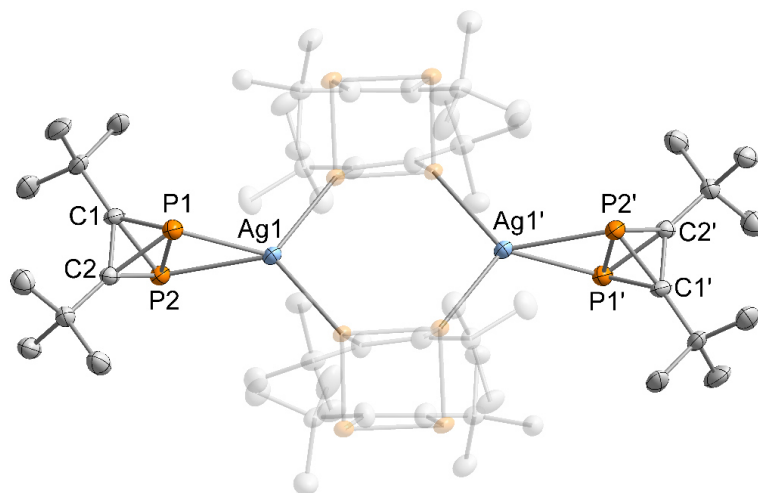
Figure 4. Molecular structure of **3** in the solid state. Thermal ellipsoids are set at the 50% probability level. Hydrogen atoms and the [pftb]⁻ counterions are omitted for clarity. Selected bond lengths [Å] and angles [°]: P1−P2 2.308(3), P1−C1 1.836(9), P1−C2 1.835(9), P2−C1 1.821(9), P2−C2 1.820(8), C1−C2 1.462(12), C1−P2−P1 51.2(3), C1−P2−C2 47.4(4), C2−P2−P1 51.1(3), C1−P1−P2 50.6(3), C2−P1−P2 50.5(3), C2−P1−C1 46.9(4), P2−C1−P1 78.3(3), C2−C1−P2 66.3(5), C2−C1−P1 66.5(5), P2−C2−P1 78.3(3), C1−C2−P2 66.4(5), C1−C2−P1 66.6(5).

In an attempt to identify possible intermediates in the formation of **1a**, the nickel tricarbonyl complexes [(NHC)Ni(CO)$_3$] (NHC = IMes, IPr, *i*Pr$_2$Im^{Me}) were reacted with one equivalent of phosphaalkyne RCP (R = *t*Bu, Ad) in *n*-hexane at ambient temperature. Each of these reactions led to an instant colour change from colourless to bright yellow and concomitant gas evolution (liberation of CO gas). For the sterically more demanding NHC ligands IPr and IMes, the phosphaalkyne complexes [(NHC)Ni(CO)(PCR)] (NHC = IMes, R = *t*Bu (**4a**), Ad (**4b**), NHC = IPr; R = *t*Bu (**4c**), Ad (**4d**)) featuring η^2-bound phosphaalkyne ligands were the sole P-containing products of these reactions (Figure 5a). Complexes **4a**–**4d** can be isolated as crystalline solids in yields from 34% to 87%, and were characterised by single crystal X-ray diffraction, multinuclear NMR spectroscopy, IR spectroscopy and elemental analysis (see the Supporting Information for details). The structural and spectroscopic data compare well to related, isoelectronic complexes [(*i*Pr$_2$Im)$_2$Ni(PC*t*Bu)] (*i*Pr$_2$Im = 1,3-di(isopropyl)imidazolin-2-ylidene) and [(trop$_2$NMe)Ni-(PCPh$_3$)}] (trop = 5*H*-dibenzo[*a,d*]cyclohepten-5-yl).[20]

Conversely, the reaction of *t*BuCP with [(*i*Pr$_2$Im^{Me})Ni(CO)$_3$] afforded a mixture of the mononuclear 1,3-diphosphacyclobutadiene complex [(*i*Pr$_2$Im^{Me})Ni(CO)(η^4-P$_2$C$_2$*t*Bu$_2$)] (**5**), the dinuclear complex [{(*i*Pr$_2$Im^{Me})Ni(CO)}$_2$(μ,η^2:η^2-*t*BuCP)] (**6**) and a tetranuclear cluster [{(*i*Pr$_2$Im^{Me})Ni$_2$(CO)$_2$(*t*BuCP)}$_2$] (**7**, Figure 5b). The three different species were identified in the ^{31}P{^{1}H} NMR spectrum and structurally authenticated by X-ray diffraction experiments after fractional crystallisation. Treatment of [(*i*Pr$_2$Im^{Me})Ni(CO)$_3$] with just 0.5 or two equivalents of *t*BuCP resulted in similar mixtures. Upon addition of *t*BuCP to one equivalent of [Ni(CO)$_4$], more than ten different species were detected by ^{31}P{^{1}H} NMR spectroscopy. The unselective nature of these reactions is in contrast to the selective formation of the η^2-bound phosphaalkyne complexes **4a-d** and presumably accounts for the lower yields in the catalytic formation of **1a**.
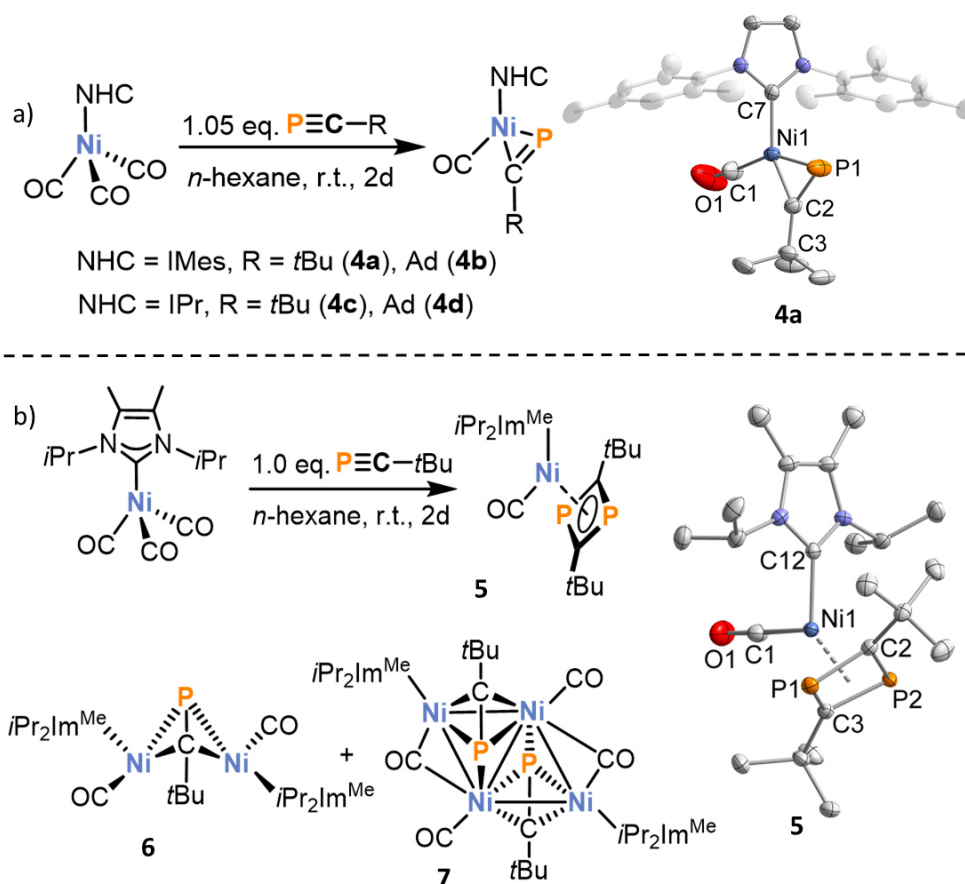
Figure 5. Synthesis of **4a-d**, **5**, **6** and **7**; and structures of **4a** and **5** in the solid state. Thermal ellipsoids are set at the 50% probability level. Hydrogen atoms and the second crystallographically independent molecule (in case of **4a**) are omitted for clarity. Selected bond lengths [Å] and angles [°] for 4a: Ni1−C1 1.777(3), Ni1−C7 1.931(2), Ni1−P1 2.1793(9), Ni1−C2 1.898(3), C1−O1 1.137(4), P1−C2 1.636(3), C3−C2−P1 144.2(2), C7−Ni1−P1 102.89(7), C2−Ni1−P1 46.67(8), C2−Ni1−C7 149.56(11), C2−P1−Ni1 57.59(10), O1−C1−Ni1 171.4(4); 5: Ni1−P1 2.3114(3), Ni1−P2 2.3113(3), Ni1−C2 2.0898(11), Ni1−C3 2.0637(11), P1−C2 1.7966(11), P1−C3 1.8143(11), P2−C2 1.8121(11), P2−C3 1.7992(11), Ni1−C1 1.7538(13), C1−O1 1.1458(17), Ni1−C12 1.9421(11), C1−Ni1−C12 94.29(5), O1−C1−Ni1 176.74(12), C2−P1−C3 78.74(5), C3−P2−C2 78.73(5), P1−C2−P2 100.90(6), P2−C3−P1 100.71(6).

With a high-yielding protocol for the preparation of **4a** in hand, the reactivity of this species was investigated. **4a** is the most potent catalyst for the dimerisation of *t*BuCP among all nickel complexes investigated. Thus, a significantly shorter reaction time for full conversion of the phosphaalkyne is required with **4a** than with [(IMes)Ni(CO)$_3$]. High temperature ^{31}P{^{1}H} NMR spectroscopic monitoring of this catalytic dimerisation reaction revealed the presence of **4a** at a constant concentration throughout the whole reaction (see the SI for further details). These observations suggest that **4a** is the resting state for the catalytic cycle. Further reaction intermediates were not detected by ^{31}P{^{1}H} NMR spectroscopy even upon monitoring the reaction at –80 °C. Also noteworthy is that treatment of **4a** with one equivalent AdCP affords the mixed-substituted diphosphatetrahedrane (P$_2$C$_2$Ad*t*Bu, **1c**), which can be identified by a ^{31}P{^{1}H} NMR singlet at −473.8 ppm.

Kinetic analysis with 0.5 to 4 mol% of **4a** indicates a first-order dependence of the dimerisation reaction in both catalyst and phosphaalkyne. The proposed rate law is therefore

$$r = \frac{d[\mathbf{1a}]}{dt} = k \cdot [\mathbf{4a}] \cdot [t\text{BuCP}].$$

These results are in good agreement with DFT calculations performed on the TPSS-D3BJ/def2-TZVP level, which suggest that the reaction between the truncated model complex [(IXy)Ni(CO)(*t*BuCP)] (**4′**, IXy = 1,3-bis(2,6-dimethylphenyl)imidazolin-2-ylidene) and a molecule of *t*BuCP initially affords the 1,3-diphosphacyclobutadiene complex **A** (Figure 5, *cf.* complex **5**, which differs only in the identity of NHC ligand; see the SI for more details).[21] However, **A** is not the global minimum of the potential hypersurface and transforms into an intermediate **B** showing an isomerised (*t*BuCP)$_2$ ligand. In the next step, a diphosphatetrahedrane complex **C** is formed. The formation of **C** has a calculated activation barrier of 26.9 kcal·mol^{-1} with respect to **A**. This is well in line with the reaction temperature of +60 °C required for the reaction to proceed at an appreciable rate (*vide supra*). Subsequent replacement of the diphosphatetrahedrane **1a** by another phosphaalkyne molecule is a downhill process and re-forms the resting state **4′** (*cf.* complex **4**, which is the only species we could identify by NMR spectroscopy in solution). Notably, a different scenario has been calculated for a further truncated model system consisting of Me−C≡P and [(IPh)Ni(CO)(PCMe)], (IPh = 1,3-diphenylimidazolin-2-ylidene, see the SI for further details). In this case, significant stabilisation of the analogous 1,3-diphosphacyclobutadiene complex (**A'**) is observed. The high activation barrier calculated for the transformation **A'** → **C'** (49.8 kcal·mol^{-1}) precludes the formation of the diphosphatetrahedrane. It appears that the steric repulsion between bulky substituents on the NHC such as Mes and Dipp and the *t*Bu groups has a destabilising effect on **A**, and this destabilisation of the 1,3-diposphacyclobutadiene complex, which is usually a thermodynamic sink in other reactions,[33] enables catalytic turnover in this particular case.
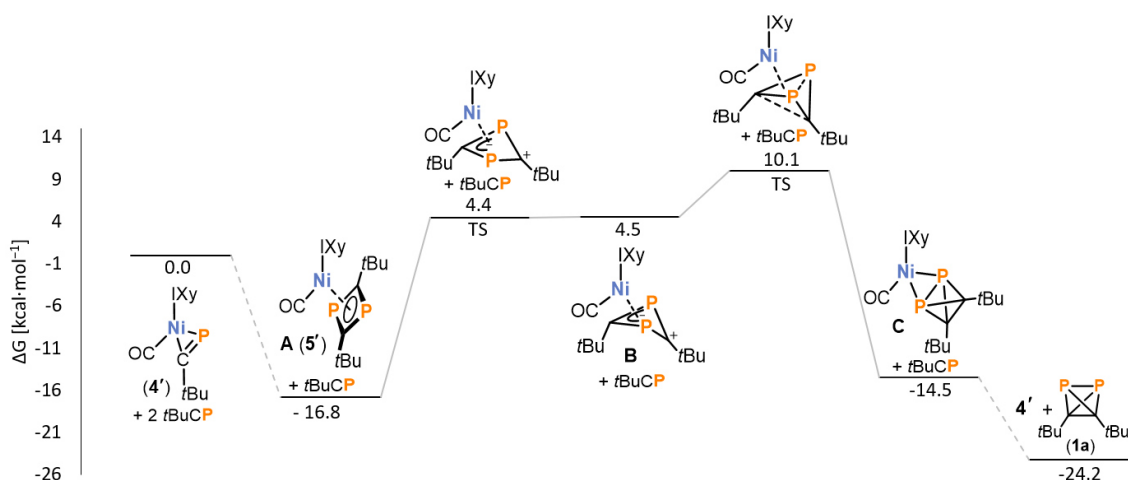

Figure 6. Reaction profile calculated with DFT at the TPSS-D3BJ/def2-TZVP level for the dimerisation of tBu−C≡P catalysed by [(IXy)Ni(PCtBu)] (IXy = 1,3-bis(2,6-dimethylphenyl)imidazolin-2-ylidene) (**4′**). Calculated Gibbs energies (in kcal·mol^{-1} at 298 K) and schematic drawings of intermediates and transition states are given.

4.3   Conclusion

In conclusion, diphosphatetrahedranes $(RCP)_2$ (R = *t*Bu, Ad) have been synthesised by an unprecedented nickel(0)-catalysed dimerisation reaction of the corresponding phosphaalkynes RCP. The *tert*-butyl-derivative $(tBuCP)_2$ (**1a**) is stable enough to be isolated and thoroughly characterised. The molecular structure of **1a** was unequivocally confirmed by single crystal X-ray diffraction experiments, which confirm the tetrahedral structure of the molecule. **1a** is a very rare 'mixed' tetrahedrane, which, moreover, represents is the hitherto elusive free phosphaalkyne dimer. Its synthesis therefore closes a significant gap in phosphaalkyne oligomer chemistry. **1a** is a metastable compound that slowly converts to the ladderane **2a**. This reaction shows that such dimers are indeed intermediates in phosphaalkyne tetramerisations as proposed previously.[25,28] Synthetic, kinetic and computational investigations suggest that a 1,3-diphosphacyclobutadiene complex is a key intermediate and that destabilisation of this complex by steric repulsion is a crucial factor in achieving catalysis. We are currently exploring the further reactivity of the remarkable small molecule **1a**.

4.4   Experimental Details

General Synthetic Methods

All reactions and product manipulations were carried out in flame-dried glassware under an inert atmosphere of argon using standard Schlenk-line or glovebox techniques (maintained at <0.1 ppm H_2O and <0.1 ppm O_2).*t*BuCP,[22] AdCP,[23] $[(NHC)Ni(CO)_3]$ (NHC = IMes, IPr, *i*Pr$_2$Im^{Me})[24,25], $[(IMes)NiP(CO)]_2$[26], $[(IMes)Ni(H_2CCHTMS)_2]$[27] and $[Ag(CH_2Cl_2)(pftb)]$[16] were prepared according to procedures previously reported in the chemical literature. $Ni(CO)_4$ in toluene (c = 0.96 M) was kindly provided by the group of Manfred Scheer. All other chemicals were purchased from commercial suppliers and used without further purification.

Solvents were dried and degassed with a MBraun SPS800solvent purification system. All dry solvents except *n*-hexane and *n*-pentane were stored under argon over activated 3 Å molecular sieves in gas-tight ampules. *n*-Hexane and *n*-pentane were stored over a potassium mirror.

General Analytical Techniques

NMR spectra were recorded on Bruker Avance 300 or 400 spectrometers at 300 K unless otherwise noted and internally referenced to residual solvent resonances (^{1}H NMR: THF-d$_8$: 1.72 ppm, C$_6$D$_6$: 7.16 ppm, CD$_2$Cl$_2$: 5.32 ppm; ^{13}C{^{1}H} NMR: THF-d$_8$: 25.31 ppm, C$_6$D$_6$: 128.06 ppm,). Chemical shifts δ are given in ppm referring to external standards of tetramethylsilane (^{1}H, ^{13}C{^{1}H}), 85% phosphorus acid (^{31}P and ^{31}P{^{1}H} spectra). ^{1}H and ^{13}C NMR signals were assigned based on 2D NMR spectra (^{1}H,^{1}H-COSY, ^{1}H,^{13}C-HSQC, ^{1}H,^{13}C-HMQC).

UV/Vis spectra were recorded on an Ocean Optics Flame spectrometer. IR spectra were recorded with a Bruker ALPHA spectrometer equipped with a diamond ATR unit. High resolution mass

spectra were recorded by the analytical department at the University of Regensburg using a Jeol AccuTOF GCX.

Yields of the catalytic and kinetic studies were determined using Gas chromatography with FID detector (GC-FID) by Shimadzu GC2010plus. H_2 was used as carrier gas. A Restek Rxi® (30m x 0.25 mm x 0.25 μm) column was used. The standard heating procedure was: 50 °C (2 min), 25 °C/min → 280 °C (5 min). **1a** was calibrated with *n*-pentadecane on the GC-FID after determination of the concentration via NMR with triphenylphosphine.

The single-crystal X-ray diffraction data of compounds **3**, **4a-d**, **5**, **6** and **7** were recorded on Rigaku Oxford Diffraction SuperNova Atlas or GV1000 Titan[S2] diffractometers with Cu-K_α radiation (λ= 1.54184 Å).

Crystals were selected under mineral oil, mounted on micromount loops and quench-cooled using an Oxford Cryosystems open flow N_2 cooling device. Either semi-empirical multi-scan absorption corrections[28] or analytical ones[29] were applied to the data. The structures were solved with SHELXT[30] solution program using dual methods and by using Olex2 as the graphical interface.[31] The models were refined with ShelXL[32] using full matrix least squares minimisation on F^2.[33]

Single-Crystal X-ray diffraction of 1a

The single-crystals X-ray diffraction data of **1a** was recorded on a Rigaku Oxford Diffraction SuperNova four-circle diffractometer with Mo-K_α radiation (λ= 0.71073Å). A mixture (approx. 1: 1) of **1a** and pentane was sucked into a capillary, the capillary was glued and placed on the diffractometer. After the first cooling below the crystallisation point of approx. 221 K, a solid forms which does not melt even at room temperature. The capillary was cooled from 221 K to 195 K with 20 K/h and an oligocrystalline material is formed, but a main domain could be determined and was measured after further cooling to 100 K. Only this domain was used for data integration and refinement. Datasets using twin integrations gave poor results. The whole molecule shows a disorder in the ratio 91:9, the carbon atoms of the minor occupied part were refined isotropically. All chemically equivalent C−C bonds were restrained to be same, hydrogen atoms were taken into account using a riding model. The structure was refined as an inversion twin with ratio 1:1.

Table S1. Crystal data and structure refinement for compound **1a**.

Empirical formula	$C_{10}H_{18}P_2$
Formula weight	200.18
Temperature/K	100.0(1)
Crystal system	monoclinic
Space group	$P2_1$
a/Å	6.1520(3)
b/Å	11.3115(5)
c/Å	8.6532(4)
α/°	90
β/°	98.903(5)
γ/°	90
Volume/Å^3	594.90(5)
Z	2
ρ_{calc}/g/cm^3	1.118
μ/mm^{-1}	0.318
F(000)	216.0
Crystal size/mm^3	0.253 × 0.215 × 0.192
Radiation	MoKα (λ = 0.71073)
2Θ range for data collection/°	4.764 to 66.264
Index ranges	-9 ≤ h ≤ 9, -17 ≤ k ≤ 17, -13 ≤ l ≤ 13
Reflections collected	21741
Independent reflections	4536 [R_{int} = 0.0614, R_{sigma} = 0.0558]
Data/restraints/parameters	4536/74/174
Goodness-of-fit on F^2	1.044
Final R indexes [I>=2σ (I)]	R_1 = 0.0379, wR_2 = 0.0739
Final R indexes [all data]	R_1 = 0.0531, wR_2 = 0.0781
Largest diff. peak/hole / e Å^{-3}	0.24/-0.20
Flack parameter	0.5

Synthesis of Compounds

(*t*BuCP)$_2$ (1a):

To a solution of [(IMes)Ni(CO)$_3$] (100 mg, 0.224 mmol, 1.0 eq.) was added *n*-hexane (25 mL) and *t*BuCP (4.4 mL, 2.56 M in O(SiMe$_3$)$_2$, 11.2 mmol, 50.0 eq.). A colour change from colourless to yellow was observed. The solution was heated to 60 °C for 18 h. Subsequently, the reaction flask was connected to a short connection tube with a Schlenk flask. The solvent was condensed into the Schlenk flask under full vacuum (p < 1·10^{-3} mbar) with the reaction flask at room temperature and the collection flask cooled to −30 °C. The condensate contains minor amounts of **1a**, *n*-hexane, O(SiMe$_3$)$_2$, residual *t*BuCP and (*t*BuCP)$_4$ (**2a**) in varying ratios. Subsequently, a new collection flask was attached to the connection tube and the collection flask was cooled to 77 K using liquid nitrogen. The reaction flask was heated to 60 °C and the product was condensed under full vacuum (p < 1·10^{-3} mbar) as a yellow liquid. The concentration of **1a** was determined

using PPh$_3$ as an internal standard via ^{31}P{^{1}H} NMR and ^{1}H NMR spectroscopy. The concentration was found to be between 3.0 and 3.5 mol/L.

1a is a yellow, pyrophoric liquid (see Figure S2). It starts smoking on contact with air and ignites organic materials (e.g. tissue paper). Neat **1a** can be stored in the freezer at −80 °C for several weeks. **1a** slowly decomposes at room temperature to **2a** within a few hours. Single crystals suitable for X-ray diffraction of **2a** were obtained by leaving the sample at room temperature for 1 week.[10]

C$_{10}$H$_{18}$P$_2$, MW = 200.20 g/mol
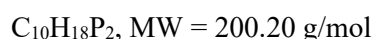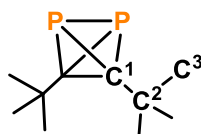
Yield: 623 mg, 0.9 mL [55% yield, determined by measurement of concentration (3.4 M)]

^{1}H NMR (400.13 MHz, 300 K, C$_6$D$_6$) δ = 1.07 (s, 18H, C^{3}H$_3$) ppm.

^{13}C{^{1}H} NMR (100.61 MHz, 300 K, C$_6$D$_6$) δ = 24.4 (t, $^1J_{CP}$ = 46.7 Hz, C^1), 25.6 (t, $^2J_{CP}$ = 5.7 Hz, C^2), 31.4 (s, C^3) ppm.

^{31}P{^{1}H} (161.98 MHz, 300 K, C$_6$D$_6$) δ = −468.2 (s) ppm.

Elemental Analysis calcd. C 59.99, H 9.06; found C 59.66, H 8.96. The liquid sample was quickly transferred into a tin capsule on air, closed with a small amount of air inside and immediately subjected to elemental analysis.

Upon prolonged air contact, the sample solidified. Elemental analysis of the solid formed were lower in carbon and hydrogen, possibly due to the formation of oxides [found C 58.85, H 8.82].

IR (ATR, cm^{-1}) ν = 2958 (vs), 2924 (w), 2901 (w), 1469 (s), 1459 (s), 1360 (s), 1267 (w), 1196 (s), 1055 (m), 919 (s), 855 (s), 823 (m), 756 (w), 645 (w), 467 (w).

melting point −32 °C.

UV/Vis (*n*-hexane): λ$_{max}$ (nm, ε$_{max}$ /L·mol^{-1}·cm^{-1}) 275 (1200), 350 (sh, 300).

HR-MS (EI-MS) m/z = 200.0879 (M$^+$, calculated 200.0878), 185.0648 (M$^+$−CH$_3$), 123.1172 (M$^+$−CH$_3$−P$_2$), 81.0705 (M$^+$−P$_2$−C*t*Bu), 57.0704 (*t*Bu).

[Ag(1a)(2a)]$_2$[pftb]$_2$ (3):

To a solution of [Ag(CH$_2$Cl$_2$)$_2$(pftb)] (0.108 g, 0.09 mmol, 1.0 eq.) in dichloromethane (2 ml) was added a solution of **1a** in toluene (40 ml, 5.0 mM, 0.200 mmol, 2.3 eq.) at room temperature. The reaction mixture was stirred for 20 min under the exclusion of light. Subsequently, the solvent was removed *in vacuo*. The beige solid was washed with *n*-hexane (3 x 10 ml) and dried under reduced pressure. The residue was dissolved in dichloromethane (1 mL) and stored at −30 °C overnight to afford colourless crystals of **3** suitable for X-ray crystallography. The crystals were isolated by decanting the supernatant solution and dried *in vacuo* to afford a colourless solid.

$C_{92}H_{108}Ag_2Al_2F_{72}O_8P_{12}$, MW = 3351.14 g/mol
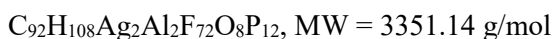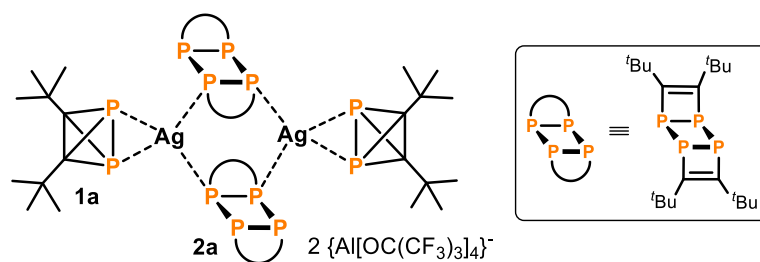
Yield: 43 mg, 29 %

^{1}H NMR (400.13 MHz, 300 K, CD_2Cl_2) δ = 1.17 (s, 36H, Ag-**1a**-H), 1.46 (s, 72H, Ag-**2a**-H) ppm.

^{31}P{^{1}H} (161.98 MHz, 300 K, CD_2Cl_2) δ = −446.8 (brs, Ag-**1a**-P), −19.9 (brs, Ag-**2a**-P) ppm.

^{19}F{^{1}H} (376.62 MHz, 300 K, CD_2Cl_2) δ = −75.6 (s, CF_3) ppm.

A **^{13}C{^{1}H} NMR** could not be obtained due to slow decomposition and the low solubility of **3** in CD_2Cl_2.

UV/Vis (CH_2Cl_2): λ_{max} (nm, ε_{max} /L·mol^{-1}·cm^{-1}) 300 (10000).

Elemental Analysis calcd. C 32.97, H 3.25; found C 33.73, H 3.24.

[(IMes)Ni(CO)(PC*t*Bu)] (4a):

To a solution of [(IMes)Ni(CO)$_3$] (50.0 mg, 0.11 mmol, 1.0 eq.) in *n*-hexane (5 mL) was added *t*BuCP (2.56 M in O(SiMe$_3$)$_2$, 44 µL, 0.12 mmol, 1.05 eq.). Gas evolution and a colour change from colourless to intense yellow were observed. After a few minutes, a yellow precipitate formed. The suspension was stirred at ambient temperature for two days. Subsequently, the solid was isolated by filtration, washed with cold hexane (−30 °C, 2 x 1 mL) and dried under reduced pressure, yielding a bright yellow powder. Crystals suitable for X-ray crystallography were grown by slow diffusion of *n*-hexane into a saturated solution of [IMesNi(CO)(PC*t*Bu)] in toluene.

$C_{27}H_{33}N_2NiOP$, MW = 491.24 g/mol
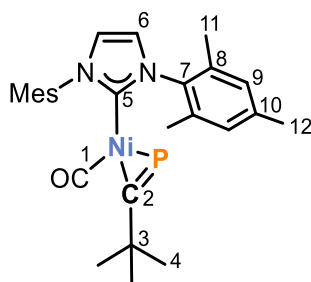
Yield: 48 mg (87%)

^{1}H NMR (400.13 MHz, 300 K, C_6D_6) δ = 1.38 (s, 9H, C^{4}H), 1.20 (s, 6H, C^{12}H), 2.18 (s, 12H, C^{11}H), 6.32 (s, 2H, C^{6}H), 6.69 (s, 4H, C^{9}H) ppm.

^{13}C{^{1}H} NMR (100.61 MHz, 300 K, C_6D_6) δ = 18.30 (s, C^{11}), 18.31 (s, C^{11}), 21.0 (s, C^{12}), 34.26 (d, $^3J_{CP}$ = 5.2 Hz, C^4), 40.82 (d, $^2J_{CP}$ = 6.9 Hz, C^3), 122.4 (s, C^6), 129.4 (s, C^9), 135.3 (s, C^8), 137.0 (s, C^7), 138.6 (s, C^{10}), 195.6 (d, $^2J_{CP}$ = 3.1 Hz, C^5), 200.8 (d, $^2J_{CP}$ = 3.4 Hz, C^1), 241.6 (d, $^1J_{CP}$ = 78.1 Hz, C^2) ppm.

**^{31}P{^{1}H}** (161.98 MHz, 300 K, C$_6$D$_6$) δ = 91.2 (s) ppm.

Elemental Analysis calcd. C 66.02, H 6.77, N 5.70; found C 66.47, H 6.50, N 5.64.

IR (ATR, cm^{-1}) 2948 (w), 2915 (w), 2856 (w), 1974 (vs), 1912 (w), 1486 (m), 1397 (m), 1323 (m), 1266 (m), 1155 (m).

UV/Vis (THF): λ_{max} (nm, ε_{max} /L·mol^{-1}·cm^{-1}) 350 (4400sh), 390 (4600).

[(IMes)Ni(CO)(PCAd)] (4b):

To a solution of [(IMes)Ni(CO)$_3$] (50.0 mg, 0.11 mmol, 1.0 eq.) in *n*-hexane (5 mL) was added AdCP (21.0 mg, 0.12 mmol, 1.05 eq.). Gas evolution and a colour change from colourless to intense yellow were observed. After a few minutes, a yellow precipitate formed. The suspension was stirred at ambient temperature for two days. Subsequently, the solvent was removed and the orange residue was dried *in vacuo*. *n*-Pentane (2 mL) was added and the suspension was stored at −30 °C in order to complete precipitation. The solid was isolated by filtration, washed with cold *n*-pentane (−30 °C, 2 x 1 mL) and dried under reduced pressure, yielding a yellow powder. A second crop of crystalline compound was obtained after reducing the volume of the filtrate further to half the volume and storing the solution at −35 °C overnight. Crystals suitable for X-ray crystallography were grown by cooling a saturated solution of [(IMes)Ni(CO)(PCAd)] in toluene from ambient temperature to −30 °C.

C$_{33}$H$_{39}$N$_2$NiOP, MW = 569.36 g/mol
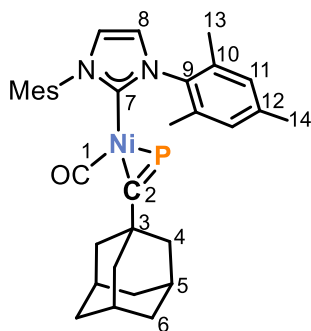
Yield: 52 mg (81%)

^{1}H NMR (400.13 MHz, 300 K, C$_6$D$_6$) δ = 1.54 (m, 6H, C^{6}H), 1.81 (s, 3H, C^5), 2.01 (overlapping s, 12H, C^{14}H + C^{4}H), 2.20 (s, 12H, C^{13}H), 6.34 (s, ^{2}H, C^{8}H), 6.71 (s, 4H, C^{11}H) ppm.

^{13}C{^{1}H} NMR (100.61 MHz, 300 K, C$_6$D$_6$) δ = 18.3 (s, C^{13}), 18.4 (s, C^{13}), 21.0 (s, C^{14}), 29.7 (s, C^5), 37.1 (s, C^6), 42.9 (d, $^2J_{CP}$ = 6.8 Hz, C^3) 47.1 (d, $^3J_{CP}$ = 5.3 Hz, C^4), 122.4 (s, C^8), 129.4 (s, C^{11}), 135.3 (s, C^{10}), 137.0 (s, C^9), 138.6 (s, C^{12}), 195.8 (d, $^2J_{CP}$ = 2.5 Hz, C^7), 201.3 (d, $^2J_{CP}$ = 2.5 Hz, C^1), 241.4 (d, $^1J_{CP}$ = 77.8 Hz, C^2) ppm.

**^{31}P{^{1}H}** (161.98 MHz, 300 K, C$_6$D$_6$) δ = 92.1 (s) ppm.

Elemental Analysis calcd. C 69.62, H 6.99, N 4.92; found C 69.92, H 7.01, N 4.76.

IR (ATR, cm^{-1}) 2900 (m), 2884 (m), 2845 (w), 1967 (m), 1964 (vs), 1919 (w), 1486 (w), 1449 (w), 1397 (w), 1323 (m), 1265 (w).

UV/Vis (THF): λ_{max} (nm, ε_{max} /L·mol^{-1}·cm^{-1}) 340 (3200sh), 390 (3200).

[(IPr)Ni(CO)(PC*t*Bu)] (4c):

To a solution of [(IPr)Ni(CO)$_3$] (100.0 mg, 0.188 mmol, 1.0 eq.) in *n*-hexane (5 mL) was added *t*BuCP (2.56 M in O(SiMe$_3$)$_2$, 77 μL, 1.05 eq.). Gas evolution and a colour change from colourless to intense yellow were observed. The yellow solution was stirred at ambient temperature for two days. Subsequently, the solution was concentrated to ca. 2 mL. Storage at −30 °C for two days afforded large yellow blocks which were isolated by filtration and dried under reduced pressure. A second crop of crystalline compound was obtained after reducing the volume of the filtrate to 1 mL and storing the solution at −35 °C overnight. Crystals suitable for X-ray crystallography were grown by cooling a saturated solution of [(IPr)Ni(CO)(PC*t*Bu)] from ambient temperature to −30 °C.
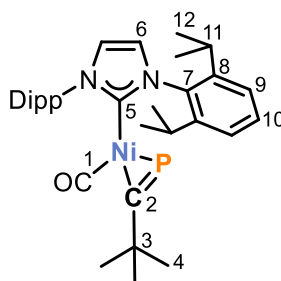
$C_{33}H_{45}N_2NiOP$, MW = 575.40 g/mol

Yield: 51 mg (47%)

^{1}H NMR (400.13 MHz, 300 K, C_6D_6) δ = 1.09 (d, $^3J_{HH}$ = 7.0 Hz, 12H, C^{12}H), 1.37 (d, $^3J_{HH}$ = 6.9 Hz, 12H, C^{12}H), 1.41 (s, 9H, C^{4}H), 3.02 (sept, $^3J_{HH}$ = 6.9 Hz, 4H, C^{11}H), 6.70 (s, 2H, C^{6}H), 7.10 (d, $^3J_{HH}$ = 7.6 Hz, 4H, C^{9}H), 7.20 (dd, $^3J_{HH}$ = 7.0 Hz, $^3J_{HH}$ = 7.6 Hz, 2H, C^{10}H) ppm.

^{13}C{^{1}H} NMR (100.61 MHz, 300 K, C_6D_6) δ = 23.4 (s, C^{12}), 25.5 (s, C^{12}), 28.9 (s, C^{11}), 34.0 (d, $^3J_{CP}$ = 5.7 Hz, C^4), 40.6 (d, $^3J_{CP}$ = 7.2 Hz, C^3), 124.0 (s, C^6), 124.3 (s, C^9), 130.1 (s, C^{10}), 137.4 (s, C^7), 146.0 (s, C^8), 197.3 (d, $^2J_{CP}$ = 3.1 Hz, C^5), 200.1 (d, $^2J_{CP}$ = 2.9 Hz, C^1), 237.8 (d, $^1J_{CP}$ = 77.7 Hz, C^2) ppm.

^{31}P{^{1}H} (161.98 MHz, 300 K, C_6D_6) δ = 93.2 (s) ppm.

Elemental Analysis calcd. C 68.88, H 7.88, N 4.87; found C 68.95, H 7.51, N 4.81.

IR (ATR, cm^{-1}) 2964 (m), 2926 (w), 2866 (w), 1970 (vs) 1459 (m) 1400 (m) 1384 (m) 1328 (m) 1178 (w), 1159 (w).

UV/Vis (THF): λ_{max} (nm, ε_{max} /L·mol^{-1}·cm^{-1}) 350 (3400sh), 400 (3500).

[(IPr)Ni(CO)(PCAd)] (4d):

To a solution of [(IPr)Ni(CO)$_3$] (100.0 mg, 0.19 mmol, 1.0 eq.) in *n*-hexane (5 mL) was added AdCP (35.2 mg, 0.20 mmol, 1.05 eq.). Gas evolution and a colour change from colourless to intense yellow were observed. The yellow solution was stirred at ambient temperature for two

days. Subsequently, the solution was concentrated to ca. 2 mL. Storage at −30 °C for two days afforded yellow crystals which were isolated by filtration and dried under reduced pressure. A second crop of crystalline compound was obtained after reducing the volume of the filtrate to 1 mL and storing the solution at −35 °C overnight. Crystals suitable for X-ray crystallography were grown by cooling a saturated solution of [(IPr)Ni(CO)(PCAd)] in *n*-hexane from ambient temperature to −30 °C.

$C_{39}H_{51}N_2NiOP$, MW = 653.52 g/mol
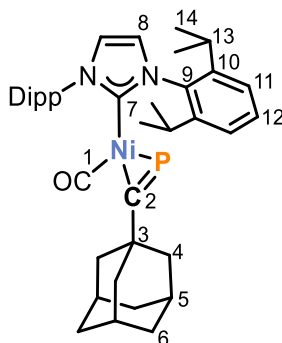
Yield: 42 mg (34%)

^{1}H NMR (400.13 MHz, 300 K, C_6D_6) δ = 1.10 (d, $^3J_{HH}$ = 6.9 Hz, 12H, $C^{14}H$), 1.40 (d, $^3J_{HH}$ = 6.9 Hz), 1.59 (m, 6H, C^6H), 1.86 (s, 3H, C^5H), 2.04 (d, $^4J_{HP}$ = 2.6 Hz, 6H, C^4H), 3.05 (sept, $^3J_{HH}$ = 6.9 Hz, $C^{13}H$), 6.71 (s, 2H, C^8H), 7.11 (d, $^3J_{HH}$ = 7.6 Hz, 4H, $C^{11}H$), 7.21 (dd, $^3J_{HH}$ = 7.1 Hz, $^3J_{HH}$ = 8.4 Hz, 2H, $C^{12}H$) ppm.

^{13}C{^{1}H} NMR (100.61 MHz, 300 K, C_6D_6) δ = 23.4 (s, C^{14}), 25.5 (s, $C^{14'}$), 28.9 (s, C^{13}), 29.7 (s, C^5), 37.2 (s, C^6), 42.7 (d, $^2J_{CP}$ = 7.7 Hz, C^3), 46.8 (d, $^3J_{CP}$ = 5.8 Hz, C^4), 123.6 (s, C^8), 124.3 (s, C^{11}), 130.0 (s, C^{12}), 137.4 (s, C^9), 146.0 (s, C^{10}), 197.5 (d, $^2J_{CP}$ = 3.0 Hz, C^7), 200.7 (d, $^2J_{CP}$ = 2.8 Hz, C^1), 237.6 (d, $^1J_{CP}$ = 78.0 Hz, C^2) ppm.

^{31}P{^{1}H} (161.98 MHz, 300 K, C_6D_6) δ = 94.1(s) ppm.

Elemental Analysis calcd. C 71.68, H 7.87, N 4.29; found C 72.02, H 7.50, N 4.23.

**IR** (ATR, cm^{-1}) 2961 (w), 2866 (w), 2847 (w), 1966 (vs), 1467 (m) 1399 (m) 1327 (m) 1179 (m)

UV/Vis (THF): λ_{max} (nm, ε_{max} /L·mol^{-1}·cm^{-1}) 350 (3600sh), 400 (3400).

[(*i*Pr$_2$Im^{Me})Ni(CO)$_3$]:

The compound was prepared analogous to the procedure for the synthesis of [(NHC)Ni(CO)$_3$] (NHC = IMes, IPr) reported by Nolan and co-workers.[24] An independent preparation was recently reported by Radius and co-workers.[25]

A cold (−60 °C) THF solution (20 mL) of *i*Pr$_2$Im^{Me} (600.0 mg, 3.33 mmol, 1.0 eq.) was added dropwise to a cold (−60 °C) THF solution (20 mL) of a [Ni(CO)$_4$] stock solution in toluene (0.96 M, 4.16 mL, 3.99 mmol, 1.2 eq.). A colour change from yellow to red and then finally to pale orange and evolution of CO gas were observed. The pale orange solution was stirred at room temperature for one hour. Subsequently, the volatiles were removed *in vacuo*. The brown solid

was washed with cold *n*-pentane (−30 °C, 3 × 15 mL), and dried in vacuo to give a beige solid. Crystals suitable for X-ray crystallography were grown by cooling a saturated solution of $[(i\text{Pr}_2\text{Im}^{\text{Me}})\text{Ni(CO)}_3]$ in toluene from ambient temperature to −30 °C.

$\text{C}_{14}\text{H}_{20}\text{N}_2\text{NiO}_3$, MW = 323.03 g/mol
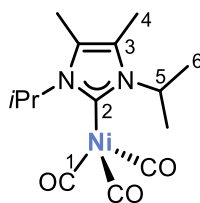
yield: 420 mg (39%)

^{1}H NMR (400.13 MHz, 300 K, C_6D_6) δ = 1.09 (d, 12H, $^3J_{\text{CH}}$ = 7.2 Hz, C^6H), 1.67 (s, 6H, C^4H), 5.45 (sept, $^3J_{\text{CH}}$ = 5.45 Hz, 2H, C^5H) ppm.

^{13}C{^{1}H} NMR (100.61 MHz, 300 K, C_6D_6) δ = 10.3 (s, C^4), 21.4 (s, C^6), 53.6 (s, C^5), 125.4 (s, C^3), 187.7 (s, C^2), 198.9 (s, C^1) ppm.

Elemental Analysis calcd. C 52.06, H 6.24, N 8.67; found C 52.58, H 6.26, N 8.76.

UV/Vis (THF): λ_{max} (nm, ε_{max} /L·mol^{-1}·cm^{-1}) 280 (12 000sh), 320 (5000sh).

IR (ATR, cm^{-1}) 2982 (w), 2938 (w), 2875 (w), 2043 (s), 1959 (s), 1913 (vs), 1868 (m), 1640 (w), 1464 (m) 1352 (w), 1332 (w), 1290 (m), 1210 (m), 1106 (w) 1021 (w).

4.5 Supporting Information

The Supporting Information of Chapter 4 can be found on the supplied CD-ROM and on https://onlinelibrary.wiley.com/doi/full/10.1002/anie.201910505. The Supporting Information contains: NMR and UV/Vis spectra, additional experiments, kinetic data, X-ray crystallography details and results of quantum chemical calculations including Cartesian coordinates of all optimised structures.
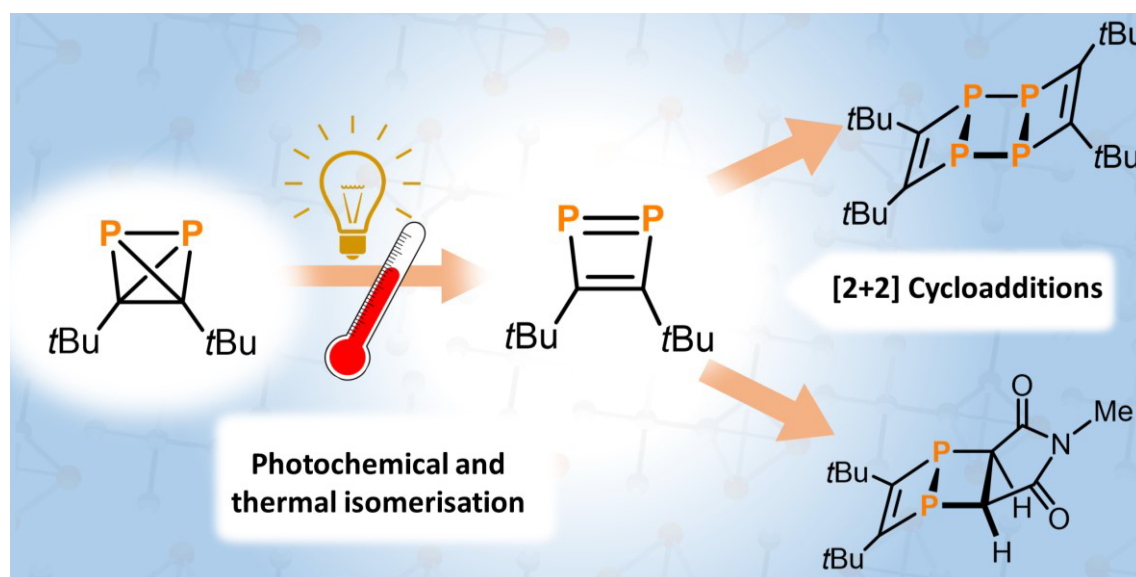
References

[1] G. Maier, *Angew. Chem. Int. Ed. Engl.* **1988**, *27*, 309.

[2] a) A. Nemirowski, H. P. Reisenauer, P. R. Schreiner, *Chem. Eur. J.* **2006**, *12*, 7411; b) R. Haunschild, G. Frenking, *Mol. Phys.* **2010**, *107*, 911.

[3] A. S. Ivanov, K. V. Bozhenko, A. I. Boldyrev, *J. Chem. Theory Comput.* **2012**, *8*, 135.

[4] T. Höltzl, D. Szieberth, M. T. Nguyen, T. Veszprémi, *Chem. Eur. J.* **2006**, *12*, 8044.

[5] G. Maier, S. Pfriem, U. Schäfer, R. Matusch, *Angew. Chem. Int. Ed. Engl.* **1978**, *17*, 520.

[6] a) A. Sekiguchi, T. Matsuo, H. Watanabe, *J. Am. Chem. Soc.* **2000**, *122*, 5652; b) Y. Kobayashi, M. Nakamoto, Y. Inagaki, A. Sekiguchi, *Angew. Chem. Int. Ed.* **2013**, *52*, 10740; c) G. Maier, J. Neudert, O. Wolf, D. Pappusch, A. Sekiguchi, M. Tanaka, T. Matsuo, *J. Am. Chem. Soc.* **2002**, *124*, 13819; d) M. Nakamoto, Y. Inagaki, M. Nishina, A. Sekiguchi, *J. Am. Chem. Soc.* **2009**, *131*, 3172; e) T. Ochiai, M. Nakamoto, Y. Inagaki, A. Sekiguchi, *J. Am. Chem. Soc.* **2011**, *133*, 11504; f) A. Sekiguchi, M. Tanaka, *J. Am. Chem. Soc.* **2003**, *125*, 12684; g) M. Tanaka, A. Sekiguchi, *Angew. Chem. Int. Ed.* **2005**, *44*, 5821.

[7] a) N. Wiberg, C. M. M. Finger, K. Polborn, *Angew. Chem. Int. Ed. Engl.* **1993**, *32*, 1054; b) W. Uhl, W. Hiller, M. Layh, W. Schwarz, *Angew. Chem. Int. Ed. Engl.* **1992**, *31*, 1364; c) T. Mennekes, P. Paetzold, R. Boese, D. Bläser, *Angew. Chem. Int. Ed. Engl.* **1991**, *30*, 173; d) C. Dohmeier, C. Robl, M. Tacke, H. Schnöckel, *Angew. Chem. Int. Ed. Engl.* **1991**, *30*, 564; e) A. Purath, C. Dohmeier, A. Ecker, H. Schnöckel, K. Amelunxen, T. Passler, N. Wiberg, *Organometallics* **1998**, *17*, 1894; f) N. Wiberg, K. Amelunxen, H.-W. Lerner, H. Nötz, W. Ponikwar, H. Schwenk, *J. Organomet. Chem.* **1999**, *574*, 246; g) W. Uhl, A. Jantschak, W. Saak, M. Kaupp, R. Wartchow, *Organometallics* **1998**, *17*, 5009; h) W. Uhl, *Angew. Chem. Int. Ed. Engl.* **1993**, *32*, 1386.

[8] B. M. Cossairt, M.-C. Diawara, C. C. Cummins, *Science* **2009**, *323*, 602.

[9] A. Chirila, R. Wolf, J. Chris Slootweg, K. Lammertsma, *Coord. Chem. Rev.* **2014**, *270-271*, 57.

[10] B. Geissler, S. Barth, U. Bergsträsser, M. Slany, J. Durkin, P. B. Hitchcock, M. Hofmann, P. Binger, J. F. Nixon, P. von Rague Schleyer, M. Regitz, *Angew. Chem. Int. Ed. Engl.* **1995**, *34*, 484.

[11] a) P. Binger, S. Leininger, J. Stannek, B. Gabor, R. Mynott, J. Bruckmann, C. Krüger, *Angew. Chem. Int. Ed. Engl.* **1995**, *34*, 2227; b) R. Bartsch, P. B. Hitchcock, J. F. Nixon, *J. Organomet. Chem.* **1989**, *375*, 31; c) T. Wettling, B. Geissler, R. Schneider, S. Barth, P. Binger, M. Regitz, *Angew. Chem. Int. Ed. Engl.* **1992**, *31*, 758; d) V. Claiman, P. B. Hitchcock, J. F. Nixon, M. Hofmann, P. von Rague Schleyer, *Angew. Chem. Int. Ed. Engl.* **1994**, *33*, 2202; e) R. Streubel, *Angew. Chem. Int. Ed. Engl.* **1995**, *34*, 436.

[12] a) R. Wolf, A. W. Ehlers, J. C. Slootweg, M. Lutz, D. Gudat, M. Hunger, A. L. Spek, K. Lammertsma, *Angew. Chem. Int. Ed.* **2008**, *47*, 4584; b) R. Wolf, J. C. Slootweg, A. W.

Ehlers, F. Hartl, B. de Bruin, M. Lutz, A. L. Spek, K. Lammertsma, *Angew. Chem. Int. Ed.* **2009**, *48*, 3104; c) R. Wolf, N. Ghavtadze, K. Weber, E.-M. Schnöckelborg, B. de Bruin, A. W. Ehlers, K. Lammertsma, *Dalton Trans.* **2010**, *39*, 1453.

[13] a) B. M. Cossairt, M.-C. Diawara, C. C. Cummins, *Science* **2009**, *323*, 602; b) B. M. Cossairt, C. C. Cummins, *J. Am. Chem. Soc.* **2009**, *131*, 15501.

[14] B. M. Cossairt, C. C. Cummins, A. R. Head, D. L. Lichtenberger, R. J. F. Berger, S. A. Hayes, N. W. Mitzel, G. Wu, *J. Am. Chem. Soc.* **2010**, *132*, 8459.

[15] H. Irngartinger, A. Goldmann, R. Jahn, M. Nixdorf, H. Rodewald, G. Maier, K.-D. Malsch, R. Emrich, *Angew. Chem. Int. Ed. Engl.* **1984**, *23*, 993.

[16] I. Krossing, *J. Am. Chem. Soc.* **2001**, *123*, 4603.

[17] C. Schwarzmaier, M. Sierka, M. Scheer, *Angew. Chem. Int. Ed.* **2013**, *52*, 858.

[18] Repeated attempts to isolate the homoleptic complex [Ag(**1a**)$_2$][pftb] were unsuccessful due to decomposition of **1a** in solution.

[19] Due to the low solubility of **3** in CD$_2$Cl$_2$ and slow decomposition in solution, a ^{13}C{^{1}H} NMR spectrum could not be obtained.

[20] a) T. Schaub, U. Radius, *Z. Anorg. Allg. Chem.* **2006**, *632*, 981; b) M. Trincado, A. J. Rosenthal, M. Vogt, H. Grützmacher, *Eur. J. Inorg. Chem.* **2014**, 1599.

[21] A possible second pathway for the formation of 1a is discussed in the Supporting Information. However, this pathway was found to be kinetically disfavoured.

[22] a) W. Rösch, T. Allspach, U. Bergsträßer, M. Regitz, W. A. Herrmann (Hrsg.) *Synthetic Methods of Organometallic and Inorganic Chemistry*, Thieme, Stuttgart, **1996**; b) G. Becker, G. Gresser, W.Uhl, *Z. Naturforsch. B* **1981**, *36*, 16.

[23] T. Allspach, M. Regitz, G. Becker, W. Becker, *Synthesis* **1986**, 31.

[24] R. Dorta, E. D. Stevens, N. M. Scott, C. Costabile, L. Cavallo, C. D. Hoff, S. P. Nolan, *J. Am. Chem. Soc.* **2005**, *127*, 2485.

[25] J. H. J. Berthel, M. W. Kuntze-Fechner, U. Radius, *Eur. J. Inorg. Chem.* **2019**, *2019*, 2618.

[26] G. Hierlmeier, A. Hinz, R. Wolf, J. M. Goicoechea, *Angew. Chem. Int. Ed.* **2018**, *57*, 431.

[27] M. R. Elsby, J. Liu, S. Zhu, L. Hu, G. Huang, S. A. Johnson, *Organometallics* **2019**, *38*, 436.

[28] a) CrysAlisPro, Scale3 Abspack, Rigaku Oxford Diffraction **2019**; b) Sheldrick, G. M. SADABS, Bruker AXS, Madison, USA **2007**.

[29] R. C. Clark, J. S. Reid, *Acta Cryst. A* **1995**, *51*, 887.

[30] G. M. Sheldrick, *Acta Cryst. A* **2015**, *71*, 3.

[31] O. V. Dolomanov, L. J. Bourhis, R. J. Gildea, J. A. K. Howard, H. Puschmann, *J .Appl. Crystallogr.* **2009**, *42*, 339.

[32] G. M. Sheldrick, *Acta Cryst. C* **2015**, *71*, 3.

[33] G. M. Sheldrick, *Acta Cryst. A* **2008**, *64*, 112.

5   Photochemistry of Di-*tert*-butyldiphosphatetrahedrane[a]

Abstract:

Di-*tert*-butyldiphosphatetrahedrane (*t*BuCP)$_2$ is a mixed carbon- and phosphorus-based tetrahedral molecule isolobal to white phosphorus (P$_4$). Inspired by the well-known (photo)chemical transformations of P$_4$, we present a detailed study on the thermal and photochemical reactivity of (*t*BuCP)$_2$. (*t*BuCP)$_2$ readily dimerises to the ladderane-type phosphaalkyne tetramer (*t*BuCP)$_4$ under irradiation with UV light. The dimerisation process was studied by NMR and stationary and transient UV/Vis absorption spectroscopy. Elevated temperatures are required for this dimerisation reaction to proceed in the dark. In both cases, an isomerisation to a 1,2-diphosphacyclobutadiene is the first step in this process. This intermediate subsequently undergoes a [2+2] cycloaddition with a second 1,2-diphosphacyclobutadiene molecule to form (*t*BuCP)$_4$. The 1,2-diphosphacyclobutadiene intermediate can be trapped chemically by addition of N-methylmaleimide as an alternative [2+2] cycloaddition partner.

5.1   Introduction

The tetrahedron is a fundamental structure motif in chemistry. Tetrahedral molecules can incorporate various elements of the periodic table, including s-, p-, and d-block elements. Among the most prominent examples are the first "organic" tetrahedrane, $(t\text{BuC})_4$ prepared by Maier and co-workers in 1978, and the first "inorganic" tetrahedrane, P_4, discovered as early as 1669.[1,2] While the chemical properties and reactivity patterns of both molecules have been studied for a long time and still fascinate the chemical community, the physical properties, in particular the thermal stability and photochemistry, of both types of species have also attracted considerable attention.[3]

The transformation of white phosphorus to its red allotrope by irradiation had already been discovered in the 19th century (Figure 1A).[4] Later on, it was proposed that this reaction takes place via photoinduced dissociation of P_4 into P_2 molecules, which then recombine to form polymeric red phosphorus.[5] The same equilibrium $P_4 \rightleftharpoons P_2$ can also be achieved thermally in the gas phase when heating P_4 to temperatures above 1000 °C.[6] Depending on the solvent system used when irradiating P_4, a radical mechanism has also been proposed for the polymerisation to red phosphorus.[7] The photochemistry of P_4 can be exploited for the synthesis of new diphosphenes *via* [2+4] cycloadditions of P_2 with dienes (see chapter 2 for further discussion).[8] The purely carbon-based tetrahedrane tetra-*tert*-butyltetrahedrane $(t\text{BuC})_4$ can be generated photochemically by irradiation of its cyclobutadiene isomer tetra-*tert*-butylcyclobutadiene ($\lambda > 300$ nm; Figure 1B).[1] Upon heating to 130 °C, colourless **1** undergoes isomerisation to give the deep red tetra-*tert*-butylcyclobutadiene.
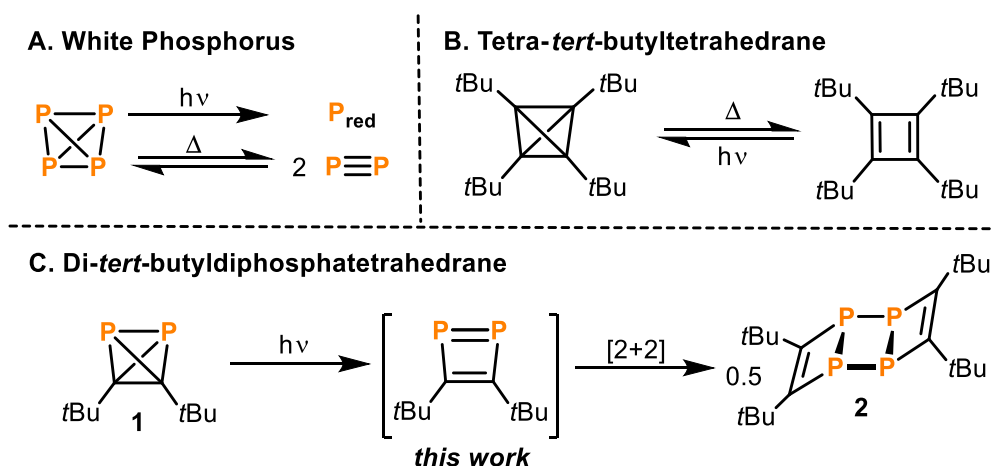

Figure 1. Thermal and photochemical reactions of group 14 / group 15 tetrahedranes.[7,1]

In recent work, some of us have described the synthesis of di-*tert*-butyldiphosphatetrahedrane (**1**), the "hybrid" of P_4 and $(t\text{BuCP})_2$ (see chapter 4).[9] This compound is readily prepared by a nickel-catalysed dimerisation reaction of *tert*-butylphosphaalkyne *t*BuCP. Diphosphatetrahedrane **1** is a metastable liquid with a melting point of −32 °C. In our earlier studies, it was reported that **1** slowly dimerises above its melting point to give the ladderane-type phosphaalkyne tetramer

(*t*BuCP)$_4$ (**2**).[10] We have now studied the temperature and light sensitivity of **1** in detail and can show that **1** indeed has an interesting photochemistry. Irradiation of **1** with UV light affords **2** via [2+2] cycloaddition of two intermediarily formed 1,2-diphosphacyclobutadienes (Figure 1C). These results give valuable first insights into the photochemical behaviour of **1** and reveal notable differences in comparison with the photochemistry of P$_4$, (*t*BuCP)$_4$ and *t*BuCP (the monomer of **1**).

5.2   Results and Discussion

To begin, the stability of **1** towards heat and light was investigated. First, the stability of a solution of **1** was studied in the dark at ambient temperature by monitoring the characteristic ^{31}P NMR signal at −468.2 ppm (Figure 2). These results show that the concentration stays constant over 15 hours and therefore, **1** can be considered thermally stable at ambient temperature in solution.
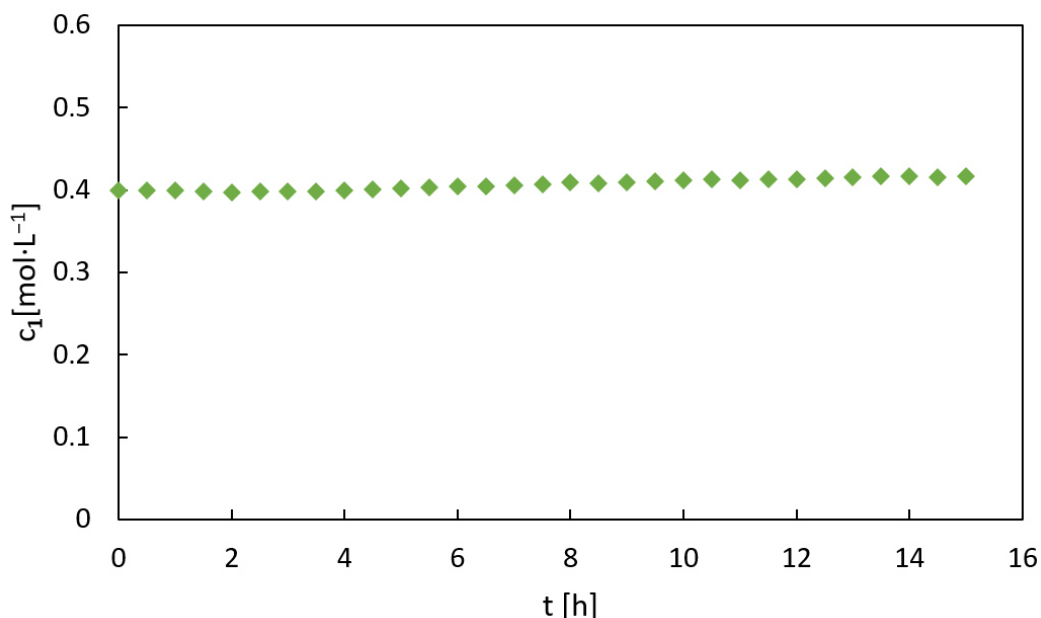
Figure 2. Change of concentration of **1** (c_1) over time at 300 K in toluene solution ($c^0 = 0.4$ mol·L^{-1}) as determined by ^{31}P NMR spectroscopy.

Following this initial stability test, a solution of **1** in toluene was slowly heated in the dark to 80 °C. At temperatures above 40 °C, the formation of (tBuCP)$_4$ (**2**) was observed as evidenced by the singlet resonance at −22.2 ppm (Figure 3).[10] The conversion of **1** to **2** increases upon increasing the temperature and keeping the solution at 80 °C for ca. 2.5 hours results in ca. 8% conversion (based on integration) of **1** to **2**.

Based on these data, it can be further concluded that, while **1** is stable in solutions at ambient temperature, it converts thermally to **2** upon heating. This more controlled experiment is in contrast to previous observations, in which the dimerisation of **1** to **2** was attributed to thermal instability of **1**.[9]
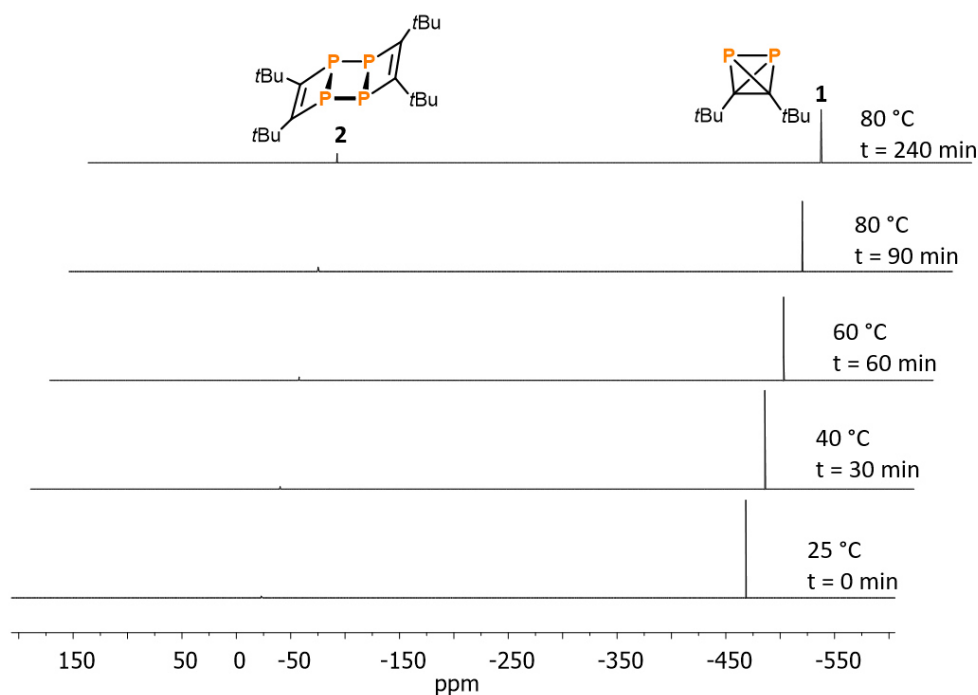
Figure 3. $^{31}P\{^{1}H\}$ NMR monitoring of a solution of **1** in toluene showing formation of **2**.

Next, the stability of **1** upon exposure to ambient light was investigated. For this purpose, two NMR samples containing **1** (with a concentration of 0.44 mol · L^{-1}) and an internal standard (PPh$_3$) in C$_6$D$_6$ were prepared, and the samples were monitored by quantitative ^{31}P NMR spectroscopy. One of these samples was stored in the dark while the other one was stored under ambient laboratory light. As expected, the change in concentration of the sample kept in the dark was negligible. The sample kept under ambient light, however, was almost completely converted into **2** after just 17 hours. A concentration of 0.04 mol·L^{-1} for **1** and of **2** 0.15 mol·L^{-1} was determined by ^{31}P NMR spectroscopy. Notably, however, the concentration of **2** was slightly lower than expected for full conversion of **1** into **2** even factoring in the 2:1 stoichiometry of the dimerisation reaction. This is presumably due to the formation of a precipitate in the NMR tube (*vide infra*).

With these initial results on the light-sensitivity of **1** in hand, *in situ* NMR illumination experiments were performed. A previously described setup with LED illumination inside the NMR tube was employed.[11] For this purpose, solutions with concentrations of 0.2 to 0.4 mol·L^{-1} of **1** and a wavelength of 365 nm were chosen, and irradiation times of less than 1 hour typically resulted in full consumption of **1** (Figure 4). The consumption of starting material is exponential and a logarithmic plot of the concentration affords linear relationships, confirming a first order photoreaction of **1** to form **2** (see experimental details). Nevertheless, plots of the concentration of **2** again revealed that the yield of **2** is not quantitative.
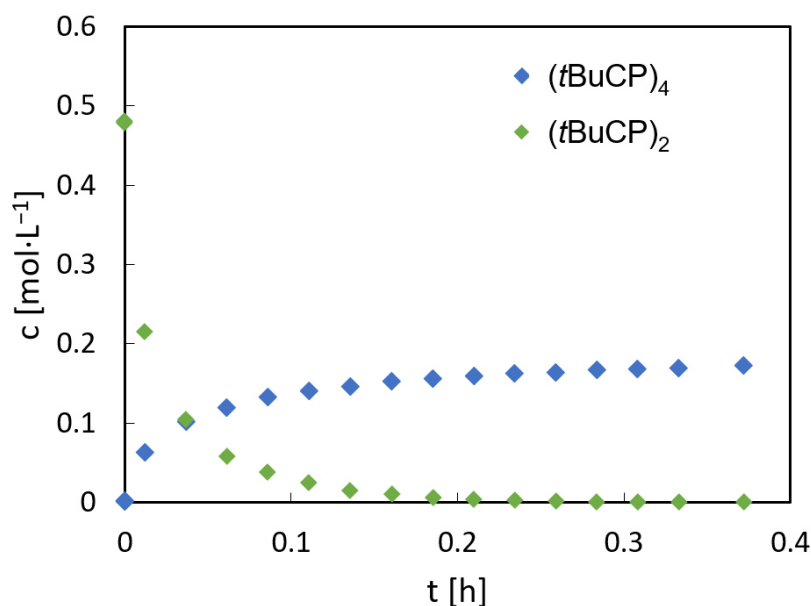
Figure 4. Change of concentration of **1** ($c^0_1 = 0.48$ mol·L^{-1}) upon *in situ* illumination ($\lambda = 365$ nm) as monitored by ^{31}P NMR spectroscopy.

In an attempt to study the photochemical behaviour of **2**, a convenient synthetic protocol for the synthesis of **2** from **1** was developed. Irradiation of solutions of **1** in THF for 3 hours using a UV lamp and subsequent extraction with benzene afforded pure **2** in 77% isolated yield (Scheme 1).
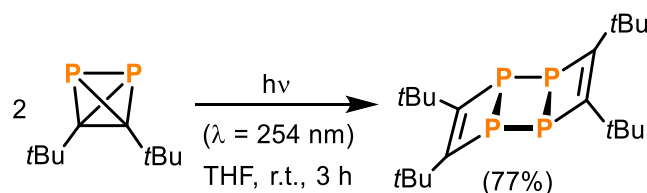
Scheme 1. Synthesis of **2** by irradiation of **1**.

Having a substantial quantity of **2** in hand, further irradiation studies were performed. Exposure of a solution of **2** in THF to LED light ($\lambda = 354$ nm or 450 nm) afforded a reaction mixture consisting of an orange precipitate and a colourless solution (Figure S4). Analysis of the solution by ^{1}H NMR spectroscopy revealed clean conversion to di-*tert*-butylacetylene as evidenced by a singlet resonance at a chemical shift of 1.34 ppm and the absence of starting material (see Figure S13). The ^{13}C{^{1}H} NMR spectrum also showed the three signals corresponding to the alkyne at chemical shifts of 27.4, 31.7 and 87.5 ppm. The ^{31}P{^{1}H} NMR spectrum showed a small amount of P$_4$ at -520.7 ppm (see Figure S15). It is therefore plausible that the orange precipitate is red phosphorus (or a related phosphorus containing polymer), which has been observed to form upon polymerisation of white phosphorus in other photoreactions (Scheme 2).[7] The fact that **2** itself undergoes photochemistry accounts for the observation that the yield of **2** from **1** was not quantitative and also accounts for the formation of a precipitate (again, presumably red phosphorus) in those samples.
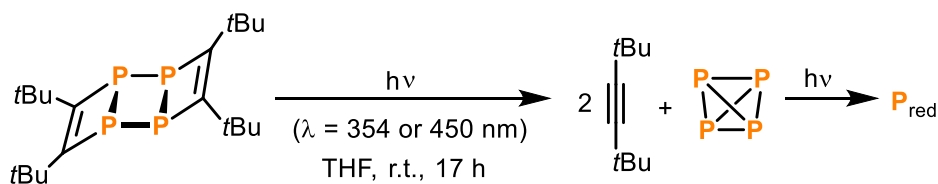
Scheme 2. Photochemistry of **2**.

After investigating the photochemistry of **1** and **2** via NMR spectroscopy, the system was studied using UV/Vis absorption spectroscopy, a spectroscopic technique with higher time resolution that should allow detection of possible short-lived intermediates. A series of experiments with **1** in different concentrations was performed.

In a first experiment, the absorption spectra of **1** were recorded after illumination at 340 nm under a defined geometry and with reproducible rectangular pulses. The pulse width is proportional to the number of emitted photons of the LED used and was varied in different experiments. Analysis of the spectra with different pulse-lengths afforded similar data; hence, only the data with pulse widths of 1 s is presented below. This pulse-wise illumination of **1** at a concentration of 500 µM in *n*-hexane resulted in the formation of a new species with an absorption spectrum with two distinct bands peaking at ca. 300 and 210 nm (Figure 5). Two isosbestic points indicate a clean photochemical conversion.
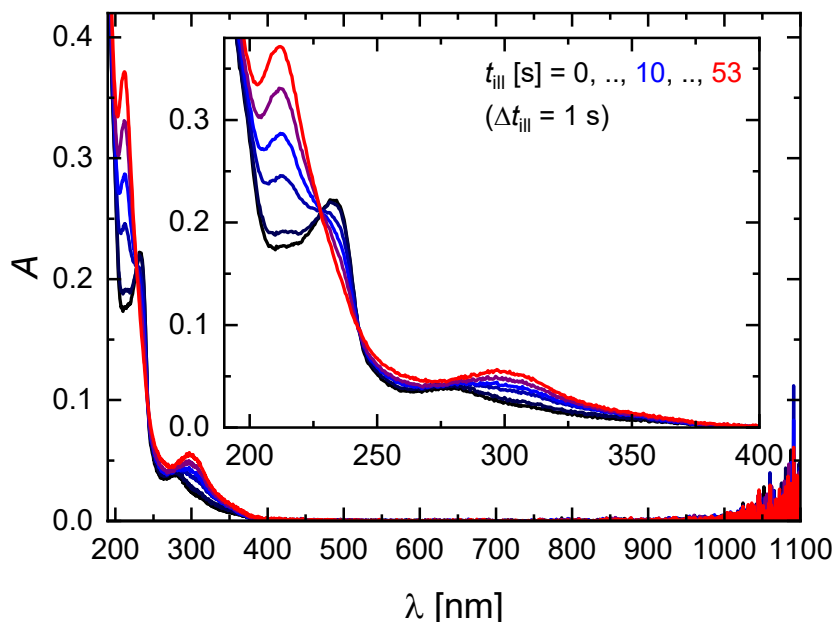

Figure 5. Sequence of absorption spectra of **1** (500 µM) in *n*-hexane after step-wise illumination at 340 nm with rectangular pulses of 1 s pulse width

The entire data set can be decomposed into the overlapping spectra of species **1** and **2**. The corresponding concentration time profiles were extracted from this data by comparison to the spectra of pure **1** and **2** (Figure 6). The spectra of the photoproduct (blue line) can be described

as a sum of the spectrum of pure synthesised **2** (orange line in Figure 6) and a scatter contribution (grey line in Figure 6), which can be explained by the observation of small insoluble particles in the sample after the experiment. This scatter contribution can be attributed to particles of P_4 or P_{red}, as shown earlier (see Scheme 2). The concentration time profile extracted from this illumination experiment is shown in Figure 6 (right) and shows a clean conversion of **1** to **2**, despite the formation of particles in the sample. Hence, it can be assumed that the photoreaction of **2** to elemental phosphorus and di-*tert*-butylacetylene is faster at higher concentrations (*vide supra*) and can be circumvented at lower concentrations. A logarithmic plot of the concentration again affords a linear relationship, confirming the reaction to be first order in **1** (see 5.4.4 for linearisation plots).
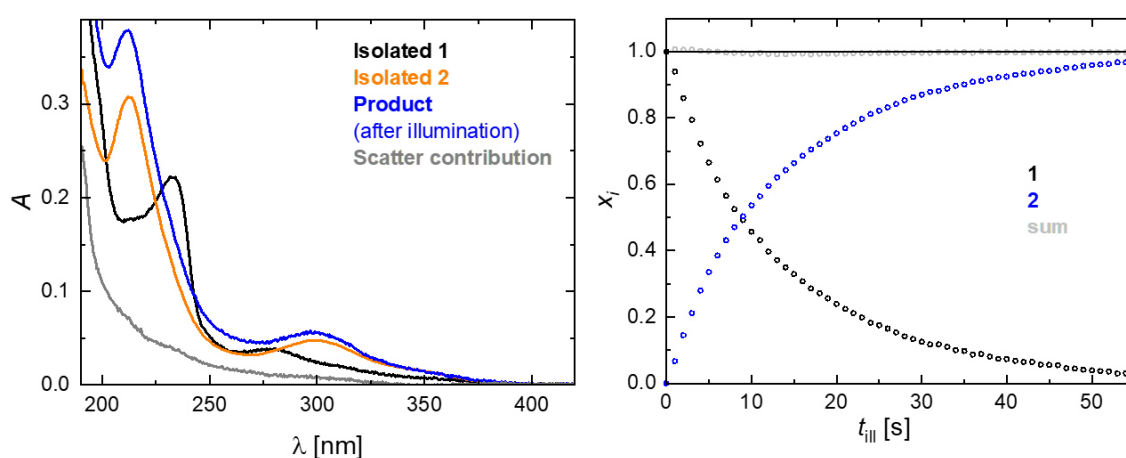

Figure 6. Different species observed in the sequence of absorption spectra (left) and concentration time profiles showing a clean photochemical conversion (right).

The photochemical conversion of **1** to **2** was further investigated by DFT calculations. Based on the structure of **2**, it was assumed that this tetracyclic P_4 compound is formed by reaction of two planar 1,2-diphosphacyclubutadienes under P−P bond formation. The overall reaction of **1** to **2** was therefore considered as a two-step process: First, the tetrahedral core of **1** isomerises to the isomeric 1,2-diphosphacyclobutadiene **1′**, which then in a second step dimerises to afford **2** (Scheme 3).
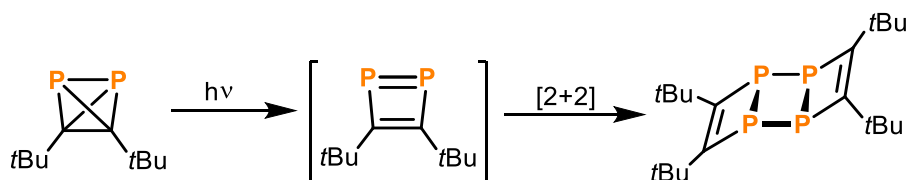
Scheme 3. Proposed mechanism for the dimerisation of **1** to **2**.

The isomerisation of **1** to **1′** was investigated by means of DFT calculations at the ωB97X-D3/def2-SVP level of theory using the Nudged Elastic Band (NEB) method (Figure 7). For comparison, the isomerisation of **1** to its 1,3-diphosphacyclobutadiene isomer (**1″**) was also

calculated. For both processes, the reaction profiles in the ground state (S_0) and the singlet excited state (S_1) were calculated. Figure 7 shows that for both isomerisations, the activation barrier is high in the S_0 state (ca. 50 kcal·mol^{-1}). In the excited state (S_1), however, the isomerisation of **1** to **1′** is energetically much more accessible. Notably, the observation that **1** dimerises in the absence of light at 80 °C contradicts such a high activation barrier. This suggests a different mechanism for the thermal process, which was not further pursued.
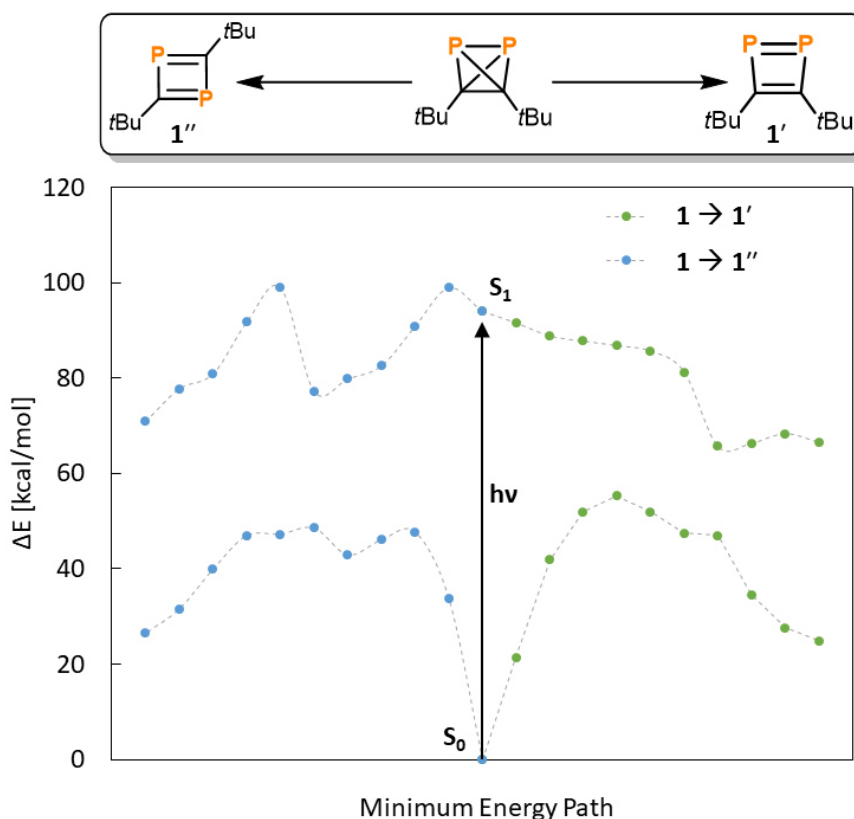
Figure 7. Calculated reaction profile for the isomerisation of **1** to **1′** and **1″** in the ground state (S_0) and the first singlet excited state (S_1). Calculations were performed at the ωB97X-D3/def2-SVP level of theory using the Nudged Elastic Band (NEB) method.

The dimerisation process of intermediate **1′** to **2** was considered to occur in the absence of light. Figure 8 shows the potential energy surface calculated on the B3LYP/def2-SVP level of theory for this process. From this energy surface, it is evident that the dimerisation of two molecules **1′** to **2** proceeds without a noticeable activation barrier and is an exothermic process. The overall thermochemical analysis reveals a total reaction enthalpy ΔH of −95.5 kcal·mol^{-1} and a Gibbs free energy ΔG of −78.8 kcal·mol^{-1}, *i.e.* the highly exothermic and exergonic dimerisation of **1′** to **2**.
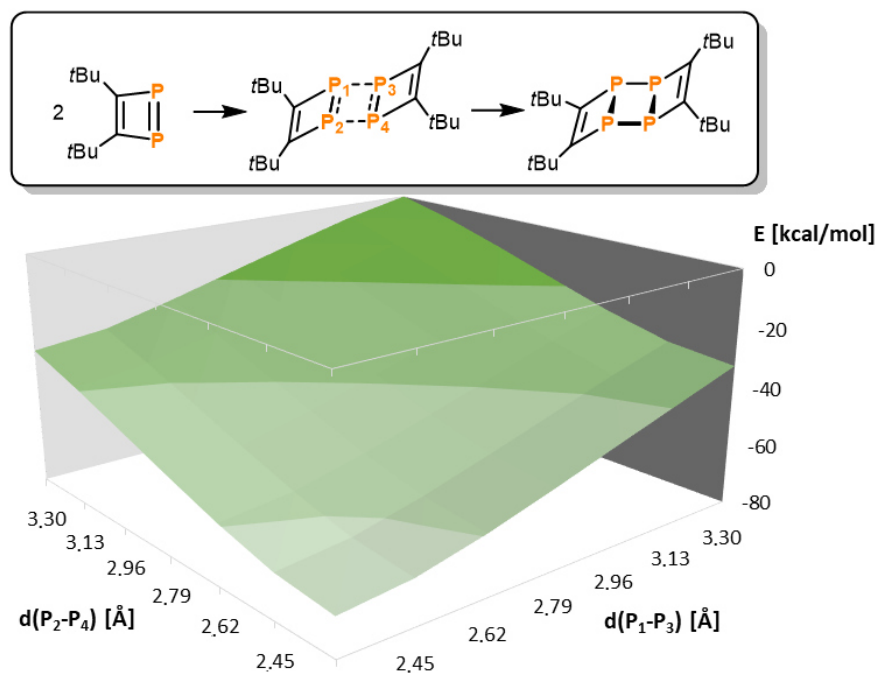
Figure 8. Energy surface plot for the dimerisation of two molecules of **1'** to **2**. Calculations were performed at the B3LYP/def2-SVP level of theory.

Given the assumption on the occurrence of a 1,2-diphosphacyclobutadiene as an intermediate in the formation of **2** from **1**, a chemical method was employed to prove the mechanism. As such the reactions of **1** with suitable trapping agents for [2+2] cycloadditions were investigated. Hence, **1** was combined with alkenes and alkynes and irradiated with a mercury vapor lamp. $^{31}P\{^1H\}$ NMR spectroscopy revealed only the previously observed dimerisation of **1** to **2** when bis(trimethylsilyl)acetylene was used as a trapping reagent. Therefore, more electron-deficient trapping reagents were employed. Maleic anhydride, however, also mainly afforded **2** due to photodimerisation of maleic anhydride itself.[12] Gratifyingly, the reaction of N-phenylmaleimide with **1** gave two singlet resonances (δ = −63.0 and −84.4 ppm) in the $^{31}P\{^1H\}$ NMR spectrum after irradiation for 2 hours (Figure S16). This reaction was more selective (affording less **2**) when excess amounts of the alkene were employed. However, removal of this excess proved difficult, due to similar solubilities and retention factors in chromatography. Therefore, subsequently, the smaller N-methylmaleimide was chosen to investigate the same reaction. The $^{31}P\{^1H\}$ NMR spectrum of the reaction of **1** with N-methylmaleimide also gave rise to two distinct signals at chemical shifts of −62.4 and −84.6 ppm. Removal of the excess N-methylmaleimide by sublimation and recrystallisation of the residue from *n*-hexane afforded single crystals of both of the isomeric [2+2] cycloaddition products **3-endo** and **3-exo** (Scheme 4). Specifically, the asymmetric unit of this crystal contained two molecules of **3-exo** and one molecule of **3-endo** (Figure 9).
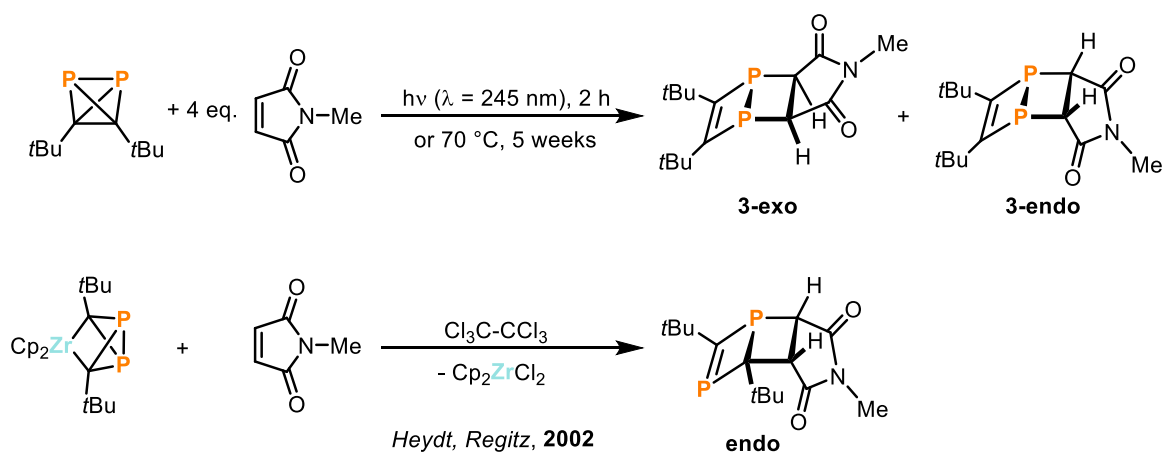
Scheme 4. [2+2]-cycloadditions of *in situ* generated 1,2- and 1,3-diphosphacyclobutadienes with N-methylmaleimide.

It is noteworthy that the groups of Heydt and Regitz described the synthesis of a related [2+2]-cycloaddition product originating from the reaction of the same maleimide with the isomeric 1,3-diphosphacyclobutadiene (Scheme 4 bottom). The formation of this product was confirmed by multinuclear (^1H, $^{13}C\{^1H\}$ and $^{31}P\{^1H\}$) NMR spectroscopy and mass spectrometry. In this case, the 1,3-diphosphacyclobutene was released by addition of hexachloroethane to a zirconium complex.

The molecular structures of **3-exo** and **3-endo** in the solid state (Figure 9) support the formation of diphosphabicyclo[2.2.0]hexene rings formed upon [2+2] cycloaddition of an *in situ* generated 1,2-diphosphacyclobutadiene with N-methylmaleimide. This is consistent with the proposed mechanism for the dimerisation of **1** to **2** via a 1,2-diphosphacyclobutadiene. In both **3-exo** and **3-endo**, the P−P bond lengths [P1−P2 2.2428(6) Å, P5−P6 2.2330(7) Å] are indicative of a single bond and the C−C bonds originating from **1** have bond lengths typical for double bonds [C1−C2 1.362(3) Å, C32−C31 1.367(3) Å].[13] The C−C bonds originating from the maleimide possess typical bond lengths for single bonds [C11−C12 1.524(2) Å, C41−C42 1.523(2) Å]. The C2-P2-C12 and C1-P1-C11 angles of 97.82(7)° and 95.54(7)°, respectively, show an almost perpendicular arrangement of the two C_2P_2 rings in **3-exo**. In **3-endo**, these angles are larger [C31-P5-C41: 100.86(8)°, C32-P6-C42: 100.74(8)°] possibly resulting from steric clash of the *tert*-butyl groups and the imide moiety.

According to the ^1H and $^{31}P\{^1H\}$ NMR spectra, **3-exo** and **3-endo** were isolated as a mixture containing ca. 53% of the endo- and 47% of the exo-isomer and further analysed by multinuclear NMR spectroscopy and mass spectrometry. The $^{31}P\{^1H\}$ NMR spectrum shows two singlet signals at chemical shifts of −85.2 and −63.1 ppm. In the proton-coupled ^{31}P NMR spectrum the signal at −85.2 ppm shows coupling to the diphosphacyclobutane protons and has the shape of a pseudo-triplet, whereas the signal at −63.1 ppm shows no coupling. DFT calculations at the TPSS pcSseg-2 level of theory confirm that the high-field resonance, which is assigned to **3-endo** in these calculations, shows higher J_{PH} coupling constants than the low-field species. This is in

agreement with the experimental values and also confirmed by a study on the effect of the lone pair conformation on P−H coupling constants.[14] Simulation of the ^{31}P NMR signal of **3-endo** reveals a $^2J_{PH}$ coupling constant of 13.1 Hz and a $^3J_{PH}$ coupling constant of −9.7 Hz.
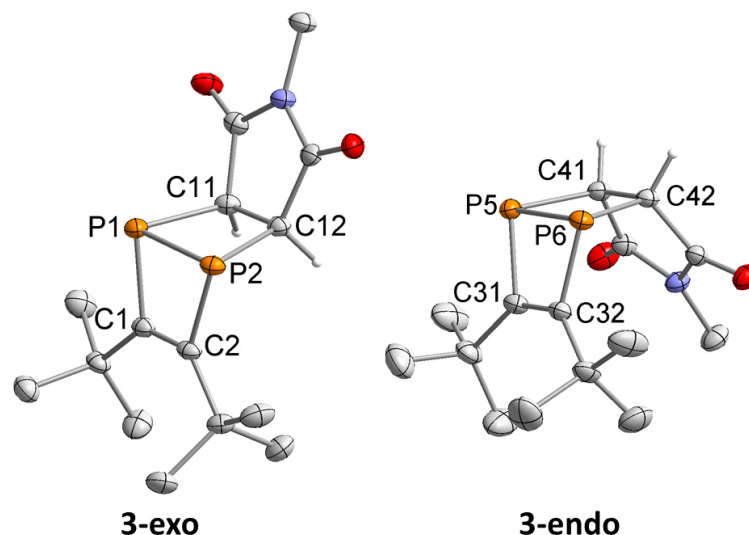

Figure 9. Molecular structures of **3-endo** and **3-exo** in the solid state. Thermal ellipsoids are set at 50% probability level. H-atoms (except for those binding to C11, C12, C41 and C42) are omitted for clarity. Selected bond lengths [Å] and angles [°]: P1−P2 2.2428(6), P1−C1 1.8440(17), P1−C11 1.9161(18), P2−C2 1.8529(17), P2−C12 1.9102(17), C1−C2 1.362(3), C11−C12 1.524(2), P5−P6 2.2330(7), P5−C31 1.8415(18), P5−C41 1.9282(19), P6−C32 1.8419(17), P6−C42 1.9239(18), C32−C31 1.367(3), C41−C42 1.523(2), C1−P1−P2 76.46(6), C2−P2−P1 75.98(6), C1−C2−P2 103.81(12), C2−C1−P1 103.74(12), C11−P1−P2 79.52(6), C12−P2−P1 78.78(6), C12−C11−P1 100.03(11), C11−C12−P2 101.54(11), C2−P2−C12 97.82(7), C1−P1−C11 95.54(7), C31−P5−P6 76.27(6), C32−P6−P5 76.53(6), C32−C31−P5 103.82(12), C31−C32−P6 103.36(12), C41−P5−P6 79.17(6), C42−P6−P5 79.57(6), C41−C42−P6 100.49(11), C42−C41−P5 100.76(11), C31−P5−C41 100.86(8), C32−P6−C42 100.74(8).

The ^{1}H NMR spectrum of the mixture of isomers **3-endo** and **3-exo** shows singlet resonances for the *tert*-butyl groups at 1.07 and 1.15 ppm and for the maleimide methyl groups at 2.65 and 2.66 ppm. Moreover, the diphosphacyclobutane proton signals arise as a singlet at 2.75 for **3-exo** and as a multiplet between 2.63 and 2.71 ppm for **3-endo**. The $^{13}C\{^1H\}$ NMR spectrum shows two singlet resonances for the maleimide methyl groups and pseudo triplet resonances for the other carbon atoms. Four low-field resonances were assigned to the diphosphacyclobutene carbon atoms at 167.7 (**3-endo**) and 168.6 ppm (**3-exo**) and the carbonyl moieties at 175.2 (**3-endo**) and 175.9 ppm (**3-exo**). Analysis of a mixture of **3-endo** and **3-exo** by GC-MS revealed two peaks at retention times of 14.28 and 14.46 min with mass spectra that show the same, expected molecular ion signal with *m/z* = 311.0.

Having studied the photoconversion of **1** to **2** by stationary absorption spectroscopy and having developed a basic mechanistic understanding, time resolved spectroscopic methods were employed in order to detect possible intermediates. Transient absorption allows to detect photochemically generated species and determine their lifetimes. In general, the change of

absorption in the sample is measured by excitation with a "pump"-pulse and measurement of the absorption with the "probe"-laser. In this experiment, the excitation wavelength was 355 nm. Applying a global fit to the TA spectra (Figure 10) allows for a separation into two species: a short-lived species with a lifetime of ca. 1.6 ms and a long-lived species with a lifetime longer than 100 ms. As Figure 11 shows, on a sub-ms time scale after excitation of **1** a very broad structureless absorption spectrum arises, which ranges over the entire spectral detection window from 350 to 750 nm within the excitation pulse width of ca. 10 ns. This spectrum is intercepted by the ground state bleach at ca. 360 nm. This broad spectrum disappears within 200 ns and another broad absorption with a single peak at ca. 400 nm remains. This new absorption spectrum does not decay over the investigated time window. It should be noted, however, that the occurrence of a short-lived species with a lifetime of ca. 1.6 ms was not observed in all preparations (see Figure S21). The reason for this is still not clear and needs further investigations.
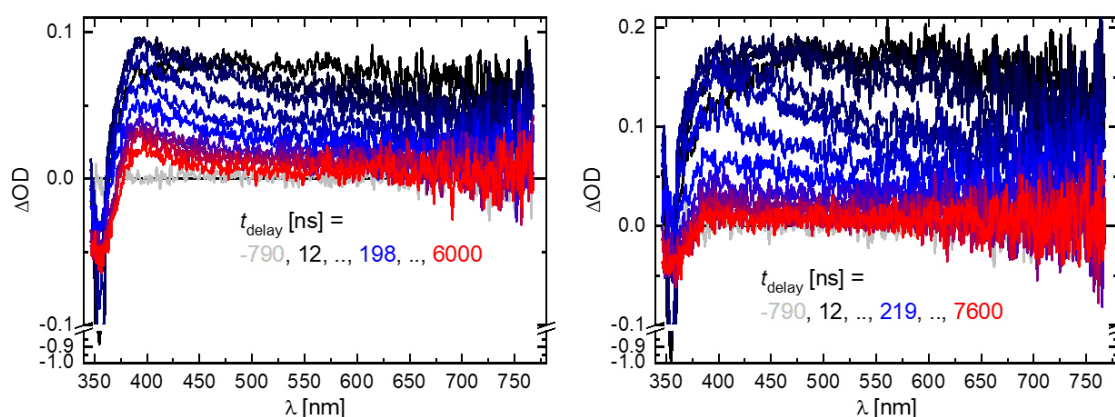

Figure 10. Transient absorption (TA) of **1** (2 mM) in molecular oxygen free *n*-hexane (sample was prepared in a glove box) after excitation at 355 nm (10 mJ). The sample volume was 3 mL (10 mm x 10 mm for pump and probe) and the sample was stirred during the measurement. 100 individual excitation cycles were performed. Left: Calculated TA when averaging over 100 individual measurements. Right: Calculated TA when averaging over only the first 10 individual measurements. As evident from different TA spectra the sample irreversibly converts, so that during the course of the measurement different accumulating species become excited.
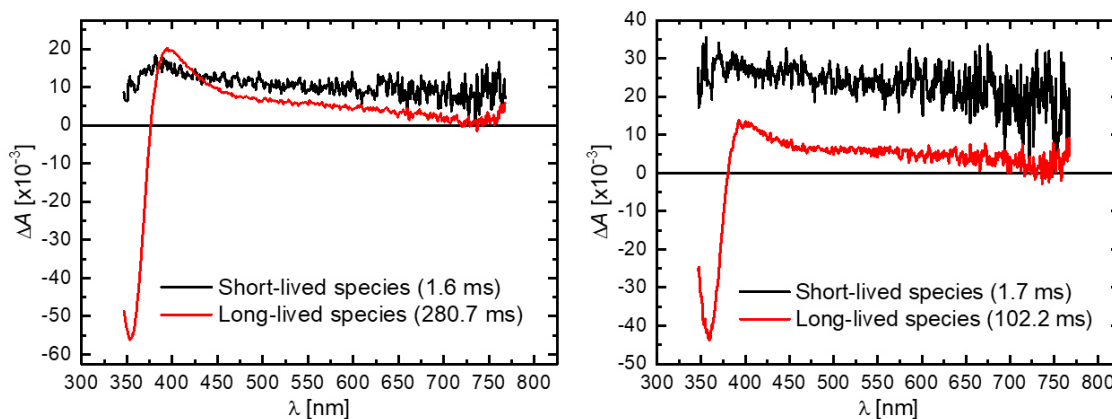

Figure 11. Decay associated differences spectra (DADS) resulting from a global fit with exponential functions on the data presented in Figure 10.

However, in all cases a longer-lived species with a lifetime of >10 ms was consistently observed. Comparison of the stationary absorption spectra before and after the TA experiment reveals that the observed spectrum after the TA experiment does not correspond to **2**, which was observed in earlier studies (see Figure 12 right).
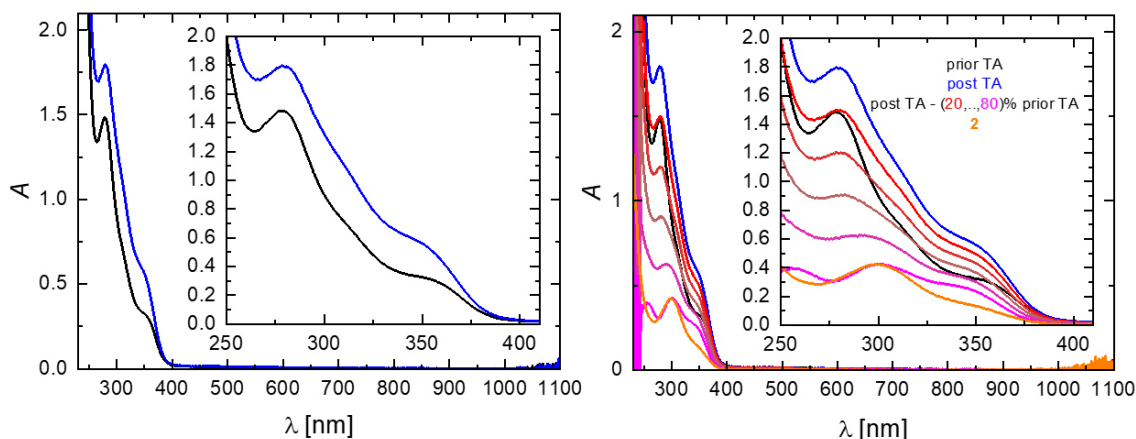

Figure 12. Stationary absorption spectra of **1** (2 mM) in molecular oxygen free *n*-hexane (sample was prepared in a glove box) prior (black) and after excitation at 355 nm during the TA experiment (blue). Subtraction of the pure spectrum of **1** of the post spectrum (red to magenta) does not result in the pure spectrum of **2** (orange) indicating the formation of an additional photoproduct.

Overall, the results of the (transient) absorption spectroscopy experiments can be summarised as follows: 1) On a ns time scale, in some cases, a broad structureless spectrum is observed; 2) On a ms time scale a species is formed that has an absorption band at ca. 400 nm; 3) On a s time scale **2** is formed; 4) In some cases or under some conditions, a pure scatter spectrum is photochemically observed, which presumably arises from formation of phosphorus particles.

5.3   Conclusion

A detailed computational and experimental study on the photochemistry of di-*tert*-butyldiphosphatetrahedrane (**1**) has been presented. ^{31}P{^{1}H} NMR spectroscopic studies have revealed that **1** is stable at ambient temperature in solutions in the dark, but converts to the ladderane-type phosphaalkyne tetramer (*t*BuCP)$_4$ (**2**) upon irradiation or at elevated temperatures. This process was studied by NMR and UV/Vis spectroscopies. For NMR studies relatively high concentrations (0.2 - 0.4 mol·L^{-1}) of **1** were necessary. Under these conditions, the formation of **2** was confirmed, but the observed yield was not 100% due to the photochemical reactivity of **2** itself, which decomposes to P$_4$ (which, in turn, is transformed into red phosphorus) and di-*tert*-butylacetylene. For absorption spectroscopic measurements, the concentration was much lower (0.5 mM for stationary and 2 mM for transient absorption) and a much cleaner photochemical conversion of **1** to **2** was observed. While the reasons for this behaviour are still unclear, one could speculate that the photoreaction of **2** to P$_4$ and di-*tert*-butylacetylene has a strong concentration dependence, affording P$_4$ much quicker at higher concentrations. Computational

analysis of the mechanism of the dimerisation reaction of **1** forming **2** reveal a possible two-step mechanism: First, **1** undergoes isomerisation to its 1,2-diphosphacyclobutadiene isomer **1′**, which has a significantly lower activation barrier in the excited state. Subsequently, [2+2] cycloaddition of two 1,2-diphosphacyclobutadienes affords **2** in a purely thermal step. However, the reaction of **1** with **1′** also represents a possible mechanism which will be elucidated computationally in future studies. Transient absorption measurements revealed the presence of a short-lived species and a long-lived species with lifetimes of 1.6 ms and >100 ms, respectively. Due to the broad, structureless spectra of these species, the assignment to any postulated intermediates (such as the 1,2-diphosphacyclobutadiene) is not possible. Further investigations on a picosecond time scale might reveal intermediates with a more defined spectrum that can be assigned and these are a future goal to further elucidate the mechanism. Finally, we were able to trap **1′** by a [2+2] cycloaddition with N-methylmaleimide. In future studies, it is anticipated that this reactivity could be expanded to a broader scope of electron-poor alkenes. Furthermore, [3+2] cycloadditions with diazomethanes could give access to new diazadiphospholines or diphosphiranes while [4+2] cycloadditions might also be feasible.

5.4   Experimental Details

General Synthetic Methods

All reactions and product manipulations were carried out in flame-dried glassware under an inert atmosphere of argon using standard Schlenk-line or glovebox techniques (maintained at <0.1 ppm H_2O and <0.1 ppm O_2). (*t*BuCP)$_2$ was prepared according to a procedure previously reported in the chemical literature.[9] All other chemicals were purchased from commercial suppliers and used without further purification.

Solvents were dried and degassed with a MBraun SPS800 solvent purification system. Fluorobenzene was dried over sodium and distilled. All dry solvents except *n*-hexane and *n*-pentane were stored under argon over activated 3 Å molecular sieves in gas-tight ampoules. *n*-Hexane and *n*-pentane were instead stored over potassium mirrors.

General Analytical Techniques

NMR spectra were recorded on Bruker Avance 300 or 400 spectrometers at 300 K unless otherwise noted and internally referenced to residual solvent resonances (^{1}H NMR: C$_6$D$_6$: 7.16 ppm; ^{13}C{^{1}H} NMR: C$_6$D$_6$: 128.06 ppm). Chemical shifts δ are given in ppm referring to external standards of tetramethylsilane (^{1}H, ^{13}C{^{1}H}) or 85% phosphoric acid (^{31}P and ^{31}P{^{1}H} spectra). ^{1}H and ^{13}C NMR signals were assigned based on 2D NMR spectra (^{1}H,^{1}H-COSY, ^{1}H,^{13}C-HSQC, ^{1}H,^{13}C-HMQC). Quantitative ^{31}P NMR spectra were recorded as previously described.[15]

Single-crystal X-ray diffraction data were recorded on a XtaLAB Synergy DW R (DW system, HyPix-Arc 150) diffractometer with Cu-K$_\alpha$ radiation (λ= 1.54184 Å). Crystals were selected under mineral oil, mounted on micromount loops and quench-cooled using an Oxford

Cryosystems open flow N_2 cooling device. Either semi-empirical multi-scan absorption corrections[16] or analytical ones[17] were applied to the data. The structures were solved with the SHELXT[18] solution program using dual methods and by using Olex2 as the graphical interface.[19] The models were refined with ShelXL[20] using full matrix least squares minimisation on F^2.[21] The hydrogen atoms were located in idealised positions and refined isotropically with a riding model.

For GC-MS an Agilent 7820A GC system with mass detector 5977B was used with H_2 as carrier gas and a HP-5MS (30m x 0.25 mm x 0.25 μm) column. The standard heating procedure was: 50 °C → 300 °C. The GC-MS analysis of the mixture of **3-endo** and **3**-exo is shown in Figure S1.
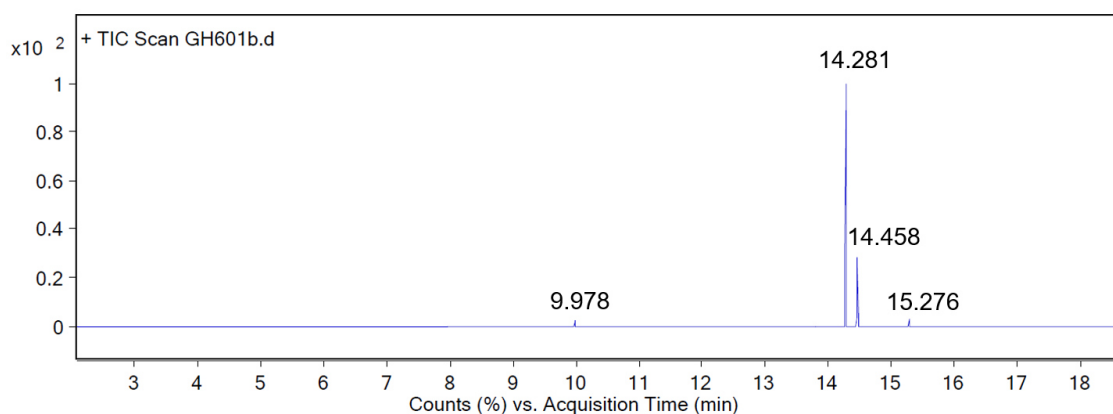
Figure S1. Chromatogram of mixture of **3-endo** and **3-exo**. The peak at 9.978 could not be identified and the peak at 15.276 can be assigned to (*t*BuCP)$_4$ (**2**).
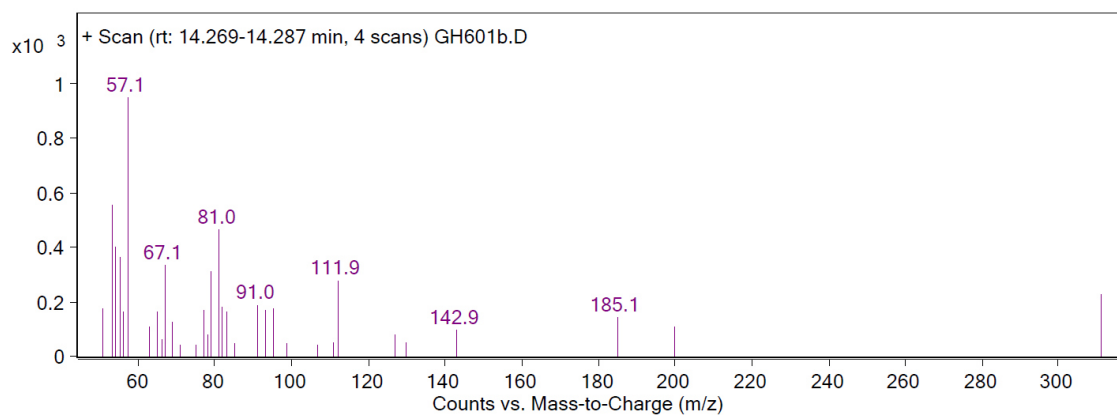

Figure S2. Mass spectrum of species arising in the chromatogram (Figure S1) at 14.281 min.
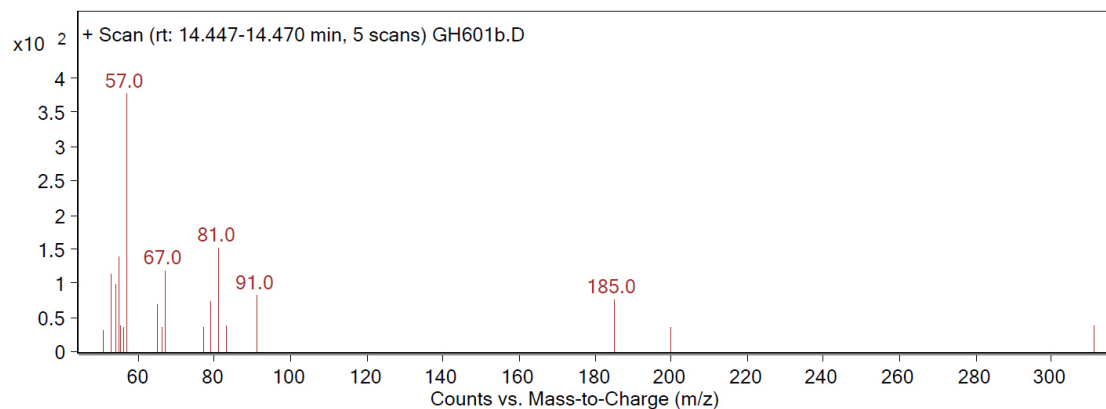
Figure S3. Mass spectrum of species arising in the chromatogram (Figure S1) at 14.458 min.


Figure S4. Image of the NMR tube after irradiation of **2** to form tBuC≡CtBu, small amounts of P$_4$ and orange precipitate.

5.4.1 Synthesis of Compounds

(tBuCP)$_4$ (2):

A solution of (tBuCP)$_2$ (0.5 mL, c = 0.6 M in toluene, 0.30 mmol) in THF (3 mL) was irradiated with a UV-lamp (λ = 254 nm; "chromatography lamp") for 3 hours while stirring. Subsequently, the solvent was removed *in vacuo* and the off-white residue was extracted with benzene (5 mL). The solvent was removed and the white powder was dried *in vacuo* to afford pure (tBuCP)$_4$ (**2**) without further purification.

C$_{20}$H$_{36}$P$_4$, MW = 400.40 g/mol
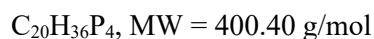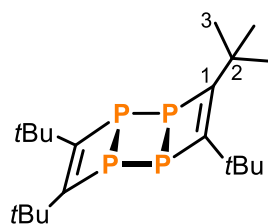
Yield: 46 mg (77%)

Analytical data was identical to the previously reported data.[10] NMR spectra are given in Figure S6 to Figure S8.

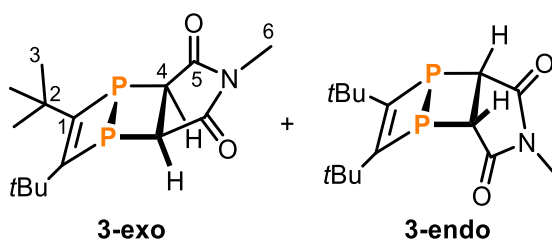**^{1}H NMR** (400 MHz, 300 K, C$_6$D$_6$) δ = 1.40 (s, 36H, C^{3}H) ppm.

^{13}C{^{1}H} NMR (100 MHz, 300 K, C$_6$D$_6$) δ = 31.6 (pseudo-t, J_{PC} = 3.1 Hz ,C^3), 39.7 (pseudo-t, J_{PC} = 2.4 H, C^2), 172.5 (s, C^1) ppm.

^{31}P{^{1}H} (162 MHz, 300 K, C$_6$D$_6$) δ = −23.0 (s) ppm.

3-exo and **3-endo**:

A solution of (*t*BuCP)$_2$ (0.6 mL, c = 2.0 M in toluene, 1.20 mmol, 1.0 eq.) and N-methyl maleimide (1333 mg, 12.0 mmol, 10.0 eq.) in toluene (15 mL) was heated to 70 °C for 5 weeks while stirring. Subsequently, the solvent was removed *in vacuo* and the residual N-methyl maleimide was removed by sublimation (oil bath at 50 °C, cooling water ca. 25 °C, pressure ca. 1·10^{-3} mbar). The crude product was recrystallised from toluene at −30 °C.

C$_{15}$H$_{23}$NO$_2$P$_2$, MW = 311.30 g/mol

Yield: 140 mg (37%)

^{1}H NMR (400 MHz, 300 K, C$_6$D$_6$) δ = 1.07 (s, 18H, C^{4}H, C^{3}H-exo), 1.15 (s, 23H, C^{3}H-endo), 2.65 (s, 3.5H, C^{6}H-endo), 2.66 (s, 3H, C^{6}H-exo), 2.63-2.71 (m, overlapping with C^{6}H-exo and C^{6}H-endo, C^{4}H-endo), 2.75 (s, 2H, C^{4}H-exo) ppm.

^{13}C{^{1}H} NMR (100 MHz, 300 K, C$_6$D$_6$) δ = 24.7 (s, C^6-exo), 24.8 (s, C^6-endo), 30.7 (ps t, J_{PC} = 9.2 Hz, C^4-endo), 31.1 (ps t, J_{PC} = 5.1 Hz, C^3-exo), 31.3 (ps t, J_{PC} = 5.0 Hz, C^3-endo), 38.5 (ps t, J_{PC} = 6.2 Hz, C^2-endo), 38.8 (ps t, J_{PC} = 6.5 Hz, C^2-exo), 42.4 (ps t, J_{PC} = 8.2 Hz, C^4-exo), 167.7 (ps t, J_{PC} = 9.3 Hz, C^1-endo), 168.6 (ps t, J_{PC} = 8.1 Hz, C^1-exo), 175.2 (ps t, J_{PC} = 3.0 Hz, C^5-endo), 175.9 (ps t, J_{PC} = 5.5 Hz, C^5-exo) ppm.

^{31}P{^{1}H} (162 MHz, 300 K, C$_6$D$_6$) δ = −85.2 (s, P-endo), −63.1(s, P-exo) ppm.

^{31}P (162 MHz, 300 K, C$_6$D$_6$) δ = −85.2 (pseudo triplet, $^2J_{PH}$ = 13.1 Hz, $^3J_{PH}$ = −9.7 Hz, P-endo), −63.1(s, P-exo) ppm.

GC-MS *m/z* = 311.0 (retention times and additional data given in Figure S1, Figure S2 and Figure S3).
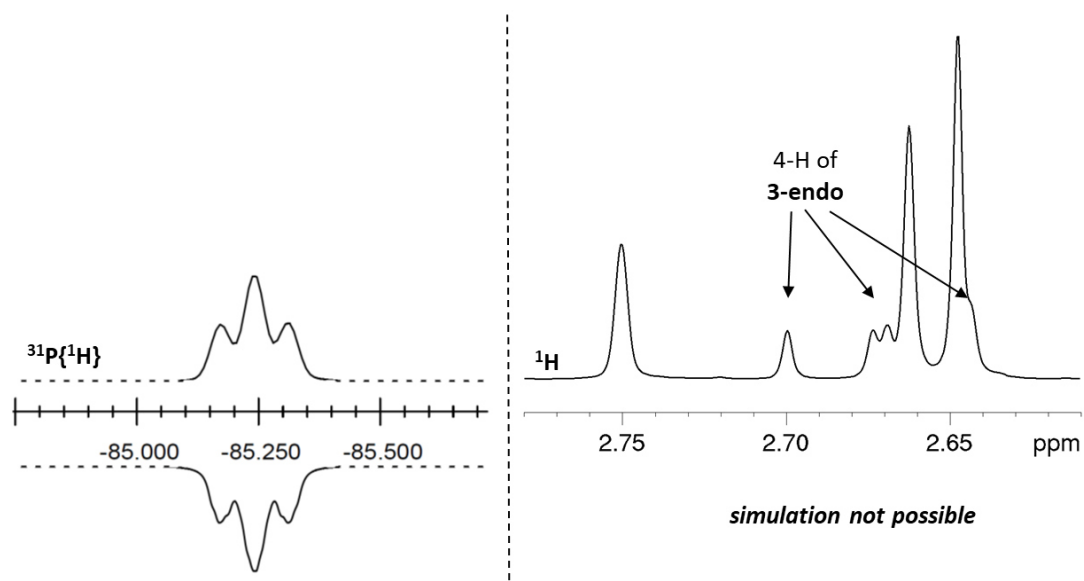
Figure S5. Left: Section of the ^{31}P NMR (162 MHz, C$_6$D$_6$, 300 K) showing the signal of **3-endo**; experimental (upwards) and simulation (downwards); right: section of the ^{1}H NMR spectrum of the mixture of **3-exo** and **3-endo** (simulation was not possible due to overlap of signals).

Table S1. Coupling constants from the iterative fit of the AA′XX′ spin system and schematic representation of **3-endo**. Only the A part (observed in the ^{31}P NMR spectrum) was simulated. The X part observed in the ^{1}H NMR spectrum was partially obscured due to signal overlap with further ^{1}H NMR signals.

δ(A) = −85.23 ppm

δ(A′) = −85.25 ppm

$^1J_{AA'}$ = 2.1 Hz

$^2J_{AX}$ = 13.1 Hz

$^3J_{A'X}$ = −9.7 Hz

$^1J_{XX'}$ = 0.1 Hz

Alternatively, **3-exo** and **3-endo** can be prepared by a photochemical reaction: A solution of (*t*BuCP)$_2$ (0.3 mL, c = 2.0 M in toluene, 0.60 mmol, 1.0 eq.) and N-methyl maleimide (500 mg, 4.5 mmol, 7.5 eq.) in toluene (100 mL) was irradiated with a Hg-lamp (photoLAB reactor from UV-Consulting Peschl®) for 5 minutes. Subsequently, the solvent was removed *in vacuo* and the sample was analysed by ^{31}P NMR spectroscopy, showing a singlet resonance at −63.1 and a triplet resonance at −85.2 ppm. Subsequently, the solvent was removed *in vacuo* and the residual N-methyl maleimide was removed by sublimation (oil bath at 50 °C, cooling water ca. 25 °C, pressure ca. 1·10^{-3} mbar). The crude product was recrystallised from toluene at −30 °C.

Single crystals of **(3-exo)$_2$(3-endo)** were obtained by slow evaporation from a saturated *n*-hexane solution of a mixture of **3-exo** and **3-endo**.

Yield: 55 mg (29%)

Analytical data was identical to the data presented above.

5.4.2 NMR Spectra
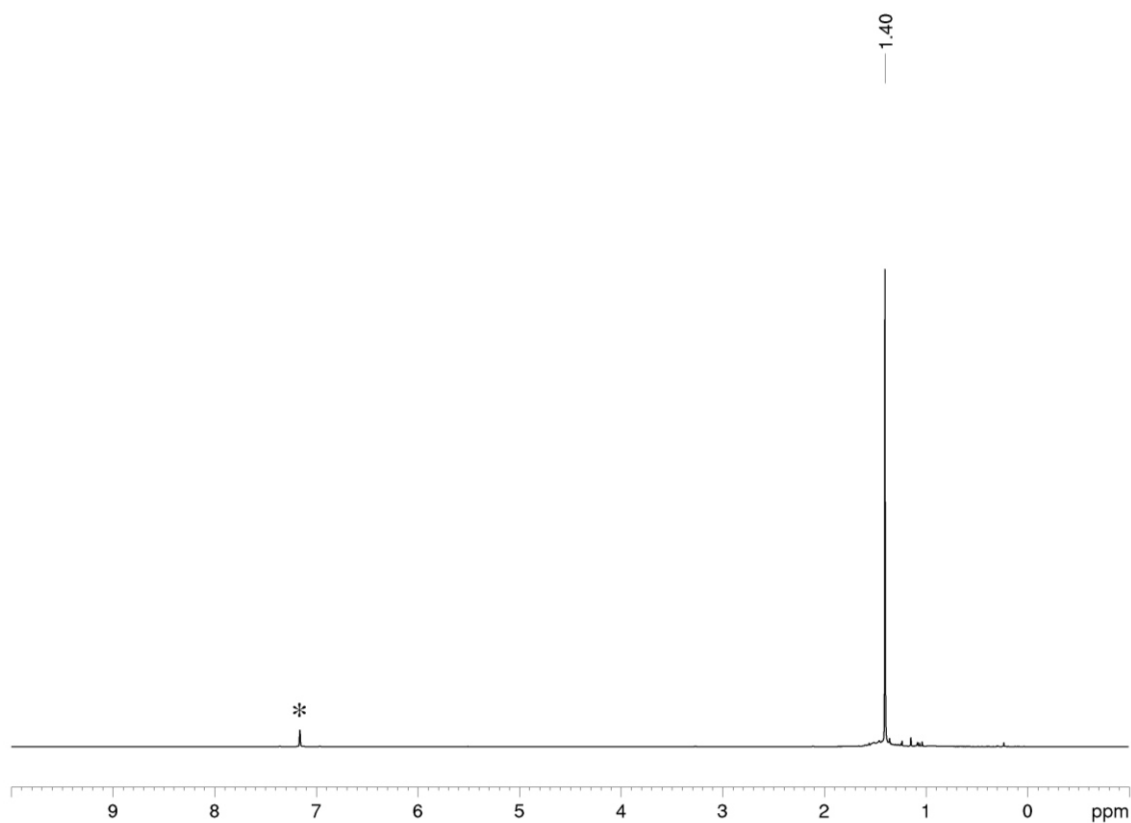
Figure S6. ^{1}H NMR spectrum (400 MHz, 300 K, C$_6$D$_6$) of **2**; *C$_6$D$_6$.
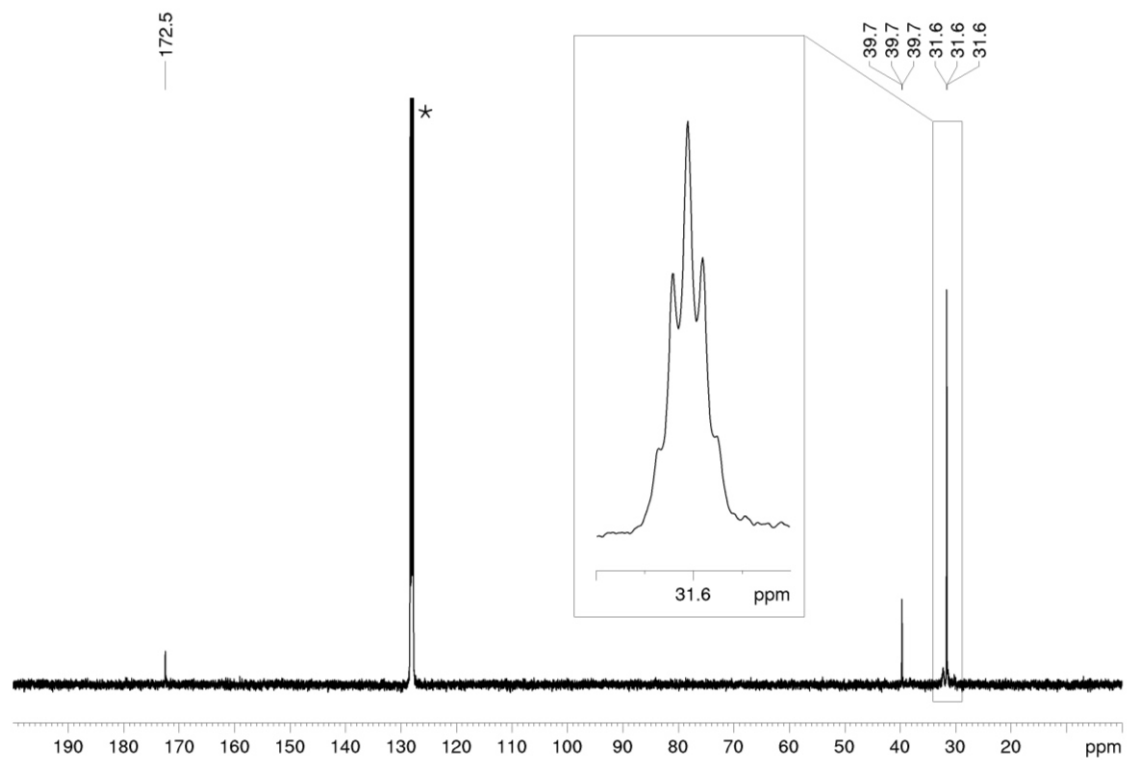
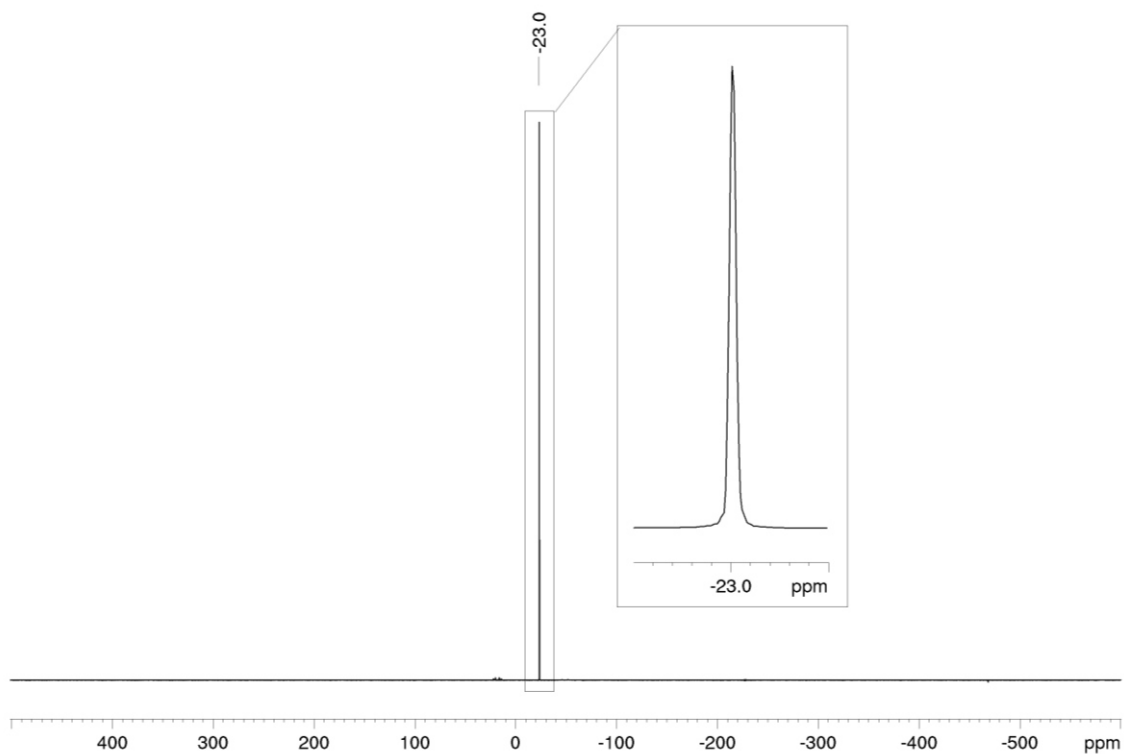**Figure S7.** ^{13}C{^{1}H} NMR spectrum (100 MHz, 300 K, C$_6$D$_6$) of **2**; *C$_6$D$_6$.

Figure S8. $^{31}P\{^1H\}$ NMR spectrum (162 MHz, 300 K, C_6D_6) of **2**.
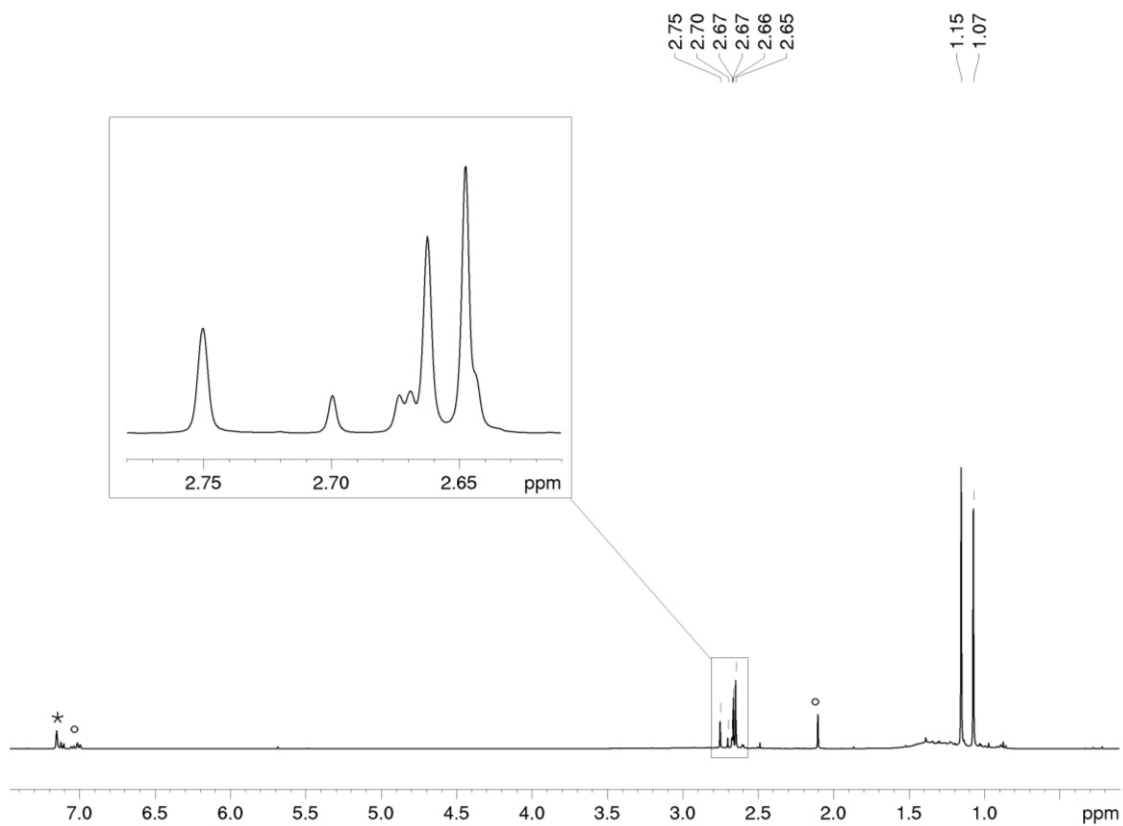

Figure S9. ^1H NMR spectrum (400 MHz, 300 K, C_6D_6) of a mixture **3-exo** and **3-endo**; *C_6D_6; °residual toluene.

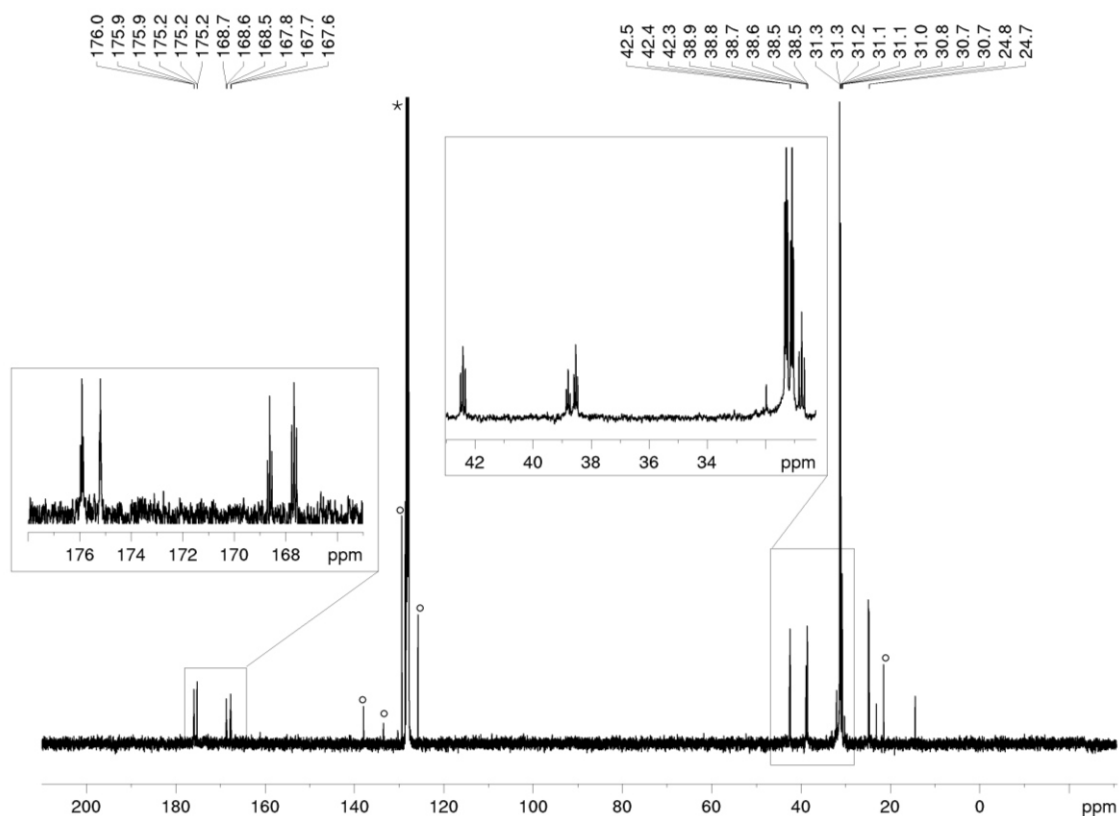**Figure S10.** $^{13}C\{^1H\}$ NMR spectrum (100 MHz, 300 K, C_6D_6) of a mixture **3-exo** and **3-endo**; *C_6D_6; °residual toluene.

Figure S11. $^{31}P\{^1H\}$ NMR spectrum (162 MHz, 300 K, C_6D_6) of a mixture **3-exo** and **3-endo**.

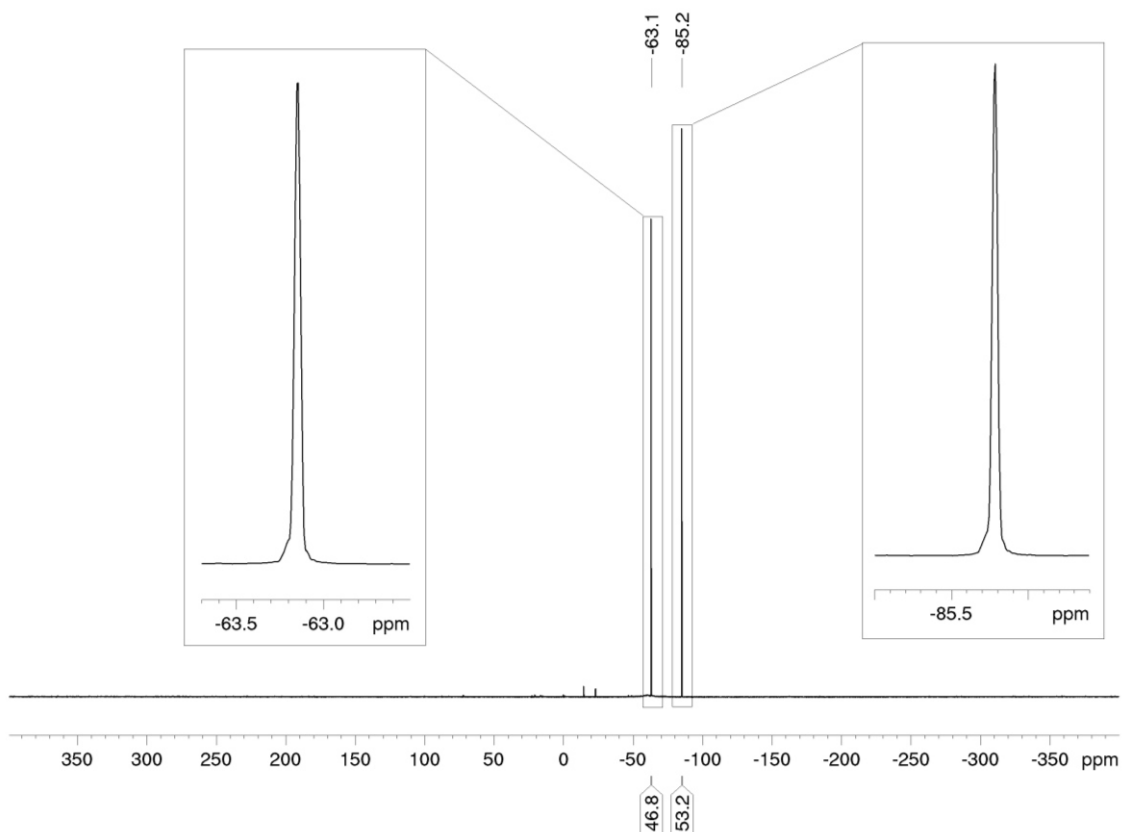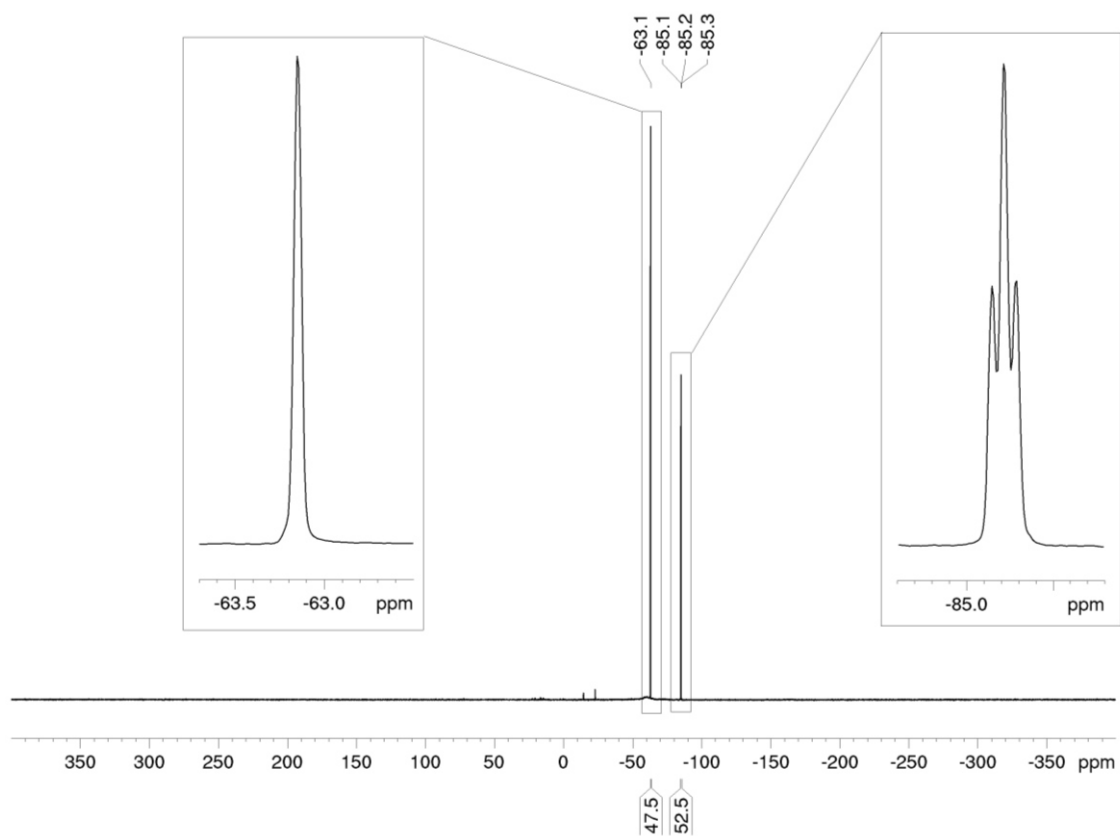**Figure S12.** ^{31}P NMR spectrum (162 MHz, 300 K, C_6D_6) of a mixture **3-exo** and **3-endo**.

Figure S13. ^1H NMR spectrum (400 MHz, 300 K, C_6D_6) after irradiation of **2** with an LED ($\lambda = 354$ nm). The main signal at 1.23 ppm corresponds to the $tBuC{\equiv}CtBu$. °PPh$_3$ (internal standard); *C_6D_6.
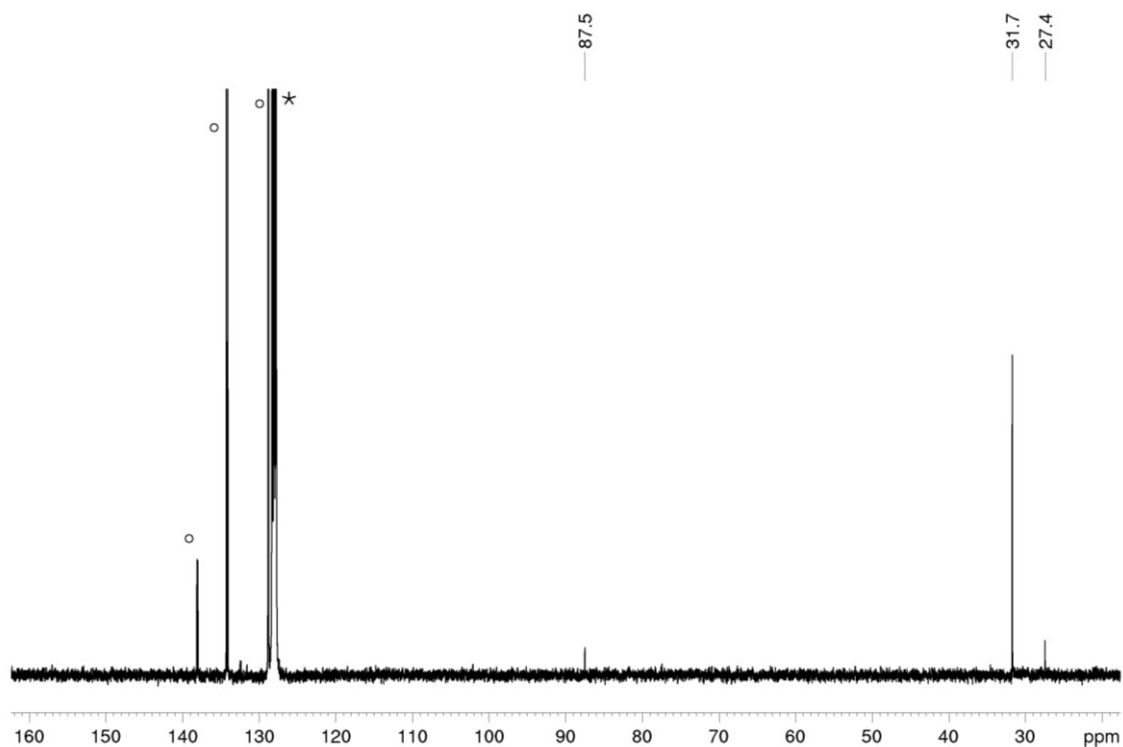
Figure S14. $^{13}C\{^1H\}$ NMR spectrum (100 MHz, 300 K, C$_6$D$_6$) after irradiation of **2** with an LED (λ = 354 nm); all marked signals belong to tBuC≡CtBu; °PPh$_3$ (internal standard), *C$_6$D$_6$.
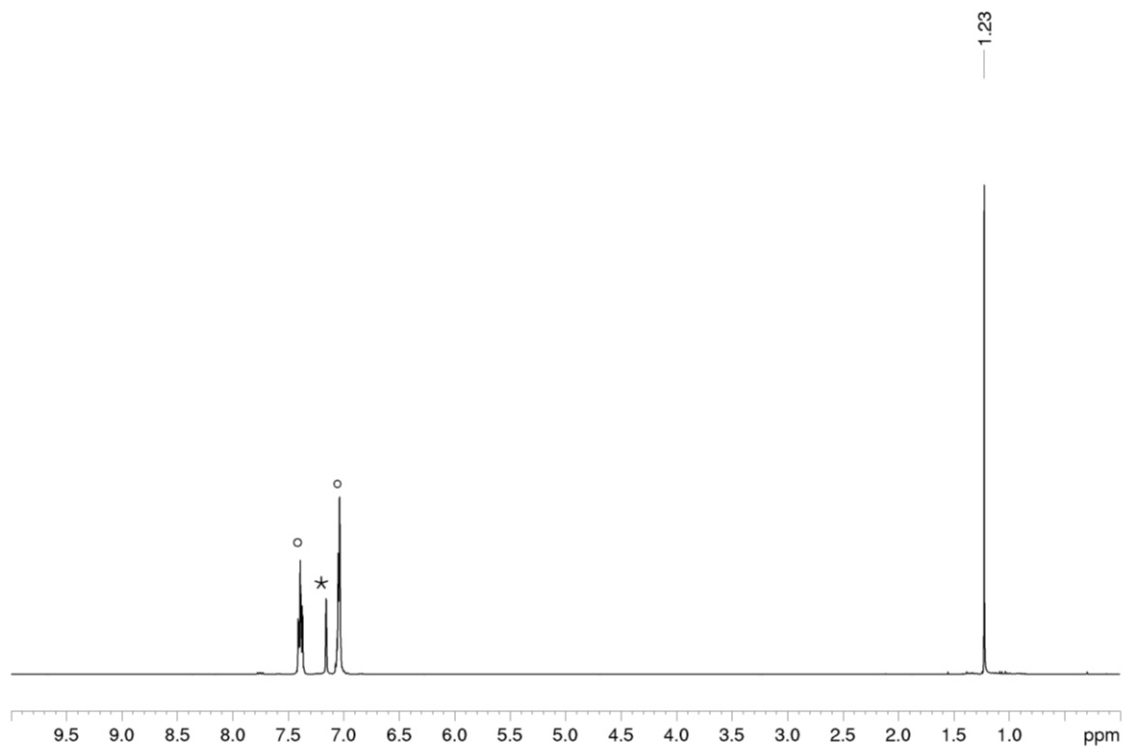

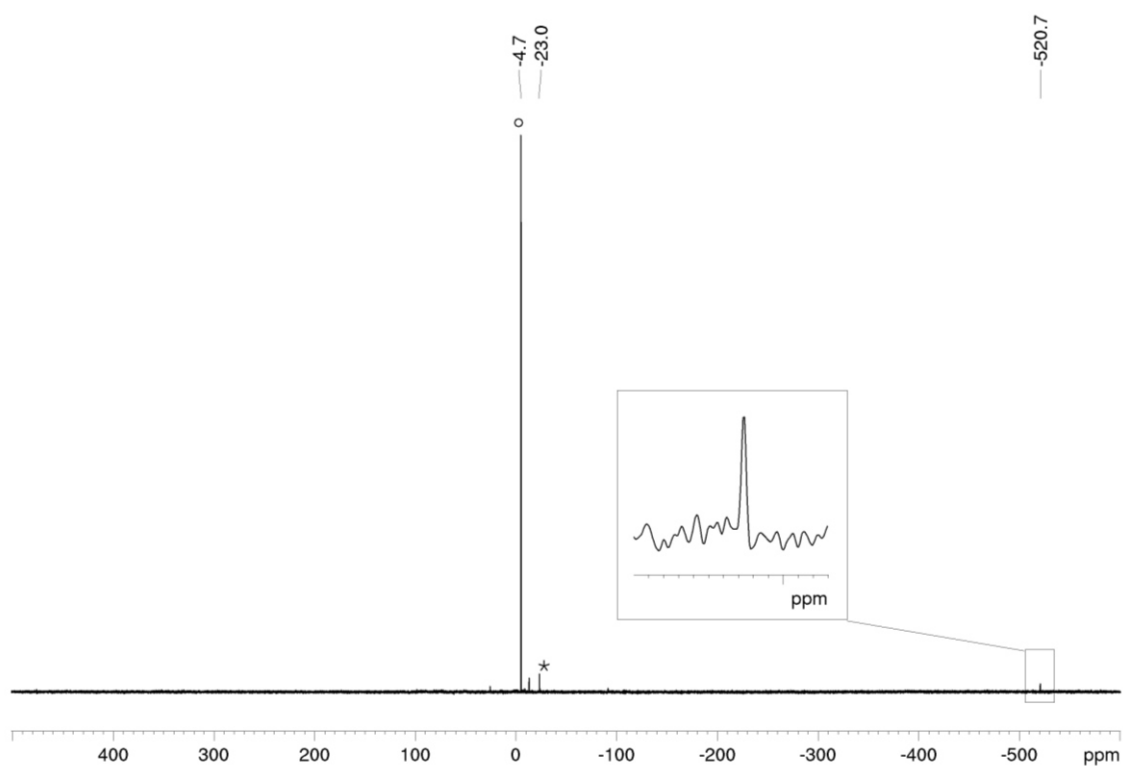**Figure S15.** ^{31}P NMR spectrum (162 MHz, 300 K, C$_6$D$_6$) after irradiation of **2** with an LED (λ = 354 nm). The signal at −520.7 ppm corresponds to P$_4$. *residual 2; °PPh$_3$ (internal standard).
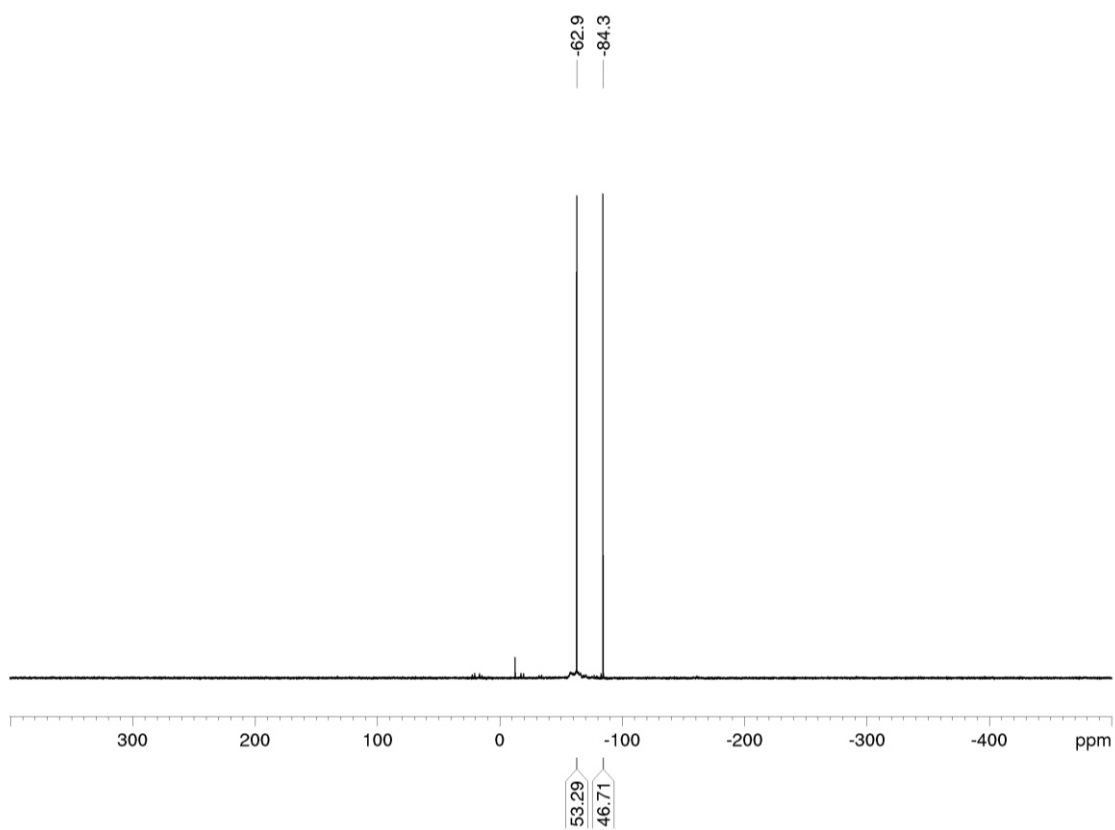
Figure S16. ^{31}P NMR spectrum (162 MHz, 300 K, C$_6$D$_6$) of the photoreaction of **1** with N-phenylmaleimide.

5.4.3   Single Crystal X-Ray Diffraction Data

Table S2. Crystal data and structure refinement for compound (**3-exo)$_2$(3-endo)**(*n*-**hexane)**.

|	(**3-exo)$_2$(3-endo)** (*n*-**hexane)**
Empirical formula	C$_{17}$H$_{27.7}$NO$_2$P$_2$
Formula weight / g mol^{-1}	340.01
Temperature/K	100.0(1)
Crystal system	monoclinic
Space group	*P*2$_1$/*c*
a/Å	7.79270(10)
b/Å	27.0421(3)
c/Å	26.5278(2)
α/°	90
β/°	96.2530(10)
γ/°	90
Volume/Å^3	5556.97(10)
Z	12
ρ$_{calc}$g/cm^3	1.219
μ/mm^{-1}	2.178
F(000)	2192.0
Crystal size/mm^3	0.286 × 0.118 × 0.063
Radiation	CuK-α (λ = 1.54184)
2Θ range for data collection/°	4.68 to 146.346
Index ranges	-5 ≤ h ≤ 9, -32 ≤ k ≤ 33, -32 ≤ l ≤ 32
Reflections collected	50947
Independent reflections	10640 [R$_{int}$ = 0.0214, R$_{sigma}$ = 0.0189]
Data/restraints/ parameters	10640/0/618
Goodness-of-fit on F^2	1.056
Final R indexes [I>=2σ (I)]	R$_1$ = 0.0390, wR$_2$ = 0.1014
Final R indexes [all data]	R$_1$ = 0.0431, wR$_2$ = 0.1040
Largest diff. peak/hole / e Å^{-3}	0.66/-0.43

5.4.4   Kinetic Data
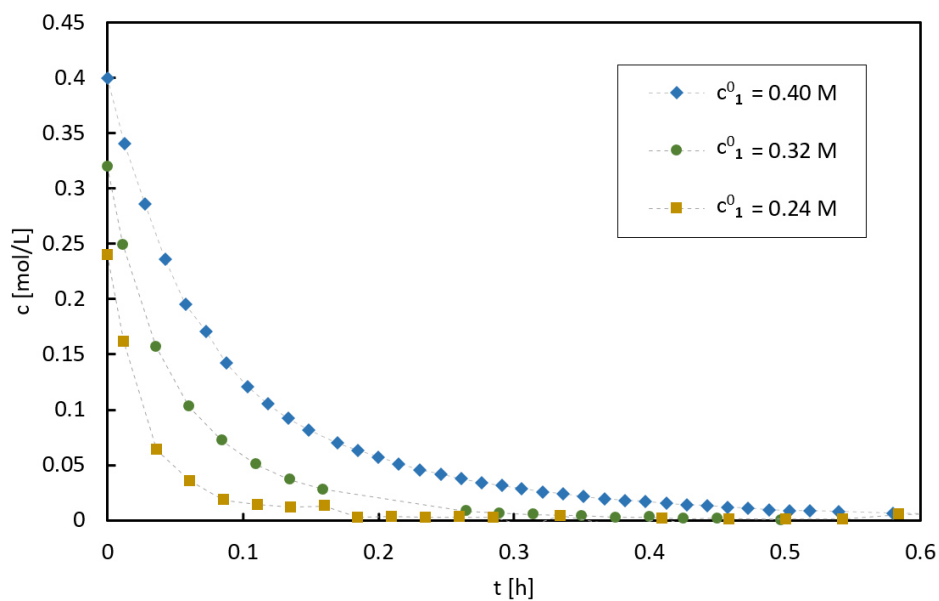
Figure S17. Decrease of concentration of **1** upon *in situ* illumination in an NMR tube.
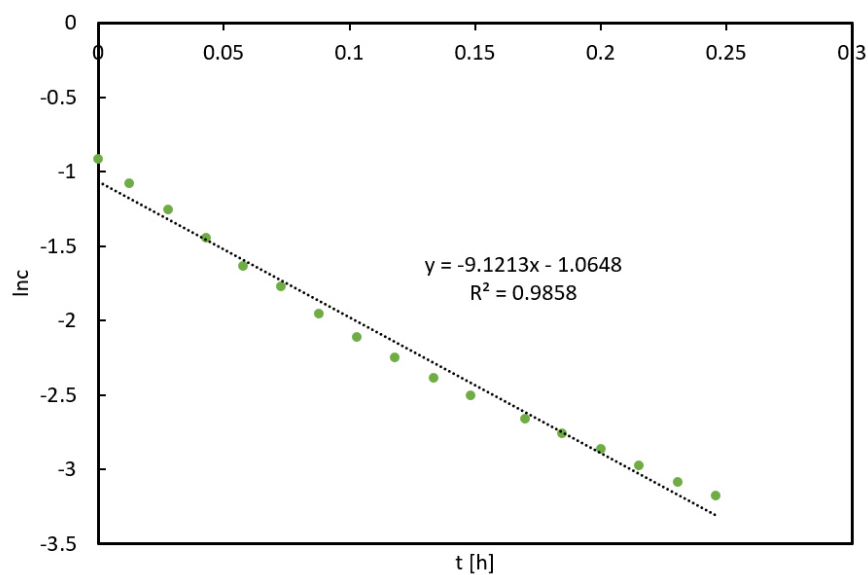

Figure S18. Logarithmic linearisation of NMR kinetic data of the decrease of concentration when irradiating a solution of **1** in toluene ($c^0 = 0.4$ M).
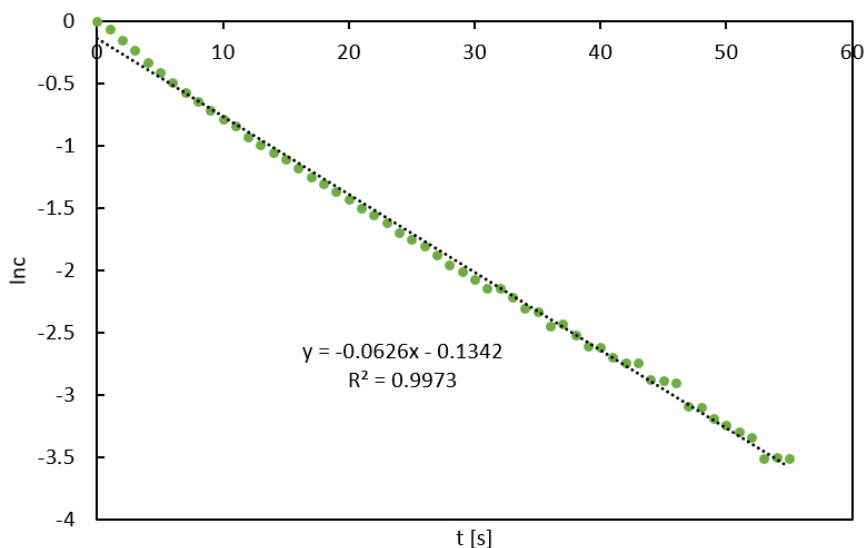
Figure S19. Logarithmic linearisation of NMR kinetic data of the decrease of concentration when irradiating a solution of **1** in *n*-hexane ($c^0 = 0.5$ mM).

5.4.5 Stationary and transient absorption spectroscopy

Stationary UV/Vis absorption and emission spectroscopy

UV/Vis absorption was recorded at room temperature using a Cary 60 UV/Vis spectrophotometer from Agilent.

Stepwise illumination and recording of absorption spectra

Stationary UV/Vis absorption spectra were recorded using an Agilent Cary 60 UV/Vis spectrophotometer in a sample cell of 1×10 mm using the 1 mm as the optical path. Samples were illuminated with an LED (Thorlabs M340L4, 340 nm, 60 mW). Light pulses with a precise pulse width were delivered onto the sample that was reproducibly positioned in a fixed geometry maintaining illumination of the entire sample volume (0.3 mL) in order to avoid diffusion effects.

Illumination of the sample for 10 s and recording spectra afterwards while keeping the sample in the dark, did not result in significant changes. Within the excitation period **2** is formed and small changes may only arise from changes in the scattering contributions altering the spectrum of **2** slightly (see Figure S20).

Figure S20. Sequence of absorption spectra of **1** (500 µM) in n-hexane after illumination for 10 s at 340 nm (left) can be decomposed into species spectra and concentration time profiles (right) showing a step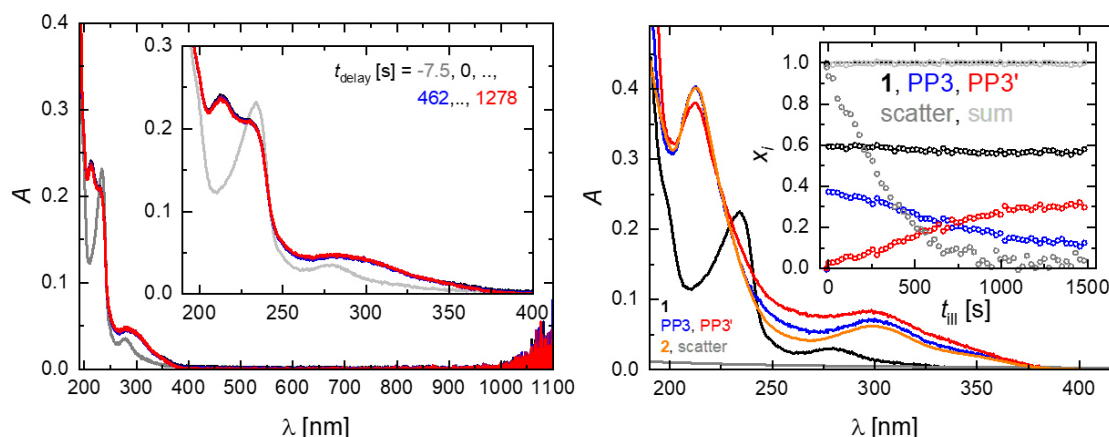-function like conversion of 1 into 2. The kinetics of the two similar photoproduct spectra arise mainly from variations in the scatter contribution in the sample that alter the spectrum of the formed **2** (orange for reference).

Ns to ms time-resolved UV/Vis absorption spectroscopy

The previously described streak camera set-up was adapted as follows.[22] The third harmonic of a Nd:YAG laser (10 Hz, Surelite II, Continuum, 355 nm, 10 mJ, ca. 10 ns) was used for sample excitation. As a probe light, a pulsed 150 W Xe-flash lamp (Applied Photophysics) was used that was focussed three times via toric mirror optics: (i) before probe shutter, (ii) into sample, and (iii) into spectrograph. The entire white light probe pulse was analysed by a combination of a spectrograph (200is, Bruker) and a streak camera (C7700, Hamamatsu Photonics). The use of mechanical shutters enabled the recording of a sequence of three individual data sets: (i) an image (D_{FL}) with both flash lamp and laser, (ii) an image (D_0) without any incoming light, and (iii) an image (D_F) only with the flash lamp. One hundred such sequences were recorded, and corresponding data sets were averaged. Then the TA was calculated as:

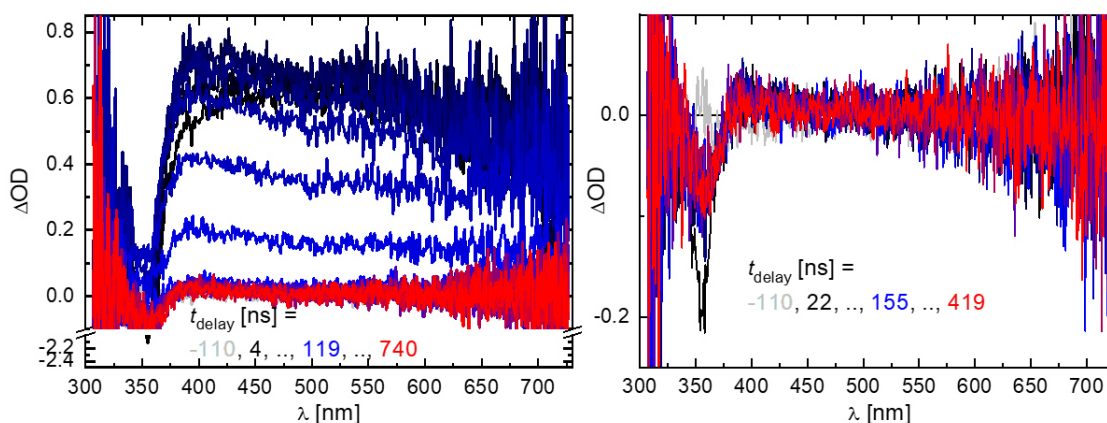$$OD = \log \left(\frac{D_F - D_0}{D_{FL} - D_0} \right)$$

Figure S21. Comparison of transient absorption (TA) data sets of **1** (2 mM) in molecular oxygen free *n*-hexane (sample was prepared in a glove box) after excitation at 355 nm (10 mJ) prepared from the same stock solution without using any particle filter. In some cases (left) a short-lived species is observed and in others not (right).

5.4.6 Quantum Chemical Calculations

General Methods

All calculations were performed with the ORCA program package.[23] All calculations were conducted in the gas phase. The RI[24] approximation was used for GGA calculations whereas the RIJCOSX approximation was used in hybrid-DFT calculations. The isomerisation process of **1** to **1′** was calculated on the ωB97X-D3/def2-SVP[25] level of theory and the thermal dimerisation of **1′** to **2** on the B3LYP/def2-SVP level of theory. Geometry optimisations of **3-endo** and **3-exo** have been carried out at the BP86-D3BJ/def2-TZVP[26] level of theory. NMR calculations of **3-endo** and **3-exo** have been carried out using the TPSS/pcSseg-2[27] level of theory and were referenced to the reported chemical shift of (*t*BuCP)$_4$.[10] Chemcraft[28] and GaussSum[29] were used to visualise the results.

TD-DFT calculations on **1′** were performed on the PBE0/def2-TZVPP level of theory and reveal an absorption spectrum with three main signals at ca. 300, 500 and 650 nm (Figure S22).
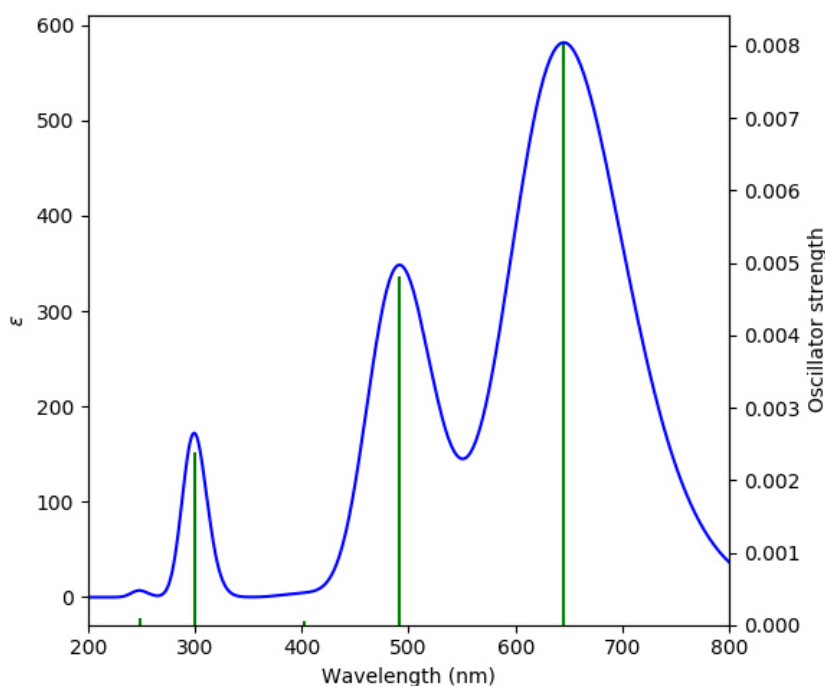
Figure S22. Calculated UV/Vis absorption spectrum for **1′** as visualised by GaussSum.

Cartesian Coordinates for Optimised Structures

1:

```
P   -5.12137783907350      0.39967169899593      0.28610730456242
C   -3.36123120451169     -0.12777555265565      0.51961291438714
C   -3.52096836044728      0.90274670987689     -0.49937014088859
P   -3.51492315387866      1.57802271846826      1.22541110778401
C   -2.63937305697805     -1.39840157122337      0.87945358653299
C   -3.06896509627181      1.36866978257099     -1.85722489925801
C   -1.55467122620358      1.64533729916710     -1.83409127302251
C   -3.82459943934436      2.66582564439220     -2.19279439363964
```

```
C  -3.39573008025164    0.29439066822668   -2.91045603237571
C  -2.96815054867160   -2.49260499465574   -0.15250610247847
C  -3.11953344476288   -1.84223309442971    2.27176455062166
C  -1.12187746672834   -1.14133310885331    0.91544111385900
H  -4.20243044037764   -2.00417522611600    2.27068000610061
H  -2.88632122512431   -1.07753972235598    3.01988080510128
H  -2.62836987628463   -2.77665664897664    2.56454083109457
H  -0.75362899305131   -0.81396346293761   -0.06137189847398
H  -0.59108359125682   -2.05932915261062    1.19121811488813
H  -0.88154486021968   -0.36665121662777    1.65084698347044
H  -1.22464358534788    2.01497873535823   -2.81131100229442
H  -0.99107438692460    0.73609181588207   -1.60460113717272
H  -1.31382743729788    2.39954818014916   -1.07784391156855
H  -3.52266457872926    3.03884371290288   -3.17755056817381
H  -3.61030944224891    3.43873379333851   -1.44742769205442
H  -4.90504260439551    2.48868610804622   -2.20421178046073
H  -3.09741755572110    0.64054586080336   -3.90629412481847
H  -4.47005136962059    0.08364479535850   -2.92319508753355
H  -2.86473257216999   -0.63876286643911   -2.69982200847138
H  -2.64784696408911   -2.19755976463992   -1.15618529965970
H  -4.04580376188614   -2.68428518098336   -0.17818056658930
H  -2.45521583813124   -3.42434596003219    0.11058060053172
```

1′:

```
P  -1.77258167023433    0.87446862715974    3.45911267022681
P  -0.11536817612046   -0.01183594861527    2.64833326807631
C  -0.48814827387111    2.32179449438996    3.59282762801891
C   0.57517133813772    1.75714288316477    2.98123360812428
C  -0.86710744229302    3.67545844054033    4.17459182626838
C   1.96617666844349    2.20454652362447    2.54244803831732
C   0.30200526093422    4.41562497972131    4.84912832867238
H   1.09633234335402    4.68921639664403    4.14569696073796
H   0.74617092680789    3.80002051898595    5.64657940544927
H  -0.06369612948686    5.34791662783851    5.30910651320313
C  -1.94848801828096    3.46373190955687    5.25686499451661
H  -1.57743877948766    2.81928070217586    6.07031756394356
H  -2.85650352440109    2.99769593062919    4.84348095577672
H  -2.23989721096646    4.43058565938071    5.69802083639018
C  -1.47052748354283    4.52284145700997    3.03120829820179
H  -1.87896680970083    5.47061814235228    3.42121491277357
H  -2.29316807859925    3.98109556482089    2.53644692552678
H  -0.71668778779167    4.75742816019632    2.26619133282817
C   1.90404102648871    3.53373202013393    1.76383986678627
H   1.23061375960805    3.44293424351683    0.89708853709519
H   2.90507833702680    3.80133553849816    1.38638036412477
H   1.54804223749738    4.36810578714485    2.37998991791164
C   2.90414426033252    2.31656813362014    3.76286891121809
H   3.91567062583642    2.61596196854936    3.43836127849257
H   2.98425575160038    1.34703279713154    4.28044900314100
H   2.54656064797057    3.05362180852310    4.49148495902646
C   2.55700328377133    1.14583739889858    1.58703945008361
H   3.54727310923134    1.46953017978338    1.22851423981361
H   1.91561289082224    0.99303644360743    0.70395827081304
H   2.67930691691344    0.17142261101672    2.08592113444153
```

2:

```
C   -3.59718567415526    -0.23084700681366     0.99257847390885
C   -2.54098809770401    -0.78350839758974     0.30052830887322
P   -3.01247239935388     1.50061813557029     1.39493420553080
P   -1.26418925177761     0.58484294645527     0.26482513758643
C   -5.02863014994854    -0.64992886846344     1.35149596238921
C   -5.53724875621072     0.24459643832148     2.50515119135503
H   -5.51544906351853     1.31903930696306     2.22699790302715
H   -4.92156998134764     0.11493396164095     3.41831653524501
H   -6.58588131181467    -0.01491674941210     2.75542348221098
C   -5.93436344424163    -0.41562554274639     0.11976210694586
H   -6.99033797818899    -0.65546393831941     0.36479107633966
H   -5.62507419493810    -1.04253715363083    -0.73758372366146
H   -5.88841330672540     0.64475442770559    -0.20153141313439
C   -5.13400707684178    -2.11009852487435     1.83290717942638
H   -6.17486807603201    -2.32339522103526     2.15094818834838
H   -4.46856620099587    -2.28587944532675     2.70120177584277
H   -4.87320111777011    -2.84090086785974     1.04669027711765
C   -2.24425482462360    -2.13707327461599    -0.35941183553933
C   -3.37746898499522    -2.60622379576199    -1.29488194818372
H   -3.58774189484182    -1.84430861794297    -2.07180543954838
H   -4.32068825863837    -2.81236168298925    -0.75591381550048
H   -3.08080500485354    -3.54490654105045    -1.80725569096658
C   -0.96308917203240    -2.01337892621065    -1.21359281780342
H   -0.09577858540668    -1.68617974560596    -0.60225520662527
H   -1.09041408032585    -1.28536382445799    -2.03969329435301
H   -0.70540747622055    -2.99724987305247    -1.65516721478127
C   -1.96856183869085    -3.18660248467808     0.74472839534401
H   -2.85582497628426    -3.36310715524874     1.37843465066784
H   -1.14309543981928    -2.84975837959520     1.40439137772653
H   -1.67227555693805    -4.15295136218243     0.28626172926390
P   -1.99910280534119     0.97134590401063     3.37571419437230
P   -0.25083646137259     0.05552989466980     2.24560567694709
C   -0.72230338565779     2.33969170946494     3.33993130232594
C    0.33393218320884     1.78697975527760     2.64797208301691
C   -1.01879528845087     3.69304611396570     4.00040029989112
C    1.76566831198580     2.20572049532370     2.28978574793543
C    0.11497532921615     4.16197539452448     4.93531104561292
H    1.05785613737047     4.36830460446381     4.39581217025910
H    0.32576558715856     3.39983605150620     5.71187597598424
H   -0.18141101318746     5.10049348445816     5.44814346535226
C   -2.29941593769142     3.56894709510393     4.85533883008208
H   -2.17149640589174     2.84068881296229     5.68113417325367
H   -3.16707045993121     3.24184347830046     4.24443798654030
H   -2.55693086624882     4.55265045224388     5.29737828427487
C   -1.29532573301119     4.74290945063263     2.89678227516718
H   -1.59144010940933     5.70906304783959     3.35576965164080
H   -2.12118146467403     4.40618829816323     2.23754120060152
H   -0.40851147391719     4.91974993856850     2.26257157635662
C    1.87170392664898     3.66574282962908     1.80809361727952
H    1.20682465527020     3.84149221012057     0.93936512262093
H    2.91281107083086     3.87868750304665     1.49061973243354
H    1.61063912839200     4.39679730683449     2.59398807416230
C    2.67056438067576     1.97157757656822     3.52215951729868
H    3.72674432498573     2.21112471000360     3.27773692725683
```

H	2.62418305687358	0.91130256421491	3.84373337058455
H	2.36085212731454	2.59881703731195	4.37913347074014
C	2.27482701986084	1.31078855015009	1.13668266293938
H	3.32367931869972	1.57000074082527	0.88702323682127
H	1.65977048861219	1.44035795284529	0.22308720529317
H	2.25260653291586	0.23641919977755	1.41509556590297

3-exo:

P	3.33976215089434	12.99294183092297	9.83535888696466
P	3.55411818006588	15.04270625074941	10.79702713929310
O	4.71098761874879	13.02450136590141	6.68860795463852
O	5.22320067898458	17.14974446755915	8.65344733407655
N	5.27275266263484	15.09001412082902	7.59153124213867
C	4.70780127347583	16.07322484740132	8.41210453789485
C	4.49973012380843	13.96962725675038	7.41045835141863
C	1.76970280225567	14.61135183190102	11.05301526328314
C	1.64811121095954	13.36028376919937	10.50351447588682
C	0.87185120192951	15.58185077182183	11.82557534975063
C	3.39123634439849	15.53273849800324	8.93246710987771
C	0.51313622081909	12.34137440114557	10.36206750231304
C	6.56393651495095	15.24512088264203	6.94591462725727
H	6.49863714802505	15.95938493587400	6.11358981921093
H	6.86498580880340	14.26340510435479	6.56383453649462
H	7.29074420266506	15.62260811638694	7.67510379078409
C	3.22932316554049	14.15776770497986	8.28612214748901
C	0.94696006964474	15.21251636095375	13.32438573101225
H	0.55389769579394	14.20448672645697	13.50842956895359
H	0.36188387769407	15.92949646768986	13.92040585330996
H	1.98751417588751	15.24126606101489	13.67821865877265
C	-0.50316052159430	12.82878300637623	9.30564823933198
H	-0.97365985544907	13.77544346646206	9.58817093655079
H	-1.29511196587309	12.07651684205124	9.17103963545986
H	-0.00816137498826	12.97116145843102	8.33407931364408
C	1.08754130070808	11.00163911261578	9.85798036576520
H	1.59299245516545	11.11527193636440	8.88663358353027
H	0.27178235547290	10.27609398469659	9.72664092622520
H	1.81375878588119	10.57854155278550	10.56601540284331
C	1.42429651793735	17.01329582729055	11.65130533645527
H	2.47705554817033	17.08884386064811	11.96336163353875
H	0.84447509238780	17.71442521047316	12.26832163871379
H	1.35269529521914	17.34734136811920	10.60622440545063
C	-0.59373347568648	15.61447448305802	11.36016626625777
H	-0.66079960610561	15.85514399946678	10.28985166303481
H	-1.13210370568256	16.39797017959896	11.91386231518165
H	-1.12049099497831	14.67103662773101	11.53606592932062
C	-0.17824155024154	12.06274186939214	11.71031385887194
H	0.55342407194448	11.71008594675866	12.45098976336558
H	-0.94072943338684	11.27945301309590	11.58412402841667
H	-0.67564224552790	12.94693766222213	12.12262151098662
H	2.59424155781761	16.27038880299752	8.78915379454531
H	2.31604862082939	13.95742801682687	7.71566957168892

3-endo:

```
P  6.93963325495231   5.23668687484793   7.96986754118070
P  6.87943304905944   7.49615801806708   7.92325857379526
O  5.45961140154652   3.86910332435512   5.11108120672352
O  5.04053677783213   8.44838734729036   5.05109512116245
N  4.95743907379257   6.13740381808845   5.01818814587821
C  5.75464386566494   5.03066753042808   5.34488554002593
C  6.85369431761202   7.08256337856472   6.01270643409337
C  5.54576920924082   7.37062311343924   5.32206832682518
C  6.97114946045608   5.56372803303586   6.04574122057826
C  5.16985876670080   5.63676572393627   8.34961479075405
C  3.67919793301442   6.03163513900324   4.34094739845036
H  3.72856321481111   6.51913405735076   3.35842443389796
H  2.89906815216691   6.52298085110650   4.93572629364754
H  3.45445134545905   4.96615949334699   4.22272103431681
C  5.14575250490932   7.01324089209184   8.36920959790548
C  4.15410732326557   4.52772540937203   8.65246547397892
C  4.14319376699958   8.09348671765743   8.78590671072592
C  4.56530187477724   9.44720073771016   8.17714780692995
H  5.57375054110011   9.73981424074998   8.50670936638735
H  3.86987627601881  10.23097314136630   8.51083942094174
H  4.55598385360638   9.41997360622257   7.07947314755093
C  3.06242394275705   4.45951755163634   7.56127234156996
C  4.87713461396563   3.16555265855926   8.65103616179971
C  4.20391313823421   8.22927280701126  10.32580227435467
C  2.70054299048850   7.82018438572199   8.32983877269861
C  3.51427463130877   4.71417933817291  10.04272637457767
H  7.89467957339106   5.12946770336405   5.64705091848708
H  5.22707594994502   8.46713005192565  10.65094860003409
H  3.89317337143452   7.30744843038130  10.83129601746267
H  2.65244222834965   7.71460401570036   7.23684256840413
H  2.06306945194801   8.67113698973271   8.61163556511722
H  2.27217807907351   6.92221818426710   8.78749771676975
H  2.55122655165864   5.41706086480369   7.42271857026310
H  2.30974780864659   3.70786768440075   7.84354826102901
H  2.87245756507002   5.60095059640624  10.09476179032749
H  4.28713740005918   4.80455388488628  10.81924811684570
H  5.36563209831599   2.97410008555323   7.68346185279897
H  4.14655443656366   2.36071549782508   8.81763325456902
H  3.54365885997241   9.04660781659856  10.65354773778001
H  5.63719505878218   3.10701541228556   9.44306941376230
H  2.89122027353957   3.83920215003387  10.28112898985355
H  3.49794649459348   4.15094528468882   6.60270040300480
H  7.67823951891610   7.62660715801389   5.53765671274036
```

References

[1] G. Maier, S. Pfriem, U. Schäfer, R. Matusch, *Angew. Chem. Int. Ed. Engl.* **1978**, *17*, 520.

[2] A. R. Jupp, J. C. Slootweg, *Angew. Chem. Int. Ed.* **2020**, *59*, 10698.

[3] a) B. M. Cossairt, N. A. Piro, C. C. Cummins, *Chem. Rev.* **2010**, *110*, 4164; b) M. Caporali, L. Gonsalvi, A. Rossin, M. Peruzzini, *Chem. Rev.* **2010**, *110*, 4178; c) M. Scheer, G. Balázs, A. Seitz, *Chem. Rev.* **2010**, *110*, 4236; d) G. Maier, *Angew. Chem. Int. Ed. Engl.* **1988**, *27*, 309.

[4] a) A. Pedler, *J. Chem. Soc., Trans.* **1890**, *57*, 599; b) M. Serrano-Ruiz, A. Romerosa, P. Lorenzo-Luis, *Eur. J. Inorg. Chem.* **2014**, *2014*, 1587.

[5] G. Rathenau, *Physica* **1937**, *4*, 503.

[6] a) O. J. Scherer, *Angew. Chem. Int. Ed.* **2000**, *39, 1029*, 1029; b) H. Bock, H. Mueller, *Inorg. Chem.* **1984**, *23*, 4365; c) N. A. Piro, J. Si Figueroa, J. T. McKellar, C. C. Cummins, *Science* **2006**, *313*, 1276.

[7] N. P. Tarasova, Y. V. Smetannikov, I. M. Artemkina, I. A. Lavrov, M. A. Sinaiskii, V. I. Ermakov, *Dokl. Chem.* **2006**, *410*, 189.

[8] a) D. Tofan, C. C. Cummins, *Angew. Chem. Int. Ed.* **2010**, *49*, 7516; b) L.-P. Wang, D. Tofan, J. Chen, T. van Voorhis, C. C. Cummins, *RSC Adv.* **2013**, *3*, 23166.

[9] G. Hierlmeier, P. Coburger, M. Bodensteiner, R. Wolf, *Angew. Chem. Int. Ed.* **2019**, *58*, 16918.

[10] B. Geissler, S. Barth, U. Bergsträsser, M. Slany, J. Durkin, P. B. Hitchcock, M. Hofmann, P. Binger, J. F. Nixon, P. von Ragué Schleyer, M. Regitz, *Angew. Chem. Int. Ed. Engl.* **1995**, *34*, 484.

[11] C. Feldmeier, H. Bartling, E. Riedle, R. M. Gschwind, *J. Magn. Reson.* **2013**, *232*, 39.

[12] T. Horie, M. Sumino, T. Tanaka, Y. Matsushita, T. Ichimura, J.-i. Yoshida, *Org. Process Res. Dev.* **2010**, *14*, 405.

[13] a) B. Cordero, V. Gómez, A. E. Platero-Prats, M. Revés, J. Echeverría, E. Cremades, F. Barragán, S. Alvarez, *Dalton Trans.* **2008**, 2832; b) P. Pyykkö, M. Atsumi, *Chem. Eur. J.* **2009**, *15*, 186; c) P. Pyykkö, *J. Phys. Chem. A* **2015**, *119*, 2326.

[14] W. H. Hersh, S. T. Lam, D. J. Moskovic, A. J. Panagiotakis, *J. Org. Chem.* **2012**, *77*, 4968.

[15] U. Lennert, P. B. Arockiam, V. Streitferdt, D. J. Scott, C. Rödl, R. M. Gschwind, R. Wolf, *Nat. Catal.* **2019**, *2*, 1101.

[16] a) Sheldrick, G. M. SADABS, Bruker AXS, Madison, USA **2007**; b) CrysAlisPro, Scale3 Abspack, Rigaku Oxford Diffraction **2019**.

[17] R. C. Clark, J. S. Reid, *Acta Cryst. A* **1995**, *51*, 887.

[18] G. M. Sheldrick, *Acta Cryst. A* **2015**, *71*, 3.

[19] O. V. Dolomanov, L. J. Bourhis, R. J. Gildea, J. A. K. Howard, H. Puschmann, *J .Appl. Crystallogr.* **2009**, *42*, 339.

[20] G. M. Sheldrick, *Acta Cryst. C* **2015**, *71*, 3.

[21] G. M. Sheldrick, *Acta Cryst. A* **2008**, *64*, 112.

[22] a) R.-J. Kutta, T. Langenbacher, U. Kensy, B. Dick, *Appl. Phys. B* **2013**, *111*, 203; b) R.-J. Kutta **2012**, *Blitzlichtphotolyse - Untersuchung zu LOV-Domänen und Photochromen Systemen. Dissertation, Naturwissenschaftliche Fakultät IV - Chemie und Pharmazie- der Universität Regensburg*.

[23] R. A. Kendall, H. A. Früchtl, *Theor. Chem. Acc.* **1997**, *97*, 158.

[24] F. Weigend, *Phys. Chem. Chem. Phys.* **2002**, *4*, 4285.

[25] F. Weigend, R. Ahlrichs, *Phys. Chem. Chem. Phys.* **2005**, *7*, 3297.

[26] a) Becke, *Physical Rev. A* **1988**, *38*, 3098; b) Perdew, *Phys. Rev. B* **1986**, *33*, 8822; c) S. Grimme, S. Ehrlich, L. Goerigk, *J. Comput. Chem.* **2011**, *32*, 1456; d) S. Grimme, J. Antony, S. Ehrlich, H. Krieg, *J. Chem. Phys.* **2010**, *132*, 154104.

[27] F. Jensen, *J. Chem. Theory Comput.* **2015**, *11*, 132.

[28] Chemcraft - graphical software for visualisation of quantum chemistry computations. https://www.chemcraftprog.com.

[29] N. M. O'Boyle, A. L. Tenderholt, K. M. Langner, *J. Comp. Chem.* **2008**, *29*, 839.

6 Di-*tert*-butyldiphosphatetrahedrane as a Building Block for Phosphaalkenes and Phosphirenes[a,b]

Abstract: The remarkable 'mixed' diphosphatetrahedrane (*t*BuCP)$_2$ (**1**) – which is both the elusive dimeric form of the phosphaalkyne *t*BuCP and an isolobal analogue of the important industrial feedstock P$_4$ – was recently isolated for the first time; however, its chemistry remains unexplored. Herein we report that treatment of **1** with various N-heterocyclic carbenes readily yields unusual, unsaturated organophosphorus motifs. These results demonstrate the significant potential of 1 as a building block for the synthesis of previously unknown organophosphorus compounds.
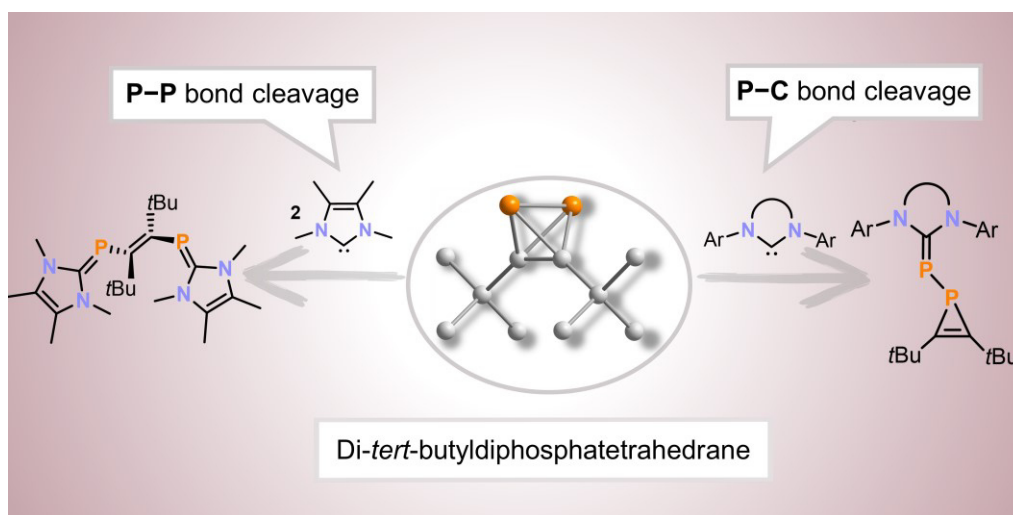
6.1 Introduction

Organophosphorus compounds (OPCs) are of high industrial and academic importance due to their widespread applications, e.g. as specialty chemicals, pharmaceuticals or ligands in homogeneous catalysis.[1] The development of suitable synthetic building blocks is a high priority for broadening the range of available OPCs. Traditional reagents available are chlorinated P compounds (e.g. PCl_3, PCl_5, and $OPCl_3$), monophosphane (PH_3),[2] and, in very selected cases, phosphoric acid and phosphates.[3] In addition, low-coordinate phosphorus compounds such as phosphaalkynes $R-C\equiv P$ (R = alkyl, aryl; see Figure 1a)[4] and, more recently, phosphacyanate salts have also received attention as versatile building blocks.[5]

Nearly all organophosphorus building blocks are ultimately derived from white phosphorus (P_4) as the single common precursor. Therefore, fundamental reactivity studies on P_4 are of high importance.[6] As early as 1963, Rauhut and Semsel reported the synthesis of (cyclo)polyphosphides and primary phosphines (e.g. phenylphosphine) after hydrolytic work-up by reacting P_4 with organolithium and -magnesium compounds.[7] This approach has gained renewed interest recently through the work of Lammertsma and Xu.[8] Bertrand and co-workers studied the reactivity of stable carbenes towards P_4 (see Figure 1b).[9–12] Both acyclic and N-heterocyclic carbenes (NHCs) were used, and the nature of the obtained products strongly depends on the steric and electronic properties of the carbene. Using a bulky menthyl- and di-*iso*-propylphenyl-substituted cyclic alkyl aminocarbene (^{Ment}CAAC) or 1,3-bis(2,6-di-*iso*-propylphenyl)imidazolin-2-ylidene (SIPr), the triphosphirene **A** was generated.[9,10] This species was trapped and characterised as a cycloaddition product with 2,3-dimethylbutadiene. Upon addition of another equivalent of carbene, **A** converts to the tetraphosphene **B**. For other NHCs, an aggregation of P_4 to larger polyphosphorus clusters and the degradation even down to monophosphorus fragments was observed.[11,12]
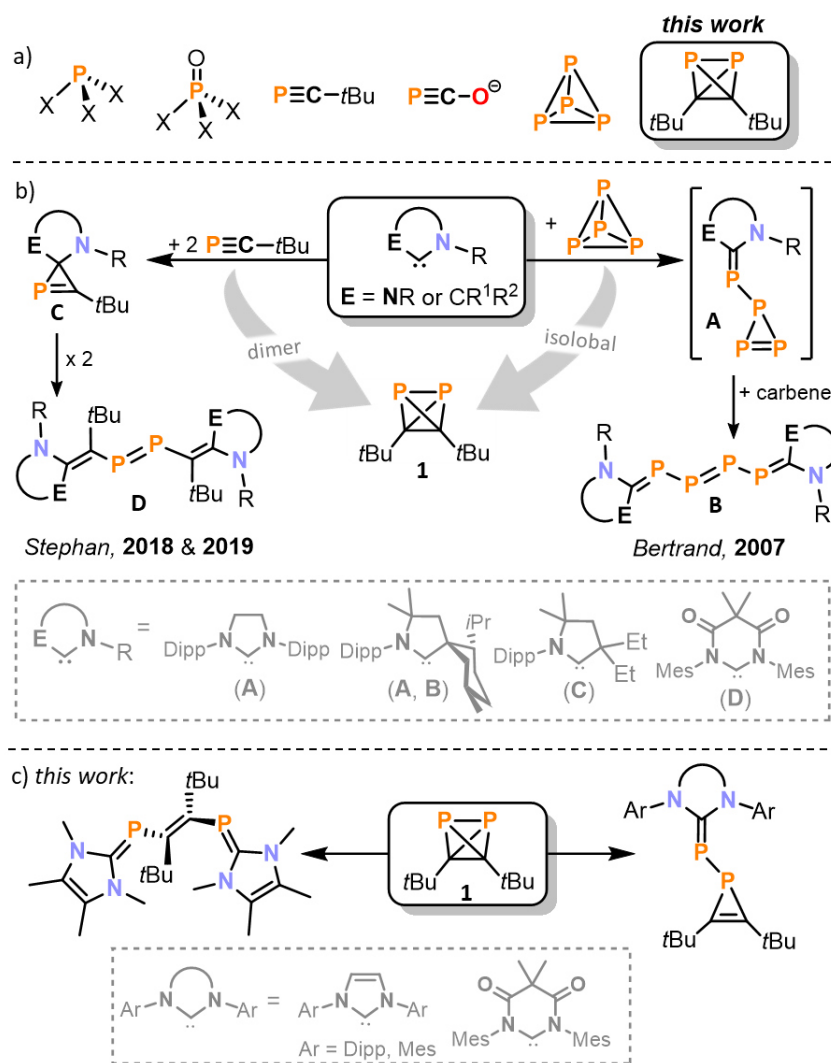
Figure 1. a) Examples of common building blocks used for the synthesis of organophosphorus compounds. X = H, Cl; b) reactivity of carbenes toward *t*BuCP, P$_4$ and (*t*BuCP)$_2$;[9,10,13,14] c) reactivity of **1** toward carbenes.

Stephan and co-workers synthesised compounds similar to **A** and **B** by reacting various NHCs with *tert*-butylphosphaalkyne (see Figure 1b).[13,14] The phosphirene structure **C** is stable and can be isolated when a diamidocarbene is used.[13] Using a specific cyclic alkylamino carbene (CAAC), the dimerisation of the phosphirene is observed, resulting in the formation of a diphosphene **D**.[14]

We recently discovered di-*tert*-butyldiphosphatetrahedrane (*t*BuCP)$_2$ (**1**), which is a rare example of a neutral tetrahedrane comprising two distinct p-block elements and the long-sought-after dimer of *t*BuCP.[15,16] The ready accessibility of **1** via a simple nickel-catalysed process, and its isolobal relationship with P$_4$, prompted us to study its reaction chemistry. For our initial investigations, we chose carbenes to examine whether **1** behaves more like the isolobal P$_4$ molecule or the parent monomer *t*BuCP.

6.2   Results and Discussion

In order to assess the impact of the steric and electronic properties of the NHC, a range of known NHCs were reacted with **1**. With 1,3-di-*iso*-propyl-4,5-dimethylimidazolin-2-ylidene (*i*Pr$_2$Im^{Me}) and menthyl-substituted ^{Ment}CAAC, ^{31}P{^{1}H} NMR spectroscopic monitoring only showed the clean formation of the ladderane (*t*BuCP)$_4$ (identified by a singlet at −23.0 ppm).[17] (*t*BuCP)$_4$ is the formal dimer of **1** and we identified this phosphaalkyne tetramer as the decomposition product of **1**.[16] However, the reaction of **1** with TMC (2,3,4,5-tetramethylimidazolin-2-ylidene) proceeds differently, affording a deep orange precipitate after 5 minutes when **1** is added to a solution of TMC in benzene. When dissolved in THF-d$_8$, this solid gives rise to a singlet at −28.4 ppm in the ^{31}P {^{1}H} NMR spectrum. Dissolution of the precipitate in THF, filtration and subsequent recrystallisation from THF yielded crystals suitable for single crystal X-ray crystallography, which revealed the molecular structure of [(TMC)PC*t*Bu]$_2$ (**2**, Figure 2b).
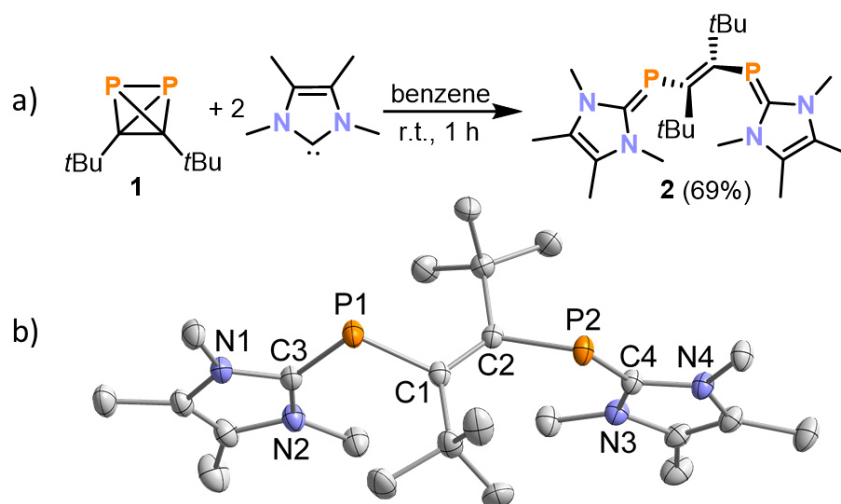

Figure 2. a) Reaction of (*t*BuCP)$_2$ with TMC; b) molecular structure of **2** in the solid state. Thermal ellipsoids are set at the 50% probability level. Hydrogen atoms are omitted for clarity. Selected bond lengths [Å] and angles [°]: C1−C2 1.366(2), P1−C1 1.8637(16), P2−C2 1.8630(15), P1−C3 1.7673(17), P2−C4 1.7660(16), N1−C3 1.376(2), N2−C3 1.368(2), N3−C4 1.371(2), N4−C4 1.371(2), C3−P1−C1 108.69(8), C4−P2−C2 108.18(7), C2−C1−P1 120.54(13), C1−C2−P2 120.37(12).

Compound **2** can be described as a vinyl-bridged bis(phosphaalkene) formed by P−P bond cleavage of the (*t*BuCP)$_2$ tetrahedron.[18] Related reactions of *t*BuCP and NHCs reported by Stephan and co-workers afford diphosphenes (e.g. **D**, Figure 1b). The formation of **2** from **1** and TMC thus highlights the distinct reactivity of **1** compared to *t*BuCP.[14]

The crystallographic analysis of **2** suggests the presence of a C1−C2 double bond (1.366(2) Å) in an *E* configuration. The P−C bonds of the TMC units (P1−C3 1.7673(17) Å and P2−C4 1.7660(16) Å) are elongated compared to common C=P double bonds,[19] while the P–C bond lengths of the vinyl group (P1−C1 1.8637(16) Å and P2−C2 1.8630(15) Å) are in the range commonly observed for P−C single bonds.[20] The P1−C3 and P2−C4 distances are similar to the values observed for IMes=PPh (1.763(6) Å) and TMC=PPh (1.794(3) Å).[21,22] Due to the

presence of two amino substituents at carbon, such "inversely polarised phosphaalkenes" show only a partial double bond character and an inverse polarity of the P=C bond compared to more common hydrocarbyl-substituted phosphaalkenes.[23] Notably, the P=C and C=C bonds in **2** are not conjugated with plane to plane twist angles of 51° (C1-P1-C3 vs. P1-C1-C2) and 53° (C2-P2-C4 vs. C1-C2-P2).

The molecular structure of **2** was well-reproduced by DFT calculations on the BP86-D3BJ/def2-TZVP level. The presence of an inverse electron density distribution ($P^{\delta-}-C^{\delta+}$) on the phosphalkene P=C π-bonds of **2** is supported by an analysis of the relevant intrinsic bond orbitals (IBO analysis, Figure 3 top).[23] Notably, the P−C σ-bond also features a slightly distorted electron density distribution, which is polarised to carbon in this case. In addition, low Mayer bond orders for these P=C bonds (1.40 for each bond) indicate a significant contribution of the resonance structure **2-II** as expected for inversely polarised phosphaalkenes (Figure 3 bottom).
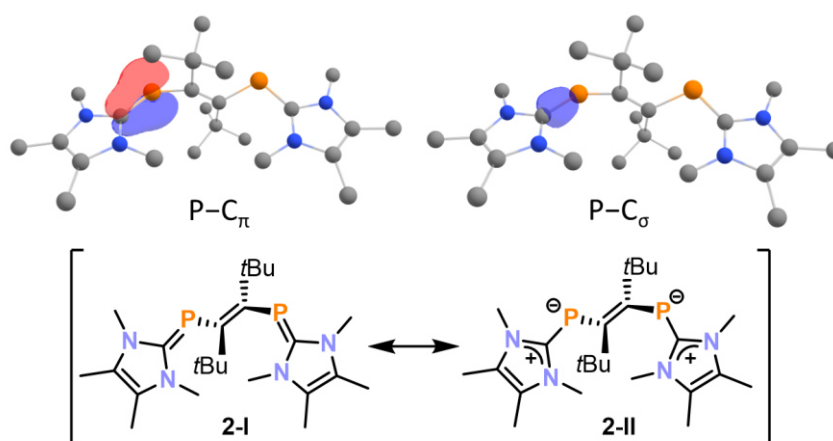

Figure 3. Intrinsic bond orbital of **2** showing the inversely polarised P=C π- and σ-bonds (top) and resonance structures of **2** (bottom).

Bis(phosphaalkene) **2** was isolated in good yield of 69% as a pure, bright orange solid. The $^{31}P\{^1H\}$ NMR spectrum of **2** in THF-d_8 exhibits a singlet resonance at −28.4 ppm, which is consistent with chemical shifts reported for IMes=PPh (−23.0 ppm) and TMC=PPh (−53.5 ppm).[21,22] The ^1H NMR spectrum shows one broad resonance assigned to the *t*Bu group and two broad signals for the Me substituents on the TMC backbone. These signals are further split into two sets of signals upon cooling (see the Supporting Information for details). This fluxional behaviour is presumably caused by slow rotation around the P=C bonds at low temperature. In agreement with the ^1H NMR data, $^{13}C\{^1H\}$ NMR data recorded at ambient temperature show only one set of resonances for the *t*Bu groups and one set of resonances for the TMC unit. The UV/Vis absorption spectrum of **1** in THF reveals three bands at 270, 340 and 450 nm, accounting for its orange colour. TD-DFT calculations at the wB97X-D3 def2-SVP level of theory show that the absorption band in the visible part of the spectrum (450 nm) is caused by

a HOMO-LUMO transition ($n_P \rightarrow \pi^*_{C-C}$; see the Supporting Information for a density difference plot).

An initial reactivity study demonstrates the high lability of the TMC moieties of **2**. Reactions with different metal complexes ([AuCl(tht)] (tht = tetrahydrothiophene), [(*p*-cymene)RuCl$_2$]$_2$, [(cod)RhCl]$_2$ (cod = 1,5-cyclooctadiene), Ag[Al{OC(CF$_3$)$_3$}$_4$]) and heterocumulenes (e.g. diphenyl diazomethane (Ph$_2$N=N) or phenyl isothiocyanate (Ph−N=C=S)) result in formation of (*t*BuCP)$_4$. The latter reactions additionally afford TMC adducts of the heterocumulene, e.g. (TMC)=N-N=CPh$_2$ and (TMC)C(S)(NPh) (see the Supporting Information for characterisation data).

It was anticipated that by increasing the size of the NHC it might be possible to favour formation of a 1:1 adduct with **1**, in contrast to the 2:1 adduct observed using TMC. Thus, **1** was reacted with bulky aryl-substituted NHCs IMes (1,3-bis(2,4,6-trimethylphenyl)imidazolin-2-ylidene), IPr (1,3-bis(2,6-di-*iso*-propylphenyl)imidazolin-2-ylidene), and ^{Mes}DAC (1,3-bis-(2,4,6-trimethylphenyl)-4,6-diketo-5,5-dimethylpyrimidin-2-ylidene, see Figure 1). ^{31}P{^{1}H} NMR spectra of the reaction mixtures reveal the presence of a distinct AX spin system in each case, which was subsequently assigned to 1*H*-phosphirenes **3a-c** (*vide infra*). (*t*BuCP)$_4$ was detected by ^{31}P NMR as the only side product. Prolonged stirring at room temperature for two weeks (for IMes and ^{Mes}DAC) or three weeks (for IPr) led to complete consumption of the NHC, and the products were subsequently crystallised from saturated *n*-hexane solutions.

Single-crystal X-ray diffraction studies revealed the molecular structures of **3a-c** (Figure 4) which result from P−C bond cleavage of **1**. The molecular structure of **3a** is very similar to those of **3b** and **3c** and so for simplicity only **3a** will be discussed below. The structural data of **3a** indicate the presence of a P1−P2 single bond (2.2200(3) Å) and a short C1=C2 double bond (1.2960(19) Å) with a low C2-P2-C1 angle (41.03(6)°). The C11−P1 bond is rather short (1.7647(12) Å) compared to the P2−C1 and P2−C2 bonds (1.8502(13) and 1.8479(13) Å) and compares well to the P1−C3 bond length in **2** (1.7673(17) Å). Overall, these bond metric data are comparable to previously reported phosphirene transition metal complexes.[24–27]
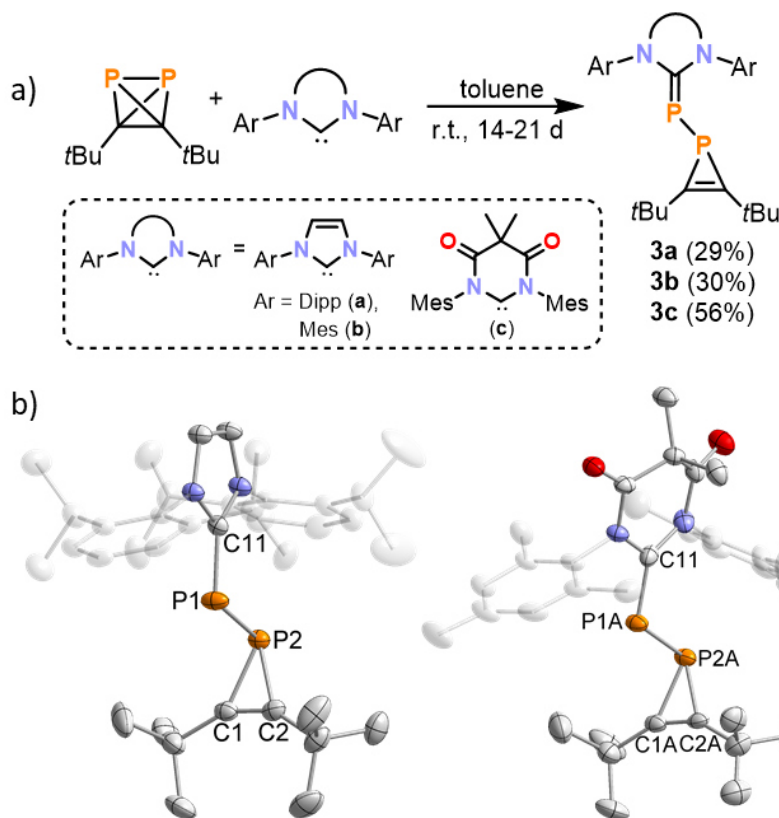
Figure 4. a) Reaction of (*t*BuCP)₂ with aryl-substituted carbenes IMes, IPr and ᴹᵉˢDAC; b) Molecular structures of **3a** and **3c** in the solid state. Thermal ellipsoids are set at the 50% probability level. Hydrogen atoms and positional disorder (in **3c**) are omitted for clarity. Selected bond lengths [Å] and angles [°] for **3a**: P1−P2 2.2200(4), P2−C1 1.8502(13), P2−C2 1.8479(13), P1−C11 1.7647(12), C1−C2 1.2960(19), C2−P2−C1 41.03(6) C1−P2−P1 98.09(4), C2−P2−P1 97.92(4), C2−C1−P2 69.39(8), C1−C2−P2 69.58(8), C11−P1−P2 109.55(4); **3c**: P1A−P2A 2.234(2), P2A−C1A 1.862(6), P2A−C2A 1.854(7), P1A−C11 1.759(5), C1A−C2A 1.290(10), C2A−P2A−C1A 40.6(3), C1A−P2A−P1A 94.7(2), C2A−P2A−P1A 96.8(2), C2A−C1A−P2A 69.3(4), C1A−C2A−P2A 70.0(4), C11−P1A−P2A 111.37(19).

Phosphinophosphirenes related to **3a-c** are scarce, and their synthesis usually requires metal coordination of the phosphino group.[25–27] An uncomplexed phosphinophosphirene was described by Bertrand and co-workers.[28] This species is formed as a minor by-product of the photolysis of bis(di-*iso*-propylamino)phosphino(trimethylsilyl)diazomethane with *t*BuCP and can also be isolated in high yield by reaction of bis(di-*iso*-propylamino)trimethylstannylphosphine with a chlorophosphirene.

The formation of **3a-c** from **1** is in stark contrast to analogous reactions of NHCs [1,3-bis(2,4,6-trimethylphenyl)imidazolidin-2-ylidene (SIMes), IMes, and IPr] with *t*BuCP. In these reactions, the formation of a 2*H*-phosphirene was observed for ᴹᵉˢDAC,[13] a triphosphole for IMes and a carbene-stabilised (*t*BuCP)₆ framework for IPr.[29] It should also be noted that three-membered heterocycles related to **3a-c** are formed in reactions of carbenes with other tetrahedranes. The triphosphirene **A** (Figure 1) is obtained from one equivalent of a CAAC or SIPr and P₄;[9,10] a

related cyclopropene is formed by reaction of tetra-*tert*-butyltetrahedrane (*t*BuC)$_4$ and tetracycanoethylene.[30]

Compounds **3a-c** were isolated as yellow solids in 29% - 56% yield after removal of the side product (*t*BuCP)$_4$ by sublimation and re-crystallisation. ^{1}H and ^{13}C{^{1}H} NMR spectra of **3a** and **3b** dissolved in C$_6$D$_6$ showed the presence of one set of signals for the carbene unit, while the spectra of **3c** show two sets of signals, indicating a hindered rotation around the P–C bond in solution at ambient temperature. For each compound, the ^{31}P{^{1}H} NMR spectra show two signals of an AX spin system with chemical shifts of −172.3/−39.4 (**3a**), −170.0/−47.2 (**3b**) and −162.9/138.9 (**3c**, see the Supporting Information). The doublet observed at high field is assigned to the phosphirene moiety. The observed $^1J_{PP}$ coupling constants ($^1J_{PP}$ = 296 Hz for **3a**, $^1J_{PP}$ = 299 Hz for **3b** , $^1J_{PP}$ = 312 Hz for **3c**) and the $^1J_{C–P}$ coupling constants of the phosphirene P-atom to the carbon ring atoms (50–52 Hz) are consistent with a covalent P–P single bond. UV/Vis absorption spectra of **3a-c** show an intense absorption band at 360 nm tailing into the visible region. This accounts for the bright yellow colour of these solids. DFT calculations on a truncated model compound (IPh)PP(C*t*Bu)$_2$ (IPh = 1,3-diphenylimidazolin-2-ylidene) show that the electronic transition corresponding to this wavelength is attributed to the HOMO-LUMO transition from the p-orbital of the phosphorus atom connected to the imidazoliumyl substituent to an empty p-orbital of the former carbene C atom (see Supporting Information for density difference plot). It seems plausible, that 1*H*-phosphirenes are intermediates in the formation of bisphosphaalkenes such as **2**. However, **3b** does not react with TMC to afford a bis(phosphaalkene); instead, a complex reaction mixture was obtained according to a ^{31}P{^{1}H} NMR spectrum.

6.3 Conclusion

In summary, the outcome of reactions of di-*tert*-butyldiphosphatetrahedrane **1** with N-heterocyclic carbenes is strongly influenced by the steric and electronic properties of the NHC. TMC, the smallest NHC used for this study, cleaves the P−P bond of **1**, selectively forming a bis(phosphaalkene) **2**. Bulkier NHCs IMes, IPr and ^{Mes}DAC afford phosphirenes **3a-c** via P−C bond cleavage. While the full mechanistic details of this dichotomous reactivity still need to be elaborated, the divergent reaction behaviour is likely attributed to the different sterics of the NHCs used. Importantly, the reactivity of **1** is clearly distinguished from its monomer *t*BuCP and resembles P$_4$, and the results suggest that **1** has significant potential for the preparation of hitherto unknown organophosphorus compounds. Further reactivity studies of **1** are in hand.

6.4   Experimental Details

General Synthetic Methods

All reactions and product manipulations were carried out in flame-dried glassware under an inert atmosphere of argon using standard Schlenk-line or glovebox techniques (maintained at <0.1 ppm H_2O and <0.1 ppm O_2). 1,3-Bis(2,4,6-trimethylphenyl)imidazolin-2-ylidene (IMes)[31], 1,3-bis(2,6-di-*iso*-propylphenyl)imidazolin-2-ylidene (IPr),[32] 1,3-bis-(2,4,6-trimethylphenyl)-4,6-diketo-5,5-dimethylpyrimidin-2-ylidene (MesDAC)[33], 1,3,4,5-tetramethylimidazolin-2-ylidene (TMC)[34], 1,3-di-*iso*-propyl-4,5-dimethylimidazolin-2-ylidene (*i*Pr₂ImMe)[35], MentCAAC[36], Ag[Al{OC(CF₃)₃}₄][37], AuCl(tht) (tht = tetrahydrothiophene)[38], Ph₂CN₂[39] and (*t*BuCP)₂ (**1**)[16] were prepared according to previously reported procedures. All other chemicals were purchased from commercial suppliers and used as received.

Solvents were dried and degassed with a MBraun SPS800solvent purification system. All dry solvents except *n*-hexane and *n*-pentane were stored under argon over activated 3 Å molecular sieves in gas-tight ampules. *n*-Hexane and *n*-pentane were stored over a potassium mirror.

General Analytical Techniques

NMR spectra were recorded on Bruker Avance 300 or 400 spectrometers at 300 K unless otherwise noted and internally referenced to residual solvent resonances (¹H NMR: THF-d₈: 1.72 ppm, C₆D₆: 7.16 ppm, toluene-d⁸: 2.08 ppm; ¹³C{¹H} NMR: THF-d₈: 25.31 ppm, C₆D₆: 128.06 ppm). Chemical shifts δ are given in ppm referring to external standards of tetramethylsilane (¹H, ¹³C{¹H}), 85% phosphoric acid (³¹P and ³¹P{¹H} spectra). ¹H and ¹³C NMR signals were assigned based on 2D NMR spectra (¹H,¹H-COSY, ¹H,¹³C-HSQC, ¹H,¹³C-HMQC). UV/Vis spectra were recorded on an Ocean Optics Flame Spectrometer. Elemental analysis was performed by the central analytics department of the University of Regensburg.

The single-crystal X-ray diffraction data were recorded on Rigaku Oxford Diffraction SuperNova Atlas diffractometers with Cu-K$_\alpha$ radiation (λ= 1.54184 Å). Crystals were selected under mineral oil, mounted on micromount loops and quench-cooled using an Oxford Cryosystems open flow N_2 cooling device. Either semi-empirical multi-scan absorption corrections[40] or analytical ones[41] were applied to the data. The structures were solved with SHELXT[42] solution program using dual methods and by using Olex2 as the graphical interface.[43] The models were refined with ShelXL[44] using full matrix least squares minimisation on F^2.[45] The hydrogen atoms were located in idealised positions and refined isotropically with a rigid model.

Synthesis of Compounds

[(TMC)PC*t*Bu]$_2$ (2)

To a solution of TMC (163.9 mg, 1.32 mmol, 1.0 eq) in toluene (3 mL) was added (*t*BuCP)$_2$ (0.58 M in toluene, 1.6 mL, 0.7 eq.). A colour change from colourless to intense orange was observed. After stirring at ambient temperature for 1 hour, a bright orange powder precipitated from the reaction mixture. Subsequently, the supernatant solution was removed by filtration and the solid was washed with toluene (0.3 mL) and dried *in vacuo*.

Crystals suitable for X-ray crystallography were grown by cooling a saturated solution of [(TMC)PC*t*Bu]$_2$ in THF from ambient temperature to −30 °C.

$C_{24}H_{42}N_4P_2$, MW = 448.58 g/mol
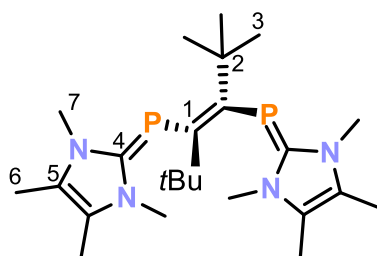
Yield: 204 mg (69%)

^{1}H NMR (400 MHz, 300 K, THF-d$_8$) δ = 1.55 (s, 18H, C^{3}H), 2.09 (s, 12H, C^{6}H), 3.36 (s, 12H, C^{7}H) ppm.

^{13}C{^{1}H} NMR (100 MHz, 300 K, C$_6$D$_6$) δ = 8.69 (s, C^6), 32.1 (t, $^3J_{CP}$ = 6.9 Hz, C^7), 33.0 (t, $^3J_{CP}$ = 6.4 Hz, C^3), 43.4 (t, $^2J_{CP}$ = 3.4 Hz, C^2), 120.9 (t, $^3J_{CP}$ = 1.7 Hz, C^5), 156.6 (dd, $^1J_{CP}$ = 73.5 Hz, $^2J_{CP}$ 14.8 Hz, C^1), 169.1 (dd, $^1J_{CP}$ = 116.13 Hz, $^4J_{CP}$ 7.1 Hz, C^4) ppm.

^{31}P{^{1}H} (162 MHz, 300 K, C$_6$D$_6$) δ = −28.4 (brs) ppm.

Elemental Analysis calcd. C 64.26, H 9.44, N 12.49; found C 64.87, H 9.14, N 12.30.

UV/Vis (THF): λ_{max} (nm, ε_{max} /L·mol^{-1}·cm^{-1}) 270 (14 000), 340 (21 000), 450 (16 000).

IPr=PP(C*t*Bu)$_2$ (3a)

To a solution of IPr (200 mg, 0.52 mmol, 1.0 eq) in toluene (10 mL) was added (*t*BuCP)$_2$ (3.6 mL, 0.58 mol/L, 2.08 mmol, 4.0 eq.). After stirring at ambient temperature for three weeks, the reaction was completed according to ^{1}H NMR monitoring. The solvent was removed and the light yellow residue was dried *in vacuo*. Recrystallisation of the residue from *n*-pentane at −30 °C overnight affords a mixture of **3a** and (*t*BuCP)$_4$ (ca. 1:1). Subsequently, (*t*BuCP)$_4$ was removed by sublimation at 120 °C on a turbomolecular pump (p < 1·10^{-4} mbar) for three days. The resulting yellow powder was pure according to NMR and elemental analysis. Single crystals suitable for X-ray crystallography were grown by cooling a saturated solution of **3a** from ambient temperature to −30 °C.
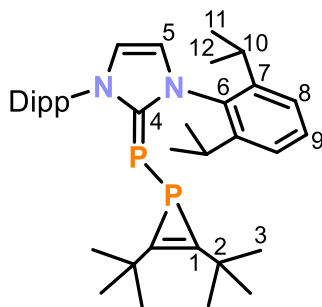
$C_{37}H_{54}N_2P_2$, MW = 588.80 g/mol

Yield: 91 mg (29%)

^{1}H NMR (400 MHz, 300 K, C_6D_6) δ = 1.20 (d, $^3J_{HH}$ = 6.9 Hz, 12H, C^{11}H), 1.23 (s, 18H, C^3H), 1.62 (d, $^3J_{HH}$ = 6.8 Hz, C^{11}H), 3.20 (sept, $^3J_{HH}$ = 6.9 Hz, 4H, C^{10}H), 6.14 (s, 2H, C^5H), 7.14 (d, $^3J_{HH}$ = 2.0 Hz, 4H, C^8H), 6.61 (dd, $^3J_{HH}$ = 6.2/8.9 Hz, 2H, C^9H) ppm.

^{13}C{^{1}H} NMR (100 MHz, 300 K, C_6D_6) δ = 23.7 (s, C^{11}), 24.7 (s, C^{12}), 29.1 (s, C^{10}), 30.9 (d, $^3J_{CP}$ = 1.8 Hz, C^3), 33.3 (dd, $^2J_{CP}$ = 6.5 Hz, $^3J_{CP}$ = 1.2 Hz, C^2), 119.8 (d, $^3J_{CP}$ = 3.7 Hz, C^5), 124.1 (dd, $^1J_{CP}$ = 50.1 Hz, $^2J_{CP}$ = 8.6 Hz, C^1), 124.6 (s, C^9), 130.3 (s, C^8), 135.8 (d, $^3J_{CP}$ = 3.4 Hz, C^6), 147.4 (s, C^7), 176.7 (dd, $^1J_{CP}$ = 115.9 Hz, $^2J_{CP}$ = 4.0 Hz, C^4) ppm.

^{31}P{^{1}H} (162 MHz, 300 K, C_6D_6) δ = −172.3 (d, $^1J_{PP}$ = 296 Hz), −39.4 (d, $^1J_{PP}$ = 296 Hz) ppm.

Elemental Analysis calcd. C 75.48, H 9.24, N 4.76; found C 75.41, H 8.98, N 4.44.

UV/Vis (THF): $λ_{max}$ (nm, $ε_{max}$ /L·mol^{-1}·cm^{-1}) 300 (10 500), 360 (15 000).

IMes=PP(C*t*Bu)$_2$ (3b)

To a solution of IMes (150 mg, 0.5 mmol, 1.0 eq) in toluene (10 mL) was added (*t*BuCP)$_2$ (0.59 M in toluene, 3.5 mL, 2.1 mmol, 4.0 eq.). After stirring at ambient temperature for two weeks, the reaction was completed according to ^{1}H NMR monitoring. The solvent was removed and the light yellow residue was dried *in vacuo*. Subsequently, (*t*BuCP)$_4$ was removed by sublimation at 120 °C on a turbomolecular pump (p < 1·10^{-4} mbar) for three days. The resulting yellow powder was pure according to NMR and elemental analysis. Single crystals suitable for X-ray crystallography were grown by cooling a saturated solution of **3b** from ambient temperature to −30 °C.
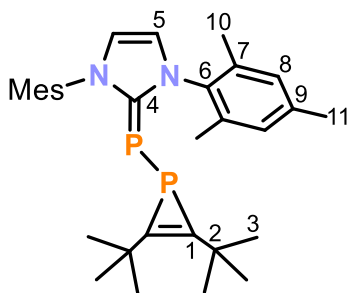
$C_{31}H_{42}N_2P_2$, MW = 504.64 g/mol

Yield: 73 mg (30%)

156

¹H NMR (400 MHz, 300 K, C_6D_6) δ = 1.23 (s, 18H, C^3H), 2.08 (s, 6H, $C^{11}H$), 2.32 (s, 12H, $C^{10}H$), 5.88 (s, 2H, C^5H), 6.78 (s, 4H, C^8H) ppm.

¹³C{¹H} NMR (100 MHz, 300 K, C_6D_6) δ = 18.7 (s, C^{10}), 21.1 (s, C^{11}), 30.8 (d $^4J_{CP}$ = 1.8 Hz C^3), 33.0 (dd, $^2J_{CP}$ = 6.6 Hz, $^3J_{CP}$ = 1.1 Hz, C^2), 118.6 (d, $^3J_{CP}$ = 3.6 Hz, C^5), 125.6 (dd, $^1J_{CP}$ = 50.4 Hz, $^2J_{CP}$ = 9.0 Hz, C^1), 129.7 (s, C^8), 135.5 (d, $^3J_{CP}$ = 2.6 Hz, C^6), 136.7 (s, C^7), 138.7 (s, C^9), 172.9 (dd, $^1J_{CP}$ = 113.9 Hz, $^2J_{CP}$ = 7.0 Hz, C^4) ppm.

³¹P{¹H} (162 MHz, 300 K, C_6D_6) δ = −169.9 (d, $^1J_{PP}$ = 299 Hz), −47.2 (d, $^1J_{PP}$ = 299 Hz) ppm.

Elemental Analysis calcd C 73.78, H 8.39, N 5.08; found C 74.05, H 8.67, N 5.43.

UV/Vis (THF): λ_{max} (nm, ε_{max} /L·mol⁻¹·cm⁻¹) 300 (15 000), 360 (15 500).

Compounds **3a** and **3b** are very sensitive towards hydrolysis, forming the known NHC=PH (NHC = IPr, IMes) compounds.[46]

ᴹᵉˢDAC=PP(C*t*Bu)₂ (3c)

To a solution of ᴹᵉˢDAC (150 mg, 0.4 mmol, 1.0 eq) in toluene (10 mL) was added (*t*BuCP)₂ (0.26 M in toluene, 1.5 mL, 0.65 mmol, 1.6 eq.). After stirring at ambient temperature for two weeks, the reaction was completed according to ¹H NMR monitoring. The solvent was removed and the light yellow residue was dried *in vacuo*. Subsequently, the residue was dissolved in benzene (5 mL) and layered with *n*-hexane (25 mL). Storage at −30 °C overnight afforded yellow crystals which were isolated by decanting the supernatant and dried under reduced pressure. ¹H NMR analysis of the material shows the presence of 0.5 equivalents of *n*-hexane (see the Supporting Information). This material was used for elemental analysis and UV/Vis spectroscopy. Further drying of the material under reduced pressure affords *n*-hexane-free **3c** which was used for NMR analysis.

Single crystals suitable for X-ray crystallography were grown by slow diffusion of *n*-hexane into a saturated solution of **3c** in benzene at ambient temperature.

$C_{34}H_{46}N_2O_2P_2$, MW = 576.70 g/mol
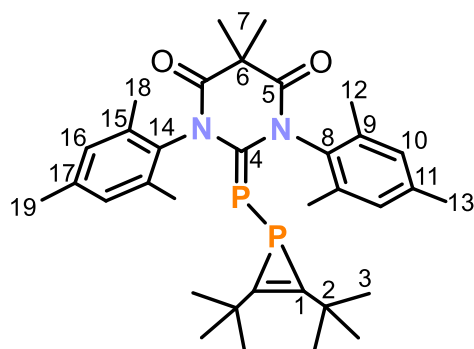
Yield: 130 mg (56%)

¹H NMR (400 MHz, 300 K, C_6D_6) δ = 0.99 (s, 18H, C^3H), 1.73 (s, 6H, C^7H), 1.99 (s, 3H $C^{13}H$), 2.07 (s, 3H, $C^{19}H$), 2.24 (s, 6H, $C^{18}H$), 2.39 (s, 6H, $C^{12}H$), 6.71 (s, 2H, $C^{10}H$), 6.89 (s, 2H, $C^{16}H$) ppm.

^{13}C{^{1}H} NMR (100 MHz, 300 K, C$_6$D$_6$) δ = 18.0 (d, $^5J_{CP}$ = 3.0 Hz, C^{18}), 18.4 (d, $^5J_{CP}$ = 1.9 Hz, C^{12}), 21.1 (s, C^{13}), 21.2 (s, C^{19}), 24.4 (s, C^7), 29.7 (d, $^4J_{CP}$ = 1.5 Hz, C^3), 32.5 (dd, $^2J_{CP}$ = 6.5 Hz, $^3J_{CP}$ = 2.0 Hz, C^2), 48.0 (s, C^6), 125.6 (dd, $^1J_{CP}$ = 51.8 Hz, $^2J_{CP}$ = 8.7 Hz, C^1), 129.8 (s, C^{10}), 131.0 (d, $^5J_{CP}$ = 2.7 Hz, C^{16}), 135.0 (d, $^3J_{CP}$ = 4.8 Hz, C^8), 135.9 (d, $^4J_{CP}$ = 4.4 Hz, C^9), 137.0 (d, $^3J_{CP}$ = 9.0 Hz, C^{14}), 137.5 (d, $^4J_{CP}$ = 8.4 Hz, C^{15}), 138.4 (s, C^{11}), 139.0 (s, C^{17}), 167.9 (d, $^3J_{CP}$ = 2.6 Hz, C^5), 168.4 (s, C$^{5'}$), 173.7 (dd, $^1J_{CP}$ = 92.5 Hz, $^2J_{CP}$ = 2.0 Hz, C^4) ppm.

^{31}P{^{1}H} (162 MHz, 300 K, C$_6$D$_6$) δ = −162.9.8 (d, $^1J_{PP}$ = 312 Hz), 139.0 (d, $^1J_{PP}$ = 312 Hz) ppm.

Elemental Analysis was performed with a sample recrystallised from *n*-hexane (containing 0.5 eq. *n*-hexane, see SI) calcd. C 71.70, H 8.62, N 4.52; found C 71.89, H 8.31, N 4.89.

UV/Vis (THF): λ_{max} (nm, ε_{max} /L·mol^{-1}·cm^{-1}) 260 (13 000sh), 360 (21 500).

(TMC)C(S)(NPh)

Phenyl isothiocyanate (0.1 mL, 113 mg, 0.84 mmol, 2.1 eq.) was added to a solution of TMC (50.0 mg, 0.4 mmol, 1.0 eq.) in 0.5 mL C$_6$D$_6$. The reaction mixture turned yellow immediately and was stirred for 18 h. Subsequently, the solvent was removed *in vacuo.* Crystallisation from toluene/*n*-hexane (1/1, 2 mL/2 mL) afforded yellow crystals of [(TMC)=C(S)(NPh)] suitable for single crystal X-ray diffraction experiments, which were isolated by decanting the supernatant and dried *in vacuo*.

C$_{14}$H$_{16}$N$_3$S, MW = 259.37 g/mol
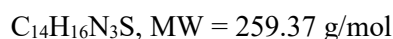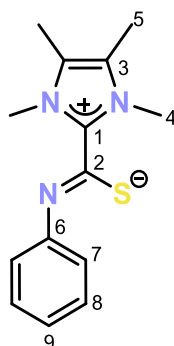
Yield: 32 mg (31%)

^{1}H NMR (400 MHz, 300 K, C$_6$D$_6$) δ = 1.00 (s, 6H, C^{5}H), 3.07 (s, 6H, C^{4}H), 7.10-7.15 (m, 1H, C^{9}H, overlapping with C$_6$D$_6$ signal), 7.47-7.55 (m, 2H, C^{8}H), 8.39-8.45 (m, 2H, C^{7}H) ppm.

^{13}C{^{1}H} NMR (100 MHz, 300 K, C$_6$D$_6$) δ = 7.27 (s, C^5), 31.4 (s, C^4), 121.7 (s, C^3), 123.7 (s, C^9), 124.3 (s, C^7), 128.6 (s, C^8), 147.0 (s, C^1), 152.4 (s, C^2), 167.8 (s, C^6) ppm.

Elemental Analysis calcd. C 64.83, H 6.41, N 16.20; found C 65.01, H 6.47, N 16.09.

UV/Vis (THF): λ_{max} (nm, ε_{max} /L·mol^{-1}·cm^{-1}) 260 (12 000sh), 340 (12 000).

(TMC)=N-N=CPh$_2$

1,1′-(Diazomethylene)bis(benzene) (78 mg, 0.4 μmol, 1.0 eq.) in C$_6$D$_6$ (0.5 mL) was added to a solution of TMC (50.0 mg, 0.4 mmol, 1.0 eq.) in C$_6$D$_6$ (0.5 mL). The orange reaction mixture was

stirred for 18 h. Subsequently, the solvent was removed *in vacuo*. Crystallisation from toluene/*n*-hexane (1/1, 2 mL/2 mL) afforded bright orange crystals of [(TMC)-N=N-CPh$_2$] suitable for single crystal X-Ray diffraction experiments, which were isolated by decanting the supernatant and dried *in vacuo*.
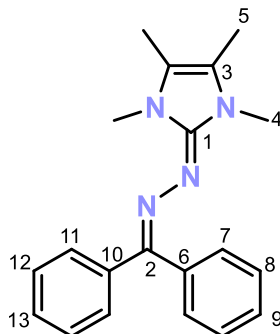
$C_{20}H_{22}N_4$, MW = 318.42 g/mol

Yield: 80 mg (63%)

^{1}H NMR (400 MHz, 300 K, C_6D_6) δ = 1.31 (s, 6H, C^5H), 3.14 (s, 6H, C^4H), 7.11-7.18 (m, 1H, C^9H), 7.19-7.25 (m, 1H, $C^{13}H$), 7.25-7.31 (m, 2H, C^8H), 7.33-7.41 (m, 2H, $C^{12}H$), 7.73-7.81 (m, 2H, $C^{11}H$), 7.91-7.98 (m, 2H, C^7H) ppm.

^{13}C{^{1}H} NMR (100 MHz, 300 K, C_6D_6) δ = 8.1 (s, C^5), 30.6 (s, C^4), 115.8 (s, C^3), 126.5 (s, C^9), 126.9 (s, C^{13}), 127.2 (s, C^7), 127.9 (s, C^{12}, overlapping with C_6D_6-signal), 128.3 (s, C^8, overlapping with C_6D_6-signal), 131.2 (s, C^{11}), 138.9 (s, C^{10}), 142.4 (s, C^6), 148.3 (s, C^2), 151.6 (s, C^1) ppm.

UV/Vis (THF): λ_{max} (nm, ε_{max} /L·mol^{-1}·cm^{-1}) 240 (16 000), 320 (8900), 400 (30 000).

Elemental Analysis calcd. C 75.44, H 6.96, N 17.60; found C 76.00, H 6.62, N 17.62.

6.5   Supporting Information

The Supporting Information of Chapter 6 can be found on the supplied CD-ROM and on https://pubs.rsc.org/en/content/articlelanding/2021/CC/D0CC07103J#!divAbstract.   The Supporting Information contains: Additional Experiments, NMR and UV/Vis spectra, X-ray crystallography details and results of quantum chemical calculations including Cartesian coordinates of all optimised structures.

References

[1] a) D. E. C. Corbridge, *Phosphorus 2000. Chemistry, Biochemistry and Technology*, (Elvesier, 2000); b) W. Schipper, *Eur. J. Inorg. Chem.* **2014**, *2014*, 1567.

[2] M. Bispinghoff, H. Grützmacher, *Chimia* **2016**, *70*, 279.

[3] M. B. Geeson, C. C. Cummins, *Science* **2018**, *359*, 1383.

[4] a) M. Regitz, *Chem. Rev.* **1990**, *90*, 191; b) A. Chirila, R. Wolf, J. Chris Slootweg, K. Lammertsma, *Coord. Chem. Rev.* **2014**, *270-271*, 57; c) W. Rösch, M. Regitz, *Angew. Chem. Int. Ed. Engl.* **1984**, *23*, 900; d) M. Regitz, W. Rösch, *Synthesis* **1987**, *112*, 689.

[5] a) A. R. Jupp, J. M. Goicoechea, *Angew. Chem. Int. Ed.* **2013**, *52*, 10064; b) D. Heift, Z. Benkő, H. Grützmacher, *Dalton Trans.* **2014**, *43*, 831; c) X. Chen, S. Alidori, F. F. Puschmann, G. Santiso-Quinones, Z. Benkő, Z. Li, G. Becker, H.-F. Grützmacher, H. Grützmacher, *Angew. Chem. Int. Ed.* **2014**, *53*, 1641.

[6] J. E. Borger, A. W. Ehlers, J. C. Slootweg, K. Lammertsma, *Chem. Eur. J.* **2017**, *23*, 11738.

[7] a) M. M. Rauhut, A. M. Semsel, *J. Org. Chem.* **1963**, *28*, 471; b) M. M. Rauhut, A. M. Semsel, *J. Org. Chem.* **1963**, *28*, 473.

[8] a) J. E. Borger, M. S. Bakker, A. W. Ehlers, M. Lutz, J. C. Slootweg, K. Lammertsma, *Chem. Commun.* **2016**, *52*, 3284; b) L. Xu, Y. Chi, S. Du, W.-X. Zhang, Z. Xi, *Angew. Chem. Int. Ed.* **2016**, *55*, 9187.

[9] J. D. Masuda, W. W. Schoeller, B. Donnadieu, G. Bertrand, *Angew. Chem. Int. Ed.* **2007**, *46*, 7052.

[10] J. D. Masuda, W. W. Schoeller, B. Donnadieu, G. Bertrand, *J. Am. Chem. Soc.* **2007**, *129*, 14180.

[11] O. Back, G. Kuchenbeiser, B. Donnadieu, G. Bertrand, *Angew. Chem. Int. Ed.* **2009**, *48*, 5530.

[12] C. D. Martin, C. M. Weinstein, C. E. Moore, A. L. Rheingold, G. Bertrand, *Chem. Commun.* **2013**, *49*, 4486.

[13] L. L. Liu, J. Zhou, L. L. Cao, R. Andrews, R. L. Falconer, C. A. Russell, D. W. Stephan, *J. Am. Chem. Soc.* **2018**, *140*, 147.

[14] L. L. Liu, L. L. Cao, J. Zhou, D. W. Stephan, *Angew. Chem. Int. Ed.* **2019**, *58*, 273.

[15] a) B. M. Cossairt, M.-C. Diawara, C. C. Cummins, *Science* **2009**, *323*, 602; b) M.-L. Y. Riu, R. L. Jones, W. J. Transue, P. Müller, C. C. Cummins, *Sci. Adv.* **2020**, *6*, eaaz3168.

[16] G. Hierlmeier, P. Coburger, M. Bodensteiner, R. Wolf, *Angew. Chem. Int. Ed.* **2019**, *58*, 16918.

[17] B. Geissler, S. Barth, U. Bergsträsser, M. Slany, J. Durkin, P. B. Hitchcock, M. Hofmann, P. Binger, J. F. Nixon, P. von Ragué Schleyer, M. Regitz, *Angew. Chem. Int. Ed. Engl.* **1995**, *34*, 484.

[18] P. Le Floch, *Coord. Chem. Rev.* **2006**, *250*, 627.

[19] P. Pyykkö, *J. Phys. Chem. A* **2015**, *119*, 2326.

[20] a) B. Cordero, V. Gómez, A. E. Platero-Prats, M. Revés, J. Echeverría, E. Cremades, F. Barragán, S. Alvarez, *Dalton Trans.* **2008**, 2832; b) P. Pyykkö, M. Atsumi, *Chem. Eur. J.* **2009**, *15*, 186.

[21] A. J. Arduengo III, J. C. Calabrese, A. H. Cowley, H. V. Rasika Dias, J. R. Goerlich, W. J. Marshall, B. Riegel, *Inorg. Chem.* **1997**, *36*, 2151.

[22] A. J. Arduengo III, H. V. Rasika Dias, J. C. Calabrese, *Chem. Lett.* **1997**, 143.

[23] L. Weber, *Eur. J. Inorg. Chem.* **2000**, 2425.

[24] F. Mathey, *Chem. Rev.* **1990**, *90*, 997.

[25] J. Foerstner, A. Kakoschke, D. Stellfeldt, H. Butenschön, R. Wartchow, *Organometallics* **1998**, *17*, 893.

[26] J. Simon, G. J. Reiß, U. Bergsträßer, H. Heydt, M. Regitz, *Eur. J. Inorg. Chem.* **2001**, 2067.

[27] A. Jayaraman, B. T. Sterenberg, *Organometallics* **2013**, *32*, 745.

[28] M. Sanchez, R. Réau, C. J. Marsden, M. Regitz, G. Bertrand, *Chem. Eur. J.* **1999**, *1*, 274.

[29] L. L. Liu, J. Zhou, Y. Kim, L. L. Cao, D. W. Stephan, *Dalton Trans.* **2019**, *48*, 14242.

[30] G. Maier, K.-A. Schneider, K.-D. Malsch, H. Irngartinger, A. Lenz, *Angew. Chem. Int. Ed. Engl.* **1982**, *21*, 437.

[31] A. J. Arduengo III, H. V. Rasika Dias, R. L. Harlow, M. Kline, *J. Am. Chem. Soc.* **1992**, *114*, 5530.

[32] P. Tang, W. Wang, T. Ritter, *J. Am. Chem. Soc.* **2011**, *133*, 11482.

[33] T. W. Hudnall, J. P. Moerdyk, C. W. Bielawski, *Chem. Commun.* **2010**, *46*, 4288.

[34] F. Hanasaka, K.-i. Fujita, R. Yamaguchi, *Organometallics* **2005**, *24*, 3422.

[35] T. K. N. Kuhn, *Synthesis* **1993**, 561.

[36] V. Lavallo, Y. Canac, C. Präsang, B. Donnadieu, G. Bertrand, *Angew. Chem. Int. Ed.* **2005**, *44*, 5705.

[37] I. Krossing, *Chem. Eur. J.* **2001**, *2*, 490.

[38] S. Ahrland, K. Dreisch, B. Noren, A. Oskarsson, *Mater. Chem. Phys.* **1993**, *35*, 281.

[39] J. B. Miller, *J. Org. Chem.* **1959**, *24*, 560.

[40] a) Sheldrick, G. M. SADABS, Bruker AXS, Madison, USA **2007**; b) CrysAlisPro, Scale3 Abspack, Rigaku Oxford Diffraction **2019**.

[41] R. C. Clark, J. S. Reid, *Acta Cryst. A* **1995**, *51*, 887.

[42] G. M. Sheldrick, *Acta Cryst. A* **2015**, *71*, 3.

[43] O. V. Dolomanov, L. J. Bourhis, R. J. Gildea, J. A. K. Howard, H. Puschmann, *J .Appl. Crystallogr.* **2009**, *42*, 339.

[44] G. M. Sheldrick, *Acta Cryst. C* **2015**, *71*, 3.

[45] G. M. Sheldrick, *Acta Cryst. A* **2008**, *64*, 112.

[46] a) A. M. Tondreau, Z. Benkő, J. R. Harmer, H. Grützmacher, *Chem. Sci.* **2014**, *5*, 1545; b) A. Doddi, D. Bockfeld, T. Bannenberg, P. G. Jones, M. Tamm, *Angew. Chem. Int. Ed.* **2014**, *53*, 13568; c) O. Lemp, C. von Hänisch, *Phosphorus, Sulfur, Silicon Relat. Elem.* **2016**, *191*, 659; d) M. Cicač-Hudi, J. Bender, S. H. Schlindwein, M. Bispinghoff, M. Nieger, H. Grützmacher, D. Gudat, *Eur. J. Inorg. Chem.* **2016**, *2016*, 649.

7 Activation of Di-tert-butyldiphosphatetrahedrane: Access to (*t*BuCP)ₙ (*n* = 2, 4) Ligand Frameworks by P–C Bond Cleavage[a,b]

Abstract: The first mixed phosphatetrahedranes were reported only recently and their reactivity is virtually unexplored. Here we present a reactivity study on di-*tert*-butyldiphosphatetrahedrane (**1**), which is the dimer of *tert*-butylphosphaalkyne. The (*t*BuCP)₂ tetrahedron is activated selectively by N-heterocyclic carbene (NHC) nickel(I) and nickel(0) complexes, resulting in novel complexes featuring diverse (*t*BuCP)ₙ-frameworks (*n* = 2, 4). Release of the (*t*BuCP)₄ framework from one of the complexes was achieved by addition of CO gas. Furthermore, **1** can be used as a source for P₂ units by elimination of di-*tert*-butylacetylene in the coordination sphere of nickel.
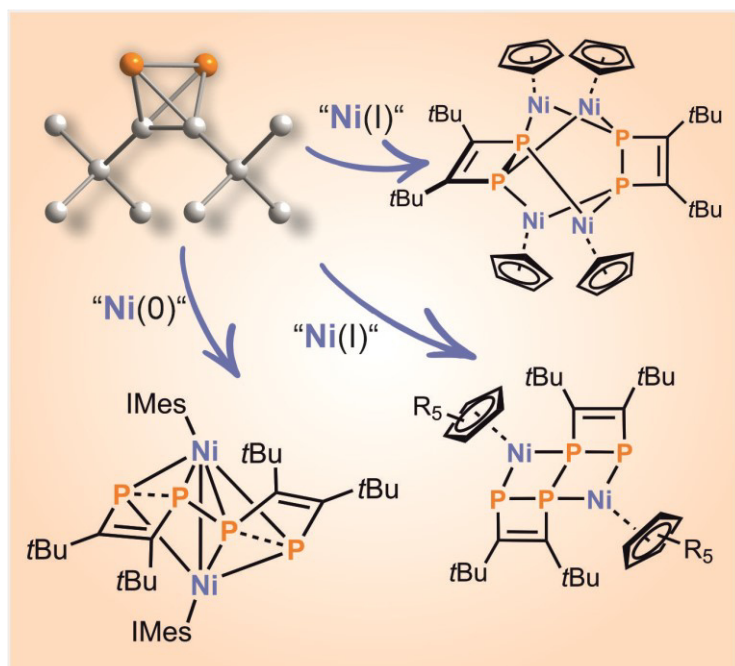
7.1 Introduction

Tetrahedranes have long fascinated the chemical community due their simple structure and typically high reactivity.[1] The first tetrahedral molecule to be prepared was white phosphorus, P_4, which was discovered as early as 1669, although its tetrahedral structure was recognised only in the early 20th century.[2] P_4 is produced on a megaton scale each year and used as the common building block for incorporation of P atoms into organophosphorus compounds.[3] The heavier homologue As_4 and the mixed interpnictogen compound AsP_3 are likewise accessible.[4] Purely carbon-based tetrahedranes are also well-known, in line with the diagonal relationship between carbon and phosphorus in the periodic table.[5] Indeed, the synthesis of $(tBuC)_4$ in 1978 was a pinnacle of organic synthesis.[5]

In contrast, the first mixed C/P tetrahedranes were only reported last year. We showed that the 'hybrid' of $(tBuC)_4$ and P_4, di-*tert*-butyldiphosphatetrahedrane $(tBuCP)_2$ (**1**), can be synthesised in a simple nickel-catalysed dimerisation reaction of *tert*-butylphosphaalkyne, *t*BuCP.[6] Shortly after our report, the synthesis of the related tri-*tert*-butylphosphatetrahedrane $(tBuC)_3P$ was published by Cummins and co-workers.[7] Given the similar molecular structures and isolobal relationship between **1** and P_4, a comparison of the reaction properties of both molecules is a tantalising prospect.[5]

Indeed, the activation of the P_4 tetrahedron by main group and transition metal complexes has attracted significant interest as a means of gaining control over its transformations, and of accessing fascinating new polyphosphorus compounds.[10] In one of our recent contributions to this area, we demonstrated the use of mononuclear cyclopentadienyl nickel(I) complexes [CpNi(NHC)] [NHC = IMes (1,3-bis(2,4,6-trimethylphenyl)imidazolin-2-ylidene), IPr (1,3-bis(2,6-di-*iso*-propylphenyl)imidazolin-2-ylidene)]. Such 'nickel(I) radicals' selectively break one P−P bond of P_4 to afford μ-η^1:η^1-bridging P_4^{2-}-ligands with a 'butterfly' type structure (Figure 1, centre left).[8] Subsequent studies demonstrated that P_4 activation by Ni(0)-NHC complexes affords unusual di- and trinuclear cluster compounds, including a *closo* $[(IPr)_3Ni_3P_8]$ cluster shown in Figure 1 (bottom left).[9]
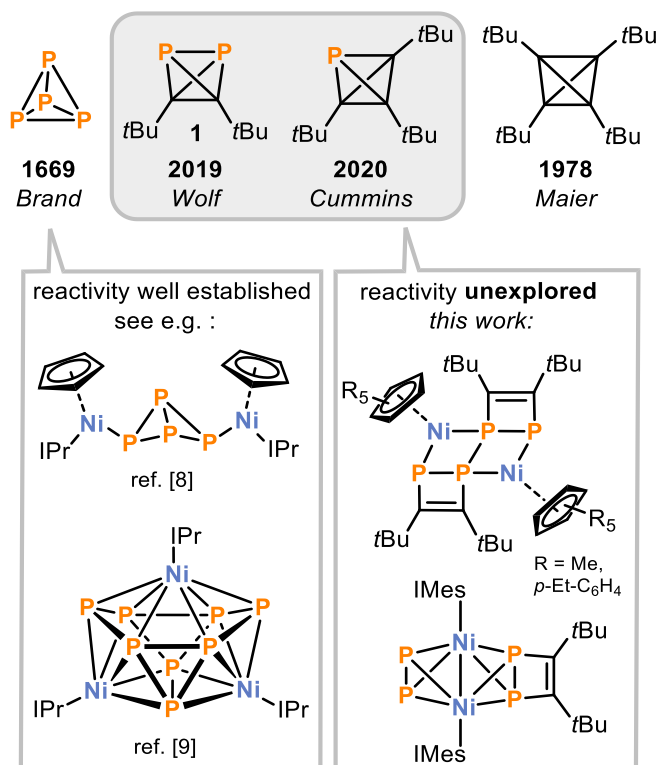
Figure 1. (Mixed) group 14/15 tetrahedranes and reactivity of P_4 with NHC-stabilised Ni(I) metalloradicals and Ni(0) complexes.[8,9]

Here, we describe a study into the reactivity of diphosphatetrahedrane **1** with the same N-heterocyclic carbene (NHC) nickel(I) and nickel(0) complexes. These investigations have led to the preparation of polynuclear nickel complexes, which incorporate a variety of (tBuCP)ₙ ($n = 2$, 4) ligands in unusual coordination modes that are not known to be accessible using other synthetic precursors. We furthermore discuss the follow-up chemistry and remarkable thermal transformation of one of these compounds. The results of this work provide a valuable first insight into the reaction behaviour of **1** toward transition metal centres and reveal that its reaction patterns are clearly distinct from those of P_4 and, indeed, also from those of tBuCP, the monomer of **1**.

7.2 Results and Discussion

This investigation commenced with the nickel(I) radical [(Cp)Ni(IPr)], which had previously been shown to react with white phosphorus under P−P bond scission (see Figure 1).[8] Reaction of two equivalents of [CpNi(IPr)] with **1** in THF instantaneously afforded a deep red solution at room temperature (Scheme 1). Analysis of the crude reaction mixture by ^{1}H NMR spectroscopy revealed consumption of the paramagnetic starting material and release of IPr. A singlet resonance at 93.0 ppm was observed in the ^{31}P{^{1}H} NMR spectrum. Crystals grown from toluene were characterised by single crystal X-ray analysis (SCXRD) as the tetranuclear complex [(CpNi)₂(tBu₂C₂P₂)]₂ (**2**, Figure 2 left) containing two 1,2-diphosphacyclobutene-1,2-diide ligands coordinated by four (CpNi) units in a realgar-type fashion. Notably, the reaction with [CpNi(IPr)] induces P−C bond cleavage to give a metalated 1,2-diphosphacyclobutene rather than forming the isomeric 'butterfly' compound [{CpNi(IPr)}₂(μ-κ^2P-tBu₂C₂P₂)] by P−P bond scission. Such a complex was observed with the valence isoelectronic P₄ molecule, see Figure 1.[9] In agreement with this, DFT calculations of the hypothetical reaction of **1** with two equivalents of a radical (methyl radical or [CpNi(IPh)]) (IPh = 1,3-diphenylimidazolin-2-ylidene) suggest that the cyclobutene compound is thermodynamically preferred over the butterfly compound (see computational details in the Supporting Information of this thesis).

Structurally characterised 1,2-diphosphacyclobutadiene transition metal complexes are scarce, and the ligand commonly coordinates via the π-system in these examples.[11] The P1−P2 bond length in **2** (2.2244(7) Å) suggests the presence of a P−P single bond, whereas the C−C bond length of 1.360(3) Å is indicative of a C=C double bond.[12] The bond metric data is thus consistent with the presence of a dianionic (tBu₂C₂P₂)$^{2-}$ ligand, which coordinates in a μ^4,η^2:η^2-mode through the lone-pairs of the P atoms, which was previously unknown for this type of ligand. Dark red, crystalline **2** was isolated in 56% yield and further analysed by NMR spectroscopy. The ^{1}H NMR spectrum of **2** showed one signal for the *t*Bu groups (δ = 1.32 ppm) and one resonance for the cyclopentadienyl ligand (δ = 5.17 ppm). In the ^{13}C{^{1}H} NMR spectrum four resonances were observed, which are consistent with the presence of a Cp and a (tBu₂C₂P₂)$^{2-}$ ligand. The UV/Vis absorption spectrum of **2** reveals two bands at 400 and 520 nm, the latter accounting for its red colour.
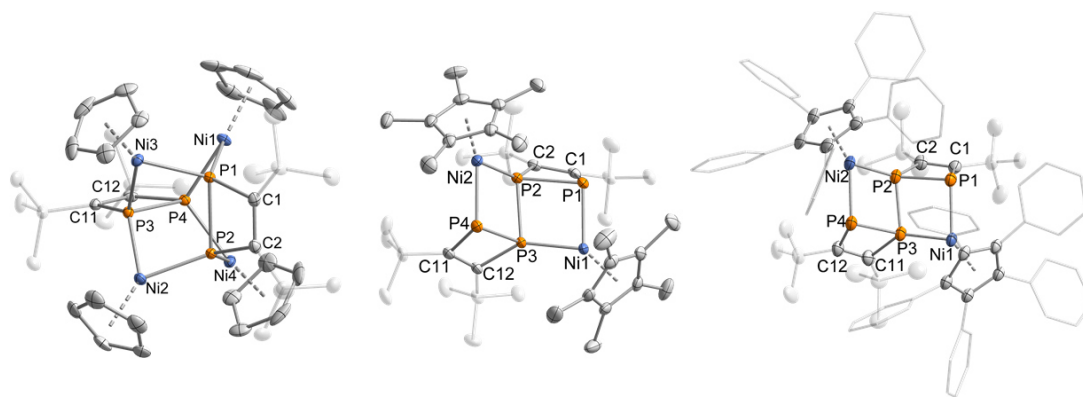
Figure 2. Molecular structures of **2** (left), **3a** (middle) and **3b** (right) in the solid state. Thermal ellipsoids are set at the 50% probability level. For **2**, only one molecule of the asymmetric unit is shown. Hydrogen atoms, solvent molecules, disorder in the aryl rings and 4-Et groups of **3b** are omitted for clarity. Selected bond lengths [Å] and angles [°] for **2**: P1−P2 2.2244(7), P3−P4 2.2199(7), P1−C1 1.854(2), P2−C2 1.864(2), C1−C2 1.360(3), Ni1−P1 2.1834(6), Ni1−P4 2.1750(6), Ni1−Cp^{centr} 1.765(1), P4−Ni1−P1 77.48(2), P7−Ni6−P6 78.03(2), C1−P1−P2 76.60(7), C2−P2−P1 76.50(7), C2−C1−P1 103.73(15), C1−C2−P2 103.11(16); **3a**: Ni1−P1 2.2376(4), Ni1−P3 2.1140(4), P1−P2 2.2211(5), P2−P3 2.1892(5), P3−P4 2.2252(5), P1−C1 1.8517(15), P2−C2 1.8214(14), C1−C2 1.372(2), Ni1−Cp^{centr} 1.746(1), P3−Ni1−P1 82.392(15), P2−P1−Ni1 95.889(16), C1−P1−Ni1 110.60(4), C2−P2−P3 111.08(5), C2−P2−P1 79.47(5), C2−P2−Ni2 143.28(5), Ni2−P2−P3 101.018(17), P3−P2−P1 81.110(16), C2−C1−P1 106.73(10), C1−C2−P2 99.52(10), Ni1−P3−P2 100.575(17), Ni1−P3−P4 124.892(19), P2−P3−P4 80.407(17); **3b**: Ni1−P1 2.2736(8), Ni1−P3 2.1230(7), P1−P2 2.2186(8), P2−P3 2.1717(9), P3−P4 2.2211(8), P1−C1 1.861(3), P2−C2 1.825(3), C1−C2 1.361(4), Ni1−Cp^{centr} 1.802(1), P3−Ni1−P1 79.33(3), P2−P1−Ni1 97.44(3), C1−P1−Ni1 113.29(9), C2−P2−P3 111.15(9), C2−P2−P1 79.86(9), C2−P2−Ni2 141.42(9), Ni2−P2−P3 103.61(3), P3−P2−P1 79.54(3), C2−C1−P1 107.38(18), C1−C2−P2 99.28(19), Ni1−P3−P2 103.63(3), Ni1−P3−P4 125.09(3), P2−P3−P4 79.74(3).

Next, we assessed the reactivity of nickel radicals bearing bulkier pentamethylcyclopentadienyl (Cp*) and pentaarylcyclopentadienyl (Cp^{BIG}) ligands (Scheme 1).[13] As with the previous reaction, deep red solutions were obtained when a 1:2 stoichiometry was used. However, analysis by ¹H NMR spectroscopy revealed broad resonances corresponding to unconsumed paramagnetic starting material, which disappeared upon addition of another equivalent of **1**.
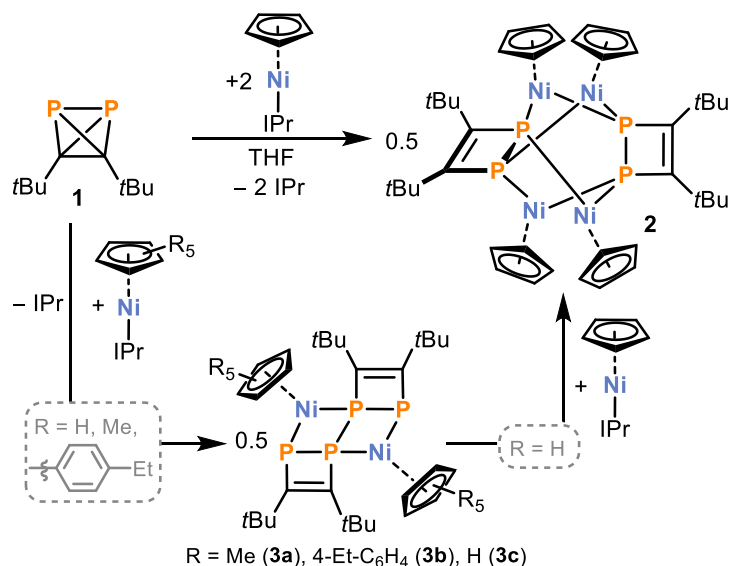
Scheme 1. Reactions of [Cp^{R}Ni(IPr)] (R = H; Me, 4-Et-C$_6$H$_4$) with (tBuCP)$_2$.

Single crystal X-ray diffraction studies revealed the formation of dinuclear species [(Cp^{R}Ni)$_2$(tBu$_4$C$_4$P$_4$)] [Cp^R = Cp* (**3a**), Cp^{BIG} (**3b**)], where two molecules of **1** have formally undergone radical coupling to produce a (tBuCP)$_4$ moiety (Scheme 1 bottom). Notably, however, compounds **2** and **3** were not formed upon reaction of the nickel complexes with the known ladderane-type phosphaalkyne tetramer (tBuCP)$_4$ (**6**), which is the known dimerisation product of **1**.[6][14] This illustrates the value of **1** as a synthetic precursor to novel P/C ligand frameworks. Compounds **3a** and **3b** were isolated in 33% (**3a**) and 44% (**3b**) yields as dark-red, crystalline solids. Single-crystal X-ray diffraction revealed a three-rung ladder structure composed of two Ni and four P atoms, which is fused with two four-membered P$_2$C$_2$ heterocycles. The P−P bond lengths range from 2.1717(9) to 2.2252(5) Å, with the shortest bond length for the P2−P3 bond, which connects the two P$_2$C$_2$ rings. Analysis of **3a** and **3b** by ^{1}H NMR spectroscopy reveal the expected signal sets for the cyclopentadienyl ligands and two singlets for the tBu groups. The ^{31}P{^{1}H} NMR spectra of both compounds show two pseudo triplet resonances. For **3a** these signals arise at −61.4 and 31.3 ppm with a coupling constant of 44.2 Hz (similar values were obtained for **3b**, see the Supporting Information for details). The signal shape likely arises from an AA′BB′ spin system with two similar $^1J_{PP}$ coupling constants and small $^2J_{PP}$ couplings. Indeed, DFT calculations at the TPSS pcSseg-2 level of theory for **3a** reproduce the two small coupling constants of 28 and 47 Hz. The absorption spectra of **3a** and **3b** show bands at 420 (**3a**) and 520 (**3b**) nm.

Considering these first insights into the reaction of **1** with [CpNi(IPr)] and bulkier metalloradicals, we reasoned that **3a** and **3b** might be intermediates in the formation of realgar-type compounds such as **2**. In order to evaluate this hypothesis, **1** was reacted with just 1.5 equivalents of [CpNi(IPr)]. Two pseudo-triplet resonances at −72.5 and 22.1 ppm were observed in the ^{31}P{^{1}H} NMR spectrum with a coupling constant of 45.5 Hz (see the Supporting Information of this thesis). In addition, formation of **2** was observed. These data are in good agreement with the

spectroscopic data obtained for **3a** and **3b** and point towards formation of [(CpNi)$_2$(tBu$_4$C$_4$P$_4$)] (**3c**). Nevertheless, all attempts to crystallise this compound failed (instead, crystals of **2** were obtained). Furthermore, no reaction occurred between **3a** and one equivalent of the smallest nickel radical [CpNi(IPr)] even when heated to temperatures of 70 °C. The sluggish reactivity of **3a** toward [CpNi(IPr)] is presumably due to the central P−P bond being shielded by the Cp* ligand. Aiming at the synthesis of further oligonuclear nickel complexes, we next investigated the reactions of **1** towards the Ni(0) complexes [(IMes)$_2$Ni] and [(IPr)Ni(η^6-toluene)].[15,16] The reactions of these complexes with P$_4$ afforded Wade-Clusters, as reported previously.[9] The reaction of **1** with [(IMes)$_2$Ni] at −80 °C afforded a brown reaction solution. Analysis by ^{31}P{^{1}H} NMR spectroscopy revealed a selective reaction and two pseudo-triplet resonances at −9.9 ppm and 299.1 ppm (J = 40.3 Hz), which is reminiscent of the (tBu$_4$C$_4$P$_4$)-framework in compounds **3a/b**. An X-ray diffraction experiment confirmed the presence of [{(IMes)Ni}$_2$(P$_4$C$_4$$tBu_4$)] (**4**), a dinuclear complex featuring a Ni−Ni bond and a (tBu$_4$C$_4$P$_4$)-moiety (Figure 3). The P−P bond lengths for the bonds within the diphosphacyclobutene ring are significantly longer compared to **3a/b**, with 2.6304(7) (P1−P2A) and 2.6702(7) Å (P3A−P4), whereas the exocyclic P2A−P3A bond is similar to that in **3a/b** (2.2445(7) Å). The Ni1−Ni2 bond distance of 2.4293(4) Å compares well to other nickel(I) dimers (e.g. [{(IPr)Ni}$_2$(μ-Cp)(μ-Cl)]: 2.4015(3) Å).[17]

The bonding situation of the truncated model complex **4′** [{(IPh)Ni}$_2$(P$_4$C$_4$$tBu_4$)] was analysed by means of intrinsic bond orbitals (IBO) on the BP86/def2-TZVP level of theory. Two of these orbitals show multicentre bonds between Ni1/P1/P2A and Ni2/P3A/P4 (see the SI for a depiction of the IBOs), which is reminiscent of the trinuclear Wade-clusters we obtained from a similar reaction with P$_4$.[9] Moreover, the Mayer bond indices for the P−P bonds are small with values of <0.1 and 0.11 for the P1−P2A and P3A−P4 bonds, suggesting only a weak interaction. The low Mayer bond index of 0.31 for the Ni1−Ni2 bond contradicts a strong covalent interaction. Compound **4** can be isolated in 28% yield by crystallisation. The ^{1}H and ^{13}C{^{1}H} NMR spectra are in agreement with the structure determined by SCXRD, showing the expected signal sets for the IMes ligand and the (tBu$_4$C$_4$P$_4$) moiety. The ^{31}P{^{1}H} NMR spectrum is inconsistent with the asymmetrical structure of **4**. However, we propose that the higher symmetry in the NMR spectrum results from a process which leads to an averaging of the signals for P1/P4 and P2/P3. Decoalescence was not observed upon cooling to 193 K. This suggests that the proposed fluxional process has a low activation barrier (see the SI for variable temperature NMR spectra).
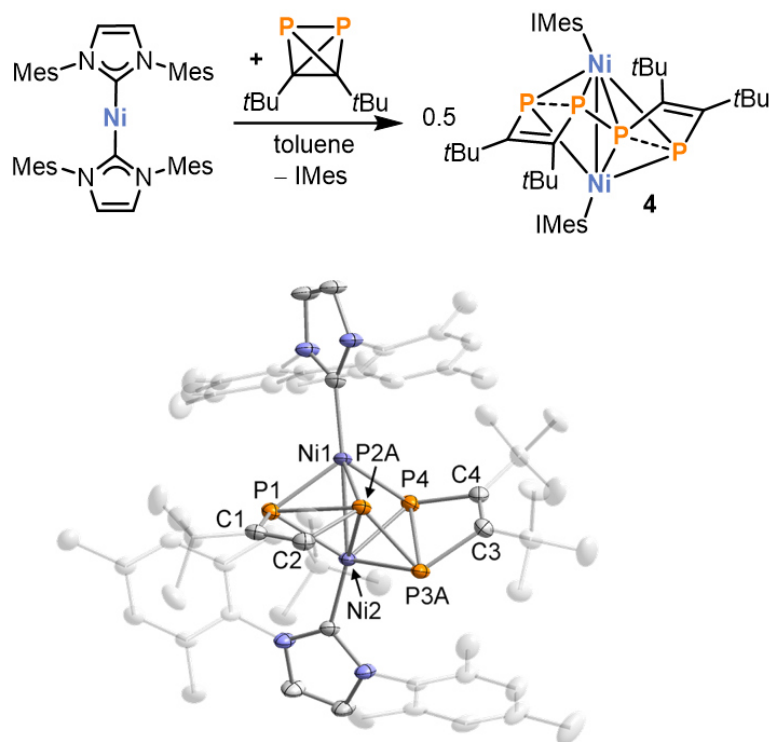
Figure 3. Dimerisation of **1** in the coordination sphere of [(IMes)₂Ni] (top) and molecular structure of **4** in the solid state (bottom). Thermal ellipsoids are set at the 50% probability level. Hydrogen atoms and solvent molecules and a minor disordered component (P2B and P3B) are omitted for clarity. Selected bond lengths [Å] and angles [°]: Ni1−Ni2 2.4293(4), Ni1−P1 2.1586(5), Ni1−P4 2.2379(5), Ni1−P2A 2.1943(5), Ni2−P1 2.2742(5), Ni2−P2A 2.5045(6), Ni2−P3A 2.2056(5), Ni2−P4 2.1530(5), P1−P2A 2.6304(7), P2A−P3A 2.2445(7), P3A−P4 2.6702(7), P1−C1 1.8645(19), P2A−C2 1.877(2), P3A−C3 1.8540(19), P4−C4 1.8396(19), C1−C2 1.353(3), C3−C4 1.353(3), C1−P1−P2A 68.78(6), C2−C1−P1 111.04(15), C1−C2−P2A 107.06(14), C2−P2A−P1 70.34(6), P3A−P2A−P1 106.75(2), P2A−P3A−P4 79.38(2), C3−P3A−P4 68.86(6), C4−P4−P3A 69.33(6), C3−C4−P4 111.00(14), C4−C3−P3A 110.78(14).

Upon storage of solutions of **4** in C_6D_6 at room temperature overnight, **4** was partially converted into a new compound according to ¹H and ³¹P{¹H} NMR spectroscopy (Scheme 2, top). Heating a mixture of **1** and [(IMes)₂Ni] to 60 °C for three hours resulted in selective formation of this new species, which is characterised by two multiplet resonances in the ³¹P{¹H} NMR spectrum at chemical shifts of 115.8 and 209.8 ppm (see the SI for a simulation). X-ray diffraction analysis of a single crystal grown from saturated *n*-hexane solutions revealed the formation of [(IMesNi)₂(P₂)(tBu₂C₂P₂)]·IMes (**5**·IMes, Figure 4). The formation of **5** involves the elimination of di-*tert*-butylacetylene, which was identified by the ¹³C{¹H} NMR resonance of the alkyne carbon atom detected at a chemical shift of 87.5 ppm. A related example of *t*BuC≡C*t*Bu elimination from a metal complex was recently reported by our group from a ruthenium complex,[18] but in contrast to that example, where the alkyne remains as η²-bound ligand in the coordination sphere of ruthenium, di-*tert*-butylacetylene was completely liberated in the reaction reported herein, which illustrates an exciting potential for **1** and its coordination compounds to act as a source of P₂ units.

Conveniently, dark brown crystals of **5** were isolated in 50% yield directly starting from [(IMes)₂Ni] and **1**. The compound initially co-crystallises with one equivalent of IMes (as compound **5·IMes**). IMes can be subsequently removed by recrystallisation from toluene/*n*-hexane. The molecular structure of **5** in the solid state confirms the presence of a $\mu\text{-}\eta^2{:}\eta^2\text{-}P_2$ dumbbell and a $\mu\text{-}\eta^2{:}\eta^2\text{-}(tBu_2C_2P_2)^{2-}$ ligand. The P1−P2 bond of the latter ligand (2.4514(4) Å) is significantly elongated in comparison to **2** (2.2244(7) Å) and the P3−P4 bond length of the P_2 ligand (2.0294(5) Å) is comparable to other complexes with a Ni_2P_2 core such as $\{(IMes)Ni(CO)\}_2(\mu\text{-}\eta^2{:}\eta^2\text{-}P_2)]$ (2.076(2) Å).[19] The $^{31}P\{^1H\}$ NMR spectrum of isolated **5** is identical to the species obtained from **4** (*vide supra*). The ^1H NMR and $^{13}C\{^1H\}$ NMR spectra are in agreement with the proposed molecular structure of **5**.
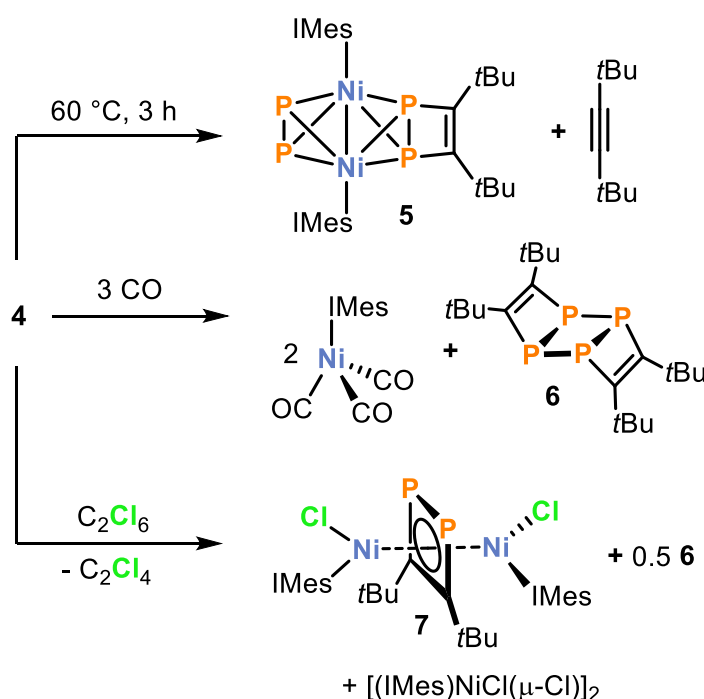
Scheme 2. Reactivity of **4** upon heating and addition of CO and hexachloroethane.

Further reactivity studies were conducted with complex **4** in order to examine the possible release and functionalisation of the $(tBuCP)_4$ framework. Treatment of a solution of **4** in C_6D_6 with carbon monoxide (1 bar) results in an instantaneous colour change of the solution from brown to pale beige and formation of $[(IMes)Ni(CO)_3]$ and the known phosphaalkyne tetramer $(tBuCP)_4$ (**6**, Scheme 2) as corroborated by ^1H and $^{31}P\{^1H\}$ NMR spectroscopy (see SI for spectra).[14] Moreover, the addition of hexachloroethane affords **6** and the chlorinated inverted sandwich complex $[\{(IMes)NiCl\}_2(\mu\text{-}tBu_2C_2P_2)]$ (**7**) as revealed by single crystal X-ray crystallography (Figure 4). Complex **7** contains a 1,2-diphosphacyclobutadiene ligand in an unusual $\mu,\eta^4{:}\eta^4$-coordination mode with a P1−P2 bond length of 2.2768(6) Å and a C1−C2 bond length of 1.437(3) Å. Unfortunately, **7** and its by-product, the dinuclear Ni(II) complex [(IMes)NiCl(μ-

Cl)]₂ could not be separated due to similar solubilities. However, we were able to crystallise [(IMes)NiCl(μ-Cl)]₂ from the reaction mixture as violet blocks (see SI for SCXRD data).
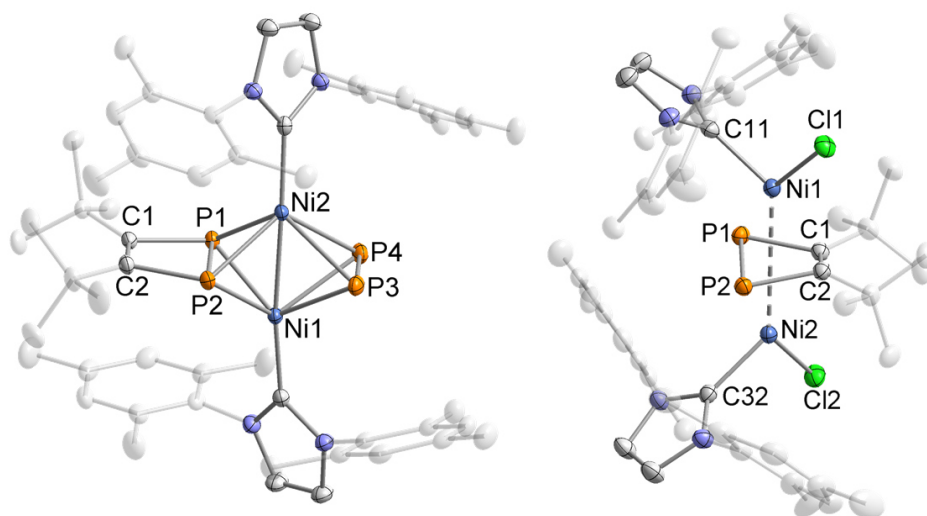

Figure 4. Molecular structures of **5** and **7** in the solid state. Thermal ellipsoids are set at the 50% probability level. Hydrogen atoms and one molecule of IMes (co-crystallising with **5**) are omitted for clarity. Selected bond lengths [Å] and angles [°] for **5**: Ni1−Ni2 2.3477(3), Ni1−P1 2.2326(4), Ni1−P2 2.2348(4), Ni1−P3 2.3002(4), Ni1−P4 2.3030(4), Ni2−P1 2.2329(4), Ni2−P2 2.2632(4), Ni2−P3 2.3034(4), Ni2−P4 2.3130(4), P1−P2 2.4514(4), P1−C1 1.8394(12), P2−C2 1.8411(13), C1−C2 1.3641(19), P3−P4 2.0294(5), C1−P1−P2 72.87(4), C2−P2−P1 72.73(4), C2−C1−P1 107.10(9), C1−C2−P2 107.22(9), Ni1−P1−Ni2 63.437(11), Ni1−P2−Ni2 62.922(11), Ni1−P3−Ni2 61.323(11), Ni1−P4−Ni2 61.141(10); for **7**: Ni1−Cl1 2.2094(4), Ni1−C11 1.9322(16), Ni2−Cl2 2.2178(4), Ni2−C32 1.9277(16), P1−C1 1.8423(16), P2−C2 1.8383(16), P1−P2 2.2770(5), C1−C2 1.438(3), Ni1−C₂P₂^centr 1.869(2), Ni2−C₂P₂^centr 1.870(2), C11-Ni1-Cl1 98.35(5), C32-Ni2-Cl2 97.67(5), C1-P1-P2 76.06(5), C2-P2-P1 76.50(5), C2-C1-P1 102.50(10), C1-C2-P2 102.11(10).

In an attempt to evaluate the influence of the steric bulk of the NHC ligand, the related, bulkier [(IPr)₂Ni] was reacted with one equivalent of **1** (Figure 5). However, ³¹P{¹H} NMR spectroscopy suggested the formation of a different product with multiplet resonances (*vide infra*). A similar spectrum was obtained when [(IPr)Ni(η⁶-toluene)] was reacted with **1** (see SI for spectra). Single crystal XRD on a crystal obtained from toluene revealed the formation of [(IPr)Ni(tBu₄C₄P₄)] (**8**), i.e. a mononuclear complex of the phosphaalkyne tetramer **6** (Figure 5).[14] The chemistry of the phosphaalkyne tetramer **6** is barely explored and, to the best of our knowledge, this is the first example of a coordination compound of **6**. **8** was also obtained by reaction of [(IPr)Ni(η⁶-toluene)] with **6** as a dark red solid and isolated in 35% yield. Considering the short time necessary (<5 minutes) to form **8** from [(IPr)₂Ni] and **1** in solution (much quicker than the known, 'background' dimerisation of **1**), we assume that coordinated **6** is formed upon dimerisation of **1** at the Ni atom.

The molecular structure of **8** reveals that the (tBuCP)₄ ligand coordinates through two lone pairs of adjacent P atoms to an (IPr)Ni fragment. As a consequence, the P1A−P2A bond is elongated (2.5821(7) Å) in comparison to the P2A−P3A bond (2.2506(8) Å, free **6**: 2.219(1) and

2.236(1) Å).[14] The ^{31}P{^{1}H} NMR spectrum of **8**, showed an AA′XX′ spin system at chemical shifts of −42.4 ppm and 102.1 ppm. The signal at high field is broad at room temperature and was resolved via variable temperature NMR at −20 °C (see the SI for spectra and simulation). The ^{1}H and ^{13}C{^{1}H} NMR spectra of **8** are in line with the molecular structure in the solid state.
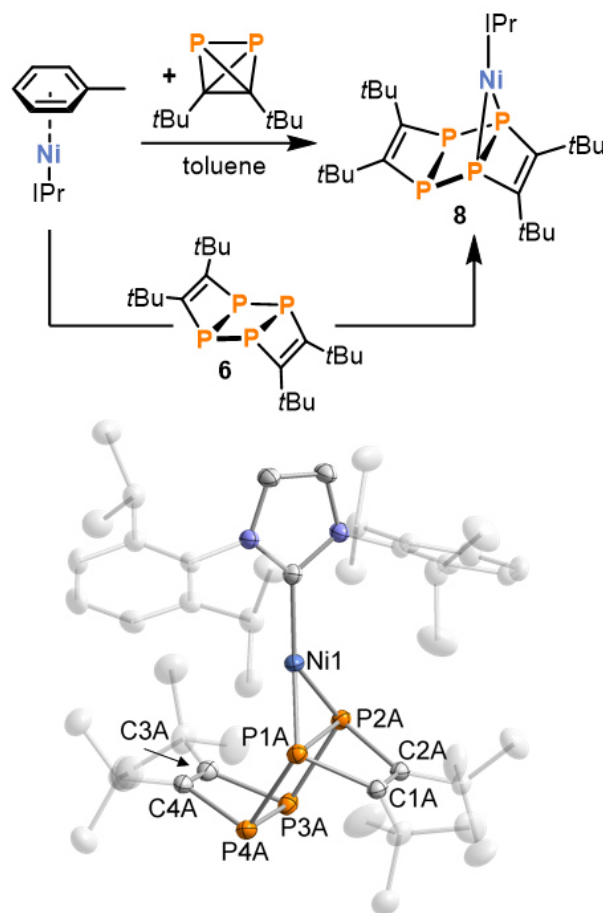

Figure 5. Formation of the ladderane complex **8** (top) and molecular structure of **8** in the solid state (bottom). Thermal ellipsoids are set at the 50% probability level. Hydrogen atoms and a minor disordered component (P1B-4B, C1B-4B) are omitted for clarity. Selected bond lengths [Å] and angles [°]: Ni1−P1A 2.1231(6), Ni1−P2A 2.1138(5), P1A−P2A 2.5821(7), P2A−P3A 2.2506(8), P1A−P4A 2.2444(7), P3A−P4A 2.2020(8), P1A−C1A 1.873(2), P2A−C2A 1.866(2), P3A−C3A 1.848(2), P4A−C4A 1.854(2), C1A−C2A 1.352(3), C3A−C4A 1.354(3), C2A−C1A−P1A 109.14(16), C1A−C2A−P2A 109.26(15), C1A−P1A−P2A 70.69(7), C2A−P2A−P1A 70.92(7), C1A−P1A−P4A 94.78(7), C2A−P2A−P3A 91.69(7), P4A−P1A−P2A 85.57(2), P3A−P2A−P1A 84.66(2), P4A−P3A−P2A 95.17(3), P3A−P4A−P1A 94.43(3), C3A−P3A−P2A 100.12(8), C4A−P4A−P1A 101.48(7), C3A−P3A−P4A 76.96(7), C4A−P4A−P3A 76.51(7), C4A−C3A−P3A 103.09(16), C3A−C4A−P4A 103.34(16).

7.3   Conclusion

In summary, reactions of di-*tert*-butyldiphosphatetrahedrane (**1**) with Ni(I)- and Ni(0)-NHC complexes afford coordination compounds with unusual $(tBuCP)_n$ (n = 2, 4) frameworks. Dimerisation of **1** on the nickel atom is a notable feature observed in several of these reactions. Moreover, elimination of di-*tert*-butylacetylene was observed from complex **5**, which has stimulated further, ongoing studies on the use of **1** as a source for P_2 fragments. It is noteworthy that complexes **2 – 4** and **8** cannot be obtained from reactions of the nickel precursors with *t*BuCP. Moreover, a comparison with the previously described reactivity of the same complexes with P_4 furthermore reveals the distinct reactivity of **1**. These promising results bode well for the future development of **1** and related phosphatetrahedranes as sources for a plethora of other previously inaccessible phosphaorganometallic molecules. Work in this direction is underway.

7.4   Experimental Details

General Synthetic Methods

All reactions and product manipulations were carried out in flame-dried glassware under an inert atmosphere of argon using standard Schlenk-line or glovebox techniques (maintained at <0.1 ppm H_2O and <0.1 ppm O_2). [CpNi(IPr)] (Cp = C_5H_5, IPr = 1,3-bis(2,6-di-*iso*-propylphenyl)imidazolin-2-ylidene),[8] [Cp*Ni(IPr)] (Cp* = C_5Me_5),[8] [Cp^{BIG}Ni(IPr)] (Cp^{BIG} = $C_5(4\text{-Et-}C_6H_4)_5$),[13] [(IMes)₂Ni] (IMes = 1,3-bis(2,4,6-trimethylphenyl)imidazolin-2-ylidene),[16] [(IPr)₂Ni],[20] [(IPr)Ni(η^6-toluene)],[15] $(tBuCP)_2$ (**1**)[6] and $(tBuCP)_4$ (**6**)[6] were prepared according to previously reported procedures. All other chemicals were purchased from commercial suppliers and used without further purification.

Solvents were dried and degassed with a MBraun SPS800 solvent purification system. All dry solvents except *n*-hexane and *n*-pentane were stored under argon over activated 3 Å molecular sieves in gas-tight ampules. *n*-Hexane and *n*-pentane were instead stored over a potassium mirror.

Analytical Techniques

NMR spectra were recorded on Bruker Avance 300 or 400 spectrometers at 300 K unless otherwise noted and internally referenced to residual solvent resonances (^1H NMR: THF-d_8: 1.72 ppm, C_6D_6: 7.16 ppm, toluene-d_8 (tol-d_8): 2.08 ppm; $^{13}C\{^1H\}$ NMR: THF-d_8: 25.31 ppm, C_6D_6: 128.06 ppm). Chemical shifts δ are given in ppm referring to external standards of tetramethylsilane (^1H, $^{13}C\{^1H\}$), 85% phosphoric acid (^{31}P and $^{31}P\{^1H\}$ spectra). ^1H and ^{13}C NMR signals were assigned based on 2D NMR spectra (^1H,^1H-COSY, ^1H,^{13}C-HSQC, ^1H,^{13}C-HMQC). UV/Vis spectra were recorded on an Ocean Optics Flame Spectrometer. Elemental analysis was performed by the central analytics department of the University of Regensburg.

The single-crystal X-ray diffraction data were recorded on Rigaku Oxford Diffraction SuperNova Atlas diffractometers with Cu-K$_\alpha$ radiation (λ= 1.54184 Å). Crystals were selected under mineral oil, mounted on micromount loops and quench-cooled using an Oxford Cryosystems open flow

N₂ cooling device. Either semi-empirical multi-scan absorption corrections[21] or analytical ones[22] were applied to the data. The structures were solved with SHELXT[23] solution program using dual methods and by using Olex2 as the graphical interface.[24] The models were refined with ShelXL[25] using full matrix least squares minimisation on F^2.[26] The hydrogen atoms were located in idealised positions and refined isotropically with a rigid model.

Synthesis of Compounds

[(CpNi)₂(tBu₂C₂P₂)]₂ (2)

To a solution of [CpNi(IPr)] (150 mg, 0.29 mmol, 1.0 eq.) in THF (3 mL) was added (tBuCP)₂ (0.5 mL, c = 2.7 M in HMDSO, 0.14 mmol, 0.5 eq.) at ambient temperature. The colour of the reaction mixture immediately changed from yellow to deep red. After stirring at ambient temperature for 18 h, the solvent was removed *in vacuo*. The dark residue was washed with *n*-hexane (3 x 3 mL) and extracted in benzene, yielding a dark red solution. Slow diffusion of *n*-hexane in the saturated benzene solution yielded dark red crystals, which were suitable for single-crystal X-ray diffraction. The crystals were isolated by filtration, washed with *n*-hexane and dried *in vacuo* (23 mg). Another crop of crystalline compound was obtained from the *n*-hexane fraction at room temperature after one week (14 mg).

$C_{40}H_{56}Ni_4P_4$, MW = 895.56 g/mol
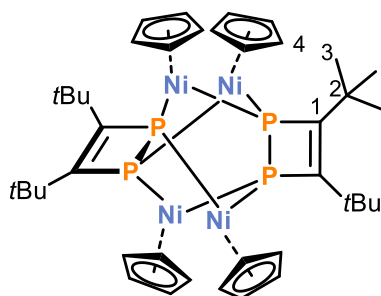
Combined Yield: 37 mg (56%)

¹H NMR (400 MHz, 300 K, C₆D₆) δ = 1.32 (s, 36H, C³H), 5.17 (s, 20H, C⁴H) ppm.

¹³C{¹H} NMR (100 MHz, 300 K, C₆D₆) δ = 32.0 (s, C³), 37.8 (m, C²), 91.2 (s, C⁴), 167.9 (s, C¹) ppm.

³¹P{¹H} (162 MHz, 300 K, C₆D₆) δ = 93.0 (s) ppm.

Elemental Analysis calcd. C 53.65, H 6.30; found C 54.20, H 6.30.

UV/Vis (THF): λ_{max} (nm, ε_{max} /L·mol⁻¹·cm⁻¹) 400 (17 200), 520 (5400).

[(Cp*Ni)₂(tBu₄C₄P₄)] (3a):

To a solution of [Cp*Ni(IPr)] (150 mg, 0.26 mmol, 1.0 eq.) in THF (2 mL) was added (tBuCP)₂ (1.4 mL, c = 0.2 M in benzene, 0.28 mmol, 1.1 eq.) at ambient temperature. The colour of the reaction mixture changed from yellow to deep red within one hour. After stirring at ambient temperature for 18 h, the solvent was removed *in vacuo*. The dark residue was extracted in *n*-hexane (5 mL) and concentrated (2 mL). Storage at ambient temperature overnight yielded dark

red crystals of **3a**, which were suitable for single-crystal X-ray diffraction. Additionally, the crystals of IPr were identified by unit cell determination. Due to similar solubilities of **3a** and IPr, purification by recrystallisation failed. IPr was removed by sublimation (oil bath: 150 °C, cold finger: ca. 20 °C, p < 1·10^{-3} mbar, 10 h). Subsequent recrystallisation of the residue from *n*-pentane afforded crystals of **3a** which were isolated by filtration and dried *in vacuo*.

C$_{40}$H$_{66}$Ni$_2$P$_4$, MW = 788.24 g/mol
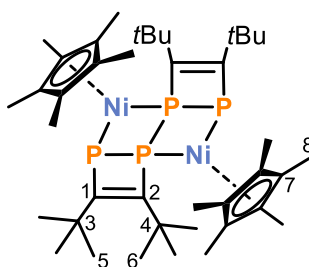
Yield: 22 mg (33%)

¹H NMR (400 MHz, 300 K, C$_6$D$_6$) δ = 1.36 (s, 18H, C$^{5/6}$H), 1.45 (s, 18H, C$^{5/6}$H), 1.86 (s, 30H, C^{8}H) ppm.

¹³C{¹H} NMR (100 MHz, 300 K, C$_6$D$_6$) δ = 10.4 (s, C^8), 31.8 (m, C$^{5\&6}$), 37.9 (t, J_{CP} = 5.4 Hz, C$^{3/4}$), 39.1 (m, C$^{3/4}$), 99.8 (s, C^7), 145.8 (m, C$^{1/2}$), 184.8 (m, C$^{1/2}$) ppm.

³¹P{¹H} (162 MHz, 300 K, C$_6$D$_6$) δ = −61.4 (pseudo-t, 2P), 31.1 (pseudo-t, 2P) ppm.

Elemental Analysis calcd. C 60.95, H 8.44; found C 61.09, H. 8.08.

UV/Vis (THF): λ_{max} (nm, ε_{max} /L·mol^{-1}·cm^{-1}) 320 (82 500), 420 (55 000).

[(Cp^{BIG}Ni)$_2$(tBu$_4$C$_4$P$_4$)] (3b):

To a solution of [Cp^{BIG}Ni(IPr)] (100 mg, 0.10 mmol, 1.0 eq.) in THF (2 mL) was added (tBuCP)$_2$ (0.53 mL, c = 0.2 M in benzene, 0.11 mmol, 1.1 eq.) at ambient temperature. The colour of the reaction mixture changed from yellow to deep red overnight. After stirring at ambient temperature for 18 h, the solvent was removed *in vacuo*. The dark residue was washed with *n*-hexane (3 x 2 mL) and extracted in toluene (2 mL). Slow diffusion of *n*-hexane in the saturated, dark red toluene solution yielded dark red crystals of X-ray quality. The crystals were washed with cold (−30 °C) *n*-hexane (ca. 2 mL) and dried *in vacuo*.

Notably, the reaction of [Cp^{BIG}Ni(^{Dipp}nacnacGa)]$^{[27]}$ with (tBuCP)$_2$ also affords **3b** along with free ^{Dipp}nacnacGa.

$C_{110}H_{126}Ni_2P_4$, MW = 1689.50 g/mol
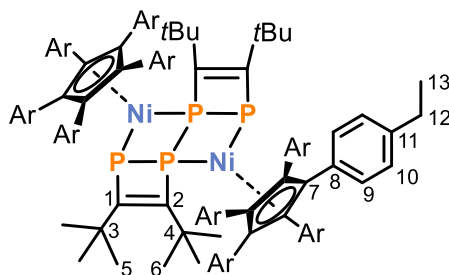
Yield: 36 mg (44%)

¹H NMR (400 MHz, 300 K, C_6D_6) δ = 1.05 (t, $^3J_{HH}$ = 7.6 Hz, 30H, $C^{13}H$), 1.27 (s, 18H, $C^{5/6}H$), 1.50 (s, 18H, $C^{5/6}H$), 2.40 (q, $^3J_{HH}$ = 7.6 Hz, 20H, $C^{13}H$), 6.75 (m, 20H, $C^{10}H$), 7.33 (m, 20H, C^9H) ppm.

¹³C{¹H} NMR (100 MHz, 300 K, C_6D_6) δ = 15.3 (s, C^{13}), 28.8 (s, C^{12}), 31.2 (br s, $C^{5/6}$), 32.4 (br s, $C^{5/6}$), 39.0 (t, $^2J_{CP}$ = 4.8 Hz, $C^{3\&4}$), 109.2 (s, C^7), 127.2 (s, C^{10}), 132.2 (s, C^8), 133.3 (s, C^9), 141.8 (s, C^{11}), 149.8 (br s, $C^{1/2}$), 182.2 (d, J = 182.2 Hz, $C^{1/2}$) ppm.

³¹P{¹H} (162 MHz, 300 K, C_6D_6) δ = −1.3 (pseudo-t, 2P), −48.9 (pseudo-t, 2P) ppm.

Elemental Analysis calcd. C 78.20 H 7.52; found C 77.82, H 7.62.

UV/Vis (THF): λ$_{max}$ (nm, ε$_{max}$ /L·mol⁻¹·cm⁻¹) 440 (33 000), 530 (25500).

[{(IMes)Ni}₂(P₄C₄tBu₄)] (4):

To a dark blue solution of [(IMes)₂Ni] (278 mg, 0.42 mmol, 1.0 eq.) in THF (2 mL) was added (tBuCP)₂ (1.2 mL, c = 0.4 M in toluene, 0.48 mmol, 1.2 eq.) at −80 °C. The colour of the reaction mixture changed to brown within 5 minutes. The mixture was stirred for 2 hours and allowed to warm to ambient temperature. Subsequently, the solvent was removed *in vacuo* and the dark brown residue was washed with *n*-hexane (3 x 3 mL) and extracted in toluene (5 mL). The solution was concentrated (ca. 3 mL) and layered with *n*-hexane (10 mL). Storage at −30 °C overnight afforded dark brown crystalline material, which was isolated by filtration and dried *in vacuo*. Single crystals suitable for X-ray diffraction were obtained by storing the *n*-hexane washings at ambient temperature overnight.

Complex **4** slowly converts to **5** when stored in toluene solution at ambient temperature.
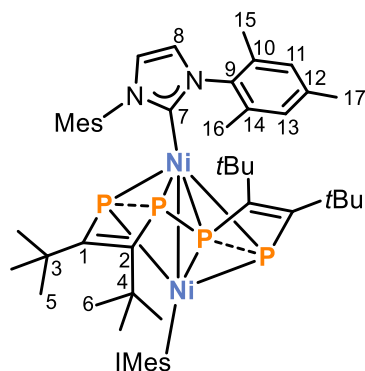
$C_{61}H_{84}N_4Ni_2P_4$, MW = 1126.66 g/mol

Yield: 70 mg (28%)

NMR spectroscopic analysis of **4** was performed at 273 K due to partial conversion to **5** at ambient temperature.

¹H NMR (400 MHz, 273 K, tol-d₈) δ = 1.22 (s, 18H, C⁵ᐟ⁶H+ *n*-hex), 1.43 (s, 18H, C⁵ᐟ⁶H), 2.16 (s, 12H, C¹⁶H), 2.21 (s, 12H,C¹⁵), 2.26 (s, 12H, C¹⁷H), 6.28 (s, 4H, C⁸H), 6.82 (s, 4H, C¹³H), 6.84 (s, 4H, C¹¹H) ppm.

¹³C{¹H} NMR (100 MHz, 273 K, tol-d₈) δ = 19.0 (s, C¹⁶), 19.5 (s, C¹⁵), 21.2 (s, C¹⁷), 32.6-32.7 (m, C⁵ᐟ⁶), 37.4 (t, ²J_{CP} = 11.3 Hz, C³ᐟ⁴), 38.4 (t, ²J_{CP} = 11.7 Hz, C³ᐟ⁴), 122.7 (s, C⁸), 129.2 (s, C¹³), 129.3 (s, C¹¹), 136.0 (s, C¹⁴), 136.2 (s, C¹⁰), 137.1 (s, C¹²), 138.0 (s, C⁹), 144.2 (t, ¹J_{CP} = 21.1 Hz, C¹ᐟ²), 154.6 (br s, C¹ᐟ²), 191.9 (br s, C⁷) ppm.

³¹P{¹H} (162 MHz, 273 K, tol-d₈) δ = −9.9 (pseudo-t, *J* = 41.2 Hz), 299.1 (pseudo-t, *J* = 41.2 Hz) ppm.

Elemental Analysis calcd. [for **4**·0.5 (*n*-hexane), see SCXRD structure] C 66.74, H 7.82, N 4.79; found C 67.09, H 7.45, N 4.67.

UV/Vis (THF): λ_{max} (nm, ε_{max} /L·mol⁻¹·cm⁻¹) 330 (19 000), 390 (12 000sh).

[(IMesNi)₂(P₂)(P₂C₂tBu₂)]·(5):

Method A:

A solution of [{(IMes)Ni}₂(P₄C₄tBu₄)] (**4**, 30 mg, 0.03 mmol, 1.0 eq.) in toluene (0.5 mL) was heated to 60 °C for 3 h. Subsequently, the reaction mixture was filtered and layered with *n*-hexane (3 mL). Storage at −30 °C overnight afforded dark brown crystals, which were isolated by filtration and dried *in vacuo*.

Yield: 15 mg (50%)

Method B:

To a dark blue solution of [(IMes)₂Ni] (120 mg, 0.18 mmol, 1.0 eq.) in THF (2 mL) was added (*t*BuCP)₂ (0.5 mL, c = 0.4 M in toluene, 0.20 mmol, 1.1 eq.) at ambient temperature. The colour of the reaction mixture changed to brown immediately. The mixture was stirred for 3 hours at 60 °C. Subsequently, the solvent was removed *in vacuo* and the dark brown residue was washed

with *n*-hexane (3 x 0.5 mL) and extracted in toluene (1 mL). The solution was concentrated to ca. 0.5 mL and layered with *n*-hexane (5 mL). Storage at ambient temperature overnight afforded dark brown crystals of **5·IMes** suitable for X-ray diffraction. The material was recrystallised by layering a toluene solution of **5·IMes** (1 mL) with *n*-hexane (5 mL) and storage at −30 °C over one week. Dark brown crystals of **5** were isolated by decanting the supernatant and dried *in vacuo*.

$C_{52}H_{66}N_4Ni_2P_4$, MW = 988.41 g/mol
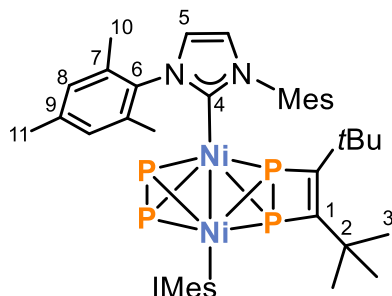
Yield: 23 mg (13%)

¹H NMR (400 MHz, 300 K, C_6D_6) δ = 1.54 (s, 18H, C^3H), 2.01 (s, 24H, $C^{10}H$), 2.16 (s, 12H, $C^{11}H$), 6.05 (s, 4H, C^5H), 6.64 (s, 8H, C^8H) ppm.

¹³C{¹H} NMR (100 MHz, 300 K, C_6D_6) δ = 18.9 (s, C^{10}), 21.2 (s, C^{11}), 31.9 (t, $^3J_{CP}$ = 5.5 Hz, C^3), 36.5 (t, $^3J_{CP}$ = 12.5 Hz, C^2), 122.5 (s, C^5), 129.4 (s, C^8), 135.4 (s, C^9), 137.5 (s, C^7), 138.1 (s, C^6), 152.2 (m, C^1), 184.9 (s, C^4) ppm.

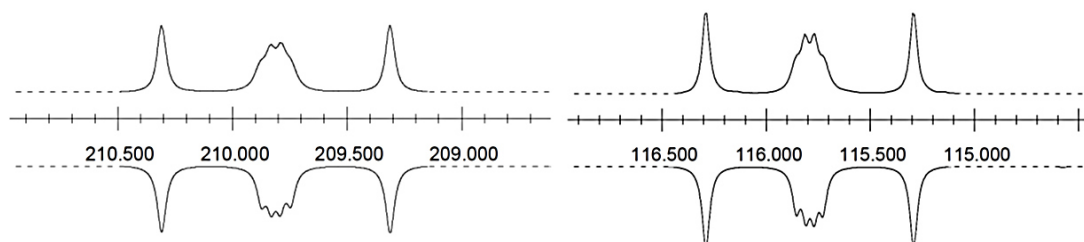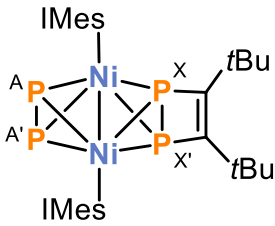**³¹P{¹H}** (162 MHz, 300 K, C_6D_6) δ = 115.6 (m), 209.6 (m) ppm.

Figure S1. Section of the ³¹P{¹H} NMR (161.98 MHz, C_6D_6, 300 K) of **5;** experimental (upwards) and simulation (downwards)

Chemical shifts were tentatively assigned on the basis of the ³¹P{¹H} NMR spectrum of compound **2** (δ = 93.0 ppm).

Table S1. Coupling constants from the iterative fit of the

AA′XX′ spin system and schematic representation of **6**.

$^1J_{AA'} = -410.8$ Hz

$^1J_{AX} = 35.41$ Hz

$^2J_{A'X} = 126.02$ Hz

$^1J_{XX'} = -224.53$ Hz

Elemental Analysis calcd. [for **5**·0.5 (toluene)] C 64.44, H 6.82, N 5.42; found C 64.98, H 6.91, N 5.56.

UV/Vis (THF): λ_{max} (nm, ε_{max} /L·mol^{-1}·cm^{-1}) 310 (19 000), 380 (12 500sh), 560 (3 500).

[(IPr)Ni(*t*Bu₄C₄P₄)] (8):

To a solution of [(IPr)Ni(η⁶-toluene)] (50 mg, 0.09 mmol, 1.0 eq.) in toluene (3 mL) was added (*t*BuCP)₄ (**6**, 41 mg, 0.10 mmol, 1.1 eq.) at ambient temperature. The solution was stirred for 5 minutes without noticeable colour change. Subsequently, the reaction mixture was filtered, concentrated (to ca. 1 mL) and layered with *n*-hexane (3 mL). Storage at −30 °C overnight afforded dark brown crystalline material, which was isolated by filtration and dried *in vacuo*. Single crystals suitable for X-ray diffraction were obtained by from saturated *n*-hexane solutions of **8**.
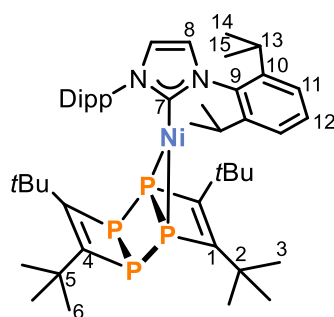
C₄₇H₇₂N₂NiP₄, MW = 847.70 g/mol

Yield: 27 mg (35%)

¹H NMR (400 MHz, 300 K, C₆D₆) δ = 1.02 (d, $^3J_{HH}$ = 6.9 Hz, 12H, C$^{14/15}$), 1.32 (s, 18H, C$^{3/6}$H), 1.48 (d, $^3J_{HH}$ = 6.9 Hz, 12H, C$^{14/15}$H), 2.85 (sept, $^3J_{HH}$ = 6.9 Hz, 4H, C^{13}), 6.32 (s, 2H, C^{8}H), 7.14 (d, $^3J_{HH}$ = 7.7 Hz, 4H, C^{11}H, overlapping with C₆D₆-signal), 7.26 (t, $^3J_{HH}$ = 7.6 Hz, 2H, C^{12}H) ppm.

¹³C{¹H} NMR (100 MHz, 300 K, C₆D₆) δ = 24.4 (s, C$^{14\&15}$), 29.0 (s, C^{13}), 31.7 (br t, coupling not resolved, C$^{3/6}$), 33.2 (br t, coupling not resolved, C$^{3/6}$), 38.6 (t, *J* = 6.7 Hz, C$^{2/5}$), 40.2 (t, *J* =

11.4 Hz, C$^{2/5}$), 123.1 (s, C^8), 124.3 (s, C^{11}), 130.1 (s, C^{12}), 136.6 (s, C^{10}), 145.5 (s, C^9), 168.5 (br t, J = 5.5 Hz, C$^{1/4}$), 187.8 (s, C^7),

^{31}P{^{1}H} (162 MHz, 300 K, C$_6$D$_6$) δ = −42.8 (m), 102.8 (m) ppm.
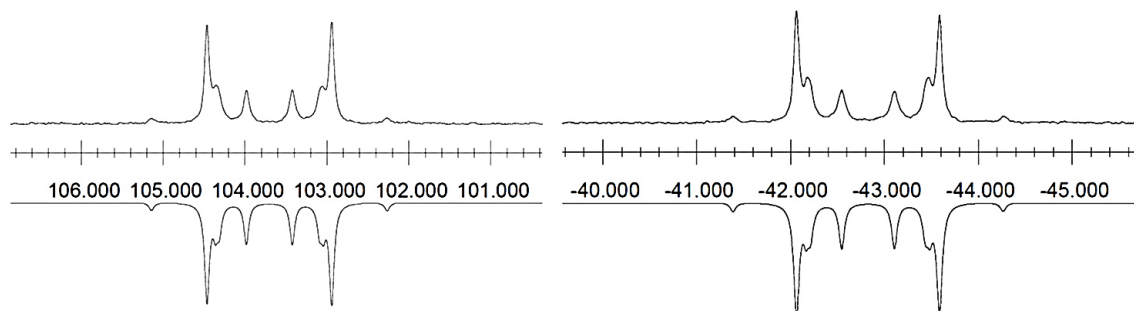

Figure S2. Section of the ^{31}P{^{1}H} NMR (161.98 MHz, tol-d$_8$, 253 K) of **8**; experimental (upwards) and simulation (downwards)

Table S2. Coupling constants from the iterative fit of the AA′XX′spin system and schematic representation of **8**.

$^1J_{AA'}$ = −90.0 Hz

$^1J_{AX}$ = −226.2 Hz

$^2J_{A'X}$ = −20.45 Hz

$^1J_{XX'}$ = −97.7 Hz

Elemental Analysis calcd. C 66.59, H 8.56, N 3.30; found C 66.56, H 8.58, N 3.06.

UV/Vis (THF): λ_{max} (nm, ε_{max} /L·mol^{-1}·cm^{-1}) 300 (11 000sh), 420 (8 000), 500 (3000sh).

7.5 Supporting Information

The Supporting Information of Chapter 7 can be found on the supplied CD-ROM and on https://onlinelibrary.wiley.com/doi/10.1002/anie.202015680. The Supporting Information contains: NMR and UV/Vis spectra, additional experiments, X-ray crystallography details and results of quantum chemical calculations including Cartesian coordinates of all optimised structures.
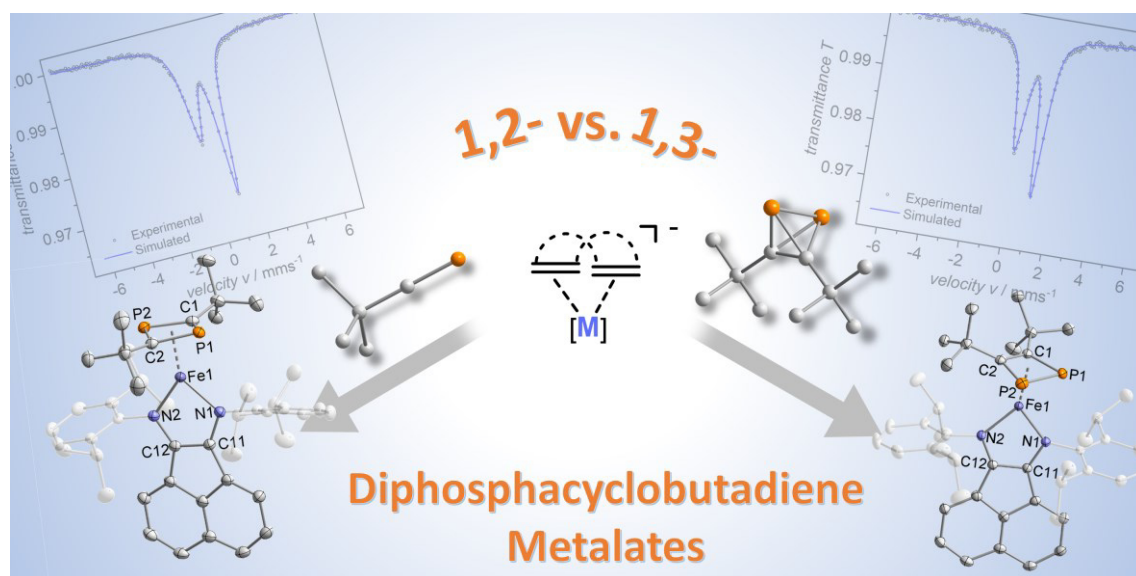
References

[1] G. Maier, *Angew. Chem. Int. Ed. Engl.* **1988**, *27*, 309.

[2] O. Reinmuth, *J. Chem. Educ.* **1928**, *5*, 1473.

[3] D. E. C. Corbridge, *Phosphorus 2000. Chemistry, Biochemistry and Technology*, (Elvesier, 2000).

[4] a) B. M. Cossairt, M.-C. Diawara, C. C. Cummins, *Science* **2009**, *323*, 602; b) M. Seidl, G. Balázs, M. Scheer, *Chem. Rev.* **2019**, *119*, 8406.

[5] A. R. Jupp, J. C. Slootweg, *Angew. Chem. Int. Ed.* **2020**, *59*, 10698.

[6] G. Hierlmeier, P. Coburger, M. Bodensteiner, R. Wolf, *Angew. Chem. Int. Ed.* **2019**, *58*, 16918.

[7] M.-L. Y. Riu, R. L. Jones, W. J. Transue, P. Müller, C. C. Cummins, *Sci. Adv.* **2020**, *6*, eaaz3168.

[8] S. Pelties, D. Herrmann, B. de Bruin, F. Hartl, R. Wolf, *Chem. Commun.* **2014**, *50*, 7014.

[9] G. Hierlmeier, P. Coburger, N. P. van Leest, B. Bruin, R. Wolf, *Angew. Chem. Int. Ed.* **2020**, *59*, 14148.

[10] a) B. M. Cossairt, N. A. Piro, C. C. Cummins, *Chem. Rev.* **2010**, *110*, 4164; b) M. Caporali, L. Gonsalvi, A. Rossin, M. Peruzzini, *Chem. Rev.* **2010**, *110*, 4178.

[11] a) A. Chirila, R. Wolf, J. Chris Slootweg, K. Lammertsma, *Coord. Chem. Rev.* **2014**, *270-271*, 57; b) C. Jones, J. A. Platts, A. F. Richards, *Chem. Commun.* **2001**, 663; c) S. Deng, C. Schwarzmaier, M. Zabel, J. F. Nixon, M. Bodensteiner, E. V. Peresypkina, G. Balázs, M. Scheer, *Eur. J. Inorg. Chem.* **2011**, *2011*, 2991; d) A. D. Burrows, A. Dransfeld, M. Green, J. C. Jeffery, C. Jones, J. M. Lynam, M.T. Nguyen, *Angew. Chem. Int. Ed.* **2001**, *40*, 3221; e) F. W. Heinemann, S. Kummer, U. Seiss-Brandl, U. Zenneck, *Organometallics* **1999**, *18*, 2021; f) C. Jones, C. Schulten, A. Stasch, *Dalton Trans.* **2006**, 3733; g) P. Binger, G. Glaser, S. Albus, C. Krüger, *Chem. Ber.* **1995**, *128*, 1261; h) E.-M. Rummel, G. Balázs, V. Heinl, M. Scheer, *Angew. Chem. Int. Ed.* **2017**, *56*, 9592.

[12] a) B. Cordero, V. Gómez, A. E. Platero-Prats, M. Revés, J. Echeverría, E. Cremades, F. Barragán, S. Alvarez, *Dalton Trans.* **2008**, 2832; b) P. Pyykkö, M. Atsumi, *Chem. Eur. J.* **2009**, *15*, 186; c) P. Pyykkö, *J. Phys. Chem. A* **2015**, *119*, 2326.

[13] U. Chakraborty, F. Urban, B. Mühldorf, C. Rebreyend, B. de Bruin, N. van Velzen, S. Harder, R. Wolf, *Organometallics* **2016**, *35*, 1624.

[14] B. Geissler, S. Barth, U. Bergsträsser, M. Slany, J. Durkin, P. B. Hitchcock, M. Hofmann, P. Binger, J. F. Nixon, P. von Ragué Schleyer, M. Regitz, *Angew. Chem. Int. Ed. Engl.* **1995**, *34*, 484.

[15] Y. Hoshimoto, Y. Hayashi, H. Suzuki, M. Ohashi, S. Ogoshi, *Organometallics* **2014**, *33*, 1276.

[16]   A. J. Arduengo III, S. F. Gamper, J. C. Calabrese, F. Davidson, *J. Am. Chem. Soc.* **1994**, *116*, 4391.

[17]   a) J. Wu, A. Nova, D. Balcells, G. W. Brudvig, W. Dai, L. M. Guard, N. Hazari, P.-H. Lin, R. Pokhrel, M. K. Takase, *Chem. Eur. J.* **2014**, *20*, 5327; b) C.-Y. Lin, P. P. Power, *Chem. Soc. Rev.* **2017**, *46*, 5347.

[18]   C. Rödl, R. Wolf, *Chem. Eur. J.* **2019**, *25*, 8332.

[19]   G. Hierlmeier, A. Hinz, R. Wolf, J. M. Goicoechea, *Angew. Chem. Int. Ed.* **2018**, *57*, 431.

[20]   J. B. Diccianni, T. Heitmann, T. Diao, *J. Org. Chem.* **2017**, *82*, 6895.

[21]   a) Sheldrick, G. M. SADABS, Bruker AXS, Madison, USA **2007**; b) CrysAlisPro, Scale3 Abspack, Rigaku Oxford Diffraction **2019**.

[22]   R. C. Clark, J. S. Reid, *Acta Cryst. A* **1995**, *51*, 887.

[23]   G. M. Sheldrick, *Acta Cryst. A* **2015**, *71*, 3.

[24]   O. V. Dolomanov, L. J. Bourhis, R. J. Gildea, J. A. K. Howard, H. Puschmann, *J .Appl. Crystallogr.* **2009**, *42*, 339.

[25]   G. M. Sheldrick, *Acta Cryst. C* **2015**, *71*, 3.

[26]   G. M. Sheldrick, *Acta Cryst. A* **2008**, *64*, 112.

[27]   U. Chakraborty, B. Mühldorf, N. J. C. van Velzen, B. de Bruin, S. Harder, R. Wolf, *Inorg. Chem.* **2016**, *55*, 3075.

8 Di-*tert*-butyldiphosphatetrahedrane as a Source of 1,2-Diphosphacyclobutadiene Ligands[a]

Abstract: Tetrahedral molecules containing carbon and phosphorus have been reported only recently, and their chemistry is largely unexplored. Herein, we describe the reactions of di-*tert*-butyldiphosphatetrahedrane (**1**) with a variety of iron and cobalt metalates. Such reactions consistently afford complexes of the rarely encountered 1,2-diphosphacyclobutadiene ligand, which have previously been very challenging synthetic targets. The subsequent reactivity of 1,2-diphosphacyclobutadiene cobaltates toward various electrophiles has also been investigated and is compared to reactions of related 1,3-diphosphacyclobutadiene ligands. The results highlight the distinct reactivity of such isomeric species, showing that the 1,2-isomers can act as precursors for previously unknown triphospholium ligands. The electronic structures of the new complexes were investigated by several methods, including NMR, EPR and Mössbauer spectroscopies and quantum chemical calculations.
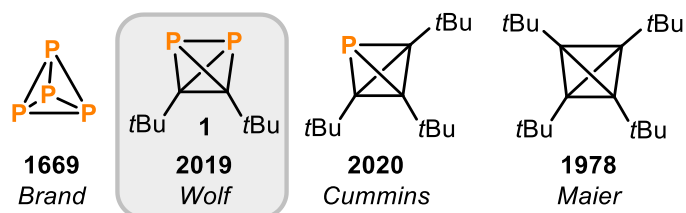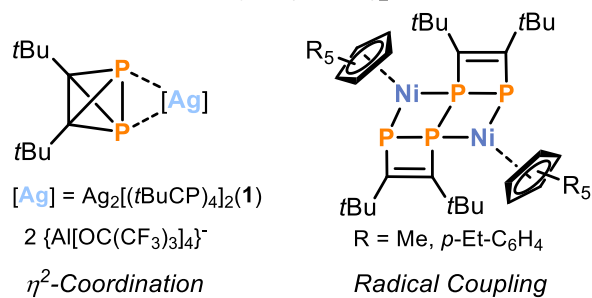
8.1 Introduction

Tetrahedranes are highly strained derivatives of the simplest platonic hydrocarbon C_4H_4.[2] The first isolated tetrahedrane was undoubtedly white phosphorus, P_4, first prepared in the 17th century. Much more recently (1978), the group of Maier showed that the carbon-based tetrahedrane tBu$_4$C$_4$ can be accessed as well.[3] Even though heavier group 14 tetrahedranes with various substituents have been prepared, mixed neutral tetrahedranes have remained scarce.[4] This is especially conspicuous considering the great number of mixed anionic tetrahedranes containing group 13, 14 or 15 elements.[5] Our group recently showed that mixed group 14 / group 15 tetrahedranes are indeed accessible.[6] A simple nickel-catalysed dimerisation reaction of tBuCP affords the phosphaalkyne dimer di-*tert*-butyldiphosphatetrahedrane (tBuCP)$_2$ (**1**, Figure 1A), which can be considered a 'hybrid' between P_4 and (tBuC)$_4$. The related tri-*tert*-butylphosphatetrahedrane was also reported shortly thereafter by Cummins and co-workers.[7]

Having been synthetically inaccessible until recently, the reactivity of these phosphatetrahedranes is still largely unexplored, although preliminary results suggest that **1** possesses a versatile coordination chemistry. For example, **1** reacts with various Ni(0) and Ni(I) complexes to form (tBuCP)$_n$ (n = 2, 4) frameworks with novel coordination modes.[8] Moreover, it coordinates in an η^2-fashion via its lone pairs to silver(I) (Figure 1B).[6] Significantly, in this latter case the behaviour of **1** is noticeably different from that of either P_4 or the monomeric *tert*-butylphosphaalkyne.[9] Furthermore, in one of our most recent contributions, the reactivity of **1** towards carbenes was investigated.[10] This study again highlighted that, while **1** appears to be reactive towards similar substrates as P_4 and tBuCP, these reactions furnish distinctly different and otherwise inaccessible products.

Based on the above results we were highly motivated to investigate the reactivity of **1** towards low-valent 3d metalates. The reactions of these species with P_4 have been extensively studied: for example, Ellis and Urněžius were able to synthesise the first completely inorganic sandwich complex $[(\eta^5\text{-}P_5)_2\text{Ti}]^{2-}$ by reaction of a titanate with P_4.[11] Our group has also contributed to this area by reaction of alkene- or arene-stabilised cobaltates and ferrates with P_4.[12,13] Many of the same metalates are also known to react with tBuCP to give 1,3-diphosphacyclobutadiene complexes of the type $[(1,3\text{-}R_2C_2P_2)_2M]^-$ (M = Fe, Co; R = tBu, tPent, Ad) by head-to-tail cyclodimerisation of the phosphaalkyne.[14,15] These 1,3-tBu$_2$C$_2$P$_2$ complexes possess versatile coordination behaviour and display much other onward reactivity, and can be used to access a diverse variety of other coordination compounds.[16] By analogy with our previous studies, it was anticipated that related reactions of metalates with **1** could provide access to similarly interesting and synthetically useful coordination complexes, that would not be accessible using established precursors.

A. Group 14/15 Tetrahedranes

1669	**2019**	**2020**	**1978**
Brand	*Wolf*	*Cummins*	*Maier*

B. Coordination Chemistry of (*t*BuCP)$_2$

[Ag] = Ag$_2$[(*t*BuCP)$_4$]$_2$(**1**)

2 {Al[OC(CF$_3$)$_3$]$_4$}$^-$

η^2-Coordination

R = Me, *p*-Et-C$_6$H$_4$

Radical Coupling

C. This work: Source of 1,2-diphosphacyclobutadiene ligands

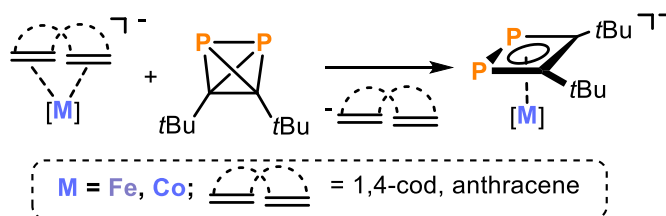**M** = **Fe**, **Co**; ⌢ = 1,4-cod, anthracene

Figure 1. Group 14/15 tetrahedranes and coordination chemistry of (*t*BuCP)$_2$.

188

8.2   Results and Discussion

Syntheses and Molecular Structures

To begin, the reaction of two equivalents of **1** with one equivalent of the anthracene ferrate [K([18]crown-6)][Fe(anthracene)$_2$] in THF was studied. Addition of **1** to a deep red solution of [K([18]crown-6)][Fe(anthracene)$_2$] in THF afforded a deep green solution after stirring the reaction overnight while allowing it to warm to room temperature. X-ray diffraction analysis on single crystals grown from benzene/*n*-hexane revealed the formation of the heteroleptic complex [K([18]crown-6)][Fe(1,2-tBu$_2$C$_2$P$_2$)(anthracene)] (**2**, Scheme 1, Figure 2). Notably, despite the 2:1 reaction stoichiometry, **2** was the only product isolated, with no observation of a homoleptic 2:1 complex. Thus, using an optimised protocol with 1:1 stoichiometry, **2** was isolated in good yields of up to 84% as a deep green powder. Compound **2** shows both a very rare η^4-coordinated 1,2-diphosphacyclobutadiene ligand (also referred to as 1,2-diphosphete) and an η^4-coordinated anthracene ligand. The bond lengths in the tBu$_2$C$_2$P$_2$ ligand compare well to those reported previously for the related cobalt complex [Cp'''Co(1,2-tBu$_2$C$_2$P$_2$)] [**2**: P1−P2 2.1738(6) Å, C1−C2 1.440(2) Å; [Cp'''Co(1,2-tBu$_2$C$_2$P$_2$)]: P−P: 2.1818(7) Å), C−C: 1.443(2) Å; Cp''' = 1,2,4-tBu$_3$C$_5$H$_3$)][17], while the bond lengths within the anthracene ligand (C11−C12 1.428(2) Å, C12−C13 1.403(2) Å, C13−C14 1.432(2) Å) indicate back donation from an Fe(I) to the π-system of the ligand. Notably, 1,2-diphosphacyclobutadiene ligands are very rare compared to their 1,3-isomers, which are commonly prepared by dimerisation of phosphaalkynes in the coordination sphere of transition metals.[17,18] The formation of complex **2** hence suggested a distinct synthetic utility of **1** in the synthesis of 1,2-diphosphacyclobutadiene complexes, for which no reliable, general synthetic routes have previously been available (*vide infra*). Notably, attempts to isolate the isomer [Fe(1,3-tBu$_2$C$_2$P$_2$)(anthracene)]$^-$ from the reaction of two equivalents of tBuCP and [K([18]crown-6)][Fe(anthracene)$_2$] have not so far been successful.

2 was characterised by UV/Vis spectroscopy, showing an intense absorption band at 650 nm, which accounts for its green colour. The NMR spectrum of isolated **2** in THF-d$_8$ shows no signals except for the deuterated solvent signals in the range from −150 to 150 ppm. Further characterisation of **2** is described in the section *Electronic Structure Analysis* (*vide infra*).
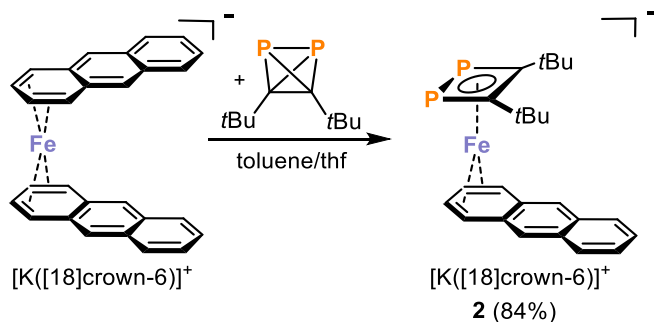
Scheme 1. Reaction of [K([18]crown-6)][Fe(anthracene)$_2$] with (tBuCP)$_2$.
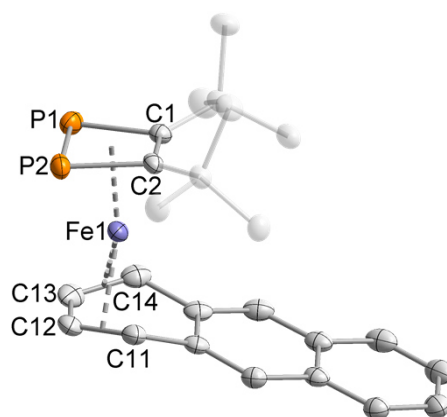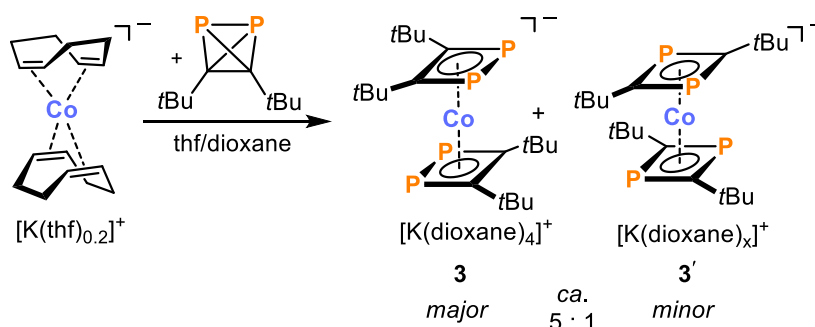
Figure 2. Molecular structure of **2** in the solid state (anion shown only). Thermal ellipsoids are set at the 50% probability level. Hydrogen atoms are omitted for clarity. Selected bond lengths [Å] and angles [°]: P1−P2 2.1738(6), P1−C1 1.8328(15), P2−C2 1.8274(14), C1−C2 1.440(2), Fe−(C$_2$P$_2^{\text{centroid}}$) 1.783(2), C11−C12 1.428(2), C12−C13 1.403(2), C13−C14 1.432(2), C1−P1−P2 78.03(5), C2−P2−P1 78.85(5), C2−C1−P1 101.97(10), C1−C2−P2 101.14(10).

To test the generality of 1,2-diphosphacyclobutadiene formation, **1** was next reacted with the cobaltate [K(thf)$_{0.2}$][Co(η^4-cod)$_2$] (cod = 1,5-cyclooctadiene). Addition of one equivalent of **1** to a THF solution at −80 °C led to the formation of an orange-brown solution. The ^{31}P{^{1}H} NMR spectrum of the reaction mixture showed two major singlet species with chemical shifts of −102.3 and 3.3 ppm in a 5:1 ratio (integration). The latter, minor shift is close to the reported value for [K([18]crown-6)(thf)$_2$][Co(1,3-tBu$_2$C$_2$P$_2$)$_2$]$^-$ (δ = 2.4 ppm).[14] And, indeed, extraction of the crude reaction mixture with 1,4-dioxane and slow diffusion of *n*-hexane afforded yellow crystals of both a 1,4-dioxane solvated salt of the previously reported cobaltate [Co(1,3-tBu$_2$C$_2$P$_2$)$_2$]$^-$ (**3′**) and the new, isomeric complex [K([18]crown-6)(1,4-dioxane)$_4$][Co(1,2-tBu$_2$C$_2$P$_2$)$_2$]$^-$ (**3**) containing a 1,2-diphosphacyclobutadiene ligand (Scheme 2).[14] The 'mixed' isomer containing both 1,2- and 1,3-diphosphacyclobutadiene ligands is not observed, which is attributed to increased steric clash between the *t*Bu groups in this isomer, as discussed in the computational details (8.4.8). Again, these results highlight both the divergent reactivity of **1** and *t*BuCP (whose reactions with [K(thf)$_{0.2}$][Co(η^4-cod)$_2$] preferentially form the 1,2-isomer **3** and the 1,3-isomer **3′**, respectively), and the ability of **1** to act as a 1,2-diphosphacyclobutadiene ligand precursor.

The solid-state molecular structure of **3** revealed a coordination polymer built upon coordination of the 1,2-diphosphacyclobutadiene ligands to [K(1,4-dioxane)$_4$]$^+$ units (Figure 3). The P−P bond length of 2.1798(6) Å as well as the C1−C2 bond length (1.443(2) Å) of the diphosphacyclobutadiene ligand compare well to **2**, as well as to the Co complex [Cp′′′Co(1,2-tBu$_2$C$_2$P$_2$)] mentioned above. The two η^4-bound tBu$_2$C$_2$P$_2$ units are in a staggered conformation with the *t*Bu groups pointing away from each other. Due to very similar solubilities, **3** could not be separated from **3′**. Moreover, heating the crude reaction mixture to 110 °C for several days did not change the integral ratio of the signals for **3** and **3′** in the ^{31}P{^{1}H} NMR spectrum. The reaction of [K(thf)$_{0.2}$][Co(η^4-cod)$_2$] with just one equivalent of **1** also afforded the

same mixture of homoleptic cobalt complexes in the $^{31}P\{^1H\}$ NMR spectrum (signals at −102.3 and 3.3 ppm) alongside unconsumed starting material, as identified in the ^1H NMR spectrum.

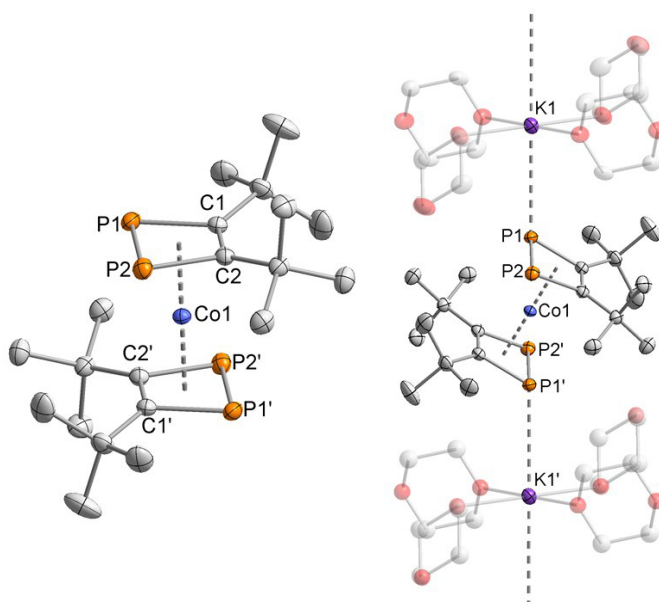**Scheme 2.** Reaction of [K(thf)$_{0.2}$][Co(η^4-cod)$_2$] with (tBuCP)$_2$.

Figure 3. Molecular structure of **3** (left: anion shown only, right: structure as coordination polymer) in the solid state. Thermal ellipsoids are set at the 50% probability level. Hydrogen atoms are omitted for clarity. Selected bond lengths [Å] and angles [°]: P1−P2 2.1798(6), P1−C1 1.8234(17), P2−C2 1.8136(17), C1−C2 1.443(2), K1−P1 3.4898(5), Co−(C$_2$P$_2$^{centroid}) 1.748(2), C1−P1−P2 78.26(6), C2−P2−P1 78.36(6), C2−C1−P1 101.39(12), C1−C2−P2 102.00(11).

To establish whether analogous results could be achieved using heteroleptic as well as homoleptic metalates, reactions were next performed using the heteroleptic BIAN (BIAN = bis(aryl)acenaphthenquinonediimine) cobaltate [K(thf)$_{1.5}$][(^{Dipp}BIAN)Co(η^4-cod)] (Dipp = 2,6-di-*iso*-propylphenyl), whose reactions with P$_4$ have previously been shown to proceed with particularly high selectivity.[19] Addition of one equivalent of **1** to a deep green solution of [K(thf)$_{1.5}$][(^{Dipp}BIAN)Co(η^4-cod)] resulted in a colour change to turquoise overnight. Reaction monitoring by $^{31}P\{^1H\}$ NMR spectroscopy revealed full consumption of **1** after stirring the reaction for 3 days at ambient temperature. Gratifyingly, the selective formation of one species with a singlet resonance at a chemical shift of −121.8 ppm was observed. Single crystal X-ray diffraction studies on crystals grown from 1,4-dioxane/*n*-hexane revealed the formation of the

heteroleptic 1,2-diphosphacyclobutadiene complex [K(1,4-dioxane)][(^{Dipp}BIAN)Co-(1,2-tBu$_2$C$_2$P$_2$)] (**4**, Scheme 3, Figure 4). In the solid state, each K$^+$ counterion is coordinated by the two P atoms of one anion, the Dipp substituent of another anion and a 1,4-dioxane molecule, resulting in a dimeric structure (see Figure S29). The bond metrical parameters of the 1,2-tBu$_2$C$_2$P$_2$ ligand resemble the data obtained for **2** and **3**. While the C−C bond length (1.403(3) Å) is in good agreement with a dianionic ^{Dipp}BIAN^{2-} ligand (1.402(4) Å in Na$_2$^{Dipp}BIAN), the N1−C11 (1.353(3) Å) and N2−C12 (1.347(3) Å) bond lengths deviate slightly from the reported values of 1.387(4) and 1.386(4) Å.[20] A more detailed analysis of the bond metric data of the BIAN ligands will be discussed below (section on *Electronic Structure Analysis*). Compound **4** was isolated in 63% crystalline yield and fully characterised by NMR and UV/Vis spectroscopies as well as elemental analysis. The ^{1}H and ^{13}C{^{1}H} NMR spectra of **4** reveal a diamagnetic compound with one signal set for the ^{Dipp}BIAN and one signal set for the tBu$_2$C$_2$P$_2$ ligand. The ^{31}P{^{1}H} NMR spectrum shows a singlet resonance at −121.8 ppm, which is comparable to **3** and to the complex [(Cp′′′Co(1,2-tBu$_2$C$_2$P$_2$)] (δ(^{31}P{^{1}H}) = −83.8 ppm).[17]
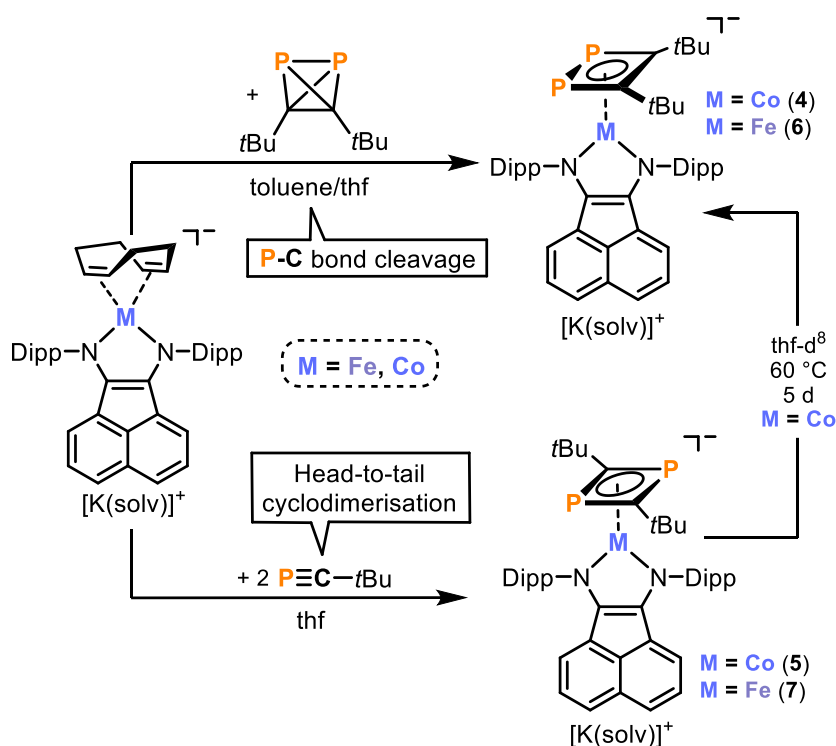
Scheme 3. Synthesis of heteroleptic [K(solv)][(^{Dipp}BIAN)M(tBu$_2$C$_2$P$_2$)] (M = Co, Fe) complexes featuring 1,2- or 1,3-(tBu$_2$C$_2$P$_2$) ligands. [K(solv)]$^+$ observed in the molecular structure determined by XRD: [K(1,4-dioxane)]$^+$ (**4**), [K(thf)$_3$]$^+$ (**5**), [K([18]crown-6)(1,4-dioxane)]$^+$ (**6**), [K([18]crown-6)(thf)$_{1.8}$(1,4-dioxane)$_{0.2}$]$^+$ (**7**). [K(solv)]$^+$ for starting materials: [K(thf)$_{1.5}$] (M = Co), [K([18]crown-6)] (M = Fe).

As noted previously, 1,3-diphosphacyclobutadiene complexes can be prepared by head-to-tail cyclodimerisation reactions. Indeed, the reaction of 2 equivalents of tBuC≡P with the same precursor [K(thf)$_{1.5}$][(^{Dipp}BIAN)Co(η^4-cod)] afforded the isomeric 1,3-diphosphacyclobutadiene complex [K(thf)$_3$][(^{Dipp}BIAN)Co(1,3-tBu$_2$C$_2$P$_2$)] (**5**) in 64% yield as turquoise crystals. The solid-

state molecular structure of **5** shows chelation of the potassium cation by one P atom of the tBu$_2$C$_2$P$_2$ ring and the phenyl ring of the Dipp group in the same anion, resulting in a monomeric structure (in contrast to **4**). The P−C bond lengths in this complex lie in the range of 1.787(4) to 1.802(4) Å and the bond metric data of the BIAN ligand will be discussed below. In the ^{31}P{^{1}H} NMR spectrum one singlet at 1.8 ppm was observed. **5** represents a rare example of a heteroleptic transition metal anion with a terminal 1,3-disphosphacyclobutadiene. The intense turquoise colouration of both **4** and **5** when dissolved in THF can be rationalised by their UV/Vis absorption spectra, with absorption bands at 630 nm (**4**) and 605 nm (**5**). When heating a solution of **5** in THF-d$_8$ for 5 days to 60 °C, the selective formation of **4** was observed. This is in line with a computational analysis on the stability of the truncated model complexes [(^{Dmp}BIAN)Co(1,2-tBu$_2$C$_2$P$_2$)]$^-$ and [(^{Dmp}BIAN)Co(1,3-tBu$_2$C$_2$P$_2$)]$^-$ (Dmp = 2,6-dimethylphenyl) at the RI-PWPB95-D3BJ/def2-TZVP level of theory. Although single point calculations using this double hybrid functional suggest little difference in energy between the isomers, the 1,2-diphosphacyclobutadiene is thermodynamically more stable than its 1,3-isomer (see section 8.4.8). A single related thermal isomerisation of a 1,3-diphosphacyclobutadiene ligand to its 1,2-isomer has been observed by Scheer and co-workers to generate [(Cp′′′Co(1,2-tBu$_2$C$_2$P$_2$)]. [17]
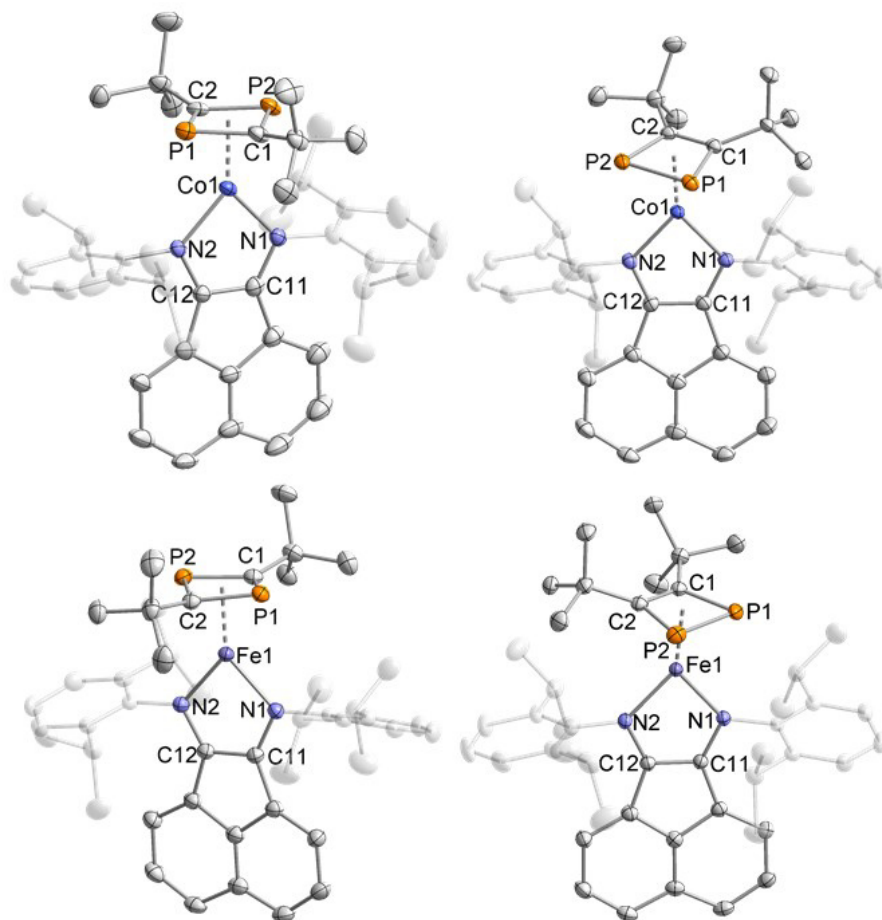
Figure 4. Molecular structures of **4-7** in the solid state. Thermal ellipsoids are set at the 50% probability level. Hydrogen atoms, cations (with sequestering agent [18]crown-6 in case of **6** and **7**) and solvent of crystallisation are omitted for clarity. For **5** and **6**, only one of two crystallographically independent molecules is shown. Selected bond lengths [Å] and angles [°]: **4**: P1−P2 2.1765(8), P1−C1 1.838(2), P2−C2 1.815(2), C1−C2 1.441(3), N1−C11 1.353(3), N2−C12 1.347(3), C12−C11 1.403(3), Co1−N1 1.9382(18), Co1−N2 1.9074(18), Co−(C₂P₂centroid) 1.775(2), C2−C1−P1 102.62(16), C1−C2−P2 100.60(16), C1−P1−P2 77.11(7), C2−P2−P1 79.66(8); **5**: P1−C1 1.802(4), P1−C2 1.787(5), P2−C1 1.787(4), P2−C2 1.802(4), N1−C11 1.358(6), N2−C12 1.352(5), C12−C11 1.397(6), Co1−N1 1.929(3), Co1−N2 1.909(4), Co−(C₂P₂centroid) 1.780(2), P2−C1−P1 98.4(2), P1−C2−P2 98.4(2), C2−P1−C1 81.45(19), C1−P2−C2 81.4(2).; **6**: P1−P2 2.173(5), P1−C1 1.819(9), P2−C2 1.776(10), C1−C2 1.434(13), N1−C11 1.369(9), N2−C12 1.350(9), C12−C11 1.413(10), Fe1−N1 1.959(6), Fe1−N2 1.958(7), Fe−(C₂P₂centroid) 1.823(3), C2−C1−P1 100.8(7), C1−C2−P2 103.0(7), C1−P1−P2 77.7(3), C2−P2−P1 78.5(3); **7**: P1−C1 1.799(2), P1−C2 1.795(2), P2−C1 1.790(2), P2−C2 1.791(2), N1−C11 1.367(3), N2−C12 1.366(2), C12−C11 1.385(3), Fe1−N1 1.9421(16), Fe1−N2 1.9331(17), Fe−(C₂P₂centroid) 1.803(3), P2−C1−P1 98.94(10), P2−C2−P1 99.01(10), C2−P1−C1 80.54(9), C1−P2−C2 80.89(10).

To probe whether these differences in reactivity could be further extended, the analogous ferrate [K([18]crown-6)][(DippBIAN)Fe(η⁴-cod)] was also reacted with *t*BuCP and its dimer **1**. Single crystals suitable for X-ray diffraction studies were obtained from both reactions which confirmed the analogous formation of two isomeric products: [K([18]crown-6)(1,4-dioxane)][(DippBIAN)Fe(1,2-*t*Bu₂C₂P₂)] (**6**, from **1**) and [K([18]crown-6)(thf)₂][(DippBIAN)Fe(1,3-*t*Bu₂C₂P₂)] (**7**, from *t*BuCP, Figure 4). **6** and **7** were isolated as dark

blue or violet crystals in 70% and 50% yield, respectively. The bond metrical data for both complexes are very similar to the values obtained for the related cobalt complexes. However, and in contrast to the cobaltates, **6** and **7** are paramagnetic and therefore reveal broad resonances in their ^{1}H NMR spectra in the region from -4 to $+12$ ppm (see experimental details for spectra).

Reactivity Studies

Having substantial quantities of the 1,2- and 1,3-tBu$_2$C$_2$P$_2$ cobaltates **4** and **5** in hand, reactions of these complexes with different electrophiles were conducted, to examine differences in their reactivities. Reactions of the 1,3-isomer **5** with HCl, Me$_3$SiCl and Cy$_2$PCl afforded only crystals of the neutral, deligated complex [(^{Dipp}BIAN)Co(μ-Cl)]$_2$ (see experimental details for molecular structure). However, we were able to detect a singlet signal in the ^{31}P{^{1}H} NMR spectrum at 194.2 ppm in some of these reactions. In reactions of **4** with HCl, MeI, Me$_3$SiCl and Ph$_2$PCl, this species was also formed and identified as [{(^{Dipp}BIAN)Co}$_2$(μ^2:η^4,η^4-tBu$_2$C$_2$P$_2$)] (**8**, Figure 5), a neutral complex featuring a μ^2-bridging 1,2-diphosphacyclobutadiene ligand. This compound was also identified as a product in the reaction of **5** with Me$_3$Si-Cl and MeI and represents another example of 1,3-tBu$_2$C$_2$P$_2$ to 1,2-tBu$_2$C$_2$P$_2$ ligand isomerisation. Bridging diphosphacyclobutadiene complexes in general are scarce, and this is the first example of the 1,2-isomer being isolated in such a bridging coordination mode. **8** could plausibly form from the reaction of 0.5 equivalents of the bridging chlorido complex [(^{Dipp}BIAN)Co(μ-Cl)]$_2$ (formed as an intermediate, *vide supra*) with one equivalent of **4** and concomitant elimination of KCl. However, due to difficulties in isolating [(^{Dipp}BIAN)Co(μ-Cl)]$_2$, this hypothesis has not yet been confirmed experimentally.

Complex **8** was isolated in 12% yield using **4** as starting material and Me$_3$Si-Cl as electrophile and characterised by X-ray crystallography, elemental analysis and NMR and UV/Vis spectroscopy. The solid-state molecular structure of **8** reveals a long P1$-$P1$'$ bond (2.3417(8) Å), two slightly elongated P1$-$C1 bonds (1.8602(16) Å) and a C1$-$C1$'$ bond length (1.449(3) Å) that compares well to complexes **4** and **5**. The Co1$\cdots$Co1$'$ distance of 3.5547(5) Å suggests no significant interaction between the metal atoms. The bond metric data of the BIAN ligand allows for a classification as monoanionic BIAN$^-$. Complex **8** is diamagnetic and features a ^{31}P{^{1}H} NMR singlet at a chemical shift of 194.2 ppm. The UV/Vis spectrum shows absorption bands at 620 and 830 nm, accounting for its dark blue colour in solution.
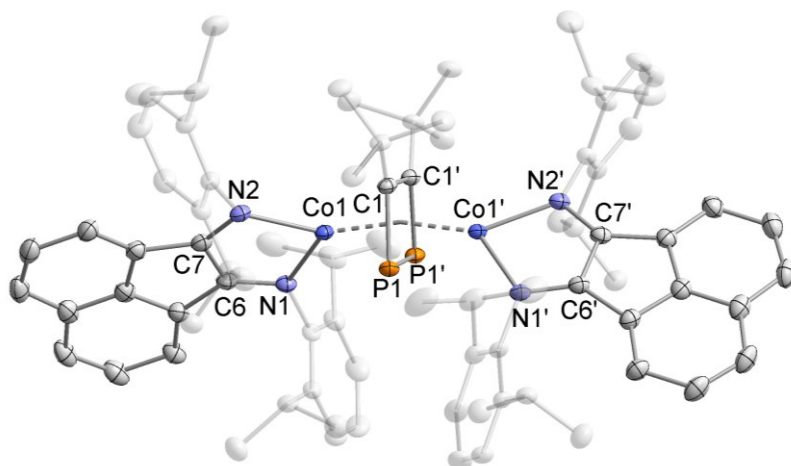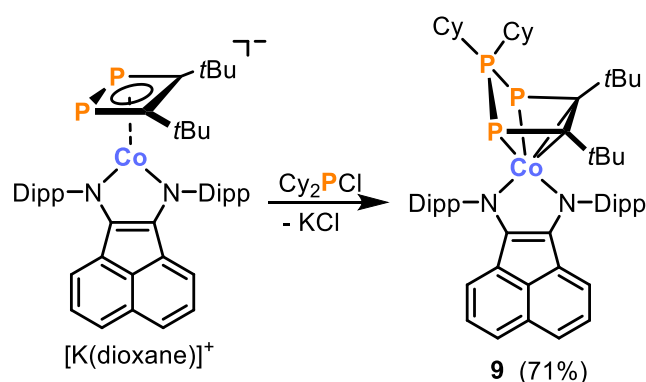
Figure 5. Molecular structure of **8** in the solid state. Thermal ellipsoids are set at the 50% probability level. Hydrogen atoms are omitted for clarity. Selected bond lengths [Å] and angles [°]: P1−P1′ 2.3417(8), P1−C1 1.8602(16), C1−C1′ 1.449(3), N1−C6 1.327(2), N2−C7 1.334(2), C6−C7 1.425(2), Co1−N1 1.9287(14), Co1−N2 1.9874(14), Co−(C2P2$^{\text{centroid}}$) 1.791(2), Co1⋯Co1′ 3.5547(5), C1−P1−P1′ 75.95(5), C1−C1′ P1−103.61(5).

The reaction of Cy$_2$PCl with **4** and **5** revealed the particular synthetic utility of **4**. The neutral complex [($^{\text{Dipp}}$BIAN)Co(η^4-tBu$_2$C$_2$P$_3$Cy$_2$)] (**9**) featuring an expanded 1,2,3-triphospholium ligand was obtained upon insertion of a PCy$_2$ fragment into the P−P bond of **4** (Scheme 4). In case of **5**, this reaction was unselective giving rise to several signals in the ^{31}P{^{1}H} NMR spectrum (see Figure S19). Even though substituted C$_2$P$_3$ rings are known (e.g. tri-organo P1,P2,P3-substituted triphospholenes), the motif of diorgano-substitution of P2 of a triphospholium ligand has not been reported to date.[21]

Scheme 4. Synthesis of the 1,2,3-triphospholium complex **9** by insertion of "PCy$_2$$^+$" into the P−P bond of **4**.

The solid-state molecular structure of **9** reveals η^4 coordination of the tBu$_2$C$_2$P$_3$Cy$_2$-ligand with P−P bond lengths (P1−P3: 2.1549(6) Å, P2−P3: 2.1535(6) Å) in the range commonly observed for P−P single bonds (Figure 6).[22] The structural parameters indicate the presence of a monoanionic BIAN$^−$ ligand (C1−C2: 1.447(3) Å, N1−C11: 1.347(2) Å, N2−C12: 1.338(2) Å *cf.* C−C: 1.446(2) Å and C−N: 1.3239(18) and 1.3326(19) Å in Na$^{\text{Dipp}}$BIAN).[20] A detailed discussion of the oxidation state of the BIAN ligand is given in the section *Electronic Structure Analysis*. Complex **9** was isolated in 71% yield as dark blue crystals and is diamagnetic in solution

as revealed by sharp resonances for the ^{Dipp}BIAN ligand and the *t*Bu and Cy groups. The $^{31}P\{^1H\}$ NMR spectrum shows two signals: a doublet at −90.3 ppm ($^1J_{PP}$ = 349.6 Hz) corresponding to the three-coordinate P-atoms and a coupled triplet resonance at 55.5 ppm, which can be assigned to the tetracoordinate P atom. The deep blue colour of **9** can be attributed to two intense absorption bands in the UV/Vis spectrum at 560 and 660 nm.
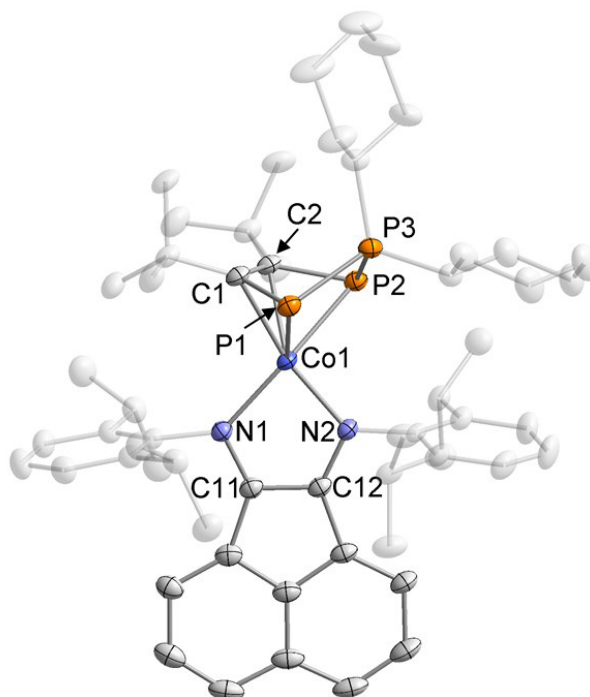

Figure 6. Molecular structure of **9** in the solid state. Thermal ellipsoids are set at the 50% probability level. Hydrogen atoms and solvent of crystallisation are omitted for clarity. Selected bond lengths [Å] and angles [°]: Co1−P1 2.3049(5), Co1−P2 2.2643(5), Co1−C1 2.1070(18), Co1−C2 2.1041(18), Co1−N1 1.9850(15), Co1−N2 1.9046(15), P1−P3 2.1549(6), P2−P3 2.1535(6), P1−C1 1.8431(18), P2−C2 1.8147(19), C1−C2 1.447(3), N1−C11 1.347(2), N2−C12 1.338(2), C12−C11 1.406(3), C1−P1−P3 91.24(6), C2−P2−P3 93.38(6), P2−P3−P1 90.79(2), C2−C1−P1 117.67(13), C1−C2−P2 114.91(13).

Electronic structure analysis

Several spectroscopic and quantum chemical methods were employed in order to analyse the electronic structure of the complexes described herein. We were especially interested in the oxidation states of the metal atoms. Therefore, the metrical oxidation states of all BIAN-containing complexes were calculated using the recently developed protocol for diazabutadiene-based ligands.[23] This method is based on a statistical analysis of bond metric data obtained from X-ray crystallography and can be used to determine a (non-integer) metrical oxidation state of the ligands and eventually the metal atom. The metrical oxidation states of the ^{Dipp}BIAN ligand for all compounds described in this study range −0.6 to −1.3, suggesting the presence of a monoanionic radical ^{Dipp}BIAN ligand in each case. However, the estimated standard deviation

was rather high in some cases, e.g. for **6** (esd: 0.24). Due to this large discrepancy, further investigations on the electronic structures were conducted.

First, the EPR spectra of paramagnetic species (**2**, **6** and **7**) were recorded, revealing rhombic signals for all systems investigated without any hyperfine couplings (see Figure 7). The spectra were simulated and the obtained *g*-values are given in Table 1. The *g*-tensors were also calculated on the CASSCF-NEVPT2/DKH-def2-TZVP level of theory for the anionic complexes [Fe(1,2-tBu$_2$C$_2$P$_2$)(anthracene)]$^-$, [(^{Dmp}BIAN)Fe(1,2-tBu$_2$C$_2$P$_2$)]$^-$ (**6′**) and [(^{Dmp}BIAN)Fe(1,3-tBu$_2$C$_2$P$_2$)]$^-$ (**7′**) . The values obtained from these calculations for **6′** and **7′** are in good agreement with the experimental values, suggesting that the calculated electronic structure fits the real structure.
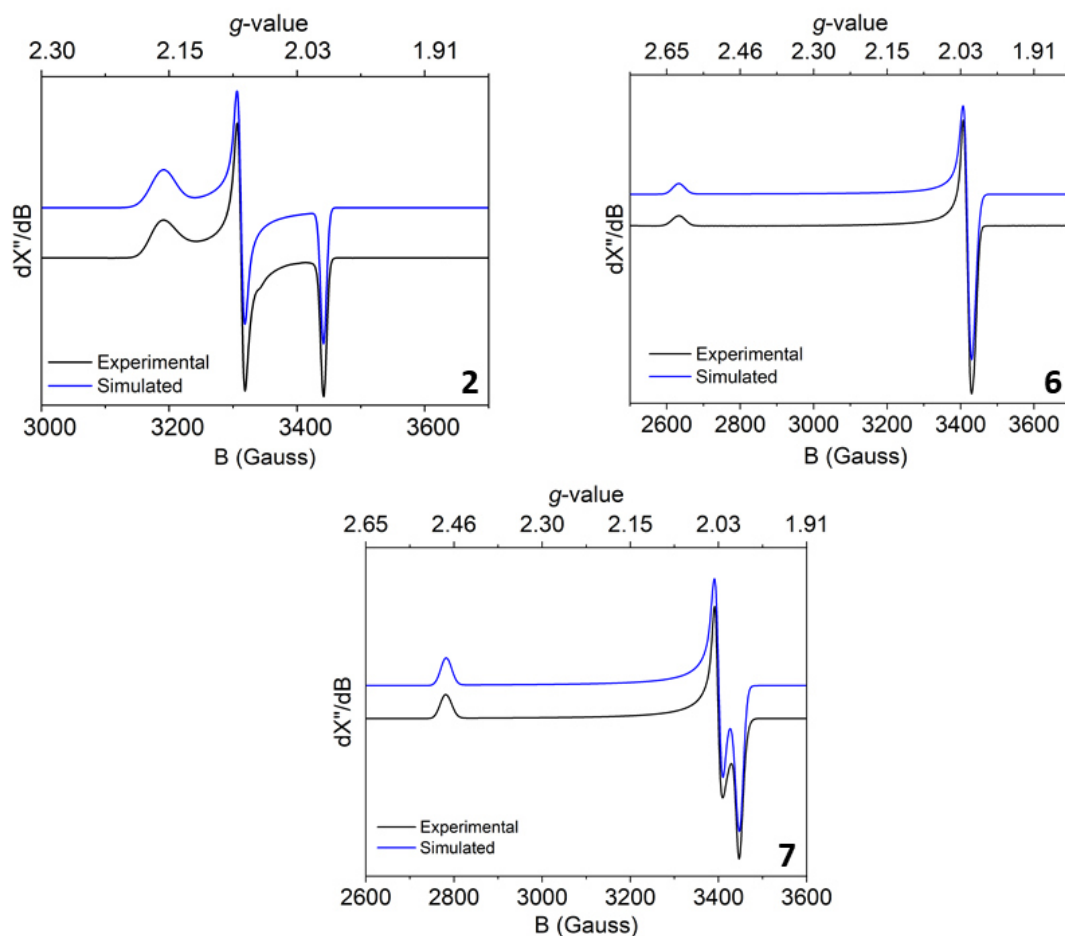

Figure 7. Experimental and simulated X-band EPR spectrum of **2** (top left), **6** (top right) and **7** (bottom) in a 2-methyl-THF glass at 20 K; **2**: temperature: 10 K, Freq. : 9.646813 GHz, 0.2000 mW, mod. 3.000 Gauss; g-tensor parameters obtained from simulations are: g_{11} = 2.003, g_{22} = 2.081, g_{33} = 2.161, 1.10 mT Gaussian line width, 0.029 MHz g_{33}-strain; **6**: temperature: 20 K, Freq.: 9.642478 GHz, 0.6325 mW, mod. 1.000 Gauss; g-tensor parameters obtained from simulations are: g_{11} = 2.617, g_{22} = 2.015, g_{33} = 2.007; **7**: temperature: 20 K, Freq. : 9.646713 GHz, 0.6325 mW, mod. 4.000 Gauss; g-tensor parameters obtained from simulations are: g_{11} = 2.478, g_{22} = 2.027, g_{33} = 1.999.

Table 1. EPR spectroscopic parameters for compounds **2**, **6** and **7**

Compound		g_{11}	g_{22}	g_{33}
2	Exp.	2.003	2.081	2.161
	Calc.	2.008	2.107	2.203
6	Exp.	2.617	2.015	2.007
	Calc.	2.600	2.004	1.997
7	Exp.	2.478	2.027	1.999
	Calc.	2.404	2.015	1.993

Next, the solution magnetic moments of **2**, **6** and **7** in THF-d$_8$ were determined using the Evans-NMR method. A magnetic moment of 1.9(1) μ_B was measured for **2**, which is close to the spin-only value for a S = ½ ground state ($\mu_B^{\text{spin-only}}$ = 1.73). Accordingly, the magnetic moments of **6** and **7** were determined as μ_{eff} = 2.0(1) μ_B in both cases. These values would be consistent with low-spin Fe(I) and Fe(III) systems.

The ^{57}Fe Mössbauer spectra of [K([18]crown-6)][Fe(1,2-tBu$_2$C$_2$P$_2$)(anthracene)] (**2**), [K([18]crown-6)(1,4-dioxane)][($^{\text{Dipp}}$BIAN)Fe(1,2-tBu$_2$C$_2$P$_2$)] (**6**) and [K([18]crown-6)(thf)$_2$][($^{\text{Dipp}}$BIAN)Fe(1,3-tBu$_2$C$_2$P$_2$)] (**7**) are shown in Figure 8. These spectra show the presence of a single species with an integral fit of the transmission in each case. The corresponding fitting parameters are listed in Table 2.
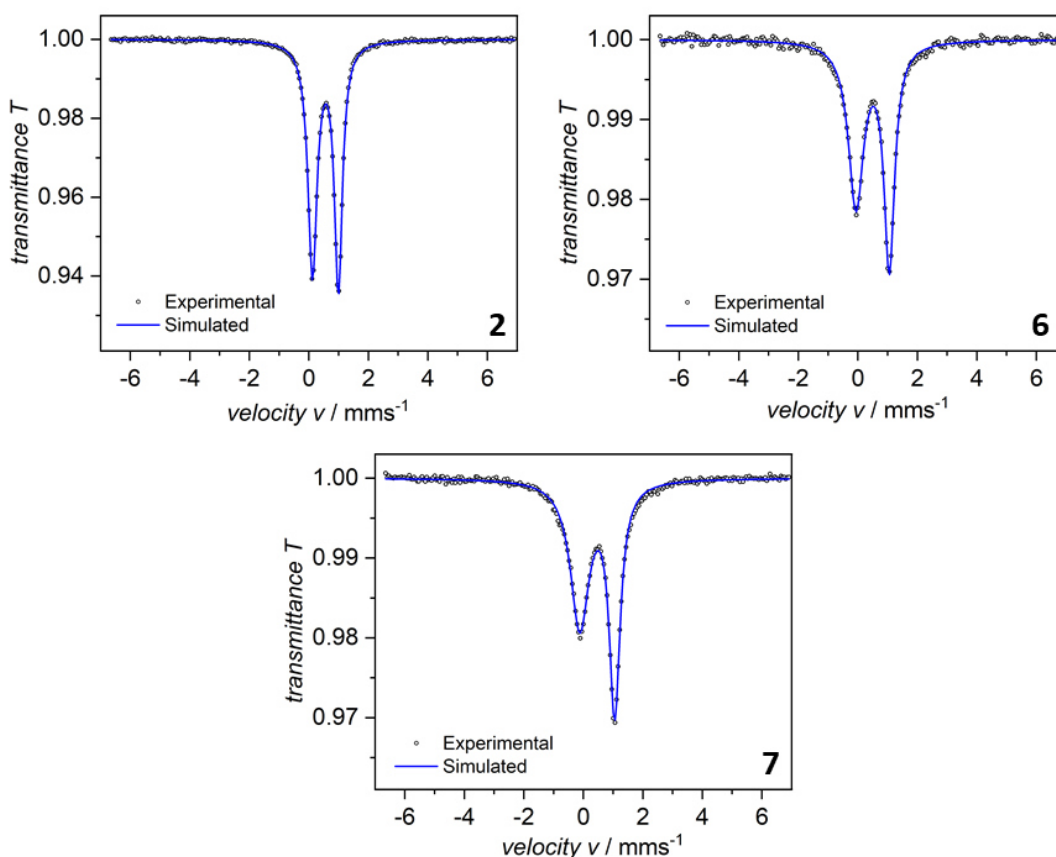

Figure 8. Experimental and simulated ^{57}Fe Mössbauer spectra of **2** (top left), **6** (top right) and **7** (bottom) recorded at 77 K.

Table 2. ^{57}Fe Mössbauer spectroscopic parameters for compounds **2**, **6** and **7**.

Compound		δ^a [mm·s^{-1}]	ρ^b [a.u.]	$\lvert \Delta E_Q^c \rvert$ [mm·s^{-1}]	$\Gamma_{fwhm}{}^d$ [mm·s^{-1}]
2	Exp.	0.55		0.87	0.37
	Calc.		11810.059	0.98	
6	Exp.	0.50		1.12	0.62
	Calc.		11810.099	1.08	
7	Exp.	0.46		1.18	0.76
	Calc		11810.475	1.20	

^{a} Isomer shift, ^{b} Calculated electron density at the nucleus (arbitrary unit, CASSCF) ^{c} Experimentally determined and calculated (CASSCF) quadrupole splittings, ^{d} Full width at half maximum.

The isomer shifts range from 0.46 (**7**) to 0.55 (**2**). The quadrupole splittings of **6** and **7** are similar (1.12 and 1.18, respectively), while the value obtained for **2** differs (0.87). The isomer shifts and quadrupole splittings of the related complexes [K([18]crown-6)][Cp*Fe(anthracene)] (Cp* = C$_5$Me$_5$; δ = 0.56 mm·s^{-1}, ΔE_Q = 2.56 mm·s^{-1}, T = 78 K), [K([18]crown-6)(thf)$_2$][Fe(1,3-tBu$_2$C$_2$P$_2$)$_2$] (δ = 0.431 mm·s^{-1}, ΔE_Q = 1.16 mm·s^{-1}, T = 85 K)[24] and [K([18]crown-6)(thf)$_{0.2}$][(^{Dipp}BIAN)Fe(1,5-cod)] (δ = 0.23 mm·s^{-1}, ΔE_Q = 2.26 mm·s^{-1}, T = 80 K) have been reported previously.[25–27] A comparison reveals that the isomer shift of the 1,2-diphosphacyclobutadiene iron complexes (**2** and **6**) are comparable to [K([18]crown-6)][Cp*Fe(anthracene)], whereas the 1,3-diphosphacyclobutadiene complex **7** compares best to the homoleptic complex [K([18]crown-6)(thf)$_2$][Fe(1,3-tBu$_2$C$_2$P$_2$)$_2$]. This comparison reveals that the iron centre in **7** has a lower electron density than in the isomeric complex **6** (Table 2), suggesting that the acceptor strength of the 1,2-diphosphacyclobutadiene ligand is higher compared to its 1,3-isomer. As shown in Table 2, the quadrupole splittings were well reproduced by CASSCF calculations. Moreover, the electron densities on the iron nuclei of all complexes were calculated, giving a similar trend as the isomer shifts. As such, the electron density on the iron atom in **2** is the lowest, which is in agreement with its rather high isomer shift.

Finally, analysis of the localised occupied orbitals in [(^{Dmp}BIAN)Co(1,2-tBu$_2$C$_2$P$_2$)]$^-$ (**4′**) and [(^{Dmp}BIAN)Co(1,3-tBu$_2$C$_2$P$_2$)]$^-$ (**5′**) by CASSCF (see Supporting Information for computational details) shows the presence of two lone pairs on the N-atoms of the ^{Dmp}BIAN ligand as well as a double bond for the C11−C12 bond (Figure S39, Figure S40) for both complexes. In addition, the Mayer bond indices in the ^{Dmp}BIAN complexes **4′**, **5′**, **6′** and **7′** for the N1−C11 and N2−C12 bonds are close to the values of single bonds (ranging from 1.13 to 1.29), whereas the values for the C11−C12 bonds range from 1.95 to 2.07, providing further evidence for the presence of a C=C double bond. Hence, the computational analyses indicate that the dianionic form BIAN^{2-} is likely present in our complexes. This is in contrast to the analysis from crystallography, which implied monoanionic BIAN$^-$ ligands, but is in line with the Mössbauer spectroscopic data.

Further analysis of the CASSCF natural orbitals shows that the tBu$_2$C$_2$P$_2$ ligands form highly covalent bonds to the metal centre for complexes **4′, 5′, 6′, 7′** and [Fe(1,2-tBu$_2$C$_2$P$_2$)(anthracene)]$^-$ (see e.g. Figure S38). Such high covalency has been observed in previous DFT studies on the electronic structure of diphosphacyclobutadiene complexes and makes the assignment of an oxidation state to the metal centres ambiguous.[26] Overall, and considering the presence of BIAN^{2-}, the bonding scenario can be described as being intermediate between two extreme cases, namely a neutral π-accepting tBu$_2$C$_2$P$_2$ ligand and a metal(I) centre or a dianionic π-donating tBu$_2$C$_2$P$_2$ ligand and a metal(III) centre.

8.3   Conclusion

In summary, we have shown that the recently reported mixed tetrahedrane (tBuCP)$_2$ (**1**) acts as a reliable source of previously difficult-to-access 1,2-diphosphacyclobutadiene ligands in reactions with cobalt and iron metalates. While these 1,2-isomers are available by P−C bond cleavage of the C$_2$P$_2$ tetrahedron, the corresponding 1,3-isomers are also available by head-to-tail cyclodimerisation of tBuCP upon reaction with the same metalates. In this manner it has been possible to rapidly prepare a family of iron and cobalt complexes, including both homoleptic and heteroleptic examples. Such convenient access to both isomers has permitted direct comparative studies of their reactivity, establishing clear differences in the behaviour of the 1,2- and 1,3-complexes. These have revealed the particular utility of 1,2-diphosphacyclobutadiene complexes for further transformations, as exemplified by unprecedented preparations of both an diorgano-substituted triphospholium ligand and a tBu$_2$C$_2$P$_2$ ligand in a μ^2:η^4,η^4-coordination mode. Further reactivity studies on the use of the new metalates in synthesis and catalysis are ongoing.

8.4   Experimental Details

General Synthetic Methods

All reactions and product manipulations were carried out in flame-dried glassware under an inert atmosphere of argon using standard Schlenk-line or glovebox techniques (maintained at <0.1 ppm H$_2$O and <0.1 ppm O$_2$). [K(thf)$_{0.2}$][Co(η^4-cod)$_2$],[28] [K([18]crown-6)][Fe(anthracene)$_2$],[29] [K(dme)$_2$][Co(anthracene)$_2$],[30] [K(thf)$_{1.5}$][(^{Dipp}BIAN)Co(η^4-cod)],[13] [K([18]crown-6)][(^{Dipp}BIAN)Fe(η^4-cod)],[27] (tBuCP)$_2$[6] and tBuCP were prepared according to previously reported procedures. All other chemicals were purchased from commercial suppliers and used without further purification.

Solvents were dried and degassed with a MBraun SPS800solvent purification system. All dry solvents except n-hexane and n-pentane were stored under argon over activated 3 Å molecular sieves in gas-tight ampules. n-Hexane and n-pentane were instead stored over a potassium mirror.

General Analytical Techniques

NMR spectra were recorded on Bruker Avance 300 or 400 spectrometers at 300 K unless otherwise noted and internally referenced to residual solvent resonances (^{1}H NMR: THF-d_8: 1.72 ppm, C_6D_6: 7.16 ppm, toluene-d_8 (tol-d_8): 2.08 ppm; $^{13}C\{^1H\}$ NMR: THF-d_8: 25.31 ppm, C_6D_6: 128.06 ppm). Chemical shifts δ are given in ppm referring to external standards of tetramethylsilane (^{1}H, $^{13}C\{^1H\}$), 85% phosphoric acid (^{31}P and $^{31}P\{^1H\}$ spectra). ^{1}H and ^{13}C NMR signals were assigned based on 2D NMR spectra (^{1}H,^{1}H-COSY, ^{1}H,^{13}C-HSQC, ^{1}H,^{13}C-HMQC). UV/Vis spectra were recorded on an Ocean Optics Flame Spectrometer. Elemental analysis were performed by the central analytics department of the University of Regensburg.

8.4.1 Synthesis of Compounds

[K([18]crown-6)][Fe(1,2-*t*Bu₂C₂P₂)(anthracene)] (2)

To a deep red, cold (−70 °C) solution of [K([18]crown-6)][Fe(anthracene)₂] (1053.4 mg, 1.23 mmol, 1.0 eq.) was added (*t*BuCP)₂ (3.0 mL, c = 0.5 M in toluene, 1.47 mmol, 1.2 eq.). After stirring overnight and allowing the solution to warm to ambient temperature, a colour change to deep green was observed. Subsequently, the solvent was removed and the dark green residue was dried *in vacuo*. The residue was washed with *n*-hexane (30 mL) and benzene (30 mL) and dried *in vacuo*. After extraction with THF (10 mL), the deep green solution was layered with *n*-hexane (60 mL). Slow diffusion over 3 days at ambient temperature afforded green blocks of [K([18]crown-6)][Fe(1,2-*t*Bu₂C₂P₂)(anthracene)] (2), which were isolated by decanting the supernatant and dried *in vacuo*. These crystals still contain residual benzene (Figure S1), which can be removed upon grinding the sample and further drying *in vacuo*.

Single crystals suitable for X-ray diffraction were obtained by slow diffusion of *n*-hexane into a saturated solution of **2** in benzene.

$C_{36}H_{52}FeKO_6P_2$, MW = 737.70 g/mol
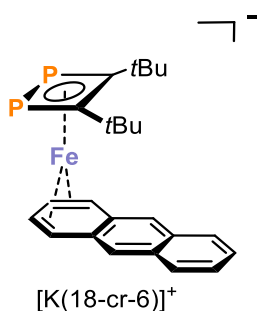
Yield: 760 mg (84%)

^{1}H NMR (400 MHz, 300 K, THF-d_8) No signal was observed in the range −150 – 150 ppm.

Evans-NMR: μ = 1.9(1) μ$_B$.

$^{31}P\{^1H\}$ (162 MHz, 300 K, C_6D_6) No signal was observed in the range −150 – 150 ppm.

Elemental Analysis calcd. C 58.61, H 7.11; found C 59.33, H 7.20.

UV/Vis (THF): λ_{max} (nm, ε_{max} /L·mol^{-1}·cm^{-1}) 330 (19 000), 440 (7 000), 650 (6 000).

[K(1,4-dioxane)][(^DippBIAN)Co(1,2-*t*Bu₂C₂P₂)] (4):

To a solution of [K(thf)$_{1.5}$][(^DippBIAN)Co(η⁴-cod)] (250 mg, 0.32 mmol, 1.0 eq) in THF (5 mL) was added (*t*BuCP)$_2$ (1.2 mL, c = 0.4 M in toluene, 0.48 mmol, 1.5 eq.). The deep green solution was stirred at ambient temperature for three days whilst turning turquoise. Subsequently, the solvent was removed *in vacuo* and the residue was washed with *n*-hexane (15 mL) and extracted with 1,4-dioxane (20 mL). The solution was concentrated to ca. 5 mL and layered with *n*-hexane (30 mL). Storage at room temperature for 5 days afforded deep turquoise crystals of [K(1,4-dioxane)][^DippBIANCo(1,2-*t*Bu₂C₂P₂)] (**4**). The supernatant was decanted and the crystals were dried *in vacuo*. Elemental analysis and the ¹H and ¹³C{¹H} NMR spectra indicate that the 1,4-dioxane molecule remains in the crystalline solid after drying.

Crystals suitable for X-ray crystallography were grown by slow diffusion of *n*-hexane into a saturated solution of **4** in 1,4-dioxane at ambient temperature.

$C_{50}H_{66}CoKN_2O_2P_2$, MW = 887.07 g/mol
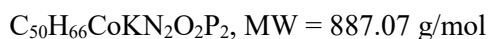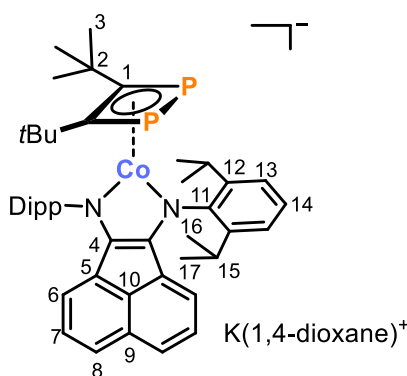
Yield: 180 mg (63%)

¹H NMR (400 MHz, 300 K, THF-d₈) δ = 0.81 (d, $^3J_{HH}$ = 6.7 Hz, 12H, C¹⁶H), 1.10 (s, 18H, C³H), 1.27 (d, $^3J_{HH}$ = 6.8 Hz, C¹⁷H), 3.55 (s, 8H, 1,4-dioxane), 4.71 (sept, $^3J_{HH}$ = 6.7 Hz, 4H, C¹⁵H), 4.99 (d, $^3J_{HH}$ = 7.0 Hz, 2H, C⁶H), 6.42 (pseudo-t, $^3J_{HH}$ = 7.6 Hz, 2H, C⁷H), 6.61 (d, $^3J_{HH}$ = 8.2 Hz, 2H, C⁸H), 7.14 (m, 6H, C¹³⁺¹⁴H) ppm.

¹³C{¹H} NMR (100 MHz, 300 K, THF-d₈) δ = 24.8 (s, C¹⁷, overlapping with THF-signal), 26.2 (s, C¹⁶), 29.0 (s, C¹⁵), 33.0 (s, C³), 37.0 (s, C²), 67.3 (s, C^{1,4-dioxane}, overlapping with THF signal), 105.2 (br s, C¹), 116.7 (s, C⁶), 119.6 (s, C⁸), 123.3 (s, C¹³), 123.8 (s, C¹⁴), 127.7 (s, C⁷), 129.5 (s, C⁹), 136.1 (s, C⁵), 137.3 (s, C¹⁰), 142.5 (s, C¹²), 150.2 (s, C⁴), 161.6 (s, C¹¹) ppm.

³¹P{¹H} (162 MHz, 300 K, THF-d₈) δ = −121.8 (s) ppm.

Elemental Analysis calcd. C 67.70, H 7.50, N 3.16; found C 67.63, H 7.45, N 3.01.

UV/Vis (THF): λ$_{max}$ (nm, ε$_{max}$ /L·mol⁻¹·cm⁻¹) 270 (17 000), 380 (5 400sh), 630 (22 000).

[K(thf)₃][(^DippBIAN)Co(1,3-*t*Bu₂C₂P₂)] (5):

A previously described protocol for the synthesis of **5** was adapted.[1]

A solution of *t*BuCP (0.18 mL, c = 3.2 M in TMS₂O, 0.58 mmol, 2.1 eq) was added dropwise to a cold (−30 °C) solution of [K(thf)$_{1.5}$][(^DippBIAN)Co(η⁴-cod)] (200 mg, 0.27 mmol, 1.0 eq) in THF

(5 mL). The green solution turned turquoise immediately and was stirred for 18 hours at ambient temperature. After removal of the solvent *in vacuo*, the residue was washed with *n*-hexane (5 mL) and extracted with THF (3.0 mL). Layering the solution with *n*-hexane (15 mL) and storage at room temperature afforded deep turquoise crystals of [K(thf)$_3$][Co(^{Dipp}BIAN)(1,3-*t*Bu$_2$C$_2$P$_2$)]. The supernatant was decanted and the crystals were dried *in vacuo*. Elemental analysis and the ^{1}H and ^{13}C{^{1}H} NMR spectra indicate that three THF molecules remain in the crystalline solid after drying.

Crystals suitable for X-ray crystallography were grown by slow diffusion of *n*-hexane into a saturated solution of [K(thf)$_3$][Co(^{Dipp}BIAN)(1,3-*t*Bu$_2$C$_2$P$_2$)] in THF at ambient temperature.

C$_{58}$H$_{82}$CoKN$_2$O$_3$P$_2$, MW = 1015.28 g/mol
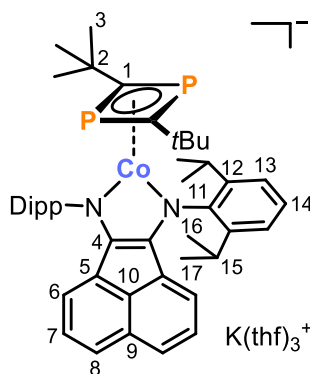
Yield: 175 mg (64%)

^{1}H NMR (400 MHz, 300 K, THF-d$_8$) δ = 0.80 (br m, 12H, C$^{16/17}$H), 0.93 (br s, 18H, C^{3}H), 1.33 (br m, 12H, C$^{16/17}$H), 5.00 (br m, 6H, C^{15}H/CH^{BIAN}), 6.36 (br m, 2H, CH^{BIAN}), 6.61 (br m, 2H, CH^{BIAN}), 7.14 (br m, 6H, C$^{13/14}$H) ppm.

^{13}C{^{1}H} NMR (100 MHz, 300 K, THF-d$_8$) δ = 25.2 (s, C$^{16/17}$), 26.4 (s, C$^{16/17}$), 28.7 (s, C^2), 32.5 (t, $^3J_{PC}$ = 4.9 Hz, C^3), 34.3 (t, $^2J_{PC}$ = 6.6 Hz, C^2), 89.4 (t, $^1J_{PC}$ = 49.5 Hz, C^1), 116.4 (s, C$^{4-10}$), 119.3 (s, C$^{4-10}$), 123.4 (s, C$^{13/14}$), 123.5 (s , C$^{13/14}$), 127.5 (s, C$^{4-10}$), 128.9 (s, C$^{4-10}$), 136.1 (s, C$^{4-10}$) 137.3 (s, C$^{4-10}$), 143.5 (s, C$^{4-10}$), 146.9 (s, C^{12}), 160.5 (s, C^{11}) ppm.

^{31}P{^{1}H} NMR (162 MHz, 300 K, THF-d$_8$) δ = 1.8 (s) ppm.

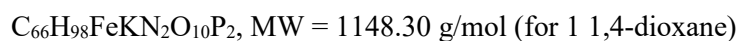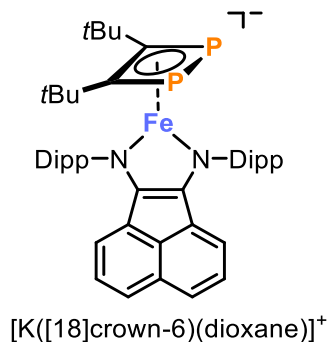**Elemental Analysis** calcd. C 68.62, H 8.14, N 2.76, found. C 68.63, H 7.96, N 2.60.

UV/Vis (THF) λ_{max} (nm, ε_{max} /L·mol^{-1}·cm^{-1}): 294 (22800), 388 (6000), 605 (16700), 738 (7800).

[K([18]crown-6)(dioxane)][(^{Dipp}BIAN)Fe(1,2-*t*Bu$_2$C$_2$P$_2$)] (6):

To a solution of [K([18]crown-6)(thf)$_2$][(^{Dipp}BIAN)Fe(η^4-cod)] (400 mg, 0.36 mmol, 1.0 eq) in THF (20 mL) was added (*t*BuCP)$_2$ (2.3 mL, c = 0.5 M in toluene, 1.14 mmol, 1.5 eq) at ambient temperature. The green solution turned dark blue after 10 minutes and was stirred at ambient temperature for 3 days. After removal of the solvent *in vacuo*, the residue was washed with *n*-hexane (50 mL) and extracted with 1,4-dioxane (200 mL). Subsequently, the solution was concentrated to ca. 50 mL and layered with *n*-hexane (400 mL). Storage at room temperature for

4 days afforded deep blue crystals of $[K([18]crown-6)(1,4-dioxane)][Fe(^{Dipp}BIAN)(1,2-tBu_2C_2P_2)]$ (**6**) The supernatant was decanted and the crystals were dried *in vacuo*. Elemental analysis and the ^1H and $^{13}C\{^1H\}$ NMR spectra indicate that the 1,4-dioxane molecule remains in the crystalline solid after drying.

Crystals suitable for X-ray crystallography were grown by slow diffusion of *n*-hexane into a saturated solution of **6** in 1,4-dioxane at ambient temperature.

$C_{66}H_{98}FeKN_2O_{10}P_2$, MW = 1148.30 g/mol (for 1 1,4-dioxane)

Yield: 290 mg (70%)

^1H NMR (400 MHz, 300 K, THF-d_8) δ = −3.86 (br s), 0.70 (br s), 2.75 (br s), 3.79 (s, 1,4-dioxane), 6.13 (br s), 7.74 (br s), 10.90 (br s) ppm.

Evans-NMR: μ = 2.0(1) $μ_B$

$^{31}P\{^1H\}$ (162 MHz, 300 K, THF-d_8) No signal was observed in the range −150 – 150 ppm.

Elemental Analysis calcd. C 64.85, H 7.90, N 2.44; found C 65.24, H 7.80, N 2.07.

UV/Vis (THF): $λ_{max}$ (nm, $ε_{max}$ /L·mol^{-1}·cm^{-1}) 280 (30 000sh), 350 (16 000sh), 430 (9 000sh), 570 (14 000), 810 (14 000).

[K([18]crown-6)(thf)₂][Fe(^{Dipp}BIAN)(1,3-*t*Bu₂C₂P₂)] (7)

A solution of *t*BuCP (0.22 mL, c = 3.5 M in TMS$_2$O, 0.28 mmol, 3.1 eq) was added dropwise to a cold (−30 °C) solution of $[K([18]crown-6)(thf)_2][(^{Dipp}BIAN)Fe(η^4-cod)]$ (400 mg, 0.36 mmol, 1.0 eq) in THF (20 mL). The green solution turned deep violet immediately and was stirred for 18 hours at ambient temperature. After removal of the solvent *in vacuo*, the residue was washed with *n*-hexane (20 mL) and extracted with THF (10 mL). Layering the solution with *n*-hexane (50 mL) and storage at room temperature afforded deep purple blocks of [K([18]crown-6)(thf)₂][Fe(^{Dipp}BIAN)(1,3-*t*Bu₂C₂P₂)]·THF. The supernatant was decanted and the crystals were dried *in vacuo*. Elemental analysis of the isolated, crystalline solid suggests a THF solvate with two K-coordinated and one additional THF molecule per formula unit.

Crystals suitable for X-ray crystallography of the 1,4-dioxane containing salt [K([18]crown-6)(thf)$_{1.8}$(1,4-dioxane)$_{0.2}$][Fe(^{Dipp}BIAN)(1,3-*t*Bu₂C₂P₂)] were grown by slow diffusion of *n*-hexane into a saturated solution of **7** in THF at ambient temperature. Minor amounts of 1,4-dioxane originated from initial crystallisation attempts with this solvent.

+ 1 THF solvate molecule

[K(18-cr-6)(thf)$_2$]$^+$
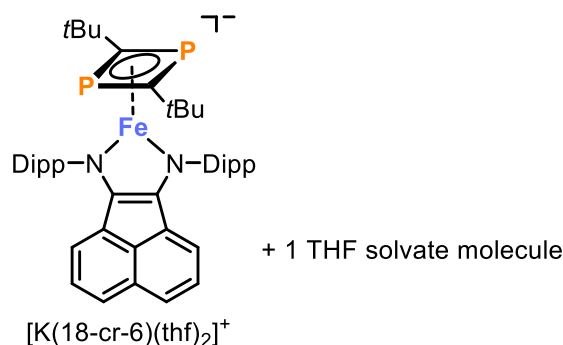
$C_{66}H_{98}FeKN_2O_8P_2 \cdot C_4H_8O$, MW = 1276.51 g/mol (for 3 THFs)

Yield: 180 mg (50%)

^{1}H NMR (400 MHz, 300 K, THF-d$_8$) δ = −3.53 (br s), −1.68 (br s), 2.17 (br s), 6.82 (br s), 7.91 (br s), 8.73 (br s), 10.62 (br s) ppm.

Evans-NMR: μ = 2.0(1) μ$_B$

**^{31}P{^{1}H}** (162 MHz, 300 K, THF-d$_8$) No signal was observed in the range −150 – 150 ppm.

Elemental Analysis calcd. for [K([18]crown-6)(thf)$_2$][Fe(^{Dipp}BIAN)(1,3-tBu$_2$C$_2$P$_2$)]·THF ($C_{66}H_{98}FeKN_2O_8P_2 \cdot C_4H_8O$) with 3 THF molecules per complex: C 65.86, H 8.37, N 2.19; found C 65.92, H 8.09, N 2.09.

UV/Vis (THF): λ_{max} (nm, ε_{max} /L·mol^{-1}·cm^{-1}) 290 (29 000), 370 (14 000sh), 540 (12 000), 800 (12 000).

[{(^{Dipp}BIAN)Co}$_2$(μ^2:η^4,η^4-tBu$_2$C$_2$P$_2$)] (8):

To a solution of [K(1,4-dioxane)][^{Dipp}BIANCo(1,2-tBu$_2$C$_2$P$_2$)] (150 mg, 0.169 mmol, 1.0 eq) in THF (5 mL) at −80 °C was added Me$_3$SiCl (0.12 mL, c = 1.58 M in toluene, 0.19 mmol, 1.1 eq.). The solution was allowed to warm to room temperature within 18 hours. During that time, the colour of the reaction solution changed from turquoise to dark blue. Subsequently, the solvent was removed *in vacuo* and the residue was extracted with *n*-hexane (5 mL). Storage at −30 °C for three days afforded dark blue crystals of [{(^{Dipp}BIAN)Co}$_2$(μ^2:η^4,η^4-tBu$_2$C$_2$P$_2$)]. The supernatant was decanted and the crystals were *in vacuo*.

Crystals suitable for X-ray crystallography were grown by storing a saturated solution of [{(^{Dipp}BIAN)Co}$_2$(μ^2:η^4,η^4-tBu$_2$C$_2$P$_2$)] in *n*-hexane at ambient temperature overnight.
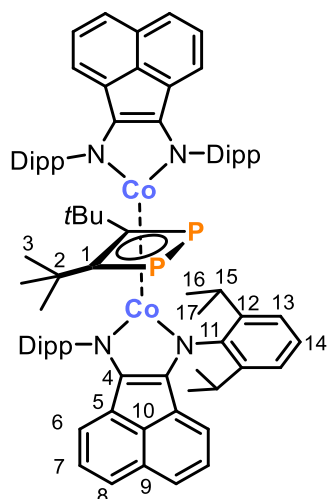
$C_{82}H_{98}Co_2N_4P_2$, MW = 1319.53 g/mol

Yield: 13 mg (12%)

^{1}H NMR (400 MHz, 300 K, C_6D_6) δ = 0.83 (d, $^3J_{HH}$ = 6.7 Hz, 24H, $C^{16}H$), 1.15 (s, 18H, C^3H), 1.20 (d, $^3J_{HH}$ = 6.7 Hz, $C^{17}H$), 3.7 (br s, 8H, $C^{15}H$), 6.55 (pseudo-t, $^3J_{HH}$ = 7.4 Hz, C^7H, overlapping with signal for C^6H), 6.58 (dd, $^3J_{HH}$ = 7.4 Hz, $^4J_{HH}$ = 1.2 Hz, C^6H), 7.11 (d, $^3J_{HH}$ = 7.8 Hz, $C^{13}H$), 7.38 (t, $^3J_{HH}$ = 7.8 Hz, $C^{14}H$), 7.89 (dd, $^3J_{HH}$ = 7.7 Hz, $^4J_{HH}$ = 1.1 Hz, C^9H) ppm.

$^{13}C\{^1H\}$ NMR (100 MHz, 300 K, C_6D_6) δ = 24.5 (s, C^{17}), 25.8 (s, C^{16}), 28.7 (s, C^{15}), 31.5 (s, C^3), 37.7 (s, C^2), 119.1 (s, C^6), 122.9 (s, C^8), 124.1 (s, C^{13}), 126.8 (s, C^{14}), 130.1 (s, C^{10}), 131.2 (s, C^7), 135.7 (s, C^{12}), 136.3 (s, C^9), 142.8 (s, C^5), 159.3 (s, C^{11}), 162.7 (s, C^4) ppm (C^1 could not be detected; ^{1}H / $^{13}C\{^1H\}$ HMBC suggests a signal at ca. 113 ppm).

**$^{31}P\{^1H\}$ NMR** (162 MHz, 300 K, C_6D_6) δ = 194.2 (s) ppm.

Elemental Analysis calcd C 74.64, H 7.49, N 4.25; found C 74.67, H 7.68, N 3.80.

UV/Vis (THF): λ_{max} (nm, ε_{max} /L·mol^{-1}·cm^{-1}) 330 (22 000sh), 480 (9 500), 620 (20 700), 830 (14 500).

[(^{Dipp}BIAN)Co(η^4-tBu$_2$C$_2$P$_3$Cy$_2$)] (9):

To a solution of [K(1,4-dioxane)][(^{Dipp}BIAN)Co(1,2-tBu$_2$C$_2$P$_2$)] (**4**, 85 mg, 0.096 mmol, 1.0 eq) in THF (3 mL) at −30 °C was added Pcy$_2$Cl (0.9 mL, c = 0.11 M in *n*-hexane, 0.10 mmol, 1.0 eq.). The turquoise solution turned dark blue immediately. After stirring for 30 minutes at ambient temperature, the solvent was removed *in vacuo*. The residue was extracted with an *n*-hexane/toluene-mixture (10:1 v/v, 5 mL). Storage at −30 °C for three days afforded dark blue crystals of [(^{Dipp}BIAN)Co(η^4-tBu$_2$C$_2$P$_3$Cy$_2$)]. The supernatant was decanted and the crystals were dried *in vacuo*. The complex crystallises as a solvate with n-hexane and toluene according to ^{1}H and $^{13}C\{^1H\}$ NMR and elemental analysis. A solvent content of 1 toluene and 0.5 n-hexane molecules per formula unit was determined.

Crystals suitable for X-ray crystallography were grown by storing a saturated solution of [(^{Dipp}BIAN)Co(η^4-tBu$_2$C$_2$P$_3$Cy$_2$)] in *n*-hexane at ambient temperature overnight.

$C_{58}H_{80}CoN_2P_3 \cdot 0.5C_6H_{14} \cdot C_7H_8$, 1092.38 g/mol
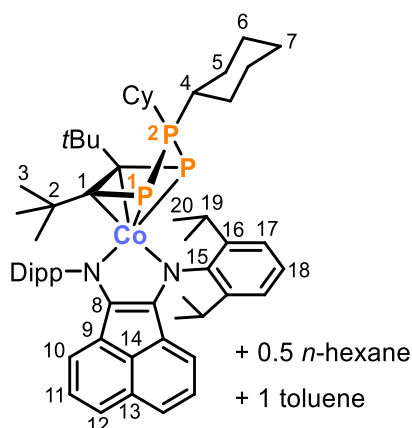
Yield: 65 mg (62%)

¹H NMR (400 MHz, 300 K, C_6D_6) δ = 0.73-0.93 (m, 9H, $C^{5-7}H$ + *n*-hexane), 0.97 (d, $^3J_{HH}$ = 6.5 Hz, 12H, $C^{20}H$), 1.13-1.63 (m, 19H, $C^{5-7}H$ + *n*-hexane), 1.67 (d, $^3J_{HH}$ = 6.5 Hz, 12H, $C^{20}H$), 1.76 (s, 18H, C^3H), 4.31 (sept, $^3J_{HH}$ = 6.5 Hz, 4H, $C^{19}H$), 5.85 (d, $^3J_{HH}$ = 7.1 Hz, 2H, $C^{10}H$), 6.77 (pseudo-t, $^3J_{HH}$ = 8.1 Hz, 2H, $C^{11}H$), 7.27 (d, $^3J_{HH}$ = 8.1 Hz, 2H, $C^{12}H$), 7.33 (d, $^3J_{HH}$ = 7.2 Hz, 4H, $C^{17}H$), 7.42 (t, $^3J_{HH}$ = 7.2 Hz, 2H, $C^{18}H$) ppm.

¹³C{¹H} NMR (100 MHz, 300 K, C_6D_6) δ = 25.2 (d, J = 4.5 Hz, C^{20}), 26.2 (m, C^{4-7}), 26.3 (s, $C^{20'}$), 27.1 (d, J = 9.5 Hz, C^{4-7}), 27.6 (d, J = 1.9 Hz, C^{4-7}), 29.0 (s, C^{19}), 30.4 (br s, C^{4-7}), 34.4 (dt, J = 24.1 Hz, 4.6 Hz, C^{4-7}), 36.8 (d, $^3J_{CP}$ = 14.5 Hz, C^3), 39.5 (d, $^2J_{CP}$ = 18.3 Hz, C^2), 40.9 (d, J = 16.4 Hz, C^{4-7}), 115.3 (m, C^1), 119.7 (s, C^{10}), 123.4 (s, C^{12}), 124.6 (s, C^{17}), 126.4 (s, C^{18}), 128.6 (s, C^{11}), 131.3 (s, C^{13}), 135.9 (s, C^9), 136.1 (s, C^{14}), 141.0 (s, C^{16}), 153.4 (s, C^8), 158.5 (s, C^{15}) ppm.

³¹P{¹H} (162 MHz, 300 K, C_6D_6) δ = −90.3 (d, $^1J_{PP}$ = 349.4 Hz, 2P, P^1), 55.5 (t, $^1J_{PP}$ = 349.6 Hz, 1P, P^2) ppm.

Elemental Analysis calcd. C 74.77, H 8.77, N 2.56; found C 75.01, H 8.62, N 2.40.

UV/Vis (THF): λ_{max} (nm, ε_{max} /L·mol⁻¹·cm⁻¹) 320 (17 000), 440 (9 300), 560 (12 000), 660 (12 500).

8.4.2   Additional Experiments

Reaction of [K(thf)₀.₂][Co(η⁴-cod)₂] with 1:

To a cold (−80 °C) solution of [K(thf)₀.₂][Co(η⁴-cod)₂] (50.0 mg, 0.15 mmol) was added (*t*BuCP)₂ (0.84 mL, 0.4 M in toluene, 0.33 mmol, 2.2 eq.). The solution was stirred overnight while allowing it to warm to ambient temperature and then analysed by ³¹P{¹H} NMR spectroscopy (Figure S16). Subsequently, the solvent was removed and the brown residue was dried *in vacuo*. The residue was washed with *n*-hexane (5 mL) and extracted with 1,4-dioxane (ca. 0.5 mL). Slow diffusion of *n*-hexane into this 1,4-dioxane solution afforded yellow crystals of both **3** and **3′**.

General procedure for reactions of [K(dioxane)][(^{Dipp}BIAN)Co(1,2-tBu$_2$C$_2$P$_2$)] (4) and [K(thf)$_3$][(^{Dipp}BIAN)Co(1,3-tBu$_2$C$_2$P$_2$)] (5) with electrophiles:

To a cold ($-80\,°C$) solution of [K(1,4-dioxane)][(^{Dipp}BIAN)Co(1,2-tBu$_2$C$_2$P$_2$)] (4) or [K(thf)$_3$][(^{Dipp}BIAN)Co(1,3-tBu$_2$C$_2$P$_2$)] (5) (ca. 0.03 mmol, 1.0 eq.) in THF (1 mL) was added reagent (see Table S1, 1.05 eq.). Subsequently, the reaction was stirred overnight while allowing it to warm to room temperature. The solution was transferred to an NMR tube and analysed by ^{31}P{^{1}H} NMR spectroscopy.

^{31}P{^{1}H} NMR spectra for the reactions are given in Figure S18 and Figure S19.

Table S1. Reagents and stock solutions used for reactivity studies of **4** and **5**.

Reagent	Stock solution
HCl	0.4 M in 1,4-dioxane
MeI	0.1 M in toluene
Me$_3$SiCl	0.5 M in toluene
Ph$_2$PCl	0.08 M in toluene
Cy$_2$PCl	0.11 M in toluene

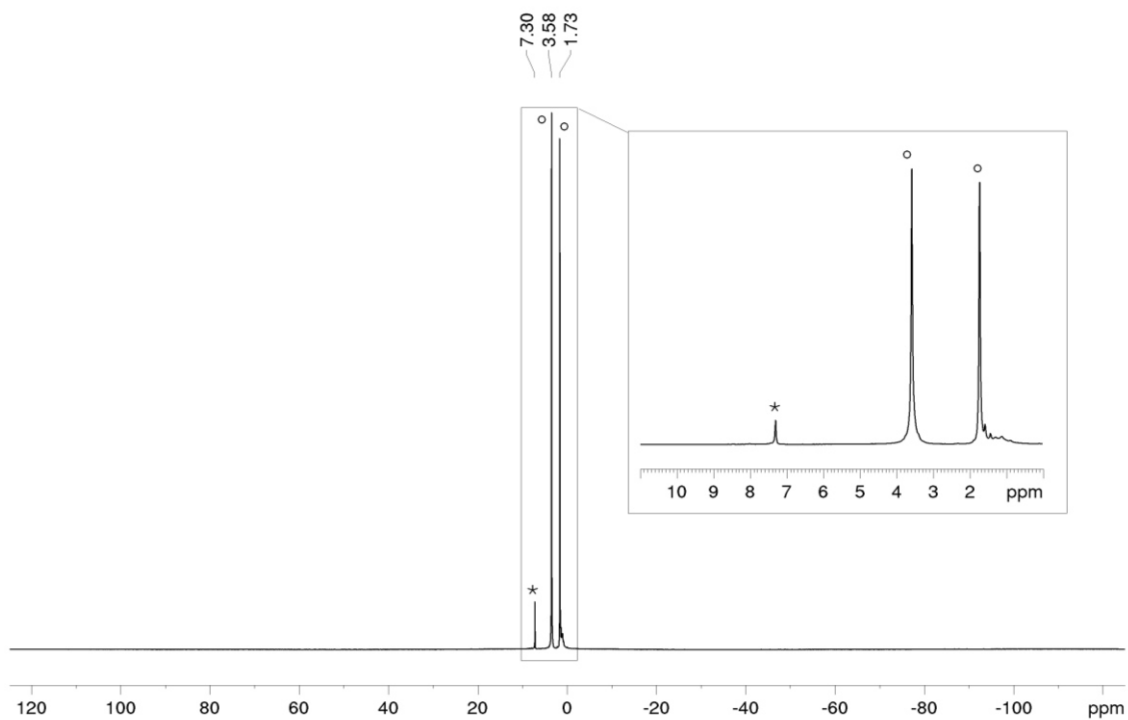### 8.4.3 NMR Spectra

Figure S1. ^{1}H NMR spectrum (400 MHz, 300 K, THF-d$_8$) of **2** *residual C$_6$H$_6$, °THF-d$_8$.
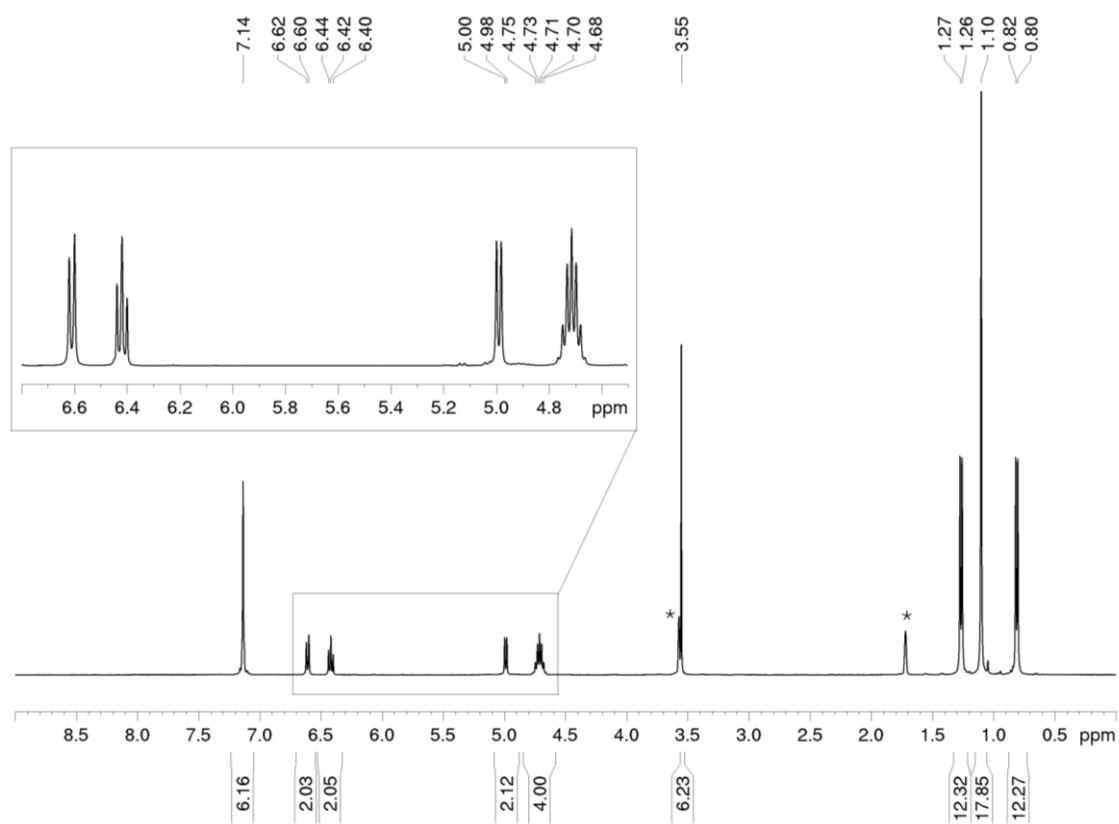
Figure S2. ^{1}H NMR spectrum (400 MHz, 300 K, THF-d$_8$) of **4** *THF-d$_8$.
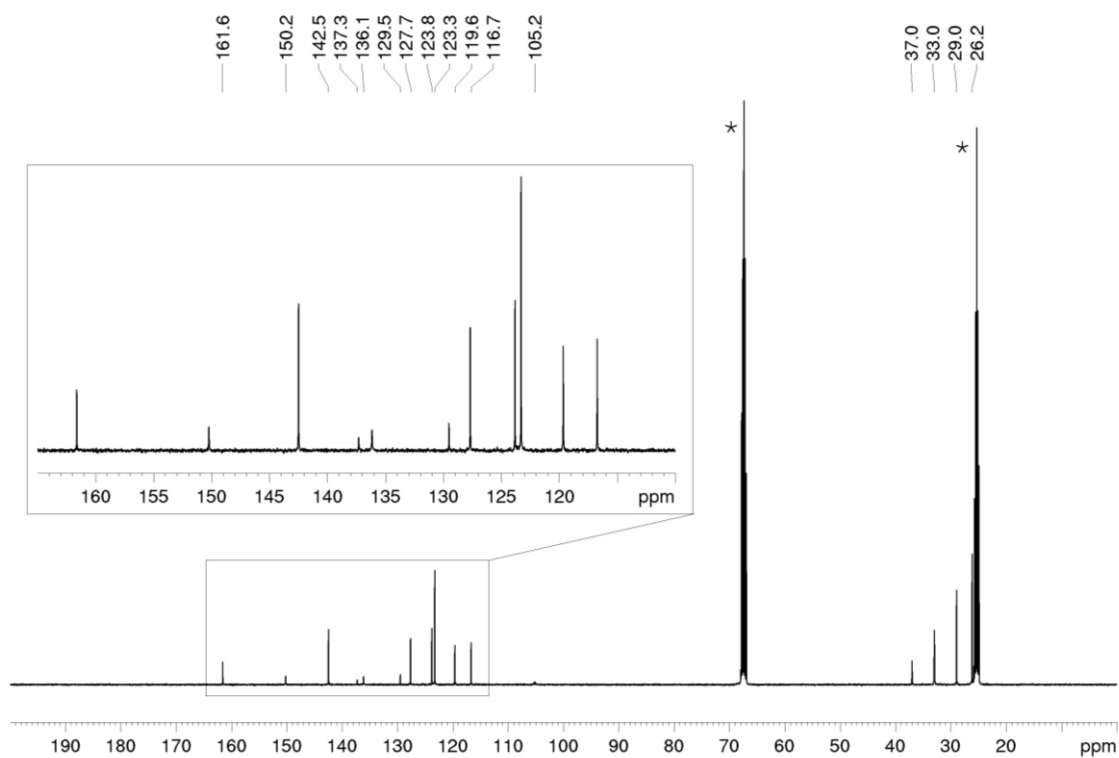
Figure S3. $^{13}C\{^{1}H\}$ NMR spectrum (100 MHz, 300 K, THF-d$_8$) of **4**; *THF-d$_8$.
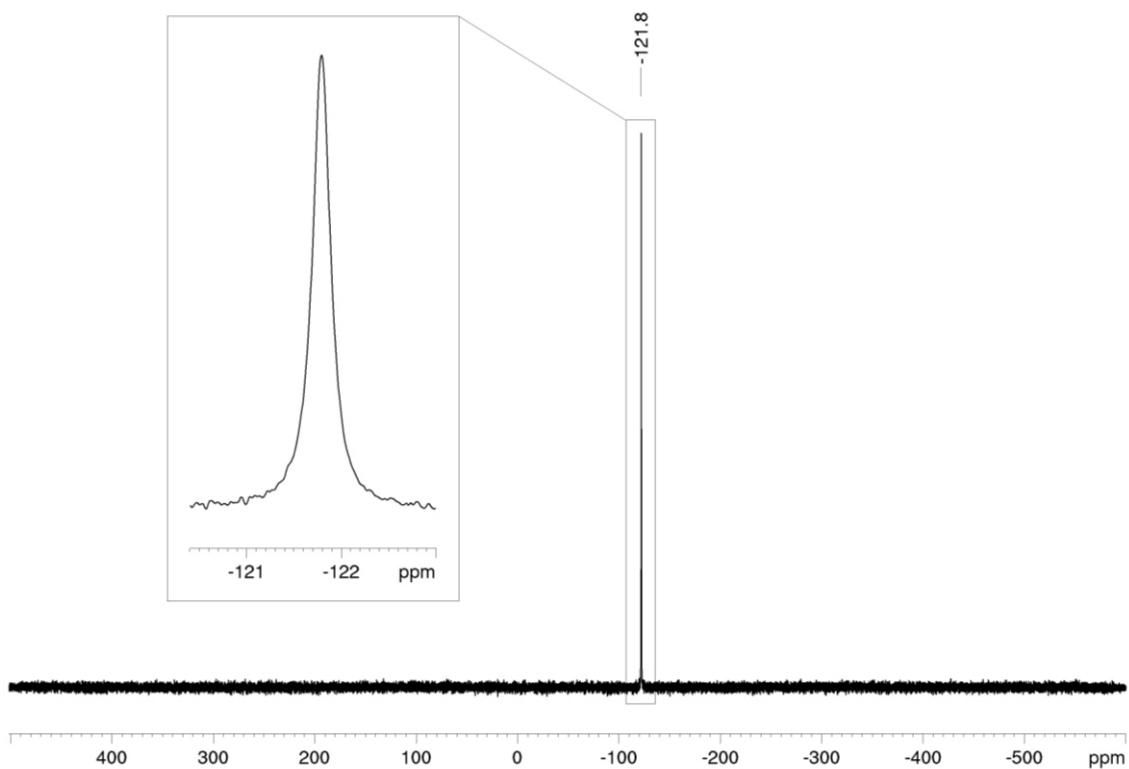
Figure S4. $^{31}P\{^{1}H\}$ NMR spectrum (162 MHz, 300 K, THF-d$_8$) of **4**.

211
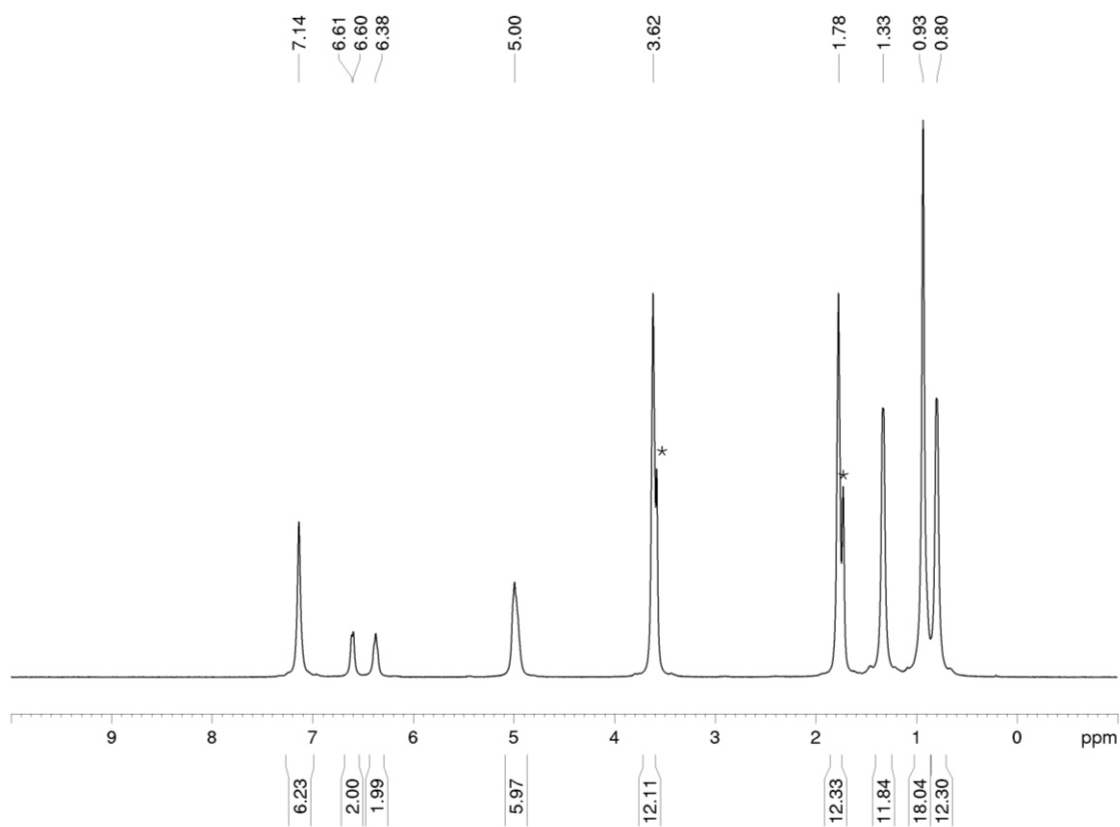
Figure S5. ^{1}H NMR spectrum (400 MHz, 300 K, THF-d$_8$) of **5** *THF-d$_8$.
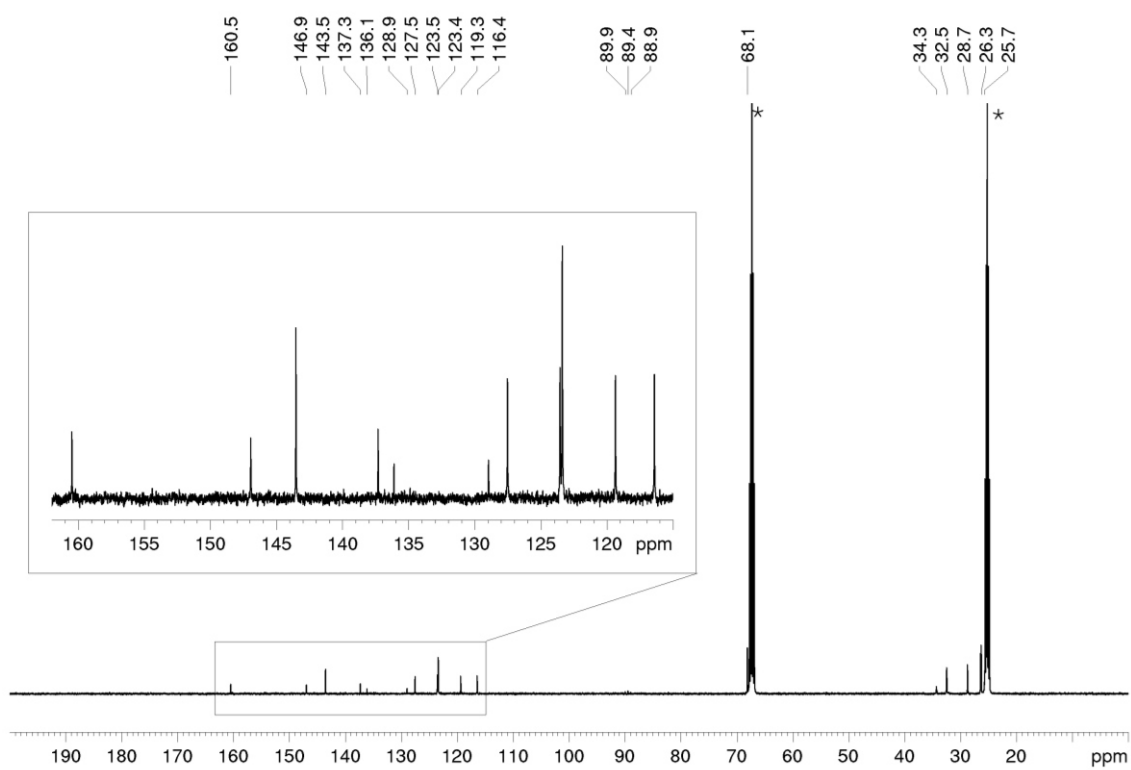
Figure S6. ^{13}C{^{1}H} NMR spectrum (100 MHz, 300 K, THF-d$_8$) of **5**; *THF-d$_8$.
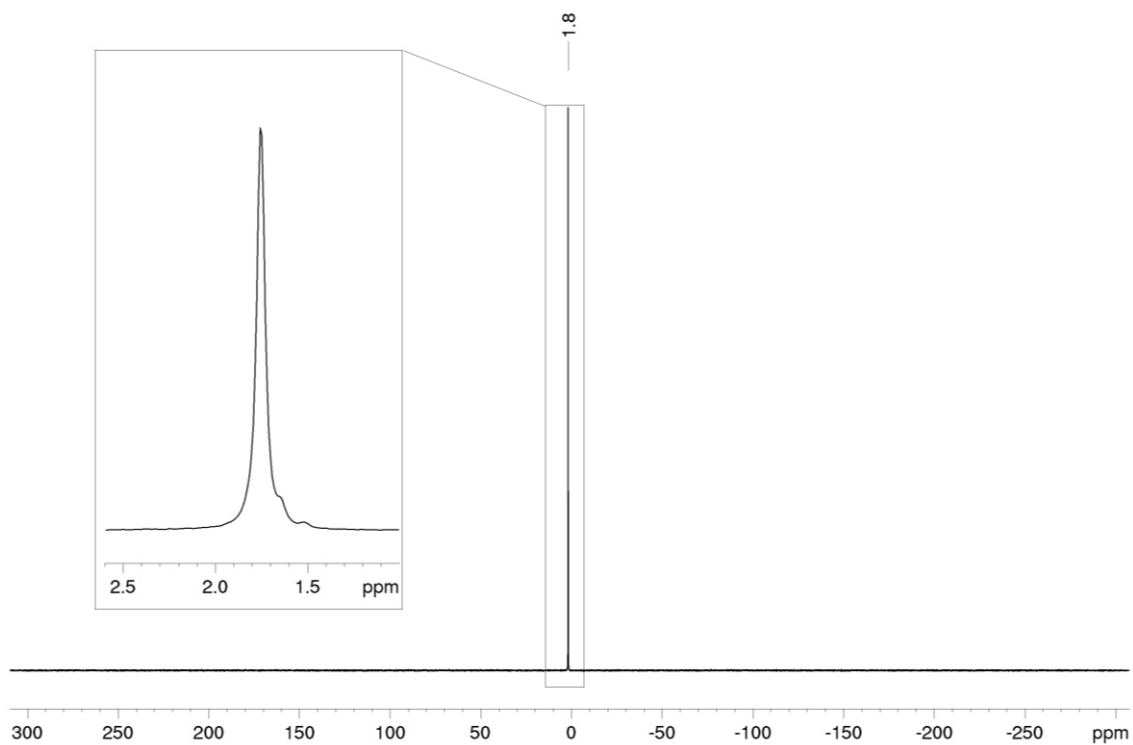
Figure S7. $^{31}P\{^1H\}$ NMR spectrum (162 MHz, 300 K, THF-d$_8$) of **5**.
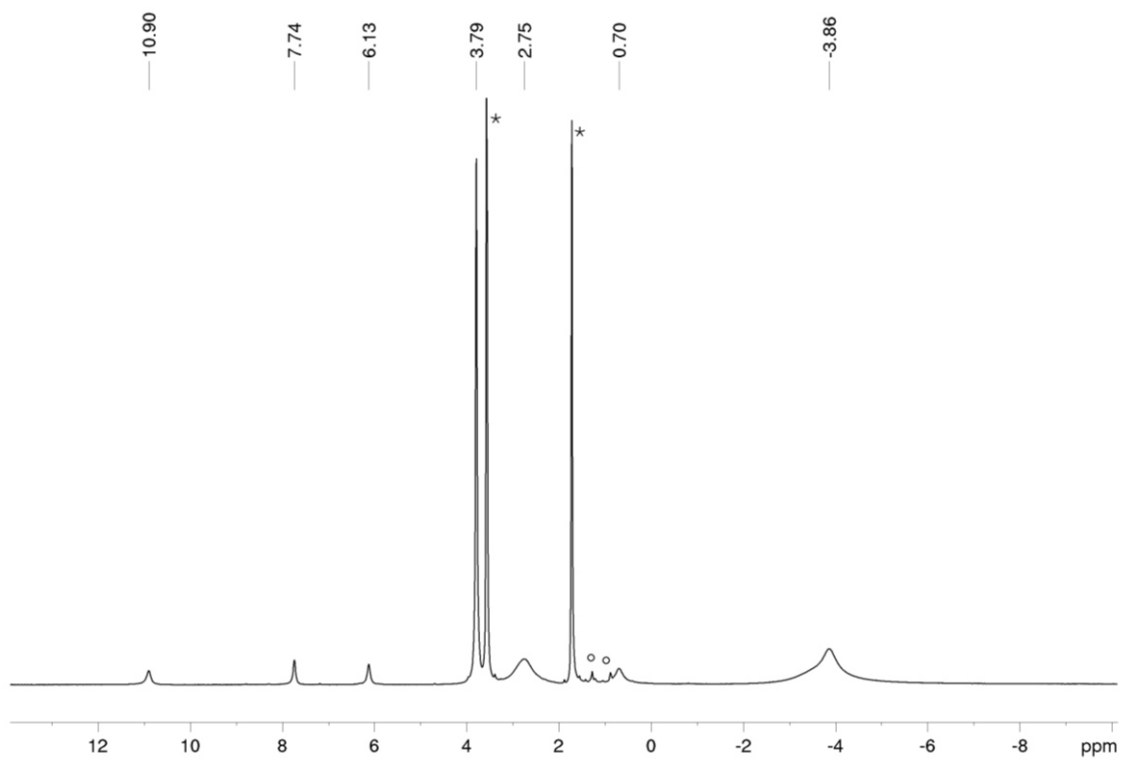
Figure S8. ^1H NMR spectrum (400 MHz, 300 K, THF-d$_8$) of **6** *THF-d$_8$, °n-hexane.
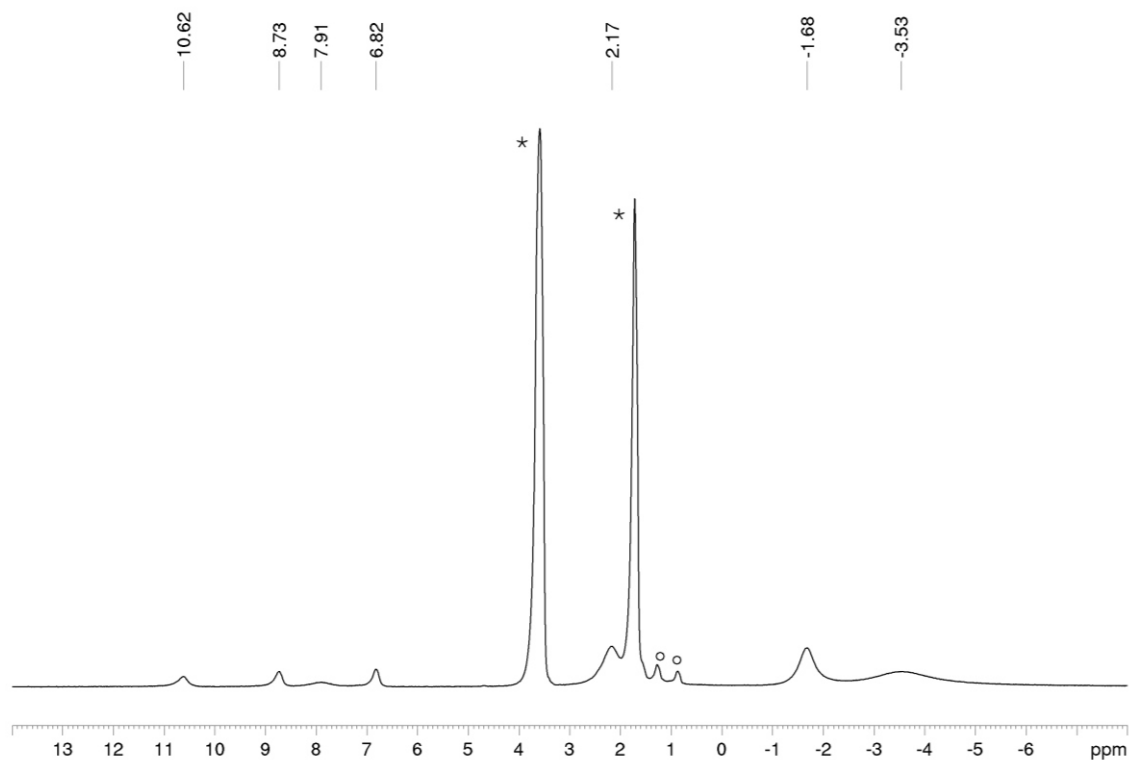
Figure S9. [^1]H NMR spectrum (400 MHz, 300 K, THF-d$_8$) of **7** *THF-d$_8$, °*n*-hexane.
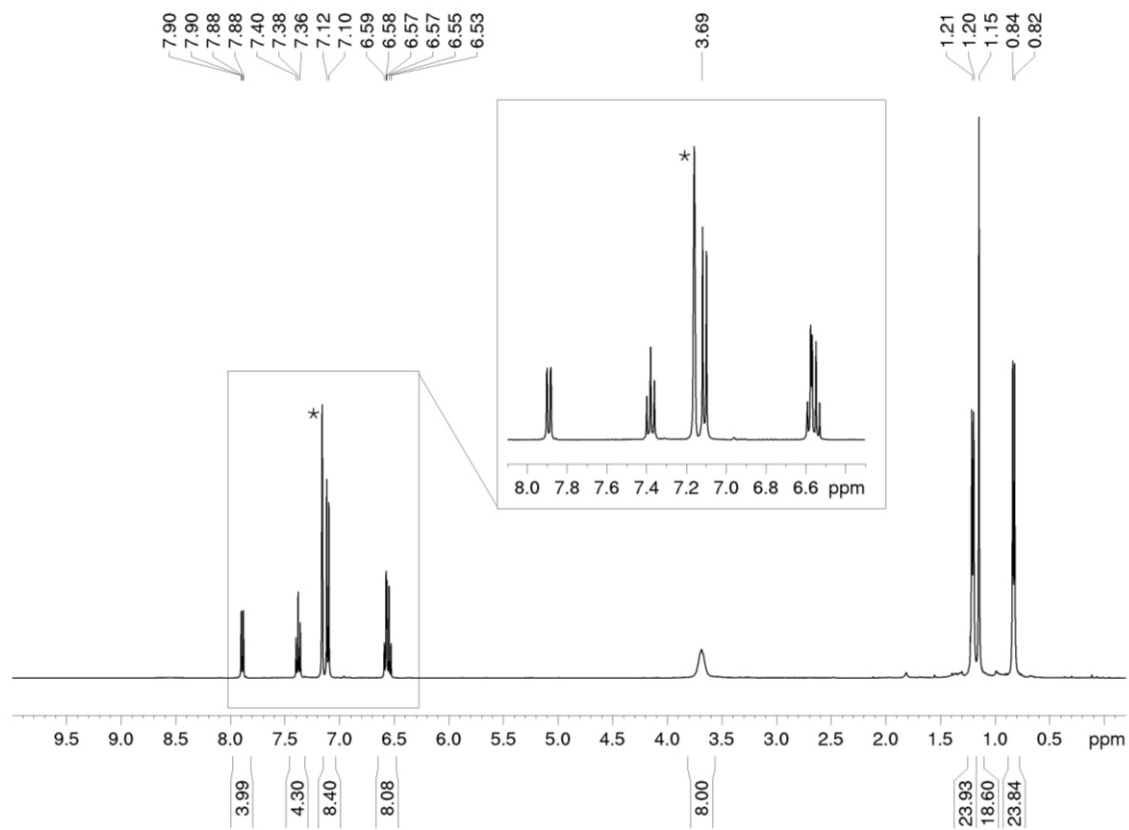
Figure S10. [^1]H NMR spectrum (400 MHz, 300 K, C$_6$D$_6$) of **8** *C$_6$D$_6$.
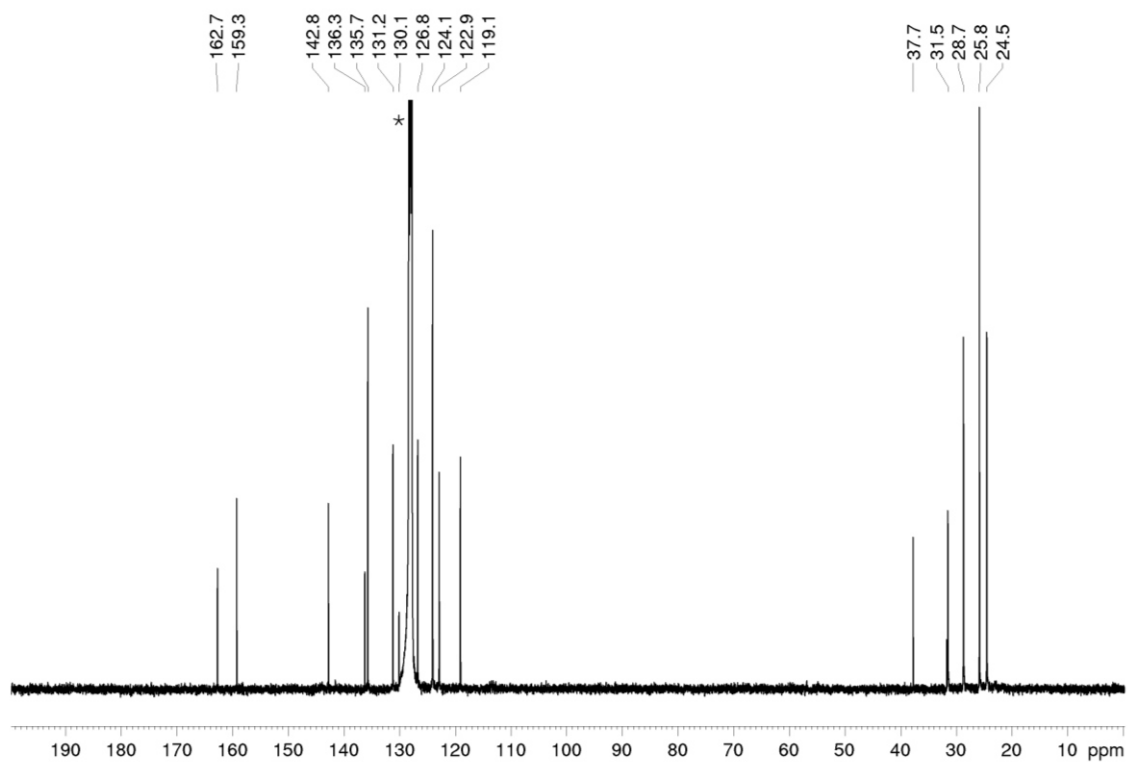
Figure S11. $^{13}C\{^1H\}$ NMR spectrum (100 MHz, 300 K, C_6D_6) of **8**; *C_6D_6.
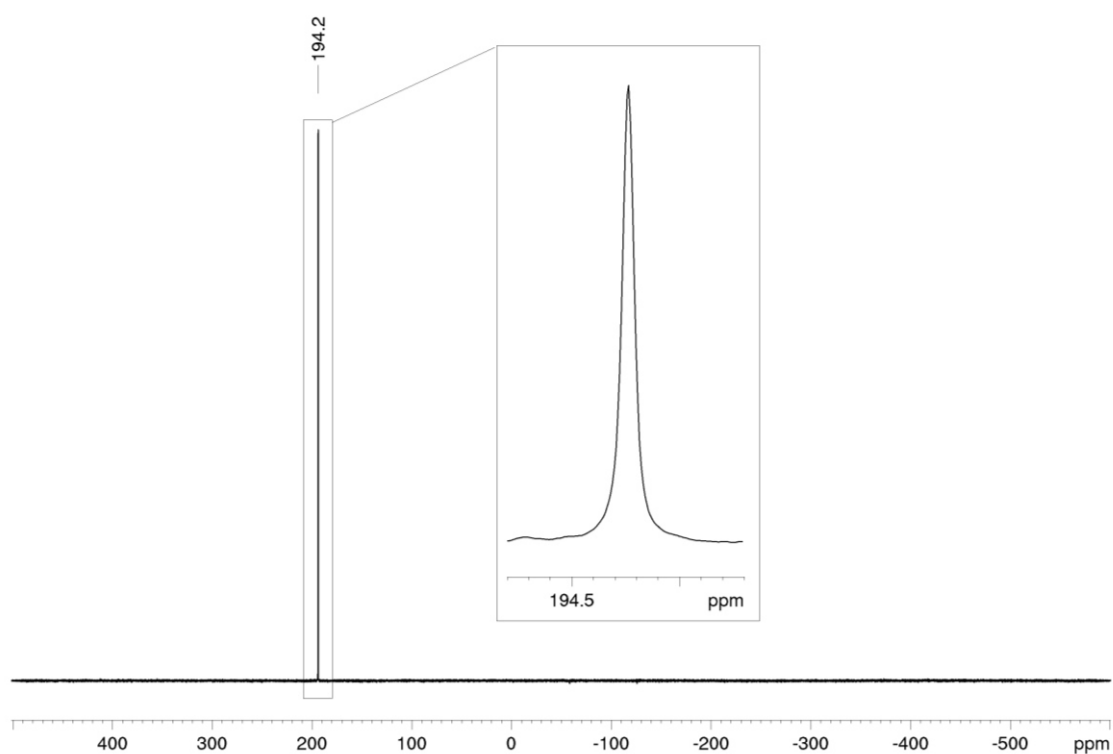
Figure S12. $^{31}P\{^1H\}$ NMR spectrum (162 MHz, 300 K, C_6D_6) of **8**.
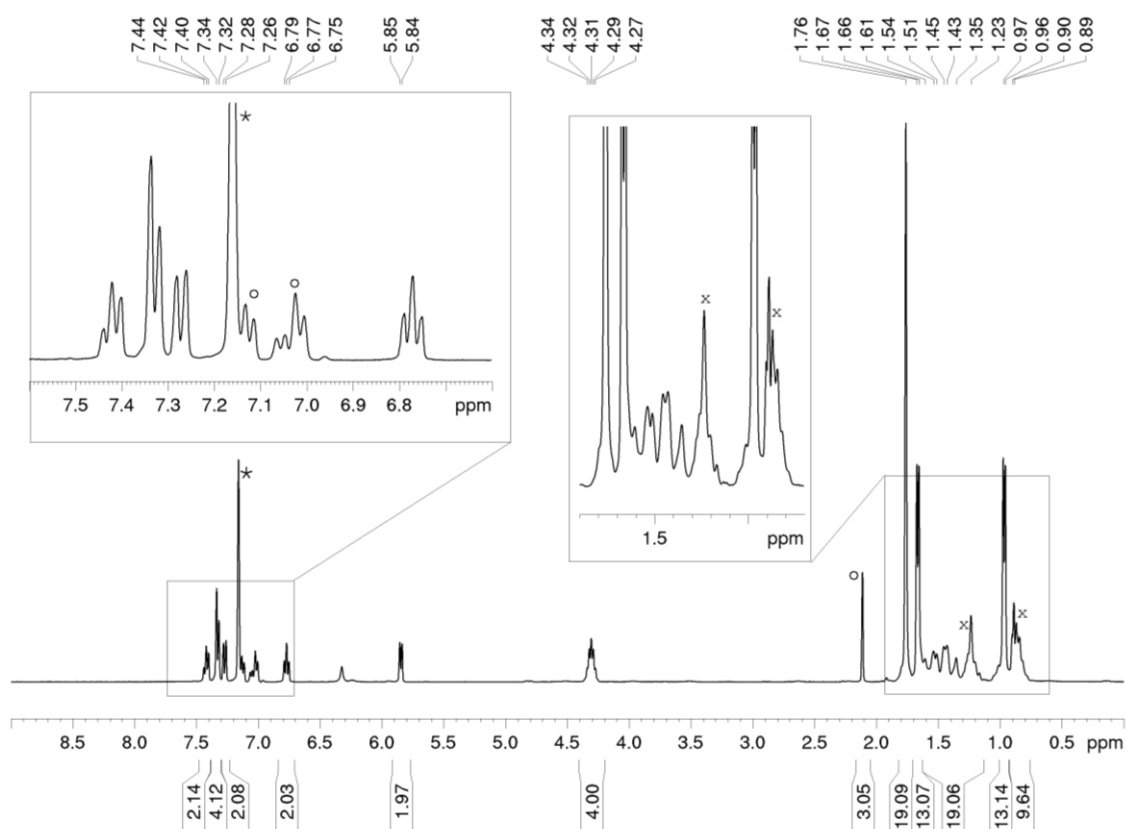
215

Figure S13. ^{1}H NMR spectrum (400 MHz, 300 K, C$_6$D$_6$) of **9** *C$_6$D$_6$, °residual toluene, ^{x}residual *n*-hexane.
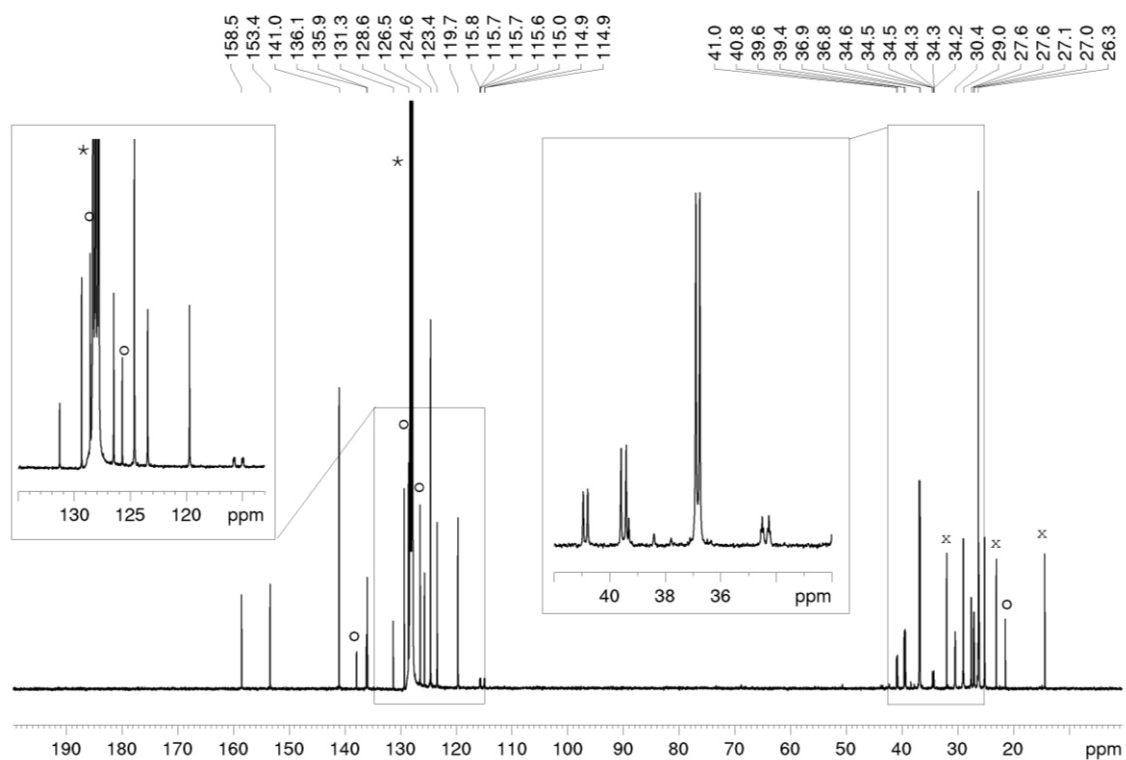
Figure S14. ^{13}C{^{1}H} NMR spectrum (100 MHz, 300 K, C$_6$D$_6$) of **9**; *C$_6$D$_6$, °residual toluene, ^{x}residual *n*-hexane.
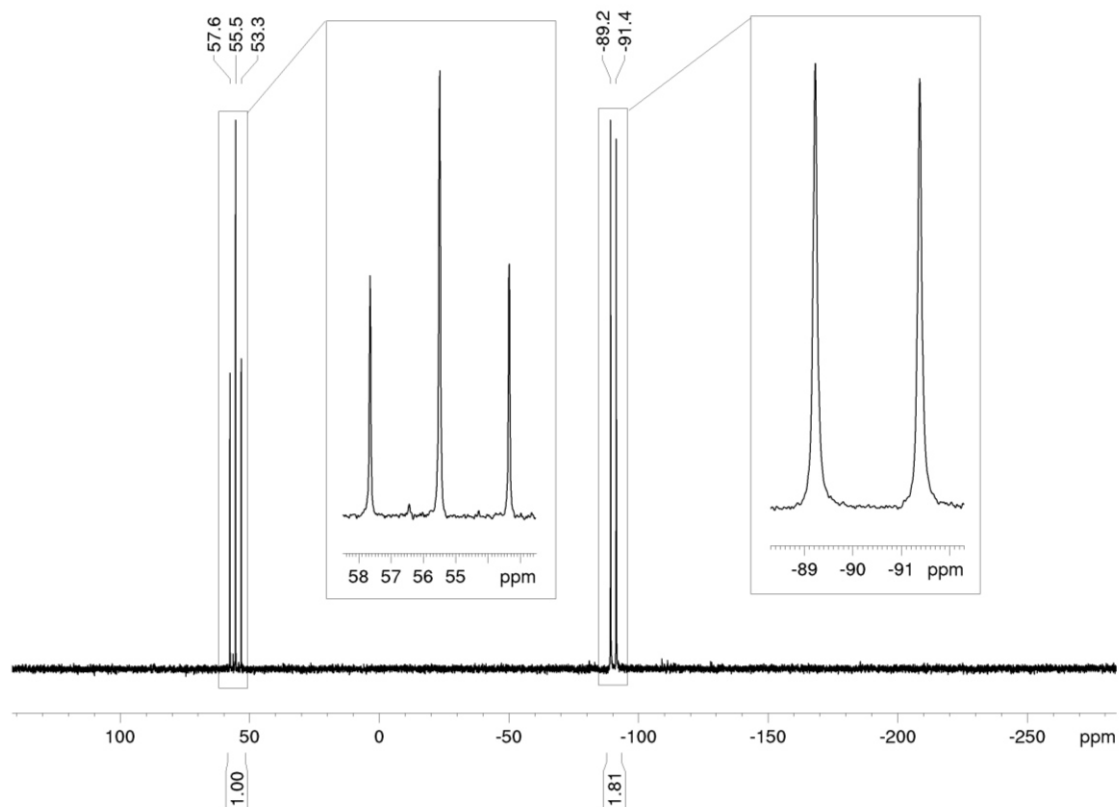
Figure S15. $^{31}P\{^1H\}$ NMR spectrum (162 MHz, 300 K, C_6D_6) of **9**.
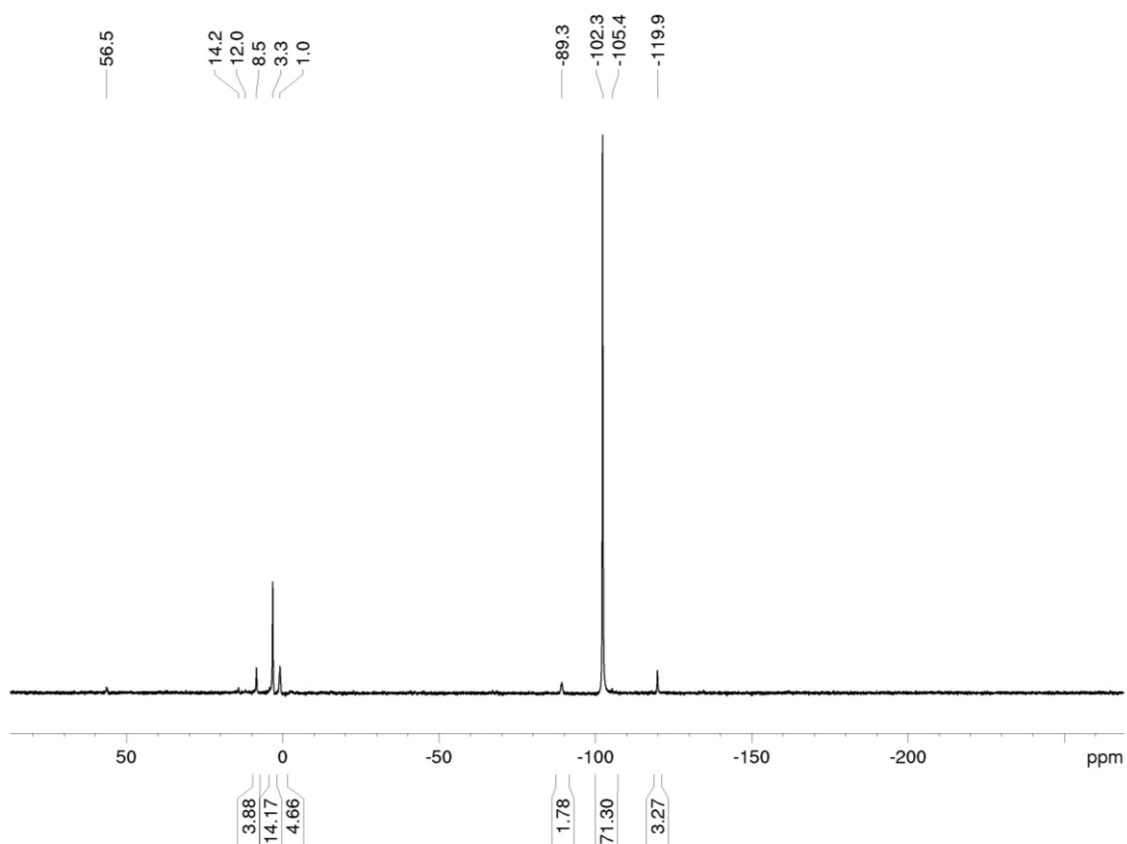
Figure S16. $^{31}P\{^1H\}$ NMR spectra (162 MHz, 300 K, C_6D_6) of the reaction of $[K(thf)_{0.2}][Co(\eta^4\text{-cod})_2]$ with **1**.

217
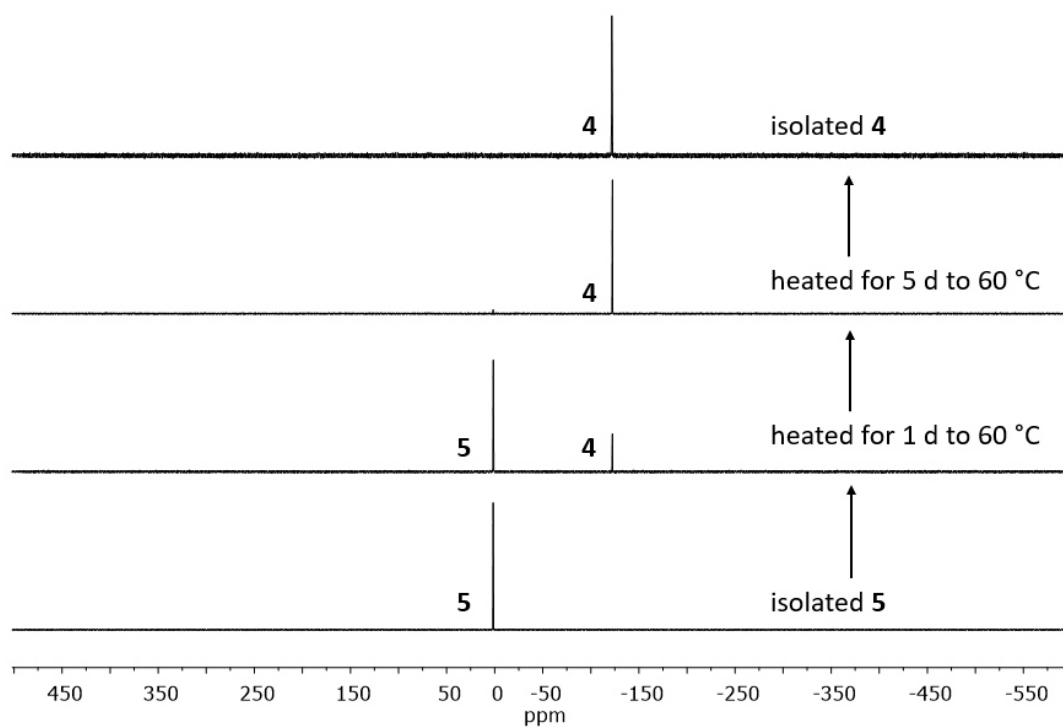
Figure S17. $^{31}P\{^{1}H\}$ NMR spectra (162 MHz, 300 K, C_6D_6) of the conversion of **5** into **4** upon heating.
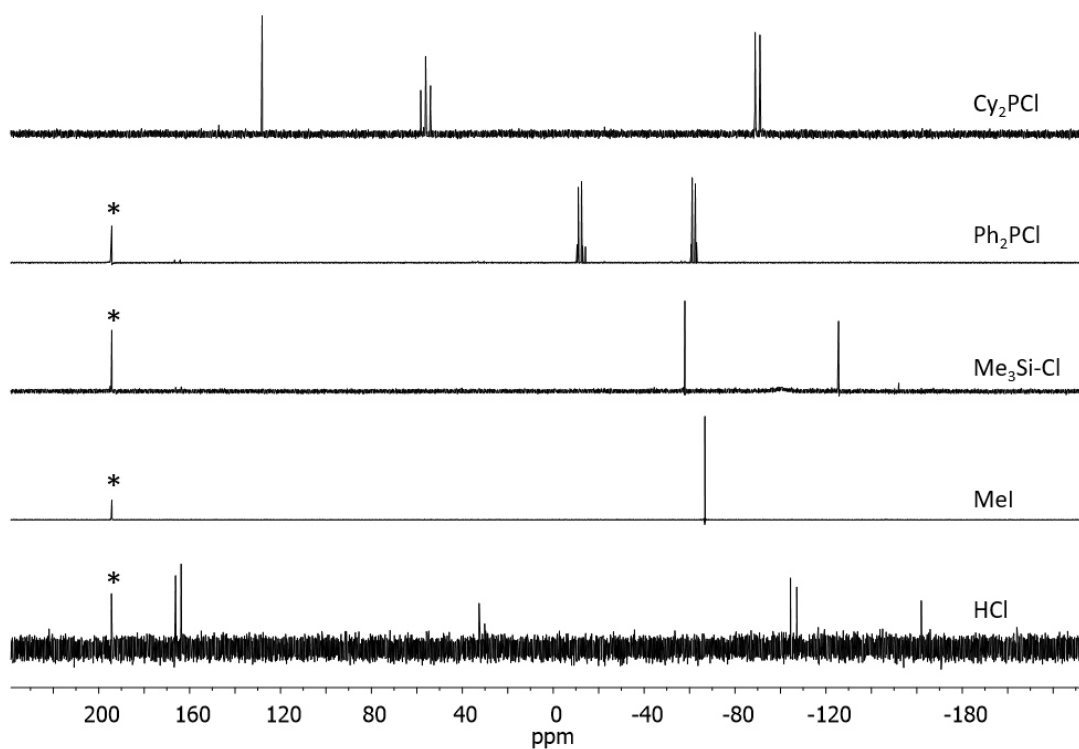
Figure S18. $^{31}P\{^{1}H\}$ NMR spectra (162 MHz, 300 K, C_6D_6) of reactions of **4** with different electrophiles; *8.
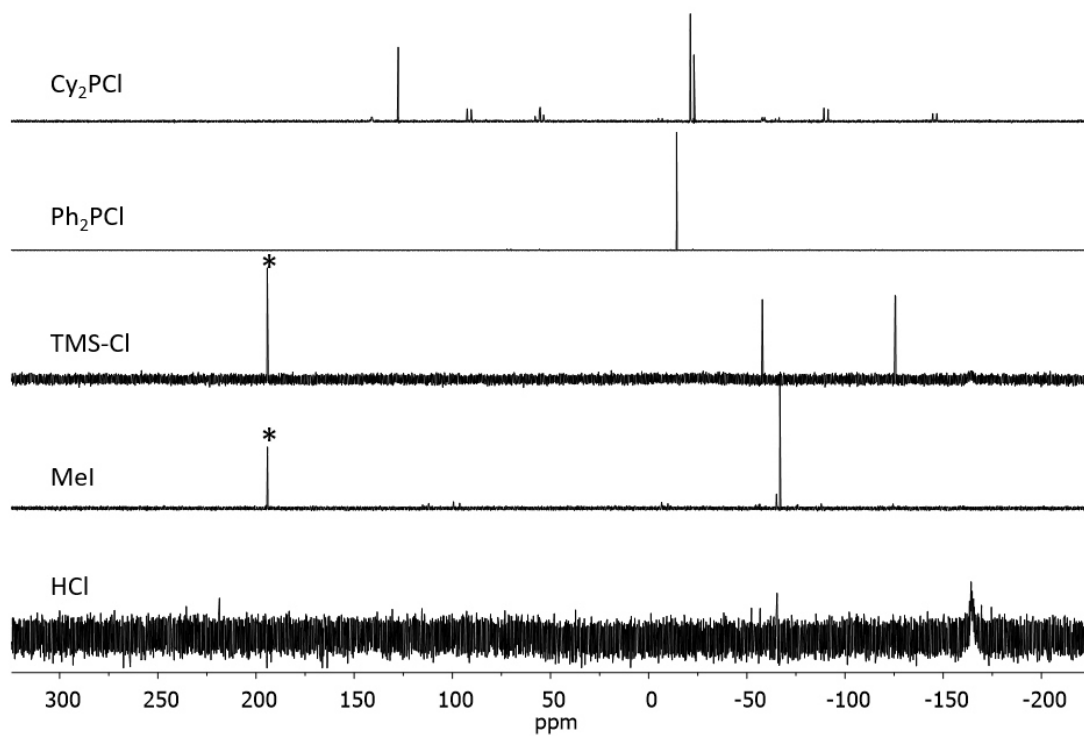
Figure S19. $^{31}P\{^1H\}$ NMR spectra (162 MHz, 300 K, C_6D_6) of reactions of **5** with different electrophiles; *8.

8.4.4   UV/Vis Spectra
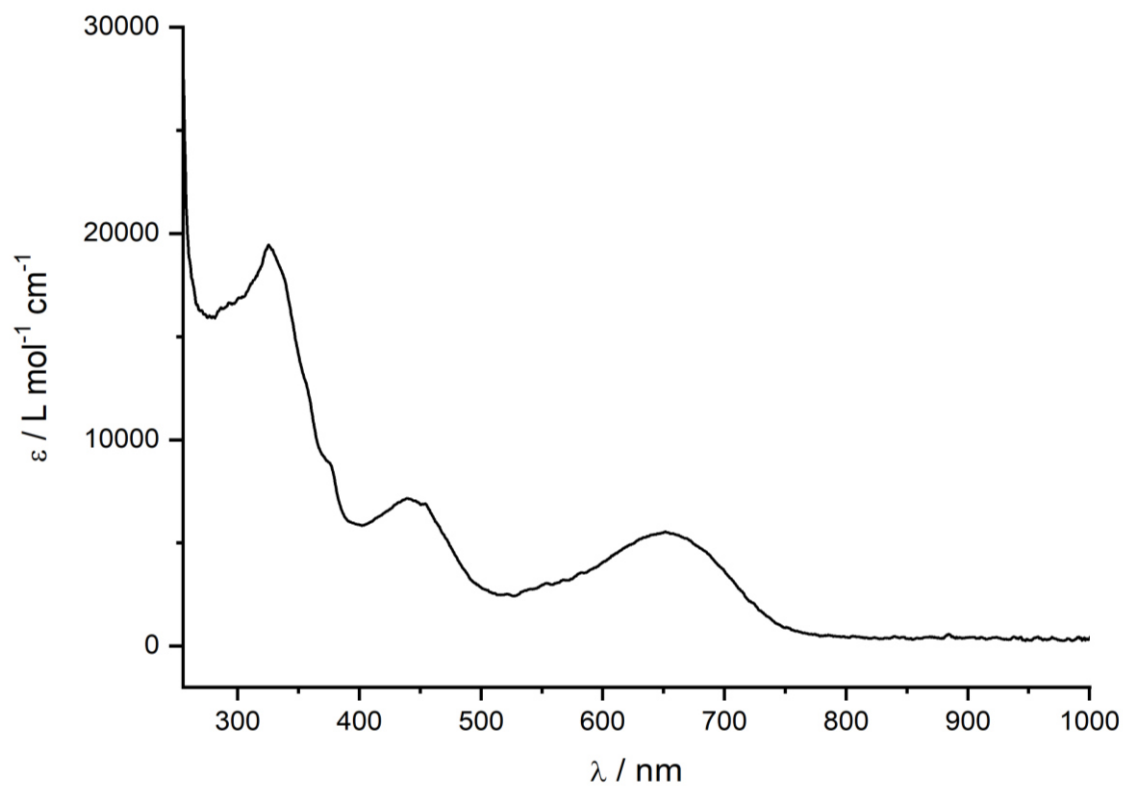
Figure S20. UV/Vis spectrum of **2** recorded in THF.
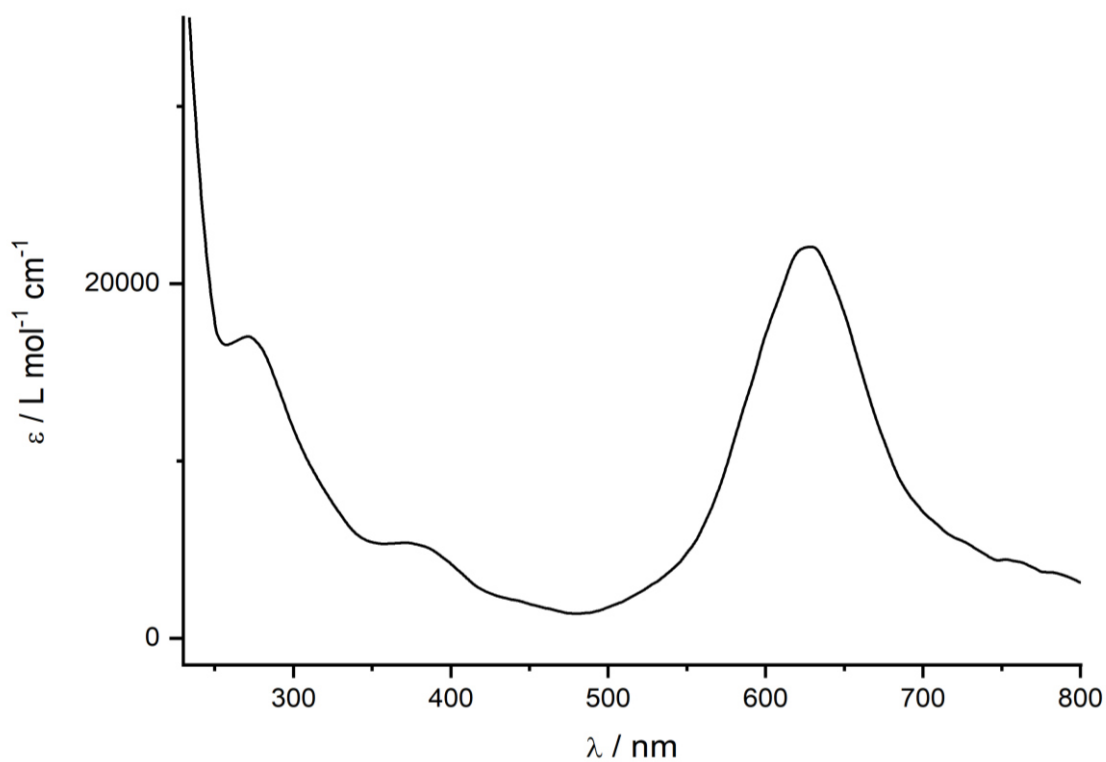
Figure S21. UV/Vis spectrum of **4** recorded in THF.
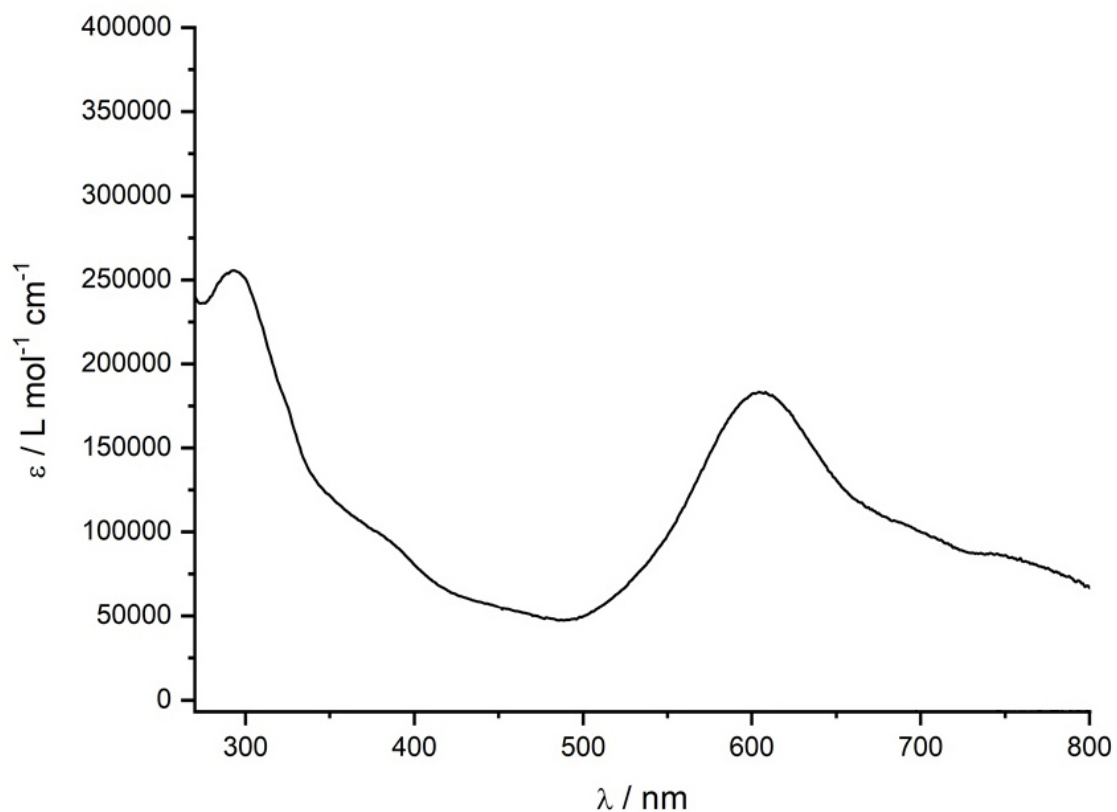
Figure S22. UV/Vis spectrum of **5** recorded in THF.
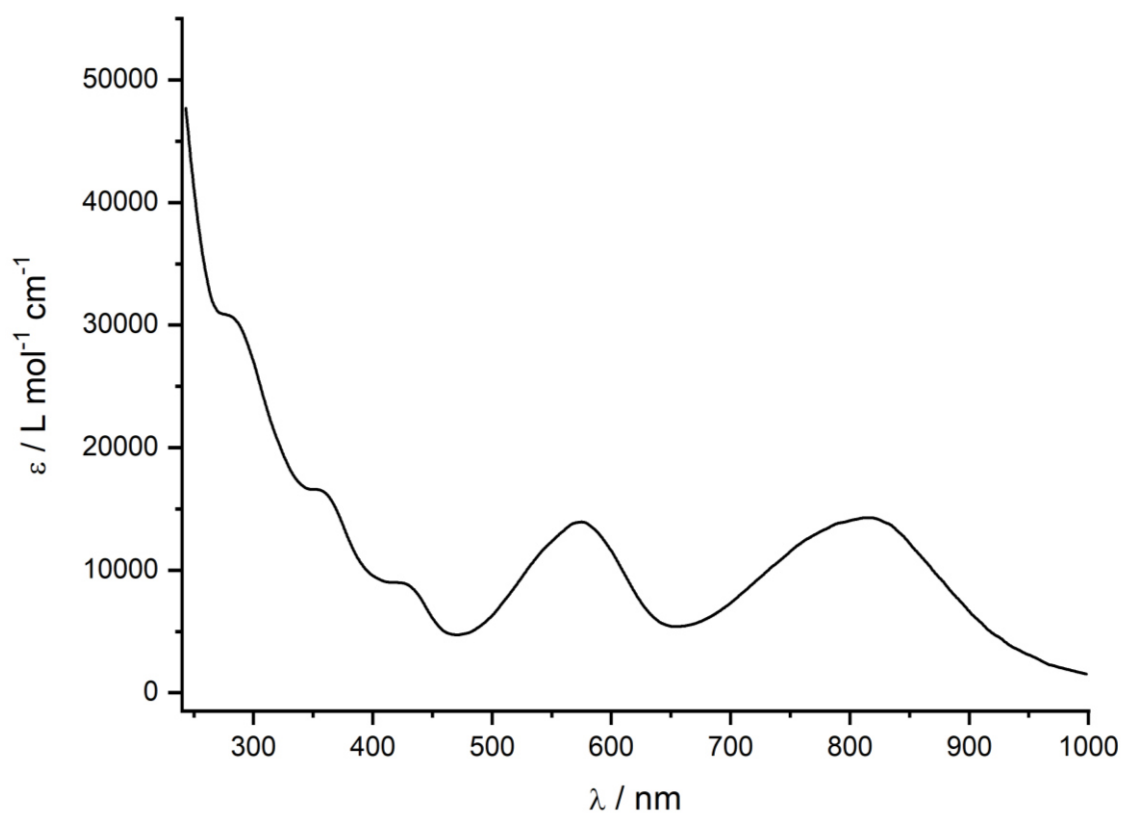
Figure S23. UV/Vis spectrum of **6** recorded in THF.
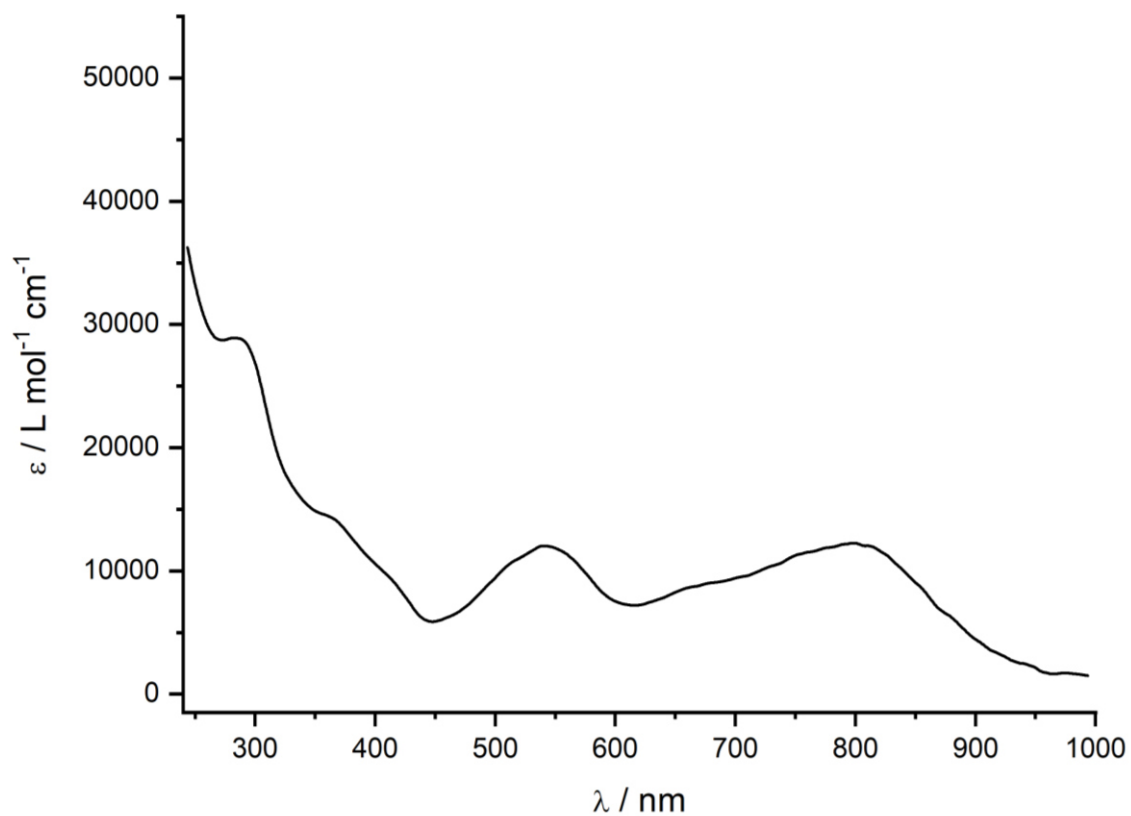
Figure S24. UV/Vis spectrum of **7** recorded in THF.
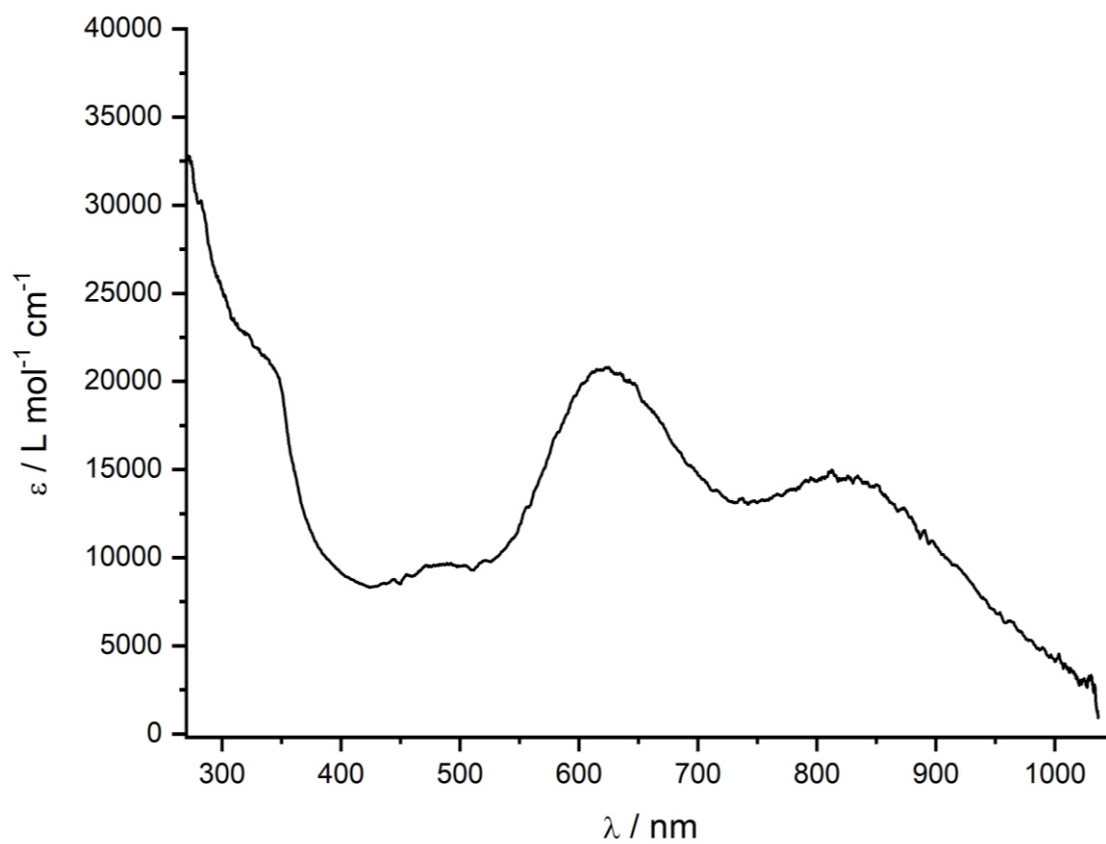
Figure S25. UV/Vis spectrum of **8** recorded in THF.
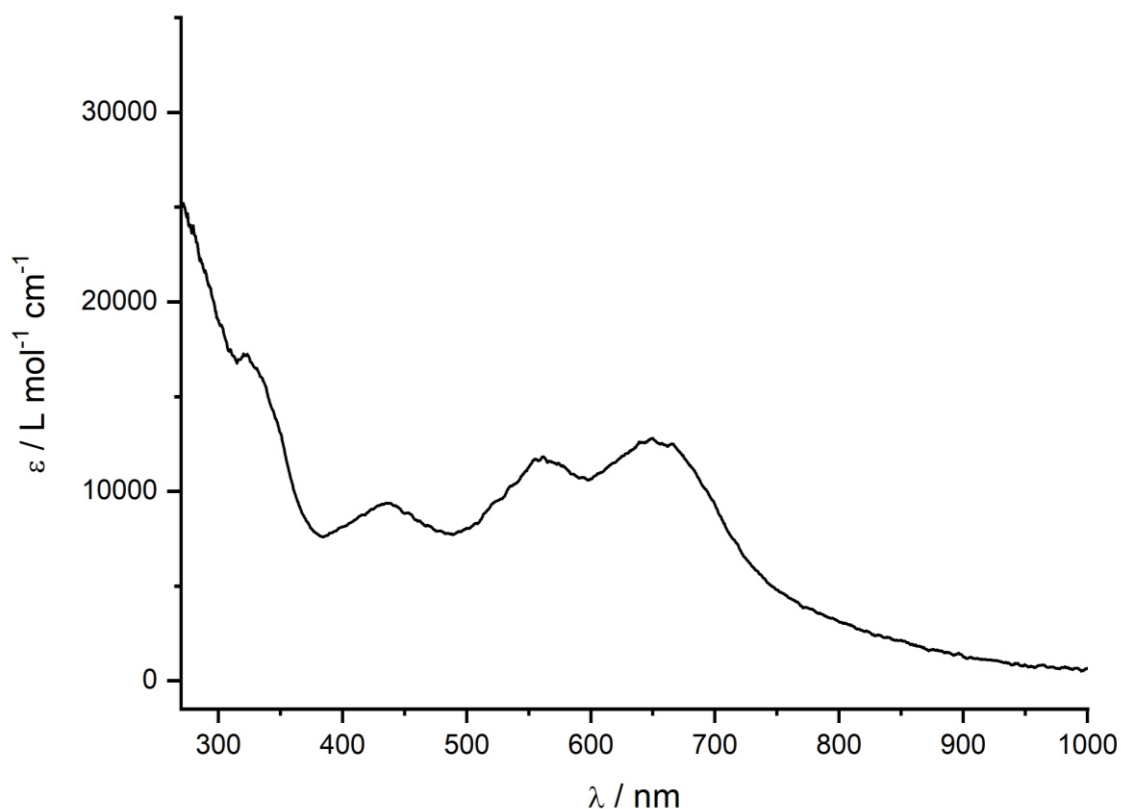
Figure S26. UV/Vis spectrum of **9** recorded in THF.

8.4.5 Zero-field ^{57}Mössbauer Spectra

Zero-field 57Fe-Mössbauer spectra were recorded on a WissEl Mössbauer spectrometer (MRG-500) at a temperature of 77 K in constant acceleration mode. ^{57}Co/Rh was used as γ-radiation source. WinNormos for Igor Pro software was used for the quantitative evaluation of the spectral parameters (least squares fitting to Lorentzian peaks). The minimum experimental line widths were 0.21 mm·s^{-1} (full width at half maximum, FWHM). The temperature of the sample was controlled by a MBBC-HE0106 MÖSSBAUER He/N2 cryostat within an accuracy of +/– 0.3 K. Least-square fitting of the Lorentzian signals was carried out with the "Mfit" software, developed by Dr. Eckhard Bill (MPI CEC, Mülheim/Ruhr). The isomer shifts were reported relative to a α-iron reference at 300 K.

8.4.6 EPR Spectroscopy

Experimental X-band EPR spectra were recorded on a Bruker EMX spectrometer (Bruker BioSpin Rheinstetten) equipped with a Helium temperature control cryostat system (Oxford Instruments). Simulations of the EPR spectra were performed by iteration of the anisotropic g-values, hyperfine coupling interactions and line widths using the EPR simulation program W95EPR developed by Prof. Dr. Frank Neese.

8.4.7 Single Crystal X-ray Diffraction Data

The single-crystal X-ray diffraction data were recorded on Rigaku Oxford Diffraction SuperNova Atlas, GV1000 Titan[S2] or Xcalibur Gemini Ultra (AtlasS2) diffractometers with Cu-K$_\alpha$ radiation (λ= 1.54184 Å). Crystals were selected under mineral oil, mounted on micromount loops and quench-cooled using an Oxford Cryosystems open flow N$_2$ cooling device. Either semi-empirical multi-scan absorption corrections[31] or analytical ones[32] were applied to the data. The structures were solved with SHELXT[33] solution program using dual methods and by using Olex2 as the graphical interface.[34] The models were refined with ShelXL[35] using full matrix least squares minimisation on F^2.[36] The hydrogen atoms were located in idealised positions and refined isotropically with a riding model.
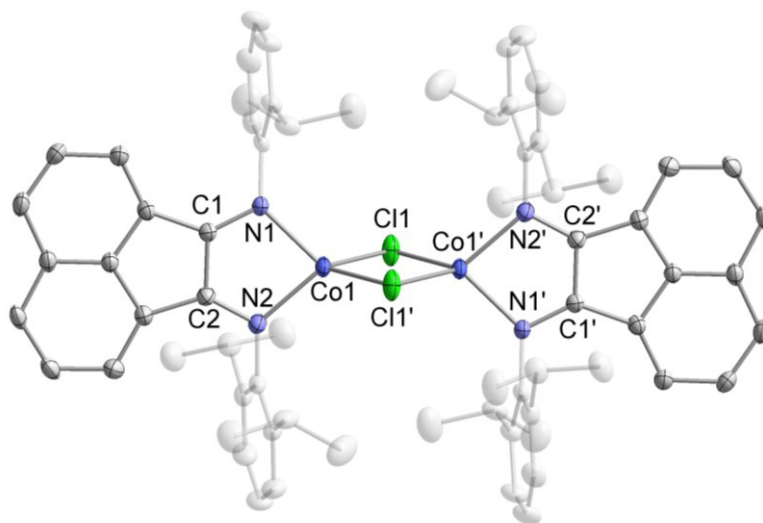
Figure S27. Molecular structure of [(^{Dipp}BIAN)CoCl]$_2$ in the solid state. Thermal ellipsoids are set at the 50% probability level. Selected bond lengths [Å] and angles [°]:Co1−Cl1 2.3000(5), Co1−Cl1′ 2.2786(5), Co1−N1 1.9606(15), Co1−N2 1.9652(17), N1−C1 1.320(2), N2−C2 1.327(3), C1−C2 1.441(2), Cl1−Co1−Cl1′ 96.169(19), N1−Co1−Cl1 126.11(5), N1−Co1−Cl1′ 112.69(5), N1−Co1−N2 85.06(7), N2−Co1−Cl1 120.69(5), N2−Co1−Cl1′ 118.54(5).

The following section provides figures of the molecular structures of metalate salts with additional potassium counterions (+ sequestering agents and solvate molecules) which were not given in section 8.2 itself.
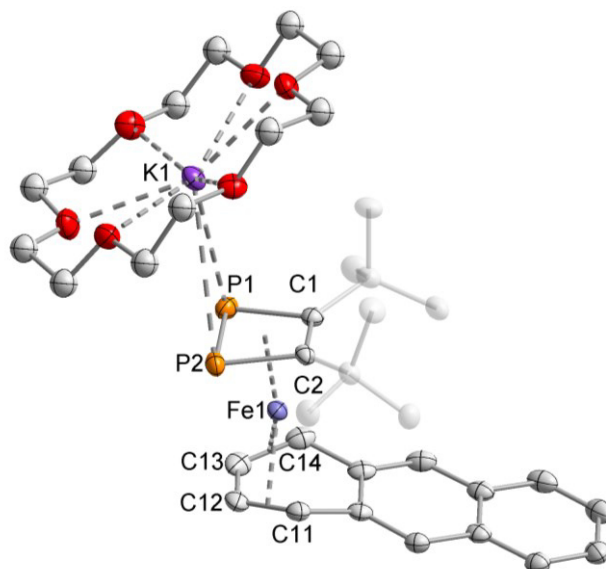
Figure S28. Molecular structure of **2** in the solid state. Thermal ellipsoids are set at the 50% probability level. Hydrogen atoms are omitted for clarity. Selected bond lengths [Å] and angles [°]: P1−P2 2.1738(6), P1−C1 1.8328(15), P2−C2 1.8274(14), C1−C2 1.440(2), Fe−(C2P2centroid) 1.783(2), C11−C12 1.428(2), C12−C13 1.403(2), C13−C14 1.432(2), P1−K1 3.4460(5), P2−K1 3.7961(5) C1−P1−P2 78.03(5), C2−P2−P1 78.85(5), C2−C1−P1 101.97(10), C1−C2−P2 101.14(10).
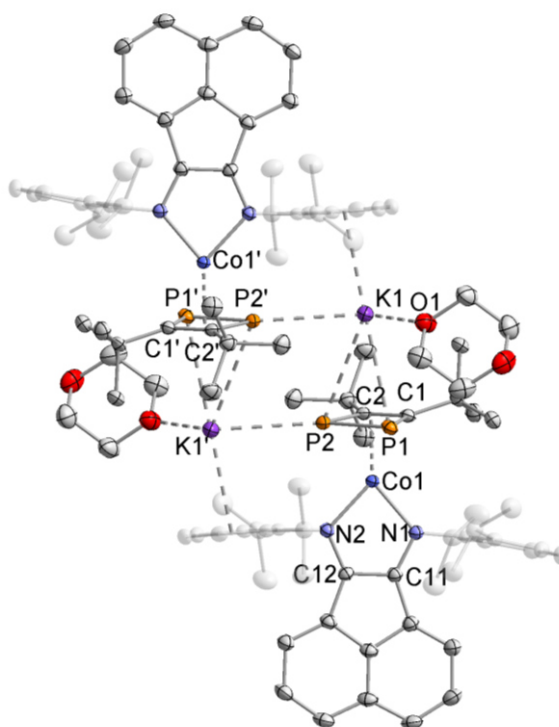
Figure S29. Molecular structure of **4** in the solid state. Thermal ellipsoids are set at the 50% probability level. Hydrogen atoms and solvent of crystallisation are omitted for clarity. Selected bond lengths [Å] and angles [°]: P1−P2 2.1765(8), P1−C1 1.838(2), P2−C2 1.815(2), C1−C2 1.441(3), N1−C11 1.353(3), N2−C12 1.347(3), C12−C11 1.403(3), Co1−N1 1.9382(18), Co1−N2 1.9074(18), Co−(C$_2$P$_2^{centroid}$) 1.775(2), K1−P1 3.3087(7), K1−P2 3.4513(7), K1−P2′ 3.2213(8), K1−O1 2.7208(19), K1−(Dipp^{centroid}) 3.002(1), C2−C1−P1 102.62(16), C1−C2−P2 100.60(16), C1−P1−P2 77.11(7), C2−P2−P1 79.66(8).
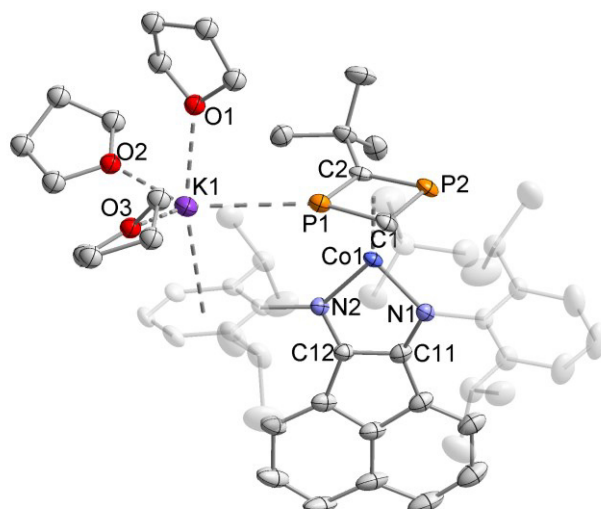
Figure S30. Molecular structure of **5**. Thermal ellipsoids are set at the 50% probability level. Hydrogen atoms and solvent of crystallisation are omitted for clarity. Only one of two crystallographically independent molecules is shown. Selected bond lengths [Å] and angles [°]: P1−C1 1.802(4), P1−C2 1.787(5), P2−C1 1.787(4), P2−C2 1.802(4), N1−C11 1.358(6), N2−C12 1.352(5), C12−C11 1.397(6), Co1−N1 1.929(3), Co1−N2 1.909(4), Co−($C_2P_2^{centroid}$) 1.780(2), K1−P1 3.3944(15), K1−O1 2.733(4), K1−O2 2.662(4), K1−O3 2.805(15), K−($Dipp^{centroid}$) 2.957(1), P2−C1−P1 98.4(2), P1−C2−P2 98.4(2), C2−P1−C1 81.45(19), C1−P2−C2 81.4(2).
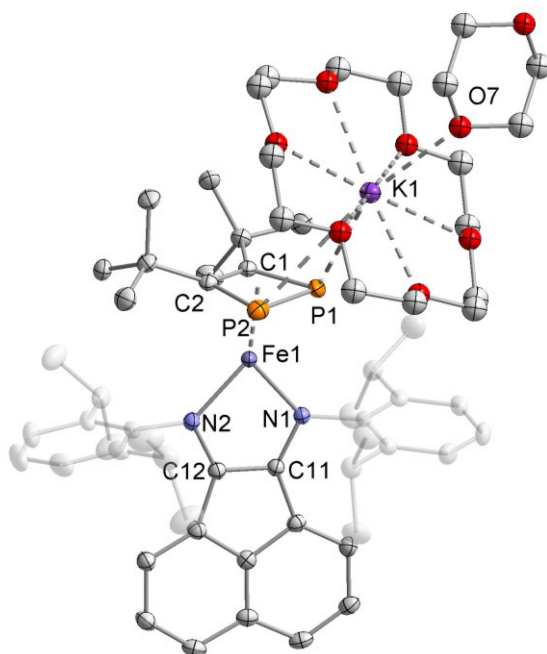
Figure S31. Molecular structure of **6** in the solid state. Thermal ellipsoids are set at the 50% probability level. Hydrogen atoms and solvent of crystallisation are omitted for clarity. Only one of two crystallographically independent molecules is shown. Selected bond lengths [Å] and angles [°]: P1−P2 2.173(5), P1−C1 1.819(9), P2−C2 1.776(10), C1−C2 1.434(13), N1−C11 1.369(9), N2−C12 1.350(9), C12−C11 1.413(10), Fe1−N1 1.959(6), Fe1−N2 1.958(7), Fe−($C_2P_2^{centroid}$) 1.823(3), K1−P1 3.3389(4), K1−P2 3.7883(4), K1−O7 2.7559(12), C2−C1−P1 100.8(7), C1−C2−P2 103.0(7), C1−P1−P2 77.7(3), C2−P2−P1 78.5(3).
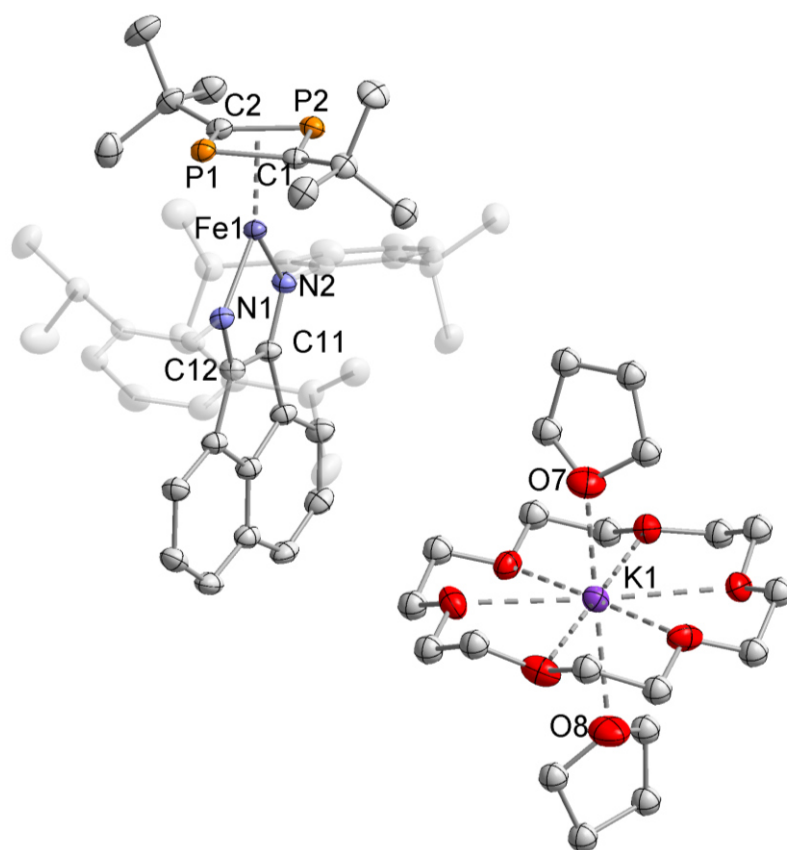
Figure S32. Molecular structure of **7** in the solid state. Thermal ellipsoids are set at the 50% probability level. Hydrogen atoms and solvent of crystallisation are omitted for clarity. Selected bond lengths [Å] and angles [°] P1−C1 1.799(2), P1−C2 1.795(2), P2−C1 1.790(2), P2−C2 1.791(2), N1−C11 1.367(3), N2−C12 1.366(2), C12−C11 1.385(3), Fe1−N1 1.9421(16), Fe1−N2 1.9331(17), Fe−($C_2P_2^{centroid}$) 1.803(3), K1−O7 2.7454(16), K1−O8 2.7333(17), P2−C1−P1 98.94(10), P2−C2−P1 99.01(10), C2−P1−C1 80.54(9), C1−P2−C2 80.89(10).

Table S2. Crystallographic data and structure refinement for compounds **2-9** and [(^{Dipp}BIAN)CoCl]$_2$

Compound	2	3	4	5	6	7	8	9	[(^{Dipp}BIAN) CoCl]$_2$
CCDC									
Empirical formula	C$_{42}$H$_{58}$FeK O$_6$P$_2$	C$_{36}$H$_{68}$CoK O$_8$P$_4$	C$_{50}$H$_{66}$CoK N$_2$O$_2$P$_2$	C$_{60}$H$_{86}$CoK N$_2$O$_{3.5}$P$_2$	C$_{62}$H$_{90}$FeK N$_2$O$_8$P$_2$	C$_{70}$H$_{105.8}$FeK N$_2$O$_{9.2}$P$_2$	C$_{82}$H$_{98}$Co$_2$N$_4$ P$_2$	C$_{61}$H$_{87}$CoN$_2$ P$_3$	C$_{72}$H$_{80}$Cl$_2$ Co$_2$N$_4$
Formula weight	815.77	850.81	887.01	1049.26	1148.24	1276.45	1664.12	1000.16	1190.16
Temperature /K	123.0(1)	123.0(1)	123.0(1)	122.9(6)	123.0(1)	123.0(1)	123.0(1)	123.0(1)	123.0(1)
Crystal system	triclinic	triclinic	monoclinic	monoclinic	monoclinic	triclinic	monoclinic	monoclinic	monoclinic
Space group	$P\bar{1}$	$P\bar{1}$	$P2_1/n$	Pn	$P2_1/c$	$P\bar{1}$	$C2/c$	$P2_1/n$	$P2_1/n$
a/Å	11.5384(4)	10.3092(4)	17.0200(3)	15.4509(2)	20.6034(2)	13.0809(4)	19.7108(3)	13.0484(2)	16.1977(2)
b/Å	13.2644(4)	10.6450(6)	12.9087(3)	21.0206(2)	14.1129(2)	14.4445(5)	22.8080(3)	12.0775(2)	12.1792(2)
c/Å	14.6464(5)	11.4046(5)	21.7442(4)	18.2194(1)	22.1268(2)	19.5071(9)	17.6768(3)	35.3534(5)	16.2781(2)
α/°	70.660(3)	73.824(4)	90	90	90	84.648(3)	90	90	90
β/°	83.052(3)	63.657(4)	95.861(2)	102.4732(9)	100.215(1)	73.288(4)	95.0430(10)	97.1380(10)	94.0090(10)
γ/°	85.943(3)	86.201(4)	90	90	90	85.656(3)	90	90	90
Volume/Å^3	2098.48(13)	1074.79(10)	4752.36(16)	5777.82(9)	6331.91(12)	3510.1(2)	7916.1(2)	5528.23(15)	3203.41(8)
Z	2	1	4	4	4	2	4	4	2
ρ$_{calc}$g/cm^3	1.291	1.314	1.240	1.206	1.205	1.208	1.396	1.202	1.234
μ/mm^{-1}	4.841	5.772	4.550	3.837	3.384	2.331	4.087	3.540	5.151
F(000)	866.0	454.0	1888.0	2248.0	2460.0	1374.0	3608.0	2156.0	1256.0
Crystal size/mm^3	0.468 × 0.152 × 0.122	0.208 × 0.123 × 0.024	0.388 × 0.214 × 0.077	0.2552 × 0.1527 × 0.0443	0.514 × 0.284 × 0.227	0.412 × 0.255 × 0.125	0.574 × 0.31 × 0.195	0.645 × 0.588 × 0.278	0.808 × 0.339 × 0.252
Radiation	CuKα (λ = 1.54184)	CuKα (λ = 1.54184)	CuKα (λ = 1.54184)	CuKα (λ = 1.54184)	CuKα (λ = 1.54184)	CuKβ (λ = 1.39222)	CuKα (λ = 1.54184)	CuKα (λ = 1.54184)	CuKα (λ = 1.54184)
2Θ range for data collection/°	7.066 to 143.938	8.668 to 147.664	6.95 to 147.086	7.212 to 133.528	7.632 to 145.78	5.556 to 120.254	8.03 to 145.366	6.978 to 145.73	7.444 to 143.542
Index ranges	-12 ≤ h ≤ 14, -16 ≤ k ≤ 16, -10 ≤ l ≤ 17	-12 ≤ h ≤ 10, -13 ≤ k ≤ 13, -12 ≤ l ≤ 14	-18 ≤ h ≤ 20, -15 ≤ k ≤ 16, -24 ≤ l ≤ 26	-18 ≤ h ≤ 18, -24 ≤ k ≤ 25, -18 ≤ l ≤ 21	-25 ≤ h ≤ 25, -16 ≤ k ≤ 17, -26 ≤ l ≤ 27	-13 ≤ h ≤ 16, -17 ≤ k ≤ 11, -23 ≤ l ≤ 24	-21 ≤ h ≤ 24, -22 ≤ k ≤ 27, -21 ≤ l ≤ 19	-16 ≤ h ≤ 16, -14 ≤ k ≤ 9, -43 ≤ l ≤ 41	-16 ≤ h ≤ 19, -10 ≤ k ≤ 14, -19 ≤ l ≤ 20
Reflections collected	14008	7017	18700	70293	26851	23140	14820	21796	14413
Independent reflections	7918 [R$_{int}$ = 0.0237, R$_{sigma}$ = 0.0343]	4178 [R$_{int}$ = 0.0287, R$_{sigma}$ = 0.0396]	9221 [R$_{int}$ = 0.0330, R$_{sigma}$ = 0.0439]	17913 [R$_{int}$ = 0.0384, R$_{sigma}$ = 0.0348]	12301 [R$_{int}$ = 0.0168, R$_{sigma}$ = 0.0202]	13609 [R$_{int}$ = 0.0200, R$_{sigma}$ = 0.0318]	7570 [R$_{int}$ = 0.0210, R$_{sigma}$ = 0.0287]	10682 [R$_{int}$ = 0.0237, R$_{sigma}$ = 0.0293]	6116 [R$_{int}$ = 0.0396, R$_{sigma}$ = 0.0389]
Data/restraints/para-meters	7918/132/521	4178/0/235	9221/0/537	17913/482/1408	12301/0/699	13609/115/846	7570/0/417	10682/0/619	6116/0/369
Goodness-of-fit on F^2	1.037	1.034	1.018	1.019	1.026	1.031	1.065	1.028	1.039
Final R indexes [I>=2σ (I)]	R$_1$ = 0.0296, wR$_2$ = 0.0733	R$_1$ = 0.0325, wR$_2$ = 0.0792	R$_1$ = 0.0420, wR$_2$ = 0.0979	R$_1$ = 0.0412, wR$_2$ = 0.1041	R$_1$ = 0.0287, wR$_2$ = 0.0726	R$_1$ = 0.0391, wR$_2$ = 0.1011	R$_1$ = 0.0383, wR$_2$ = 0.1022	R$_1$ = 0.0401, wR$_2$ = 0.1015	R$_1$ = 0.0483, wR$_2$ = 0.1283
Final R indexes [all data]	R$_1$ = 0.0316, wR$_2$ = 0.0747	R$_1$ = 0.0357, wR$_2$ = 0.0822	R$_1$ = 0.0515, wR$_2$ = 0.1032	R$_1$ = 0.0472, wR$_2$ = 0.1081	R$_1$ = 0.0307, wR$_2$ = 0.0740	R$_1$ = 0.0442, wR$_2$ = 0.1056	R$_1$ = 0.0405, wR$_2$ = 0.1040	R$_1$ = 0.0433, wR$_2$ = 0.1040	R$_1$ = 0.0501, wR$_2$ = 0.1307
Largest diff. peak/hole / e Å^{-3}	0.38/-0.21	0.30/-0.30	0.44/-0.47	0.78/-0.47	0.29/-0.24	0.61/-0.69	0.32/-0.36	0.56/-0.40	0.60/-0.49
Flack parameter	/		/	-0.0329(14)	/	/	/	/	/

8.4.8   Quantum Chemical Calculations

General Methods

All calculations were performed with the ORCA program package.[37] All geometry optimisations were performed at the BP86-D3BJ/def2-TZVP level of theory in the gas phase.[38–40,41] Density fitting techniques, also called resolution-of-identity approximation (RI)[42] were used for GGA calculations, whereas the RIJCOSX[43] approximation was used for hybrid-DFT and CASSCF calculations

Calculations were performed on the anions only (cations were omitted). In addition, the aryl substituents at the 2,6-di-*iso*-propylphenyl (Dipp) moieties were truncated to 2,6-dimethylphenyl rings (Dmp). Single point calculations on the energies of $[(^{Dmp}BIAN)Co(1,2\text{-}t\text{Bu}_2\text{C}_2\text{P}_2)]^-$ and $[(^{Dmp}BIAN)Co(1,3\text{-}t\text{Bu}_2\text{C}_2\text{P}_2)]^-$ have been carried out at the RI-PWPB95/def2-TZVP level of theory. The differences in energies for $[(^{Dmp}BIAN)Co(1,2\text{-}t\text{Bu}_2\text{C}_2\text{P}_2)]^-$ and $[(^{Dmp}BIAN)Co(1,3\text{-}t\text{Bu}_2\text{C}_2\text{P}_2)]^-$ are smaller than 1 kcal·mol^{-1}.

Frequency analysis of **3**, **3′** and the mixed isomer $[Co(1,2\text{-}t\text{Bu}_2\text{C}_2\text{P}_2)(1,3\text{-}t\text{Bu}_2\text{C}_2\text{P}_2)]^-$ were performed on the BP86-D3BJ/def2-TZVP level of theory.[38–40] The minimum structures and corresponding energies are depicted in Figure S33.

EPR parameters were calculated at the CASSCF-NEVPT2/DKH-def2-TZVP level of theory. For the iron complexes **6** and **7** an active space of nine electrons in nine orbitals were chosen. Here, the initial guess orbitals consisted of the five 3d-orbitals of Fe, two ligand orbitals and two orbitals of the 4d-shell of Fe (so called double-shell). The resulting orbitals are shown in Figure S34 and Figure S35. For **2**, the guess orbitals consisted of the five 3d orbitals on Fe, two ligand orbitals and three orbitals of the 4d-shell of Fe. The resulting orbitals are shown in Figure S36. For all complexes, the experimental g-tensors are well reproduced when 14 excited states were included in the spin-orbit coupling procedure.

For the calculation of Mössbauer parameters, the ground-states of the three iron complexes were calculated using the TZVP basis on C, H, N and P and the CP(PPP)[44] basis on Fe. The active spaces were constructed in the same manner as described above.

The active space of the cobalt complexes consists of ten electrons in ten orbitals (using TZVP on C, H, N and P and CP(PPP) on Co). The initial guess orbitals consisted of the five 3d orbitals on Co, two ligand orbitals and three orbitals of the 4d-shell of Co. The resulting orbitals are shown in Figure S37 and Figure S38.

$[Co(1,2\text{-}t\text{Bu}_2\text{C}_2\text{P}_2)_2]^-$ $[Co(1,3\text{-}t\text{Bu}_2\text{C}_2\text{P}_2)_2]^-$ $[Co(1,2\text{-}t\text{Bu}_2\text{C}_2\text{P}_2)$
$(1,3\text{-}t\text{Bu}_2\text{C}_2\text{P}_2)]^-$

ΔG [kcal·mol^{-1}]:	2.4	0.0	6.4
ΔH [kcal·mol^{-1}]:	0.5	0.0	6.0
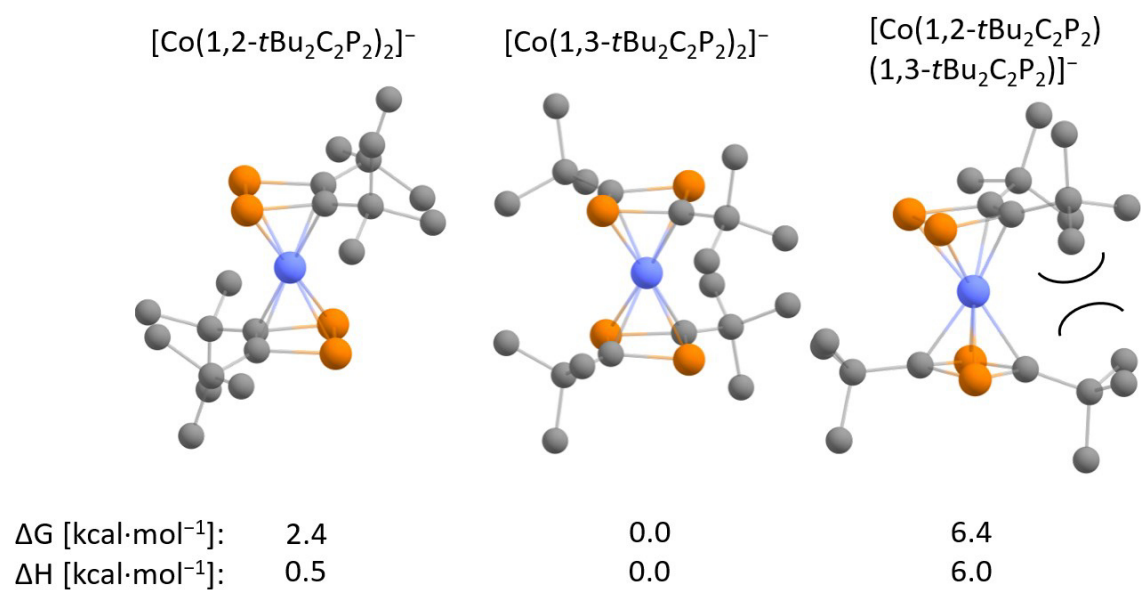
Figure S33. Optimised geometries, enthalpies and Gibb's energies for [Co(1,2-*t*Bu₂C₂P₂)₂]⁻, [Co(1,3-*t*Bu₂C₂P₂)₂]⁻ and the mixed isomer [Co(1,2-*t*Bu₂C₂P₂)(1,3-*t*Bu₂C₂P₂)]⁻ calculated at the BP86-D3BJ/def2-TZVP level of theory.
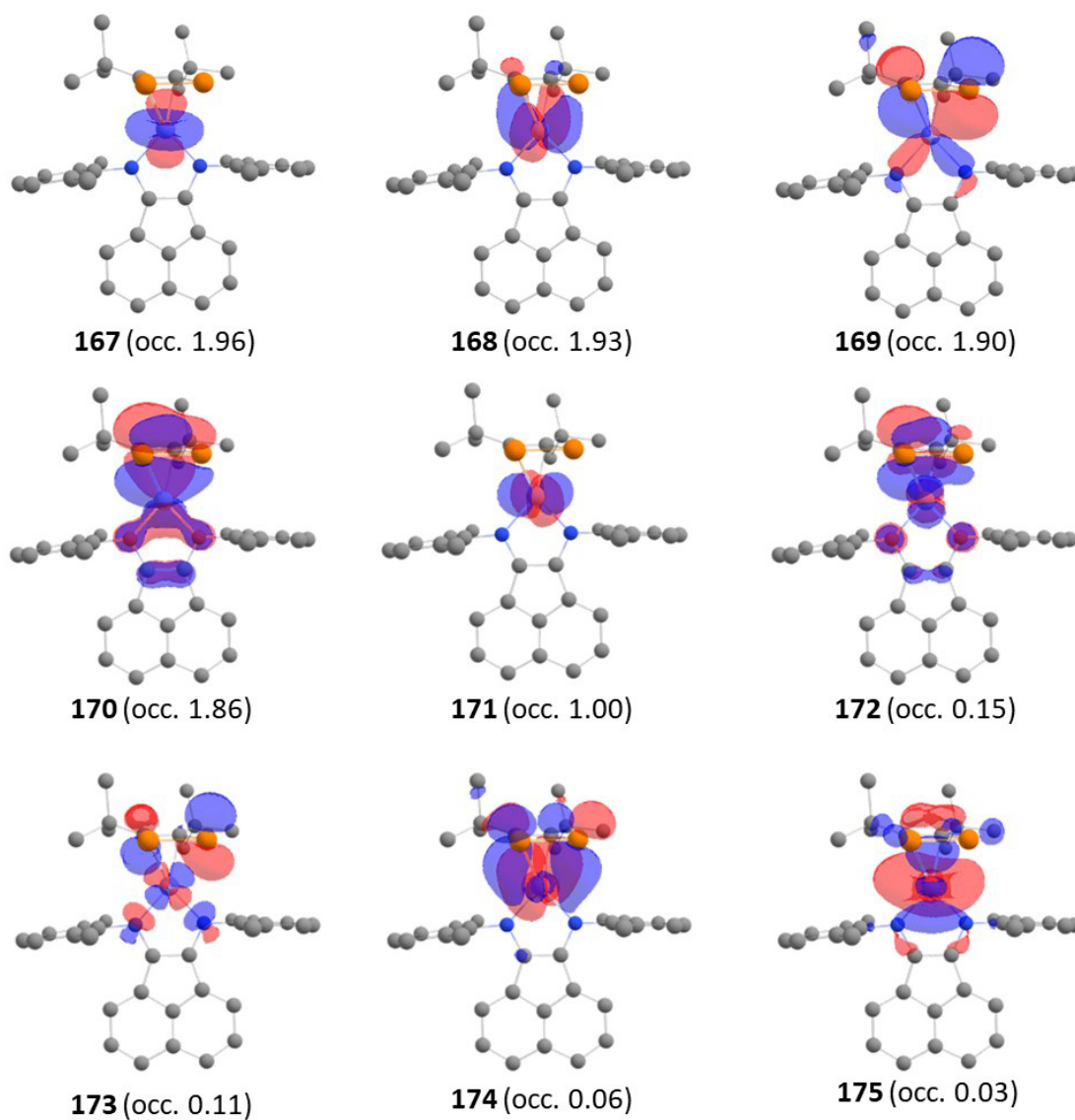
Figure S34. Natural orbitals of the active space of a CASSCF calculation [RIJCOSX/TZVP-def2/JK, CP(PPP) on Fe] on [(^{Dmp}BIAN)Fe(1,2-tBu$_2$C$_2$P$_2$)]$^-$. The occupancy of each orbital is given in parentheses. Surface isovalue = 0.03.
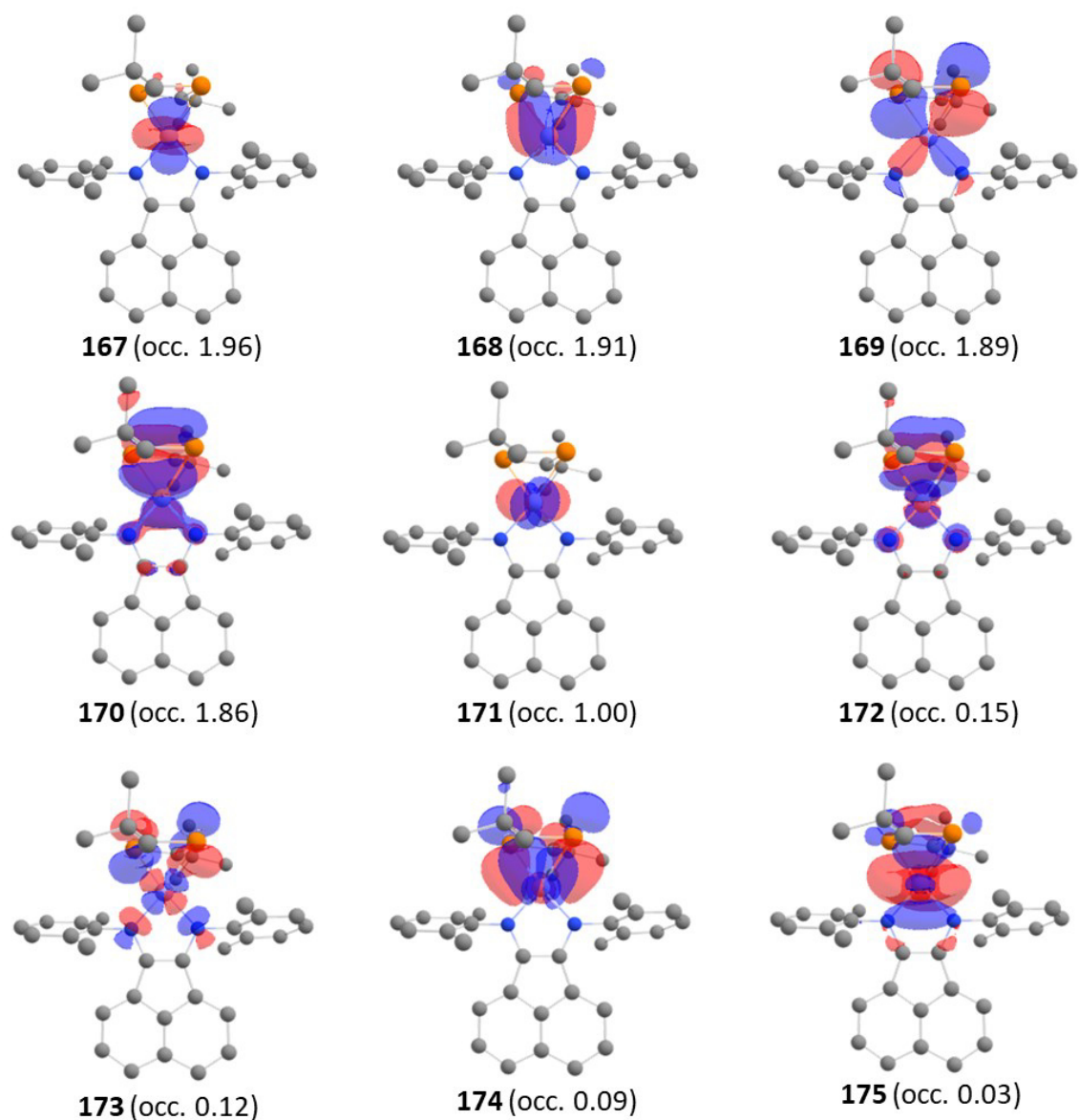
Figure S35. Natural orbitals of the active space of a CASSCF calculation [RIJCOSX/TZVP-def2/JK, CP(PPP) on Fe] on [(^{Dmp}BIAN)Fe(1,3-tBu$_2$C$_2$P$_2$)]$^-$. The occupancy of each orbital is given in parentheses. Surface isovalue = 0.03.
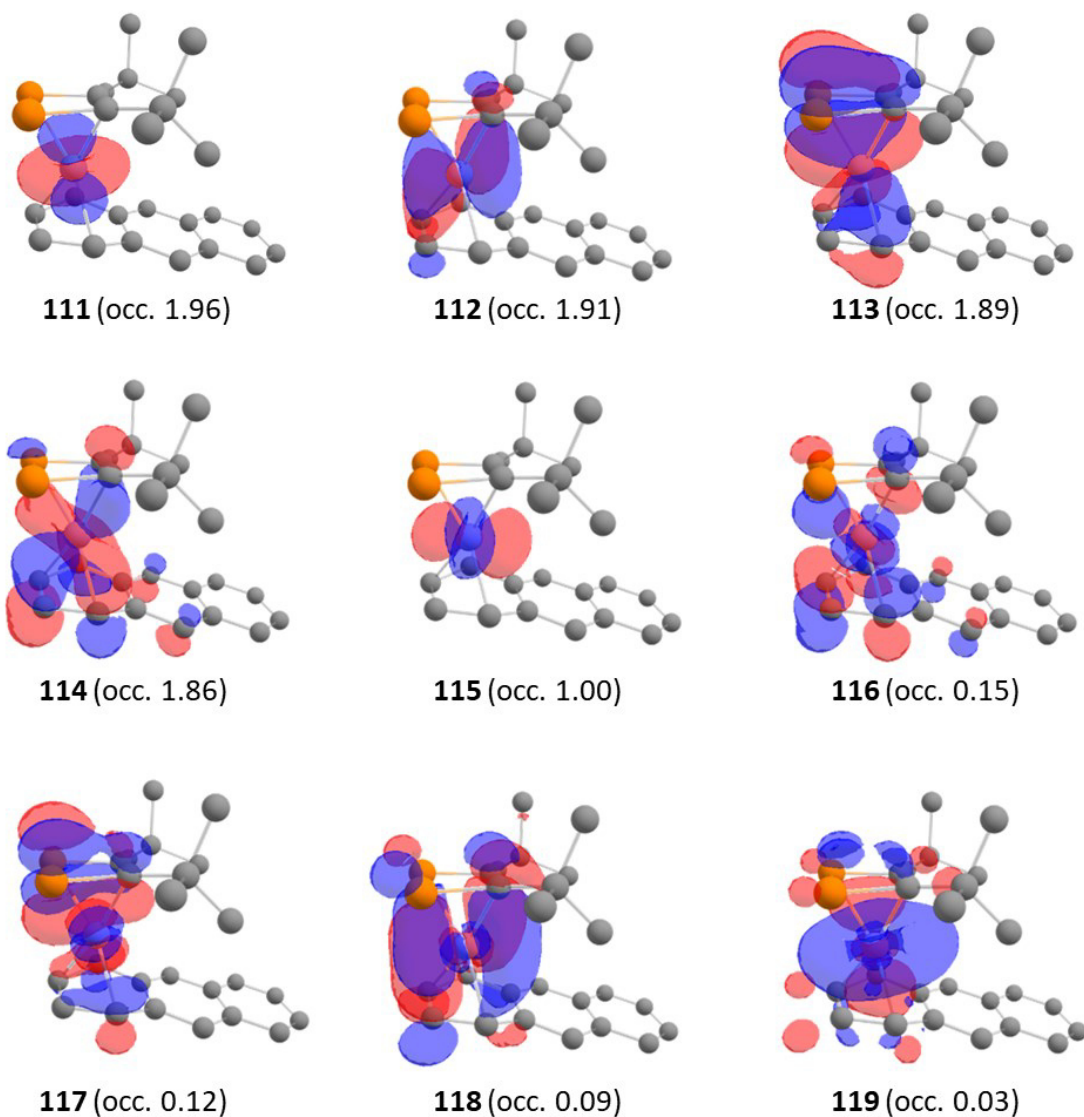
Figure S36. Natural orbitals of the active space of a CASSCF calculation [RIJCOSX/TZVP-def2/JK, CP(PPP) on Fe] on [Fe(1,2-tBu$_2$C$_2$P$_2$)(anthracene)]$^-$. The occupancy of each orbital is given in parentheses. Surface isovalue = 0.03.

167 (occ. 1.97)   **168** (occ. 1.96)   **169** (occ. 1.94)

170 (occ. 1.91)   **171** (occ. 1.89)   **172** (occ. 0.12)

173 (occ. 0.10)   **174** (occ. 0.05)   **175** (occ. 0.03)

176 (occ. 0.02)
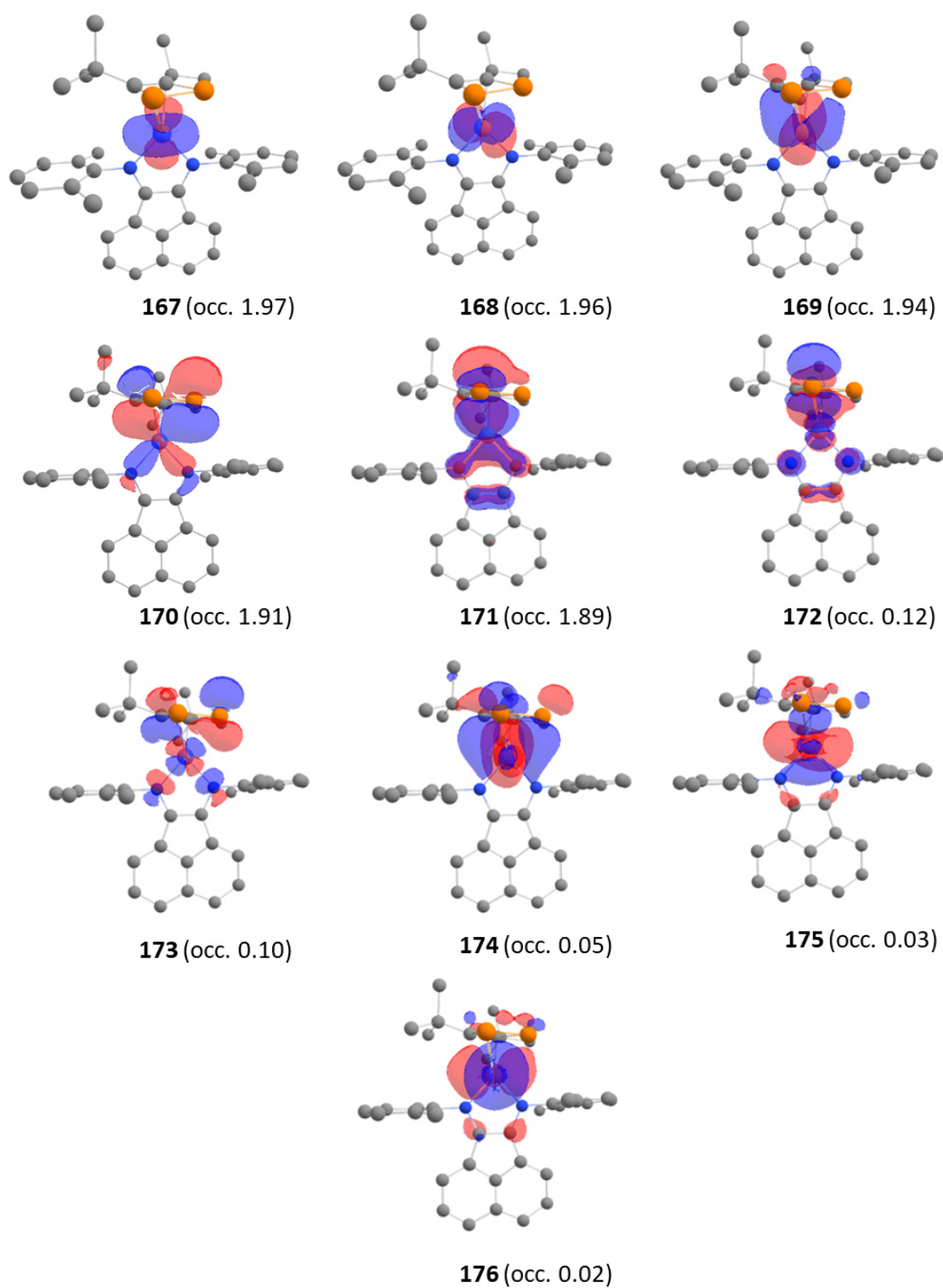
Figure S37. Natural orbitals of the active space of a CASSCF calculation [RIJCOSX/TZVP-def2/JK, CP(PPP) on Co] on [(^{Dmp}BIAN)Co(1,2-tBu$_2$C$_2$P$_2$)]$^-$. The occupancy of each orbital is given in parentheses. Surface isovalue = 0.03.

167 (occ. 1.97) **168** (occ. 1.96) **169** (occ. 1.93)

170 (occ. 1.91) **171** (occ. 1.88) **172** (occ. 0.13)

173 (occ. 0.10) **174** (occ. 0.06) **175** (occ. 0.03)

176 (occ. 0.02)
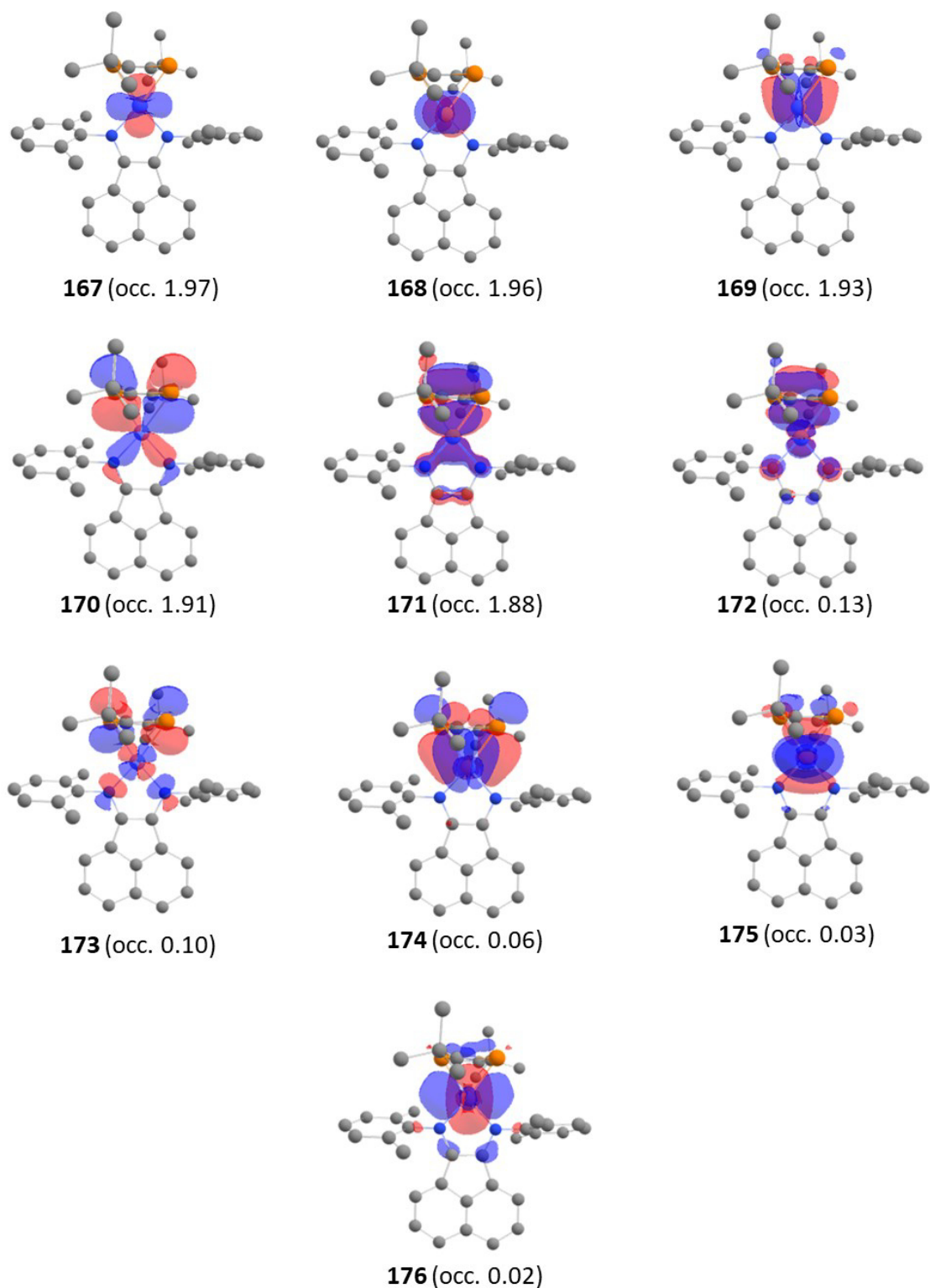
Figure S38. Natural orbitals of the active space of a CASSCF calculation [RIJCOSX/TZVP-def2/JK, CP(PPP) on Co] on [(^{Dmp}BIAN)Co(1,3-tBu$_2$C$_2$P$_2$)]$^-$. The occupancy of each orbital is given in parentheses. Surface isovalue = 0.03.

22 (occ. 2.0)
isosurface value
0.0075

23 (occ. 2.0)
isosurface value
0.0075

84 (occ. 2.0)
isosurface value
0.06

85 (occ. 2.0)
isosurface value
0.06
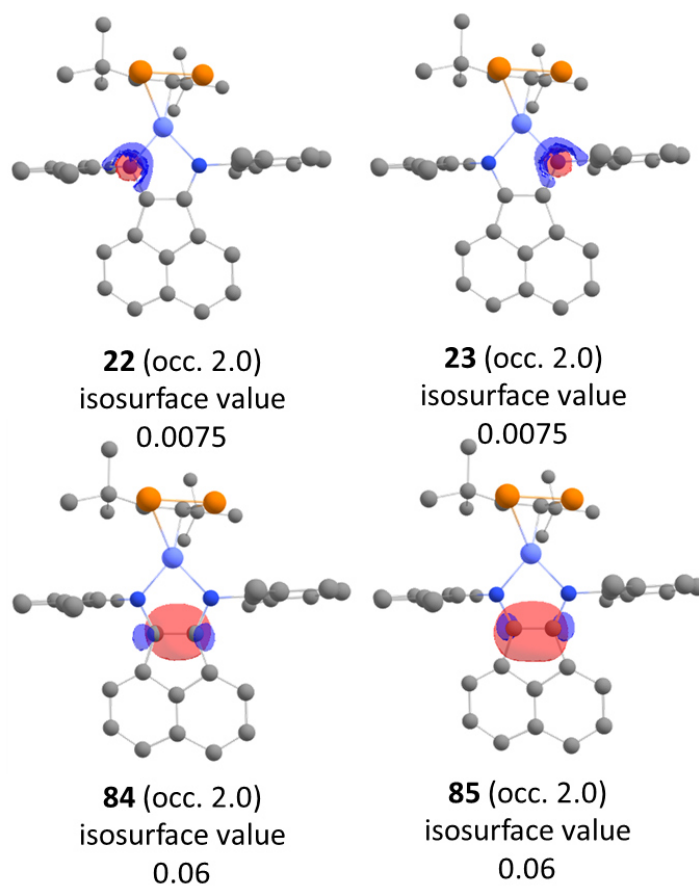
Figure S39. Selected localised molecular orbitals below the active space of a CASSCF calculation [RIJCOSX/TZVP-def2/JK, CP(PPP) on Co] on [(^{Dmp}BIAN)Co(1,2-tBu$_2$C$_2$P$_2$)]$^-$. The occupancy of each orbital is given in parentheses (2.0). These orbitals represent the lone pairs on the N atoms as well as the connecting C=C double bond of the ^{Dmp}BIAN ligand.

22 (occ. 2.0)
isosurface value 0.0075

23 (occ. 2.0)
isosurface value 0.0075

89 (occ. 2.0)
isosurface value 0.06

90 (occ. 2.0)
isosurface value 0.06
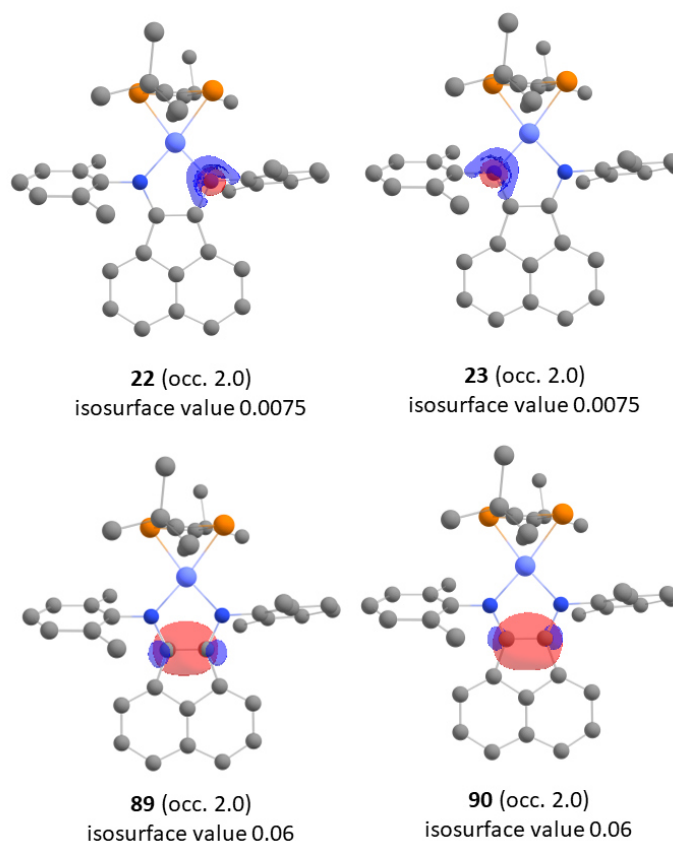
Figure S40. Selected localised molecular orbitals below the active space of a CASSCF calculation [RIJCOSX/TZVP-def2/JK, CP(PPP) on Co] on [(^{Dmp}BIAN)Co(1,3-*t*Bu$_2$C$_2$P$_2$)]⁻. The occupancy of each orbital is given in parentheses (2.0). These orbitals represent the lone pairs on the N atoms as well as the connecting C=C double bond of the ^{Dmp}BIAN ligand.

Cartesian Coordinates for Optimised Structures

[(^{Dmp}BIAN)Co(1,2-*t*Bu$_2$C$_2$P$_2$)]⁻:

```
Co  6.90410033514340    6.15330831951012   11.35984907085909
P   6.85052854423478    5.02699910811742    9.37339781624692
P   8.72160413127847    5.04152986710298   10.52207610126049
N   7.11729654968343    6.87669170275783   13.11422124236625
N   5.19967926345825    5.61041152469170   11.99296201596355
C   6.03546147308029    6.65470670107382   13.90116183541723
C   5.69307966541484    6.90911031101124   15.29818310409287
C   5.57983610799920    7.54458678549787   17.63204603906584
H   6.05786196493332    8.02430118106321   18.48945396099681
C   4.31854638067479    6.98954199565647   17.79012281460207
H   3.81425846066238    7.03153339184449   18.75825425010385
C   6.28960865519491    7.51529229353724   16.39817786365691
H   7.28376620440376    7.95843239880452   16.33379840849716
C   2.67065578533189    5.11334892988506   14.29375310727060
H   2.25791345004648    4.62516116028709   13.41031342867678
C   3.91518567994650    5.73349710631086   14.26279184468772
C   4.38828588288716    6.33809843281035   15.47657067287007
C   8.21960644408367    7.49306845893977   13.75466467072679
C   4.97299090749219    5.95858349281301   13.28370087976165
C   3.67883331108848    6.35111311807890   16.68141699693368
```

C	2.39829836889404	5.71325474735205	16.67445420838340
H	1.79616825870646	5.69157879720472	17.58557771198745
C	9.09564792592480	5.19232500251529	14.31238375742943
C	4.30532646293926	3.47540782467546	11.20327526030827
C	4.17698172760161	4.87563705537802	11.33783436644646
C	1.93227075706501	5.11907696991361	15.51087216970452
H	0.95490959864066	4.63067096039952	15.52174192294777
C	2.03430578203762	4.79826256455945	10.21474043883759
H	1.14739759963273	5.31579447037871	9.84027561783998
C	8.27353041601097	8.89923753300532	13.84539499762759
C	2.16791579952016	3.42172605433411	10.03848958265284
H	1.39309337830857	2.85633352845760	9.51715014262881
C	3.02033513688691	5.54113987786466	10.87778702577472
C	9.66014090580130	7.79137095772047	10.19244122413044
C	9.21096464187680	6.68798981007203	14.35755730672035
C	3.29398803402248	2.76879263918342	10.54539148809664
H	3.39444045412690	1.68631426728574	10.43411180832682
C	8.47933064854831	6.81737504059852	10.16027518543820
C	10.28600032672213	7.31794331483808	14.99546814005030
H	11.06135067048445	6.70091907219318	15.45579836343070
C	2.82701793092870	7.00925860998901	11.14064965128964
C	7.12966003520770	9.72612461664466	13.32810094009418
C	5.49670100230115	2.76819165164850	11.78287449028547
C	5.95521800230328	9.00817376781846	9.68782482435734
H	5.28841733332040	9.71434261246803	9.16601746843397
H	6.81839145841181	9.56633931962791	10.06226359079489
H	5.42529420763196	8.59805688805060	10.55759077839453
C	6.36836258100917	7.86437228828989	8.74461207509880
C	5.07914881460985	7.19232821488153	8.23378432482787
H	4.54703720013848	6.68144321987435	9.04667872605347
H	5.30195775318358	6.44168686874887	7.46182908832248
H	4.40710303598199	7.94856218104746	7.79897882431884
C	7.21784624922063	6.80536177584284	9.45106124075678
C	9.37364629082458	9.49211597181150	14.47719056792766
H	9.42842947029165	10.58212122843928	14.53302725649262
C	7.10774131808402	8.43428052680847	7.51674631420465
H	6.43497097332104	9.08566801919175	6.93504689231894
H	7.44640106375585	7.61774123117723	6.86185720614343
H	7.98497003742150	9.02851942072771	7.80234930929246
C	9.30732779208324	9.27436110847634	10.38095449707712
H	8.74432021292652	9.67872012154368	9.53141887975804
H	10.23415327145906	9.86315231296276	10.47261360725231
H	8.72414096867807	9.42506646407745	11.29597447778957
C	10.38084419573862	8.71023300182208	15.04422569290436
H	11.23430481817923	9.18491494977524	15.53199896825722
C	10.40032613076916	7.61748004964382	8.84313333852055
H	10.74547475875469	6.57892730675396	8.73638028986237
H	11.27661968938951	8.28558229853713	8.79901678549293
H	9.74599719533527	7.84351304454778	7.99162800497466
C	10.64572250593740	7.40656208143785	11.30858740914122
H	10.24208297316871	7.63887905978487	12.29816474707218
H	11.58654846632526	7.96508519398348	11.18250069499626
H	10.87990220207467	6.33168561012090	11.27641047274199
H	9.05319002450067	4.83761543703108	13.26986034439762
H	8.16228629089701	4.85660311881229	14.78915363554364
H	9.94487316172646	4.71964135839062	14.82446169971786

```
H   2.10924263757336      7.44490648627380     10.43186712405042
H   3.77753305044713      7.55152978123594     11.06788254188388
H   2.44713840613536      7.17550478256274     12.16171242771999
H   6.74937196410896      9.32292709095073     12.38085901264360
H   7.42797085034573     10.77431509577731     13.18794286342728
H   6.28668901477806      9.69947408977570     14.03767323423495
H   5.39758194352531      1.67989055282199     11.66953417236452
H   5.61560962368729      3.00764505297470     12.84985668989972
H   6.42507700271857      3.09864936911372     11.29333797604913
```

[(^{Dmp}BIAN)Co(1,3-*t*Bu₂C₂P₂)]⁻:

```
Co  6.26070922590476     11.32572283032820      5.27742212988500
P   4.15004124365782     11.88083782934124      4.67375583633794
P   4.95161832354998     10.69317144382055      7.01216813378952
N   7.19410913413078     11.43645665370285      3.61996476909215
N   8.00182066578069     11.28072041184108      6.04948723416630
C   8.40997627371591     11.32386518502813      7.40521951536092
C   6.71297040212706     11.38648782118310      2.28879735323745
C   9.70278957711900     11.49879973191258      2.89396066833462
C  12.17238199668425     11.43823782793786      3.31843095343529
C   4.49847392936869     10.23602958719674      5.32674019418981
C   8.37029160870586     10.15690533777094      8.19960540652490
C   6.15915994591103     12.53765119328885      1.68694936446094
C   8.54386694592435     11.43037727798221      3.78109628375868
C  10.84605141819635     11.41796658205538      3.75816537219258
C  10.44818416306416     11.31294695790180      5.13347177956961
C   5.68841207113831     12.44929188316975      0.37137952031082
H   5.26066174112437     13.34036797563761     -0.09497411088058
C  11.45260664868216     11.21088546978924      6.08855981097496
H  11.21978217348819     11.12555948844768      7.15047716164138
C   9.93451488728607     11.61945219153466      1.52904259376566
H   9.11116187678216     11.68817668611841      0.81731698031860
C   6.84266038528203     10.18423894907579      1.55356241483093
C   8.98749480674103     11.34131907711872      5.11507790451288
C   7.93047240051437      8.84757732748992      7.61213272871789
C   8.90910290848689     12.53673390698074      7.93682850908277
C   4.14236893721438      8.88111715874395      4.76778857045525
C   4.77297753515159     12.34153134608666      6.30246922838082
C  13.18083017530498     11.33613796024787      4.32841592698277
H  14.23621130357948     11.34654281012139      4.04682279651896
C   6.35537848945507     10.13662488500324      0.24227295156273
H   6.43693023002657      9.20117404111779     -0.31690503884364
C  12.37464146513130     11.55813021179551      1.90693953151579
H  13.38900026753220     11.57863926860433      1.50211623078903
C  11.27969106832394     11.64729258492849      1.06102405929190
H  11.44841344321545     11.74028422063766     -0.01446388679544
C   6.10560212358216     13.83881669095645      2.43344308641720
C   9.30022935913000     12.57704870641757      9.28021118318387
H   9.66550352056267     13.51987621099466      9.69498203428875
C   5.77271869409800     11.25743814274555     -0.34972880446930
H   5.39584642027239     11.20589657025590     -1.37302508000354
C   2.77461134732039      8.46595642985899      5.35599596034576
H   2.82898346843725      8.40381238019685      6.45264821909972
H   2.45925253549329      7.48502626602982      4.96245002486285
H   2.00707690323936      9.20971768935697      5.09610956414294
```

```
C   8.77609227238991    10.23853941585278    9.53706637348503
H   8.74620419094751     9.33523805488181   10.15155266469840
C   4.77043314323634    13.69008760921619    6.97809272038279
C   9.03972256145406    13.75621073535978    7.06610911124945
C   5.19647011067122     7.83949577125819    5.17753635540594
H   6.19291109811242     8.14243415529574    4.83106676664316
H   4.95608586783250     6.84905074497259    4.75862583046194
H   5.24117961715978     7.74497778671151    6.27285667971607
C  12.81108141827137    11.22397145439638    5.65999242845187
H  13.59129843641451    11.14481476990055    6.42076439631871
C   7.51242295239111     8.98407186816339    2.16489803492622
C   5.59013837039656    13.63956006219034    8.27562434359800
H   5.16571282505645    12.90160808809139    8.97300205872536
H   5.59388332992412    14.62181134566617    8.77460817361273
H   6.62665931183725    13.34422287619785    8.08084921556305
C   4.02002519827140     8.94866705104892    3.23838630319529
H   3.23084951277362     9.65751429588513    2.94526925844012
H   3.76649711149304     7.96053952734941    2.82253992460327
H   4.95210088945249     9.29223068877473    2.77728024530570
C   3.30814304132676    14.04802581535552    7.32782144000039
H   2.69505923687511    14.09914003982877    6.41624739575107
H   3.25534253271155    15.02146971000822    7.84360704314154
H   2.87475340971093    13.28017398182852    7.98536857096486
C   9.22918945826373    11.43955257703991   10.08459443572310
H   9.53670259988344    11.48565940628420   11.13108482427860
C   5.33206233462841    14.76246311375892    6.03029055696141
H   6.35215033356020    14.50356331614193    5.71874759078093
H   5.34501008684248    15.75139599493458    6.51624610878880
H   4.71679834323045    14.83616047336357    5.12091783126813
H   8.31110369877002     8.72369030052822    6.58972138231443
H   6.83246017984148     8.81204735486507    7.54211668632731
H   8.27202680486504     8.00711778030914    8.23289988805403
H   5.98586214347861    14.68246784335297    1.73893720727513
H   7.01181640962606    13.98763990946257    3.03502865144446
H   5.26008170636710    13.83989925440149    3.13862330615467
H   8.22962986579658    13.79545981482346    6.32612467849636
H   9.98364431253846    13.73313195347533    6.49877089464700
H   9.02370676670528    14.67351008650868    7.67094398892545
H   7.16317353701814     8.05600273000463    1.69135389593471
H   7.31591994931777     8.93715130745064    3.24405506371785
H   8.60599299011997     9.04202773430712    2.04538260892928
```

[(^{Dmp}BIAN)Fe(1,3-tBu$_2$C$_2$P$_2$)]$^-$:

```
Fe  6.24556596645472    11.32929160284019    5.28185116683388
P   4.09761759421678    11.89817126437982    4.69559311838341
P   4.90049629740832    10.67921605894511    7.02760697663079
N   7.19565114125721    11.42298583672634    3.60543826045029
N   8.01124235125749    11.29645121302279    6.05832826275177
C   8.42894374155150    11.34259768713790    7.41093908539656
C   6.72677640650530    11.36559949523953    2.26999499172361
C   9.70901742228471    11.50685549449432    2.89202144757708
C  12.17792488212975    11.43976192623314    3.31210420959331
C   4.46842164440188    10.24658975754285    5.32526778464737
C   8.38408912207884    10.18021713883584    8.21208424460460
C   6.16985417898182    12.51074095312424    1.65871889723631
```

```
C  8.54943921285927    11.43038676783484     3.78061116747738
C  10.85352499075242   11.41953311977669     3.75257857081753
C  10.45454851560004   11.30834995990963     5.12636665006077
C  5.70672185482344    12.41357571965859     0.34117017670838
H  5.27508724504410    13.29951876497470    -0.13138808521137
C  11.45849296405191   11.20053458451407     6.07985156458191
H  11.22637987385832   11.11055663384509     7.14157681626179
C  9.93806338164895    11.63336627870689     1.52825060939022
H  9.11382835428210    11.70732072644562     0.81809770837577
C  6.86688689019575    10.16088555208873     1.54095158771478
C  8.99250212834393    11.34639945767869     5.11017145994339
C  7.93641930153422    8.87026837935619      7.63130106217014
C  8.93513166222887    12.55553377245447     7.93628462073608
C  4.10831784754053    8.89704932383821      4.75104472957316
C  4.74897907423150    12.33539127546023     6.32518949105606
C  13.18791282906480   11.32982849341405     4.32071854049299
H  14.24303739078913   11.33707177590740     4.03813377109643
C  6.38919136903038    10.10451155730909     0.22638298850088
H  6.48016059374794    9.16719223639531     -0.32830203398458
C  12.37906963887025   11.56727071535603     1.90058072110183
H  13.39307381894990   11.59114865476036     1.49498107062947
C  11.28371490608600   11.66219752174879     1.05722257044387
H  11.45009172688724   11.76142720167598    -0.01800096565004
C  6.10775442981389    13.81419115244378     2.40048479011386
C  9.33040805957833    12.60038633642241     9.27807971475229
H  9.70227005940249    13.54328887766435     9.68700417823503
C  5.80363611191885    11.21907721457693    -0.37444923769906
H  5.43257778891646    11.16040946047251    -1.39950179918278
C  2.73254855814399    8.48154749133635      5.31913109207684
H  2.77382713061813    8.41050123210725      6.41587335567937
H  2.41809625500908    7.50501901121867      4.91401938913698
H  1.97104687282251    9.23045166273813      5.05672486620329
C  8.79215988692082    10.26658510390205     9.54874448820842
H  8.75733537542857    9.36706261830467     10.16860132963427
C  4.75314025411568    13.67758062413302     7.01732646118588
C  9.06329600141103    13.77103831404556     7.05973744135095
C  5.15383535073911    7.84782483795217      5.16406934222381
H  6.15318677226066    8.14043189905169      4.81573676355492
H  4.90607297870821    6.85866252374527      4.74630436010712
H  5.19771419218002    7.75443382239862      6.25964659857152
C  12.81840459802740   11.21230080878398     5.65099110461329
H  13.59798844810182   11.12671973906139     6.41165263287546
C  7.53659773519968    8.96679333167522      2.16385319779246
C  5.58813547812664    13.61156787788666     8.30443235197568
H  5.17517775218940    12.86132536775004     8.99566832632849
H  5.59311251578442    14.58608552158728     8.81826678477905
H  6.62378695100841    13.32389118519102     8.09360835776894
C  4.00647310710742    8.97858491726728      3.22080692249488
H  3.23011085978754    9.69959314048442      2.92321780329299
H  3.74624558922647    7.99724297401715      2.79307215980824
H  4.94913750653484    9.31404241317282      2.77537664871111
C  3.29608711551360    14.03563312923269     7.38722300556243
H  2.67252737475615    14.09729835682511     6.48337788645793
H  3.25072424501385    15.00373490743920     7.91379259089185
H  2.86855017564099    13.26153982539598     8.04115199768633
C  9.25459341503735    11.46743503943770     10.08881279214908
```

H	9.56366343231172	11.51726584418401	11.13467525267805
C	5.30761174791537	14.75903042489849	6.07524102876976
H	6.33375134993314	14.51455260631928	5.76996550932795
H	5.30769616957735	15.74644147805333	6.56447252473309
H	4.69660688320881	14.82917243754355	5.16254544936491
H	8.34696269971417	8.72199913700051	6.62333601204151
H	6.84033003607792	8.85584987658449	7.52738685428083
H	8.24211302356423	8.03306746586583	8.27457556969878
H	5.88080579885077	14.64331310984981	1.71569787614014
H	7.05446405524736	14.02160400418841	2.91824268865599
H	5.32957280719415	13.77108563722090	3.17791377992951
H	8.23980719778001	13.81736936636713	6.33461292589188
H	9.99536915969733	13.73614575413703	6.47379992456961
H	9.06828846728205	14.69009692643507	7.66187391395561
H	7.20703244106628	8.03622667803505	1.68127842578633
H	7.31734854166093	8.91454930035522	3.23859294477791
H	8.63182092492524	9.03579233360872	2.06843838394143

[(^{Dmp}BIAN)Fe(1,2-tBu$_2$C$_2$P$_2$)]$^-$:

Fe	6.95933952896180	6.12005865212629	11.38242106026567
P	6.97214841134604	4.96648613498811	9.36619641316097
P	8.83919599227014	5.07967634310467	10.53044211100740
N	7.16166486276801	6.79716828463087	13.17457611913803
N	5.19452082762216	5.63510767625741	11.98584855147564
C	6.03627593103217	6.63360372832158	13.92578107932763
C	5.66536142327007	6.91296268529047	15.31311182220455
C	5.51856582195918	7.55760554330462	17.64394131056465
H	5.99280313861942	8.02507743176316	18.51007342443224
C	4.23712336865899	7.04647416159285	17.77397276394843
H	3.71056301705265	7.11050501509820	18.72889372025779
C	6.25560558242183	7.49935571401458	16.42508027744439
H	7.26525010548129	7.90913634827053	16.38287884616559
C	2.62086315714437	5.20286744298693	14.24781857190061
H	2.21700519224207	4.71645507544459	13.35928569748799
C	3.88031095351229	5.78911006550822	14.24244394197955
C	4.33931086201521	6.38640500833943	15.46432050125815
C	8.26148518977445	7.41166541066242	13.81874968089696
C	4.96909648766364	5.98016254279599	13.28547148137423
C	3.60440520345126	6.42457766360337	16.65097499846557
C	2.30618348378729	5.82280964870985	16.61797377813978
H	1.68394447656267	5.82045701404169	17.51574297619942
C	9.25248338193897	5.11799833151745	14.27728581938408
C	4.29513863148711	3.50077421051104	11.19891737617360
C	4.17029579047025	4.90258155115756	11.32958214928092
C	1.85201682083112	5.23583316744472	15.44769212103935
H	0.86259192486109	4.77260209473963	15.43706667677175
C	2.03083871694465	4.82218096102531	10.19570130419419
H	1.14576685474955	5.33963980357510	9.81671350719236
C	8.29251172356508	8.82050632806498	13.93669847361471
C	2.16383605553988	3.44545866929213	10.02267909892350
H	1.39136633643952	2.87952481911517	9.49840114775085
C	3.01509821105510	5.56583094411613	10.86077826580859
C	9.65467747551857	7.86342952314550	10.18973200250734
C	9.29624209198223	6.61972377156898	14.36068718980522
C	3.28701004716759	2.79342766244038	10.53641824625682

H	3.38681021279844	1.71054812676783	10.42868568276222
C	8.51200635515251	6.84260019773478	10.16724794829527
C	10.37843755927535	7.26224375820934	14.97705244405615
H	11.18581144551830	6.65395921230832	15.39265224563027
C	2.81444704832003	7.03372225772881	11.11944409090006
C	7.13433525437166	9.64066425568708	13.44063898517612
C	5.47648941809030	2.78827650716197	11.79253378756301
C	5.92083077954573	8.92631633335064	9.67063879375951
H	5.22019579410920	9.59888062489288	9.14876423384628
H	6.76504381546997	9.52421042479906	10.02617403766483
H	5.41641179014252	8.50996759457774	10.55255572490402
C	6.36539992651192	7.78521404870296	8.73720993466081
C	5.09655991286044	7.06688790264958	8.24111424874668
H	4.57490282841821	6.56368986150383	9.06530773512292
H	5.34165152578288	6.30285855302875	7.48914988122877
H	4.40601185809855	7.79316912301511	7.78445301280226
C	7.25379742998338	6.76174664639580	9.45133761751222
C	9.39743191833264	9.42385525944716	14.54604506139592
H	9.43365312632968	10.51370765893260	14.61811538894572
C	7.08155247131255	8.36649553062168	7.50146027988308
H	6.39009278067254	8.99935603728650	6.92112006204877
H	7.43583402599178	7.55475844445971	6.84896867818400
H	7.94632861545995	8.98216159657574	7.77959374728294
C	9.24177890760063	9.33212206207921	10.36943118876332
H	8.67546368966684	9.71339490414007	9.51104498823605
H	10.14397366662706	9.95670322275463	10.47095665686771
H	8.64071812365814	9.46292457469241	11.27675950646105
C	10.44116444167564	8.65269294478662	15.06254222943712
H	11.29929100965682	9.13587446608958	15.53352311418075
C	10.40927601063921	7.71376477068382	8.84576969884152
H	10.80574648966611	6.69259303048510	8.75116692205435
H	11.25141383905756	8.42433178875541	8.79721036126768
H	9.74838730023857	7.89731855956736	7.98919683898990
C	10.64940075859293	7.52796007205560	11.31403214463431
H	10.22579713575366	7.73898672037568	12.30012343616788
H	11.56231024707199	8.13261610106071	11.19599312922729
H	10.93710719428469	6.46610009815787	11.28325769957640
H	8.26196672707425	4.76717995736582	13.96989273665821
H	9.51423694273974	4.66918267672395	15.24753096504622
H	9.96694623635642	4.74856924966059	13.52516196397598
H	2.12615223592508	7.47308900463545	10.38419308864734
H	3.76681916973853	7.57488876154881	11.08553277963112
H	2.39371858253851	7.19748895009172	12.12481967830459
H	6.75976553912832	9.25222176218941	12.48394236618136
H	7.41971207440929	10.69486443072638	13.32015417830058
H	6.29021099338836	9.59082684980550	14.14715225582453
H	5.37611911263758	1.70071916590530	11.67323460084858
H	5.58062491477752	3.02169361043654	12.86256795414981
H	6.41110568438037	3.11738288081863	11.31376338955604

[Fe(1,2-*t*Bu₂C₂P₂)(anthracene)]⁻:

Fe	5.42992338896547	10.21329259797338	4.09655246495137
P	3.27081912469223	9.37074297810374	3.88260991763509
P	4.71462146743912	8.23481996598950	5.06855804286578
C	8.75893610634255	12.32604842142458	1.50258150806364

C	5.54014543097296	8.28562032369459	3.43340444799700
C	9.06964322496417	11.04561880204657	3.58394123244978
H	9.70313536155170	10.42758732850495	4.22608779934441
C	5.51726888730192	12.24124760088973	3.50485015137721
H	4.83834281913736	12.73893131970857	2.80900995158177
C	7.76284188319901	11.31980536132664	3.97969350717611
C	6.91353552165672	12.12086978550977	3.11512082974346
C	7.43747581846268	12.62337250404024	1.92973466437242
H	6.80018913780467	13.22655790272626	1.27723649256286
C	9.59482022297998	11.50956036933791	2.34927373978894
C	4.40291201004026	9.31757749313681	1.14872477852717
C	5.10837478779764	12.07905321555021	4.86529298930349
H	4.12986165877882	12.42255482522647	5.20013906772663
C	9.28714766728218	12.78974406262612	0.27296216281347
H	8.64774540556294	13.40249223160152	-0.36791670310972
C	4.58430704658751	9.04199446632838	2.64768049829269
C	5.52454154543554	10.16934050410594	0.53152610606912
H	5.48052396793526	11.18996467553065	0.92677158871565
H	5.40890397159222	10.21756811426729	-0.56451556056025
H	6.52421798009941	9.78845990622380	0.75286573696628
C	6.75573639660870	7.41167888354831	3.12029991955503
C	5.94549887691943	11.32385256020950	5.72100536783477
H	5.63195637664804	11.07316350822020	6.73405338263058
C	7.14074777466973	10.76332556169740	5.16537276875521
H	7.73677957305419	10.09367492316436	5.78735458170814
C	6.25257530836751	5.98863561159257	2.78726256281905
H	5.68268177761453	5.58239048518786	3.63566589593460
H	7.10001032707451	5.31506929171676	2.57660365926648
H	5.59001736627465	5.99531643470544	1.91177323787653
C	3.09278598345542	10.10281632821169	0.94591418359401
H	2.21751841709211	9.51387435698520	1.25558950100181
H	2.97693409969083	10.37342457719761	-0.11577399377262
H	3.10304656562731	11.02860263391476	1.53978884166466
C	10.90743569794161	11.20414263362206	1.91142534432964
H	11.53538813684963	10.57872868797772	2.55130047953862
C	10.58101402466190	12.47861746671254	-0.12415713861945
H	10.96461791871884	12.84840400560212	-1.07716195927714
C	7.64101211700184	7.92550247155637	1.97441596959691
H	7.13341859676342	7.87737942579475	1.00368754961084
H	8.54847049922447	7.30418772764594	1.90020859126669
H	7.95809965098120	8.96119370595715	2.15778009867135
C	11.39723761242334	11.67881428833602	0.70200196973623
H	12.41299760075058	11.42971084918711	0.38825973579620
C	4.26913669751848	7.98153376151916	0.39041201193845
H	5.21451453211875	7.42411386822805	0.38498894602883
H	3.97830228677105	8.16090458166007	-0.65796545687338
H	3.50305724548729	7.34782270355695	0.86128464914671
C	7.64693319508260	7.31854023495724	4.37305686827100
H	8.11873189224048	8.28648839904366	4.58065687025429
H	8.43786473039856	6.56739538319608	4.21866949613474
H	7.06074428538640	7.02756989322120	5.25794065092669

[Co(1,2-*t*Bu₂C₂P₂)₂]⁻:

P	6.64938391058229	7.55525715681854	8.00177373498066
P	4.49445918522593	7.91779672906008	7.73986252497686

C	6.49510260587596	9.30413377752347	8.52056972282425
C	5.07642909999820	9.53631892693298	8.34011995774395
C	4.51947211114347	11.90099945722442	9.23398232335246
H	4.63464686108104	11.51740937753246	10.25727074739976
H	3.71277542217134	12.65220509769370	9.23269695057302
H	5.44320091168956	12.41204660368133	8.93420166662225
C	4.16060121524240	10.75917427860493	8.27492444761793
C	4.18994544820989	11.28673079470589	6.82121149155081
H	5.20615102363349	11.58125951611109	6.52542652990906
H	3.52870246902273	12.16274572359091	6.71344811486487
H	3.85191006159741	10.50263275100064	6.12830451932694
C	7.71631259251636	10.20396288945178	8.75142928881772
C	2.71647301594247	10.33081742711116	8.59684075049428
H	2.40814037512657	9.47668821407003	7.97425990861737
H	2.02402793182692	11.16621386031512	8.40339655343891
H	2.63662444198264	10.03292441781177	9.65121836948773
C	8.96633315851741	9.31300661708705	8.88423560451054
H	8.86199415728061	8.64239675437981	9.74848500012303
H	9.85888589209567	9.94057549159707	9.03596591613360
H	9.12120212169748	8.69710437839624	7.98642488591223
C	7.68038197010441	11.07783947214667	10.01826890510897
H	6.82365882887970	11.75442329164771	10.04789514977531
H	8.59768140163681	11.68920763658929	10.06664788407832
H	7.63524571933187	10.43767999534191	10.90937339436188
C	7.89245295365262	11.10324861744877	7.50892953942038
H	7.89993818663448	10.49487070131208	6.59233314853057
H	8.84030782859175	11.66352041059897	7.56706379499048
H	7.07353860106217	11.83107613323309	7.42763967246027
Co	5.41335595384599	8.15892285419413	9.81538667086170
P	4.17730265537511	8.76256466205733	11.62899081900202
P	6.33222662184621	8.40005835068470	11.89091738400542
C	4.33160823843264	7.01369336811577	11.11018700334786
C	5.75029193821326	6.78152599577879	11.29065549920037
C	6.30755145858268	4.41686284206775	10.39680166953154
H	6.19240658766219	4.80044875584104	9.37350876073599
H	7.11434906275918	3.66576567801498	10.39814352068256
H	5.38387081665006	3.90568877880106	10.69650486943530
C	6.66619589849060	5.55872117400287	11.35590026935190
C	6.63677734486310	5.03114809861139	12.80960562273374
H	5.62057277804889	4.73652948209645	13.10530390460146
H	7.29808769694851	4.15518962916903	12.91741486372818
H	6.97468799751399	5.81526862835548	13.50254785312610
C	3.11036345745693	6.11390930269720	10.87931217890680
C	8.11031367509772	5.98721070732250	11.03412520345048
H	8.41850765922480	6.84136543301499	11.65673971131119
H	8.80281786139917	5.15187738886849	11.22763203226719
H	8.19023579207773	6.28511557421947	9.97975664788824
C	1.86038728119064	7.00494641105136	10.74665318325479
H	1.96471177361531	7.67561831459174	9.88244993606924
H	0.96778932665142	6.37744025516681	10.59493017192588
H	1.70561222887339	7.62078704307267	11.64452246983146
C	3.14613807066714	5.24014890955145	9.61238768454899
H	4.00277864956505	4.56347451082967	9.58265099730100
H	2.22876845685474	4.62888743520280	9.56399869155777
H	3.19129789739262	5.88038763028657	8.72134062109439
C	2.93423305905211	5.21453984569190	12.12175508297020

245

H 2.92682381738597   5.82285071945895   13.03839639001513
H 1.98634546420044   4.65432342120910   12.06362338224147
H 3.75311097770871   4.48666230095461   12.20295640701719

[Co(1,3-*t*Bu₂C₂P₂)₂]⁻:

Co 4.77915327914802   5.96659674678014   6.20688184845955
P   6.61071027853583   5.12606097718256   7.25523026189821
P   4.34180269677009   3.76340978665667   6.45123519877359
P   3.52266194963722   7.74424807387785   6.80558102541787
P   4.65238307755447   7.23628133839241   4.34302735393108
C   4.95626774347235   4.73849117856493   7.84570280871896
C   5.92090665425435   4.31563124972012   5.76261328825507
C   5.08982631998917   7.97930437933080   5.93311973530431
C   3.16033925494209   6.83606022882922   5.28408803325726
C   4.40712632526285   4.85589769469377   9.24688794626532
C   4.86141619162523   3.60512196954168   10.03422024858716
H   4.48532477833418   2.69211042108751   9.54990863042658
H   4.48708652404900   3.63400637151311   11.07113704035608
H   5.95945398810515   3.54701117858377   10.05822895817323
C   4.95259760200757   6.11334318383000   9.94140040134323
H   6.05330097484440   6.11873621451569   9.93181870460180
H   4.61782304664716   6.15559394240598   10.99065265633964
H   4.60118908739832   7.01259813903854   9.41855463637295
C   2.87147299308306   4.90800851432951   9.22855074564522
H   2.53427980632277   5.82455015041354   8.72683994134914
H   2.46823277176504   4.89148185797072   10.25425705585169
H   2.45758643958417   4.04649214834811   8.68272755462687
C   6.60918046897777   3.88729717139428   4.48931720222079
C   7.33113960799416   2.55023790090350   4.77447463930693
H   8.06618061290823   2.67878985365208   5.58237719726348
H   7.85538283891393   2.18528480179243   3.87552971903304
H   6.60743035974953   1.78633633959965   5.09423807755114
C   7.64468571878370   4.93371680190296   4.04883024020361
H   7.13955531011073   5.87192719000585   3.78416850473572
H   8.21436655243888   4.57577767712225   3.17570317374844
H   8.35762350251913   5.14514956623090   4.86039064489023
C   5.58605043658680   3.67705484677485   3.36223019396852
H   4.81044223924124   2.95780927241032   3.66704677131487
H   6.07866454107417   3.28814988451818   2.45623742911043
H   5.09398291552751   4.62846698240850   3.12063860439856
C   6.25637972978233   8.87001960400489   6.28581542200284
C   6.50899444374711   8.86287598742107   7.80157640775408
H   5.59314389496568   9.12869460380764   8.35139406001029
H   7.29395093360803   9.58873508731667   8.06957256822736
H   6.82319318825104   7.86143666507462   8.12401396035566
C   7.52887615856476   8.41628617642127   5.55392913337091
H   7.81876686873882   7.41296153694629   5.89278001335167
H   8.36007947942707   9.11344990918804   5.74874914079995
H   7.36187799332342   8.37674478255677   4.46661040459239
C   5.90040447035283   10.30675636492637   5.83929582506229
H   5.70784907051968   10.33346797890953   4.75680863575349
H   6.72163737437596   11.00604997459824   6.06888248299517
H   4.99111886617228   10.65143041796471   6.35303253780776
C   1.85275999530321   6.25440387894149   4.80390874416271
C   2.09556893546767   5.17900392993694   3.73330261531901

```
H   2.69449639743522     5.58237348584655     2.90243062404069
H   1.13993035150073     4.81437911389806     3.32250345286983
H   2.64181071635812     4.33287180336028     4.17053810363977
C   1.06646697041145     5.64145995980781     5.97338490127615
H   1.61332789585157     4.78258515999564     6.38415295205155
H   0.07073350958321     5.30634638173749     5.64010642733725
H   0.92903504672394     6.37701485090235     6.78057611477055
C   1.02590562618793     7.40586963993404     4.18736132779061
H   0.84062619118932     8.18748511169779     4.93863916115960
H   0.05539421220542     7.03876659056682     3.81392971002435
H   1.57354479179491     7.86459696991624     3.35105880177348
```

[Co(1,2-*t*Bu₂C₂P₂)(1,3-*t*Bu₂C₂P₂)]⁻:

```
P   7.20418158499781     7.79485466349769     8.44774990855626
P   5.05488928320007     7.66107954504914     7.99442538308555
C   6.68129509846732     9.53886757383435     8.61537729760361
C   5.27257491397685     9.45560337023367     8.30532972909033
C   4.26372983816780    11.81641946801524     8.58036483728892
H   4.31265295157375    11.70554497905687     9.67030686054394
H   3.36900607416202    12.41110911522929     8.33414905060018
H   5.14120600522142    12.38843586960155     8.25309515891487
C   4.18553014788925    10.44503544227665     7.89646353429595
C   4.27895361643435    10.64964658736817     6.36602147338073
H   5.25159458884145    11.07401455993212     6.08106718034433
H   3.48584843267751    11.33116341818638     6.01482840914716
H   4.16810218123028     9.68506198367601     5.85021723539291
C   7.69707090677457    10.67548854492578     8.76951688104048
C   2.81142717516135     9.82386619193288     8.20975302193320
H   2.69481960258403     8.85902677392538     7.69388395122117
H   2.00220680272113    10.49475133353598     7.87889952944151
H   2.70671909830448     9.63128394030434     9.28393694248276
C   9.08152805285340    10.06612222476179     9.06608167194825
H   9.03850120762814     9.45017893559143     9.97618399579329
H   9.81861228806667    10.87021176223574     9.22097614946153
H   9.42763272055877     9.43060057849915     8.23831173492039
C   7.38994110528164    11.62774554877640     9.93396012925499
H   6.41941799761203    12.11894089313429     9.82649468314196
H   8.16373706954934    12.41151660718870     9.99763752762636
H   7.38237315756835    11.06041811853722    10.87292826366941
C   7.79363986418102    11.45826044917251     7.44457681166666
H   7.99621084748397    10.77145136482640     6.60931941607113
H   8.60733718625451    12.20107127684680     7.49044706588591
H   6.86047550812124    11.99300577738958     7.22309599305666
Co  5.69672699939180     8.42038418099407    10.02703995132127
P   6.59496704473718     8.39704792942191    12.09309816261063
C   5.81976732196286     6.91940352372522    11.39043598991059
C   5.75659079124251     4.78667876474564    10.05766550653011
H   6.12505207160999     5.23957872424945     9.12733937700964
H   6.03110425446006     3.71845674970949    10.06302604812025
H   4.65917720255900     4.86391668524682    10.05301887880051
C   6.34964005608019     5.50778664372072    11.27952688740929
C   5.92096719232715     4.75262258249800    12.55999269312719
H   4.82419756949841     4.72186522638064    12.63806846113489
H   6.30394538520184     3.71825809853108    12.55387957281593
H   6.30893572778226     5.26567711366666    13.45238923327834
```

```
C  7.88436872173649     5.50004742238514    11.19559015091548
H  8.32266797466788     6.00757737405836    12.06900237561862
H  8.26628914613990     4.46611962338033    11.17058571680001
H  8.21824093848613     6.02876184500308    10.29229333598866
C  4.91064102881199     9.02788411439613    11.88193237893699
P  4.10775526125241     7.50614839246665    11.32451106990744
C  4.24364641514248    10.18816207369655    12.59374882762676
C  4.03001246320984     9.75075123478088    14.06421107531365
H  3.41330316594468     8.84125254325311    14.10494177920825
H  3.52865887158419    10.54556244988692    14.64292380069710
H  4.99626581020444     9.52470970687079    14.53777122836311
C  5.11639349306834    11.45088584492622    12.59398237735008
H  6.12026885685338    11.22865036139558    12.98664551250920
H  4.66650968056359    12.23470567669299    13.25540436421371
H  5.23524126561692    11.84808496614559    11.57996243516065
C  2.86723752680400    10.50417397801979    11.98791718165785
H  2.24211390042749     9.59857590699798    11.95780276310292
H  2.96128804031358    10.88199102242848    10.96341295037234
H  2.34258051477450    11.26494234278417    12.58883008732809
```

References

[1]   S. Pelties **2016**, *Synthesis, Characterization, and Reactivity Studies of Low-valent 3d Metal Complexes with N-Heterocyclic Carbene and α-Diimine Ligands. Dissertation, Naturwissenschaftliche Fakultät IV -Chemie und Pharmazie - der Universität Regensburg.*

[2]   G. Maier, *Angew. Chem. Int. Ed. Engl.* **1988**, *27*, 309.

[3]   G. Maier, S. Pfriem, U. Schäfer, R. Matusch, *Angew. Chem. Int. Ed. Engl.* **1978**, *17*, 520.

[4]   A. R. Jupp, J. C. Slootweg, *Angew. Chem. Int. Ed.* **2020**, *59*, 10698.

[5]   a) R. J. Wilson, N. Lichtenberger, B. Weinert, S. Dehnen, *Chem. Rev.* **2019**, *119*, 8506; b) S. Scharfe, F. Kraus, S. Stegmaier, A. Schier, T. F. Fässler, *Angew. Chem. Int. Ed.* **2011**, *50*, 3630; c) K. Mayer, J. Weßing, T. F. Fässler, R. A. Fischer, *Angew. Chem. Int. Ed.* **2018**, *57*, 14372; d) T. F. Fässler, *Zintl Ions: Principles and Recent Developments*, Springer, **2011**; e) R. Ababei, J. Heine, M. Hołyńska, G. Thiele, B. Weinert, X. Xie, F. Weigend, S. Dehnen, *Chem. Commun.* **2012**, *48*, 11295; f) U. Friedrich, M. Neumeier, C. Koch, N. Korber, *Chem. Commun.* **2012**, *48*, 10544; g) S. Mitzinger, J. Bandemehr, K. Reiter, J. Scott McIndoe, X. Xie, F. Weigend, J. F. Corrigan, S. Dehnen, *Chem. Commun.* **2018**, *54*, 1421; h) S. Mitzinger, L. Broeckaert, W. Massa, F. Weigend, S. Dehnen, *Nat. Commun.* **2016**, *7*, 10480; i) S. C. Critchlow, J. D. Corbett, *Inorg. Chem.* **1985**, *24*, 979; j) G. C. W. Blase, *Z. Kristallogr. – Cryst. Mater.* **1991**, *196*, 207; k) L. Xu, S. C. Sevov, *Inorg. Chem.* **2000**, *39*, 5383; l) S. C. Critchlow, J. D. Corbett, *Inorg. Chem.* **1982**, *21*, 3286; m) F. Lips, I. Schellenberg, R. Pöttgen, S. Dehnen, *Chem. Eur. J.* **2009**, *15*, 12968; n) F. Lips, M. Raupach, W. Massa, S. Dehnen, *Z. Anorg. Allg. Chem.* **2011**, *637*, 859.

[6]   G. Hierlmeier, P. Coburger, M. Bodensteiner, R. Wolf, *Angew. Chem. Int. Ed.* **2019**, *58*, 16918.

[7]   M.-L. Y. Riu, R. L. Jones, W. J. Transue, P. Müller, C. C. Cummins, *Sci. Adv.* **2020**, *6*, eaaz3168.

[8]   G. Hierlmeier, R. Wolf, *Angew. Chem. Int. Ed.* **2021**, *60*, 6435.

[9]   Which react with Ag$^+$ to give homoleptic complexes [AgL$_2$]+ (L = η^2-P$_4$, η^2-tBuCP): a) E.-M. Rummel, P. Mastrorilli, S. Todisco, M. Latronico, G. Balázs, A. V. Virovets, M. Scheer, *Angew. Chem. Int. Ed.* **2016**, *55*, 13301–13305; b) I. Krossing, *J. Am. Chem. Soc.* **2001**, *123*, 4603–4604.

[10]   G. Hierlmeier, M. K. Uttendorfer, R. Wolf, *Chem. Commun.* **2021**, *57*, 2356.

[11]   E. Urnėžius, W. W. Brennessel, C. J. Cramer, J. E. Ellis, P. v. R. Schleyer, *Science* **2002**, *295*, 832.

[12]   a) E.-M. Schnöckelborg, J. J. Weigand, R. Wolf, *Angew. Chem. Int. Ed.* **2011**, *50*, 6657; b) C. M. Hoidn, T. M. Maier, K. Trabitsch, J. J. Weigand, R. Wolf, *Angew. Chem. Int. Ed.* **2019**, *58*, 18931.

[13]   S. Pelties, T. Maier, D. Herrmann, B. de Bruin, C. Rebreyend, S. Gärtner, I. G. Shenderovich, R. Wolf, *Chem. Eur. J.* **2017**, *23*, 6094.

[14]   R. Wolf, A. W. Ehlers, J. C. Slootweg, M. Lutz, D. Gudat, M. Hunger, A. L. Spek, K. Lammertsma, *Angew. Chem. Int. Ed.* **2008**, *47*, 4584.

[15]   R. Wolf, J. C. Slootweg, A. W. Ehlers, F. Hartl, B. de Bruin, M. Lutz, A. L. Spek, K. Lammertsma, *Angew. Chem. Int. Ed.* **2009**, *48*, 3104.

[16]   a) J. Malberg, T. Wiegand, H. Eckert, M. Bodensteiner, R. Wolf, *Chem. Eur. J.* **2013**, *19*, 2356; b) J. Malberg, M. Bodensteiner, D. Paul, T. Wiegand, H. Eckert, R. Wolf, *Angew. Chem. Int. Ed.* **2014**, *53*, 2771; c) J. Malberg, T. Wiegand, H. Eckert, M. Bodensteiner, R. Wolf, *Eur. J. Inorg. Chem.* **2014**, *2014*, 1638; d) C. Rödl, R. Wolf, *Eur. J. Inorg. Chem.* **2016**, *2016*, 736; e) C. Rödl, J. B. n. Malberg, R. Wolf, *Z. Naturforsch. B* **2018**, *73*, 895; f) C. Rödl, K. Schwedtmann, J. J. Weigand, R. Wolf, *Chem. Eur. J.* **2019**, *25*, 6180; g) C. Rödl, R. Wolf, *Chem. Eur. J.* **2019**, *25*, 8332.

[17]   E.-M. Rummel, G. Balázs, V. Heinl, M. Scheer, *Angew. Chem. Int. Ed.* **2017**, *56*, 9592.

[18]   a) P. Binger, G. Glaser, S. Albus, C. Krüger, *Chem. Ber.* **1995**, *128*, 1261; b) F. W. Heinemann, S. Kummer, U. Seiss-Brandl, U. Zenneck, *Organometallics* **1999**, *18*, 2021; c) A. D. Burrows, A. Dransfeld, M. Green, J. C. Jeffery, C. Jones, J. M. Lynam, M.T. Nguyen, *Angew. Chem. Int. Ed.* **2001**, *40*, 3221; d) C. Jones, C. Schulten, A. Stasch, *Dalton Trans.* **2006**, 3733; e) S. Deng, C. Schwarzmaier, M. Zabel, J. F. Nixon, M. Bodensteiner, E. V. Peresypkina, G. Balázs, M. Scheer, *Eur. J. Inorg. Chem.* **2011**, *2011*, 2991.

[19]   S. Pelties, T. Maier, D. Herrmann, B. de Bruin, C. Rebreyend, S. Gärtner, I. G. Shenderovich, R. Wolf, *Chem. Eur. J.* **2017**, *23*, 6094.

[20]   I. L. Fedushkin, A. A. Skatova, V. A. Chudakova, G. K. Fukin, *Angew. Chem. Int. Ed.* **2003**, *42*, 3294.

[21]   a) T. L. Breen, D. W. Stephan, *Organometallics* **1997**, *16*, 365; b) H. G. Ang, S. G. Ang, X. Wang, *J. Chem. Soc., Dalton Trans.* **2000**, 3429.

[22]   a) P. Pyykkö, *J. Phys. Chem. A* **2015**, *119*, 2326; b) P. Pyykkö, M. Atsumi, *Chem. Eur. J.* **2009**, *15*, 186.

[23]   F. J. de Zwart, B. Reus, A. A. H. Laporte, V. Sinha, B. de Bruin, *Inorg. Chem.* **2021**, *60*, 3274.

[24]   Note that the Mössbauer spectrum of this compound was not recorded at 77 K. However, the isomer shift at 4.2 K ($0.431 \ mms^{-1}$) suggests that there is only a small difference upon further cooling down the sample.

[25]   E.-M. Schnöckelborg, M. M. Khusniyarov, B. de Bruin, F. Hartl, T. Langer, M. Eul, S. Schulz, R. Pöttgen, R. Wolf, *Inorg. Chem.* **2012**, *51*, 6719.

[26]   R. Wolf, A. W. Ehlers, M. M. Khusniyarov, F. Hartl, B. de Bruin, G. J. Long, F. Grandjean, F. M. Schappacher, R. Pöttgen, J. C. Slootweg, M. Lutz, A. L. Spek, K. Lammertsma, *Chem. Eur. J.* **2010**, *16*, 14322.

[27]   T. M. Maier, M. Gawron, P. Coburger, M. Bodensteiner, R. Wolf, N. P. van Leest, B. de Bruin, S. Demeshko, F. Meyer, *Inorg. Chem.* **2020**, *59*, 16035.

[28]   K. Jonas, R. Mynott, C. Krüger, J. C. Sekutowski, Y.-H. Tsay, *Angew. Chem. Int. Ed. Engl.* **1976**, *15*, 767.

[29]   W. W. Brennessel, R. E. Jilek, J. E. Ellis, *Angew. Chem. Int. Ed.* **2007**, *46*, 6132.

[30]   W. W. Brennessel, J. V. G. Young, J. E. Ellis, *Angew. Chem. Int. Ed.* **2002**, *41*, 1211.

[31]   a) CrysAlisPro, Scale3 Abspack, Rigaku Oxford Diffraction **2019**; b) Sheldrick, G. M. SADABS, Bruker AXS, Madison, USA **2007**.

[32]   R. C. Clark, J. S. Reid, *Acta Cryst. A* **1995**, *51*, 887.

[33]   G. M. Sheldrick, *Acta Cryst. A* **2015**, *71*, 3.

[34]   O. V. Dolomanov, L. J. Bourhis, R. J. Gildea, J. A. K. Howard, H. Puschmann, *J .Appl. Crystallogr.* **2009**, *42*, 339.

[35]   G. M. Sheldrick, *Acta Cryst. C* **2015**, *71*, 3.

[36]   G. M. Sheldrick, *Acta Cryst. A* **2008**, *64*, 112.

[37]   a) F. Neese, *WIREs Comput. Mol. Sci.* **2012**, *2*, 73; b) F. Neese, *WIREs Comput. Mol. Sci.* **2018**, *8*, 1327.

[38]   S. Grimme, S. Ehrlich, L. Goerigk, *J. Comput. Chem.* **2011**, *32*, 1456.

[39]   S. Grimme, J. Antony, S. Ehrlich, H. Krieg, *J. Chem. Phys.* **2010**, *132*, 154104.

[40]   F. Weigend, R. Ahlrichs, *Phys. Chem. Chem. Phys.* **2005**, *7*, 3297.

[41]   a) Becke, *Physical Rev. A* **1988**, *38*, 3098; b) Perdew, *Phys. Rev. B* **1986**, *33*, 8822.

[42]   J. L. Whitten, *J. Chem. Phys.* **1973**, *58*, 4496.

[43]   F. Neese, F. Wennmohs, A. Hansen, U. Becker, *Chem. Phys.* **2009**, *356*, 98.

[44]   F. Neese, *Inorg. Chim. Acta* **2002**, *337*, 181.

9   Bulking up Cp^{BIG}: A Penta-Terphenyl Cyclopentadienyl Ligand[a]

Abstract:

The modification of cyclopentadienyl ligands with carefully selected substituents is a widely used strategy to modify their steric and electronic properties. We describe the synthesis of an extremely bulky penta-terphenyl cyclopentadienyl ligand (Cp^{T5}) by arylation of cyclopentadiene. Deprotonation reactions with different group 1 metals and bases afforded a complete series of alkali metal salts MCp^{T5} with M = Li to Cs. The potassium salt KCp^{T5} reveals a dimeric structure in the solid state. Dimerisation is achieved by coordination of potassium ions by the terphenyl substituents. Moreover, iron-, cobalt- and nickel complexes of Cp^{T5} were synthesised and the potential formation of dimetallocenes by reduction with KC_8 was investigated.
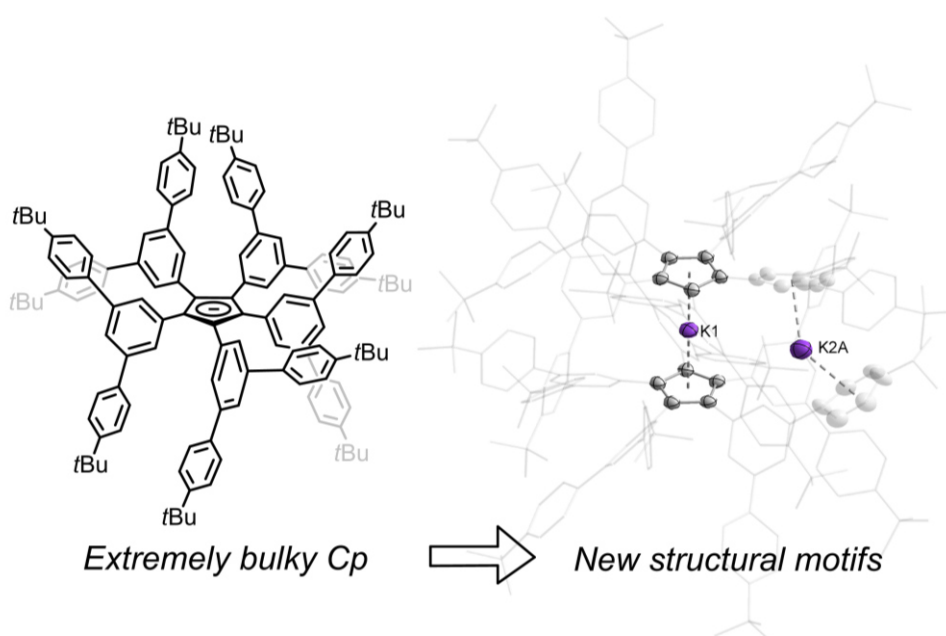
Extremely bulky Cp ⟹ New structural motifs

9.1   Introduction

Since the discovery of ferrocene in 1951,[1] cyclopentadienyl ligands have developed into one of the most fundamental ligand families in organometallic chemistry and have found widespread use in (asymmetric) catalysis,[2] small molecule activation,[3] and coordination chemistry (e.g. for the synthesis of single molecule magnets).[4] Cyclopentadienyl ligands are classical 'spectator'-ligands and their steric and electronic properties can be readily modified by introducing one or more substituents on the carbon atoms. These substitutions have dramatic effects, including slower rotational dynamics in the five-membered ring as well as higher steric protection of the coordinated metal centre. As a consequence, the resulting metal complexes can be more stable compared to their unsubstituted analogues or possess higher catalytic activity.[5]

The permethylated pentamethylcyclopentadienyl C_5Me_5 (Cp*, Figure 1A) was introduced in 1960 and has developed to a ubiquitous ligand due to its higher steric demand and stronger donating properties.[6] These properties led to isolation of metal complexes which were previously unstable with Cp ligands, e.g. decamethyltitanocene (Figure 1B).[7] Moreover, the introduction of even bulkier substituents such as *tert*-butyl or *iso*-propyl groups has led to cyclopentadienyls with still higher steric demand such as $C_5H_2tBu_3$ (Cp‴) and C_5iPr_5.[8,9] The latter ligand has recently received attention through its capability to stabilise the linear uranocene $[(\eta^5-C_5iPr_5)_2U]$.[10]

Apart from bulky alkyl substituents, the introduction of aryl substituents on the cyclopentadienyl ring has also been a major focus in this research field. As such, the coordination chemistry of the (nowadays commercially available) pentaphenylcyclopentadienyl ligand has been investigated, affording fascinating new structural motifs (Figure 1).[11] For instance, the introduction of a pentaphenylcyclopentadienyl ligand caused the formation of a linear stannocene, whose structure is in contrast to those of Cp_2Sn and $Cp*_2Sn$, which are significantly bent (33 and 25°, respectively).[12,13] Moreover, the isolation of a linkage isomer of decaphenylferrocene was accomplished.[11,14] Due to poor solubility of pentaphenylcyclopentadienyl complexes in common organic solvents, recent studies focused on the introduction of substituted arene rings in order to increase solubility. For instance, Harder and co-workers employed the so-called Cp^BIG ligand featuring *para-n*-butyl groups on the arene rings.[15] Due to high solubility even in *n*-hexane, which commonly hinders purification, and severe disorder in crystallography caused by the *n*-butyl groups, the related *p*-ethyl-substituted ligand has been introduced.[16] Furthermore, 3,5-substitution on the arene rings (using groups such as Me, *i*Pr or *t*Bu) has been achieved.[17,18] It is worth noting that the stability of complexes containing pentaarylcyclopentadienyl ligands is provided not only by steric protection of the metal centre, but attractive dispersion interactions between the cyclopentadienyl ligands also play a crucial role.[19]
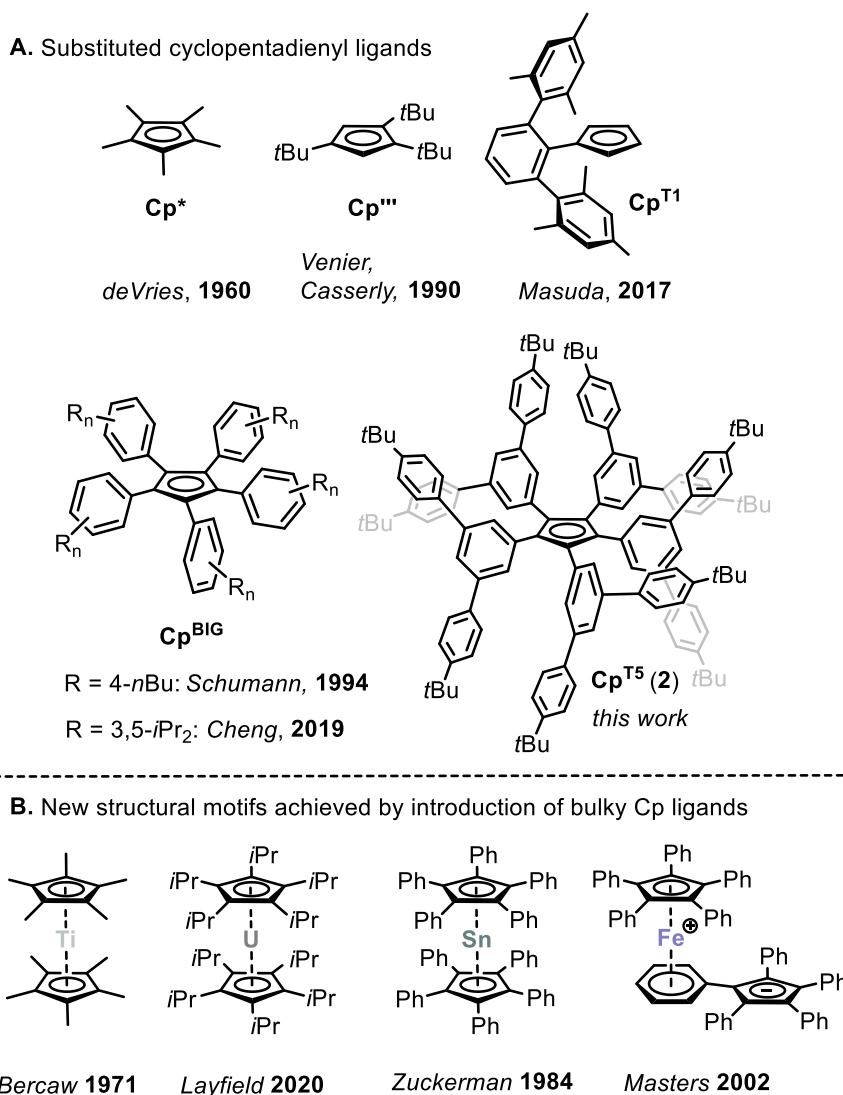
Figure 1. Examples of alkyl- and aryl-substituted cyclopentadienyl ligands (A) and structural motifs stabilised by introduction of bulky cyclopentadienyl ligands.[6–10,13–15,17,20]

Moreover, the arene rings in pentaarylcyclopentadienyl ligands are not co-planar with the cyclopentadienyl ring, but exhibit slight distortion resulting in propeller-shaped geometries. A higher plane-to-plane twist angle of 55.24(11)° was achieved for mono-terphenyl cyclopentadienyl ligands such as Cp^{T1} through additional interactions with the terphenyl aryl moieties (Figure 1A, angle is given for Cp^{T1}H).[21,20] In this case, the coupling of a 2,6-terphenyl to a cyclopentadienyl ring resulted in a ligand capable of chelating alkali metal cations. However, and despite the three-dimensional nature of this ligand, the steric protection of the metal centre is limited due to the mono-substitution of the Cp ring.

Our group recently showed that the reaction of [4-Et-Cp^{BIG}NiBr]$_2$ with two equivalents of KC$_8$ afforded a deep green solution that acts as a source of a (4-Et-Cp^{BIG})Ni(I) species that could be trapped with various reagents, including N-heterocyclic carbenes and TEMPO (Figure 2).[22] Unfortunately, the structure of this presumed Ni(I) compound has remained elusive. However, the Ni(I) species shows a well-resolved ^{1}H NMR spectrum, which indicates that it is diamagnetic.

A possible explanation for the diamagnetism is the presence of two magnetically coupled Ni(I) centres in a dimetallocene type structure. While dizincocenes discovered by Carmona are still the only class of dimetallocenes described in chemical literature,[23] computational studies suggest that dinickelocenes are an "interesting and reasonable synthetic objective".[24] Indeed, several groups have investigated reduction reactions of nickelocene with lithium and magnesium alkyls, and sodium naphthalenide.[25] Such experiments resulted in the isolation of trinuclear species [(CpNi)$_3$(CR)] (R = CH(CH$_3$)Ph) and octahedral (CpNi)$_6$.
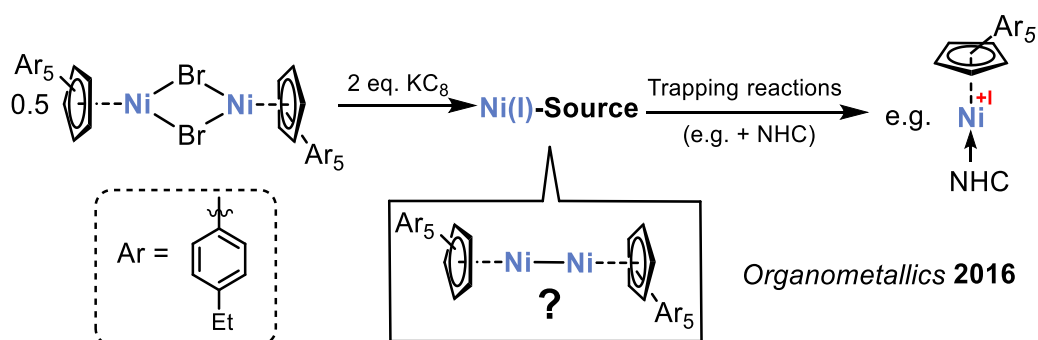
Figure 2. Reaction of [4-Et-Cp^{BIG}NiBr]$_2$ with KC$_8$ and trapping reactions.[22]

Herein, we describe the development of a penta-terphenyl cyclopentadienyl ligand with a large three-dimensional profile. For this purpose, a suitable 3,5-terphenyl substituent was chosen in order to achieve penta-substitution of the cyclopentadiene ring. This ligand is deprotonated by alkali metals or alkali metal bases. The resulting cyclopentadienyl anion forms a remarkable dimeric structure in combination with potassium. Furthermore, the synthesis of iron-, cobalt- and nickel bromido complexes is described and the putative formation of dimetallocenes from these complexes was investigated.

9.2 Results and Discussion

This study started with the investigation of the palladium-catalysed Heck reaction of suitable 3,5-terphenyl bromides with cyclopentadiene according to the protocol developed by Dyker and Miura.[26] After synthesising three different 3,5-terphenyl bromides $3,5-R_2-C_6H_3Br$ (R = 4-tBu-C_6H_4, $3,5-t$Bu$_2-C_6H_3$ and $2,4,6-Me_3-C_4H_2$),[27,28] their behaviour in the Heck reaction was investigated. After work-up, the solids obtained were characterised by ^{1}H NMR spectroscopy. While the products from the mono- and di-*tert*-butyl substituted terphenyls (R = 4-tBu-C_6H_4 and $3,5-t$Bu$_2-C_6H_3$) gave a single set of signals in the alkyl-region, the product from the arylation reaction with the mesityl-substituted terphenyl bromide (R = $2,4,6-Me_3-C_4H_2$) contained more than one species, suggesting an unselective reaction which was not pursued further. Analysis of the products from the arylation reactions with $3,5-R_2-C_6H_3Br$ (R = 4-tBu-C_6H_4 and $3,5-t$Bu$_2-C_6H_3$) by LIFDI-MS revealed the formation of the pentaarylated $C_5[3,5-(4-t$Bu-$C_6H_4)_2C_6H_3]_5$H (**1-H**, Scheme 1) as evidenced by a molecular ion peak at m/z = 1768.262 and the tetraarylated $C_5[3,5-(3,5-t$Bu$_2-C_6H_3)_2C_6H_3]_4$H$_2$ (m/z = 1876.448).
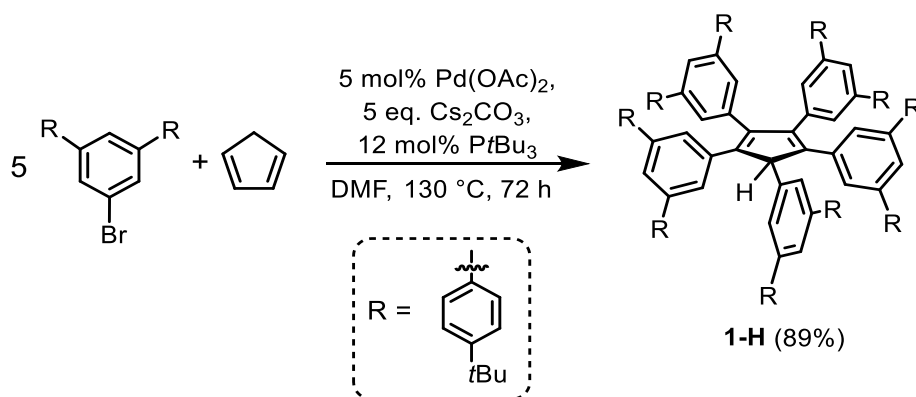
Scheme 1. Synthesis of the penta-terphenyl cyclopentadiene **1-H**.

1-H was synthesised on a multi-gram scale in up to 89% yield as a beige solid using freshly distilled cyclopentadiene as the Cp-source. Notably, when Cp_2ZrCl_2 was employed as an alternative Cp-source, significant amounts of the hydrodehalogenation product $3,5-(4-t$Bu-$C_6H_4)_2C_6H_4$ were observed.

Single crystals grown from *n*-hexane confirm the molecular structure of **1-H** (Figure 3). The bond lengths show the expected values for C−C single and double bonds [C2−C3: 1.3599(17) and C4−C5: 1.3592(17) Å, C1−C2: 1.5173(17) Å, C3−C4 1.4741(18) Å, C5−C1 1.5200(17) Å]. The cyclopentadiene to arene plane-to-plane twist angles range from 18.0 to 87.8°, which confirms a significant deviation from co-planarity and suggests a sufficient three-dimensional structure for stabilisation of low-coordinate transition metal complexes. The ^{1}H and ^{13}C{^{1}H} NMR spectra of **1-H** show the presence of three signals for the *t*Bu-substituents (δ = 1.33-1.34 ppm). This is in line with the molecular structure determined by X-ray crystallography (*vide supra*) with three inequivalent terphenyl environments. Notably, however, the observation of three signal sets is in

contrast to the ^{1}H NMR spectrum obtained for the 4-Et-Cp^{BIG} ligand, which features only one signal set for the aryl-substituents due to the fast [1,5]-sigmatropic shift of the hydrogen atom bound to the five-membered cyclopentadiene ring. The cyclopentadiene proton of **1-H** was observed at a chemical shift of 5.60 ppm.
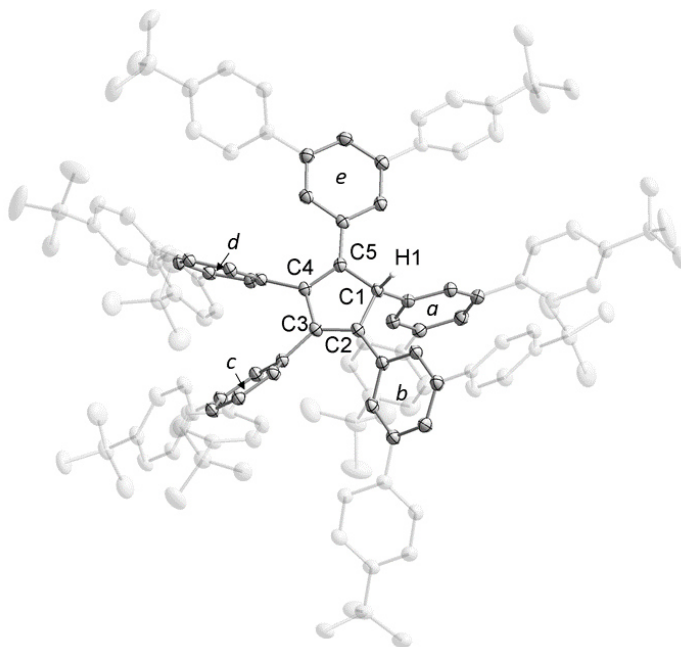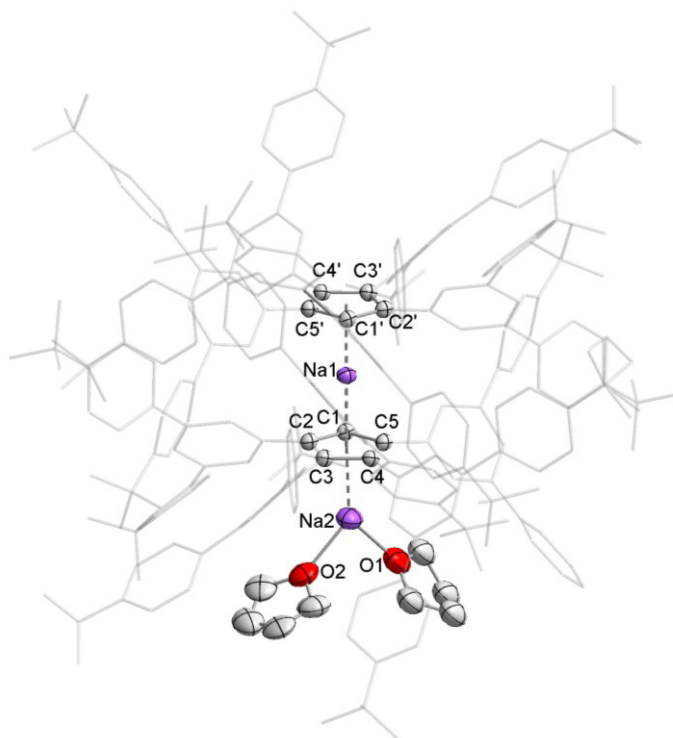

Figure 3. Molecular structure of **1-H** in the solid state. Thermal ellipsoids are set at the 50% probability level. Hydrogen atoms (except for H1) and solvent molecules are omitted for clarity. Selected bond lengths [Å] and angles [°]:C1−C2 1.5173(17), C2−C3 1.3599(17), C3−C4 1.4741(18), C4−C5 1.3592(17), C5−C1 1.5200(17), C5−C1−C6 112.08(10), C3−C2−C1 108.87(11), C2−C3−C4 109.01(11) C5−C4−C3 110.21(11), C4−C5−C1 108.07(11); plane-to-plane twist angles [°]: a/C1−C5 87.8, b/C1−C5 36.9, c/C1−C5 58.0, d/C1−C5 72.8, e/C1−C5 18.0.

Having substantial amounts of this super-bulky ligand precursor in hand, deprotonation reactions with a variety of alkali metals or alkali metal bases were investigated. The reaction of **1-H** with *n*BuLi proceeded extremely slow even at elevated temperatures. After stirring for four weeks at ambient temperature, a light green solid was obtained. Analysis by ^{1}H NMR spectroscopy showed just a single aryl-environment similar to that observed in the terphenyl bromide 3,5-*t*Bu$_2$-C$_6$H$_3$Br. The observation of a single set of aryl signals can be explained by planarisation of the Cp^{T5} ligand and equivalence of the terphenyl substituents and thus is consistent with the formation of Cp^{T5}Li (**1-Li**). Crystals of **1-Li** were obtained from *n*-hexane solutions at ambient temperature and reveal a [(Cp^{T5})Li]$^-$ sandwich. Due to poor low angle date, the position of the second lithium atom could not be detected and further analysis of the molecular structure is not possible. Nevertheless, the dimeric nature of **1-Li** is evident from the experiment (Figure 4).
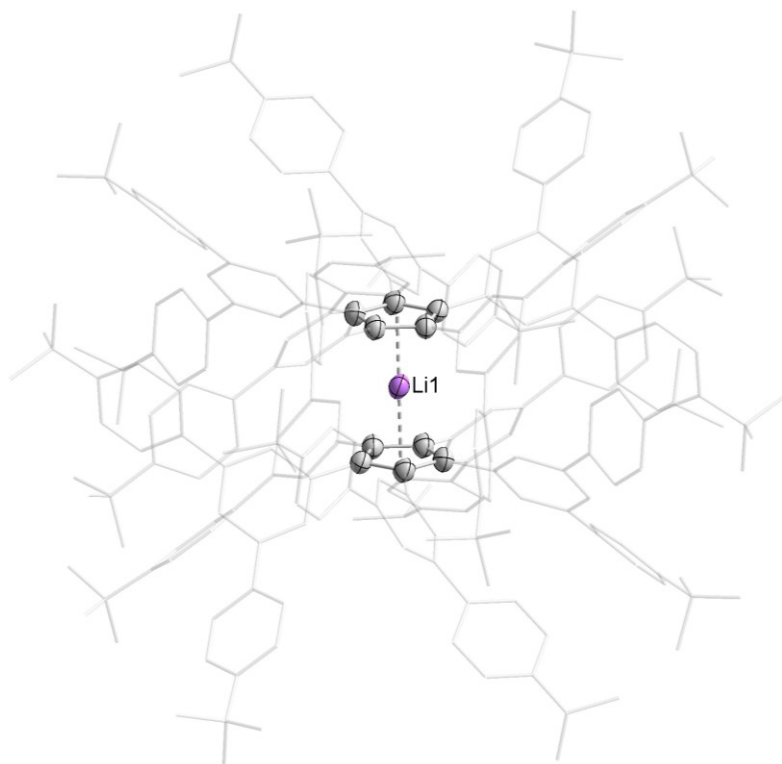
Figure 4. Structural drawing of $[(Cp^{T5})Li]^-$ as part of the structure of **1-Li** from a single crystal X-ray diffraction experiment. The position of the second Li^+ cation was not determined due to strong disorder of this cation. Thermal ellipsoids are set at the 50% probability level. Hydrogen atoms are omitted for clarity. Bond lengths and angles are not given due to poor refinement data.

Next, we assessed the deprotonation reaction of **1-H** with sodium and sodium bases. Na metal did not react with **1-H** even at elevated temperatures of 80 °C. However, the reaction of sodium hexamethyldisilazide (NaHMDS) with **1-H** in THF produced a light green solid after stirring at 80 °C overnight. Analysis of this solid by ^1H and $^{13}C\{^1H\}$ NMR spectroscopy revealed the formation of five equivalent terphenyl groups. This is indicative for the formation of $Cp^{T5}Na$ (**1-Na**), which was isolated in 21% yield.

Upon crystallisation, crystals of **1-Na·thf** were obtained, which show a Na^+ cation (Na1) sandwiched between the cyclopentadienyl rings of two anionic Cp^{T5} ligands. The second Na^+ cation (Na2) is coordinated by only one Cp^{T5} ligand, and, surprisingly, by two additional THF molecules (Figure 5). The exact source of the THF observed in the molecular structure of **1-Na** is presently unclear, but it seems to have been adventitiously introduced during synthesis and work-up. No traces of THF were observed in the NMR or elemental analysis of **1-Na** before crystallisation. Unfortunately, attempts to grow suitable THF-free crystals of **1-Na** have been unsuccessful so far. This suggests that the presence of THF greatly facilitates the formation of single crystals. In the structure of **1-Na·thf**, the Na−Cp(centroid) distances are 2.359(1) [Na1−Cp(centroid)] and 2.488(1) Å [Na2−Cp(centroid)], The Na1−Cp(centroid) distance compares very well to the Na−Cp(centroid) distance observed in NaCp (2.357 Å).[29]

The C−C bond lengths within the cyclopentadienyl ring range 1.416(3) to 1.430(3) Å and are in the area typically observed for cyclopentadienyl compounds.[29–33] The dimeric structure of **1-Na·thf** is distinct compared to the structures of other sodium salts of cyclopentadienide salts. Solvent-free NaCp itself features a chain-like structure,[29] and addition of donor-solvents such as THF or DME (1,2-dimethoxyethane) typically break up these chains to afford compounds with a piano-stool structure, e.g. [Cp^RNa(thf)₃] (Cp^R = C₅Me₄-C≡C-SiMe₃).[31–33] **1-Na·thf**, in contrast, features a dimeric structure with a μ²-bridging Cp^T5 ligand.

Figure 5. Molecular structure of **1-Na·thf** in the solid state. Thermal ellipsoids are set at the 50% probability level. Hydrogen atoms and non-coordinating solvent molecules are omitted for clarity. Selected bond lengths [Å] and angles [°]: C1−C2 1.426(3), C2−C3 1.426(3), C3−C4 1.416(3), C4−C5 1.430(3), C5−C1 1.420(3), Na2−O1 2.363(8), Na2−O2 2.236(9), Na1−Cp(centroid) 2.359(3), Na2−Cp(centroid) 2.488(3), Na1−Cp(centroid)−Na2 174.51(3), C5−C1−C2 108.2(2), C1−C2−C3 107.8(2), C4−C3−C2 108.1(2), C3−C4−C5 108.2(2), C1−C5−C4 107.7(2).

Despite many reports of the use of sodium cyclopentadienides for salt metathesis reactions to produce transition metal complexes, the potassium salts of bulky cyclopentadienides (e.g. 4-Et-Cp^BIGK, 4-*n*-Bu-Cp^BIGK) are far more commonly employed. The corresponding potassium salt was therefore also synthesised by deprotonation with KH in THF.[34] Full consumption of **1-H** was observed after stirring the reaction for 18 hours at 60 °C. Analysis of the yellow powder obtained after work-up by ¹H NMR spectroscopy again revealed the formation of one distinct terphenyl environment. THF could not be removed completely from the product *in vacuo* and presumably coordinates to the potassium ion to form either a solvent-separated ion pair or a piano-stool complex.[35] Despite the lack of a definite structural proof by XRD for this compound, **1-K·(thf)**_x (with *x* = 2-4 THF molecules) was isolated in a high yield (95%) on a gram scale. The

THF content varies for every batch and was individually determined by integration in ^{1}H NMR (as an example, see Figure S10). The ^{1}H and ^{13}C{^{1}H} NMR data in C_6D_6 are similar to **1-Li** and **1-Na** and the elemental analysis on a sample with three coordinating THF molecules supports the THF content determined by ^{1}H NMR spectroscopy.

Next, we sought to deprotonate **1-H** with a potassium base in a non-coordinating solvent. As such, the reaction of **1-H** with potassium metal in *n*-hexane produced a light green powder, which possesses a similar ^{1}H NMR spectrum in C_6D_6 to **1-K·(thf)₃**, with the only difference being the absence of THF. Single crystal X-ray diffraction on a crystal grown from benzene/*n*-hexane revealed the solvate-free structure of **1-K**. The structure shows a dimeric arrangement of two Cp^{T5}K units. One potassium ion (K1) is sandwiched between two symmetry-related cyclopentadienyl moieties in a staggered conformation with a K1−Cp(centroid) distance of 2.708(3) Å. A second potassium ion (K2) is sandwiched between the aryl rings of several terphenyl substituents and disordered over three positions (K2A-K2C). As a consequence, the C−C bond lengths in these arene rings are slightly elongated (C−C bond lenghts in arene ring C84-C89: 1.403(2)-1.388(3) Å, see Figure 6). The dimeric structure of **1-K** is particularly fascinating considering the distinct (bent) chain-like arrangement of solvent-free 4-*n*-Bu-Cp^{BIG}K in the solid state (Figure 6, bottom).[34] The higher degree of aggregation is presumably prevented by the high steric bulk of **2**. In comparison to the structure of 4-*n*-Bu-Cp^{BIG}K, **1-K** features a slightly longer K1−Cp(centroid) distance (**1-K**: 2.708(3) Å, 4-*n*-Bu-Cp^{BIG}K: K1−Cp(centroid): 2.6464(17) Å; K3−Cp(centroid) 2.6601(16) Å), K2−Cp(centroid) 2.6738(19) Å).[34]
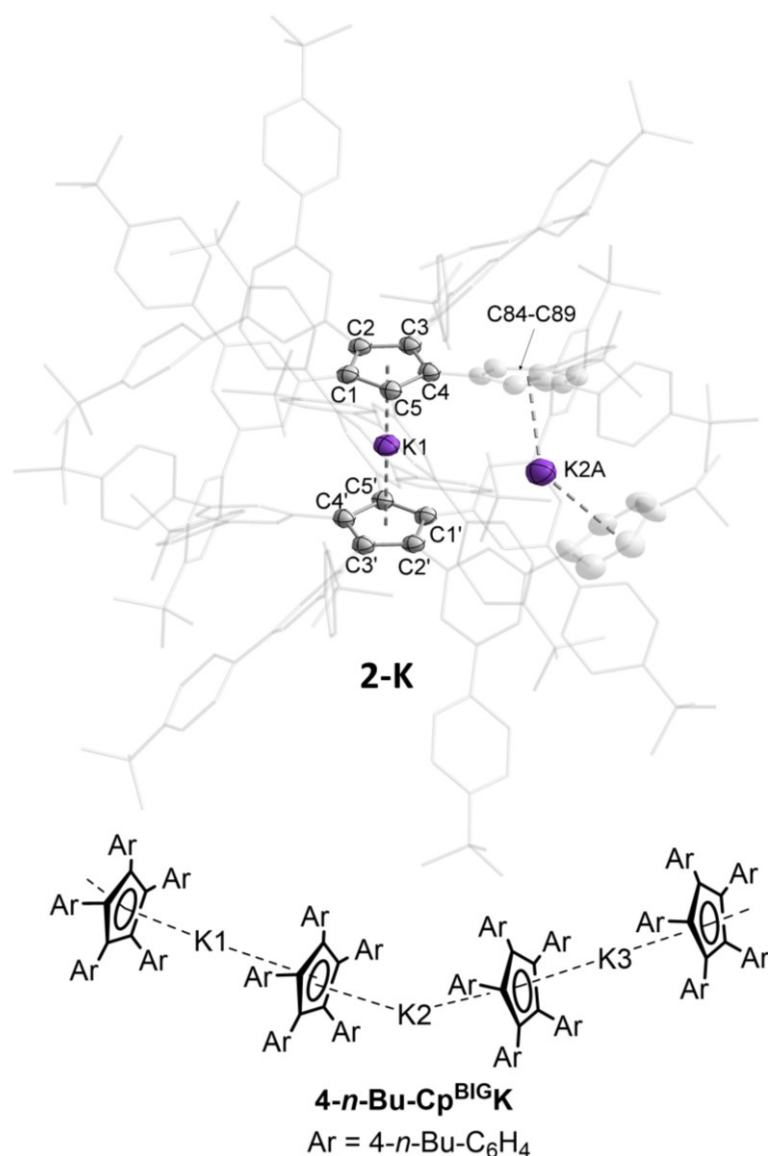
Figure 6. Molecular structure of **1-K** in the solid state (top) and schematic drawing of the structure of the related compound 4-*n*-Bu-Cp^{BIG}K in the solid state.[34] Thermal ellipsoids are set at the 50% probability level. Hydrogen atoms and non-coordinating solvent molecules are omitted for clarity. Selected bond lengths [Å] and angles [°]: C1−C2 1.425(2), C2−C3 1.418(3), C3−C4 1.416(3), C4−C5 1.421(2), C5−C1 1.417(3), C84−C85 1.403(2), C85−C86 1.391(3), C86−C87 1.388(3), C87−C88 1.400(3), C89−C88 1.397(3), C89−C84 1.394(3), K1−Cp(centroid) 2.708(3), K2A−C38−C42(centroid) 2.867(2), K2A−C85−C89(centroid) 2.826(3), C5−C1−C2 107.77(15), C3−C2−C1 108.15(16), C4−C3−C2 107.84(14), C3−C4−C5 108.27(16), C1−C5−C4 107.98(15).

Other dimeric cyclopentadienyl group 1 compounds are known in the literature.[36,37] The group of Paquette could show that lithium cyclopentadienyl compounds are speciated in the dimeric form [Li(thf)$_4$][Cp′$_2$Li] (Cp′ = *iso*-dicyclopentadienide) at low temperature by means of variable-temperature NMR studies.[38] Such species can be isolated by introduction of a sterically demanding 4-*t*Bu-Cp^{BIG} ligand, as recently demonstrated by the group of Schulz.[37] Moreover, Harder and co-workers showed that substitution of 0.5 equivalents of the lithium cations with the non-coordination cation PPh$_4^+$ results in discrete lithocene anions [Cp$_2$Li]$^−$ in the solid state.[39]

However, the formation of such dimeric units in the solid state has not been observed previously for binary alkali cyclopentadienyl salts. This observation can be attributed to the exceptional bulk of **1** and its ability to coordinate additional metal ions with the terphenyl substituents.

DOSY NMR measurements suggest that the dimeric structure of **1-K** is not preserved in solution. Using the experimentally observed diffusion coefficient ($4.00 \cdot 10^{-10}$ m^2·s^{-1}), the hydrodynamic radius of **1-H** in C$_6$D$_6$ was determined using the Stokes-Einstein equation as 9.93 Å.[40] This is well in line with the molecular structure in the solid state, featuring Cp(centroid)-C(tBu) distances of 8.92 to 10.38 Å. The hydrodynamic radii of **1-K·(thf)$_{2.3}$** and **1-K** dissolved in C$_6$D$_6$ were then determined as 10.30 and 10.37 Å, respectively (see the experimental details). These data compare well to the radius determined for **1-H** and thus strongly indicate the formation of monomers in solution.

Considering the intriguing structure of compound **1-K**, the corresponding rubidium and caesium compounds were also prepared by reacting **1-H** with the elemental alkali metals. The desired salts **1-Rb** and **1-Cs** could be isolated in excellent yields (M = Rb: 94% and M = Cs: 89%) as analytically pure powders according to NMR spectroscopy and elemental analysis. Unfortunately, crystals of neither of these compounds could be obtained.

The entire series of alkali metal salts was also characterised by UV/Vis absorption spectroscopy. All compounds feature absorption bands in the range from 350-370 nm, which account for their yellow colours in solution (Figure S24 to Figure S29).

After synthesising the series of alkali metal compounds **1-M** (**M** = Li-Cs), we were interested in using these in salt metathesis reactions for the preparation of transition metal complexes containing the Cp^{5T} ligand. For this purpose, we chose **1-K·(thf)$_x$** (x = 2-4) as the preferred cyclopentadienide source due to its simple and high yielding preparation (*vide supra*). The reactions of **1-K·(thf)$_x$** with FeBr$_2$ and CoBr$_2$ produced brown solids that feature broad resonances in the ^{1}H NMR spectrum, which is indicative for the formation of paramagnetic complexes. Similarly, the reaction with NiBr$_2$ resulted in the formation of a new, paramagnetic species, although this reaction required heating to 60 °C for 18 hours for completion. Complexes **2** and **3** were isolated by crystallisation from *n*-hexane in 49% and 39% yields as yellow and brown powders, respectively. The putative cobalt complex [Cp^{T5}CoBr]$_2$ (**4**) was isolated in 29% yield as a brown powder.

Crystals obtained from *n*-hexane and single crystal X-ray diffraction analysis revealed the formation of the complexes [Cp^{T5}FeBr(thf)]$_2$ (**2**) and [Cp^{T5}NiBr]$_2$ (**3**, Scheme 2). For the cobalt complex, no crystals suitable for structure determination were obtained, but elemental analysis is consistent with the formation of [Cp^{T5}CoBr]$_2$ (**4**).
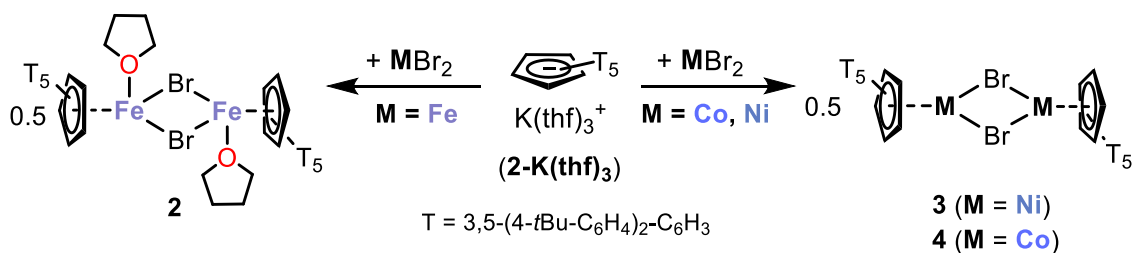
Scheme 2. Synthesis of Fe, Co and Ni-complexes (**2-4**) incorporating Cp^{T5} ligands by salt metathesis.

The molecular structures of **2** and **3** (Figure 7) reveal dimeric complexes formed upon coordination of μ^2-bridging bromido ligands. Dimeric cyclopentadienyl halido complexes are well known in the literature and typically require a bulky ligand.[16,41]

In the case of **3**, each iron atom is additionally coordinated by one THF molecule. The Fe$_2$Br$_2$ core in **3** is nearly planar and the cyclopentadienyl ligands are in a staggered conformation. As a consequence, the terphenyl substituents are arranged in a "zipper"-like way to create a pocket for the central Fe$_2$Br$_2$ moiety. The plane-to-plane twist angles range from 59.42 to 70.11° for four of the five terphenyl substituents. The fifth substituent is significantly less twisted (23.73°) as it is located directly above the Fe-bound THF molecule, which limits its available positions. The Fe−Br bond lengths (Fe1−Br1 2.5585(6) Å, Fe1−Br1′ 2.6529(5) Å) compare well to the related complex [4-Et-Cp^{BIG}FeBr(thf)]$_2$ (2.5870(6)-2.5688(6) Å) and the Fe1−Cp(centroid) distance of 2.062(2) Å is also similar.[16] The long Fe1···Fe1′ distance of 3.8085(5) Å indicates the absence of a bond.

The structure of **3** similarly contains a planar Ni$_2$Br$_2$ core, but the cyclopentadienyl ligands are in an eclipsed conformation. Nevertheless, the terphenyl moieties are tilted and arrange in a similar "zipper"-like way. The arene to cyclopentadienyl plane-to-plane twist angles lie in between 45.68 and 73.22° and the Ni1···Ni1′ distance of 3.4772(5) Å is also significantly longer than in nickel complexes featuring a covalent interaction. The Ni1−Cp(centroid) distance of 1.803(2) Å is the same as in [4-Et-Cp^{BIG}NiBr]$_2$ (1.803(1) Å).

The ^{1}H NMR spectra of complexes **2-4** feature broad resonances with no resolved coupling as a result of their paramagnetism. In case of the iron complex **2**, six resonances were observed in the range from −63 to 5 ppm. The nickel complex **3**, gives rise to five signals in the ^{1}H NMR spectrum from −15 to 10 ppm. The presence of five resonances is well in line with the spectra observed for diamagnetic complexes **1-Li-1-Cs**, which feature five resonances each. For the iron complex **2**, two additional signals for the coordinated THF molecule are expected. Nevertheless, only six instead of seven signals were observed. Similarly, the cobalt complex **4** only exhibits four resonances between 1 and 8 ppm in the ^{1}H NMR spectrum. Magnetic moments of compounds **2-4** were determined by the Evans-NMR method from solutions in C$_6$D$_6$ at 300 K. The iron complex **2** exhibits a magnetic moment of 7.2(1) μ_B, which is close to the value determined for [4-Et-Cp^{BIG}FeBr]$_2$ (μ = 7.8(1) μ_B) and indicates the presence of two high spin Fe^{2+} centres with four unpaired electrons each.[16] The magnetic moments for **3** and **4** were determined as 4.1(1) μ_B (*cf.*

265

[4-Et-Cp^{BIG}NiBr]$_2$ 4.1(1) μ_B) and 3.4(1) μ_B (*cf.* [4-Et-Cp^{BIG}CoBr]$_2$ 2.9(1) μ_B). These values also compare well to the previously determined values for related complexes featuring smaller 4-Et-Cp^{BIG} ligands and hint towards the presence of two unpaired electrons per nickel atom in **3** and one unpaired electron per cobalt atom in **4**. The UV/Vis absorption spectra of compounds **2-4** reveal absorption bands at 280 and broad shoulders at 350-360 nm. These data explain the pale yellow colour of the complexes in dilute solution, which arise from tailing of the bands into the visible region.
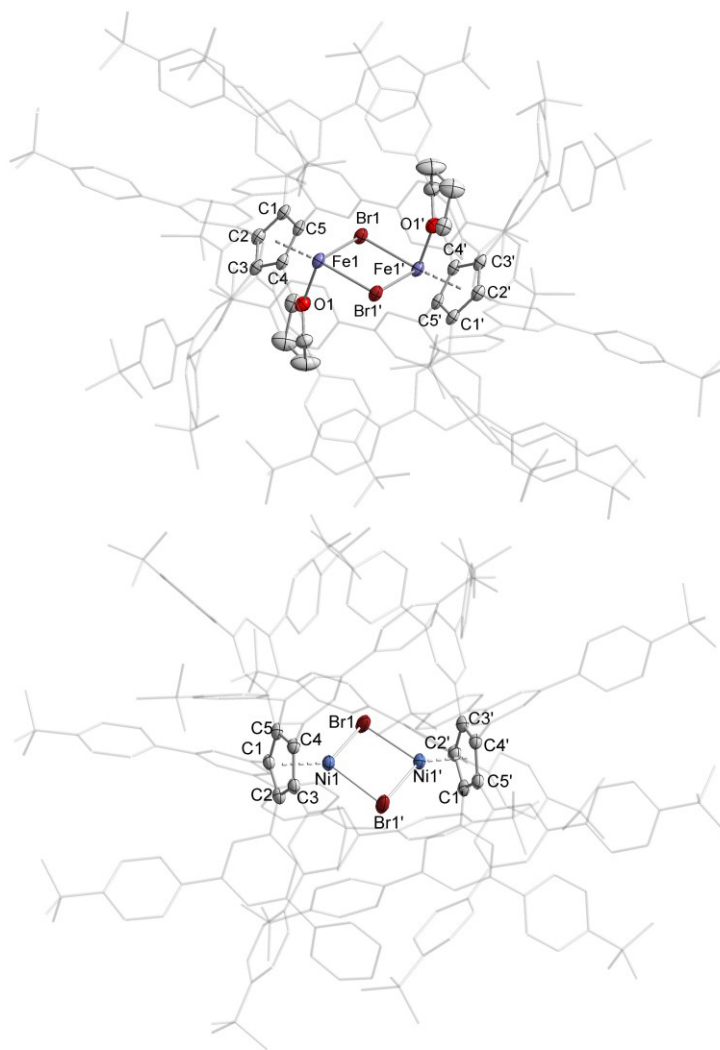
Figure 7. Molecular structures of **2** (top) and **3** (bottom) in the solid state. Thermal ellipsoids are set at the 50% probability level. Hydrogen atoms and non-coordinating solvent molecules are omitted for clarity. Selected bond lengths [Å] and angles [°] for **2**: Fe1…Fe1′ 3.8085(5), Fe1−Br1 2.5585(6), Fe1−Br1′ 2.6529(5), Fe1−O1 2.091(2), Fe1−Cp(centroid) 2.062(2), C1−C2 1.416(5), C2−C3 1.432(4), C3−C4 1.430(4), C4−C5 1.416(5), C5−C1 1.434(4), O1−Fe1−Br1 93.26(6), O1−Fe1−Br1′ 94.56(6), Br1−Fe1−Br1′ 86.107(16), Fe1−Br1−Fe1′ 93.894(16), C2−C1−C5 108.0(3), C1−C2−C3 108.8(2), C4 C3 C2 106.5(3), C5 C4 C3 109.2(3), C4 C5 C1 107.4(3) ; for **3**: Ni1…Ni1′ 3.4772(5), Ni1−Br1 2.3905(4), Ni1−Br1′ 2.4370(4) Ni1−Cp(centroid) 1.803(2), C1−C2 1.432(3), C2−C3 1.428(3), C3−C4 1.434(3), C4−C5 1.422(3), C5−C1 1.431(3), Ni1−Br1−Ni1′ 92.156(14), Br1−Ni1−Br1′ 87.503(13), C5−C1−C2 107.98(18), C3−C2−C1 107.39(18), C2−C3−C4 108.66(19), C5−C4−C3 107.35(18) C4−C5−C1 108.51(18).

We next set out to investigate the reactivity of complexes **2–4** in reduction reactions, aiming at the synthesis of dimetallocenes or related low coordinate metal(I) complexes. The reactions of the iron and cobalt complexes **2** and **4** with 2 equivalents of KC_8 afforded complex intractable reaction mixtures featuring multiple sets of signals in the ^{1}H NMR spectra (see Figure S22 and Figure S23). The reaction of the nickel complex **3** with KC_8 in C_6D_6 did not proceed at reasonable rates at ambient temperature and heating to 50 °C was required in order to observe new signals in the ^{1}H NMR spectrum. These signals lie in the region between −13 and 8 ppm and are broad, indicating the formation of another paramagnetic complex (Figure S21) which is inconsistent with the formation of a diamagnetic Ni(I) dimer.[42] After stirring for 24 hours at 50 °C, the reaction was completed as evidenced by the absence of signals of **3** in the ^{1}H NMR spectrum. Filtration of the reaction mixture afforded a bright orange solution. Orange crystals suitable for X-ray crystallography were obtained by slow evaporation from a benzene solution and revealed the formation of the nickelocene $[(Cp^{T5})_2Ni]$ (**5**, Scheme 3). Product **5** likely forms through disproportionation of an intermediate $Cp^{T5}Ni(I)$ species to **5** and nickel(0) particles. The molecular structure of **5** clearly reflects its connectivity. However, severe disorder in the Cp^{T5} moieties resulted in poor refinement values. As consequence, the precision on the structural parameters is rather low and therefore bond lengths and angles are not discussed here.
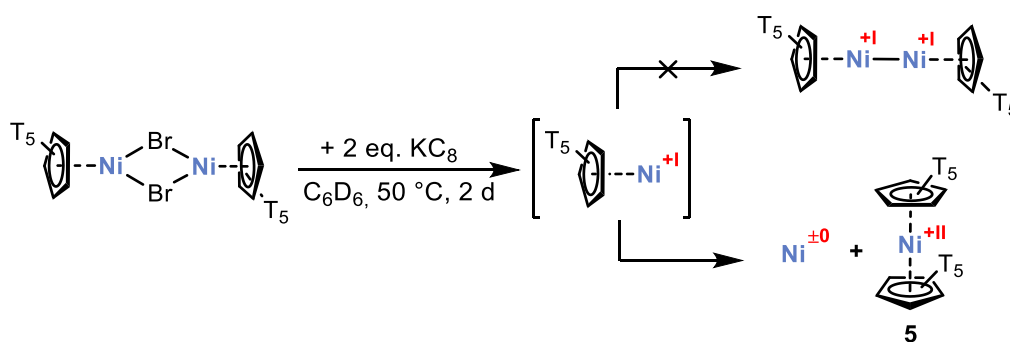
Scheme 3. Reduction of $[Cp^{T5}NiBr]_2$ with KC_8 and putative disproportionation of a Ni(I) species to nickelocene (**5**).
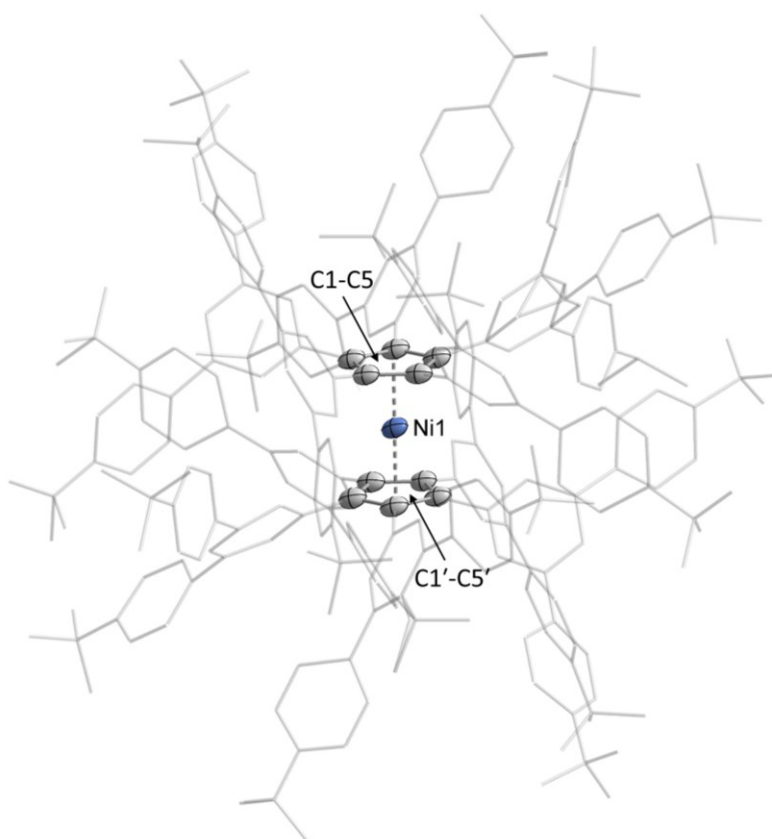
Figure 8. Structural drawing of **5** from a single crystal X-ray diffraction experiment. Thermal ellipsoids are set at the 50% probability level. Hydrogen atoms and non-coordinating solvent molecules are omitted for clarity. Bond lengths and angles are not given due to poor refinement data.

9.3   Conclusion

The extremely bulky cyclopentadienyl ligand Cp^{5T} (**2**) featuring five 3,5-terphenyl substituents can be synthesised in high yield by arylation of cyclopentadiene with the corresponding terphenyl bromide. The cyclopentadiene **1-H** can be deprotonated by alkali metals or alkali metal bases to afford compounds **1-M** (**M** = Li-Cs). However, in some cases (**M** = Li, Na), these deprotonation reactions require long reaction times and heating. The need for such harsh conditions can presumably be attributed to the steric protection and inaccessibility of the cyclopentadiene proton. X-ray structure determination on the lithium, sodium and the potassium salt reveal dimers of Cp^{T5}M units in the solid state which result in a metallocene sandwich. The second alkali metal could not be located in case of **1-Li**. In **1-Na**, the second sodium cation was coordinated to one cyclopentadienyl ring and two additional THF molecule. The potassium salt **1-K** features a sandwich structure where one potassium cation is coordinated by cyclopentadienyl rings and the other potassium cation is sandwich by arene rings of terphenyl substituents from opposite Cp^{T5} ligands. Subsequently, we have shown that **1-K·(thf)**$_x$ (x = 2-4) is a suitable precursor for salt metathesis reactions with transition metal precursors. The dimeric halido complexes [Cp^{T5}FeBr(thf)]$_2$ (**2**) and [Cp^{T5}MBr]$_2$ [M = Ni (**3**), Co (**4**)] were synthesised and their reduction reactions with KC$_8$ were investigated. The reduction of **3** afforded the nickelocene **5**, presumably

by disproportionation of an initial Ni(I) compound. Our results demonstrate that the high steric demand of Cp^{T5} in combination with its ability to additionally coordinate metal ions gave access to new structural motifs, e.g. the dimeric metallocene structure of **1-K**. Nevertheless, the reactions with MBr_2 (M = Fe, Ni) afforded complexes which were similar to previously reported complexes.[16] It is therefore tempting to speculate, that **1** preferentially forms metallocene structures due to strong dispersion interactions between the bulky terphenyl substituents on the cyclopentadienyl rings. In future studies, this stabilising effect could be exploited for the synthesis of metallocene anions, where the cations are coordinated by arene rings of the terphenyl substituents.

9.4   Experimental Details

General Synthetic Methods

All reactions and product manipulations were carried out in flame-dried glassware under an inert atmosphere of argon using standard Schlenk-line or glovebox techniques (maintained at <0.1 ppm H_2O and <0.1 ppm O_2). $3,5-R_2-C_6H_3Br$ (R = $4\text{-}t\text{Bu-}C_6H_4$,[27] $3,5\text{-}t\text{Bu}_2\text{-}C_6H_3$[27] and $2,4,6\text{-}Me_3\text{-}C_4H_2$[28]), $PtBu_3$,[43] and KC_8[44] were prepared according to procedures previously reported in the chemical literature. Cyclopentadiene was obtained from dicyclopentadiene according to a previously reported procedure.[45] It was stored at −30 °C and re-distilled before use. Elemental rubidium and caesium were kindly provided by the group of Prof. Dr. Nikolaus Korber. All other chemicals were purchased from commercial suppliers and used without further purification.

Solvents were dried and degassed with a MBraun SPS800 solvent purification system. All dry solvents except *n*-hexane and *n*-pentane were stored under argon over activated 3 Å molecular sieves in gas-tight ampules. *n*-Hexane and *n*-pentane were instead stored over potassium mirrors.

General Analytical Techniques

NMR spectra were recorded on Bruker Avance 300 or 400 spectrometers at 300 K unless otherwise noted and were internally referenced to residual solvent resonances (^{1}H NMR: THF-d_8: 1.72 ppm, C_6D_6: 7.16 ppm; ^{13}C{^{1}H} NMR: THF-d_8: 25.31 ppm, C_6D_6: 128.06 ppm). ^{7}Li NMR spectra were externally referenced to LiCl in D_2O. Chemical shifts, δ, are given in ppm referring to external standards of tetramethylsilane (^{1}H, ^{13}C{^{1}H}). ^{1}H and ^{13}C NMR signals were assigned based on 2D NMR spectra (^{1}H,^{1}H-COSY, ^{1}H,^{13}C-HSQC, ^{1}H,^{13}C-HMQC).

UV/Vis spectra were recorded on an Ocean Optics Flame Spectrometer. Mass spectra were recorded by the analytical department at the University of Regensburg using a Jeol AccuTOF GCX. Elemental analysis and mass spectrometry were performed by the Central Analytics Department of the University of Regensburg.

Single-crystal X-ray diffraction data were recorded on Rigaku Oxford Diffraction SuperNova Atlas, Rigaku GV 1000 or XtaLAB Synergy R (DW system, Hypix-Arc 150) devices with Cu-K$_\alpha$ radiation (λ= 1.54184 Å). Crystals were selected under mineral oil, mounted on micromount loops

and quench-cooled using an Oxford Cryosystems open flow N_2 cooling device. Either semi-empirical multi-scan absorption corrections[46] or analytical ones[47] were applied to the data. The structures were solved with SHELXT[48] solution program using dual methods and by using Olex2 as the graphical interface.[49] The models were refined with ShelXL[50] using full matrix least squares minimisation on F^2.[51] The hydrogen atoms were located in idealised positions and refined isotropically with a riding model.

9.4.1 DOSY NMR

DOSY (diffusion-ordered spectroscopy) spectra were recorded on an Avance III 600 (600.25 MHz) spectrometer equipped with a z-gradient (53.5 Gauss/cm), 5 mm TXI cryo probe and BVT 3000 unit at 298 K.

The NMR spectra were processed with the Bruker program TopSpin® 3.2 and the diffusion coefficients were calculated applying the Bruker software *T1/T2* relaxation module. For the calibration of the diffusion coefficients using temperature and viscosity corrections, TMS (tetramethylsilane) was added as standard.

The ^{1}H-diffusion measurement was performed with the convection suppressing DSTE (double stimulated echo) pulse sequence, developed by Mueller and Jerschow[52] in a pseudo 2D mode. 120 dummy scans and 16 scans were used with a relaxation delay of 2 s. Sinusoidal shapes were used for the gradient and a linear gradient ramp with 20 increments between 5 and 95 % of the maximum gradient strength was applied. Regarding the homospoil gradient strengths, −13.17, 20 and −17.13 G cm^{-1} were used. The length of the gradient pulse δ was adjusted for every species in the sample, giving δ values of 2.4 ms for TMS, 5.0 ms (**1-H**, **1-K·(thf)$_{2.3}$**,) and 5.4 ms (**1-K**) for the complexes. A diffusion time Δ of 50 ms was applied.

From DOSY experiments the translational self-diffusion coefficients D of molecules in solution can be calculated according to the Stejskal-Tanner equation.[53] The obtained values were: $4.00 \cdot 10^{-10}$ m^2·s^{-1} (**1-H**), $3.94 \cdot 10^{-10}$ m^2·s^{-1} (**1-K**) and $3.97 \cdot 10^{-10}$ m^2·s^{-1} (**1-K·(thf)$_{2.3}$**). With the diffusion coefficients D of the analyte and TMS (standard for viscosity referencing), the hydrodynamic radius r_H of the analyte can be estimated following the Stokes-Einstein equation.[40] The correction factor c of the Stokes-Einstein equation was calculated according to the semi-empirical modification according to Chen.[54]

For the present work r_H = 9.93 Å for Cp^{T5}H, r_H = 10.30 Å for **1-K** and r_H = 10.37 Å **1-K·(thf)$_{2.3}$** were obtained. This in very good agreement with the crystal derived radii of 8.92 to 10.38 Å (for Cp(centroid)-CtBu in **1-H**) in the solid state. Therefore, these results clearly indicate the presence of monomeric structures in solution.

9.4.2 Synthesis of Compounds

Cp^{T5}H (1-H):

This compound was prepared according to an adapted literature procedure from Dyker and Miura.[26] Only four equivalents of 3,5-(4-tBu-C_6H_4)$_2C_6H_3$Br referring to cyclopentadiene were used, because earlier experiments had shown that use of five equivalents resulted in unconsumed starting material, which proved to be difficult to separate from the product.

Solid 3,5-(4-tBu-C_6H_4)$_2C_6H_3$Br (**1**, 10.0 g, 23.7 mmol, 5.0 eq.), Pd(OAc)$_2$ (67.0 mg, 5.9 mmol, 0.05 eq.) and Cs$_2$CO$_3$ (9.7 g, 29.7 mmol, 6.3 eq.) were combined. Subsequently, freshly distilled cyclopentadiene (0.5 mL, 5.9 mmol, 1.2 eq.), PtBu$_3$ (144.0 mg, 0.7 mmol, 0.15 eq.) and DMF (35 mL) were added. The reaction mixture was heated for 72 hours to 130 °C, affording a deep green suspension. After cooling to ambient temperature, DCM (300 mL) and *para*-toluenesulfonic acid monohydrate (9.0 g, 47.4 mmol, 10.0 eq.) were added. The red-brown suspension was filtered over silica (5 cm x 20 cm) using DCM as eluent. DCM was removed under reduced pressure. The DMF-containing brown oil was added dropwise to water (500 mL), affording a light brown solid which was isolated by filtration and dried at 80 °C *in vacuo*.

Crystals suitable for single crystal X-ray diffraction were obtained from a saturated solution of **1-H** in *n*-hexane.

$C_{135}H_{146}$, MW = 1768.65 g/mol
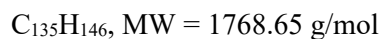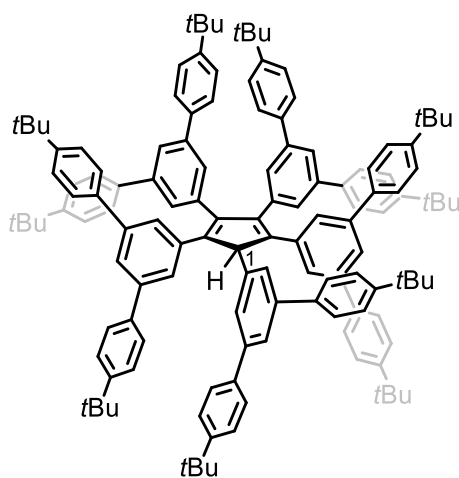
Yield: 7.5 g (89%, referenced to terphenyl bromide)

^{1}H NMR (400 MHz, 300 K, CDCl$_3$) δ = 1.33 (s, 36H, tBu), 1.33 (s, 36H, tBu), 1.34 (s, 18H, tBu), 5.60 (s, 1H, C^{1}H), 7.26-7-66 (s, 33H, C^{Ar}H), 7.75 (t, J_{HH} = 1.60 Hz, 2H, C^{Ar}H) ppm.

^{13}C{^{1}H} NMR (100 MHz, 300 K, CDCl$_3$) δ = 31.5 (s, C-CH_3), 34.6 (s, C-CH$_3$), 34.7 (s, C-CH$_3$), 62.4 (s, C^1), 123.9 (s, CH^{Ar}), 124.7 (s, CH^{Ar}), 125.7 (s, CH^{Ar}), 125.9 (s, CH^{Ar}), 126.7 (s, CH^{Ar}), 126.9 (s, CH^{Ar}), 127.0 (s, CH^{Ar}), 127.15 (s, CH^{Ar}), 127.21 (s, CH^{Ar}), 128.4 (s, CH^{Ar}), 136.1 (s, C$^{Ar/Cp}$), 137.7 (s, C$^{Ar/Cp}$), 138.4 (s, C$^{Ar/Cp}$), 138.5 (s, C$^{Ar/Cp}$), 138.5 (s, C$^{Ar/Cp}$), 139.8 (s, C$^{Ar/Cp}$), 141.0 (s, C$^{Ar/Cp}$), 141.9 (s, C$^{Ar/Cp}$), 142.0 (s, C$^{Ar/Cp}$), 145.3 (s, C$^{Ar/Cp}$), 146.5 (s, C$^{Ar/Cp}$), 150.1 (s, C$^{Ar/Cp}$), 150.28 (s, C$^{Ar/Cp}$), 150.37 (s, C$^{Ar/Cp}$) ppm. In the region from 123 to 151 ppm 24 signals were detected (26 expected). Unfortunately, these signals could not be assigned by 2D NMR spectra

due to partial overlap. However, we expect these signals to arise from three chemically different terphenyl substituents (8 signals each) and from overlapping cyclopentadiene signals expected for C_{2v} symmetrical **1-H**. In particular, the signals of the aromatic C-H carbon atoms (assigned by DEPT-135) overlap partially and therefore two resonances of these carbon atoms were likely not detected (Figure S2).

Elemental Analysis calcd. C 91.68, H 8.32; found C 91.70, H 8.31.

LIFDI-MS m/z = 1768.262.

1-Li:

To a solution of Cp^{T5}H (200 mg, 0.114 mmol, 1. eq.) in n-hexane (3 mL) was added nBuLi (2.5 M in hexanes, 0.05 mL, 0.13 mmol, 1.1 eq.) at ambient temperature. The solution was stirred for 4 weeks and a yellow-green solid precipitated. The solid was isolated by filtration and dried *in vacuo* to afford analytically pure **1-Li**.

$C_{135}H_{145}Li$, MW = 1774.59 g/mol
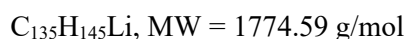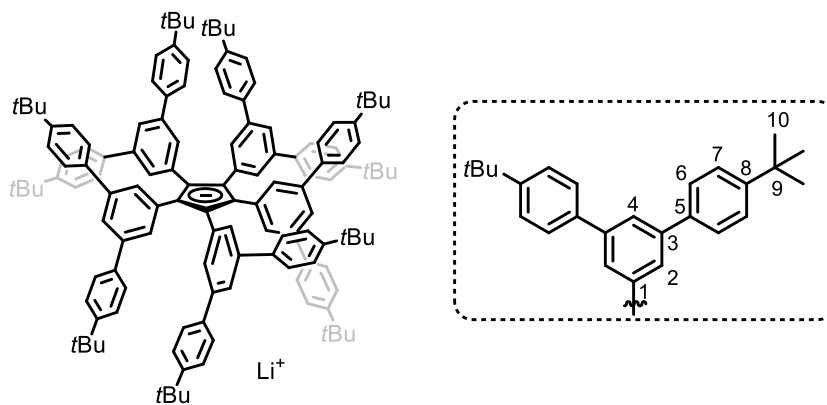
Yield: 164 mg (81%)

^{1}H NMR (400 MHz, 300 K, C$_6$D$_6$) δ = 1.16 (s, 90H, C^{10}H), 7.33 (m, 20H, C^{7}H), 7.63 (m, 20H, C^{6}H), 7.77 (d, $^3J_{HH}$ = 1.60 Hz, 10H, C^{2}H), 8.04 (t, $^3J_{HH}$ = 1.60 Hz, C^{4}H) ppm.

^{13}C{^{1}H} NMR (100 MHz, 300 K, C$_6$D$_6$) δ = 31.4 (s, C^{10}), 34.4 (s, C^9), 120.2 (s, C^1), 122.6 (s, C^4), 126.2 (s, C^7), 127.4 (s, C^6), 130.3 (s, C^2), 139.7 (s, C^5), 139.8 (s, C^{Cp}), 141.9 (s, C^3), 150.0 (s, C^8) ppm.

^{7}Li NMR (155 MHz, 300 K, C$_6$D$_6$) δ = −5.3 ppm.

Elemental Analysis calcd. C 91.37, H 8.24; found C 90.68, H 8.22.

UV/Vis (n-hexane): λ_{max} (nm, ε_{max} /L·mol^{-1}·cm^{-1}) 220 (200 000), 255 (290 000), 350sh (27 000).

1-Na:

To a mixture of Cp^{T5}H (366 mg, 0.207 mmol, 1.0 eq.) and NaHMDS (38.0 mg, 0.21 mmol, 1.0 eq.) was added n-hexane (3 mL). The reaction was heated to 75 °C overnight to afford a light green precipitate. The solid was isolated by filtration, washed with cold (−20 °C) n-hexane (2 x 3 mL) and dried *in vacuo* to afford analytically pure **1-Na**. Single crystals suitable for X-ray

diffraction were grown by slow diffusion of *n*-hexane into a saturated solution of **1-Na** in C_6H_6. Despite several crystallisation attempts, the presence of minor amounts of THF (presumably contaminations from the atmosphere of the glove box) caused crystallisation of **1-Na·thf**. Attempts to crystallise **1-Na** from freshly distilled benzene and *n*-hexane did not afford crystals.

$C_{135}H_{145}Na$, MW = 1790.63 g/mol
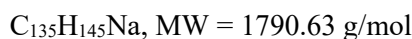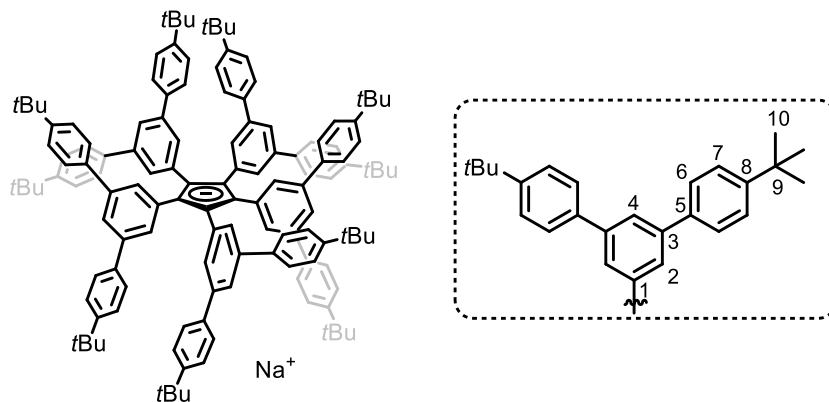
Yield: 76 mg (21%)

¹H NMR (400 MHz, 300 K, C_6D_6) δ = 1.16 (s, 90H, $C^{10}H$), 7.32 (m, 20H, C^7H), 7.64 (m, 20H, C^6H), 7.85 (d, $^3J_{HH}$ = 1.50 Hz, 10H, C^2H), 8.01 (t, $^3J_{HH}$ = 1.50 Hz, C^4H) ppm.

¹³C{¹H} NMR (100 MHz, 300 K, C_6D_6) δ = 31.4 (s, C^{10}), 34.4 (s, C^9), 121.2 (s, C^4), 121.9 (s, C^1), 126.1 (s, C^7), 127.5 (s, C^6), 130.5 (s, C^2), 139.9 (s, C^5), 141.5 (s, C^3), 142.0 (s, C^{Cp}), 149.9 (s, C^8) ppm.

Elemental Analysis calcd. C 90.55, H 8.16; found C 89.55, H 8.04.

UV/Vis (*n*-hexane): λ_{max} (nm, ε_{max} /L·mol⁻¹·cm⁻¹) 220 (140 000), 255 (220 000), 350sh (24 000).

1-K:

To a mixture of $Cp^{T5}H$ (461.4 mg, 0.26 mmol, 1.0 eq.) and potassium (10.2 mg, 0.26 mmol, 1.0 eq.) was added *n*-hexane (2 mL). After stirring at ambient temperature overnight, only a small amount of precipitate formed. The reaction was then heated to at 50 °C for 6 hours and formation of more green precipitate was observed. The solid was isolated by filtration, washed with cold (−20 °C) *n*-hexane (3 x 1.5 mL) and dried *in vacuo* to afford analytically pure **1-K**. Single crystals suitable for X-ray diffraction were grown by slow diffusion of *n*-hexane into a saturated solution of **1-K** in C_6H_6.

$C_{135}H_{145}K$, MW = 1806.74 g/mol
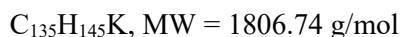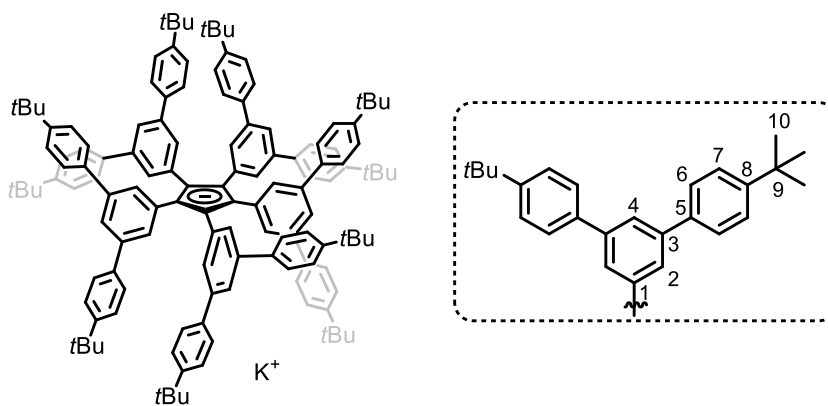
Yield: 65 mg (14%)

¹H NMR (400 MHz, 300 K, C_6D_6) δ = 1.16 (s, 90H, $C^{10}H$), 7.31 (m, 20H, C^7H), 7.66 (m, 20H, C^6H), 7.88 (d, $^4J_{HH}$ = 1.63 Hz, 10H, C^2H), 8.00 (t, $^4J_{HH}$ = 1.60 Hz, 5H, C^4H) ppm.

¹³C{¹H} NMR (100 MHz, 300 K, $CDCl_3$) δ = 31.4 (s, C^{10}), 34.4 (s, C^9), 121.6 (s, C^4), 122.4 (s, C^1), 126.0 (s, C^7), 127.5 (s, C^6), 130.5 (s, C^2), 140.0 (s, C^5), 142.0 (s, C^3), 142.2 (s, C^{Cp}), 149.9 (s, C^8) ppm.

Elemental Analysis calcd. C 89.75, H 8.09; found C 87.40, H 8.17.

UV/Vis (*n*-hexane): λ_{max} (nm, ε_{max} /L·mol⁻¹·cm⁻¹) 220 (160 000), 250 (250 000), 360 (31 000).

1-K·(thf)$_x$ (x = 2-4):

To a mixture of $Cp^{T5}H$ (6.0 g, 3.4 mmol, 1.0 eq.) and KH (0.54 g, 6.8 mmol, 4.0 eq.) was added THF (120 mL). The green suspension was stirred at 60 °C for 18 hours. Subsequently, the suspension was filtered (P4 frit) and the solvent was removed *in vacuo*. The remaining solid was dried under reduced pressure. The product was isolated as a yellow powder with variable THF content (x = 2-4).

$C_{135}H_{145}K(C_4H_8)_n$, n = 3-4, MW = 2023.06 g/mol (n = 3)
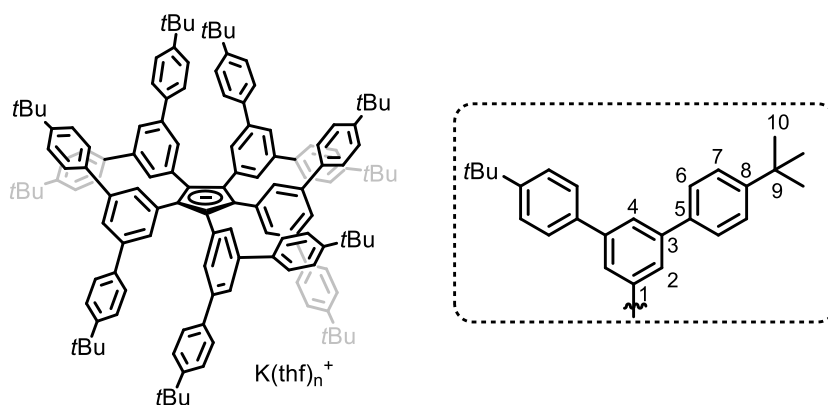
Yield: 6.52 g (95%)

For full characterisation of this compound, a sample with THF-content of n = 3 was chosen (determined by integration of the ¹H NMR signals, see Figure S10)

¹H NMR (400 MHz, 300 K, C₆D₆) δ = 1.16 (s, 90H, C¹⁰H), 1.26 (m, 12H, THF), 3.32 (m, 12H, THF), 7.30 (m, 20H, C⁷H), 7.64 (m, 20H, C⁶H), 7.90 (d, ⁴J_{HH} = 1.50 Hz, 10H, C²H), 7.98 (t, ⁴J_{HH} = 1.50 Hz, 5H, C⁴H) ppm.

¹³C{¹H} NMR (100 MHz, 300 K, CDCl₃) δ = 25.6 (s, THF), 31.4 (s, C¹⁰), 34.4 (s, C⁹), 67.8 (s, THF), 121.2 (s, C⁴), 122.3 (s, C¹), 126.0 (s, C⁷), 127.5 (s, C⁶), 130.6 (s, C²), 140.2 (s, C⁵), 141.8 (s, C³), 142.5 (s, C^{Cp}), 149.7 (s, C⁸) ppm.

Elemental Analysis calcd. C 87.27, H 8.42; found C 87.40, H 8.17.

UV/Vis (*n*-hexane): λ_{max} (nm, ε_{max} /L·mol⁻¹·cm⁻¹) 220 (190 000), 255 (280 000), 355 (45 000).

1-Rb:

To a mixture of Cp^{T5}H (378.0 mg, 0.214 mmol, 1.0 eq.) and rubidium (20.1 mg, 0.24 mmol, 1.1 eq.) was added *n*-hexane. The mixture was sonicated at 50 °C for 1.5 hours to afford a suspension of a green precipitate. Subsequently, the solvent was removed *in vacuo* and the remaining green solid was extracted with toluene (ca. 5 mL). The solvent was again removed *in vacuo* and the green powder was dried under reduced pressure to afford analytically pure **1-Rb**.

C₁₃₅H₁₄₅Rb, MW = 1853.11 g/mol
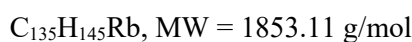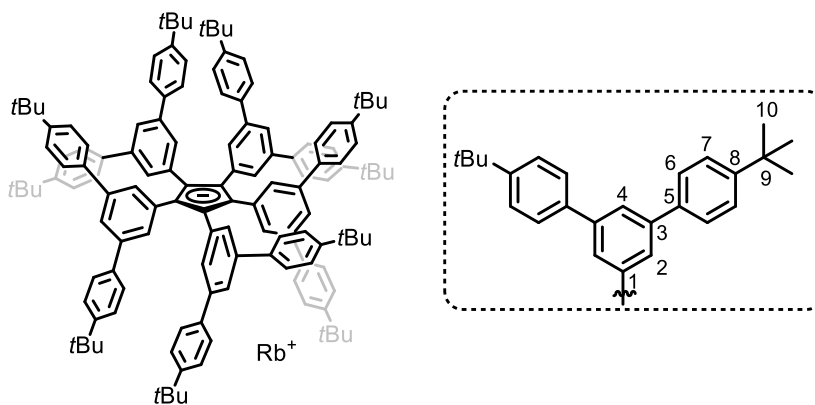
Yield: 372 mg (94%)

¹H NMR (400 MHz, 300 K, C₆D₆) δ = 1.15 (s, 90H, C¹⁰H), 7.32 (m, 20H, C⁷H), 7.66 (m, 20H, C⁶H), 7.86 (br s, 10H, C²H), 8.01 (br s, C⁴H) ppm.

¹³C{¹H} NMR (100 MHz, 300 K, C₆D₆) δ = 31.4 (s, C¹⁰), 34.4 (s, C⁹), 121.4 (s, C⁴), 122.6 (s, C¹), 126.0 (s, C⁷), 127.6 (s, C⁶), 130.5 (s, C²), 140.1 (s, C⁵), 141.9 (s, C³), 142.4 (s, C^{Cp}), 149.9 (s, C⁸) ppm.

Elemental Analysis calcd. C 87.50, H 7.89; found C 87.81, H 7.84.

UV/Vis (C₆H₆): λ_{max} (nm, ε_{max} /L·mol⁻¹·cm⁻¹) 280 (180 000), 340 (49 000), 370sh (44 000).

1-Cs:

To a mixture of Cp^{T5}H (411.3 mg, 0.233 mmol, 1.0 eq.) and caesium (34 mg, 0.26 mmol, 1.1 eq.) was added *n*-hexane. The mixture was sonicated at 50 °C for 1.5 hours to afford a suspension of a green precipitate. Subsequently, the solvent was removed *in vacuo* and the remaining green

solid was extracted with toluene (ca. 5 mL). The solvent was again removed *in vacuo* and the green powder was dried under reduced pressure to afford analytically pure **1-Cs**.

$C_{135}H_{145}Cs$, MW = 1900.55 g/mol
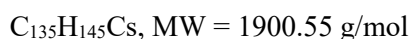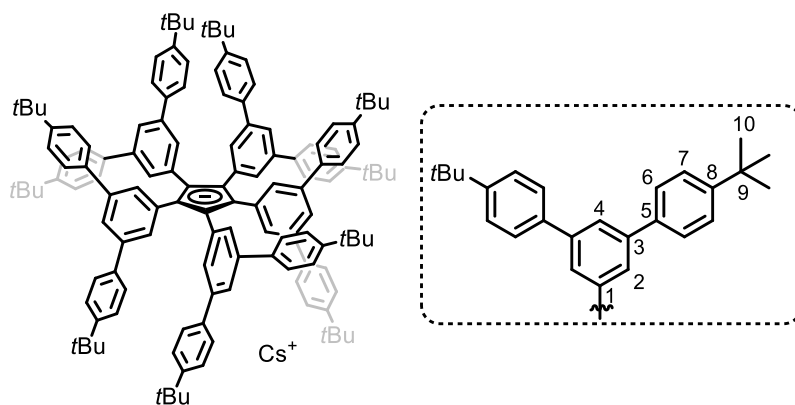
Yield: 394 mg (89%)

^{1}H NMR (400 MHz, 300 K, C_6D_6) δ = 1.15 (s, 90H, $C^{10}H$), 7.32 (m, 20H, C^7H), 7.67 (m, 20H, C^7H), 7.81 (br s, $^3J_{HH}$ not resolved, 10H, C^2H), 8.02 (br s, 5H, C^4H) ppm.

^{13}C{^{1}H} NMR (100 MHz, 300 K, $CDCl_3$) δ = 31.4 (s, C^{10}), 34.4 (s, C^9), 121.4 (s, C^4), 123.0 (s, C^1), 126.0 (s, C^7), 127.6 (s, C^6), 130.5 (s, C^2), 140.1 (s, C^5), 141.9 (s, C^3), 142.4 (s, C^{Cp}), 149.9 (s, C^8) ppm.

Elemental Analysis calcd. C 85.32, H 7.69; found C 85.28, H 7.91.

UV/Vis (C_6H_6): λ_{max} (nm, ε_{max} /L·mol^{-1}·cm^{-1}) 280 (150 000), 340 (45 000), 370sh (41 000).

[Cp^{T5}FeBr(thf)]$_2$ (2):

To a mixture of Cp^{T5}K·(thf)$_{2.2}$ (500.0 mg, 0.25 mmol, 1.0 eq.) and FeBr$_2$ (60.2 mg, 0.28 mmol, 1.1 eq.) was added THF (15 mL). The brown suspension was stirred over night at ambient temperature to afford an orange-red solution. Subsequently, the solvent was removed and the brown residue was dried *in vacuo*. The residue was extracted with *n*-hexane (2 x 10 mL) and the resulting orange-brown solution was concentrated to half the volume. Storage at −30 °C for four days afforded a yellow powder which was isolated by decanting the supernatant and dried *in vacuo* for ca. 5 minutes. When **3** was dried for longer times, the THF-free complex [Cp^{T5}FeBr]$_2$ is formed upon THF loss, which gives rise to a second set of signals in the ^{1}H NMR spectrum (Figure S17).

Single crystals suitable for X-ray diffraction were grown by storage of a saturated solution of **3** in *n*-hexane overnight.

T = 3,5-(4-*t*Bu-C_6H_4)$_2$-C_6H_3

$C_{278}H_{306}Br_2Fe_2O_2$, MW = 3951.00 g/mol
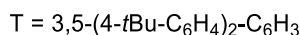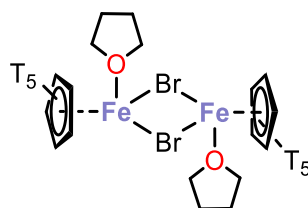
Yield: 240 mg (49%)

¹H NMR (400 MHz, 300 K, C_6D_6) δ = −23.08 (br s), −20.84 (br s), −2.51 (br s), 0.00 (br s), 3.54 (br s) ppm.

Evans NMR μ_{eff} = 7.8(1) μ_B.

Elemental Analysis calcd. for (**3** · 2 *n*-hexane, see SCXRD data) C 84.47, H 8.16; found C 84.86, H 7.82.

UV/Vis (C_6H_6): λ_{max} (nm, ε_{max} /L·mol⁻¹·cm⁻¹) 280 (360 000), 350sh (34 000).

[Cp^{T5}NiBr]₂ (3):

To a mixture of Cp^{T5}K·(thf)$_{3.2}$ (1000.0 mg, 0.49 mmol, 1.0 eq.) and NiBr$_2$ (112.6 mg, 0.52 mmol, 1.1 eq.) was added THF (30 mL). The brown suspension was stirred at 60 °C for four days. Subsequently, the solvent was removed and the brown residue was dried *in vacuo*. The residue was extracted with *n*-hexane (2 x 25 mL) and the resulting brown solution was concentrated by ca. 20 mL. Storage at −30 °C overnight afforded brown needles suitable for X-ray diffraction of **3**. The crystals were isolated by decanting the supernatant and dried *in vacuo*. Another batch of crystalline solid was obtained upon concentrating the supernatant solution and crystallisation at −30 °C.

T = 3,5-(4-*t*Bu-C_6H_4)$_2$-C_6H_3

$C_{270}H_{290}Br_2Ni_2$, MW = 3812.48 g/mol
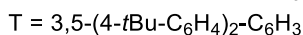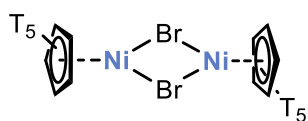
Yield: 362 mg (39%)

¹H NMR (400 MHz, 300 K, C_6D_6) δ = −15.20 (br s), −13.7 (br s), 1.30 (br s), 7.33 (s), 9.80 (br s) ppm.

Evans NMR μ_{eff} = 4.1(1) μ_B.

Elemental Analysis calc. C 85.06, H 7.67; found C 85.65, H 7.39.

UV/Vis (C_6H_6): λ_{max} (nm, ε_{max} /L·mol⁻¹·cm⁻¹) 280 (340 000), 350sh (36 000).

[Cp^{T5}CoBr]$_2$ (4):

To a mixture of Cp^{T5}K·(thf)$_{2.3}$ (300.0 mg, 0.15 mmol, 1.0 eq.) and CoBr$_2$ (36.7 mg, 0.17 mmol, 1.1 eq.) was added THF (10 mL). The brown suspension was stirred at ambient temperature overnight. Subsequently, the solvent was removed and the brown residue was dried *in vacuo*. The residue was extracted with *n*-hexane (5 mL) and the resulting brown solution was concentrated to ca. 3 mL. Storage at −30 °C overnight afforded a brown microcrystalline powder of **5**. The solid was isolated by decanting the supernatant and dried *in vacuo*. Another batch of crystalline solid was obtained upon concentrating the supernatant solution and crystallisation at −30 °C.

T = 3,5-(4-*t*Bu-C$_6$H$_4$)$_2$-C$_6$H$_3$

C$_{270}$H$_{290}$Br$_2$Co$_2$, MW = 3812.96 g/mol
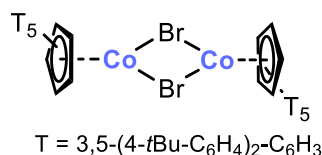
Yield: 83.0 mg (29%)

^{1}H NMR (400 MHz, 300 K, C$_6$D$_6$) δ = 1.07 (s), 5.61 (br s), 7.07 (br s), 7.93 (br s) ppm.

Evans NMR μ_{eff} = 3.4(1) μ_B.

Elemental Analysis calc C 85.05, H 7.67; found C 85.74, H 7.51.

UV/Vis (C$_6$H$_6$): λ_{max} (nm, ε_{max} /L·mol^{-1}·cm^{-1}) 280 (205 000), 360sh (13 000).

Reduction Reactions of [Cp^{T5}MBr]$_2$ (M = Fe(thf), Co, Ni)

The reduction reactions were carried out for iron, cobalt and nickel complexes (**2-4**). Only the procedure for the nickel complex is presented below. The procedures for reductions of **2** and **4** were performed on a similar scale at −30 °C. NMR spectra for the reduction reactions with **2** and **4** are depicted in Figure S31 and Figure S32, respectively.

To a solution of [Cp^{T5}NiBr]$_2$ (50.0 mg, 0.013 mmol, 1.0 eq.) in C$_6$D$_6$ (0.5 mL) was added KC$_8$ (3.7 mg, 0.027 mmol, 2.1 eq.). The brown suspension was heated to 50 °C for 24 h while stirring. Subsequently, the suspension was filtered and the solvent was removed *in vacuo*. The orange residue was washed with *n*-hexane (2 x 0.5 mL) and extracted in benzene. Single crystals suitable for X-ray diffraction were grown by slow evaporation from a benzene solution of [(Cp^{T5})$_2$Ni] (**6**).

T = 3,5-(4-*t*Bu-C$_6$H$_4$)$_2$-C$_6$H$_3$

C$_{270}$H$_{290}$Ni, MW = 3532.56 g/mol
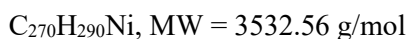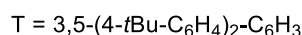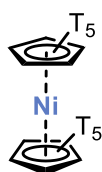
^{1}H NMR (400 MHz, 300 K, C$_6$D$_6$) δ = −12.94 (br s), −8.78 (br s), 1.03 (s), 1.10 (s), 6.88 (s), 8.03 (br s), 8.46 (br s) ppm.

A larger scale preparation and further characterisation of **5** was not pursued.

9.4.3 NMR Spectra
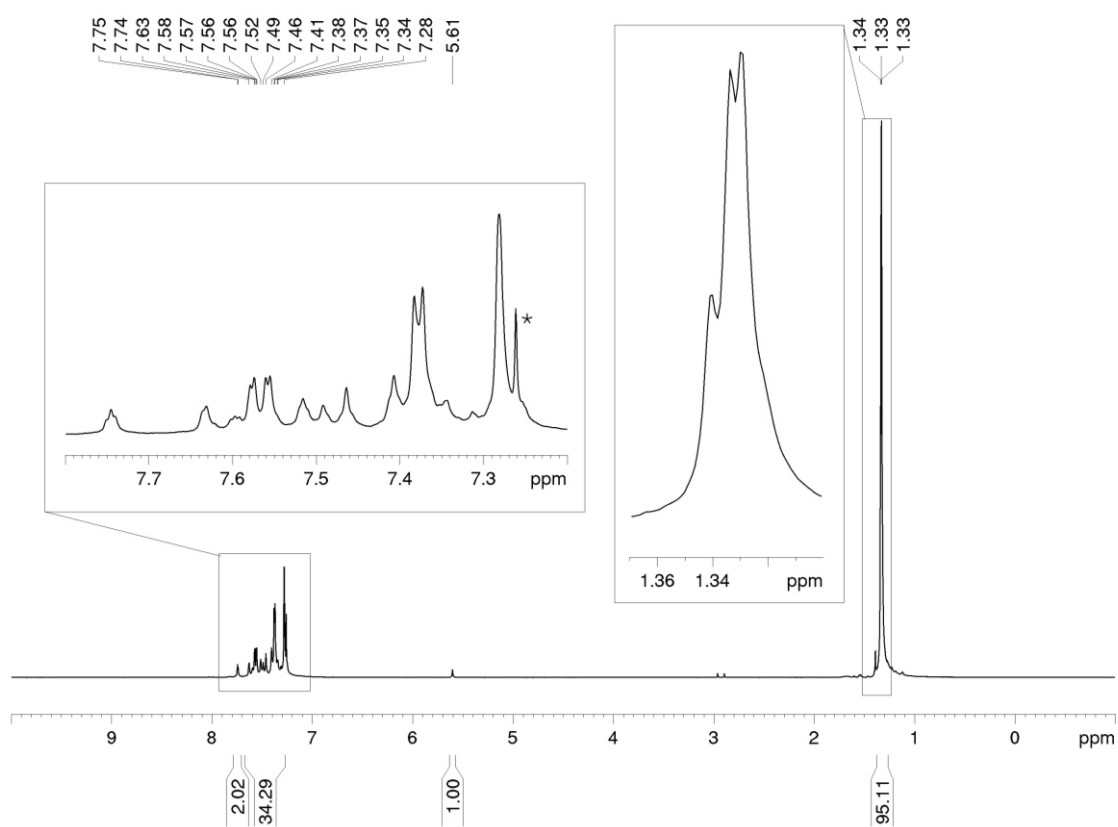
Figure S1. ^{1}H NMR spectrum (400 MHz, 300 K, CDCl$_3$) of **1-H**; *CDCl$_3$.
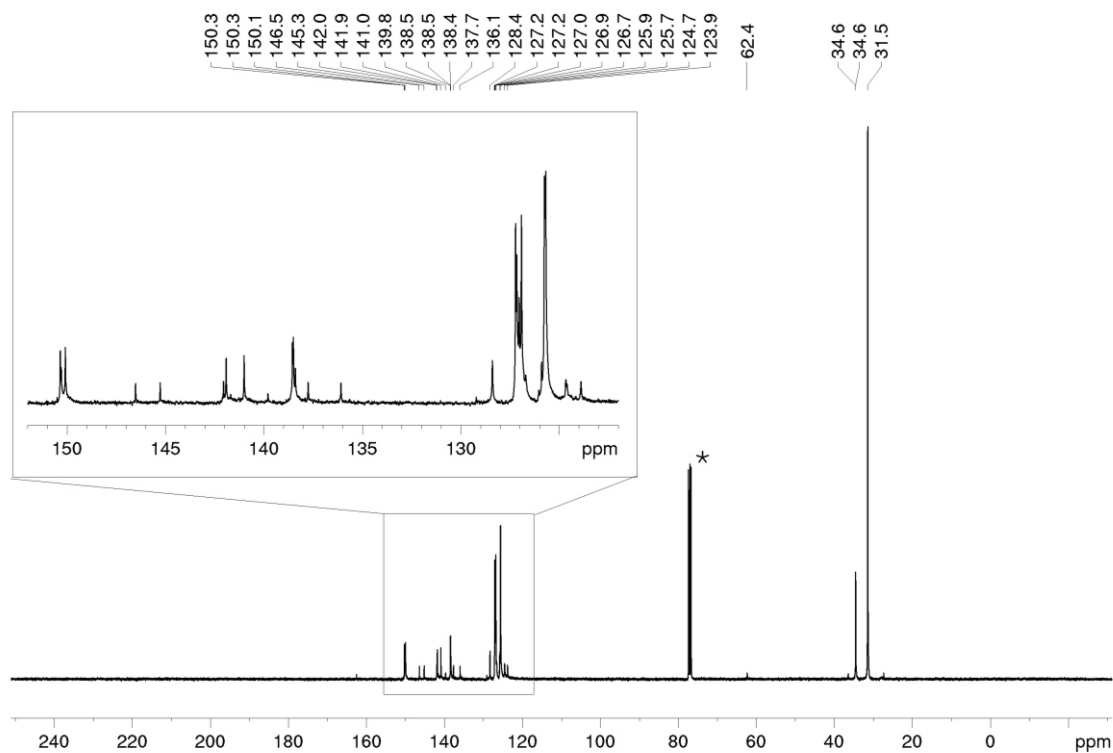
Figure S2. ^{13}C{^{1}H} NMR spectrum (100 MHz, 300 K, CDCl$_3$) of **1-H**; *CDCl$_3$.
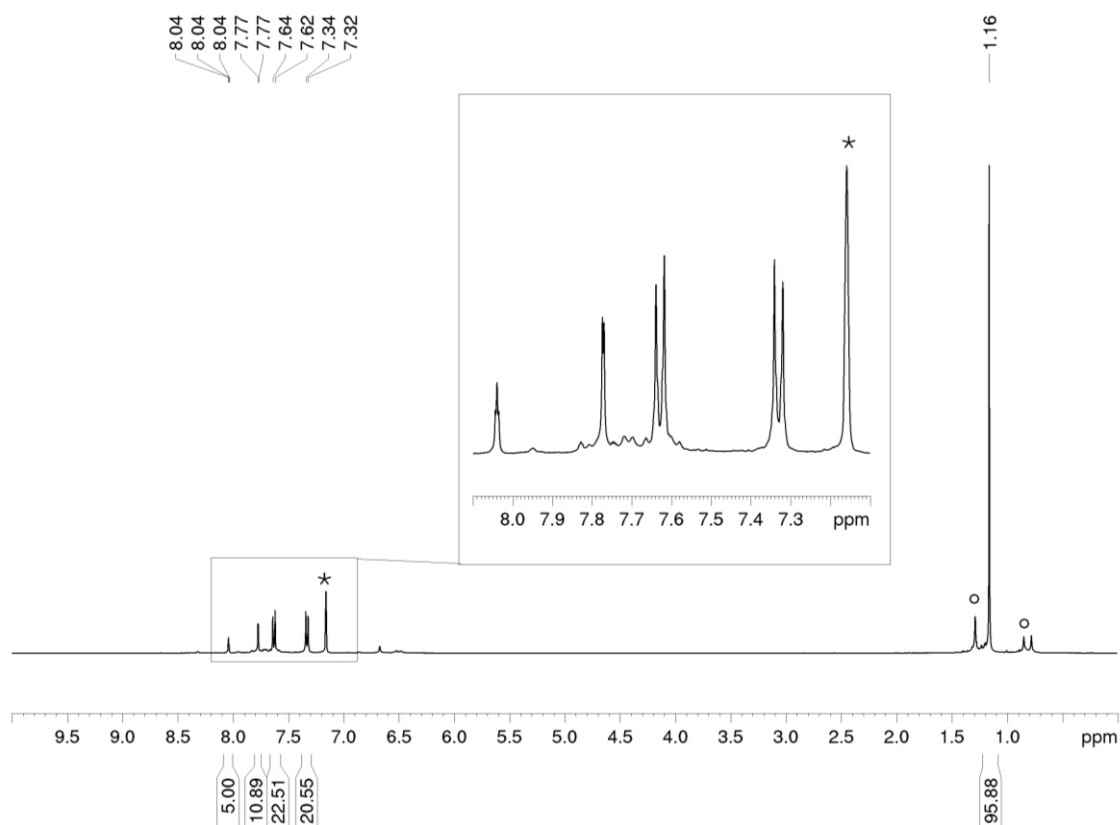
Figure S3. ^{1}H NMR spectrum (400 MHz, 300 K, C$_6$D$_6$) of **1-Li**; *C$_6$D$_6$; °unidentified impurity.
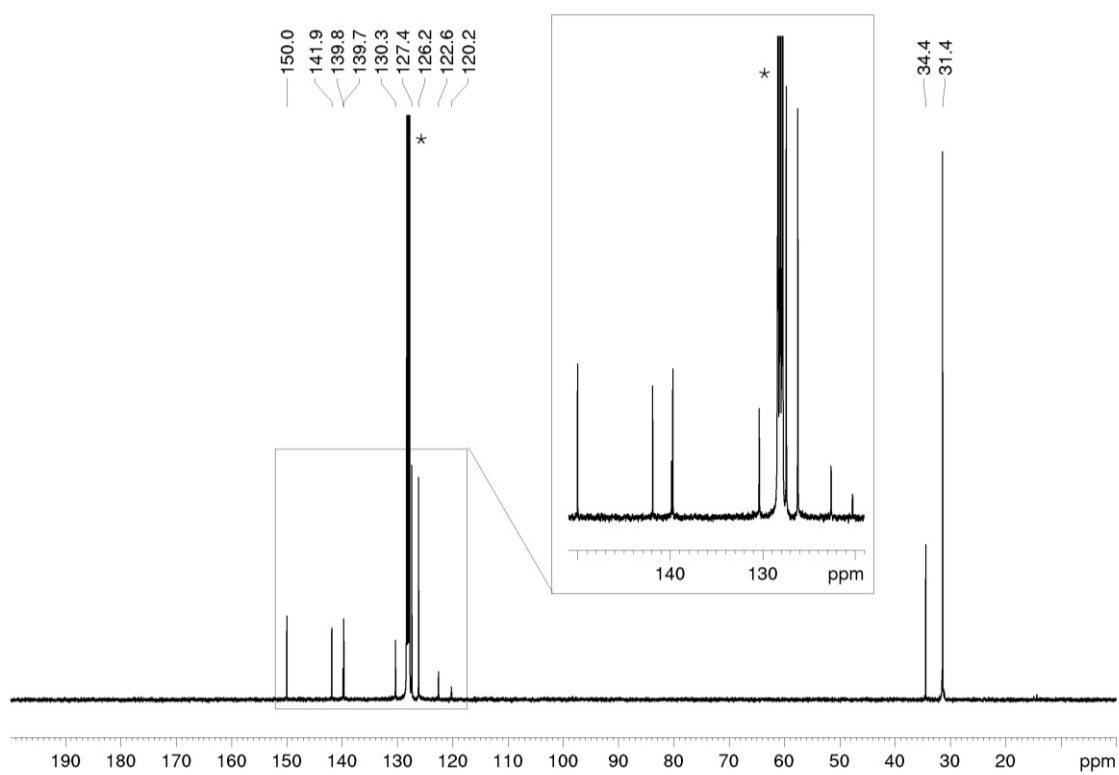
Figure S4. ^{13}C{^{1}H} NMR spectrum (100 MHz, 300 K, C$_6$D$_6$) of **1-Li**; *C$_6$D$_6$.
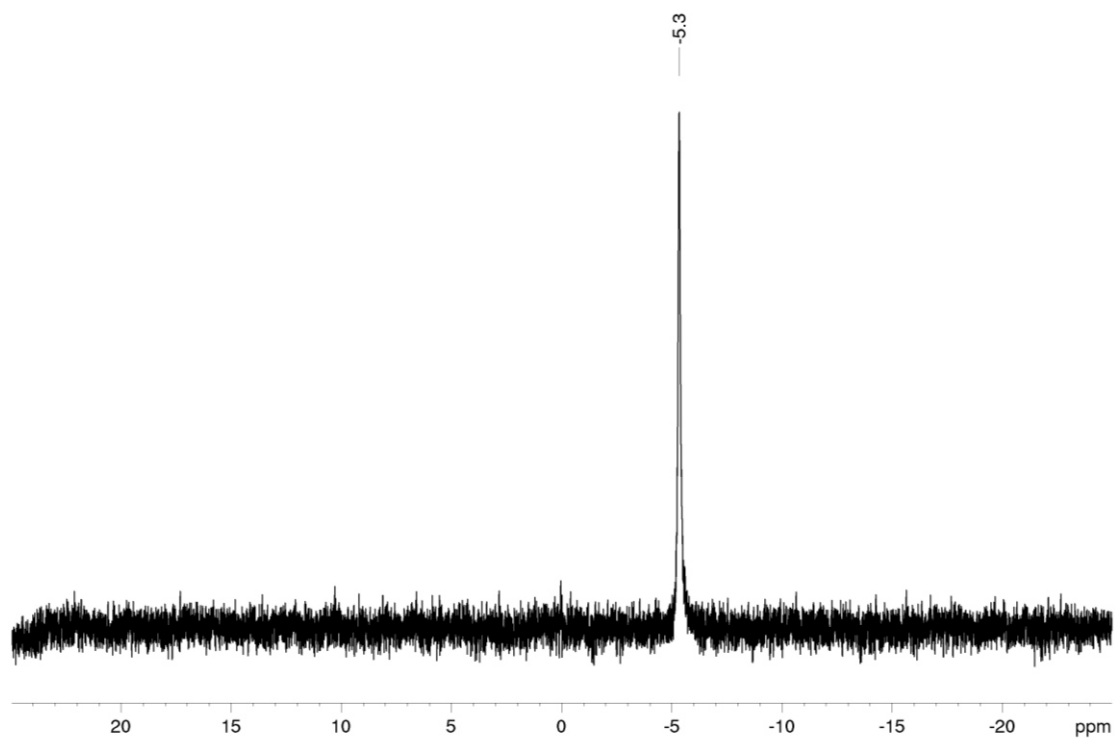
Figure S5. ^{7}Li NMR spectrum (155 MHz, 300 K, C$_6$D) of **1-Li**.
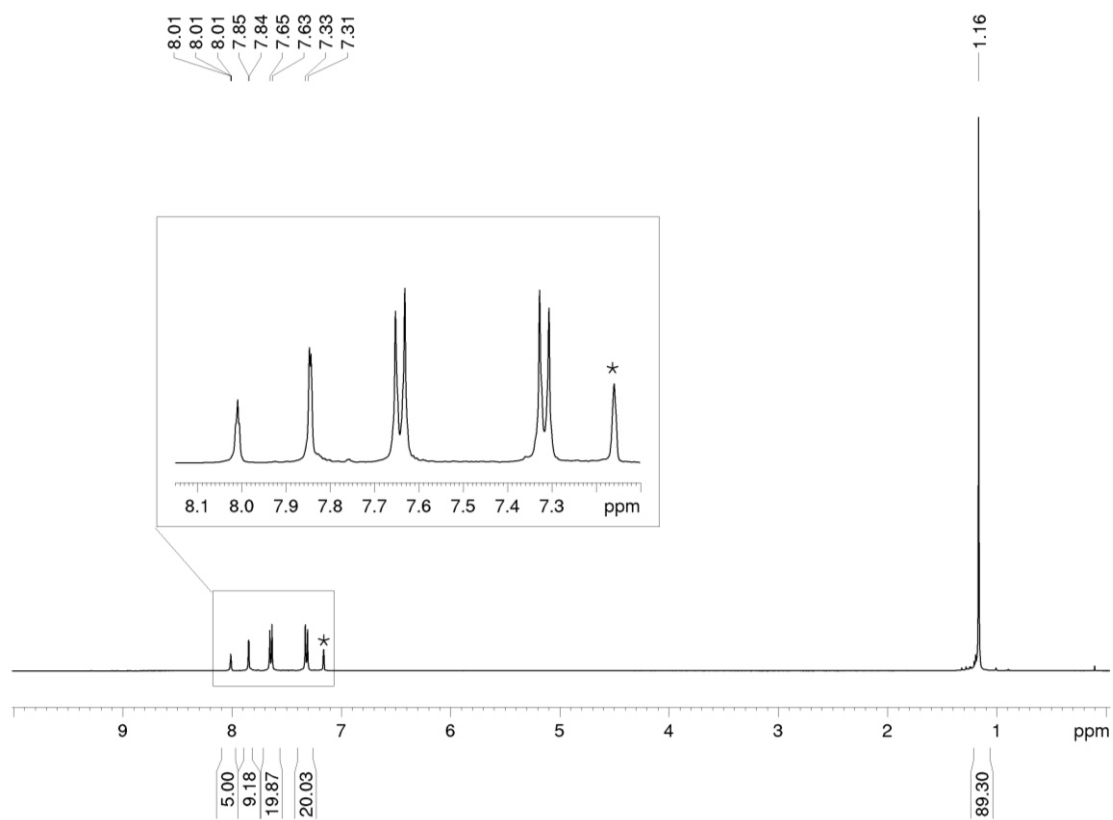
Figure S6. ^{1}H NMR spectrum (400 MHz, 300 K, C$_6$D$_6$) of **1-Na**; *C$_6$D$_6$.
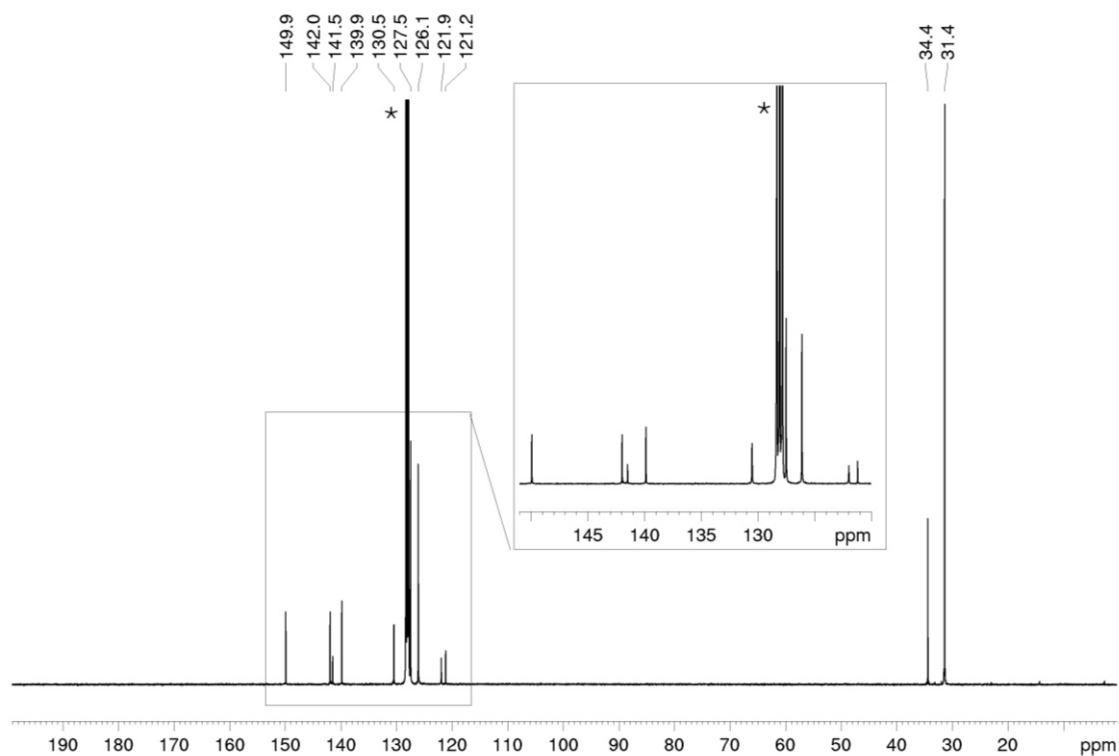
Figure S7. $^{13}C\{^1H\}$ NMR spectrum (100 MHz, 300 K, C_6D_6) of **1-Na**; *C_6D_6.
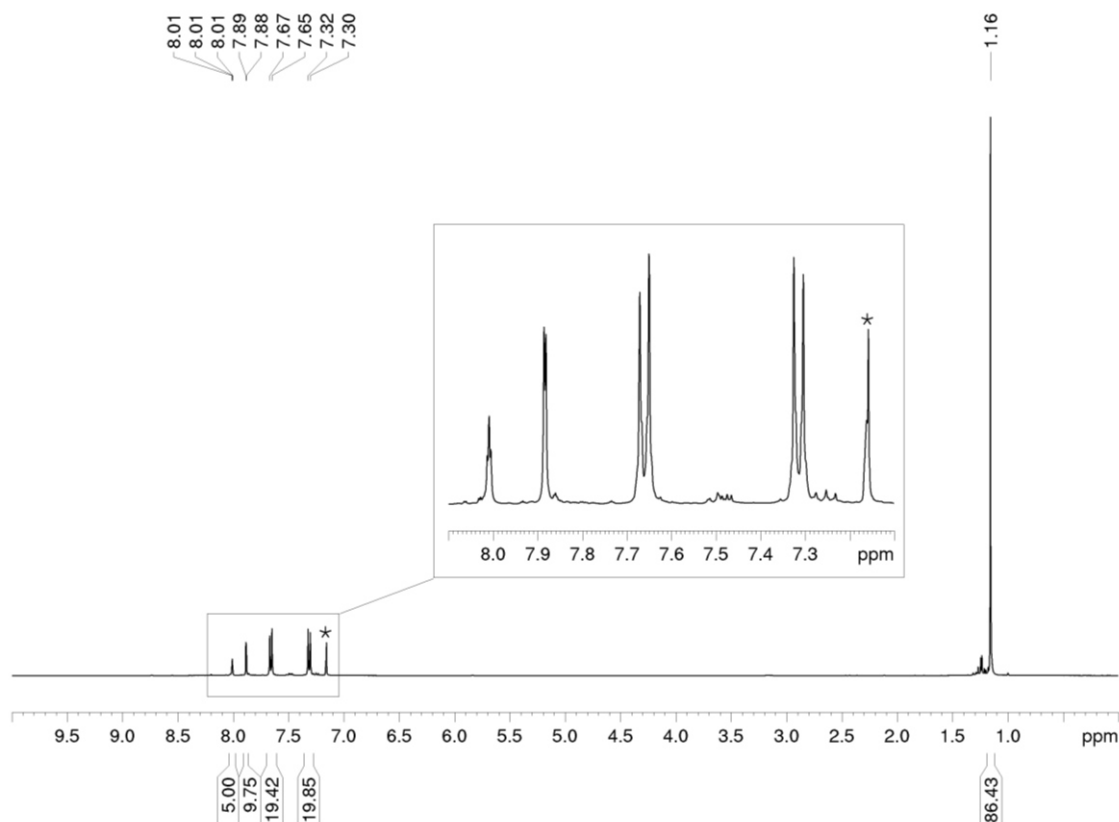
Figure S8. ^1H NMR spectrum (400 MHz, 300 K, C_6D_6) of **1-K**; *C_6D_6.
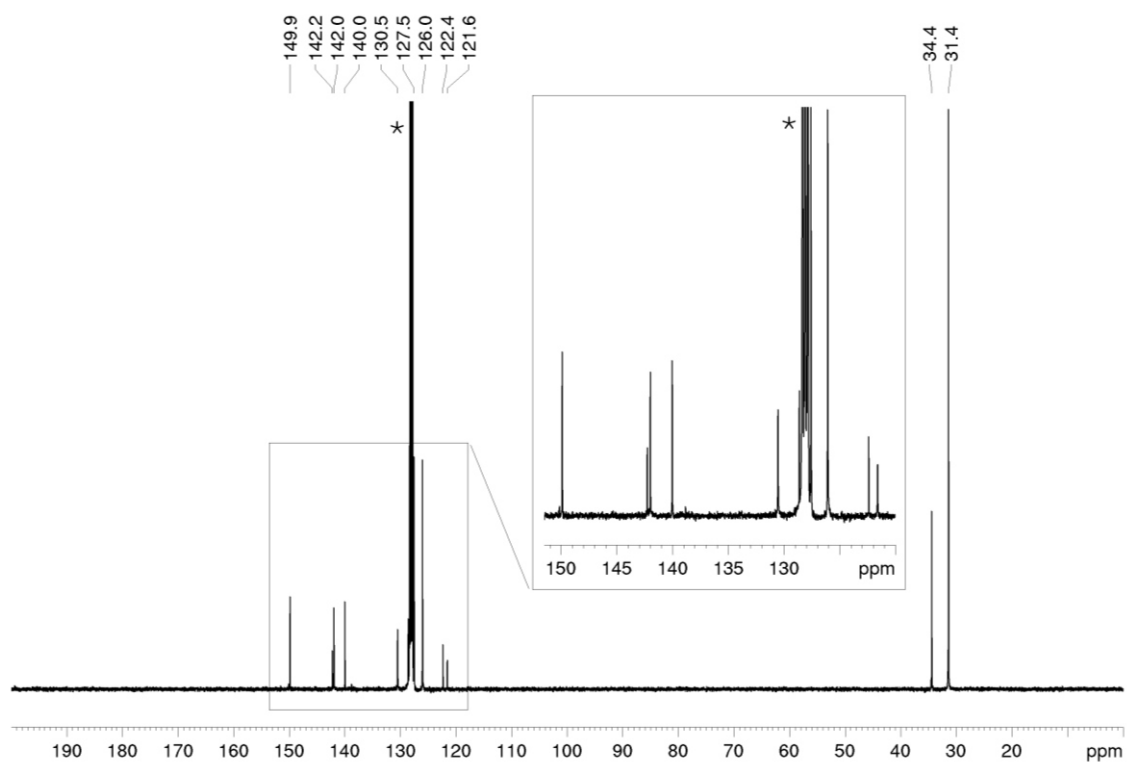
Figure S9. $^{13}C\{^1H\}$ NMR spectrum (100 MHz, 300 K, C$_6$D$_6$) of **1-K**; *C$_6$D$_6$.
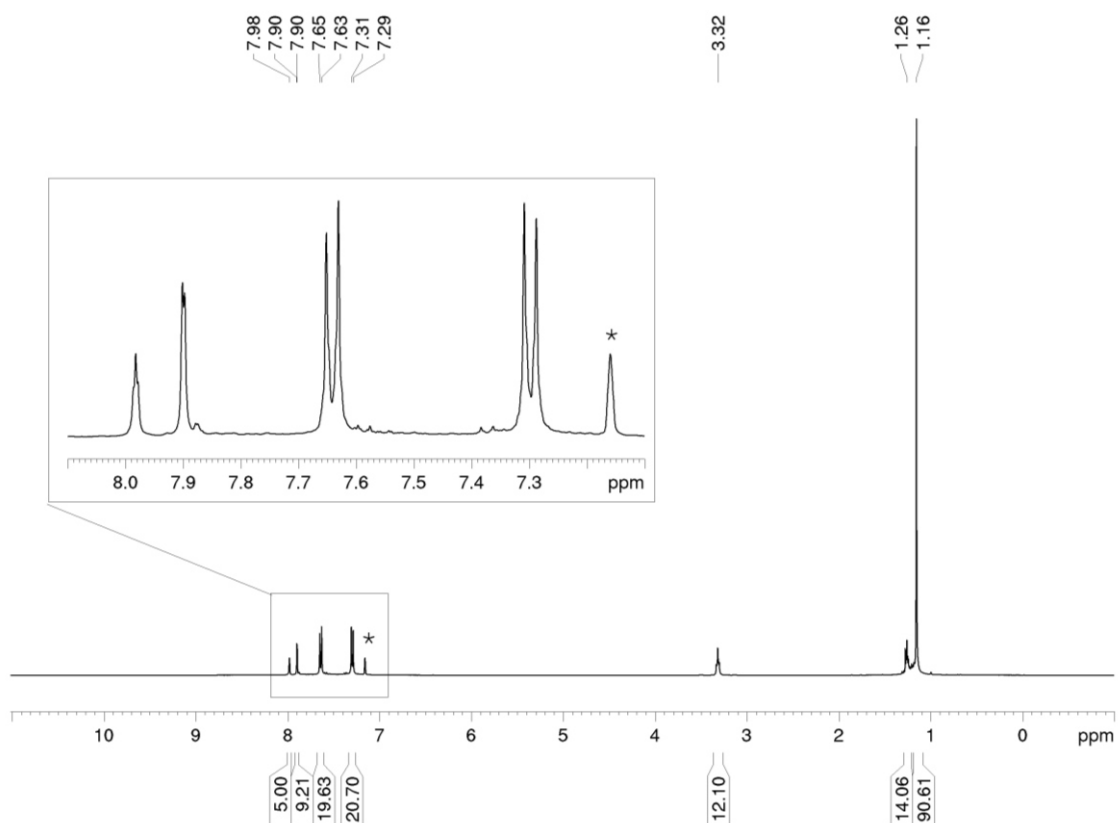
Figure S10. ^1H NMR spectrum (400 MHz, 300 K, C$_6$D$_6$) of **1-K·(thf)$_3$**; *C$_6$D$_6$.
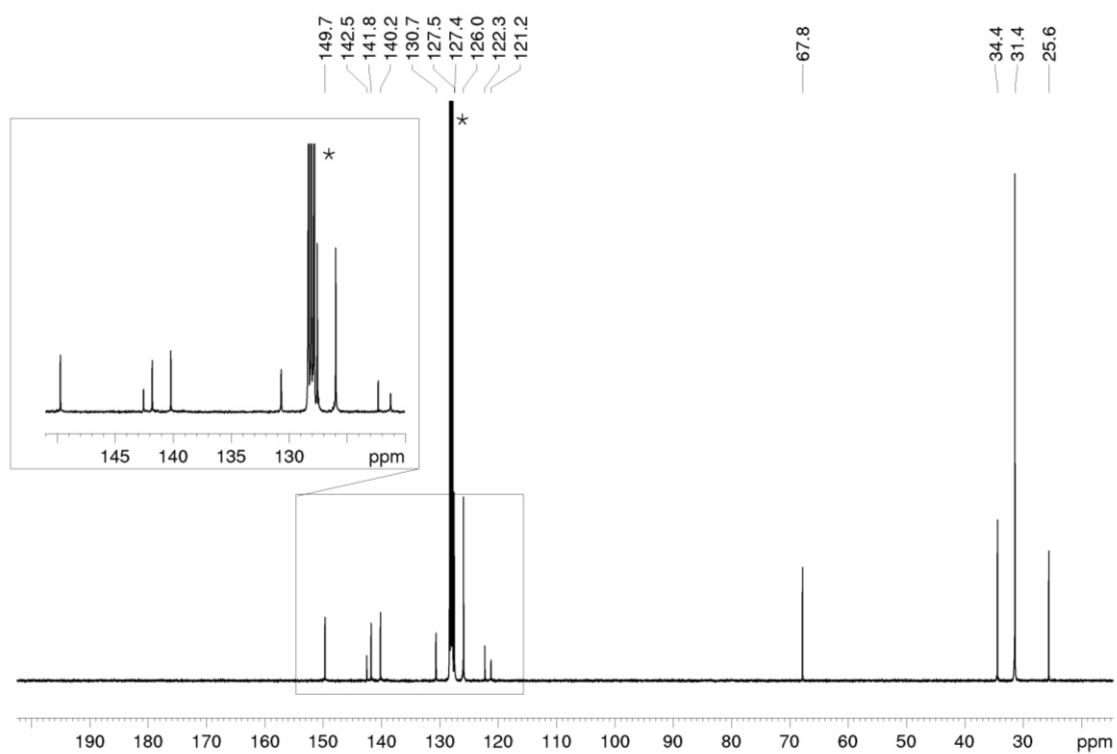
Figure S11. $^{13}C\{^1H\}$ NMR spectrum (100 MHz, 300 K, C_6D_6) of **1-K·(thf)₃**; *C_6D_6.
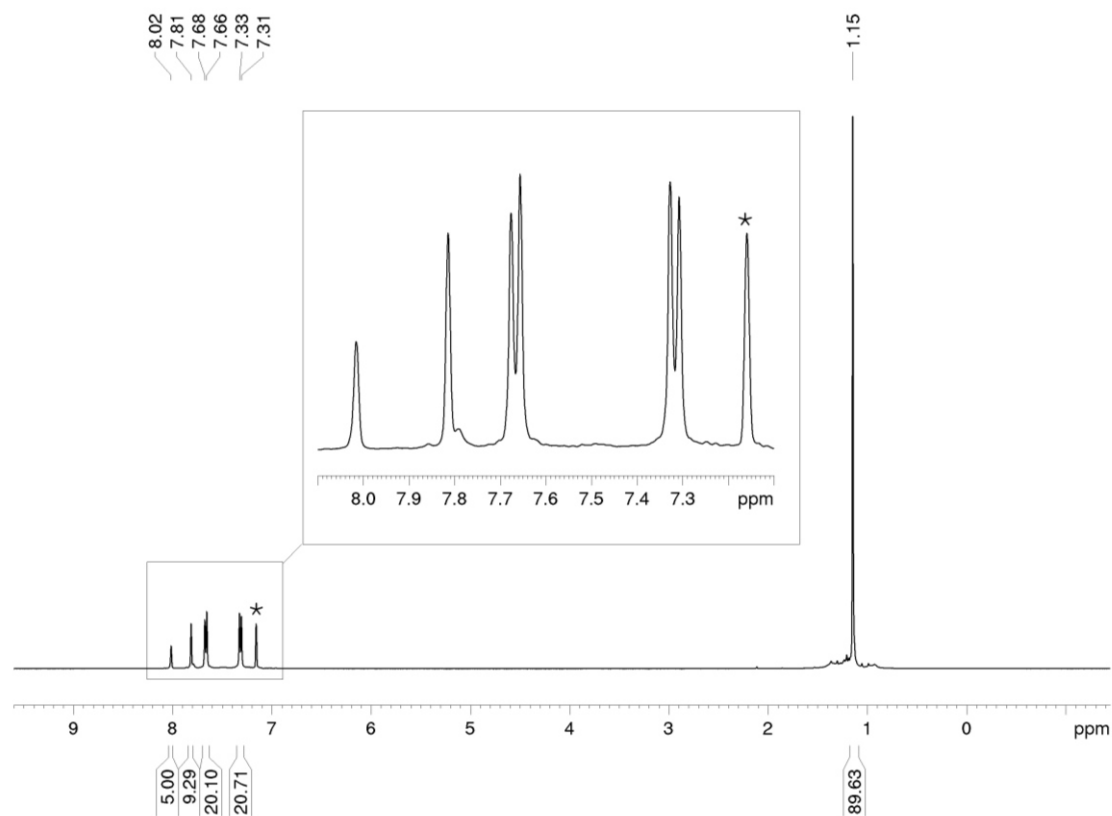
Figure S12. ^1H NMR spectrum (400 MHz, 300 K, C_6D_6) of **1-Rb**; *C_6D_6.
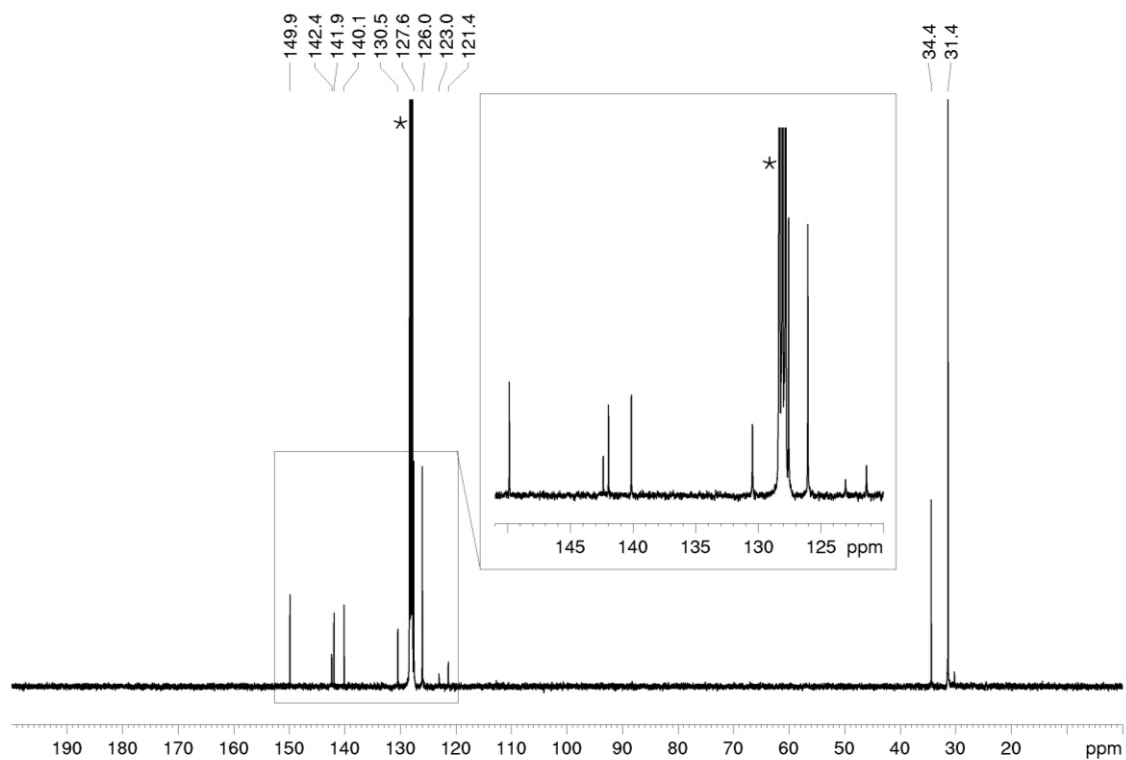
Figure S13. ^{13}C{^{1}H} NMR spectrum (100 MHz, 300 K, C$_6$D$_6$) of **1-Rb**; *C$_6$D$_6$.
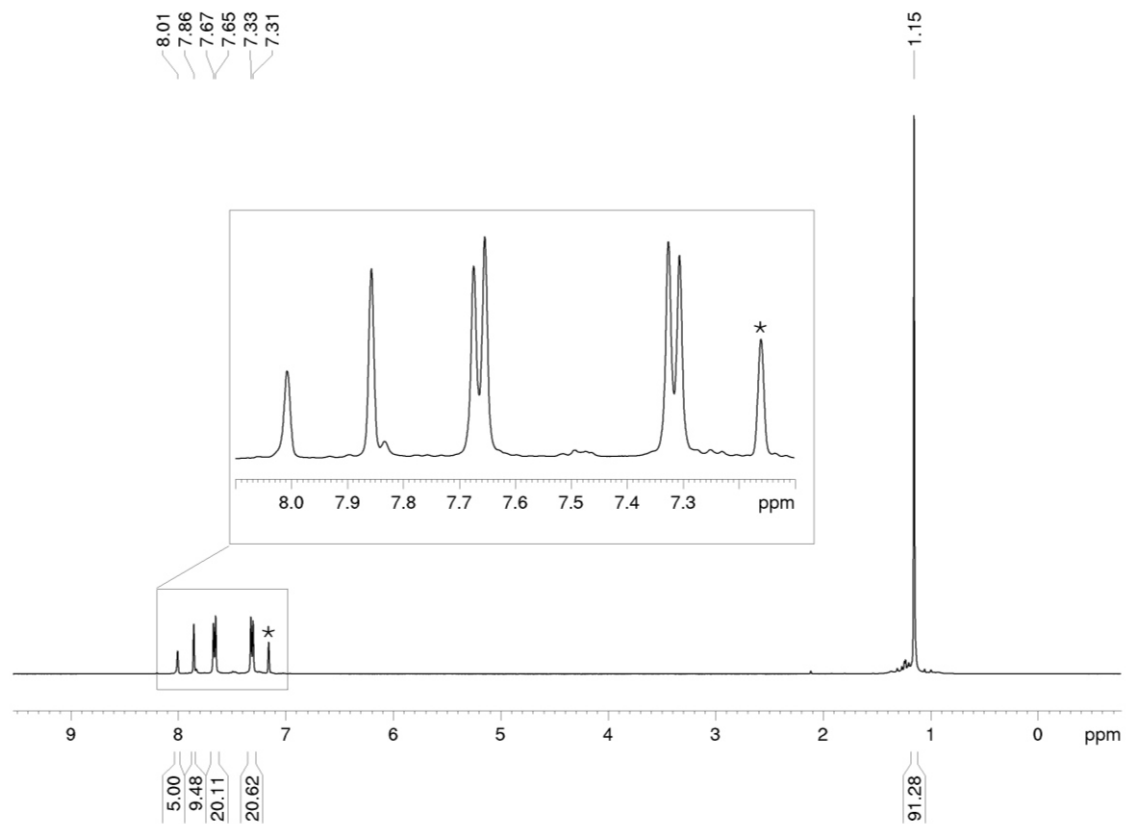
Figure S14. ^{1}H NMR spectrum (400 MHz, 300 K, C$_6$D$_6$) of **1-Cs**; *C$_6$D$_6$.

285
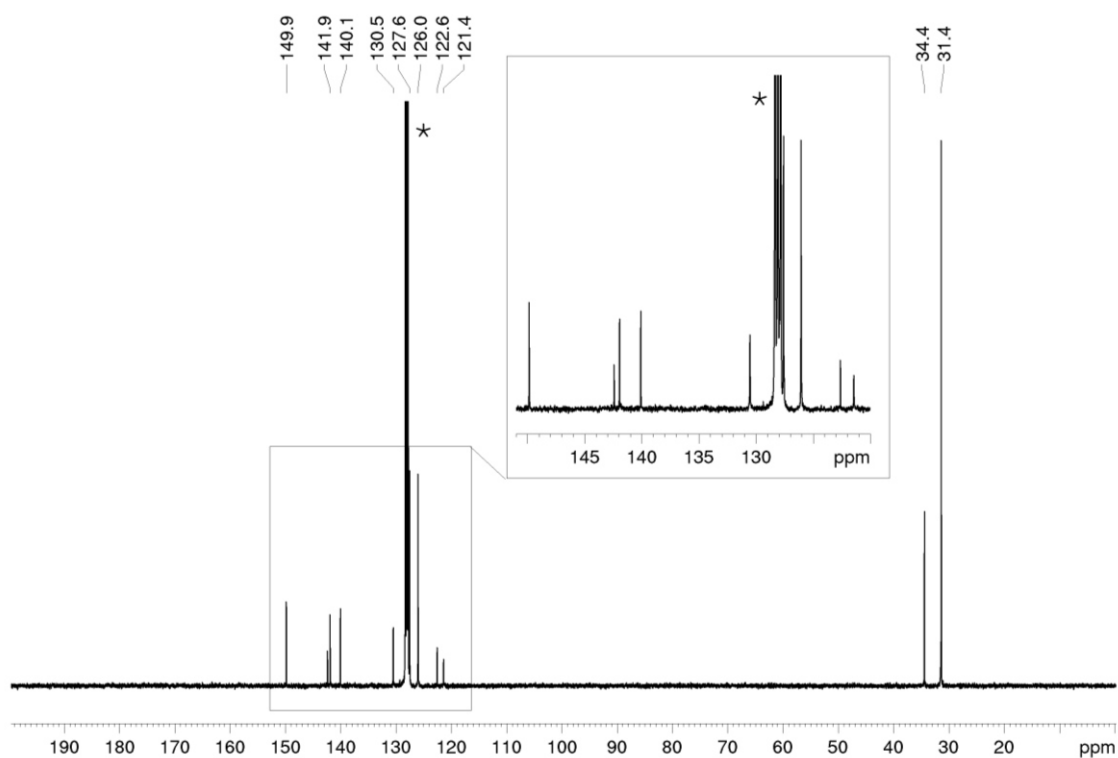
Figure S15. $^{13}C\{^1H\}$ NMR spectrum (100 MHz, 300 K, C_6D_6) of **1-Cs**; *C_6D_6.
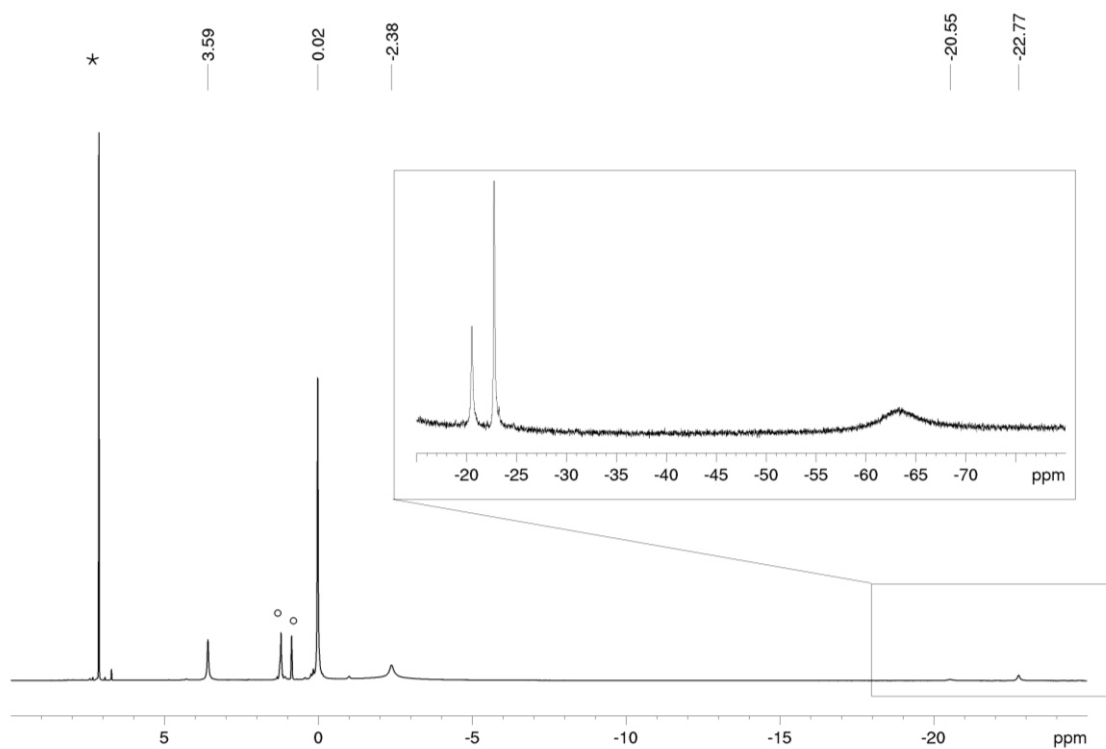
Figure S16. ^1H NMR spectrum (400 MHz, 300 K, C_6D_6) of **2**; *C_6D_6; °*n*-hexane.
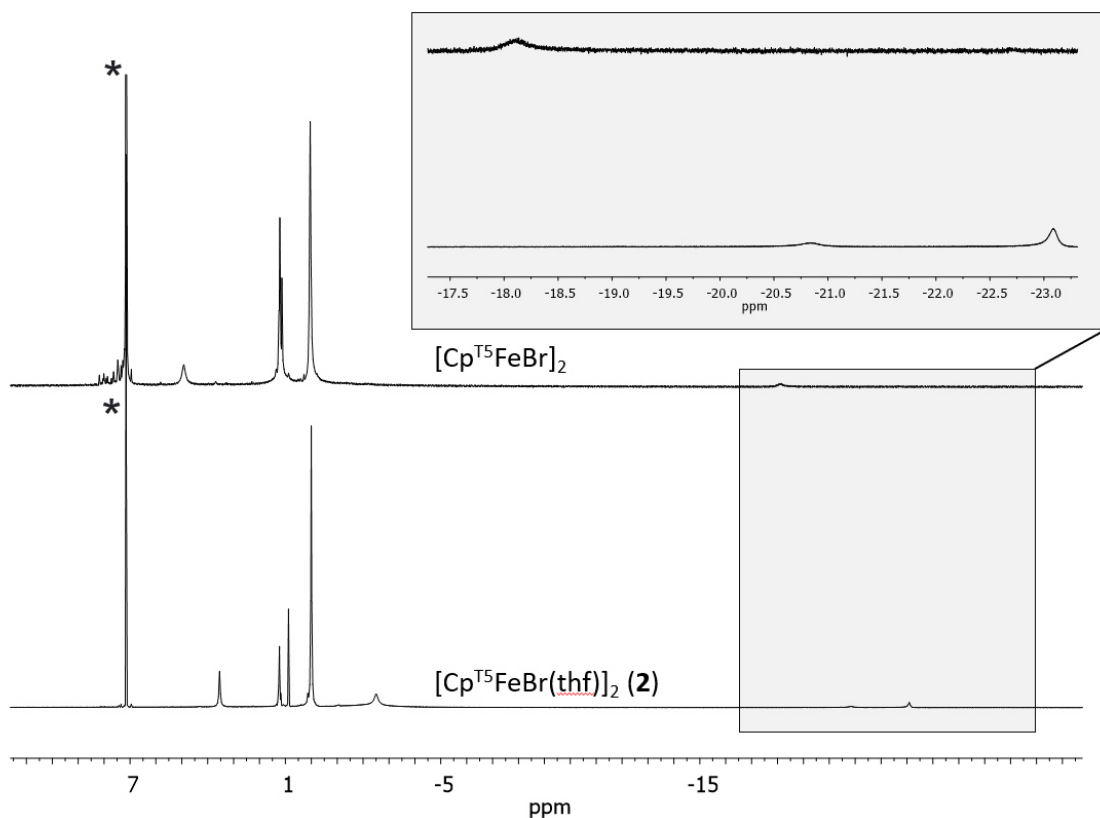
Figure S17. ^{1}H NMR spectrum (400 MHz, 300 K, CDCl$_3$) of **2** (with coordinated THF) and the putative THF-free complex [Cp^{T5}FeBr]$_2$; *C$_6$D$_6$.
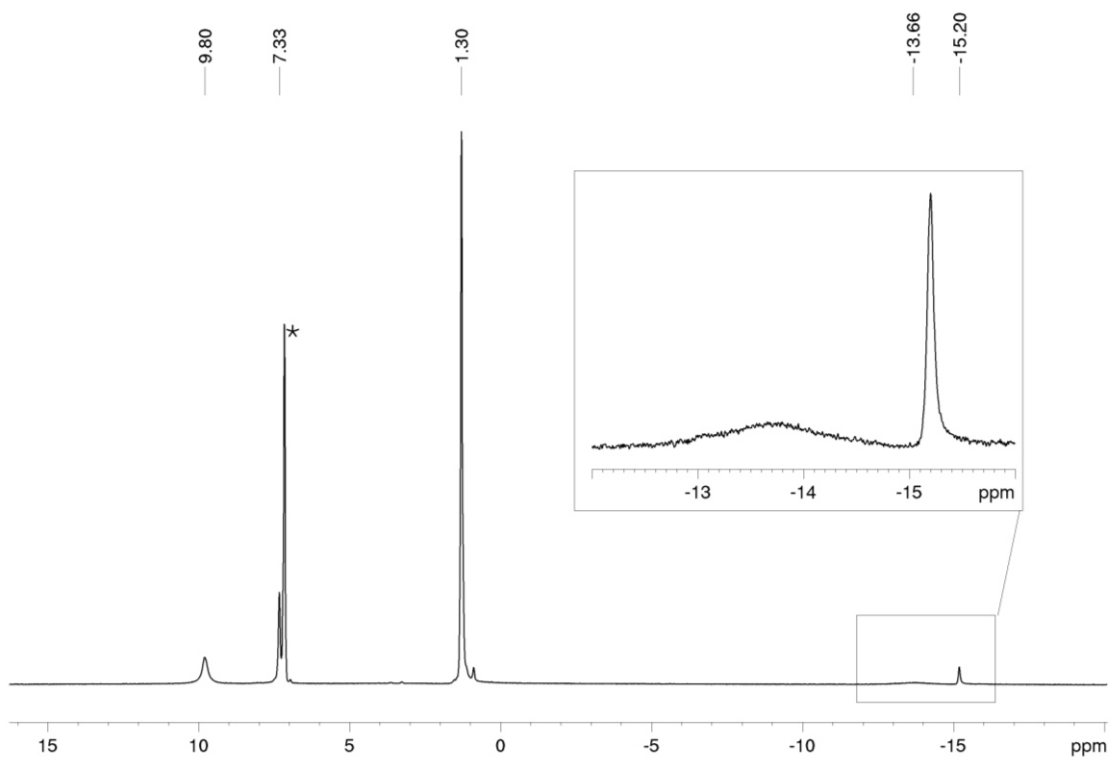
Figure S18. ^{1}H NMR spectrum (400 MHz, 300 K, CDCl$_3$) of **3**; *C$_6$D$_6$.

Figure S19. ^{1}H NMR spectrum (400 MHz, 300 K, CDCl$_3$) of **4**; *C$_6$D$_6$.

Figure S20. ^{1}H NMR spectrum (400 MHz, 300 K, C$_6$D$_6$) of **5**; *C$_6$D$_6$.
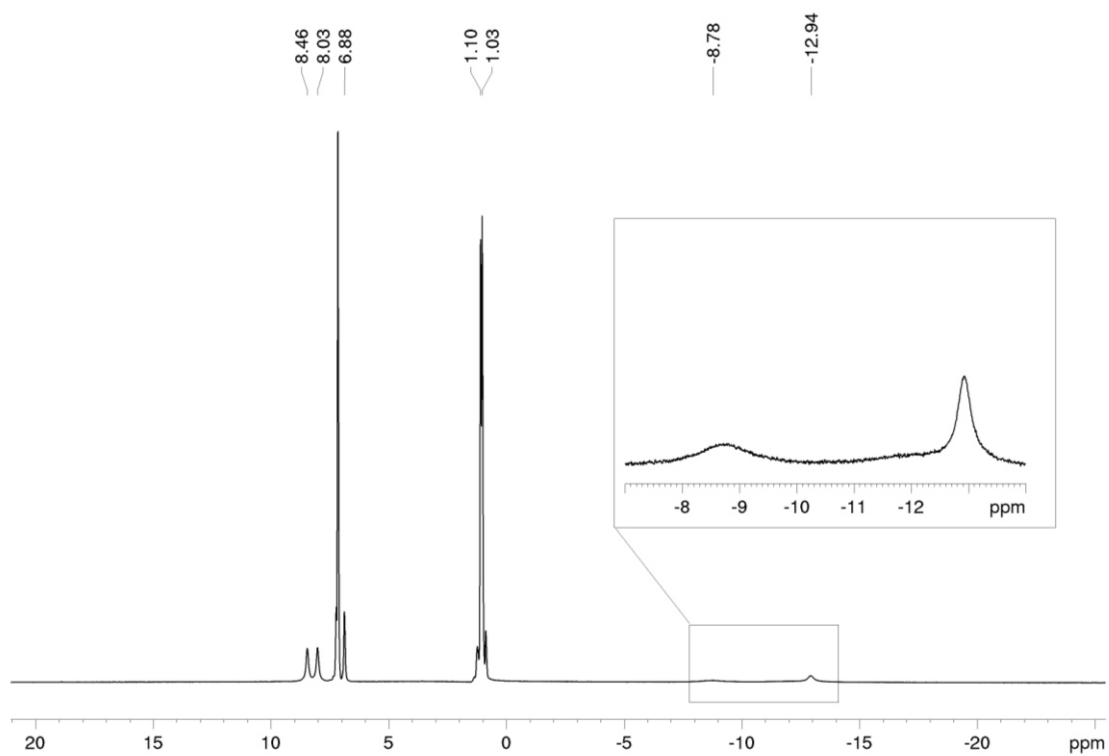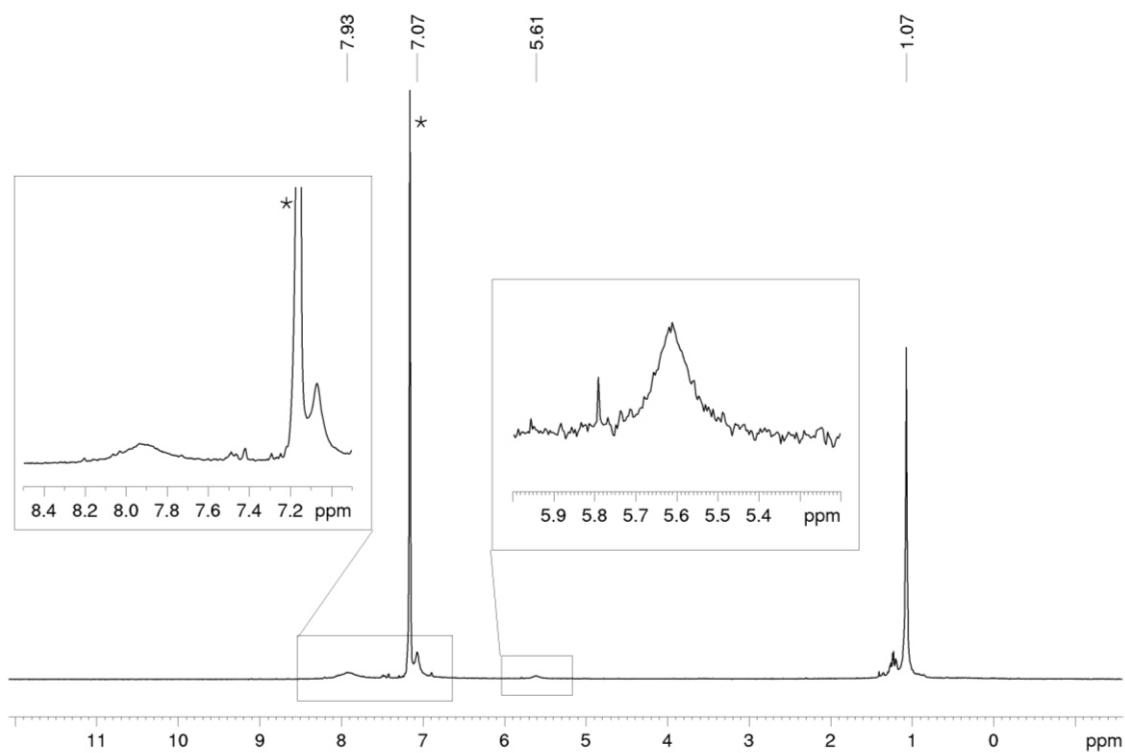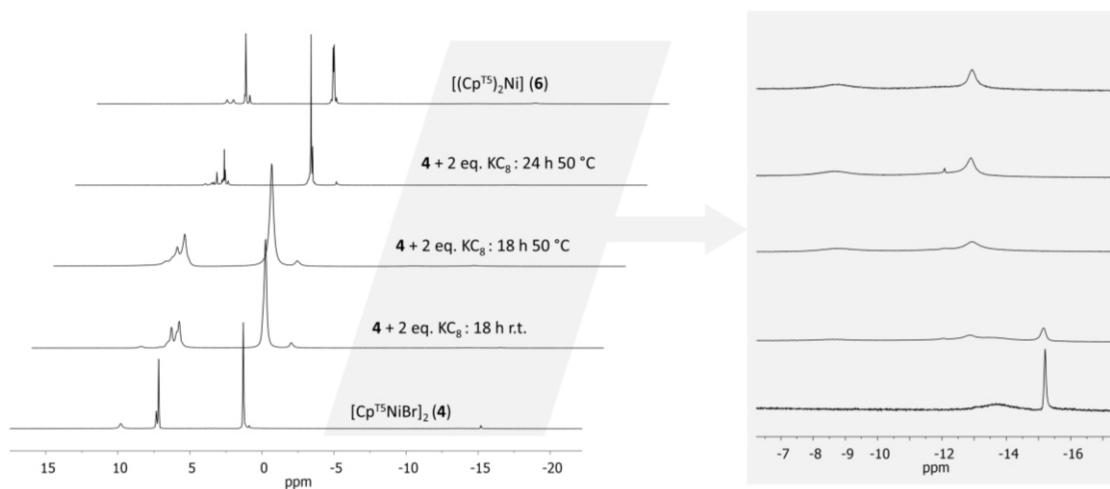
Figure S21. ^{1}H NMR spectra (400 MHz, 300 K, C_6D_6) of the reaction of **3** with 2 eq. KC$_8$.
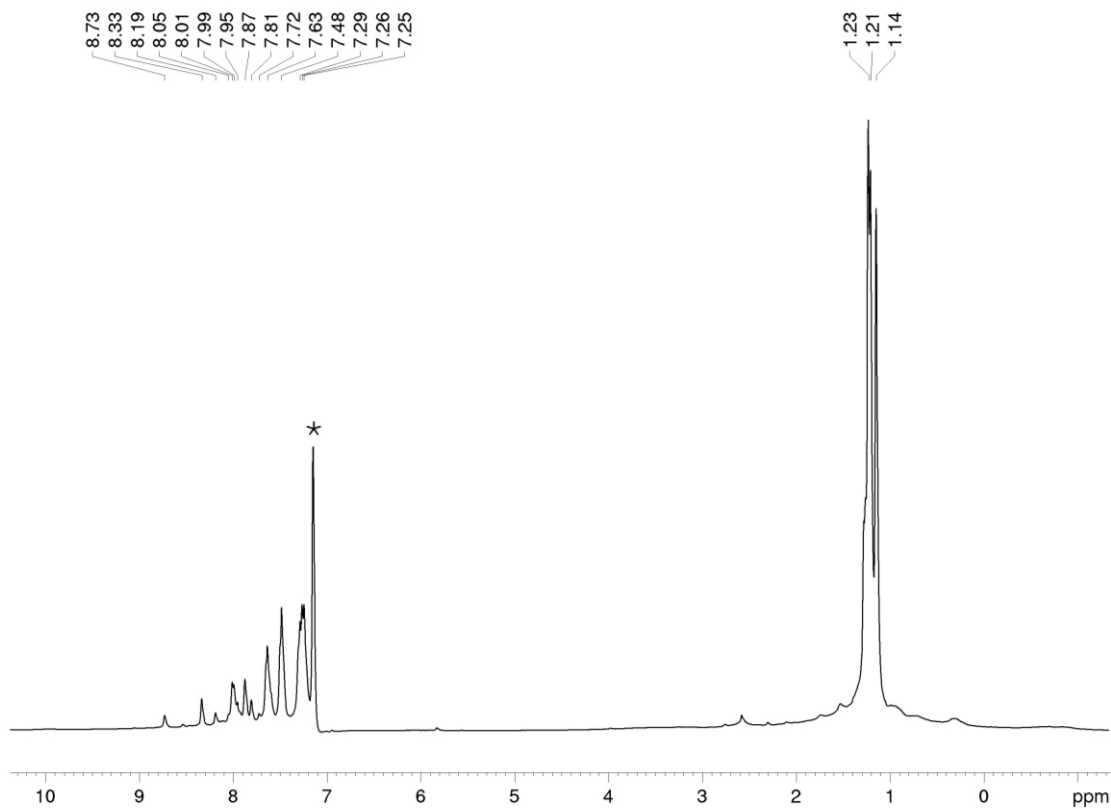
Figure S22. ^{1}H NMR spectrum (400 MHz, 300 K, C_6D_6) of the reaction of **2** with 2 eq. KC$_8$; C_6D_6.
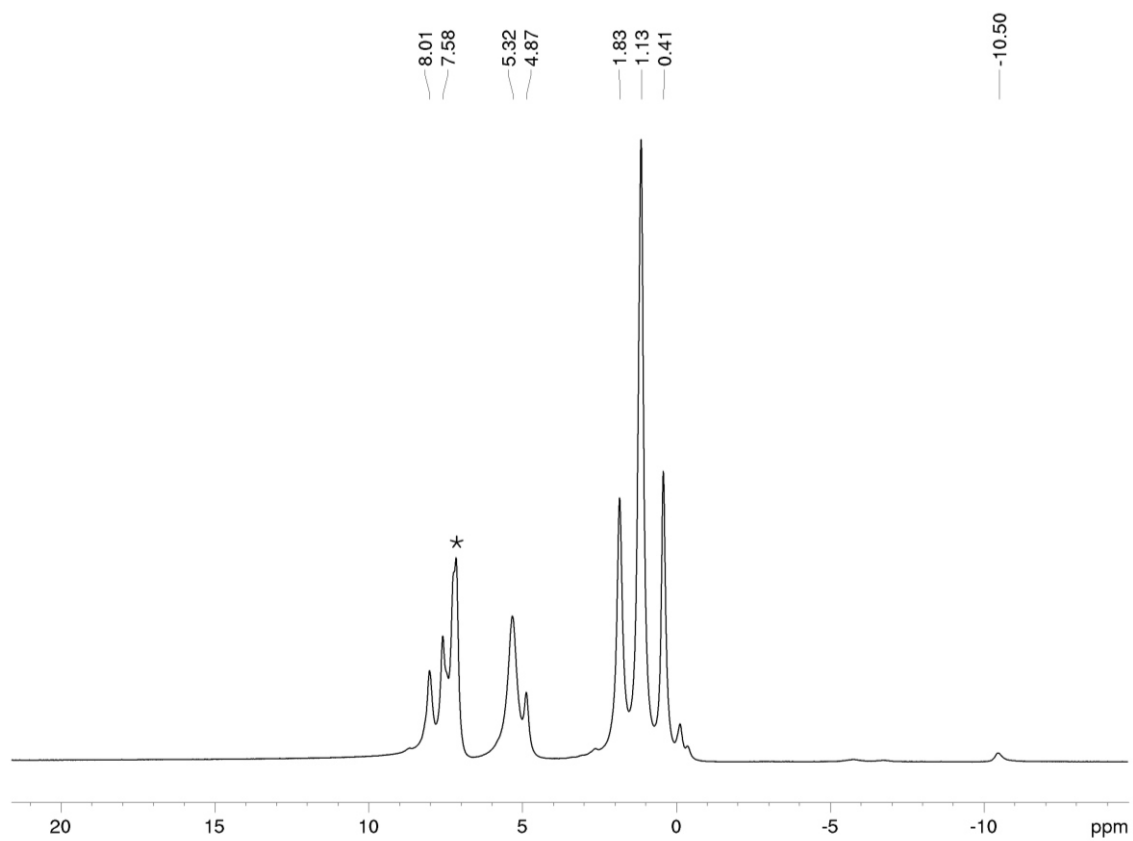
Figure S23. ^{1}H NMR spectrum (400 MHz, 300 K, C_6D_6) of the reaction of **4** with 2 eq. KC_8; C_6D_6.

9.4.4 UV/Vis Spectra
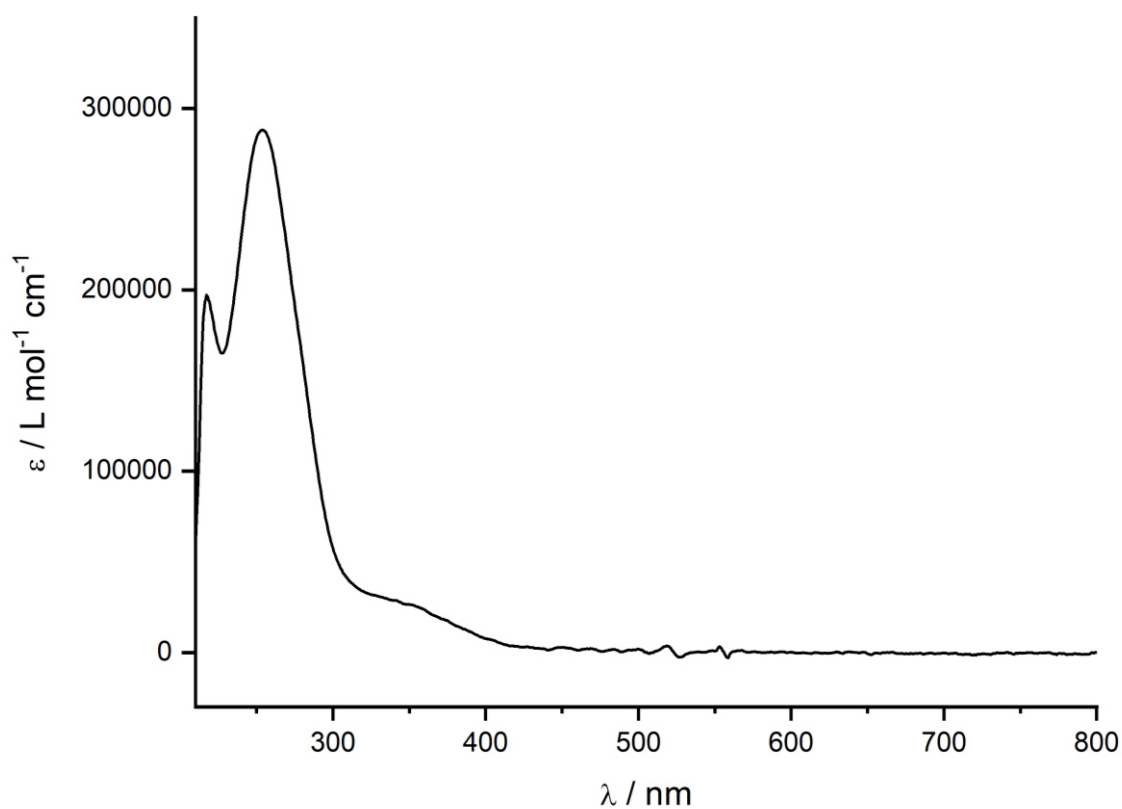
Figure S24. UV/Vis spectrum of **1-Li** recorded in *n*-hexane.
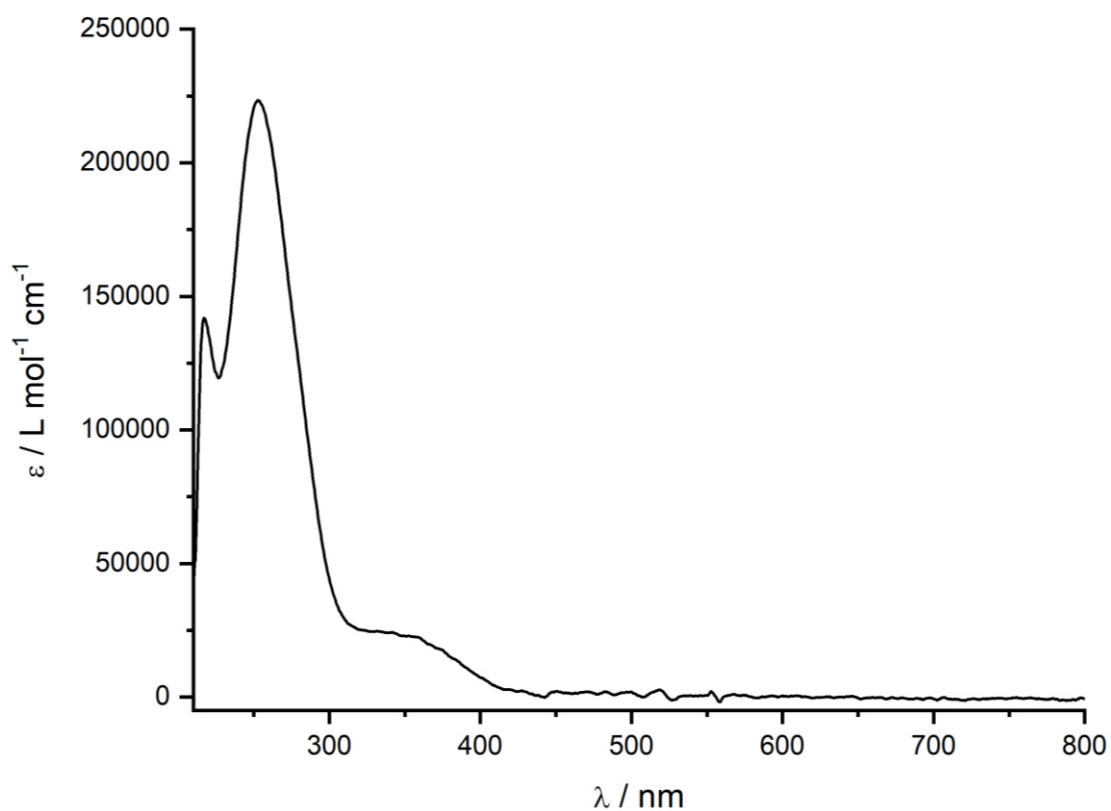
Figure S25. UV/Vis spectrum of **1-Na** recorded in *n*-hexane.
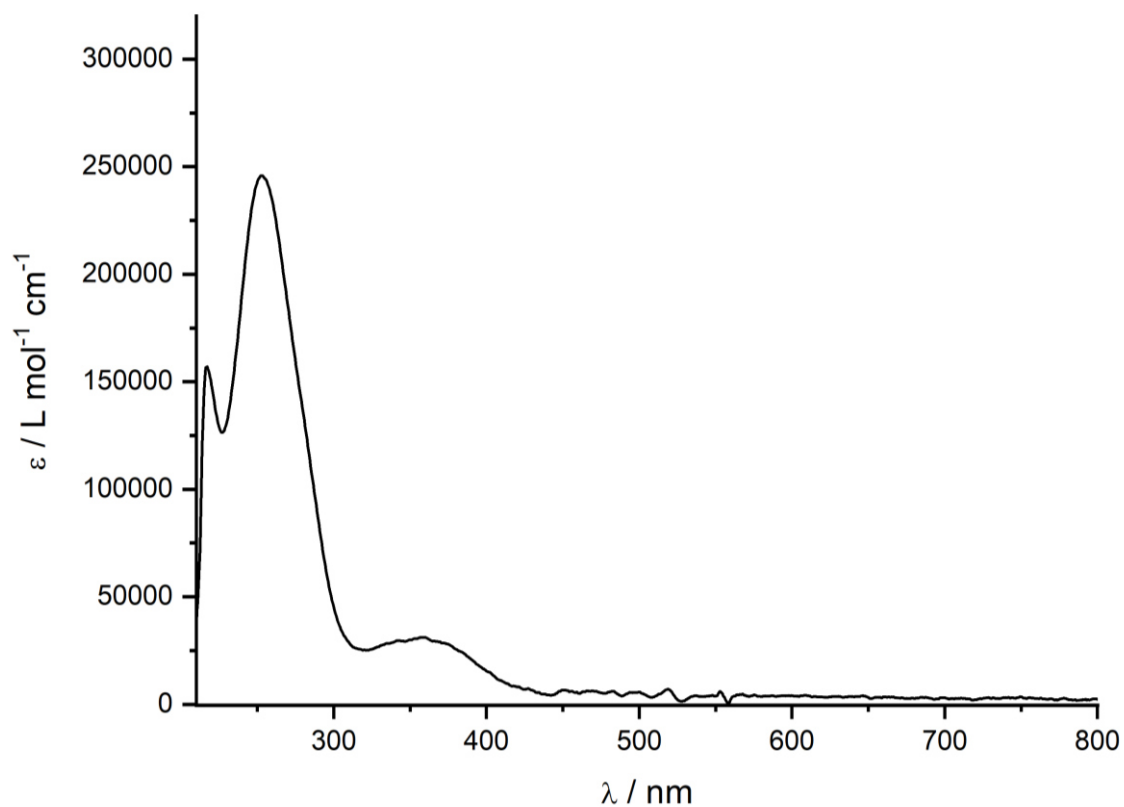
Figure S26. UV/Vis spectrum of **1-K** recorded in *n*-hexane.
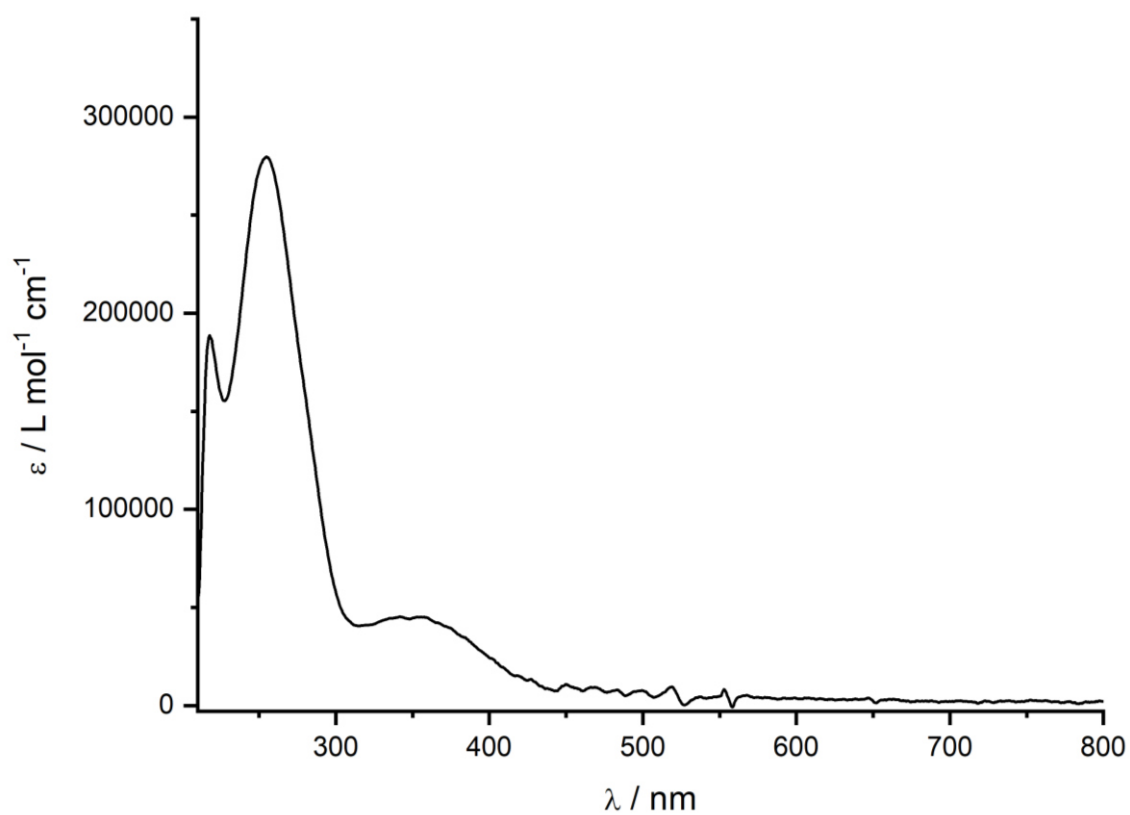
Figure S27. UV/Vis spectrum of **1-K·(thf)₃** recorded in *n*-hexane.
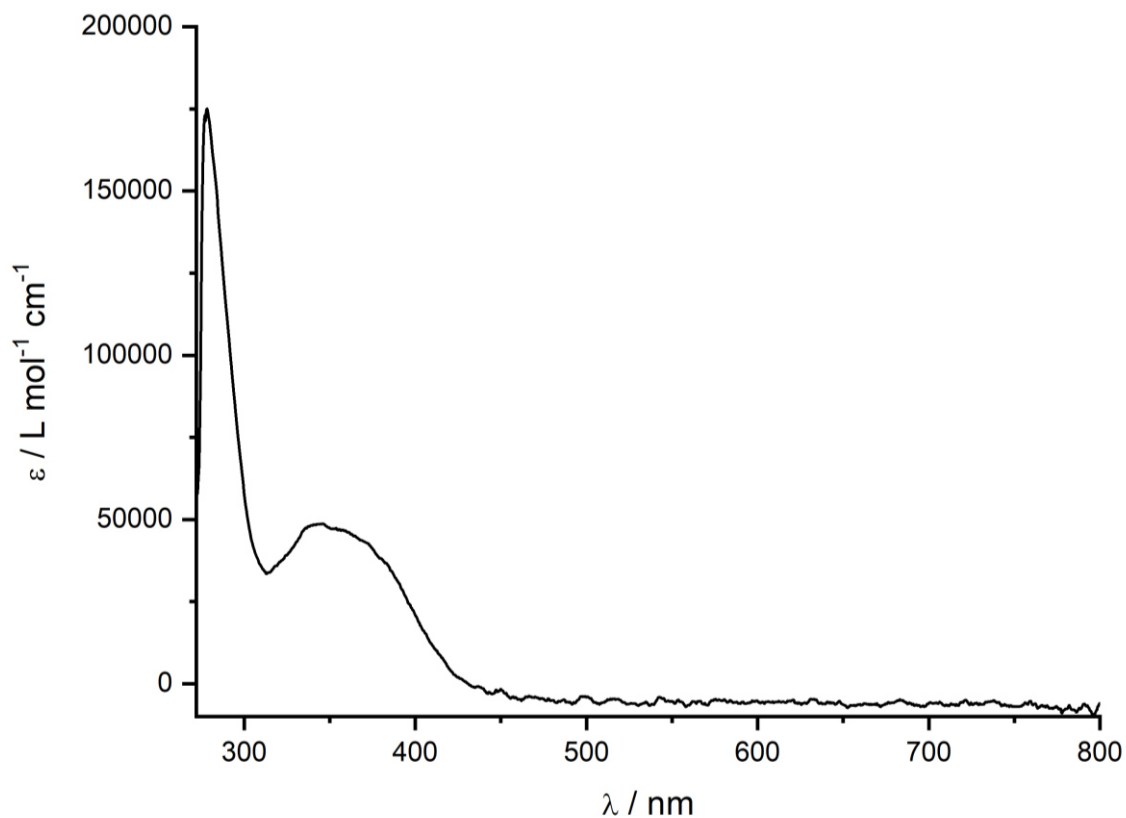
Figure S28. UV/Vis spectrum of **1-Rb** recorded in benzene.
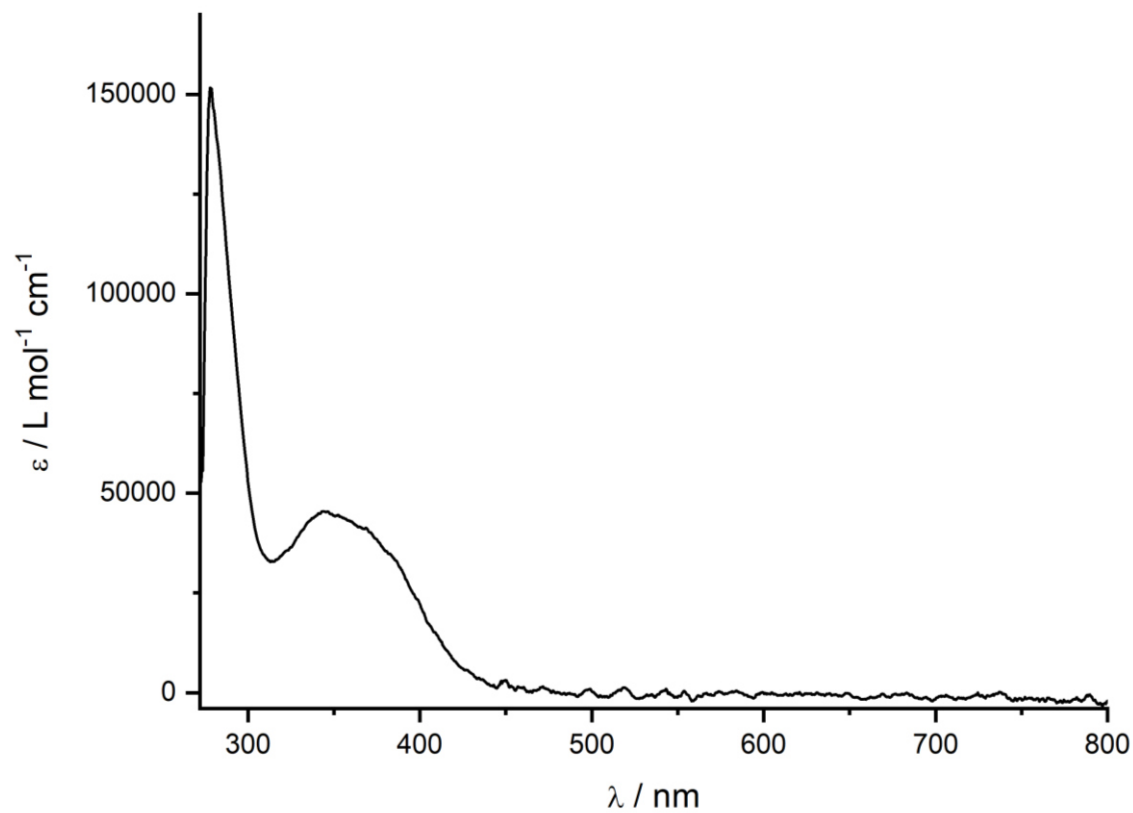
Figure S29. UV/Vis spectrum of **1-Cs** recorded in benzene.
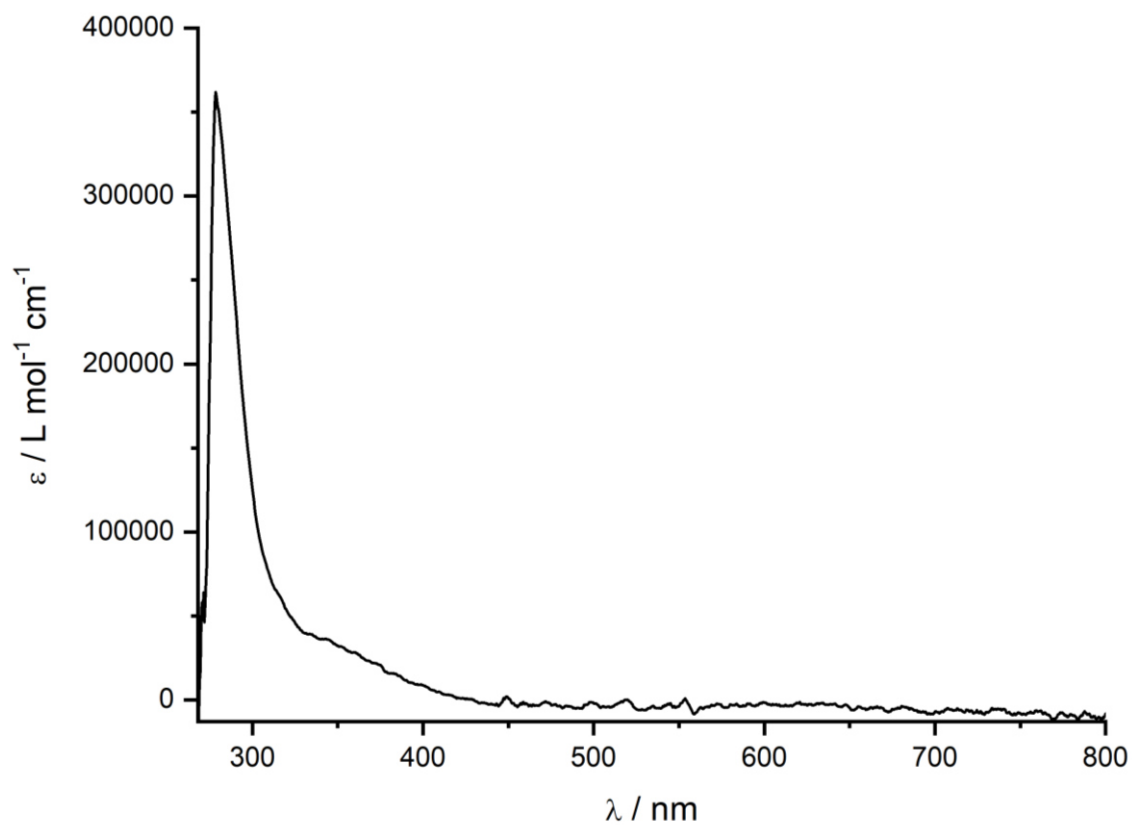
Figure S30. UV/Vis spectrum of $[Cp^{T5}FeBr(thf)]_2$ (**2**) recorded in benzene.
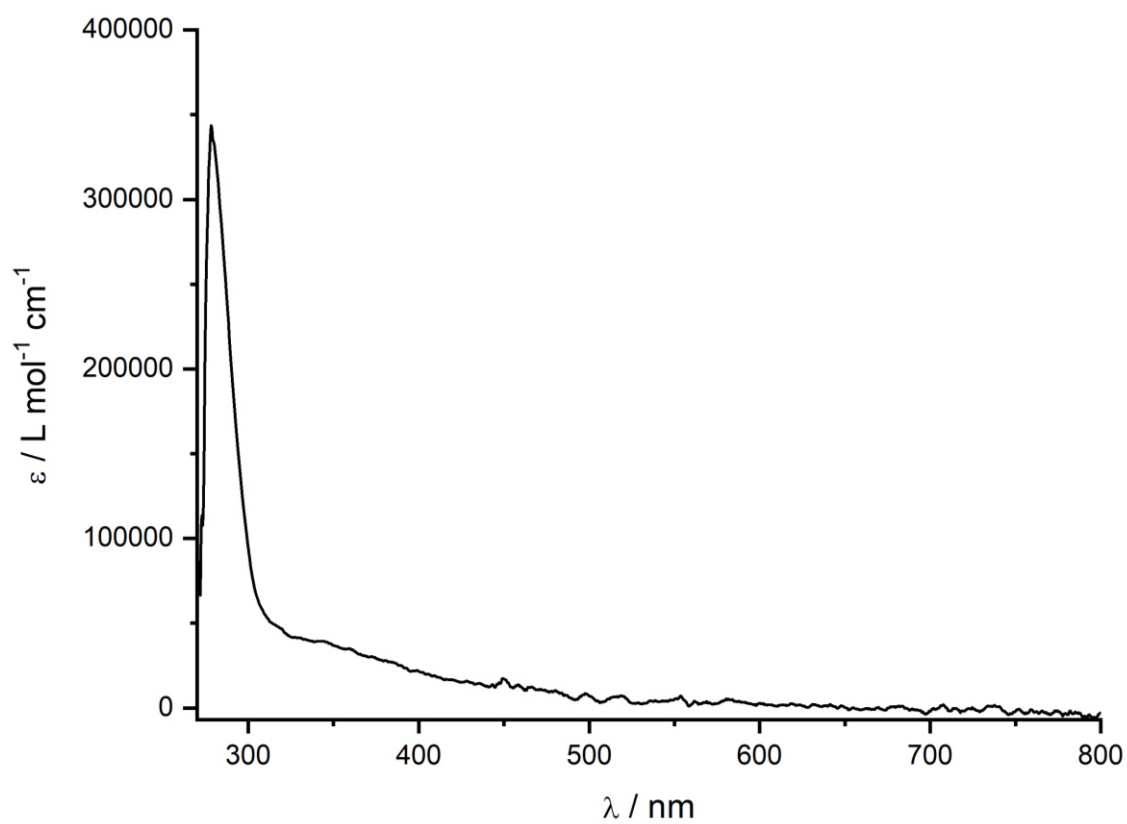
Figure S31. UV/Vis spectrum of $[Cp^{T5}NiBr]_2$ (**3**) recorded in benzene.
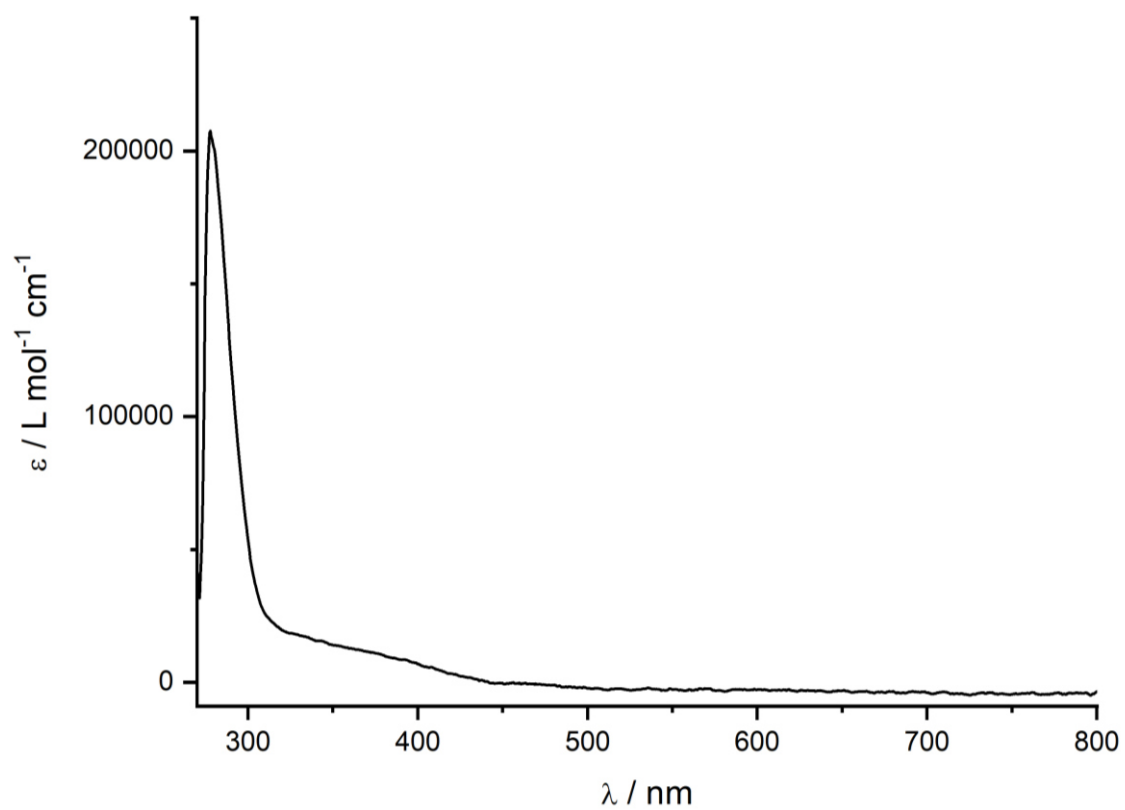
Figure S32. UV/Vis spectrum of [Cp^{T5}CoBr]$_2$ (**4**) recorded in benzene.

9.4.5   Single Crystal X-Ray Diffraction Data

Table S1. Crystal data and structure refinement for compounds **1-H**, **1-Na·thf**, **1-K**, **2**, **3** and **5**.

	1-H	1-Li	1-Na·thf	1-K	2	3	5
Empirical formula	$C_{135}H_{146}$	$C_{135}H_{145}Li$	$C_{139}H_{152}NaO$	$C_{270}H_{290}K_2$	$C_{284}H_{320}Br_2Fe_2O_2$	$C_{138}H_{152}BrNi$	$C_{270}H_{290}Ni$
Formula weight	1768.51	1774.59	1861.59	3612.42	4036.90	1949.21	3584.73
Temperature/K	103(4)	100.0(1)	123.0(1)	123.0(1)	123.0(1)	123.0(1)	123.0(1)
Crystal system	monoclinic	triclinic	triclinic	triclinic	triclinic	monoclinic	triclinic
Space group	$P2_1/c$	$P\bar{1}$	$P\bar{1}$	$P\bar{1}$	$P\bar{1}$	$C2/c$	$P\bar{1}$
a/Å	21.63770(10)	20.3564(1)	18.5068(5)	18.8155(3)	16.0293(3)	35.0175(11)	17.5659(7)
b/Å	16.39610(10)	29.73115(2)	19.9199(5)	19.8622(6)	18.4106(3)	29.7551(11)	20.1415(9)
c/Å	32.7835(2)	36.9472(2)	20.2850(5)	20.2449(4)	21.1275(4)	28.2685(9)	20.5156(10)
α/°	90	106.741(1)	112.104(2)	113.502(3)	90.8080(10)	90	107.449(4)
β/°	103.2790(10)	90.538	95.334(2)	110.1512(18)	95.259(2)	112.771(4)	109.895(4)
γ/°	90	108.902(1)	110.497(2)	94.7561(18)	102.310(2)	90	103.234(4)
Volume/Å³	11319.76(12)	20128.3(3)	6268.5(3)	6296.6(3)	6062.3(2)	27158.6(17)	6051.8(5)
Z	4	8	2	1	1	8	1
ρ_{calc}g/cm³	1.038	1.171	0.986	0.953	1.106	0.953	0.984
μ/mm⁻¹	0.432	0.451	0.448	0.684	1.748	0.856	0.482
F(000)	3824.0	7664.000	2010.0	1948.0	2162.0	8344.0	1933.0
Crystal size/mm³	0.319 × 0.127 × 0.062	0.272 x 0.159 x 0.128	0.685 × 0.38 × 0.248	0.698 × 0.361 × 0.246	0.143 × 0.126 × 0.112	0.456 × 0.098 × 0.083	0.463 × 0.301 × 0.194
Radiation	Cu Kα (λ = 1.54184)	Cu Kα (λ = 1.54184)	CuKα (λ = 1.54184)	CuKα (λ = 1.54184)	CuKα (λ = 1.54184)	CuKα (λ = 1.54184)	CuKα (λ = 1.54184)
2Θ range for data collection/°	4.196 to 146.43	2.3300 to 73.7890	8.058 to 150.022	6.804 to 147.122	7.67 to 152.568	6.924 to 149.384	7.548 to 147.194
Index ranges	-26 ≤ h ≤ 23, -20 ≤ k ≤ 19, -40 ≤ l ≤ 39	-25 ≤ h ≤ 25, -37 ≤ k ≤ 34, -44 ≤ l ≤ 45	-22 ≤ h ≤ 21, -24 ≤ k ≤ 20, -23 ≤ l ≤ 24	-23 ≤ h ≤ 22, -24 ≤ k ≤ 21, -18 ≤ l ≤ 24	-17 ≤ h ≤ 20, -23 ≤ k ≤ 23, -26 ≤ l ≤ 26	-43 ≤ h ≤ 29, -36 ≤ k ≤ 32, -35 ≤ l ≤ 30	-21 ≤ h ≤ 21, -24 ≤ k ≤ 24, -20 ≤ l ≤ 25
Reflections collected	79494	428141	43348	41369	91780	48465	46298
Independent reflections	21764 [R_{int} = 0.0196, R_{sigma} = 0.0165]	114607 [R_{int} =0.0414, R_{sigma} = 0.0355]	24365 [R_{int} = 0.0229, R_{sigma} = 0.0303]	24258 [R_{int} = 0.0271, R_{sigma} = 0.0341]	24971 [R_{int} = 0.0680, R_{sigma} = 0.0619]	26240 [R_{int} = 0.0305, R_{sigma} = 0.0474]	23411 [R_{int} = 0.0409, R_{sigma} = 0.0474]
Data/restraints/ parameters	21764/24/1277	81439/36/3914	24365/117/1369	24258/309/1597	24971/72/1417	26240/235/1522	23411/743/1769
Goodness-of-fit on F²	1.032	1.513	1.074	1.041	1.046	1.039	1.369
Final R indexes [I>=2σ (I)]	R_1 = 0.0467, wR_2 = 0.1237	R_1 = 0.1275, wR_2 = 0.3997	R_1 = 0.0948, wR_2 = 0.2542	R_1 = 0.0697, wR_2 = 0.1917	R_1 = 0.0720, wR_2 = 0.1865	R_1 = 0.0553, wR_2 = 0.1467	R_1 = 0.1226, wR_2 = 0.3433
Final R indexes [all data]	R_1 = 0.0523, wR_2 = 0.1279	R_1 = 0.16122, wR_2 = 0.4234	R_1 = 0.1003, wR_2 = 0.2586	R_1 = 0.0785, wR_2 = 0.2010	R_1 = 0.0933, wR_2 = 0.2073	R_1 = 0.0740, wR_2 = 0.1605	R_1 = 0.1569, wR_2 = 0.3822
Largest diff. peak/hole / e Å⁻³	0.58/-0.36	1.80/-0.80	0.97/-0.88	0.87/-0.42	1.62/-0.76	0.67/-0.68	0.85/-0.56

References

[1] a) T. J. Kealy, P. L. Pauson, *Nature* **1951**, *168*, 1039; b) S. A. Miller, J. A. Tebboth, J. F. Tremaine, *J. Chem. Soc.* **1952**, 632.

[2] a) H. G. Alt, A. Köppl, *Chem. Rev.* **2000**, *100*, 1205; b) R. L. Halterman, *Chem. Rev.* **1992**, *92*, 965.

[3] S. Heinl, S. Reisinger, C. Schwarzmaier, M. Bodensteiner, M. Scheer, *Angew. Chem. Int. Ed.* **2014**, *53*, 7639.

[4] a) B. M. Day, F.-S. Guo, R. A. Layfield, *Acc. Chem. Res* **2018**, *51*, 1880; b) F.-S. Guo, B. M. Day, Y.-C. Chen, M.-L. Tong, A. Mansikkamäki, R. A. Layfield, *Science* **2018**, *362*, 1400.

[5] J. Craig Ruble, Hallie A. Latham, and Gregory C. Fu, *J. Am. Chem. Soc.* **1997**, *119*, 1492.

[6] L. deVries, *J. Org. Chem.* **1960**, *25*, 1838.

[7] H. Brintzinger, J. E. Bercaw, *J. Am. Chem. Soc.* **1971**, *93*, 2045.

[8] H. Sitzmann, *Z. Naturforsch. B* **1989**, *44*, 1293.

[9] Clifford G. Venier, Edward W. Casserly, *J. Am. Chem. Soc.* **1990**, *112*, 2809.

[10] F.-S. Guo, N. Tsoureas, G.-Z. Huang, M.-L. Tong, A. Mansikkamäki, R. A. Layfield, *Angew. Chem. Int. Ed.* **2020**, 2299.

[11] L. D. Field, C. M. Lindall, A. F. Masters, G. K.B. Clentsmith, *Coord. Chem. Rev.* **2011**, *255*, 1733.

[12] a) J. L. Atwood, W. E. Hunter, A. H. Cowley, R. A. Jones, C. E. Stewart, *J. Chem. Soc., Chem. Commun.* **1981**, 925; b) P. Jutzi, F. Kohl, P. Hofmann, C. Krüger, Y.-H. Tsay, *Chem. Ber.* **1980**, *113*, 757.

[13] M. J. Heeg, C. Janiak, J. J. Zuckerman, *J. Am. Chem. Soc.* **1984**, *106*, 4259.

[14] L. D. Field, T. W. Hambley, P. A. Humphrey, A. F. Masters, P. Turner, *Inorg. Chem.* **2002**, *41*, 4618.

[15] C. Ruspic, J. R. Moss, M. Schürmann, S. Harder, *Angew. Chem. Int. Ed.* **2008**, *47*, 2121.

[16] U. Chakraborty, M. Modl, B. Mühldorf, M. Bodensteiner, S. Demeshko, N. J. C. van Velzen, M. Scheer, S. Harder, R. Wolf, *Inorg. Chem.* **2016**, *55*, 3065.

[17] X. Shi, G. Qin, Y. Wang, L. Zhao, Z. Liu, J. Cheng, *Angew. Chem. Int. Ed.* **2019**.

[18] G. R. Giesbrecht, J. C. Gordon, D. L. Clark, B. L. Scott, *Dalton Trans.* **2003**, 2658.

[19] D. Kuchenbecker, S. Harder, G. Jansen, *Z. Anorg. Allg. Chem.* **2010**, *636*, 2257.

[20] A. J. Veinot, A. D. K. Todd, J. D. Masuda, *Angew. Chem. Int. Ed.* **2017**, *56*, 11615.

[21] O. J. Curnow, G. M. Fern, D. Wöll, *Inorg. Chem. Commun.* **2003**, *6*, 1201.

[22] U. Chakraborty, F. Urban, B. Mühldorf, C. Rebreyend, B. de Bruin, N. van Velzen, S. Harder, R. Wolf, *Organometallics* **2016**, *35*, 1624.

[23] I. Resa, E. Carmona, E. Gutierrez-Puebla, A. Monge, *Science* **2004**, *305*, 1136.

[24]   Yaoming Xie, Henry F. Schaefer III, and, and R. Bruce King, *J. Am. Chem. Soc.* **2005**, *127*, 2818.

[25]   a) Michael S. Paquette, Lawrence F. Dahl, *J. Am. Chem. Soc.* **1980**, *102*, 6623; b) S. Pasynkiewicz, A. Pietrzykowski, L. Trojanowska, P. Sobota, L Jerzykiewicz, *J. Organomet. Chem.* **1998**, *550*, 111.

[26]   G. Dyker, J. Heiermann, M. Miura, J.-I. Inoh, S. Pivsa-Art, T. Satoh, M. Nomura, *Chem. Eur. J.* **2000**, *6*, 3426.

[27]   G. E. Greco, R. R. Schrock, *Inorg. Chem.* **2001**, *40*, 3850.

[28]   C. J. F. Du, H. Hart, K. K. D. Ng, *J. Org. Chem.* **1986**, *51*, 3162.

[29]   Robert E. Dinnebier, Ulrich Behrens, Falk Olbrich, *Organometallics* **1997**, *16*, 3855.

[30]   C. Näther, T. Hauck and H. Bock, *Acta Cryst. C* **1996**, *52*, 570.

[31]   H. Bock, T. Hauck, C. Näther, Z. Havlas, *Z. Naturforsch. B* **1997**, *52*, 524.

[32]   T. Nishinaga, D. Yamazaki, H. Stahr, A. Wakamiya, K. Komatsu, *J. Am. Chem. Soc.* **2003**, *125*, 7324.

[33]   Tim Seifert and Peter W. Roesky, *Inorganics* **2017**, *5*, 28.

[34]   S. Harder, C. Ruspic, *J. Organomet. Chem.* **2009**, *694*, 1180.

[35]   J. Lorberth, S.-H. Shin, S. Wocadlo, W. Massa, *Angew. Chem. Int. Ed. Engl.* **1989**, *28*, 735.

[36]   P. Jutzi, N. Burford, *Chem. Rev.* **1999**, *99*, 969.

[37]   Y. Schulte, C. Stienen, C. Wölper, S. Schulz, *Organometallics* **2019**, *38*, 2381.

[38]   Leo A. Paquette, Walter Bauer, Mark R. Sivik, Michael Buehl, Martin Feigel, Paul von Ragué Schleyer, *J. Am. Chem. Soc.* **1990**, *112*, 8776.

[39]   S. Harder, M. H. Prosenc, *Angew. Chem. Int. Ed. Engl.* **1994**, *33*, 1744-1746.

[40]   A. Macchioni, G. Ciancaleoni, C. Zuccaccia, D. Zuccaccia, *Chem. Soc. Rev.* **2008**, 479.

[41]   a) J. J. Schneider, R. Goddard, C. Krüger, *Z. Naturforsch. B* **1995**, *50*, 448; b) F. Baumann, E. Dormann, Y. Ehleiter, W. Kaim, J. Kärcher, M. Kelemen, R. Krammer, D. Saurenz, D. Stalke, C. Wachter et al., *J. Organomet. Chem.* **1999**, *587*, 267; c) H. Sitzmann, D. Saurenz, G. Wolmershäuser, A. Klein, R. Boese, *Organometallics* **2001**, *20*, 700; d) M. D. Walter, P. S. White, *New J. Chem.* **2011**, *35*, 1842; e) D. Weismann, D. Saurenz, R. Boese, D. Bläser, G. Wolmershäuser, Y. Sun, H. Sitzmann, *Organometallics* **2011**, *30*, 6351; f) M. Wallasch, G. Wolmershäuser, H. Sitzmann, *Angew. Chem. Int. Ed.* **2005**, *44*, 2597; g) M. Schär, D. Saurenz, F. Zimmer, I. Schädlich, G. Wolmershäuser, S. Demeshko, F. Meyer, H. Sitzmann, O. M. Heigl, F. H. Köhler, *Organometallics* **2013**, *32*, 6298; h) H. Bauer, D. Weismann, G. Wolmershäuser, Y. Sun, H. Sitzmann, *Eur. J. Inorg. Chem.* **2014**, *2014*, 3072; i) M. Reiners, D. Baabe, K. Harms, M. Maekawa, C. G. Daniliuc, M. Freytag, P. G. Jones, M. D. Walter, *Inorg. Chem. Front.* **2016**, *3*, 250.

[42]   C.-Y. Lin, P. P. Power, *Chem. Soc. Rev.* **2017**, *46*, 5347.

[43]   H. Hoffmann, P. Schellenbeck, *Chem. Ber.* **1967**, *100*, 692.

[44] H. Podall, W. E. Foster, A. P. Giraitis, *J. Org. Chem.* **1958**, *23*, 82.

[45] R. S. Dickson, B. J. Dobney, F. W. Eastwood, *J. Chem. Educ.* **1987**, *64*, 898.

[46] a) Sheldrick, G. M. SADABS, Bruker AXS, Madison, USA **2007**; b) CrysAlisPro, Scale3 Abspack, Rigaku Oxford Diffraction **2019**.

[47] R. C. Clark, J. S. Reid, *Acta Cryst. A* **1995**, *51*, 887.

[48] G. M. Sheldrick, *Acta Cryst. A* **2015**, *71*, 3.

[49] O. V. Dolomanov, L. J. Bourhis, R. J. Gildea, J. A. K. Howard, H. Puschmann, *J .Appl. Crystallogr.* **2009**, *42*, 339.

[50] G. M. Sheldrick, *Acta Cryst. C* **2015**, *71*, 3.

[51] G. M. Sheldrick, *Acta Cryst. A* **2008**, *64*, 112.

[52] A. Jerschow, N. Müller, *J. Magn. Reson.* **1997**, *125*, 372.

[53] a) C. S. Johnson, *Prog. Nucl. Magn. Reson. Spectrosc.* **1999**, *34*, 203; b) E. O. Stejskal, J. E. Tanner, 1965, 42, 288-292., *J. Chem. Phys.* **1965**, *42*, 288; c) W. S. Price, *Concepts Magn. Reson* **1998**, *10*, 197.

[54] S.-H. C. H.-C. Chen, *J. Phys. Chem.* **1984**, *88*, 5118.

10   Summary and Conclusion

Chapter 1. *Tetrahedranes Composed of p-Block Elements: Topical Molecules with a Long History*

Tetrahedral structures are ubiquitous within chemistry. They range from elusive laboratory curiosities such as the parent tetrahedrane C_4H_4 to long-known allotropes of the elements, for instance white phosphorus (P_4). The introductory chapter of this thesis reviews the chemistry of tetrahedranes composed of main group elements. The aim of this chapter is to give an overview of tetrahedrally-structured cage compounds in the p-block of the periodic table and to provide the context for further classification of phosphorus-containing tetrahedranes covered in this thesis (Figure 1).
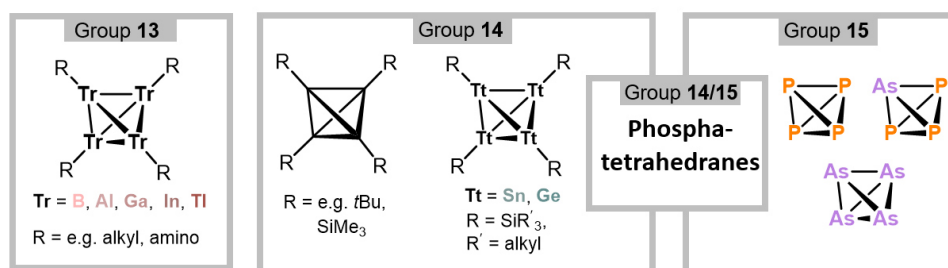
Figure 1. Selected p-block tetrahedranes.

After a brief introduction and classification of these tetrahedranes, this review is subdivided into a description of the special bonding situations found in different p-block tetrahedranes followed by an account of their synthesis and properties. While homoatomic tetrahedranes are scarce, the incorporation of two different elements into the tetrahedrane motif is particularly intriguing and synthetically very challenging. Numerous tetrahedranes with more than one element in the core appear viable, yet little progress has been made in this field. This omission provided the central motivation for the investigations of diphosphatetrahedranes described in this thesis.

Chapter 2. *Release of P_2 Units from a Nickel Butterfly Complex*

The use of P_2 as a synthon for the synthesis of organophosphorus compounds has been a longstanding goal in organometallic chemistry and provides a potential strategy for the synthesis of cyclic diphosphines by [4+2] cycloaddition with dienes. In chapter 2, the nickel butterfly complex [{(IMes)Ni(CO)}$_2$(μ^2:η^2:η^2-P_2)] (IMes = 1,3-bis(2,4,6-trimethylphenyl)imidazolin-2-ylidene) has been investigated as a source of P_2 units. The results are summarised in Scheme 1. Reaction of [{(IMes)Ni(CO)}$_2$(μ^2:η^2:η^2-P_2)] with 2,3,4,5-tetramethylimidazolin-2-ylidene

(TMC) afforded [{(TMC)$_2$Ni}$_2$(μ^2:η^2:η^2-P$_2$)] (**2-1**). Thus, CO and NHC ligand substitution were unexpectedly observed, while the Ni$_2$P$_2$ butterfly core was retained.

Furthermore, the reactivity of [{(IMes)Ni(CO)}$_2$(μ^2:η^2:η^2-P$_2$)] toward sulfur-containing heterocumulenes was investigated. Reactions of [{(IMes)Ni(CO)}$_2$(μ^2:η^2:η^2-P$_2$)] with aryl isothiocyanates afford mononuclear nickel complexes with trimerised aryl isothiocyanate ligand scaffolds [(IMes)Ni(η^3-ArNCS)$_3$] [Ar = Ph (**2-2a**); 2,6-Me$_2$-C$_6$H$_3$ (**2-2b**)]. The obtained pincer-type ligands can be classified as *Fischer*-type carbenes, which coordinate via two sulfur atoms and the central carbon atom. The reaction of [{(IMes)Ni(CO)}$_2$(μ^2:η^2:η^2-P$_2$)] with CS$_2$ led to formation of the dinuclear complex [{(IMes)Ni(μ^2,η^2:η^2-CS$_2$)}$_2$] (**2-3**). The observation of P$_4$ in these reactions suggests the desired formation of reactive P$_2$ fragments. Further work on trapping the P$_2$ fragments seems a worthwhile goal. Moreover, the universal use of pincer-complexes in catalysis and the simple preparation of the pincer-complexes **2-2** renders them promising precursors for catalytic applications.
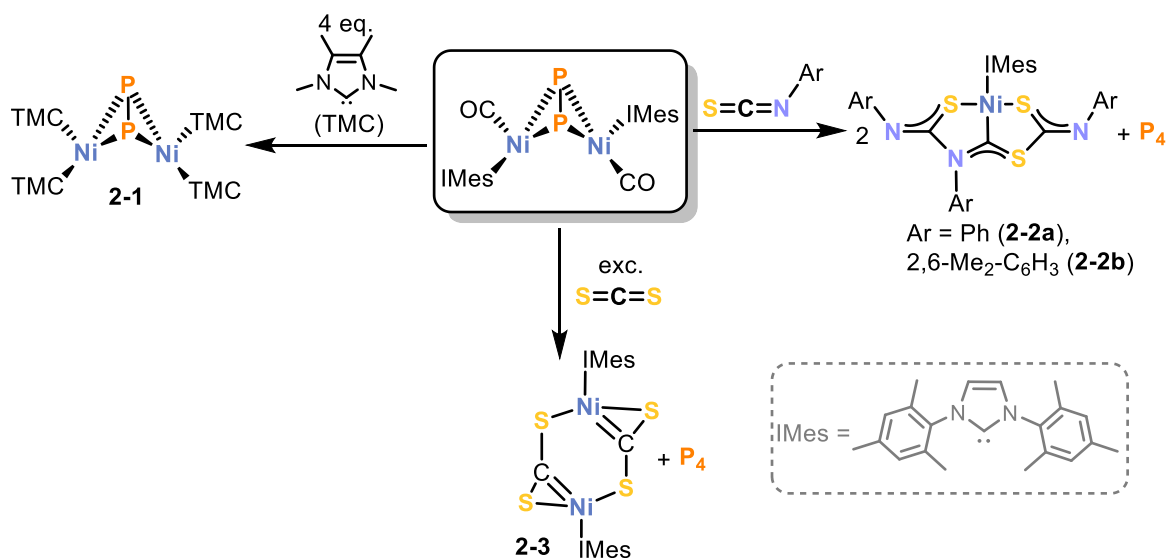
Scheme 1. Reactivity of [{(IMes)Ni(CO)}$_2$(μ^2:η^2:η^2-P$_2$)] toward 2,3,4,5-tetramethylimidazolin-2-ylidene (TMC), aryl isothiocyanates and carbon disulfide.

Chapter 3. *Aggregation and Degradation of White Phosphorus Mediated by N-Heterocyclic Carbene Nickel(0) Complexes*

Nickel phosphides are efficient catalysts for the hydrogen evolution reaction. The preparation of convenient single source precursors would enable efficient synthetic routes toward novel and powerful Ni-P catalysts. Only few reports on the activation of white phosphorus with nickel(0) complexes have been described and the structural motifs and Ni/P ratios were limited. In this chapter, the reactivity of white phosphorus toward simple N-heterocyclic carbene Ni(0) complexes was investigated, which resulted in the isolation of unprecedented oligonuclear polyphosphide clusters. Our studies revealed the steric impact of the carbene as well as the

influence of solvent effects on the nature of the products, ultimately allowing the controlled synthesis of several nickel phosphide clusters with variable Ni/P ratios (Scheme 2).
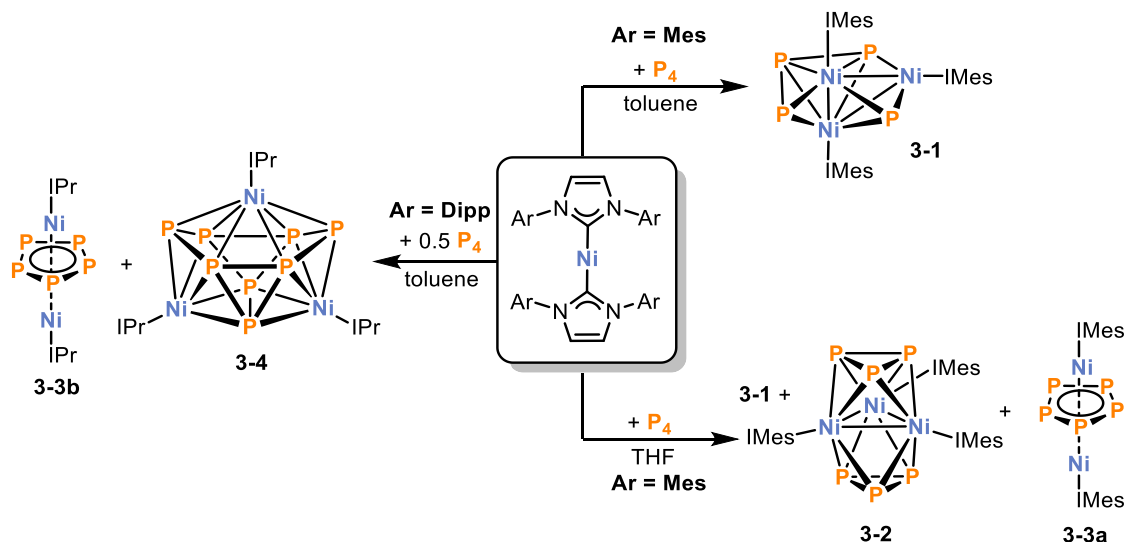
Scheme 2. Reactivity of low-coordinate Ni(0)-NHC complexes toward P₄.

Reaction of [(IMes)$_2$Ni] with 0.5 equivalents of white phosphorus in toluene afforded the trinuclear compound [(IMes)$_3$Ni$_3$P$_4$] (**3-1**) as the main product. Complex **3-1** possesses 12 cluster electrons and can therefore be classified as a *superhypercloso*-cluster according to the Wade-Mingos rules, which is an particularly scarce structural motif. By changing the polarity of the solvent, dramatic effects on the selectivity were observed. Apart from **3-1**, two other nickel phosphorus complexes were obtained when using THF: trinuclear [(IMes)$_3$Ni$_3$P$_6$] (**3-2**) and the dinuclear inverse sandwich complex [(IMes)$_2$Ni$_2$P$_5$] (**3-3a**). Compound **3-2** consists of two Ni$_3$P$_3$ octahedra sharing a Ni$_3$-face. **3-2** can also be described as a *hypercloso*-cluster with 18 cluster electrons. Modifying the steric demand of the N-heterocyclic carbene ligand from IMes to IPr (IPr = 1,3-bis(2,6-di-*iso*-propylphenyl)imidazolin-2-ylidene) again changes the outcome of the reaction. Using [(IPr)$_2$Ni] (or, more conveniently, [(IPr)Ni(η^6-toluene)]), the homoquadricyclane-like cluster [(IPr)$_3$Ni$_3$P$_8$] (**3-4**) was obtained as the main product. **3-4** is a *closo*-cluster according to the Wade-Mingos rules with an octadecahedral geometry. An inverse-sandwich complex similar to **3-3a** [(IPr)$_2$Ni$_2$(P$_5$)] was identified as a side product.

The future use of the NHC-stabilised nickel phosphide complexes as single-source precursors for the preparation of nickel phosphide nanoparticles is envisioned. Dissociation of the free carbene upon heating is expected to afford P-rich nanoparticles under mild conditions.

Chapter 4.   *Di-tert-butyldiphosphatetrahedrane: Catalytic Synthesis of the Elusive*
                   Phosphaalkyne Dimer

Although P_4 and $(tBuC)_4$ are two of the most significant tetrahedral molecules ever synthesised, 'hybrids' of these species comprising phosphorus *and* carbon in the tetrahedral scaffold have remained elusive. Due to their extremely challenging synthesis, this field has been unexplored in the past.

Chapter 4 describes the synthesis and characterisation of di-*tert*-butyldiphosphatetrahedrane **4-1**, via a very simple nickel-catalysed dimerisation reaction of *tert*-butylphosphaalkyne. Remarkably, $(tBuCP)_2$ not only represents the first example of a neutral, 'mixed' group 14/15 tetrahedrane, but it is also the first stable phosphaalkyne dimer to be isolated and structurally characterised (including sophisticated X-ray diffraction experiments). As such, diphosphatetrahedrane **4-1** fills an important gap in the series of phosphaalkyne oligomers $(tBuCP)_n$ (n = 2-6, Figure 2).
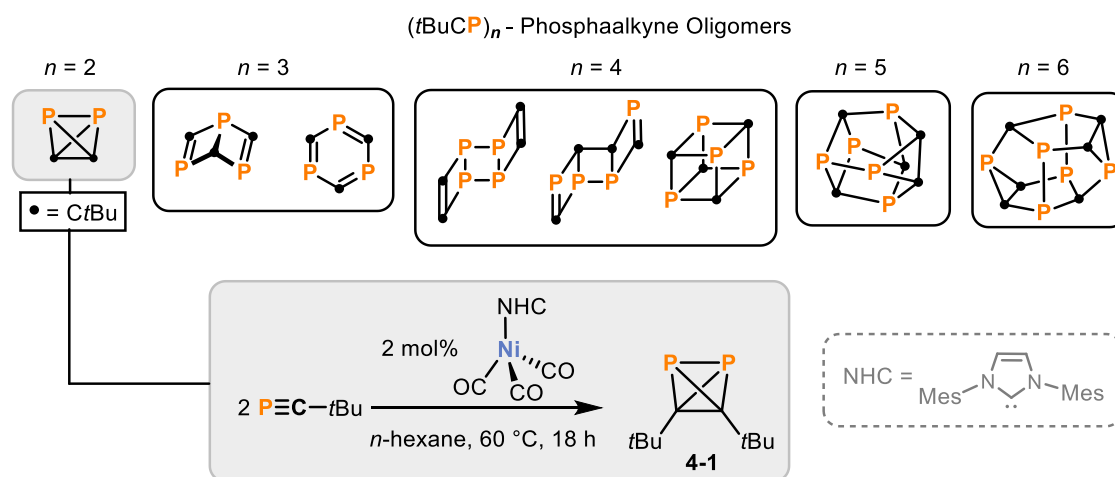
Figure 2. Phosphaalkyne oligomers (top) and nickel-catalysed synthesis of
di-*tert*-butyldiphosphatetrahedrane (bottom).

4-1 was isolated in yields of up to 55% as a yellow, pyrophoric liquid. A characteristic, high-field singlet resonance is observed for **4-1** in the $^{31}P\{^1H\}$ NMR spectrum at a chemical shift of −468.2 ppm. Moreover, **4-1** was characterised by X-ray crystallography by *in situ* crystallisation in a capillary.

The mechanism of formation of **4-1** was analysed thoroughly by stoichiometric experiments, kinetic investigations and rationalised by DFT computations, which revealed the catalytic cycle shown in Scheme 3. In a first step, the η^2-phosphaalkyne complex **4-2** reacts with a second equivalent of *t*BuCP to form the 1,3-diphosphacyclobutadiene complex **4-3**. The planar ring of this complex subsequently undergoes isomerisation through P−P and C−C bond formation to form **4-4**, which is a complex of η^2-coordinated **4-1**. Diphosphatetrahedrane **4-1** is finally liberated by addition of another equivalent of *t*BuCP, which leads to reformation of **4-2**.
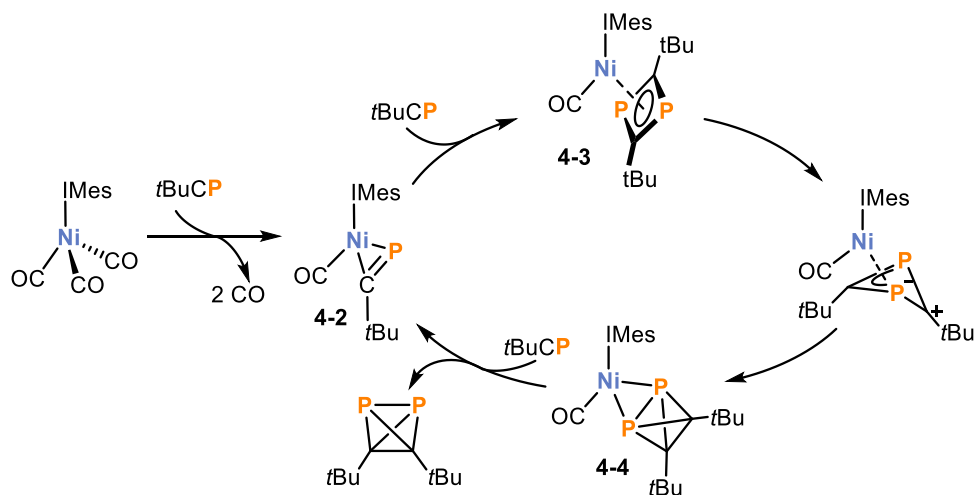
Scheme 3. Mechanism of the nickel-catalysed synthesis of (*t*BuCP)₂ elucidated by preparative experiments, kinetic studies and DFT calculations.

Due to the novel structure and now facile accessibility of **4-1**, it was of great interest to study the reactivity of this highly unusual tetrahedral molecule. To this end, studies toward the stability and photochemistry of **4-1** were conducted, and the results are discussed in chapter 5. Inspired by the diverse chemistry of white phosphorus, the reactivity of **4-2** toward N-heterocyclic carbenes and its coordination ability were also investigated, and revealed a distinct and reactive organophosphorus building block. These studies are described in chapters 6 to 8.

Chapter 5. Photochemistry of Di-tert-butyldiphosphatetrahedrane

Fundamental investigations on the stability of (*t*BuCP)₂ are essential for its effective handling in the laboratory, as well as to provide a foundation for further reactivity studies. In chapter 6, the thermal stability and photochemistry of **4-1** are described. It was found that **4-1** is stable at room temperature in the dark, while it slowly dimerises to form the ladderane **5-1** upon heating to temperatures above 40 °C. Upon exposure to ambient light, however, **4-1** forms **5-1** much more rapidly even at ambient temperature.
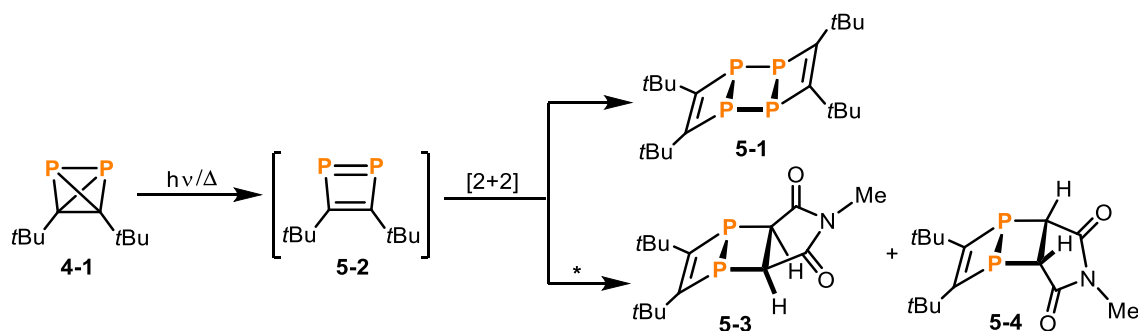
Scheme 4. Isomerisation of (*t*BuCP)₂ to a 1,2-diphosphacyclobutadiene and subsequent [2+2]-cycloadditions;
* N-methylmaleimide.

Furthermore, the mechanism of this dimerisation reaction was studied by UV/Vis absorption spectroscopy and quantum chemical calculations. These studies suggest that **4-1** initially isomerises to the 1,2-diphosphacyclobutadiene **5-2**, which then undergoes a [2+2] cycloaddition to form **5-1**. Inspired by these mechanistic insights it was attempted to intercept the unstable intermediate **5-2** by [2+2] cycloaddition reactions. **5-2** was successfully trapped with an electron-poor alkene to afford **5-3** and its endo-isomer **5-4**, thus providing further evidence for the proposed mechanism.

The photochemistry of **4-1** emerging from this chapter suggests the use of **4-1** (via the short-lived intermediate **5-2**) for further photochemical cycloadditions, potentially affording new phosphorus-containing heterocycles by not only [2+2], but also [3+2] and [4+2] cycloadditions.

Chapter 6. *Di-tert-butyldiphosphatetrahedrane as a Building Block for Phosphaalkenes and Phosphirenes*

Previous literature reports revealed a rich reactivity of both P_4 and *t*BuCP with N-heterocyclic carbenes (NHCs). Based on this prior knowledge and considering the similarity of (*t*BuCP)$_2$ (**4-1**) with P_4, NHCs were chosen for an initial reactivity study. Chapter 6 describes how such reactions give access to novel unsaturated phosphaorganic frameworks (Scheme 5).

The reaction of the smallest carbene used in this study, 2,3,4,5-tetramethylimidazolin-2-ylidene (TMC) resulted in P−P bond cleavage of **4-1**, affording the bis(phosphaalkene) **6-1**. When bulkier, aryl-substituted carbenes were reacted with **4-1**, the selective formation of the phosphinophosphirenes **6-2** was observed. These compounds resulted from P−C bond cleavage in the (*t*BuCP)$_2$ tetrahedron. Thus, the steric effects of the carbene play an important role in these reactions and the outcomes can be controlled by varying the size. The formation of **6-1** and **6-2** contrasts with the products formed from reactions of carbenes with *t*BuCP itself. Hence, the reactivity of **4-1** with carbenes highlights the utility of **4-1** for the synthesis of previously unknown organophosphorus compounds.
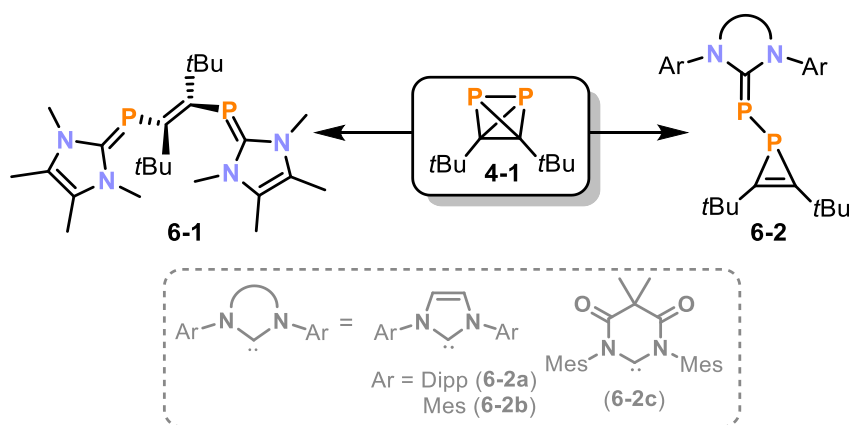
**Scheme 5.** Reactivity of (*t*BuCP)$_2$ with carbenes.

Chapter 7. *Activation of Di-tert-butyldiphosphatetrahedrane: Access to (tBuCP)$_n$ (n = 2, 4)*
Ligand Frameworks by P–C Bond Cleavage

Inspired by previous reactivity studies with white phosphorus (P$_4$, see chapter 3), the coordination chemistry of (*t*BuCP)$_2$ (**4-1**) was studied toward a range of organometallic N-heterocyclic carbene (NHC) complexes of nickel(I) and nickel(0). The first part of chapter 7 presents the reactivity of **4-1** towards cyclopentadienyl nickel(I) radicals of the type [CpNi(NHC)]. Such 'nickel(I) radicals' have recently been shown to selectively activate white phosphorus by P−P bond cleavage. In reactions of **4-1** with the nickel(I) radical [CpNi(IPr)], however, the cleavage of P−C bonds was observed, and the 1,2-diphosphacyclobutadienediide complex **7-1** was isolated (Scheme 6). Furthermore, the effect of different cyclopentadienyl ligands was investigated. When the size of the cyclopentadienyl ligand increases from C$_5$H$_5$ to C$_5$Me$_5$ and C$_5$Ar$_5$ (Ar = 4-Et-C$_6$H$_4$), a coupling of two molecules of (*t*BuCP)$_2$ occurs and a new P−P bond is formed (presumably via a radical pathway). The resulting complexes **7-2** and **7-3** feature dimeric (*t*Bu$_4$C$_4$P$_4$)$^{2-}$ ligands.
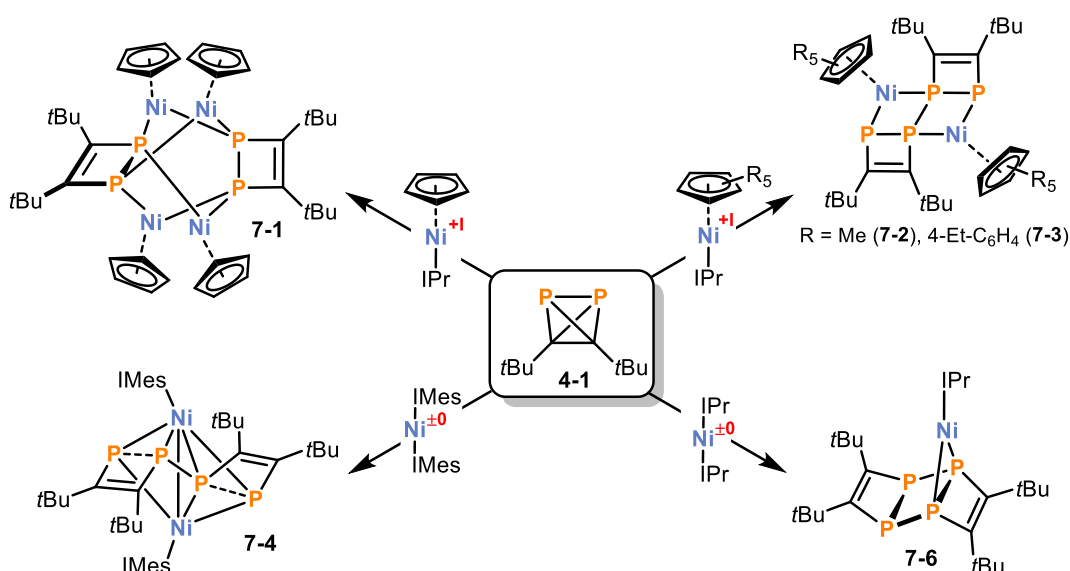
Scheme 6. Reactivity of **8** toward Ni(I)- and Ni(0)-NHC complexes.

Furthermore, reactions of (*t*BuCP)$_2$ (**4-1**) with nickel(0) complexes are described in this chapter. The reactivity of the same complexes with P$_4$ is described in chapter 3. A comparison of the results reveals marked differences between the behaviour of (*t*BuCP)$_2$ and P$_4$. [(IMes)$_2$Ni] reacted with **4-1** to give the dinuclear nickel complex **7-4**, which features a (*t*BuCP)$_4$ scaffold. The reactivity of **7-4** was further studied. Surprisingly, the elimination of *t*BuC≡C*t*Bu was observed upon heating and the P$_2$ complex **7-5** was isolated as a result (Scheme 7). In contrast, the reaction of **4-1** with the slightly bulkier NHC complex [(IPr)$_2$Ni] (or, similarly, [(IPr)Ni(η^6-toluene)]) afforded the mononuclear complex **7-6** featuring a ladderane-type ligand. This compound was also obtained when (*t*BuCP)$_4$ itself was reacted with [(IPr)Ni(η^6-toluene)].
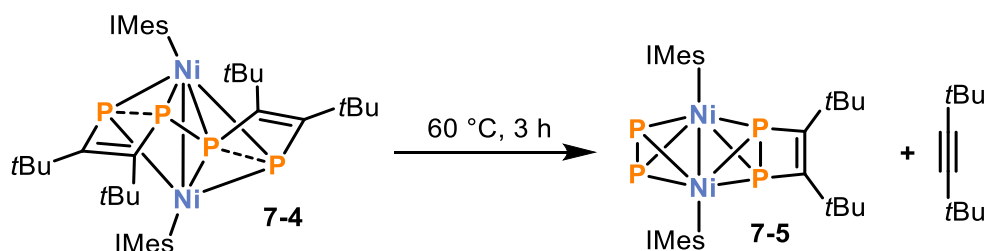
**Scheme 7.** Elimination of di-*tert*-butylacetylene from complex **7-4**.

These results are clear examples of the distinct reactivity of **4-2** compared to its monomer *t*BuCP, while they also reveal first insights into coordination chemistry of this tetrahedral compound. The dominant features are P−C bond cleavage of the tetrahedron and dimerisation of two diphosphatetrahedrane moieties to form unusual (*t*BuCP)$_n$ ($n = 2, 4$) frameworks.

Chapter 8. Di-tert-butyldiphosphatetrahedrane as a Source of 1,2-Diphosphacyclobutadiene Ligands

Chapters 6 and 7 investigated reactions of **4-1** with N-heterocyclic carbenes and Ni(I/0) complexes in order to compare its reactivity with those of P$_4$ and *t*BuCP, and it has been shown that **4-1** shows a distinct reactivity in comparison with these well-investigated molecules. Chapter 8 of this thesis further extends these studies by describing the reactivity of (*t*BuCP)$_2$ (**4-1**) toward highly reduced metalate anions. Reactions of **4-1** with a range of ferrates and cobaltates according to Scheme 8 afford 1,2-diphosphacyclobutadiene complexes **8-1**, **8-2**, **8-4** and **8-5**. Those complexes are formed by P−C bond cleavage of the diphosphatetrahedrane core, which is in contrast to the formation of 1,3-diphosphacyclobutadiene complexes by analogous reactions of "monomeric" phosphaalkynes (e.g. **8-6** and **8-7** shown in Scheme 9). Comparison of the reactivity of **8-4** and **8-6** toward a series of electrophiles revealed that the 1,2-isomer is particularly useful for the selective preparation of the triphospholium complex **8-8**, while the 1,3-diphosphacyclobutadiene complex **8-6** mainly afforded a deligated chlorido complex.
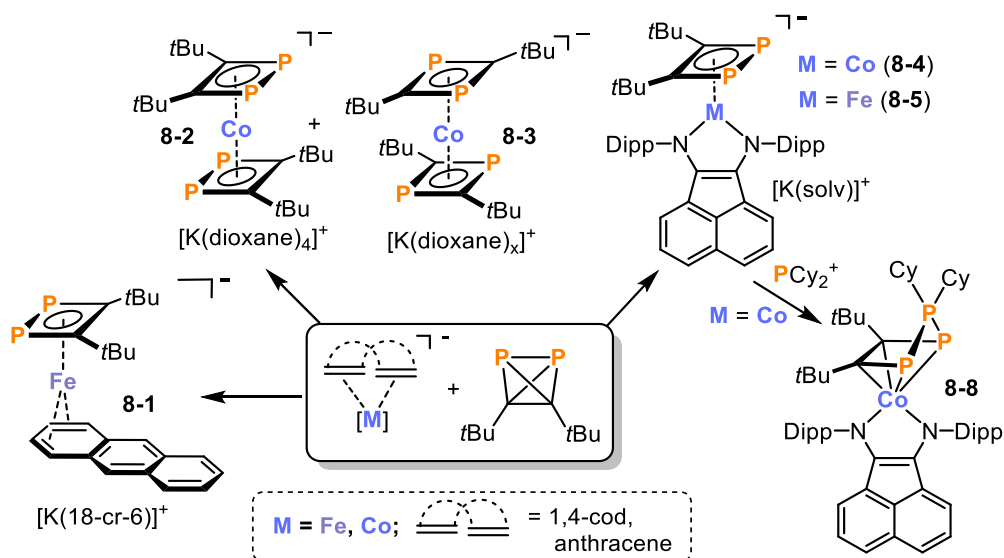
Scheme 8. Reactivity of **4-2** toward metalates and formal insertion of PCy_2^+ into a 1,2-diphosphacyclobutadiene ligand.
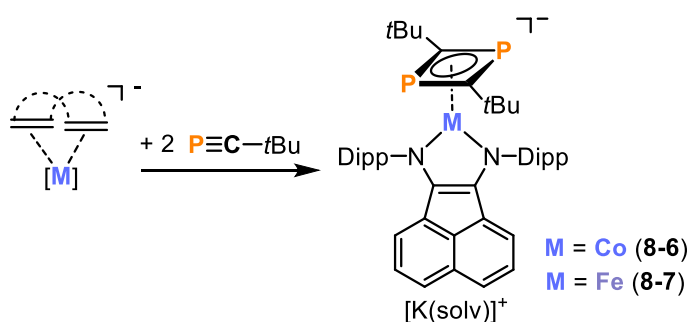
Scheme 9. Synthesis of 1,3-diphosphacyclobutadiene metalates each containing a BIAN-ligand.

The electronic structures of the novel paramagnetic iron complexes **8-1**, **8-5** and **8-7** were additionally investigated by Mössbauer spectroscopy. Analysis of the isomer shifts of **8-5** and **8-7** revealed that the 1,2-diphosphacyclobutadiene ligand is a stronger π-acceptor than its 1,3-isomer. This study of the bonding properties of isomeric diphosphacyclobutadiene ligands provided a valuable insight into their coordination chemistry.

Overall, the use of **4-1** allows for the facile preparation of a family of iron and cobalt complexes incorporating 1,2-diphosphacyclobutadiene ligands, which have previously been observed only rarely in comparison to their 1,3-isomers. It appears that this approach is a new, reliable strategy for the preparation of such 1,2-diphosphacyclobutadiene compounds (see also the synthesis of related Ni complexes reported in chapter 7). These results further highlight the synthetic value and distinct coordination chemistry of **4-1** compared to its monomer *t*BuCP.

Chapter 9.   *Bulking up Cp^{BIG}: A Penta-Terphenyl Cyclopentadienyl Ligand*

Finally, chapter 9 of this thesis covers the synthesis of a novel and extremely sterically demanding penta-terphenyl cyclopentadienyl ligand, which was intended for use in the stabilisation of low-coordinate transition metal complexes. The new ligand **9-1** was synthesised on a multi-gram scale by a Heck reaction (Figure 3). Deprotonation reactions with alkali metal bases afforded dimeric compounds in the solid state. The structure of the potassium salt **9-1** is particularly interesting, considering that it differs from the chain-like arrangement seen for many comparable compounds.

A. Penta-terphenyl-cyclopentadienyl ligand

B. Dimeric potassium salt in the solid state

C. Reduction of nickel(II)-bromido complex
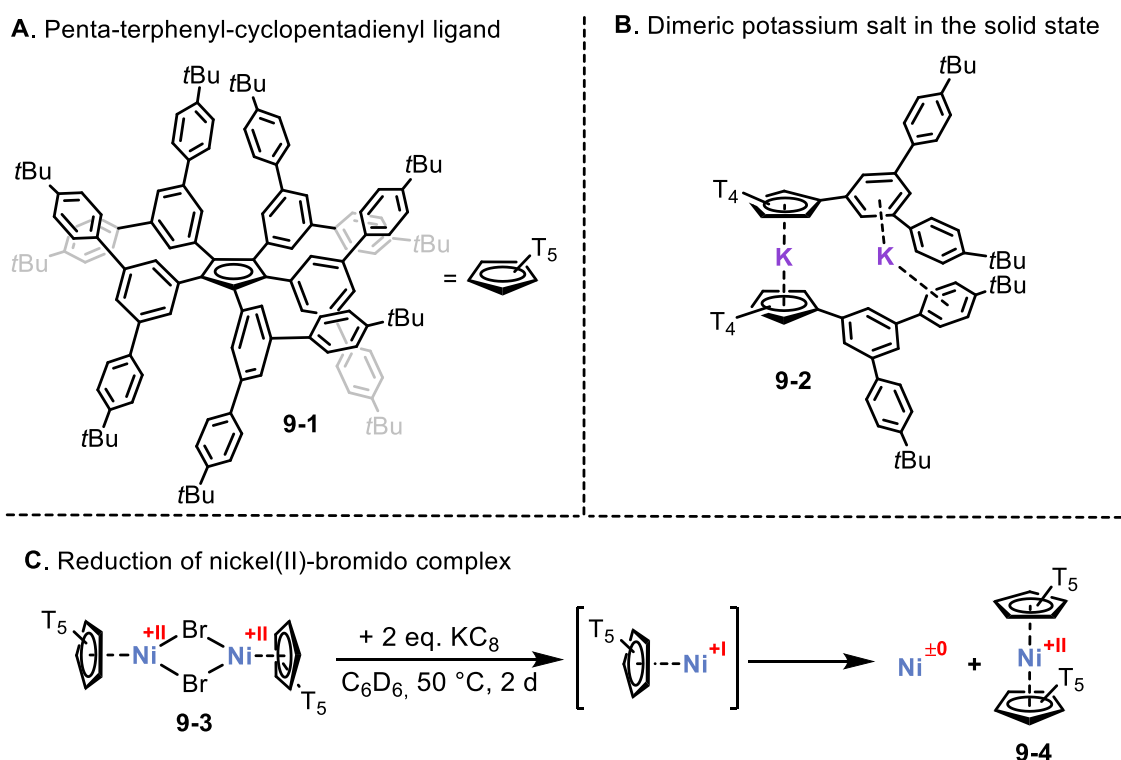
Figure 3. A penta-terphenyl cyclopentadienyl ligand **9-1**, its potassium salt **9-2** and reduction of the nickel(II)-bromido complex **9-3**.

Furthermore, the dimeric bromido complexes [Cp^{T5}MBr]$_2$ [M = Fe(thf), Br, Ni (**9-3**)] were synthesised and their reduction reactions with KC$_8$ were studied, aiming at the preparation of dimetallocenes [Cp^{T5}M]$_2$ or related metal(I) species. Unfortunately, the desired products could not be isolated during initial studies. Instead, the formation of the bulky nickelocene **9-4** was observed upon reduction of **9-3** with two equivalents of KC$_8$. While the initially targeted dimetallocenes were not obtained so far, it is nevertheless expected that this super-bulky ligand offers sufficient steric protection for the preparation of as-yet-undiscovered structural motifs such as reduced metallocenes or pseudo-monocoordinate metal complexes.

Conclusion

In summary, this doctoral thesis highlights the myriad opportunities available in the so far underexplored field of phosphatetrahedranes. For example, even though the reactivity of white phosphorus has been studied for decades, reactions with simple Ni(0) complexes readily afforded nickel phosphorus clusters with valuable new structural motifs. In future studies, the use of these species as readily accessible single source precursors for binary nickel phosphide nanomaterials will be explored. A particular highlight of the work described in this thesis was the discovery of di-*tert*-butyldiphosphatetrahedrane (**4-1**). This molecule is not only the hybrid of two long-known tetrahedranes [P$_4$ and (*t*BuC)$_4$], but also the long-sought-after free phosphaalkyne dimer. The facile preparation of this remarkable molecule has opened a new vista in phosphorus chemistry. As an illustration of the exciting potential of this compound as a new organophosphorus precursor, exploratory studies focused on reactions of **4-1** with N-heterocyclic carbenes, nickel(0) and nickel(I) complexes, and low-oxidation state ferrate and cobaltate salts. The results show that **4-1** is a wellspring of novel reactivity and a versatile source of previously inaccessible compounds. As such, it can be confidently predicted that, many more exciting aspects and applications of the reactivity of this striking molecule are still waiting to be discovered. Thus, in addition to the results already described herein, this thesis has also laid the foundation for the future synthesis of many other novel compounds which are of interest in fundamental and applied research, spanning further mixed (phospha-)tetrahedranes, organophosphorus compounds, transition metal phosphide clusters and phosphorus-based materials.

11 Acknowledgements

All meinen Freunden sowie meinen Geschwistern Lisa und Tobias und meinen Eltern Hermine und Franz-Xaver gilt ganz besonderer Dank für ihr großes Verständnis und die Unterstützung in vielerlei Hinsicht.

Zuletzt möchte ich mich bei meinem Partner Sebastian für die Geduld und den Rückhalt während meiner Promotionszeit bedanken. Danke, dass du mich in schwierigen Phasen unterstützt hast und in guten Phasen meine Freude und Euphorie geteilt hast.

12   Curriculum Vitae

Education

November 2017 to present:	<u>University of Regensburg, Germany:</u> PhD thesis in the group of Prof. Dr. Robert Wolf
April to September 2017:	<u>University of Oxford, UK:</u> Master's thesis with Prof. Jose M. Goicoechea, title: "*Using Heavier Group 15 Cyanate Analogues for the Synthesis of New Metal Pnictogen Complexes*"
2015 to 2017:	<u>University of Regensburg:</u> M. Sc. Chemistry, average grade 1.0
2012 to 2015:	<u>University of Regensburg:</u> B. Sc. Chemistry, average grade 1.0
2004 – 2012:	<u>Donau-Gymnasium Kelheim:</u> High school diploma ("Abitur"), average grade 1.2

Awards and Scholarships

- Best oral presentation awards at *Online Workshop on Phosphorus Chemistry* (OWPC, 3/2021), *Koordinationschemikertagung* (Coordination Chemistry Conference, KCT), Freiburg, Germany (3/2020) and European Workshop on Phosphorus Chemistry"(EWPC) at Uppsala, Sweden (3/2018).

- Finanzielles Anreizsystem zur Förderung der Gleichstellung (Women's Equality Scholarship) for a 6-week research project at the University of Sussex, UK

- Kékulé-Stipendium scholarship of the Fonds der Chemischen Industrie (FCI) for PhD (7/2018 - 6/2020)

- DAAD scholarship for *International Conference on Coordination Chemistry* in Sendai, Japan (8/2018)

- Dr. Alfons Paulus award for the best final grade of chemistry students in Regensburg for B.Sc. and M.Sc. (2016 and 2018)

- Otto-Bayer scholarship (Bayer AG) for a research stay at the University of Oxford (4/2017-9/2017)

- August-Wilhelm-von-Hofmann-Stiftung and Deutschlandstipendium scholarships for B. Sc. and M. Sc. (2013-2017)

Conference Contributions

- 3/2021: *Online Workshop on Phosphorus Chemistry* (OWPC), oral presentation

- 6/2020: *P-Chemistry Webinar Series*, oral presentation

- 3/2020: *Koordinationschemikertagung* (Coordination Chemistry Conference, KCT) in Freiburg, Germany, oral presentation

- 12/2019: *Christmas Colloquium* in Regensburg, Germany, oral presentation

- 8/2019: *Hirschegg-Kolloquium* in Hirschegg, Austria, oral presentation

- 4/2019: *European Workshop in Phosphorus Chemistry* (EWPC) in Bristol, UK, session chair and poster presentation

- 10/2018: *Wöhlertagung* in Regensburg, Germany, poster presentation

- 8/2018: *International Conference on Coordination Chemistry* (ICCC) in Sendai, Japan, oral presentation

- 3/2018: *European Workshop in Phosphorus Chemistry* (EWPC) in Uppsala, Sweden, oral presentation

- 9/2017: *RSC Main Group Interest Annual Meeting* in London, UK, poster presentation

- 9/2017: *Dalton Younger Members Event* in Bath, UK, poster presentation

13   List of Publications

8)   <u>G. Hierlmeier</u>, R. Wolf, "Activation of Di-*tert*-butyldiphosphatetrahedrane: Access to (*t*BuCP)*ₙ* (*n* = 2, 4) Ligand Frameworks by P–C Bond Cleavage", *Angew. Chem. Int. Ed.* **2021**, *60*, 6435–6440; *Angew. Chem.* **2021**, *113*, 6507–6512.

7)   <u>G. Hierlmeier</u>, M. K. Uttendorfer, R. Wolf, "Di-*tert*-butyldiphosphatetrahedrane as a building block for phosphaalkenes and phosphirenes", *Chem. Commun.* **2021**, *57*, 2356–2359.

6)   C. G. P. Ziegler, C. Taube, J. A. Kelly, <u>G. Hierlmeier</u>, M. Uttendorfer, J. J. Weigand, R. Wolf, "An unusual $Ni_2Si_2P_8$ cluster formed by complexation and thermolysis", *Chem. Commun. 2020, 56,* 14071–14074.

5)   J. Leitl, P. Coburger, D. J. Scott, N. P. van Leest, C. G. P. Ziegler, <u>G. Hierlmeier</u>, B. de Bruin, C. Müller, R. Wolf, "Phosphorus-Analogues of [Ni(bpy)₂]: Synthesis and Application in Carbon-Halogen Bond Activation", *Inorg. Chem.* **2020**, *59*, *14*, 9951–9961.

4)   <u>G. Hierlmeier</u>, P. Coburger, N. P. van Leest, B. de Bruin, R. Wolf, "Aggregation and Degradation of White Phosphorus Mediated by 12 Valence Electron Nickel(0) Fragments", *Angew. Chem. Int. Ed.* **2020**, *59*, 14148–14153; *Angew. Chem.* **2020**, *132*, 14252–14257. (highlighted in *Nachr. Chem.* **2021**, *69*, 66–80)

3)   <u>G. Hierlmeier</u>, P. Coburger, M. Bodensteiner, R. Wolf, "Di-*tert*-butyldiphospha-tetrahedrane: Catalytic Synthesis of the Elusive Phosphaalkyne Dimer", *Angew. Chem. Int. Ed.* **2019**, *58*, 16918–16922 ; *Angew. Chem.* **2019**, *131*, 17074-17078. front cover: *Angew. Chem. Int. Ed*. **2019**, *58*, 16699. (highlighted in *ChemistryViews* and *Angew. Chem. Int. Ed*. **2020**, *59*, 10698–10700; *Angew. Chem.* **2020**, *132*, 10786–10788.)

2)   <u>G. Hierlmeier</u>, A. Hinz, R. Wolf, J. M. Goicoechea, "Synthesis and Reactivity of Nickel-Stabilised $\mu^2{:}\eta^2{,}\eta^2$-P_2, As_2 and PAs Units", *Angew. Chem. Int. Ed.* **2018**, *57*, 431–436; *Angew. Chem.* **2018**, *130*, 439–444. (highlighted in *Nachr. Chem*. **2019**, *67*, 46–64 and *Nachr. Chem*. **2019**, *67*, 65–80)

1)   L. R. Collins, <u>G. Hierlmeier</u>, M. F. Mahon, I. M. Riddlestone, M. K. Whittesey "Unexpected Migratory Insertion Reactions of M(alkyl)₂ (M=Zn, Cd)", *Chem. Eur. J.* **2015**, *21*, 3215–3218.

Supporting Information

The Supporting Information of this thesis contains the supporting information of all published material (chapters 3, 4, 6 and 7). It contains analytical data (NMR spectra, UV/Vis spectra, IR spectra, EPR spectra, X-ray crystallography and cyclic voltammograms) as well as details on quantum chemical calculations. The pdf file is stored on an external CD-ROM, which is supplied with this thesis.

Eidesstattliche Erklärung

Ich erkläre hiermit an Eides statt, dass ich die vorliegende Arbeit ohne unzulässige Hilfe Dritter und ohne Benutzung anderer als der angegebenen Hilfsmittel angefertigt habe; die aus anderen Quellen direkt oder indirekt übernommenen Daten und Konzepte sind unter Angabe des Literaturzitats gekennzeichnet. Die Arbeit wurde bisher weder im In- noch im Ausland in gleicher oder ähnlicher Form einer anderen Prüfungsbehörde vorgelegt.

_____

Gabriele Hierlmeier